SCHOLARLY PUBLICATIONS

A CURRENT AWARENESS BULLETIN
OF RESEARCH OUTPUT

@DTU

(23rd Edition)

NOVEMBER 2014

BY: CENTRAL LIBRARY

DELHI TECHNOLOGICAL UNIVERSITY
(FORMERLY *DELHI COLLEGE OF ENGINEERING)*
GOVT. OF N.C.T. OF DELHI
SHAHBAD DAULATPUR, MAIN BAWANA ROAD
DELHI 110042

PREFACE

This is the Twenty third Issue of Current Awareness Bulletin started by Delhi Technological University, Central Library. The aim of the bulletin is to compile, preserve and disseminate information published by the faculty, students and alumni for mutual benefits. The bulletin also aims to propagate the intellectual contribution of Delhi Technological University (DTU) as a whole to the academia.

The bulletin contains information resources available in the internet in the form of articles, reports, presentations published in international journals, websites, etc. by the faculty and students of DTU. The publications of faculty and student which are not covered in this bulletin may be because of the reason that the full text either was not accessible or could not be searched by the search engine used by the library for this purpose.

The learned faculty and students are requested to provide their uncovered publications to the library either through email or in CD, etc to make the bulletin more comprehensive.

This issue contains the information published during November 2014. The arrangement of the contents is alphabetical. The full text of the article which is either subscribed by the university or available in the web is provided in this bulletin.

Central Library

CONTENTS

1. A visionary in-vitro analysis for anti-bacterial potential using seeds of a deciduous shrub, Punica granatum, Hemant Kr. Sharma, Anjali Sharma, Yunus Parvez, Harshit K. Shrivastava and ***Shashank Kr. Singh***, Deptt. of Biotechnology, DTU

2. An approach to generate students' response on learning environment using Association Rule Mining, Jindal Rajni and ***Dutta Borah Malaya***, Computer Engineering, DTU

3. Analysis of Optimal Carrier Sensing Range in Wireless, Ad Hoc Networks with Order Dependent Capture Capability, Mayur M. Vegad, Swades De and ***#Brejesh Lall***, B.E. and M.E. in electronics and communication engineering, DTU

4. APPLICATION OF GREEN CHEMISTRY PRICIPLES IN ORGANO-GRIGNARD REACTIONS, ***INVESTIGATION OF FREQUENCY DEPENDENT PARAMETER OF GEWE-SiNW MOSFET FOR MICROWAVE AND RF APPLICATIONS*** (From pg. 61 onwards), ****Neha Gupta, *Ajay Kumar*** and ****Rishu Chaujar***, Engineering Physics, DTU

5. CDTA BASED CURRENT MODE ADC, ****Neeta Pandey, *Rajeshwari Pandey, *Ranjana Sridhar, *Veepsa Bhatia, *Alok Kumar Singh*** and ****Pradeep Kumar***, Electronics and Communication Engineering, DTU

6. Control of DC-Fault-Resilient Voltage Source Converter Based HVDC Transmission System under DC Fault Operating Condition, Nima Yousefpoor, Student Member, IEEE, ***#Ajit Narwal***, and Subhashish Bhattacharya

7. Defect Collection and Reporting System for Git based Open Source Software, ****Ruchika Malhotra, *Nakul Pritam, *Kanishk Nagpal*** and ****Prakarsh Upmanyu***, Computer Engineering, DTU

8. Design and analyze the Refractive Index sensor having the discontinuity between sensing region and cladding area by large core diameter, ****Himanshu Mohan***, Gopal, Ajeet Kumar, DTU

9. DESIGN AND STUDY OF A SOLAR THERMAL SYPHON PUMP Md. Zishan Akhter, Md. Sarwar Khan, Md Sameer Farooque, ***@Kaushalendra K. Dubey***, Gopal P. Sinha, DTU

10. Design of CDTA and VDTA Based Frequency Agile Filters, ****Neeta Pandey1, *Aseem Sayal2, *Richa Choudhary3, *Rajeshwari Pandey4,*** 1,4Deptartment of Electronics and Communication Engineering, 2,3Deptartment of Electrical Engineering, DTU

11. DETECTION CLASSIFICATION AND LOCATION OF FAULTS ON 220 KV TRANSMISSION LINE WITH STATCOM USING WAVELET TRANSFORM AND NEURAL NETWORK, R.P. Hasabe1, A. P. Vaidya2, (From pg. 67 onwards) ***INVESTIGATIONS ON EFFECT OF INCORPORATION OF PHOTOVOLTAIC SYSTEM WITH COMBINED CYCLE GAS TURBINEPLANT,*** Naimul Hasan, ****B.B .Arora***, J.N. Rai, Mechanical Engineering, DTU

12. DUAL MODE BIQUADRATIC FILTER USING SINGLE VDTA, ****Navin Singhal *Rajeshwari Pandey*** and ****Neeta Pandey***, Electronics and Communication, DTU

13. Electrical Prototype Model of Pantograph-Catenary System, ****Rachana Garg***, ****Priya Mahajan***, ****Parmod Kumar*** and ****Vidushi Gupta***, Deptt. of Electrical Engg, DTU

14. Empirical Validation of Website Quality Using Statistical and Machine Learning Methods, ****Poonam Dhiman*** and ****Anjali****, Software Engineering, DTU

15. Forward Osmosis in India: Status and Comparison with Other Desalination Technologies, ****DhruvMehta, *Lovleen Gupta***, and ****Rijul Dhingra***, Environmental Engineering, DTU

16. INVESTIGATIONS ON EFFECT OF INCORPORATION OF PHOTOVOLTAIC SYSTEM WITH COMBINED CYCLE GAS TURBINEPLANT, Naimul Hasan, ****B.B .Arora***, J.N. Rai, Department of Mechanical Engineering, DTU

17. Luminous TCAD Analysis of Transparent ITO Gate Recessed Channel MOSFET using Elliptical Lenslet, ****Anuj Kumar Sinha***, and ****Rishu Chaujar***, Microelectronics Research Lab, Department of Engineering Physics, DTU

18. MODELING OF 5-LEVEL CHB AS DSTATCOM FOR COMPENSATION OF POWER QUALITY ISSUES ***(DESIGN AND STUDY OF A SOLAR THERMAL SYPHON PUMP)*** (From pg. 46 onwards) Md. Zishan Akhter, Md. Sarwar Khan, Md Sameer Farooque, ***@Kaushalendra K. Dubey***, Gopal P. Sinha, Dept of Mechanical, Production, Industrial & Automobile Engg, DTU

19. NOVEL OSCILLATORS IN SUBTHRESHOLD REGIME, ****Neeta Pandey, *Kirti Gupta, *Rajeshwari Pandey, *Rishi Pandey*** and ****Tanvi Mittal***, Electronics and Communication Engineering, DTU

20. Numerical Study of the generic Sports Utility Vehicle design with a drag reduction add-on device, ****Shubham Singha, *M. Zunaid, *Naushad Ahmad Ansari, *Shikha Bahirani, *Sumit Dhall*** and ****Sandeep Kumar***, Department of Mechanical engineering, DTU

21. Optimization of Tool Wear: A Review, Ramakant Rana, Kunal Rajput, Rohit Saini, ****Roop Lal,*** Mechanical Engineering, DTU

22. Spectroscopic studies of Nd3+ doped lead tungsten tellurite glasses for the NIR emission at 1062 nm, M. Venkateswarlu, Sk. Mahamuda, K. Swapna, M.V.V.K.S. Prasad, ****A. Srinivasa Rao***, A. Mohan Babu, Suman Shakya, G. Vijaya Prakash, Applied Physics

23. Status of E-Waste in India - A Review, Mahesh C. Vats and ****Santosh K. Singh***, Professor & Dean, Department of Environmental Engineering, DTU

24. Throughput Calculation according to User Location in LTE-A Network, Kishor Pratap Singh, ***#Pradeep Kumar Chopra,*** DTU

***Faculty** **@Research Scholar** **$PG Scholar**
#Alumni **£Undergraduate Student** **~ Ex Faculty**
! Teaching-cum-Research Fellow **<Ex Research Scholar** **>Ex PG Scholar**

Available online at www.pelagiaresearchlibrary.com

Pelagia Research Library

European Journal of Experimental Biology, 2014, 4(5):117-122

ISSN: 2248 –9215
CODEN (USA): EJEBAU

A visionary *in-vitro* analysis for anti-bacterial potential using seeds of a deciduous shrub *Punica granatum*

Hemant Kr. Sharma[1*], Anjali Sharma[3], Yunus Parvez[3], Harshit K. Shrivastava[3] and Shashank Kr. Singh[2]

[1]*Cytogene Research & Development, LLP, Indira Nagar, Lucknow, U.P., India*
[2]*Deptt. of Biotechnology, Delhi Technological University, New Delhi, India*
[3]*Deptt. of Biosciences, Faculty of Applied Science, Integral University, Lucknow, U.P., India*

ABSTRACT

Punica granatum i.e., pomegranate plays a very important role in Indian fruit market. From very ancient times pomegranate has been used for many medicinal purposes to cure many short term as well as long term disorders. The current study proves that Punica granatum is having a very strong anti-bacterial activity. For the present study firstly, we have used granatum seeds, pericarp (peel) as well as juice to evaluate the antibacterial activity of the fruits against enteric bacteria i.e. E. coli. For the detection of antibacterial activity agar gel diffusion method was used. As a result zone of inhibition was only shown by seed. On the other hand, zone of inhibition was not observed in juice and peel. So it was concluded that, the granatum seeds persists the anti-bacterial property. Secondly, solvent extract of the pomegranate peel i.e. water, ethanol and methanol extracts were prepared and antibacterial activity was tested against enteric bacteria E. coli by the method of agar diffusion method. As a result, methanol and ethanol extract showed almost same zone of inhibition (21 mm) while water extract showed comparatively less zone of inhibition (13 mm) with respect to control ofloxacin (32 mm) at 150 ppm.

Keywords: *Punica granatum*, Deciduous, Zone of Inhibition, Ofloxacin, Agar Diffusion.

INTRODUCTION

Punica granatum Linn. (Pomegranate) is a member of family *Punicaceae* which is a deciduous spreading shrub or small tree and has thorns with it. This plant is found all over India. Pomegranate peel is an inedible part obtained during processing of Pomegranate juice. Pomegranate peel is a rich source of tannins, flavonoids, polyphenols and some anthocyanins as Delphinidins, Cyanidins, etc. [1]. Antioxidant and antibacterial properties of pomegranate peel in in-vitro model systems have been reported [2][3][4].The compounds of pomegranate peels are reported to have therapeutic properties.

The objectives of present study were to evaluate the antibacterial activity of different parts of pomegranate fruit. During the experiment different parts of pomegranate i.e. pericarp, juice and and seeds were separated. They were grounded into fine paste by incorporating water. The mixture was filtered and the supernatant was used to detect the antibacterial activity by the agar diffusion method. As a result pericarp and fruit juice did not showed any zone of

inhibition where as seed showed clear zone of inhibition which was measured out to be 17mm in comparison to zone of inhibition of ofloxacin which was measured to be 32mm.

Further the pericarp of the fruit was peeled out. It was sundried to exclude moisture or water content. The pericarp was grounded into fine powder with the help of mixer grinder. Solvent extracts of the powdered peel was prepared in water, methanol, and ethanol.

The antibacterial activity of the three solvent extracts were detected by using agar diffusion method in which methanol and ethanol extract showed almost equal zone of inhibition (21 mm) whereas water extract showed lesser zone of inhibition (13 mm) as compared to zone of inhibition of ofloxacin (32mm) at 150ppm.

MATERIALS AND METHODS

Collection of Sample :
Pomegranate was collected from local market in Lucknow . The fruit was first washed with tap water followed by washing with distilled water.

The fruit was cut to separate out its peel, juice, and seed. The peel and seed were grinded by incorporating distilled water with the help of mixer grinder. The fruit juice, seed and peel extract were then filtered by whatmann's filter paper no. 1 and the filtrate were collected which were used to study antibacterial property.

Figure 1 : Powdered Pericarp

In the other section of the study fruit peels were cut into smaller pieces and then first washed with tap water followed by distilled water. It was then dried under sunlight until water droplets got completely evaporated. Pericarp or peel was then completely dried in microwave. Dried pericarp was then taken for grinding by the help of mixer grinder. The powdered pericarp was used throughout the study.

Model organisms:
Anti-bacterial property of *Punica granatum* was tested against enteric bacteria *Escherichia coli*.

Media Preparation:
A) Nutrient Agar Media : Nutrient agar media was found to be suitable for the growth of bacteria. Nutrient Agar 28 gm, in 1000 ml distilled water. Nutrient agar media preparation must be performed in the following order -
1. 2.8 gm of Nutrient agar dissolved in 100ml distill water.
2. The media was sterilized at 15 lbs (121˚C) for 15 minutes in an autoclave.
3. In the laminar flow poured the media in Petri dish, amount of nutrient agar is 25 ml in each Petri dish.
4. Leave the Petri dish in laminar air flow for 2-3 hrs for solidification.
5. Solidified media is prepared for spreading/streaking, take *E. coli* culture and spread / streak on the plate surface.
6. The plate was kept in the incubator for overnight at 37^{o}C temperature
7. After overnight incubation, colonies were well developed in the Petri dish

8. *E. coli* plates were prepared. It is used when necessary.

B) Nutrient Broth :- Preparation of Nutrient broth in 100 ml.Nutrient broth performed in the following order.
1. 3gm of Nutrient Broth was taken and dissolved in 100ml Distilled Water.
2. Autoclaved it at 121^{o}C for 15 minutes.
3. Cool the nutrient broth at room temperature.
4. One colony isolated from the master plate.
5. This colony inoculated in the nutrient broth by inoculated loop.
6. Left the prepared flask in the Incubator for overnight at 37^{o} C.
7. Nutrient broth culture is prepared for culturing.

MATERIALS AND METHODS

A) Extraction procedure:- The powdered pericarp was dissolved in different solvents. The solvents used were methanol, ethanol and water. 5gm of ground pericarp was added to 50ml of hot boiling water and left in hot water bath for an hour at 70 degree Celsius so that secondary metabolites got completely extracted. The extract was then filtered with the help of whatmann's filter paper no.1 and kept in microwave for drying. Similarly ethanoic and methanoic extraction were carried out where 5 gm of dried powder was added to 50ml of 80% methanol and 70% methanol and kept in dark for 3 to 4 days. The solvent extracts were filtered and resultant was used to get the antibacterial activity.

Figure 2 : Solvent Extracts of Powdered Pericarp

Figure 3 : Antibacterial Sensitivity Of Seed Part By Kirby Bauer Method

B) Screening of the fruit part for antibacterial activity: Antibacterial activity was assessed by agar well diffusion method by Kirby Bauer where in nutrient agar plates were prepared and were spread with 20 µl of *E. coli* broth culture. Wells of 8mm diameter were bored. Wells were loaded with ofloxacin as standard and distilled water as negative control and the resultant of fruit parts i.e. fruit juice, peel and seed extract.

C) Screening of the extracts for antibacterial activity: Antibacterial activity was assessed by agar well diffusion method of Kirby Bauer where nutrient agar plates were prepared and were spread with 20 µl *E. coli* broth culture in 100 mm petri dish. Wells of 8 mm diameter were bored. Wells were loaded with ofloxacin as standard, distilled water as negative control and solvent extract of fruit pericarp.

Figure 4: Antibacterial Sensitivity of Solvent Extracts By Kirby Bauer Method

RESULTS AND DISCUSSION

The development of drug resistance in many microorganisms against commonly used antibiotics laid the basis for search of new antimicrobials of plant origin. As in this study pomegranate was screened for anti-bacterial activity. The results of the study are observed as follows:-

Figure 5 : Inhibition zone By Water Extract Of Pericarp

Figure 6 : Inhibition zone by Ethanol Extract Of Pericarp

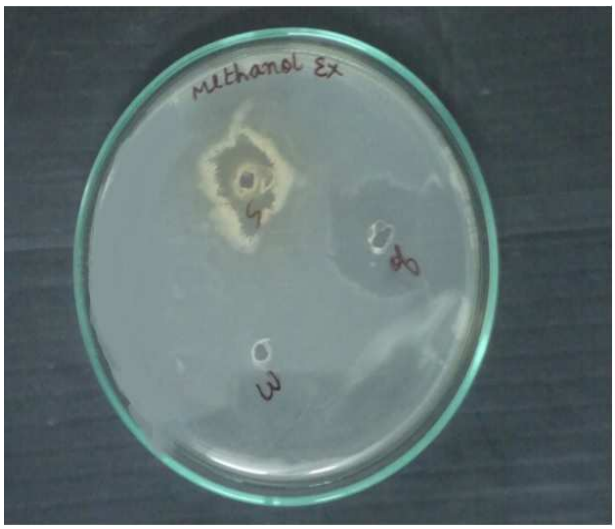

Figure 7 : Inhibition zone By Methanol Extract Of Pericarp

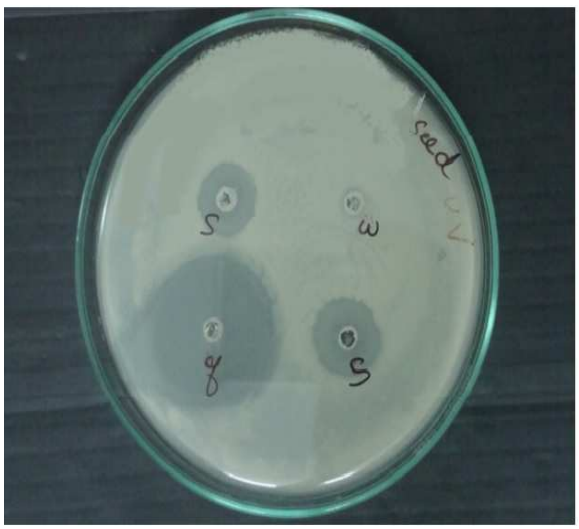

Figure 8 : Inhibition Zone by Seed

1)Antibacterial Activity Of Fruit Parts :

Table 1 :

TEST ORGANISM	Sr. No.	PARTS OF FRUIT	INHIBITION Zone OF OFLOXACIN(+VE control)	INHIBITION Zone OF FRUIT PART WITHOUT SOLVENT EXTRACT
E.coli	1	Juice	32mm	-
E. coli	2	Seed	32mm	17mm
E. coli	3	Peel (pericarp)	32mm	-

2)Antibacterial Activity Of Solvent Extracts Of Fruit Pericarp:

Table 2 :

Hot aqueous extract of pericarp		Methanolic extract of pericarp		Ethanolic extract of pericarp	
INHIBITION ZONE BY OFLOXACIN(+VE control)	INHIBITION ZONE BY SAMPLE	INHIBITION ZONE BY OFLOXACIN(+VE control)	INHIBITION ZONE BY SAMPLE	INHIBITION ZONE BY OFLOXACIN(+VE control)	INHIBITION ZONE BY SAMPLE
31mm	13mm	33mm	21mm	32mm	21mm

Nearly 80% of the world populations depends on the traditional medicine for primary health care, mainly including the use of natural products. Researchers have extensively studied the biological properties of *Punica granatum* and their results showed that this plant is ethno medically valuable. *Punica granatum* peel extracts are currently used for treatment of respiratory diseases and in the preparation of therapeutic formulae. The tannin rich ell-agitannins and phenolic acids of *Punica granatum* have antibacterial, antifungal and anti-protozoal activity.

In the current study the hot aqueous extract of pericarp showed zone of inhibition of 13 mm, methanolic and ethanolic extracts of *Punica granatum* showed almost equal zone of inhibition of 21 mm against *enteric bacteria E. coli.*

In the other section of the study the seed of pomegranate exhibited clear zone of inhibition of 17 mm on the other hand the other parts of the fruit i.e. pericarp and juice did not showed any zone of inhibition. Broad spectrum anti-microbial compounds that act against both gram +ve and gram –ve bacteria. Ethanolic extracts and Methanolic extracts exhibited higher degree of antibacterial activity as compared to that of hot aqueous extracts tested against bacteria that cause gut infection, stomachache, diarrhoea. It is reported that *Punica granatum* contains large amount of tannins (25 %) and antibacterial activity may be indicative of presence of secondary metabolites.

CONCLUSION

Plant extracts are complex and isolating bioactive compound is challenging. Only a few extracts have generally been used for extracting antibacterial compounds from plants. In the present study, the organic solvents proved to be much better than that of aqueous extracts in inhibiting enteric bacteria *E. coli.*

On the other hand, seed of *Punica granatum* inhibited the enteric bacteria *E. coli*. Hence it can be concluded that "seed part" of pomegranate have anti-bacterial properties.

Acknowledgement
We are extremely indebted to our close friends and colleagues for their constant support during the whole of this research work. Special thanks to Ms. Anjali Sharma for her kind support and dedication. God bless them all.

REFERENCES

[1] Li, Y., Guo, C., Yang, J., Wei, J., Xu, J., Cheng, S., *Food Chemistry, Elsevier* (**2006*)***, 2, 96, 254-260.
[2] Negi, P.S., Jayaprakasha, G.K., Jena, B.S., *Food Chemistry*, *Elsevier* (**2003*)***, 3, 80, 393-397.
[3] Opara, L.U., Al-Ani, M.R., Al-Shuaibi, Y.R., *J. of Food and Bioprocess Tech.* (**2009*)***, 3, 2, 315-321.
[4] Al-Zoreky, N.S., *Int. J. of Food Microbio. (****2009*)***, 3, 134, 244-248.

An approach to generate students' response on learning environment using Association Rule Mining

Jindal Rajni
Department of IT
Indira Gandhi Delhi Technical University for Women
Delhi-110006, India
rajnijindal@dce.ac.in

Dutta Borah Malaya
Department of Computer Engineering
Delhi Technological University, Delhi-110042, India
malayadutta@dce.ac.in

Abstract— **To enhance the quality and cost effectiveness of the education, students participation and a better understanding of the learning is important. The proliferation of learning innovations such as distributed and heterogeneous applications and resources requires the adoption of appropriate technique to deal with the various information flows to support learning. Association Rule Mining is one the prominent Data Mining technique that helps to find out the items frequently appears in the dataset, relationships among different attributes in a large search space. The focal point of this work is to measure learner's beliefs, interests in particular subjects and ultimately generate students' response in on learning environment using Association Rule Mining. For training and testing purpose, we used the 'Motivation and Metacognition in Chinese Vocabulary Learning, Experiment 3 (27,421 transactions) & 5 (72,249 transactions) dataset accessed via DataShop.**

Keywords*— *Data Mining; Association Rule Mining; Learning; Students response

I. INTRODUCTION

In today's competitive world, right place, right times are the crucial factors to ensure right decision from large amount [1]. To deal with the large amount of data stored in the database, Data Mining (DM) has been introduced. In literature, it can also refer as data archaeology, data pattern processing, information discovery, and information harvesting and knowledge extraction [2]. It deals with the data, explores, built the model and finally provides the knowledge that helps decision makers for better decisions. Various DM techniques are in literature. Association Rule Mining, Classification, Clustering and Neural Networks are few of them.

DM in educational domain plays a vital rule by providing intrinsic knowledge of teaching and learning process for effective education planning [3][4][5]

Proliferation of learning innovations such as personal devices, distributed and heterogeneous applications and resources, requires the adoption of appropriate approaches to deal with information flows in learning environments. Such approaches are beneficial to identify students at risk, to analysis of performance, to provide guidance and to create measures for future decision making process [6]. It is to quite challenging to find out effectively and efficiently the interestingness, association of students' participation and obtain their response for a particular event on online teaching and learning environment[7][8]. Association Rule Mining (ARM) is one the prominent DM technique that helps to find out the items frequently appearing in the dataset, relationships among different attributes in a learning environment.

In this paper, we are exploring applicability of ARM in learning environment, measuring learner's beliefs, and interests in particular lesson and finally generating students' response in on line learning environment.

The paper is organized in 4 sections. : section 2 is about related research works, section 3 presents approach used to generate students response, and in section 4 gives the conclusion of our work.

II. RELATED WORKS

This section discusses related research works about ARM followed by its applicability in educational (learning) domain.

In 1993, the concept of Association Rule was introduced by R. Agrawal et al. [9] for mining transactional database. It finds the frequent pattern, co-relations and associations among itemsets presents in a database. The idea behind the Agrawal research is as follows:

"Let I = {i1, i2, ..., in} be a set of n binary attributes called items. Let D = {t1, t2, ..., tn} be a set of Transactions called the database. Each transaction in D has a unique transaction ID and contains a subset of the items in I. A rule is defined as an implication of the form X→Y where X, Y □ I and X ∩Y=□. The sets of items X and Y are called antecedent (left-hand-side and consequent (right-hand-side) of the rule respectively."

Other terminologies used in this approach are as follows:

- user defined minimum support (Support(X)= no. of transactions which contain the itemset X / total no. of transactions) and
- Confidence (Conf (X→Y)=Support(X U Y)/ Support(X)).

These measures of interestingness are suitable for finding out frequent itemsets and useful rules from a set of possible rules. The base algorithm in ARM is Apriori algorithm which is a level wise, iterative, down ward closure algorithm [10]. The key concept of this algorithm is that for a frequent itemset, all its subsets are also frequent. It is a two way process: one is to generation of candidate set and second is to find out the frequent itemset from those candidate itemset with a user defined minimum support.

For mining quantitative attributes, a distance based discretization method was introduced [11].This method is useful

978-1-4799-4674-7/14/ $ 31.00@2014 IEEE

for two-dimensional association rules and clustering. Utility factors such as density and frequency are important factor in ARM that can be defined as weighted ARM [12].

Another concept of ARM is Multiple Level ARM [13]. In a real world problem, data are lying in multidimensional space. It is difficult to find out the suitable rules in low level abstraction where at higher level it may be novel to some other users. Hence there is a possibility to find strong/ suitable rules at "intra" and "inter" level of abstraction. To mine different level of abstraction, Multiple Level ARM is used.

In context of educational domain [14], ARM has been successfully applied [15] [16]. Most of the work was based on Apriori algorithm [17]. E.g.: To find the relationships among rules of course which is significant for curriculum development, to discover behaviours and strategies for learner and teacher [18] [19].

Association rules found to be very important in practical applications. To measure the interesting rules, in [20], discovered association rules compared with existing users knowledge. A process of discovery of association rules without parameters were described in [21]. It plays vital rules in collaborative recommender systems [22]. This system is based by experts' opinions and suggestion is made for better solution which is based on overall experience.

Our work is based on the discovery of generalised association rules in learning environment. It is different from the previous works in the sense that large amount of data (72,249 transactions) has been used for training and testing purpose, and association rules with 100% confidence are considered that are efficient in decision making process in learning environment.

III. APPROACH USED TO GENERATE STUDENTS' RESPONSE

To enhance the quality and cost effectiveness of the education it is necessary to measure the expectations of students in learning environment. Learning is process that governs by many factors such as [23][24]:

- Skills
- Attitudes
- Knowledge
- Participation and
- better understanding of the learning process by students

Though all the mentioned factors are important, students' participation and a better understanding of the learning process should be considered as integral part in online environment.

In traditional learning system, face to face interaction and continual process of evaluation (assignments, semester examination etc) are the way to measure the way of learning of students. But in online learning, Students' expectation and measurement of those expectations is mainly based on the students' participation and generate the students' response accordingly.

The approach used for generating Students response in a particular subject is shown in figure 1. The steps involved are as follows:

- Input data from learning lab
- Pre processing
- Capture the knowledge component and build the model
- Pattern Evaluation and Generate Students Response

Fig. 1 Workflow for Generating Students Response Type

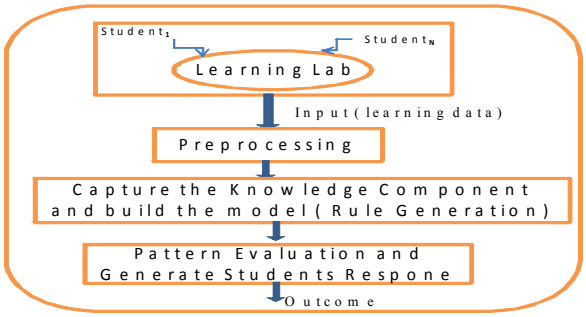

We apply each step to learning lab dataset [25]. Each step is explained in detail below:

A. *Input data from learning lab*

We used the 'Motivation and Metacognition in Chinese Vocabulary Learning, Experiment 3 (27,421 transactions) & 5 (72,249 transactions) dataset accessed via DataShop [25]. Some of the attributes in the dataset are shown in Table 1:

TABLE I. ATTRIBUTES IN LEARNING DATASET

Sl. No	Attributes	Descriptions
1.	Row	1 to N
2.	Sample name	All data (Vocabulary Learning) in learning lab
3.	Anon Student Id	Student Identity
4.	Session Id	Session and lesson for a specific user
5.	Problem start/ session Time	HH:MM:SS
6.	Time Zone	US/Eastern
7.	Duration	Seconds
8.	Student Response Type	Attempt a problem
9.	Student Response sub Type	Event/ Drill
10.	Tutor Response	Suggestions/ Feedback
11.	Problem name	Specific lesson
12.	Problem view	No of times viewing the problem
13.	Condition	Random difficulty
14.	Total Num Hints	No of hits achieved
15.	Knowledge component	Default (lesson), ChineseMM10Fall etc.

The datasets were trained and tested in SPSS Clementine 11.1 environment. A partial view of this environment is shown in figure 2.

Fig. 2 A partial view of SPSS environment

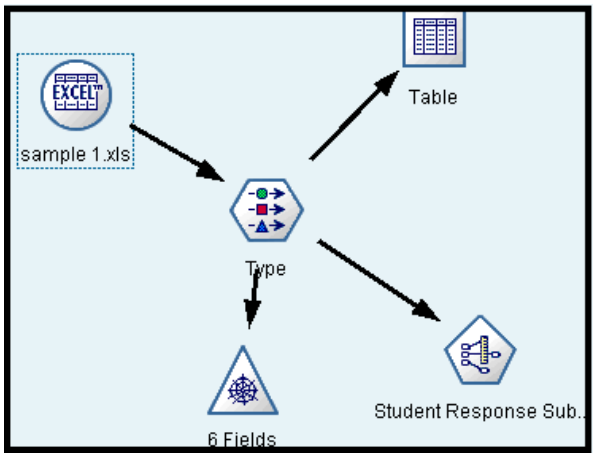

B. *Pre processing*

To provide the suitable data for effective training and testing purpose, there is a necessity to cleanse, integrate and transform of the original data. A major step performed in this process is as follows:

- Identify missing values, special characters, question marks, blanks etc. using "Null Rule"
- Filter out the attributes those are not so important to in model building process (ARM). E.g.: Row, Sample name, Anon Student Id etc.

The resultant snapshot is shown in figure 3.

Fig. 3 Resultant list after pre-processing step

Session Id	Duration (sec)	Student Response Subtype	Level(UNIT)	Problem Name	Problem View	Problem Start Time
session-Lesson8-user4	2.00000000000000E+000	DRILL	Lesson8	9_9_Lesson8	9.000	23:21:46
session-Lesson8-user4	2.00000000000000E+000	EVENT	Lesson8	LAST_SINOGRAPH 8	10.000	23:21:46
session-Lesson8-user4	2.50000000000000E+000	DRILL	Lesson8	9_9_Lesson8	10.000	23:21:51
session-Lesson8-user4	2.50000000000000E+000	EVENT	Lesson8	LAST_SINOGRAPH 8	10.000	23:21:46
session-Lesson8-user4	3.00000000000000E+000	DRILL	Lesson8	1_1_Lesson8	8.000	23:21:51
session-Lesson8-user4	1.00000000000000E+000	EVENT	Lesson8	LAST_SINOGRAPH 0	8.000	23:21:54
session-Lesson8-user4	1.00000000000000E+000	DRILL	Lesson8	12_12_Lesson8	8.000	23:21:57
session-Lesson8-user4	1.00000000000000E+000	EVENT	Lesson8	LAST_SINOGRAPH...	8.000	23:21:57
session-Lesson8-user4	4.00000000000000E+000	DRILL	Lesson8	4_4_Lesson8	7.000	23:22:05
session-Lesson8-user4	4.00000000000000E+000	EVENT	Lesson8	LAST_SINOGRAPH 3	7.000	23:21:57
session-Lesson8-user4	7.00000000000000E+000	DRILL	Lesson8	15_15_Lesson8	7.000	23:22:19
session-Lesson8-user4	7.00000000000000E+000	EVENT	Lesson8	LAST_SINOGRAPH...	7.000	23:22:05
session-Lesson8-user4	5.00000000000000E+000	EVENT	Lesson8	RETIRED_SINOGR...	4.000	23:22:19
session-Lesson8-user4	6.00000000000000E+000	DRILL	Lesson8	2_2_Lesson8	10.000	23:22:30
session-Lesson8-user4	1.00000000000000E+000	EVENT	Lesson8	LAST_SINOGRAPH 1	10.000	23:22:30
session-Lesson8-user4	3.00000000000000E+000	DRILL	Lesson8	14_14_Lesson8	10.000	23:22:37
session-Lesson8-user4	3.00000000000000E+000	EVENT	Lesson8	LAST_SINOGRAPH...	11.000	23:22:37
session-Lesson0-user4	6.00000000000000E+000	DRILL	Lesson0	0_0_Lesson0	10.000	23:22:37
session-Lesson8-user4	1.00000000000000E+000	EVENT	Lesson8	LAST_SINOGRAPH 7	10.000	23:22:43
session-Lesson8-user4	5.00000000000000E+000	EVENT	Lesson8	RETIRED_SINOGR...	5.000	23:22:48

C. *Capture the knowledge component and build the model*

In online learning environment is important to the educators to understand students' behaviour and related view in a particular subject matter. This will help for future enhancements of teaching program. To understand their participation, following parameters are important:

- Capture: Capture students interaction/ knowledge component (input data collected from learning lab)
- Build the Model: Apply DM technique(e.g.: ARM)and
- Provide learning outcome (Generate students response)

After capturing the components that is useful to provide knowledge to the user (see figure 3) from learning lab, next step is to build the model using ARM technique (Apriori algorithm). "Building the model" is important step as it fully explains the relationships among important parameters. It is a two way approach:

- Generate all itemsets whose support greater than or equal to user defined minimum support and
- Generate Association Rules from each frequent itemset

The appropriate values for the support and confidence thresholds of association rules depend on the application and the data.

D. *Pattern Evaluation and Generate Students Response*

An ARM technique has a capacity to generate high number of patterns. A Research question based on this matter is that "are all of the patterns interesting"? han, J. Et al, 2007 in [2], defines that a pattern is interesting if it easily understood, Valid on test data, potentially useful, Novel in nature and ultimately provide knowledge to the user.

"Although frequent patterns are interesting in their own right, the end goal of association analysis is often the efficient generation of association rules [9]".

In [26], stated that the rule generated from high confidence from each frequent patterns are efficient. Hence we have considered 100% confidence to efficiently derive the association among learning parameters (see figure 4)

Fig. 4 Outcome after applying ARM technique

Consequent	Antecedent	Support %	Confidence %
Student Response S...	Outcome = EVENT	54.43	100.0
Student Response S...	Level(UNIT) Outcome = EVENT	20.51	100.0
Student Response S...	Duration (sec) = 1.0... Outcome = EVENT	19.8	100.0
Student Response S...	Duration (sec) = 1.0... Problem View < 10.5... Outcome = EVENT	15.33	100.0
Student Response S...	Duration (sec) = 1.0... Level(UNIT) Outcome = EVENT	6.97	100.0
Student Response S...	Session Id = sessio... Outcome = EVENT	1.59	100.0
Student Response S...	Session Id = sessio... Outcome = EVENT	1.59	100.0
Student Response S...	Session Id = sessio... Outcome = EVENT	1.33	100.0

Mapping of associations between different parameters are shown in figure 5. It shows that students' response for a particular lesson tightly associated with outcome "Event".

Fig. 5 Association between Consequent and Antecedent

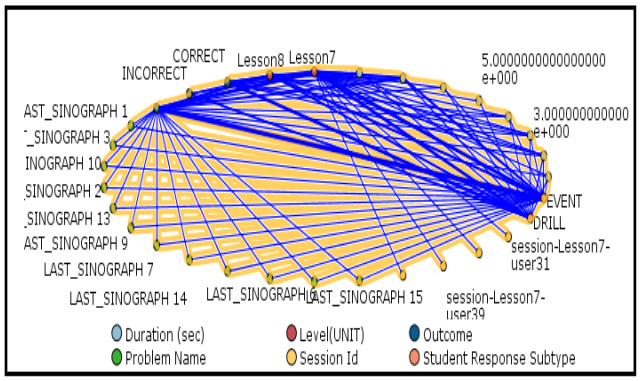

And finally resultant rules to generate appropriate students response are shown in figure 6. "Duration, outcome, problem view and event" are identified as main parameter to generate desired result i.e student response.

E. Results

As an outcome of this approach, twenty numbers of association rules were generated. We have found that "problem view" and "duration" of attempting a lesson are most interesting parameters during rule generation (see rule3, 4 and 5 from figure6). Summarizing the resultant association rules, we get that student response for a particular lesson is mainly based on the following categories:

- Students with "outcome=event" is directly associated with "student response to event"
- Students those were exercising lesson 8 (assigned lesson) and "outcome is event" is associated with "student response to event" and
- Duration for hit a particular lesson is 1.0 sec and viewing a problem is less than 10 no. than "student response is associated with event"

Educators' can use the discovered knowledge from the rules for decision making process.

Fig. 6 Important resultant Rules

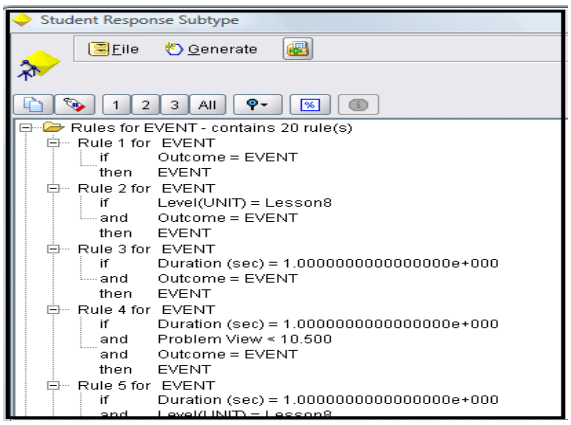

IV. CONCLUSIONS

This paper discusses about the generation of students' response for a particular lesson by:

- Assessing the interestingness of patterns and
- Finding suitable rules using Association Rule Mining technique.

The finding of the work was that ARM generates lots of rules where all are not so important to derive proper knowledge. Hence this work considers rules having 100% confidence.

The knowledge discovered from this rule is beneficial for students as well as educators/ education planners such that

- Students should improve their learning by exercising the target lesson within less amount of time
- Educators can monitor students' participation. E,g.: identifying learners patterns that actively participating, finding frequent mistake level and risk level of students and
- Providing the guidance/ feedback to the students for their future participation and knowledge improvement.

As a future work, we will consider new measures and in exploring which measures are most suitable for incremental data.

REFERENCES

[1] Amy H.L. Lim, Chien-Sing Lee , "Processing online analytics with classification and association rule mining", in Knowledge-Based Systems, vol. 23 ,pp. 248–255, 2010.

[2] Han,J., Cheng,H., Xin,D., Yan,X., "Frequent pattern mining: current status and future directions" in Data Minining and Knowledge Discovery, 15:55–86, DOI: 10.1007/s10618-006-0059-1, 2007.

[3] Divna Krpan, Slavomir Stankov, " Educational Data Mining for Grouping Students in E-learning System", In Proc. of ITI 2012 34th Int. Conf. on Information Technology Interfaces, June 2012

[4] Jindal R., Dutta Borah M., "A Survey on Educational Data Mining and Research Trends",in International Journal of Database Management Systems (IJDMS), vol.5, no.3, pp.53-74, June 2013.

[5] Winne, P.H., Baker, R.S.J.d. ,The Potentials of Educational Data Mining for Researching Metacognition, Motivation, and Self-Regulated Learning. Journal of Educational Data Mining, 5 (1), 1-8,2013.

[6] Perry J. Samson, "Analyzing student notes and questions to create personalized study guides", In Proc. of the Fourth International Conference on Learning Analytics And Knowledge, Pages 263-264 ,ACM: New York, USA, doi:10.1145/2567574.2567576, 2014.

[7] Gowda, S.M., Baker, R.S.J.d., Corbett, A.T., Rossi, L.M., "Towards Automatically Detecting Whether Student Learning is Shallow".in International Journal of Artificial Intelligence in Education, vol.23, no.1,pp. 50-70, 2013.

[8] Jian Wang, Zhubin Lu, Weihua Wu and Yuzhou Li, "The Application of Data Mining Technology based on Teaching Information", ICCSE 2012.

[9] Agrawal Rakesh, Imilienski T., and Swami Arun. "Mining association rules between sets of items in large datasets", in Proc. of the ACM SIGMOD Conference on Management of Data, 207-216, 1993.

[10] Srikant R, Agrawal R, "Mining generalized association rules". In: Proc. of the 1995 international conference on very large data bases (VLDB'95), Zurich, Switzerland, pp 407–419, 1995.

[11] Lent B, Swami A,Widom J, "Clustering association rules", In: Proc. of the 1997 international conference on data engineering (ICDE'97), Birmingham, England, pp 220–231,1997.

[12] Yun U, New Approaches to weighted frequent pattern mining, December 2005.

[13] Han J, Pei J, Yin Y, "Mining frequent patterns without candidate generation", In: Proc. of the 2000 ACM-SIGMOD international

conference on management of data (SIGMOD'00), Dallas, TX, pp 1–12,2000.

[14] Jayshree Jha and Leena Ragha, "Educational Data Mining using Improved Apriori Algorithm", International Journal of Information and Computation Technology.ISSN 0974-2239 Volume 3, Number 5 pp. 411-418, 2013

[15] Stefanos Ougiaroglou, Giorgos Paschalis, 2012 "Association Rules Mining from the Educational Data of ESOG Web-Based Application", Artificial Intelligence Applications and Innovations IFIP Advances in Information and Communication Technology vol. 382, pp 105-114, 2012.

[16] Qiang Yang, Yanhong Hu , "Application of Improved Apriori Algorithm on Educational Information" , in Fifth International Conference on Genetic and Evolutionary Computing , DOI: 10.1109/ICGEC.2011.82 , pp. 330 – 332,2011.

[17] Deng, Jiabin ; Hu, JuanLi ; Chi, Hehua ; Wu, Juebo, "An Apriori-Based Approach for Teaching Evaluation", In 2nd International Symposium on Information Engineering and Electronic Commerce (IEEC),pp.1-4,DOI: 10.1109/IEEC.2010.5533217,2010.

[18] Pan qingxian ; Qu Linjie ; Lou Lanfang , "Data mining and application of teaching evaluationbased on association rules ," 4th International Conference on Computer Science & Education, pp.1404-1407, DOI: 10.1109/ICCSE.2009.5228194, 2009.

[19] Lanfang Lou ; Qingxian 2009Pan ; Xiuqin Qiu "New Application of Association Rules in Teaching Evaluation System", In International Conference on Computer and Information Application (ICCIA), pp.13-16,DOI: 10.1109/ICCIA.2010.6141524 ,2010.

[20] Liu, B., H. Wynne, C. Shu and M. Yiming, "Analyzing the Subjective Interestingness of Association Rules", in IEEE Inteligent System, vol. 15,no.5,pp. 47-55, DOI : 10.1109/5254.889106,2000.

[21] García, E., Romero, C., Ventura, S., de Castro, C., An architecture for making recommendations to courseware authors through association rule mining and collaborative filtering, in UMUAI: User Modelling and User Adapted Interaction, 19(1-2), pp. 99-132, 2009.

[22] Mobasher, B., Data Mining for Web Personalization, The Adaptive Web: Methods and Strategies of Web Personalization. Lecture Notes in Computer Science 4321, Brusilovsky, P., Kobsa, A., Nejdl, W. (eds.), Heidelberg: Springer-Verlag, pp. 90-135, 2006.

[23] Romero, C., and Ventura S., " Data Mining in Education". WIREs Data Mining and Know.Dis.,vol.3,pp.12-27,2013.

[24] Romero, C. and Ventura, S., "Educational data mining: A survey from 1995 to 2005", in Expert Systems with Applications, vol.33,no.,pp. 1135–146, 2007.

[25] Koedinger, K.R., Baker, R.S.J.d., Cunningham, K., Skogsholm, A., Leber, B., Stamper, J.. A Data Repository for the EDM community: The PSLC DataShop. In Romero, C., Ventura, S., Pechenizkiy, M., Baker, R.S.J.d. (Eds.) Handbook of Educational Data Mining. Boca Raton, FL: CRC Press,2010.

[26] Michael Steinbach, Pang-ning Tan, Hui Xiong and Vipin Kumar, 2000 , Mathematics Subject Classification. Primary 62-07, 68P99; Secondary 62P10, 2007 American Mathematical Society, Accessed on : Jan 2014, Available in :.researchgate.net% 2Fpublication % 2F228787492_Objective_measures_for_association_pattern_analysis%2Ffile%2F72e7e5182f2bdd2555.pdf&ei=n_FYU4n9BoXPrQff3oHoDQ&usg=AFQjCNFH9c65SyAyW51VaTbEPB2zA_AnJg&bvm=bv.65397613,d.bmk

Wireless Pers Commun
DOI 10.1007/s11277-014-2138-8

Analysis of Optimal Carrier Sensing Range in Wireless Ad Hoc Networks with Order Dependent Capture Capability

Mayur M. Vegad · Swades De · Brejesh Lall

© Springer Science+Business Media New York 2014

Abstract IEEE 802.11 wireless ad hoc network performance in distributed coordination function mode is limited by hidden and exposed terminals problem. Request-to-send/clear-to-send based hand shake reduces the problem to some extent, but the network performance is a function of nodal carrier sense (CS) range and interference range. While a large CS range compared to the interference range can reduce the collision related throughput loss, it has a negative impact of increased exposed terminals. Via experimental studies it was recently demonstrated that, the effect of interference to a reception process differs depending on arrival order of the desired signal and interfering signal. In view of this frame arrival order dependent capture (ODC) capability of receivers, in this paper we investigate the optimal choice of CS range and explore the possibility of maximizing the network performance. Via mathematical analysis, supported by extensive network simulations, we demonstrate the network performance benefit of ODC dependent optimal CS range. The distinctive characteristic of ODC diminishes at higher data rates, and as a result the performance gain with optimal CS range reduces. Nevertheless, at low-to-moderately-high data rates, the performance gain is shown to be quite significant.

Keywords Medium access control · Optimal carrier sensing · Order dependent capture · Mathematical modeling · Hidden terminals · Exposed terminals

M. M. Vegad
Department of Electrical Engineering, Indian Institute of Technology Delhi, New Delhi, India
e-mail: mayur8374@gmail.com

Present Address
M. M. Vegad
BVM Engineering College, Gujarat, India

S. De (✉) · B. Lall
Department of Electrical Engineering and Bharti School of Telecommunication,
Indian Institute of Technology Delhi, New Delhi, India
e-mail: swadesd@ee.iitd.ac.in

B. Lall
e-mail: brejesh@ee.iitd.ac.in

Published online: 09 November 2014

1 Introduction

Medium access control (MAC) protocol plays an important role of coordinating the users' access to the shared medium in wireless networks. Though IEEE 802.11 [4] is a standard protocol suit for the wireless local area networks (LANs), its distributed coordination function (DCF) has also been studied and widely adopted in wireless ad hoc networks. DCF is a kind of carrier sense multiple access with collision avoidance (CSMA/CA) MAC protocol wherein the carrier sensing (CS) is the fundamental aspect. Each user senses the medium before making a transmission attempt and defers the transmission if the medium is sensed busy. The 802.11 suggests two types of CS: physical carrier sensing (PCS) and virtual carrier sensing (VCS). In PCS, the medium is determined to be busy if the signal power is larger than a threshold called CS threshold Γ_c; otherwise it is considered idle. A given value of threshold Γ_c determines the corresponding CS range R_c which is the minimum distance allowed between two concurrent transmitters. In VCS, each user regards the channel as busy for the duration mentioned in the MAC header of the received frames, such as, request to send (RTS), clear to send (CTS), Data, and acknowledgment (ACK) [4]. One objective of CS (both PCS and VCS) is to cover possible interferers in the sensing range so as to avoid collisions. A potential interferer left uncovered by CS is called a hidden terminal.

The interfering range R_i (within which a transmitted frame can cause collision to an ongoing reception) around a receiver increases with the sender–receiver separation distance d. Therefore, one way to reduce the hidden regions is to keep d small, so that the farthest potential interferer is covered within a given CS range of the sender [26]. Alternatively, one may increase the value of CS range R_c [8] so as to cover the farthest possible interferer for the largest value of d (= the nodal transmission range, R_t). But, this approach may not be preferable, as it increases the number of exposed terminals, and hence reduces the spatial reuse. This negative impact becomes quite significant at high data rates because of increase in R_i with the data rates. Increasing the CS threshold Γ_c (thereby reducing R_c) arbitrarily would solve the exposed terminals problem but at the cost of increasing the hidden terminals problem. The excessive collisions due to hidden terminals result in false link/route failure alarms, resulting in unnecessarily triggering the corresponding recovery mechanisms at routing and transport layers. This in turn either increases network traffic by flooded broadcast packets or slows down some flows to starvation, creating unfairness amongst the competing flows. Thus, there is some trade-off and the value of Γ_c (and hence R_c) must be set optimally so as to have a favorable balance between desired spatial reuse and allowable interference.

When more than one frame are received at a receiver in overlapped fashion, one of them can be successfully decoded if the signal-to-interference (SIR) ratio is above a threshold, called capture threshold δ. While the dependence of δ on data rate and other physical parameters, such as the modulation scheme, are well known, recent experimental results [12,21] have shown that, the value of δ also depends on the arrival order of the overlapping frames. Typically, δ is significantly small when the intended frame arrives earlier than an interfering frame (**S**ender's **F**irst, or SF case), otherwise it is large (**S**ender's **L**ast, or SL case). The SF case leads to a much smaller value of R_i around a node that has started receiving a signal. This SF/SL phenomenon motivates us to take into account the frame arrival order dependent capture (ODC) while considering the optimization of CS threshold, so as to increase the network throughput.

There have been significant prior research works (e.g., [6,27,31,32]) that suggest different approaches towards the optimization of the CS threshold to achieve enhanced network performance. On the other hand, a few researchers [21,23] have proposed exploiting ODC

at the physical layer (PHY) for improving the network performance by reordering the transmissions at the MAC layer. *To the best of our knowledge, no work has been reported in the literature that studies the role of ODC in the optimization of CS threshold.*

Note that, the value of δ is still higher in SL cases, and it may appear that the step to arbitrarily reducing R_c involves a risk of leaving the fate (success/failure) of a transmitted frame to pure chance. That is, a frame will be successful, only if it is received either in isolation or in SF overlap fashion. But actually, the VCS plays a significant role. In our prior work [25] we have shown that, once the RTS/CTS exchange is successful, the interfering range in SL case is reduced significantly. It was further shown that, with ODC at PHY it is possible to safely reduce the CS range. *However, the claims in* [25] *were purely based on simulations and lacked any theoretical justification. Moreover, the evaluation was carried out only at the basic (1 Mbps) data rate of 802.11b.*

In this paper, we develop an analytical framework to characterize the impact of ODC in optimizing the CS threshold at different data rates of IEEE 802.11a. The key contributions of this work are as follows: (a) An analytical model is developed with ODC at PHY for the RTS/CTS based access scheme of IEEE 802.11 standard, and the results are supported by rigorous ns2 simulations; (b) the significance of considering ODC on the CS threshold decision at the MAC layer is demonstrated through numerical and simulation results at different data rates of IEEE 802.11a.

The remaining paper is organized as follows: Sect. 2 surveys the related works. After building some background on nodal ranges and order dependent capture capability in Sect. 3, we develop the analytical model with incorporation of ODC in Sect. 4. In Sect. 5, we validate the model through network simulations in ns2. In Sect. 6, we use the developed analytical model to evaluate the impact of ODC on the consideration of PCS threshold at different data rates of IEEE 802.11a. Finally, Sect. 7 concludes the paper.

2 Related Works

Improving spatial reuse through variations of VCS Some researchers [14,26,28] have proposed to improve spatial reuse through some variations in the VCS mechanism while assuming a fixed PCS threshold. Depending upon the value of δ, one can define a critical sender–receiver distance d beyond which the R_i becomes larger than the R_t. For a d larger than the critical distance, the above phenomenon makes the RTS/CTS ineffective in mitigating the hidden terminals that are located outside the transmission range. To solve this problem, it was proposed in [26] that a RTS is responded only if it is received from a distance that is lower than the critical distance. As per the basic IEEE 802.11 standard, every node respects all the overheard frames by deferring its own transmissions until the duration mentioned in the overheard frames. Targeting improved spatial reuse through mitigation of exposed terminals, the authors in [28] suggested that a node needs to respect an overheard RTS or CTS only if it is received in isolation (i.e., only RTS or only CTS). While this approach works better for a smaller d, the throughput performance significantly deteriorates as d increases. When an overheard frame is erroneous (or sensed only), the exact duration by which a node should defer its transmission may not be known. In such a case, according to the basic IEEE 802.11 standard a node defers blindly for a fixed duration (represented by extended inter-frame space or EIFS) without discriminating amongst the different types of overheard frames. An enhanced carrier sensing approach in [14] distinguishes among the types of erroneous frames based on their lengths, and thus it allows the overhearing nodes to defer their transmissions accordingly. None of [26,28], and [14] considered ODC at PHY.

Tuning of CS threshold Several researchers [6,19,24,27,31,32] have recommended tuning of PCS threshold in order to achieve a trade-off between spatial reuse and probability of frame collisions, though none of them have considered the role of ODC in their works. To our knowledge [6] was the first to suggest the tuning of PCS threshold against the fixed one, which was assumed in earlier works [14,26] and is being used widely in some network simulators [3]. The authors in [27] argued for accounting bandwidth independent and bandwidth dependent MAC overhead while determining an optimal Γ_c. In [31] it was demonstrated that, PCS enhanced with tunable Γ_c can avoid interference, thereby obviating the need of VCS altogether. The analytical model in [32] computed an optimal PCS threshold and also suggested a PCS tuning algorithm for adapting the PCS threshold to varying network conditions. In [18], the authors proposed an algorithm that differentiates the packet losses due to hidden and non-hidden interferers and tunes PCS adaptively. The analytical model in [19] showed that, a close-to-optimal CS range is equal to the interference range R_i. To achieve a control over variable R_i in practical networks (where d is random), they proposed a rate-to-link allocation scheme based on rendering the R_i equal for all links, allowing a single CS range to be used in the whole network. The effect of PCS on multi-rate and multi-hop wireless ad hoc networks was studied in [29]. In determining an optimal Γ_c, they considered several factors, like variable transmission ranges and receiver sensitivities for different data rates, impact of multi-hop forwarding, node topology, and bidirectional handshake. From a different angle, in [24], the authors used the framework of IEEE 802.11k Radio Resource Management on each node to enable on-line tuning of CS threshold.

Spatial reuse through power control The level of spatial reuse can also be enhanced by reducing the level of transmit power. To improve spatial reuse, the experimental study in [9] presented an interesting comparison of two approaches, namely, tuning of transmit power and CS threshold. Similarly, the analytical model in [15] addressed the joint tuning of PHY (transmit power and data rate) and MAC (contention window size) parameters to optimize the network throughput by determining appropriate data rate for a given signal-to-interference-and-noise ratio (SINR). These works however, did not exploit ODC at PHY.

Experimentation and exploitation of ODC Usefulness of capture capability in IEEE 802.11 based wireless networks was experimentally evaluated in [10,12]. Particularly, the *Message-in-Message* feature of modern wireless receivers and the corresponding ODC effect at various data rates of IEEE 802.11a was studied by [12,13,21] through test-bed experimentations. At low data rates, for very small sender–receiver separation distances, the interference range can be smaller than the communication range. Observing this fact, the study in [23] exploited the ODC to effect concurrent transmissions even within a communication range through *properly staggering* the different transmissions. This approach however requires a considerable modification in the existing 802.11 MAC. Further, it did not consider the role of CS range, and hence the exposed terminals that are out of communication range of the sender and receiver were not addressed. Through another set of test-bed experiments the authors in [21] emphasized the importance of frame reception order (SF vs. SL) and proposed a link layer protocol that achieves ODC aware *reordering* of transmissions for optimal network throughput. The authors in [30] have distinguished the SL and SF type of collisions (identified respectively as H_1 and H_2 collisions) and proposed solutions to each of these types. The analytical study in [11] has quantified the gains from the concurrency by exploiting MIM-capture in IEEE 802.11 WLANs. ODC has also been studied experimentally in wireless sensor networks (WSNs) [16,20]. In [16], the authors have shown that due to the capture effect enabled concurrent transmissions, it is possible to expedite the network flooding in WSNs. The authors

in [20] suggested a new MAC protocol for WSNs based on MIM-capture that allows parallel transmissions—leading to enhanced throughput and reduced power consumption.

To complement the prior studies, in our work we aim at increasing the spatial reuse, and as a result network throughput, by judiciously exploiting the ODC in determining the optimal CS range. In contrast to the approach in [23], our approach does not impose any restriction on the sender–receiver distance. Our claims on the impact of ODC on the choice of CS threshold is based on a probabilistic mathematical model and backed by ns2 based extensive simulations.

3 Background Concepts

We develop some background to appreciate the analytical treatment in the following section.

3.1 Nodal Ranges

Transmission range R_t and CS range R_c When a sender **S** transmits a frame with power P_T, following standard path loss model [22], the received signal strength P_r at a receiver **R** is given as:

$$P_r = P_0 \left(\frac{d_0}{d_{SR}} \right)^{\alpha}, \tag{1}$$

where P_0 is the received signal strength measured at a reference distance d_0, d_{SR} indicates the separation distance of nodes **S** and **R**, and α is the path loss exponent (usually $2 \leq \alpha \leq 4$).

Let Γ_t be the minimum power level required for successful decoding of a received frame. Then the distance from the transmitter at which, the received signal strength equals Γ_t is called the transmission range R_t. Using (1) it can be given as

$$R_t = d_0 \left(\frac{P_0}{\Gamma_t} \right)^{\frac{1}{\alpha}}.$$

In a CSMA/CA MAC protocol (e.g., DCF of IEEE 802.11), all the participating nodes follow *listen before talk* policy and ensures the availability of medium before using it for its own transmission. To this end, besides Γ_t, each node maintains another threshold called CS threshold Γ_c. When the sensed power level is above Γ_c, the medium is identified as busy and a transmission aspirant node defers its own transmission [4]. This leads to a definition of CS range R_c around the transmitter which is the minimum distance between two permitted concurrent transmissions. From (1),

$$R_c = d_0 \left(\frac{P_0}{\Gamma_c} \right)^{\frac{1}{\alpha}}.$$

Since, P_0 is proportional to the transmit power P_T, R_t and R_c are also the functions of P_T as well as of the respective thresholds.

Interference range R_i For a successful frame reception, the SIR at **R** should be above a capture threshold δ. Let P_s and P_i be the respective signal strengths from sender **S** and interferer **I** at **R**. Under the assumption of homogeneous transmit power being used for all (data and control) frames at all participating nodes, from (1) the minimum SIR condition can be given as:

$$\frac{P_s}{P_i} = \left(\frac{d_{IR}}{d_{SR}} \right)^{\alpha} \geq \delta. \tag{2}$$

The condition in (2) gives us the interference range R_i. Therefore,

$$R_i = (\delta)^{\frac{1}{\alpha}} \cdot d_{SR} = K \cdot d_{SR}, \tag{3}$$

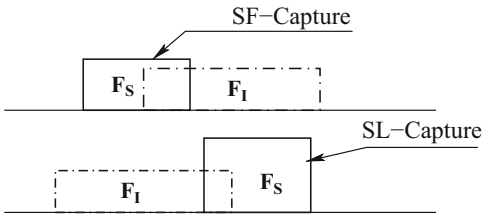

Fig. 1 SF and SL overlaps. F_S and F_I are signal and interfering frames, respectively. Note that, the signal power of F_S required for signal capture in SF case is lower than that in SL case

Table 1 The values of δ for SF and SL cases at different data rates of IEEE 802.11a [12,13]

Data rate (Mbps)	6	9	12	18	24	36	48	54
δ^{SF} (dB)	0	3	4	7	11	15	21	23
δ^{SL} (dB)	10	10	10	10	12	16	22	23

where $K \triangleq \delta^{\frac{1}{\alpha}}$. Thus, $R_i \propto d_{SR}$ and is maximum when $d_{SR} = R_t$. That is,

$$R_{i_{max}} = K \cdot R_t.$$

From (3) it is clear that, when $K > 1$, even for a moderately large value of d_{SR} the interference range can be larger than the transmission range.

3.2 Order Dependent Capture (ODC)

Interference in wireless networks can be better handled with *message-in-message* (MIM) feature of modern wireless receivers [1]. The test-bed experimental studies with MIM-capable wireless nodes have found that the value of capture threshold δ depends on order of arrival of the overlapping frames [12,13,21]. This dependence is in addition to the transmission rate and other physical parameters (such as modulation scheme). Figure 1 shows two possible frame arrival orders: **S**ender's **F**irst SF case and **S**ender's **L**ast SL case. It was experimentally found in [12,13,21] that, the value of δ differs in the above two cases, the difference being larger at low data rates. The reference values of δ for SF and SL cases[1] at different data rates are depicted in Table 1.

4 Analytical Model for RTS/CTS Access Scheme of IEEE 802.11

We consider a network with N users deployed over a two dimensional (2-D) plane obeying homogeneous spatial Poisson distribution with node density λ. Each data frame is preceded with RTS/CTS exchange. Saturated traffic scenario is considered where all nodes have always a data packet to transmit. The model assumes no action by upper layers in response to the MAC failures. CTS and ACK packets are transmitted by a receiver after successfully receiving RTS and data frames, respectively. Further, both of these control packets are very small and transmitted at the lowest (reliable) data rate. So, our model neglects the loss probabilities of CTS and ACK frames.

In IEEE 802.11 standard, when a node finds the channel busy, it freezes its back-off counter. This leads to a variable time interval between two consecutive time slot beginnings.

[1] Besides SF and SL overlap cases, the authors in [12] have also experimented with a third possible case (called SLG capture case) where the first arriving frame (from the interferer) is already *garbled*. Because of relatively less probability of such overlaps, we do not consider SLG capture case in our work.

Hence, it is convenient to define a generic time slot T_{gen} [5], which could be much longer than the system time slot. In the subsequent developments, we use only 'time slot' to refer to the generic time slot.

4.1 Description of State Model

The basic access scheme of IEEE 802.11 (without RTS/CTS) can be captured through an analytical node level model consisting of following 4 states: Idle (node is idle), DATA-Success (node is engaged in a successful transmission attempt), DATA-Failure (node is engaged in an unsuccessful transmission attempt), or Deferring (node is deferring due to busy medium reported by PCS) [17]. In our study, to obtain the optimal CS range based on the nodal ODC capability, we need to develop a model for RTS/CTS based access scheme. The prior exchange of two small frames (i.e., RTS, CTS) leads to the nodal behavior that is more complex than that without RTS/CTS exchange. Consequently, the corresponding analytical model needs 3 more states to capture the behavior of a generic node.

Figure 2 shows the resulting 7-state node level model which is constructed from the perspective of a generic reference node $\mathbf{n}_0$ in the system. In a given time slot, $\mathbf{n}_0$ can be in any of the following 7 states:

Idle (I) State: A node remains in Idle state if neither the $\mathbf{n}_0$ node nor any other node in its CS range transmits. The duration T_I, for which $\mathbf{n}_0$ stays in the Idle state, is the length of system time slot defined in IEEE 802.11 standard (e.g., in 802.11a, $T_I = 9\,\mu$S).

RTS-Success (RS) State: $\mathbf{n}_0$ node transmits a RTS frame which is successfully responded with a CTS from its intended receiver. If a transmission attempt by $\mathbf{n}_0$ results in a successful response of CTS by the intended receiver, it transits from Idle state to RTS-Success state. Here, the success of a RTS frame requires for both of the following events to occur: (i) RTS is not lost in collisions at the receiver, and (ii) The network allocation vector (NAV) [4] of receiver is zero when the RTS is received. The duration (in micro seconds or μS), for which a node stays in this state is given as:

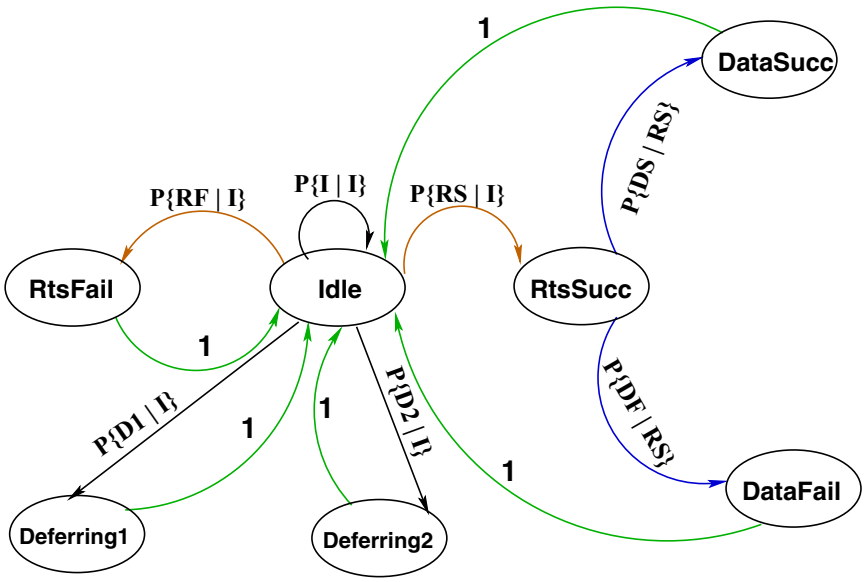

Fig. 2 A 7-state nodal model for RTS/CTS access scheme of IEEE 802.11

$$T_{RS} = T_{RTS} + SIFS + \sigma + T_{CTS} + DIFS + \sigma\ \mu\text{S},$$

where σ is the propagation delay. In 802.11a, T_{RTS} and T_{CTS} are calculated as:

$$T_{RTS} = 20 + 4\left\lceil \frac{182}{4\nu_h} \right\rceil \mu\text{S}, \text{ and } T_{CTS} = 20 + 4\left\lceil \frac{134}{4\nu_h} \right\rceil \mu\text{S}.$$

where ν_h is control frame transmission rate in Mbps.

RTS-Failure (RF) State: $\mathbf{n}_0$ transmits a RTS frame which is not responded with a CTS from its intended receiver. If a RTS transmission does not get a CTS in response, the node transits from Idle to RTS-Failure state. Here, a RTS failure implies occurrence of any of the following events: (i) RTS is lost in collisions at the receiver, or (ii) The NAV of receiver is non-zero when the RTS is received. Before confirming the non-reception of a valid CTS frame, $\mathbf{n}_0$ waits for a timeout period which is almost equal to the transmission time of a CTS frame [4]. Therefore, $T_{RF} \approx T_{RS}\ \mu\text{S}$.

DATA-Success (DS) State: After successful reception of CTS, $\mathbf{n}_0$ transmits data frame and receives an ACK successfully from the receiver. For such scenarios, $\mathbf{n}_0$ moves from RTS-Success to Data-Success state. This implies that, data frame reaches the receiver without any collisions. Recall that, we have assumed that ACK collisions are negligible.[2] The duration of this state is

$$T_{DS} = T_{data} + SIFS + \sigma + T_{ACK} + SIFS + \sigma\ \mu\text{S}.$$

The time durations of a data frame T_{data} and an ACK frame T_{ACK} can be derived as:

$$T_{data} = 20 + 4\left\lceil \frac{294 + L_{dt}}{4\nu} \right\rceil \mu\text{S}, \text{ and } T_{ACK} = 20 + 4\left\lceil \frac{134}{4\nu_h} \right\rceil \mu\text{S},$$

where L_{dt} (in bits) is length of data frame and ν is the data frame transmission rate in Mbps.

DATA-Failure (DF) State: After successful reception of CTS, $\mathbf{n}_0$ transmits data frame but does not receive an ACK from the receiver. Here, $\mathbf{n}_0$ transitions from RTS-Success state to Data-Failure state. This happens when the data frame is lost in collision at the receiver. Before confirming the non-reception of a valid ACK frame, $\mathbf{n}_0$ waits for a timeout period which is almost equal to the transmission time of an ACK frame [4]. Thus, $T_{DF} \approx T_{DS}\ \mu\text{S}$.

Deferring-1 (D1) State: In a time slot the node $\mathbf{n}_0$ transitions from Idle to this state if in that time slot $\mathbf{n}_0$ itself does not initiate a transmission but it starts receiving a RTS frame for the case when the RTS/CTS exchange results in a successful data transmission. It results in a successful communication session consisting of the complete 4-way exchange of RTS-CTS-data-ACK between a sender–receiver pair, for which both or at least the sender is located in its CS range. Note that, this completes the reception aspect of $\mathbf{n}_0$ as well. The duration in this state is: $T_{D_1} = T_{RS} + T_{DS}\ \mu\text{S}$.

Deferring-2 (D2) State: In a time slot the node $\mathbf{n}_0$ transitions from Idle to this state if in that time slot, $\mathbf{n}_0$ itself does not initiate a transmission but, starts receiving a RTS frame, either destined to itself or an overheard frame, and for the case when this RTS results in to a failure. The duration for which $\mathbf{n}_0$ stays in this state can be obtained as follows. If the received RTS is decoded successfully at $\mathbf{n}_0$, then according to IEEE 802.11 standard, $\mathbf{n}_0$ will update its NAV and respectfully defer for a duration mentioned in the RTS frame irrespective of the consequences (success or failure) of that RTS, and hence, $T_{D_2} = T_{D_1}$. However, if a failed (decodable) RTS was destined to $\mathbf{n}_0$ then $T_{D2} = T_{RF} \approx T_{RS}$. Further, if a failed RTS was received as a 'sensed only' frame at $\mathbf{n}_0$, then according to the *EIFS mechanism*,

[2] Also note that, as per IEEE 802.11 standard [4], having received a data frame successfully, a receiver sends the ACK without any type of carrier sensing, neither PCS nor VCS.

$T_{D_2} = T_{RTS} + EIFS \approx T_{RS}$. To simplify the analysis we take only one value of the duration as: $T_{D_2} = T_{RS}\,\mu$S.

To derive the steady state and transition probabilities, let Π_S denote the steady state probability of state S and $P\{S_2|S_1\}$ denote a transition probability from state S_1 to state S_2. Then each of the steady state probabilities can be described in terms of the steady state probability of Idle state as:

$$\Pi_{RS} = \Pi_I P\{RS|I\}, \tag{4a}$$
$$\Pi_{RF} = \Pi_I P\{RF|I\}, \tag{4b}$$
$$\Pi_{DS} = \Pi_{RS} P\{DS|RS\} = \Pi_I P\{RS|I\} P\{DS|RS\}, \tag{4c}$$
$$\Pi_{DF} = \Pi_{RS} P\{DF|RS\} = \Pi_I P\{RS|I\} P\{DF|RS\}, \tag{4d}$$
$$\Pi_{D1} = \Pi_I P\{D1|I\}, \tag{4e}$$
$$\Pi_{D2} = \Pi_I P\{D2|I\}. \tag{4f}$$

Assuming time-homogeneity of the Markov chain in Fig. 2, we have for the idle state:$\Pi_I = P\{I|I\}\Pi_I + P\{I|RF\}\Pi_{RF} + P\{I|D1\}\Pi_{D1} + P\{I|D2\}\Pi_{D2} + P\{I|DS\}\Pi_{DS} + P\{I|DF\}\Pi_{DF}$. Observing that a node moves to Idle from RF, D1, D2, DS, and DF with probability 1, we obtain:

$$\Pi_I = P\{I|I\}\Pi_I + \Pi_{RF} + \Pi_{D1} + \Pi_{D2} + \Pi_{DS} + \Pi_{DF}. \tag{5}$$

Substitutions from (4b) to (4f) into (5) and simplification yields

$$P\{I|I\} + P\{RF|I\} + P\{RS|I\}\,(P\{DS|RS\} + P\{DF|RS\}) + P\{D1|I\} + P\{D2|I\} = 1. \tag{6}$$

The model also assumes, after receiving a CTS successfully a node always transmits a data frame, which results either in a success or a failure, i.e.,

$$P\{DS|RS\} + P\{DF|RS\} = 1 \tag{7}$$

Further, we denote τ_R as the probability of RTS transmission by any node from its Idle state. So,

$$\tau_R = P\{RS|I\} + P\{RF|I\} \tag{8}$$

Using substitutions from (7) and (8), (6) simplifies to

$$P\{I|I\} + \tau_R + P\{D1|I\} + P\{D2|I\} = 1. \tag{9}$$

For simplicity, we assume no retransmission of RTS or data. This implies no exponential back-off in DCF and hence, use of a fixed contention window CW. Therefore, τ_R is given as [5]:

$$\tau_R = \frac{2}{CW + 1}. \tag{10}$$

Since the channel is shared with all neighbors of the reference node $\mathbf{n}_0$, the status of surrounding nodes is required to be considered while computing the transition probabilities. When every node in the network is within the CS range of every other node (as assumed in [5]), all nodes in the CS range of $\mathbf{n}_0$ perceive the channel status same as $\mathbf{n}_0$, and hence, it is reasonable to consider that, the RTS-transmission probability of all neighbors, given they are in Idle state, is the same (i.e., τ_R). Note that, this is possible only if all nodes are at the same physical location or if the CS range of each node is large enough to cover the farthest node in the system. When such is not the case, the network environment (or the channel status) 'seen' by one node greatly differs from the one 'seen' by other node. Further, with increasing distances between them or with reducing CS range (or with both), the difference between

their channel status becomes pronounced because of their large non-overlapping CS regions. Therefore, the RTS-transmission probability ρ in the next time slot of these nodes cannot be taken same as that of $\mathbf{n}_0$. Rather, it has to be computed as the average RTS-transmission probability per generic slot derived as:

$$\rho = \Pi_{RS} + \Pi_{RF} = \Pi_I \tau_R. \tag{11}$$

To compute the transition probabilities of our model, as in [17] we consider that, when the channel around node $\mathbf{n}_0$ is sensed Idle, the nodes within the transmission range of $\mathbf{n}_0$ share the same channel status and hence, have the same RTS-transmission probability τ_R. On the other hand, the status of other CS range neighbors that are outside the transmission range of $\mathbf{n}_0$ is independent of the status of $\mathbf{n}_0$ and hence, they transmit RTS with generic RTS-transmission probability ρ.

Note that, at any instant the node can be in any one of the seven states. So,

$$\Pi_I + \Pi_{DS} + \Pi_{DF} + \Pi_{RS} + \Pi_{RF} + \Pi_{D1} + \Pi_{D2} = 1. \tag{12}$$

Substituting from (4a) to (4f) in (12), and subsequently using (7) and (8), we get

$$\Pi_I = \frac{1}{(1 + P\{RS|I\} + \tau_R + P\{D1|I\} + P\{D2|I\})}. \tag{13}$$

The generic slot time can be derived as: $T_{gen} = \Pi_I T_I + \Pi_{DS} T_{DS} + \Pi_{DF} T_{DF} + \Pi_{RS} T_{RS} + \Pi_{RF} T_{RF} + \Pi_{D1} T_{D1} + \Pi_{D2} T_{D2}$. Using (4a)–(4f), (7), and (8), and substituting $T_{DS} = T_{DF}$, $T_{RS} = T_{RF} = T_{D2}$ and $T_{D1} = T_{RS} + T_{DS}$ we get,

$$T_{gen} = \Pi_I \big(T_I + T_{DS}(P\{RS|I\} + P\{D1|I\}) + T_{RS}(\tau_R + P\{D1|I\} + P\{D2|I\})\big). \tag{14}$$

In the following, we determine the probability of receiving a CTS in response to a RTS frame.

4.2 Analysis of Success/Failure of RTS Frame

A transmitted RTS may not be responded with a CTS by its intended receiver for two reasons. First, the RTS may be lost due to collision, and second, the receiver may not respond to RTS because it finds the channel not available. Hence, we investigate the collision vulnerability of RTS frame and also determine the probability that a RTS is not responded with a CTS. Eventually, we obtain an equation for probability of successful RTS transmission.

4.2.1 Collisions of a RTS Frame

A RTS frame is said to be lost due to collision if it is received at the receiver in overlapped fashion with another frame being transmitted from within interference range of the receiver. Accordingly, all the nodes within the interference range of node **R** are potential interferers in Fig. 3.

One objective of carrier sensing in CSMA/CA based protocols is to avoid collisions by possibly covering all potential interferers within its (physical or virtual) CS range. Any interferer that is left uncovered is a potential hidden interferer. Obviously, VCS is not applicable for a RTS frame and hence, all potential interferers that are outside CS range of $\mathbf{n}_0$ are hidden. Such a zone containing hidden interferers for RTS frame is shown with horizontally dashed region in Fig. 3.

Note that, a transmission from an interferer located within CS range of $\mathbf{n}_0$ can also corrupt an RTS reception at **R**, if such an interference signal is initiated in the same time slot in which the transmission of RTS began. Such interferers are referred to as *non-hidden* interferers. The

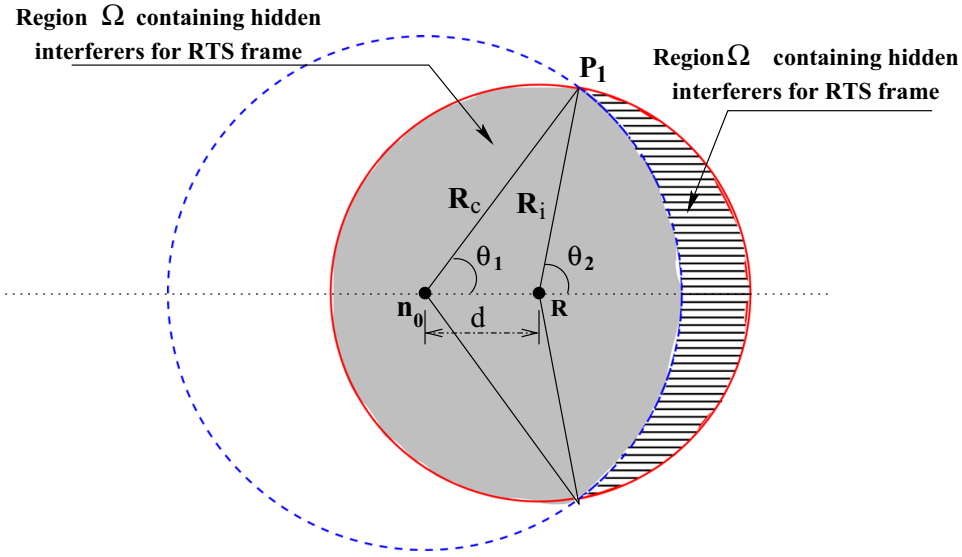

Fig. 3 The nodes in the horizontal-dashed region are potential hidden interferers for an $\mathbf{n}_0$ to **R** RTS frame

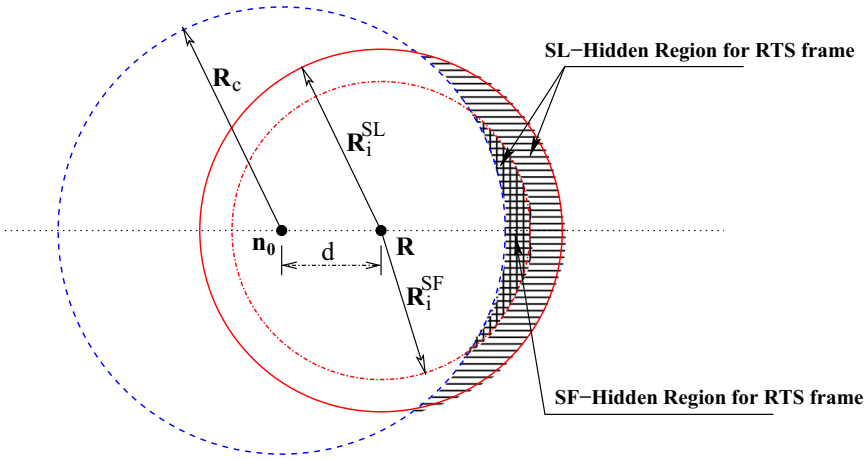

Fig. 4 Effect of ODC on the hidden region for RTS frames

shaded zone in Fig. 3 depicts such a zone that contains non-hidden interferers for RTS frame. Calculation of areas of the above regions as a function of S–R distance d are carried out in "Appendix".

As discussed in Sect. 3.2, two different values of δ for SF and SL cases lead to two different interfering ranges, even for a given data rate and a given d. As shown in Fig. 4, depending upon the relative values of δ, the hidden region for an RTS frame could significantly be reduced when it is received in SF-overlapping fashion. Note that, the effect of frame arrival order dependent capture is to effectively reduce the hidden area through reduction in interference range for SF case. We will treat the two overlapping cases (SF and SL) separately in the analysis of collisions.

Now, we proceed to derive the probability of successful reception of RTS frame by considering probabilities of collisions of RTS due to hidden or non-hidden interference.

As stated in the beginning of Sect. 4, in a network with homogeneous spatial Poisson distributed nodes with density λ, the probability of number of nodes in an area A being n is given by: $Prob(N = n) = \frac{(\lambda A)^n}{n!} e^{-\lambda A}$. Hence, if τ is the transmission probability of a node, the probability that none of the nodes in an area A initiates a transmission in a given time slot is given as:

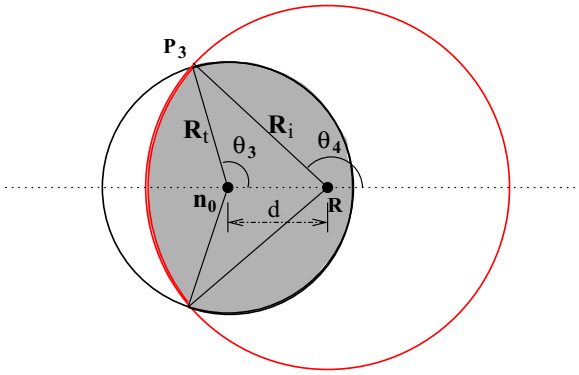

Fig. 5 The intersection of non-hidden region for RTS frames and transmission range of node n_0 is denoted as Ψ

$$Prob\{\text{No node in area A transmits in a given time slot}\}$$
$$= \sum_{k=0}^{\infty} (1-\tau)^k \frac{(\lambda A)^k}{k!} e^{-\lambda A} = e^{-\lambda \tau A} \tag{15}$$

Let A_Ω denote the area of region Ω containing hidden interferers for RTS frame. Then, from Fig. 3, $\pi R_i^2 - A_\Omega$ is the area of the region containing non-hidden interferers for RTS frame. Referring to Fig. 5, we denote A_Ψ as the area of a sub-region Ψ of the 'non-hidden-region' that also falls in the transmission range of the reference node $\mathbf{n}_0$. The areas A_Ω and A_Ψ as functions of d are computed in "Appendix".

As noted Sect. 4.1, a RTS frame from $\mathbf{n}_0$ will not be subjected to any non-hidden interference if none of the nodes within the area $\pi R_i^2 - A_\Omega$ initiates a transmission in the same time slot in which the RTS transmission from $\mathbf{n}_0$ has begun. Accordingly, we use different transmission probabilities, τ_R and ρ, inside and outside the transmission range of node $\mathbf{n}_0$. Denoting p_{nh} as the probability of no-collisions due to non-hidden interferers and considering such interference as an SF case, p_{nh} as a function of S–R distance d, can be computed as:

$$\begin{aligned} & p_{nh}(d) \\ & = \sum_{k=0}^{\infty} \left[(1-\rho)^k \frac{\left(\left(\pi \left(R_i^{SF}(d) \right)^2 - A_\Omega^{SF}(d) - A_\Psi^{SF}(d) \right) \lambda \right)^k}{k!} \right. \\ & \quad \left. \times e^{-\left(\pi \left(R_i^{SF}(d) \right)^2 - A_\Omega^{SF}(d) - A_\Psi^{SF}(d) \right) \lambda} \right] \\ & \quad \cdot \sum_{k=0}^{\infty} (1-\tau_R)^k \frac{\left(A_\Psi^{SF}(d) \lambda \right)^k}{k!} e^{-\left(A_\Psi^{SF}(d) \right) \lambda} \\ & = e^{-\lambda \rho \left(\pi \left(R_i^{SF}(d) \right)^2 - A_\Omega^{SF}(d) - A_\Psi^{SF}(d) \right) - \lambda \tau_R A_\Psi^{SF}(d),} \end{aligned} \tag{16}$$

We now analyze the loss of RTS frame due to collisions with hidden interference. Figure 6 can be used to describe the possible overlaps of RTS frame with an interfering frame F from a hidden terminal. A hidden interfering node is completely unaware of the transmission initiation from $\mathbf{n}_0$ and hence, unlike non-hidden interference, here the F can begin in any of the (vulnerable) slots such that it overlaps with the RTS frame at least in one time slot. Further note that, F could be any of the four frames (RTS, CTS, data, ACK) from the interferer. However, as both, the transmission probability and the length of CTS and ACK frames, are relatively negligible, for simplicity of the analysis we consider only two possibilities of F:

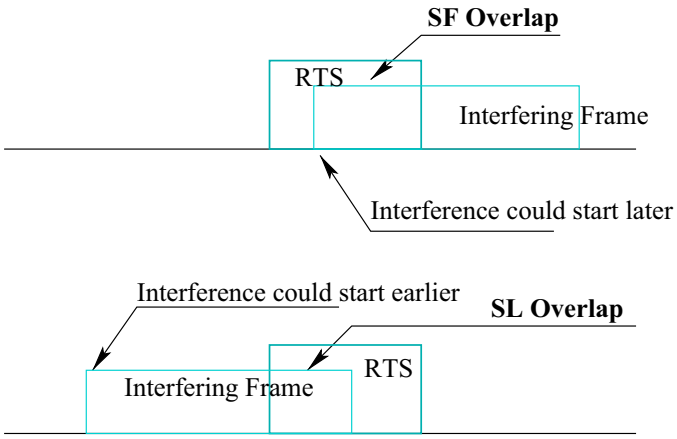

Fig. 6 Possible overlaps of a RTS frame with hidden interferences

RTS and data. To incorporate the effect of ODC in our analysis we need to consider the number of vulnerable slots separately for SF and SL cases.

We denote $N_{F_1-F_2}$ as the number of vulnerable slots for an overlap between the intended signal frames F_1 and F_2 in SF and SL cases, respectively. From Fig. 6 it is clear that, in SF case the number of vulnerable slots are independent of the type of interfering frame and hence,

$$N^{SF}_{RTS-F} = \left\lceil \frac{T_{RTS}}{T_{gen}} \right\rceil, \quad F \in \{RTS, data\}, \tag{17}$$

where $\lceil . \rceil$ is the ceiling function. On the other hand, the number of vulnerable slots in SL case will equal the number of slots in the interfering frame F. That is,

$$N^{SL}_{F-RTS} = \left\lceil \frac{T_F}{T_{gen}} \right\rceil, \quad F \in \{RTS, data\}. \tag{18}$$

As the hidden interferer will always be located outside the transmission range from the sender, it is clear that an interfering RTS frame will be transmitted with the generic RTS-transmission probability ρ. An interfering data frame will be transmitted by a node only if it has reached its own RTS-Success state, i.e., with a transmission probability $\Pi_{RS} = \Pi_I P\{RS|I\}$.

Probability of no-collision of SF (SL) type with a frame F is same as the probability that no node in the area A^{SF}_{Ω} (A^{SL}_{Ω}) transmits frame F (with probability τ_F) in the vulnerable period N^{SF}_{RTS-F} (N^{SL}_{F-RTS}). So, $Prob\{\text{No SF-Collision of RTS with F}\}(d) = e^{-\tau_F \lambda A^{SF}_{\Omega}(d) N^{SF}_{RTS-F}}$, and $Prob\{\text{No SL-Collision of RTS with F}\}(d) = e^{-\tau_F \lambda A^{SL}_{\Omega}(d) N^{SL}_{F-RTS}}$.

Thus, the probability $p_h(d)$ that RTS is not lost due to collisions with hidden interferences is:

$$\begin{aligned} p_h(d) = {} & Prob\{\text{No SF-Collision of RTS with RTS}\}(d) \cdot Prob\{\text{No SF-Collision of RTS with data}\}(d) \\ & \cdot Prob\{\text{No SL-Collision of RTS with RTS}\}(d) \cdot Prob\{\text{No SL-Collision of RTS with data}\}(d) \end{aligned}$$

Eventually, for a successful RTS reception, it should not face any collisions due to non-hidden or hidden interference. Hence,

$$Prob\{\text{successful reception of RTS}\}(d) = Prob\{\text{no collision of RTS}\} = p_{nh}(d) p_h(d).$$

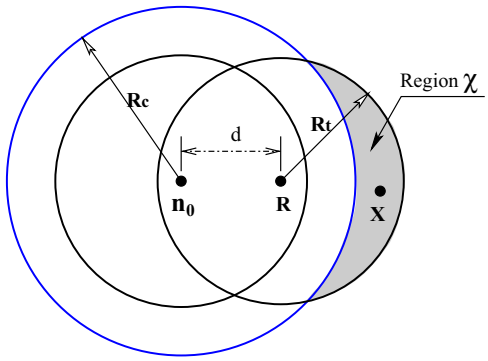

Fig. 7 Depiction of the case when a RTS from $\mathbf{n}_0$ is not responded with a CTS by **R**. **R** overheard a frame F from **X** and set its NAV. It remains non-zero when it receives a RTS from $\mathbf{n}_0$, and hence it does not respond with a CTS

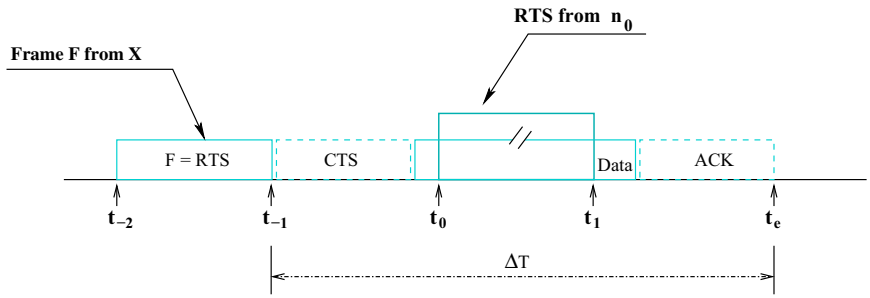

Fig. 8 Timing diagram illustrating the case of no-CTS-response where a RTS frame from **X** does not allow **R** to respond to the sender $\mathbf{n}_0$. The vulnerability period in which the RTS from node **X** may begin is $\Delta T - T_{RTS}$

4.2.2 CTS Response to a RTS

Consider the event when **R** does not respond to a successfully received RTS with a CTS. To derive the probability of this event we use an illustrative scenario of Fig. 7. A possible sequence of transmission events is shown in Fig. 8. The receiver **R** will not respond to the RTS from $\mathbf{n}_0$ if it finds its NAV non-zero at time SIFS after t_1. As shown in Fig. 7, let **X** be such a node whose transmitted frame F gets the NAV of **R** loaded with a duration value ΔT which does not expire at t_1. If reception of F is completed at time t_{-1}, then for **R** to be non-responding to $\mathbf{n}_0$

$$\Delta T > (t_1 + SIFS) - t_{-1}. \tag{19}$$

It is obvious that, F from **X** and RTS from $\mathbf{n}_0$ must be received at **R** in non-overlapped fashion and hence, $t_{-1} < t_0$ where t_0 is the starting time of RTS frame from $\mathbf{n}_0$. Thus, as $t_1 - t_0 = T_{RTS}$, $t_1 - t_{-1} \geq T_{RTS}$. Therefore, the condition in (19) becomes

$$\Delta T > T_{RTS} + SIFS. \tag{20}$$

The duration value in any data frame is always equal to $T_{ACK} + SIFS$ and in any ACK frame it is always *zero*. Thus, the condition in (20) rules out the possibility of F being a data or an ACK because of very low values of ΔT in such cases. Further, we ignore the possibility of F being a *sensed-only* frame as in that case the value of ΔT would be EIFS which is almost equal to the required lower bound in (20). For example in 802.11a at 6 Mbps data rate, $EIFS = 100\,\mu$S and $T_{RTS} + SIFS = 66\,\mu$S. Therefore, F is either a RTS or a CTS, and **X** must be located outside CS range of $\mathbf{n}_0$ but within transmission range of **R**. This leaves the remaining region χ (shaded region in Fig. 7) in which nodes like **X** may lie. For simplicity of the analysis we ignore the case where $F = CTS$ as the probability of a RTS transmission is relatively higher than that of CTS.

Figure 8 shows the timing relationship when $F = RTS$. ΔT for a RTS frame will be $\Delta T = SIFS + T_{CTS} + SIFS + T_{data} + SIFS + T_{ACK}$, which expires at t_e. Obviously, ΔT would

not expire at t_1 if following conditions are satisfied: (i) t_1 occurs after t_{-1}, (ii) t_1 occurs before t_e, (iii) t_0 occurs after t_{-1}, and (iv) t_0 occurs at least T_{RTS} before t_e. From above, it is easy to deduce that, the vulnerable period in which the transmission of F may begin is $\Delta T - T_{RTS}$. Therefore, the probability $p_{cr} = Prob\{\text{Received RTS responded with CTS}\}$ that **R** responds to $\mathbf{n}_0$ with a CTS given that it has received the RTS from $\mathbf{n}_0$ successfully is equivalent to saying that, no node in the area A_χ transmits a RTS in any of the time slots during a period of $\Delta T - T_{RTS}$. Hence p_{cr} as a function of d can be expressed as: $p_{cr}(d) = e^{-\rho\lambda A_\chi(d)\left\lceil \frac{(\Delta T - T_{RTS})}{T_{gen}} \right\rceil}$, where $\lceil\cdot\rceil$ is the ceiling function.

We denote $rtsSucc$ as the event that a transmitted RTS is responded by a successful CTS. Then,

$$\begin{aligned} Prob\{\text{rtsSucc}\}(d) &= Prob\{\text{Receiver does not transmit in next slot}\} \\ &\quad \cdot Prob\{\text{successful reception of RTS}\}(d) \\ &\quad \cdot Prob\{\text{Received RTS responded with CTS}\}(d) \\ &= (1-\tau_R)\cdot p_{nh}(d)\cdot p_h(d)\cdot p_{cr}(d). \end{aligned}$$

Note that, $Prob\{\text{rtsSucc}\}(d)$ is a function of S–R distance d which is a random variable. Therefore, for all equations involving this term, we need to find an expected value based on the probability distribution (pdf) of d. Assuming that a node chooses any of its neighbors as its destination within its transmission range equiprobably, assuming 2-D Poisson distribution for the number of nodes in a given area, we obtain the pdf $f(d)$ of the distance between a node and its neighboring nodes within the transmission range R_t as: $f(d) = \frac{2d}{R_t^2}$, for $0 \le d \le R_t$. Hence, the average RTS frame success probability is obtained as:

$$Prob\{\text{rtsSucc}\} = \int_0^{R_t} Prob\{\text{rtsSucc}\}(x)\, f(x)\, dx.$$

4.3 Analysis of Success/Failure of Data Frame

For the derivation of transition probability for the transition from RTS-Success state to data-Success (or data-Failure) state, we need to determine the probability of receiving an ACK frame in response to a data frame. As we neglect the possibility of ACK collisions, loss of data frame in collisions is the only remaining reason due to which a transmitted data may not be acknowledged by its intended receiver. In this section, we investigate the collision vulnerability of data frame.

A data frame is said to be lost due to collision if it is received at the receiver in overlapped fashion with another frame being transmitted from within interference range of the receiver. Accordingly, all the nodes within the interference range of node **R** are potential interferers in Fig. 9. However, due to prior transmission of a RTS frame, there would not be any non-hidden interferer for the subsequent data frame. Further, the nodes within region Φ (in Fig. 9) should have received CTS from **R** successfully, and hence they would not initiate any transmission until the ACK is transmitted by **R**. Thus, the union of regions Θ_i and Θ_o is the hidden region[3] for the data frames. Further, all the nodes within region Θ_i will defer for EIFS after CTS completion, i.e., they will be hidden for a shorter (vulnerable) period. However, the nodes within region Θ_o will function as hidden terminals for a longer vulnerable period, because a potential interfering transmitter is free to transmit at any time, which will cause

[3] Note that, the area of hidden region depends on the value of CS range and the S–R separation distance d. Figure 9 shows a typical scenario where this region is the union of the two *non-zero* sub-regions Θ_i and Θ_o.

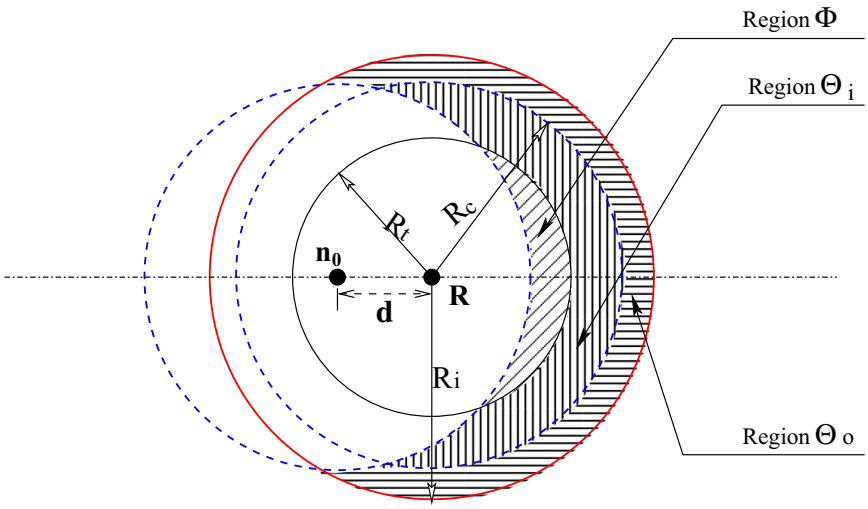

Fig. 9 The nodes within region Φ should have received CTS from **R** successfully, and hence, would no more be hidden for the subsequent data frame

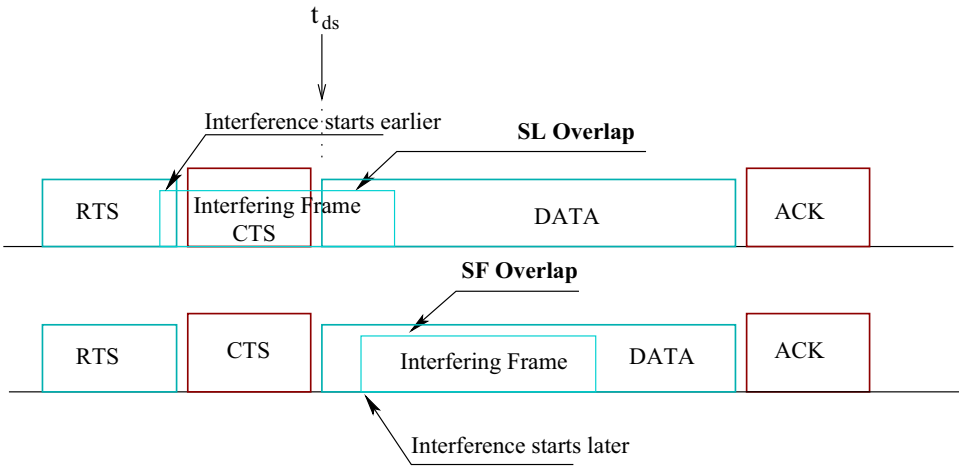

Fig. 10 Possible overlaps of data frame with hidden interferences

interference at **R**. Calculation of areas A_{Φ}, A_{Θ_i}, and A_{Θ_o} as a function of d is carried out in "Appendix". The effect of ODC is to effectively reduce the area of hidden zone through reduction in interference range for SF case. The two overlapping cases (SF and SL) will be treated separately in the collision analysis.

Now we determine the vulnerable periods for SF and SL types of overlaps of data frame. Figure 10 shows the SF and SL types of overlaps of data frame with interference from a hidden transmitter. For SF collision the interfering RTS frame has to start after t_{ds}. Due to EIFS mechanism the number of vulnerable slots in SF-collisions can be given as:

$$N^{SF}_{data-F} = \begin{cases} \left\lceil \frac{(T_{data}-EIFS)}{T_{gen}} \right\rceil & \text{if } \mathbf{X}\text{is within}\Theta_i \\ \left\lceil \frac{T_{data}}{T_{gen}} \right\rceil & \text{if } \mathbf{X}\text{is within}\Theta_o, \end{cases}$$

where $\lceil \cdot \rceil$ is the ceiling function. Note that, for SF case the number of vulnerable slots do not change with the type of interfering frame. As the transmission probability of the interfering RTS frame is larger than that of a data frame, we consider only the RTS frame as a possible source of SF-collisions. Denoting $F_{in}(F_{out})$ as the interfering frame from a node in region Θ_i (Θ_o), the data frame will not be subjected to any SF collision if none of the hidden nodes

within region Θ_i (Θ_o) initiates a transmission of frame F_{in} (F_{out}) in any of the corresponding vulnerable slots. Hence,

$$\begin{aligned} Prob\{\text{no SF Collisions of data}\}(d) &= Prob\{\text{no SF Collisions of type } data - F_{in}\}(d) \\ &\quad \cdot Prob\{\text{no SF Collisions of type } data - F_{out}\}(d) \\ &= e^{\left(-\rho\lambda A^{SF}_{\Theta_i}(d) N^{SF}_{data-F_{in}}\right)} \cdot e^{\left(-\rho\lambda A^{SF}_{\Theta_o}(d) N^{SF}_{data-F_{out}}\right)}. \end{aligned}$$

As observed in Fig. 10, for qualifying as an SL-interference, the interfering frame F must have started before t_{ds}. We consider the cases of F to be either RTS or data and ignore the other two cases of it being CTS or ACK. The vulnerable number of slots can be obtained as:

$$N^{SL}_{F-data} = \begin{cases} \left\lceil \frac{T_{RTS}}{T_{gen}} \right\rceil & \text{for } F = RTS, \\ \left\lceil \frac{(T_{RTS}+SIFS+T_{CTS}+SIFS)}{T_{gen}} \right\rceil & \text{for } F = data. \end{cases}$$

$F = RTS$ is intuitive from the explanation for (17), while the value for $F = data$ needs some explanation. Given that the RTS from $\mathbf{n}_0$ was received at $\mathbf{R}$ without any collision, the transmission of F must not have started before the starting instant of RTS from $\mathbf{n}_0$. Hence, the vulnerable number of slots for $F = data$ is justified in above equation.

Next, we discuss about the possible location of an interferer causing SL type of collision to the data frame. As $T_{RTS} \approx T_{CTS}$, with very high probability, the transmission of $F = RTS$ starts after the beginning of CTS. Therefore, the location of interferer is limited within Θ_o region, as otherwise it would not have initiated its RTS. The frame $F = data$ could have started either during RTS or during CTS. If it started during RTS, the interferer could lie anywhere in Θ_i or Θ_o but outside R_i^{SF} of receiver $\mathbf{R}$. And if it started during CTS, it could lie only in region Θ_o. Thus, a region other than Θ_o from where the interference can occur is negligibly small. Hence, for simplicity of the analysis, we consider A_{Θ_o} as the area of the SL-interference zone. Accordingly,

$$\begin{aligned} Prob\{\text{no SL Collisions of data}\}(d) &= Prob\{\text{no SL Collisions of type RTS-data}\}(d) \\ &\quad \cdot Prob\{\text{no SL Collisions of type data-data}\}(d) \\ &= e^{\left(-\rho\lambda A^{SL}_{\Theta_o}(d) N^{SL}_{RTS-data}\right)} \cdot e^{\left(-\Pi_{RS}\lambda A^{SL}_{\Theta_o}(d) N^{SL}_{data-data}\right)}. \end{aligned}$$

Finally, denoting $dataSucc$ as the event that, given a successful exchange of RTS/CTS, the subsequent data frame reaches the intended receiver without any collisions,

$$\begin{aligned} Prob\{\text{dataSucc}\}(d) = Prob\{&\text{no SF Collisions of data}\}(d) \\ &\cdot Prob\{\text{no SL Collisions of data}\}(d). \end{aligned}$$

Based on the descriptions of various states of the model in Fig. 2, the transition probabilities $P\{RS|I\}$, $P\{RF|I\}$, $P\{D1|I\}$, and $P\{D2|I\}$ can be expressed in terms of $Prob\{\text{rtsSucc}\}$ as:

$$P\{RS|I\} = \int_0^{R_t} f(x) \cdot \tau_R \cdot Prob\{\text{rtsSucc}\}(x)\mathrm{d}x, \tag{21}$$

$$P\{RF|I\} = \tau_R - P\{RS|I\}, \tag{22}$$

$$P\{D1|I\} = \int_0^{R_t} f(x) \cdot (1-\tau_R) \cdot (1-\tau') \cdot Prob\{\text{rtsSucc}\}(x)\mathrm{d}x, \tag{23}$$

$$P\{D2|I\} = \int_0^{R_t} f(x) \cdot (1-\tau_R) \cdot (1-\tau') \cdot (1 - Prob\{\text{rtsSucc}\}(x))\mathrm{d}x, \tag{24}$$

where, in the last two equations, τ' is the probability that no node in the so called *transmission deferral zone* (denoted as κ) initiates a transmission attempt in next time slot. As the name suggests, the κ zone is the region in which a node is prevented from transmission by an on-going transmission of a data frame. Clearly, besides covering the nodes within CS range of the sender, this zone also covers the nodes within transmission range of the sender as well as that of the receiver. Nodes within transmission range will have received either a RTS or a CTS and hence will defer their own transmission due to VCS. On the other hand, the nodes within CS range of both the sender and the receiver, will be receiving each of the four frames, at least as *sensed-only* frames and hence, will be deferring their own transmission due to PCS. Nodes located exclusively within CS range of the sender such that they receive only 'sense-only' frames transmitted by the sender only (i.e., RTS and data only and not CTS and ACK), they will also defer their own transmission until the ACK reception is completed at the receiver due to PCS and EIFS mechanism. However, the nodes that are located exclusively within CS range of the receiver such that they receive only 'sense-only' frames transmitted by the receiver only (i.e., CTS and ACK only and not RTS and data) will defer their transmission but for a limited time (EIFS) after each of the overheard frame. And hence, we do not include such nodes in the transmission deferral zone. Denoting the area of transmission deferral zone as A_κ, τ' can be expressed as:

$$\tau' = e^{(-\tau_R \lambda A_\kappa)}.$$

Thus, the term $(1 - \tau')$ in (23) and (24) stands for $\mathbb{P}$(at least one node in the CS range transmits) to cause the transition of node $\mathbf{n}_0$ from Idle state to a Deferring state. Now, we have six equations ((9), (13), (14), (21), (23), and (24)) with six unknowns (p_{ii}, Π_I, T_{gen}, $P\{RS|I\}$, $P\{D1|I\}$, and $P\{D2|I\}$). This system of non-linear equations can be solved to find the values of all these six parameters for given values of λ and R_c.

As we have neglected the ACK collisions, the transition probability $P\{DS|RS\}$ becomes:

$$P\{DS|RS\} = \int_0^{R_t} f(x) Prob\{\text{dataSucc}\}(x)\text{d}x,$$

and hence,

$$P\{DF|RS\} = 1 - P\{DS|RS\}.$$

Having determined the steady state probability Π_I, other steady state probabilities can be found easily from Eqs. (4a) to (4f).

Let TH_n denote the throughput per user, defined as the successfully transmitted average payload by an arbitrary user in a generic time slot, which is given by

$$TH_n = \frac{\Pi_{DS} L_{dt}}{T_{gen}}, \tag{25}$$

where, L_{dt} is the (constant) length of all data frames in bits.

5 Validation of the Model

In this section, we validate the analytical model through ns2 simulations. We noted that, the default IEEE 802.11 MAC implementation in ns2 does not support the scenarios where the interfering range is greater than the CS range. After incorporating the necessary changes to accommodate $R_i > R_c$ cases, the MAC and PHY layer codes were modified to incorporate ODC at PHY.

Further modifications were carried out in ns2 to reflect the corresponding assumptions in the analysis. The network topology and other system parameters chosen to match the parameters for analytical results were: Fixed CW of 1,024 system slots with no retransmission; fixed MAC data payload size 1,018 Bytes; 6 Mbps data rate for control packets and 6, 9, 12, 18, 24, 36, 48, and 54 Mbps data rates for data packets. Nodes were randomly deployed in an area of 2,000 m $\times$ 2,000 m with node density of $\lambda = 5 \times 10^{-5}$ nodes/m^2. This corresponds to around 9 to 10 nodes within a transmission radius of 250 m. Every node arbitrarily selects one of its R_t-neighbors (1-hop) as a receiver if it finds at least one. CBR traffic was generated from upper layer using UDP at the transport layer. At routing layer NO-Ad-Hoc (NOAH) protocol [2] was used with Time-To-Live set to 1. The choice of UDP at transport layer and NOAH at routing layer guarantees no reactions from higher layers for the happenings at the MAC layer. The chosen rate of CBR traffic is sufficient to keep the node always backlogged at the link layer. Both, the short and long retry limits were made 1 and the binary exponential back-off was stopped and a fixed contention window was used. Though, (almost) all the nodes are active transmitters, in calculating the throughput we consider only those sender–receiver pairs that are within the inner square of 1,000 m $\times$ 1,000 m to avoid boundary effects.

Figure 11 shows the per node throughput versus R_c/R_t ratio at 6 Mbps data rate with and without ODC. Though the simulation and analysis curves do not match at well, the trend is more or less the same. It can be noted that, the difference between simulation and analysis is higher when R_c/R_t is lower. We analyzed the reason and found the following: Many of earlier analytical works (e.g., the seminal work in [5]) assume that, all nodes are within the CS range of every other node in the system, and hence, the transmission probability of every node is the same as every node senses the same environment around itself. However, this assumption of uniform transmission probability is no more valid with the increase in the separation between two nodes and/or with the reduction in the CS range. As discussed in Sect. 4.1 [Ref. (10) and (11)], we addressed this problem by assuming two different transmission probabilities, pw and ρ, for nodes within transmission range and for those nodes outside transmission range (but within CS range), respectively. However, this also, not being entirely accurate, does not work well when CS range is small. The accurate analysis is found to be difficult [7] and

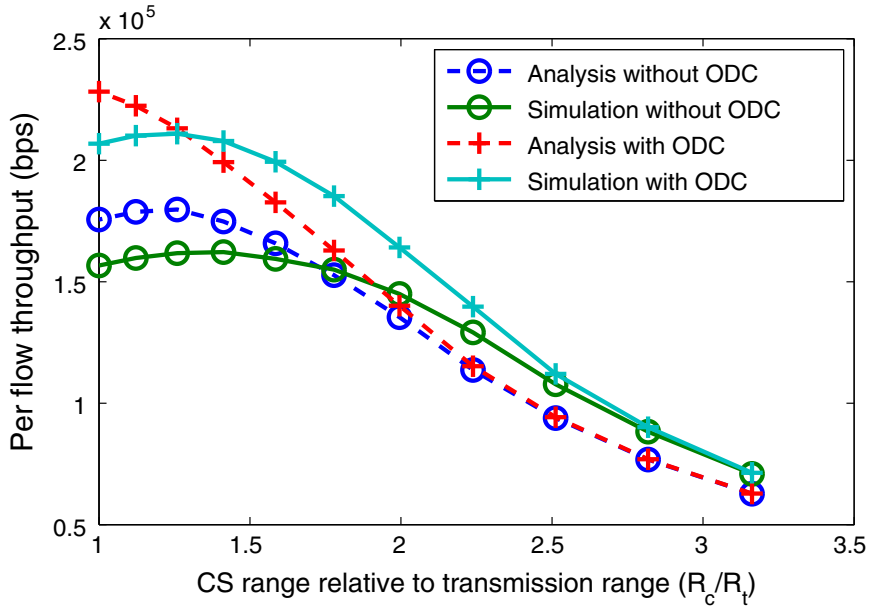

Fig. 11 Validation of analysis: per flow throughput versus R_c/R_t ratio at 6 Mbps data rate

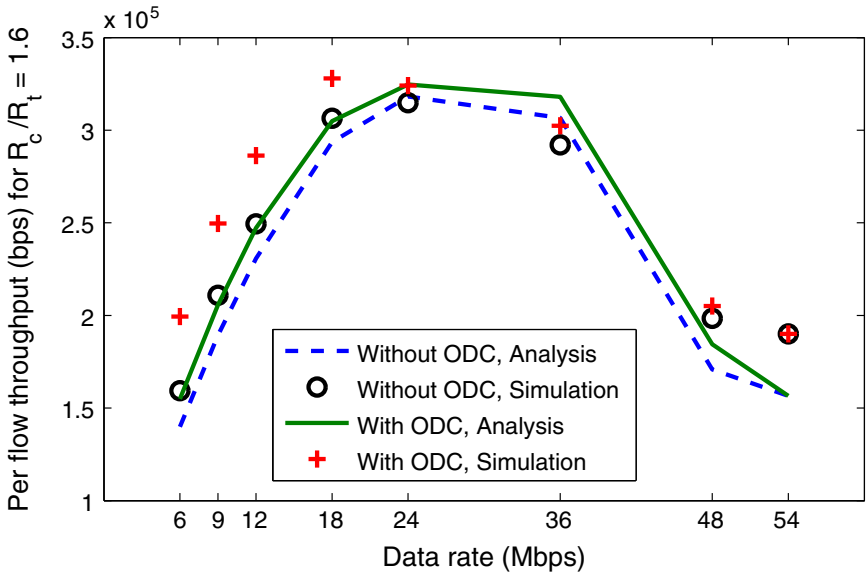

Fig. 12 Validating the analytical model at higher data rates. The *plots* are for typical value of $R_c/R_t = 1.6$. We have verified at other values of R_c/R_t as well

most existing analysis [17,32] assume constant transmission probability for all nodes in the system. The focus of our work is on the effect of ODC on deciding the CS threshold which is brought out by the trends shown in Fig. 11.

To validate the analysis at higher data rates, further simulation are carried out at higher data rates of IEEE 802.11a. Figure 12 shows per flow throughput at a typical value of R_c/R_t ($= 1.6$) with different data rates. Here also, though the analysis does not match exactly, the trend is more or less the same.

6 Impact of ODC on the Choice of CS Threshold

In this section, we use the analytical model developed in Sect. 4 to evaluate the impact of ODC on the choice of optimum CS threshold. As the significance of ODC diminishes with increase in operating data rates, we expect the gain due to ODC also to reduce with increase in data rate. To see this effect we plot and discuss the analytical results at various data rates of IEEE 802.11a. The system parameters considered are as follows: CW size: 1,024 and 128 system slots, with no retransmission option; node density λ: 5×10^{-5}, 1×10^{-4} nodes/m^2; fixed MAC payload size 1,018 Bytes; rate for control packets: 6 Mbps (802.11**a** basic rate for RTS, CST, ACK); rate for data frames: 6, 9, 12, 18, 24, 36, 48, 54 Mbps (802.11**a** data rates). Reduction in exposed terminals results in enhanced network throughput while possibly increasing the number of frame losses due to the increase in the number of hidden terminals. Therefore, following two performance metrics become important for evaluating the trade-off involved: per user throughput and frame loss rate. Per user throughput was already derived in (25). Using the notation Π_{DF} for steady state probability of DF state, the data frame loss rate (FLR) can be obtained as:

$$FLR = \frac{\Pi_{DF}}{\Pi_{DS} + \Pi_{DF}} = \frac{P\{DF|RS\}}{P\{DS|RS\} + P\{DF|RS\}}.$$

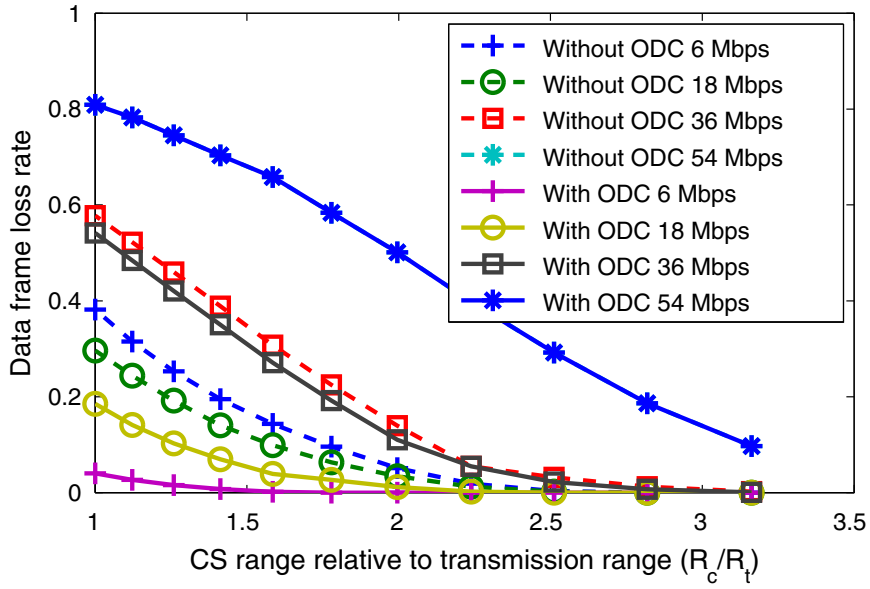

Fig. 13 Frame loss rate for data frames versus normalized CS range. CW = 128 and $\lambda = 5 \times 10^{-5}$ nodes/m^2

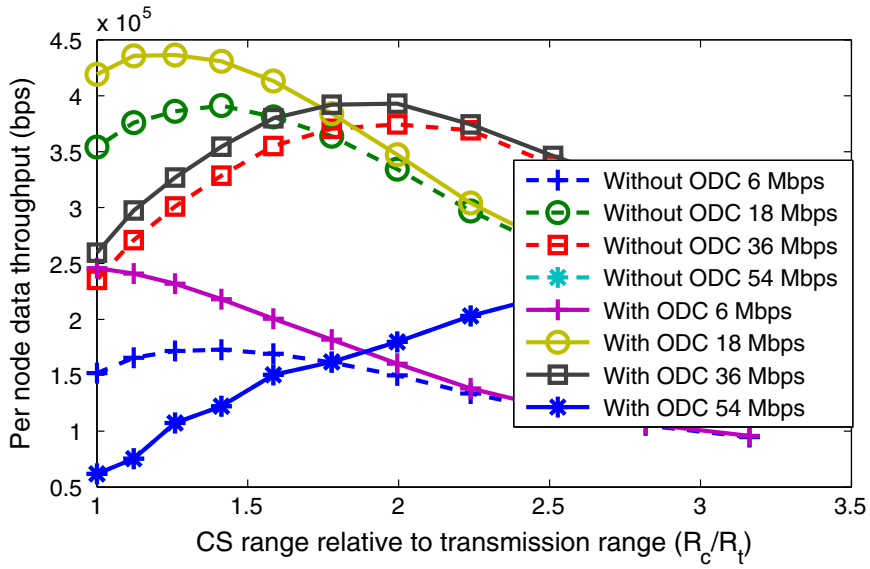

Fig. 14 Per-node throughput versus normalized CS range. CW = 128 and $\lambda = 5 \times 10^{-5}$ nodes/m^2

As our interest is to see the impact of ODC on the optimality of CS threshold, we plot the above performance metrics against different values of R_c for different data rates of IEEE 802.11a.

6.1 Impact of ODC on CS Threshold at Different Data Rates

Figures 13 and 14 respectively show frame loss rate and average per-node throughput versus R_c/R_t for a fixed CW 128 slots and node density of 5×10^{-5} (which corresponds to around 10 nodes in $R_t = 250$ m). Both the figures show results at four representative data rates (Mbps) of 802.11a: 6, 18, 36, and 54, with and without ODC.

As discussed in Sect. 4.3, at low data rates, the number of SL collision of data frames is reduced due to VCS, while the number of SF collisions are less due to the lower value of capture threshold in SF case (δ^{SF}). This has resulted in significant reduction in frame loss

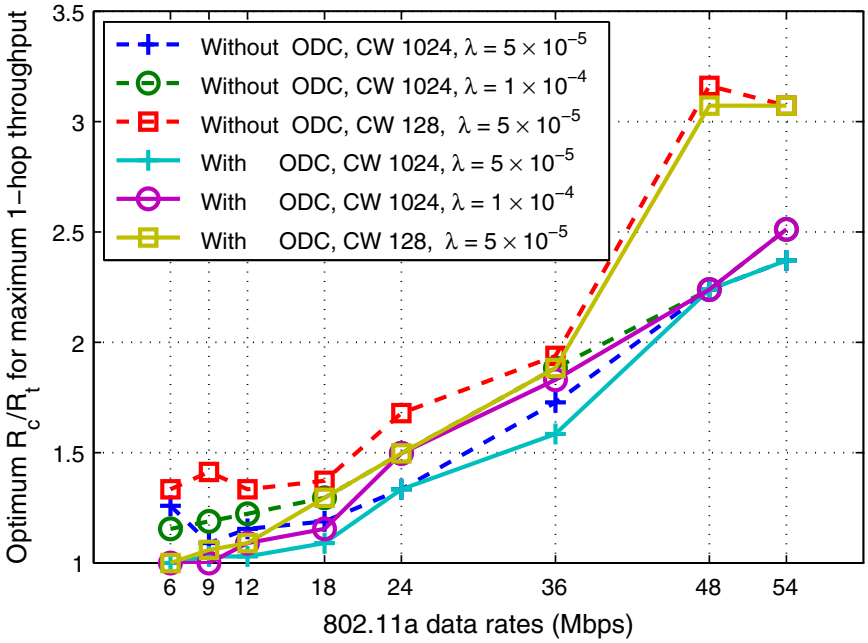

Fig. 15 Optimum value of R_c/R_t versus different data rates of 802.11a for different combinations of CW and λ

rate at low data rates (up to 18 Mbps) with ODC, as observed in Fig. 13. Though the frame loss rate plots show almost monotonic decreasing trend due to reduction in interference with the R_c/R_t, the throughput curves show a very different trend with an optimum R_c/R_t. This is due to the fact that, hidden terminals dominate towards lower value of R_c/R_t (i.e., $=$ 1.0) while exposed terminals dominate towards higher value of R_c/R_t (i.e., $= 3.5$). In other words, a lower value of R_c leads to the improvement in spatial reuse through reduction in exposed terminals while increasing the probability of collision due to increased number of potential hidden terminals. The impact of ODC is clear from the throughput curves of Fig. 14 as well. At low data rates there is a shift in the optimum PCS threshold. As the data rate increases beyond 18 Mbps, the difference between δ^{SF} and δ^{SL} (cf. Table 1) reduces, and so the difference between the two corresponding curves (with and without ODC) also becomes small. At 54 Mbps, the performance graphs for the two cases nearly overlap as the difference between the corresponding capture thresholds becomes quite small.

To study the impact of ODC on the amount of shift in optimum PCS threshold, we obtain the optimum value of R_c/R_t ratio for which the throughput is maximum at different data rate. Figure 15 shows these results with and without ODC for different combinations of λ and CW. The significant impact of ODC in low data rate region can be observed in all the curves.

6.2 Multi-hop Network Performance

While the numerical results serve the purpose of mathematical demonstration of the effect of ODC on the choice of CS threshold, it involves some constraining assumptions on network parameters. Hence, we further conducted simulation based network performance evaluation by considering more realistic system parameters. Though in multi-hop networks the optimum value of CS range shifts from its value in single hop networks [29], the effect of ODC should be prevailing irrespective of number of the hops in a flow. To verify this intuition we chose multi-hop networks for further evaluations.

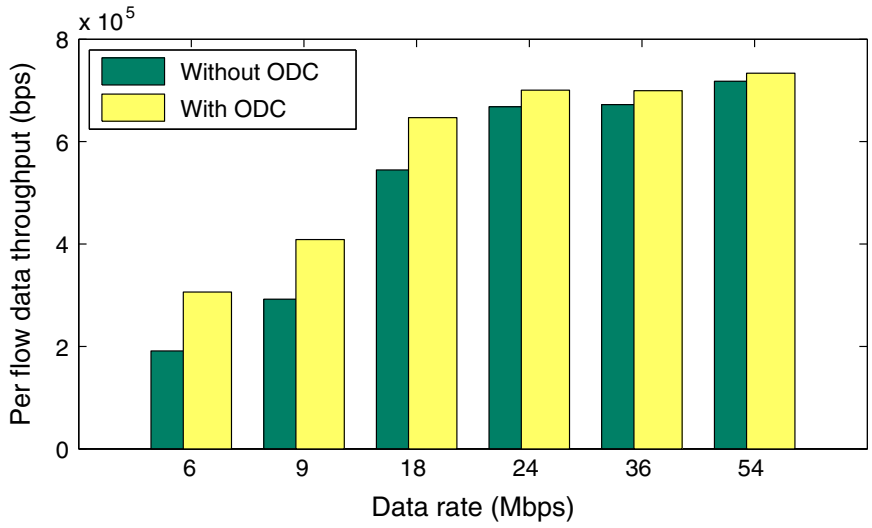

Fig. 16 Simulated multi-hop network performance at different data rates of IEEE 802.11a

To avoid excessively high run time, we consider a relatively small number of nodes in the network. We deployed 80 nodes in a 1,250 m × 1,250 m area. Thus, the node density is around 10 nodes in a transmission range of 250 m. Varying number of flows were established between arbitrarily chosen sender–receiver pairs, with end-to-end source–destination distance randomly selected 500–600 m. We used AODV routing protocol which tries to establish a route with minimum number of hops, and hence, the above end-to-end source–destination separation corresponds to around 3 hops. Each of these flows was sourced with a constant bit rate (CBR) traffic at the application layer, offering fixed sized packets of 1,000 bytes. Standard back-off algorithm with CW in the range of 15 to 1,023 was used with short and long retry limits set to 7 and 4, respectively. The CS thresholds at different data rates were set such that, R_c/R_t is set to the optimum values for 'with ODC' case at CW = 127 and $\lambda = 5 \times 10^{-5}$ from Fig. 15. Each data point was generated by taking an average of 50 simulation runs.

Figure 16 shows per flow throughput at various data rates of 802.11a. Similar to the observations in single hop network performance, the performance gain in multi-hop network scenario with ODC decreases at higher data rates. For example, the plots in Fig. 16 affirm that, per flow throughput gain with ODC are respectively around 60, 40, 19, 5, 4, and 2 % at 6, 9, 18, 24, 36, and 54 Mbps data rates. The reason for decreased gain at higher data rates is due to reduced difference in arrival order dependent capture threshold.

Figure 17 shows per flow throughput versus number of flows at data rates up to 18 Mbps. It can be observed that, the gain with ODC increases from 6, 4, and 3 % to 71, 45, and 20 % at 6, 12, and 18 Mbps, respectively, when number of simultaneous network flows increases from 1 to 11. Here, the increase in number of flows leads to an increased interference due to higher network activities. This results in an increased positive effect of ODC exploitation approximately up to 7 number of flows, after which the gain tends to saturate.

7 Concluding Remarks

In this paper, we have developed a 7-state model to analytically capture the network performance of RTS/CTS enabled distributed control wireless ad hoc networks with the nodes having ODC capability. Validation of the analytical model has been carried out through ns2

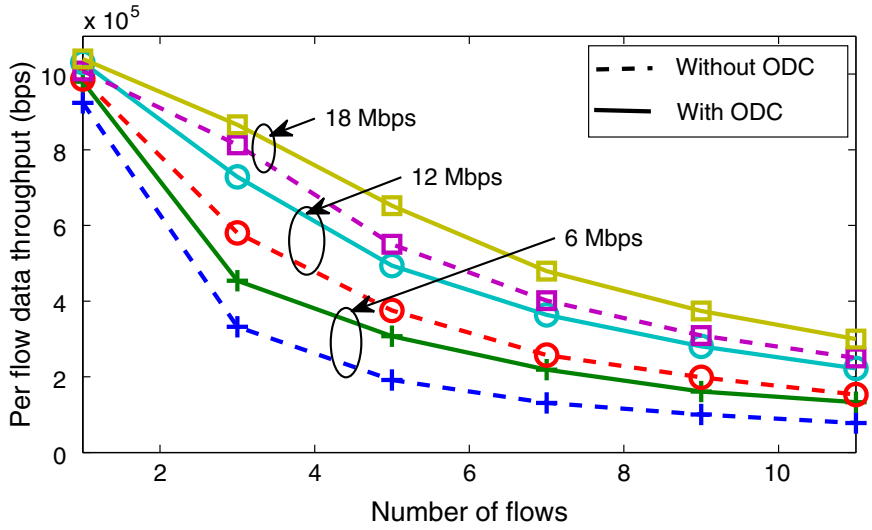

Fig. 17 Simulated multi-hop network performance for different number of flows

simulations after incorporating appropriate changes to accommodate the ODC capability of the nodes.

Utilizing the developed analytical framework, we have investigated the impact of considering ODC capability on the optimal choice of CS range in IEEE 802.11a wireless ad hoc networks with decentralized control. With the optimal CS range, the throughput performance gain up to moderately high data rates has been shown to be quite significant—up to 41 %. Since the order-dependence of capture threshold is less prominent at higher data rates, correspondingly the performance gain with ODC is also reduced.

Although the performance studies in this paper has been based on 802.11a standard, the results indicate that the ODC capability can be exploited to achieve significantly improved network performance in relatively low rate wireless ad hoc networks, such as WSNs.

Acknowledgments This research was partly supported by the Dept. of Science and Technology (DST) under the grant no. SR/S3/EECE/054/2007.

Appendix: Derivation of Different Areas

Area of Hidden Region for RTS Frames: A_{Ω}

A_{Ω} refers to the area of the horizontal-dashed region in Fig. 3. Let d_0 and d_1 be defined as: $d_0 = \frac{R_c}{K+1}$ and $d_1 = \frac{R_c}{K-1}$. Then, the hidden area for RTS frames can be obtained as:

$$A_{\Omega}(d) = \begin{cases} 0 & \text{for } 0 \le d \le d_0 \\ \theta_2(d)R_i^2(d) - \theta_1(d)R_c^2 + 2A_{\triangle(n_0RP_1)} & \text{for } d_0 < d \le \min(d_1, R_t) \\ \pi\left(R_i^2(d) - R_c^2\right) & \text{for } d_1 < d \le R_t, \end{cases} \quad (26)$$

where, $\theta_1(d)$, $\theta_2(d)$, and $A_{\triangle(n_0RP_1)}$ are derived as follows:

$$\theta_1(d) = \cos^{-1}\left(\frac{R_c^2 + d^2 - R_i^2(d)}{2R_c d}\right) \text{ and } \theta_2(d) = \pi - \cos^{-1}\left(\frac{d^2 + R_i^2(d) - R_c^2}{2dR_i(d)}\right).$$

Denoting $s(d) = \frac{R_c + R_i(d) + d}{2}$, we get

$$A_{\triangle(n_0 R P_1)} = \sqrt{s(d)(s(d) - R_c)(s(d) - R_i(d))(s(d) - d)}.$$

Area of Non-hidden Region for RTS Frames Covered by the Transmission Range of Sender: A_Ψ

Refer to Fig. 5. Let $d_2 = \frac{R_t}{K+1}$ and $d_3 = \frac{R_t}{K-1}$. Then,

$$A_\Psi(d) = \begin{cases} \pi R_i^2(d) & \text{for } 0 \le d \le d_2 \\ \pi R_i^2(d) - \theta_4(d) R_i^2(d) + \theta_3(d) R_t^2 & \\ \quad -2\sqrt{s(d)(s(d) - R_t)(s(d) - R_i(d))(s(d) - d)} & \text{for } d_2 < d \le \min(d_3, R_t) \\ \pi R_t^2 & \text{for } d_3 < d \le R_t \end{cases} \tag{27}$$

where, $s(d) = \frac{R_t + R_i(d) + d}{2}$ and $\theta_3(d)$ and $\theta_4(d)$ are calculated as follows:

$$\theta_3(d) = \cos^{-1}\left(\frac{R_t^2 + d^2 - R_i^2(d)}{2 R_t d}\right) \text{ and } \theta_4(d) = \pi - \cos^{-1}\left(\frac{d^2 + R_i^2(d) - R_t^2}{2 d R_i(d)}\right),$$

Area of Hidden Region for Data Frames: A_Θ

Referring to Fig. 9, $A_\Theta = A_\Omega - A_\Phi$, where A_Φ ($= A_\chi$, discussed in Sect. 4.2.2) is non-zero only if $d > R_c - R_t$ and its derivation is similar to that of A_Ω in (26). The hidden area for the data frames A_Θ has two sub-regions A_{Θ_i} and A_{Θ_o}. Let $d_c = \frac{R_c}{K}$. The area of A_{Θ_i} can be determined as:

$$A_{\Theta_i} = \begin{cases} A_\Theta & \text{for } d \le d_c \\ \pi R_c^2 - A_\Upsilon & \text{for } d > d_c, \end{cases} \tag{28}$$

where A_Υ is the area of intersection of two circles having same radius R_c whose centers are d distance apart. It is given by: $A_\Upsilon = 2R_c^2 \cos^{-1}\left(\frac{d}{2R_c}\right) - \frac{1}{2} d\sqrt{4R_c^2 - d^2}$. Finally, A_{Θ_o} is derived as:

$$A_{\Theta_o} = \begin{cases} 0 & \text{for } d \le d_c, \\ A_\Theta - A_{\Theta_i} & \text{for } d > d_c. \end{cases} \tag{29}$$

References

1. Atheros Communications. http://www.atheros.com/
2. NO Ad-Hoc Routing Agent (NOAH). http://icapeople.epfl.ch/widmer/uwb/ns-2/noah/
3. VINT Group: Network simulator ns-2 (version 2.33). http://www.isi.edu/nsnam/ns
4. IEEE std 802.11: Wireless LAN Medium Access Control (MAC) and Physical Layer (PHY) Specifications (2007)
5. Bianchi, G. (2000). Performance analysis of the IEEE 802.11 distributed coordination function. *IEEE Journal on Selected Areas in Communications*, *18*(3), 535–547.
6. Deng, J., Liang, B., & Varshney, P. (2004). Tuning the carrier sensing range of IEEE 802.11 MAC. In *Proceedings of IEEE international conference on global telecommunications (GLOBECOM)*, Dallas, USA.
7. He, J., Kaleshi, D., Munro, A., Wang, Y., Doufexi, A., McGeehan, J., & Fan, Z. (2005). Performance investigation of IEEE 802.11 MAC in multihop wireless networks. In *Proceedings of 8th ACM international symposium on modeling, analysis and simulation of wireless and mobile systems (MSWiM)*, New York, NY, USA.

8. Jiang, L. B., & Liew, S. C. (2007). Hidden-node removal and its application in cellular WiFi networks. *IEEE Transactions on Vehicular Technology*, *56*(5), 2641–2654.
9. Kim, T. S., Lim, H., & Hou, J. C. (2006). Improving spatial reuse through tuning transmit power, carrier sense threshold, and data rate in multihop wireless networks. In *Proceedings of the 12th annual international conference on mobile computing and networking, MobiCom '06*, ACM, New York, NY.
10. Kochut, A., Vasan, A., Shankar, A., & Agrawala, A. (2004). Sniffing out the correct physical layer capture model in 802.11b. In *Proceedings of IEEE international conference on network protocols (ICNP)*, Berlin, Germany.
11. Lee, J., Kang, Y. M., Lee, S., & Kim, C. K. (2011). Opportunities of MIM capture in IEEE 802.11 WLANs: Analytic study. In *Proceedings of ACM international conference on ubiquitous information management and communication (ICUIMC)*, Seoul, Korea.
12. Lee, J., Kim, W., Lee, S. J., Jo, D., Ryu, J., Kwon, T., & Choi, Y. (2007). An experimental study on the capture effect in 802.11a networks. In *Proceedings of ACM international workshop on wireless network testbeds, experimental evaluation and characterization*, New York, NY, USA.
13. Lee, J., Ryu, J., Lee, S. J., & Kwon, T. T. (2010). Improved modeling of IEEE 802.11a PHY through fine-grained measurements. ACM. *Computer Networks*, *54*, 641–657.
14. Li, Z., Nandi, S., & Gupta, A. K. (2005). ECS: An enhanced carrier sensing mechanism for wireless ad hoc networks. *Elsevier Computer Communications*, *28*(17), 1970–1984.
15. Lin, T. Y., & Hou, J. (2007). Interplay of spatial reuse and SINR-determined data rates in CSMA/CA-based, multi-hop, multi-rate wireless networks. In *26th IEEE international conference on computer communications (INFOCOM)*.
16. Lu, J., & Whitehouse, K. (2009). Flash flooding: Exploiting the capture effect for rapid flooding in wireless sensor networks. In *Proceedings of IEEE international conference on computer communications (INFOCOM)*, Rio de Janeiro, Brazil.
17. Ma, H., Alazemi, H., & Roy, S. (2005). A stochastic model for optimizing physical carrier sensing and spatial reuse in wireless ad hoc networks. In *Proceedings of IEEE International conference on mobile ad hoc and sensor systems (MASS)*, Washington, DC, USA.
18. Ma, H., Shin, S. Y., & Roy, S. (2007). Optimizing throughput with carrier sensing adaptation for IEEE 802.11 mesh networks based on loss differentiation. In *IEEE international conference on communications (ICC)*, Glasgow, UK.
19. Ma, H., Vijayakumar, R., Roy, S., & Zhu, J. (2009). Optimizing 802.11 wireless mesh networks based on physical carrier sensing. *IEEE/ACM Transactions on Networking*, *17*(5), 1550–1563.
20. Ma, Q., Liu, K., Miao, X., & Liu, Y. (2011). Opportunistic concurrency: A MAC protocol for wireless sensor networks. In *IEEE international conference on distributed computing in sensor systems and workshops (DCOSS)*, Barcelona, Spain.
21. Manweiler, J., Santhapuri, N., Sen, S., Roy Choudhury, R., Nelakuditi, S., & Munagala, K. (2009). Order matters: Transmission reordering in wireless networks. In *Proceedings of ACM international conference on mobile computing and networking (MOBICOM)*, ACM, Beijing.
22. Rappaport, T. (2001). *Wireless communications: Principles and practice* (2nd ed.). Englewood Cliffs: Prentice Hall.
23. Santhapuri, N., Nelakuditi, S., & Choudhury, R. R. (2008). On spatial reuse and capture in ad hoc networks. In *Proceedings of IEEE wireless communications and networking conference (WCNC)*, Las Vegas, USA.
24. Thorpe, C., Murphy, S., & Murphy, L. (2011). IEEE 802.11k enabled adaptive carrier sense management mechanism (kapcs2). In *IFIP/IEEE international symposium on integrated network management (IM)*, Dublin, Ireland.
25. Vegad, M. M., De, S., & Lall, B. (2009). Reconsideration of carrier sensing range for wireless ad hoc networks. In *Proceedings of 3rd IEEE international symposium on advanced networks and telecommunication systems (ANTS)*, New Delhi, India.
26. Xu, K., Gerla, M., & Bae, S. (2002). How effective is the IEEE 802.11 RTS/CTS handshake in ad hoc networks. In *Proceedings of IEEE international conference on global telecommunications (GLOBECOM)*, Taipei, Taiwan.
27. Yang, X., & Vaidya, N. (2005). On physical carrier sensing in wireless ad hoc networks. In *Proceedings of IEEE international conference on computer communications (INFOCOM)*.
28. Ye, F., Yi, S., & Sikdar, B. (2003). Improving spatial reuse of IEEE 802.11 based ad hoc networks. In *Proceedings of IEEE international conference on global telecommunications (GLOBECOM)*, San Francisco, USA.
29. Zhai, H., & Fang, Y. (2006). Physical carrier sensing and spatial reuse in multirate and multihop wireless ad hoc networks. In *25th IEEE international conference on computer communications (INFOCOM)*.

30. Zhang, Y., Assi, C., Alawieh, B., & Alazemi, H. (2011). A spatiotemporal contention resolution for enhancing spatial reuse in wireless networks. *IEEE Transactions on Vehicular Technology*, *60*(2), 680–691.
31. Zhu, J., Guo, X., Yang, L., & Conner, W. (2004). Leveraging spatial reuse in 802.11 mesh networks with enhanced physical carrier sensing. In *Proceedings of IEEE international conference on communications (ICC)*, Paris, France.
32. Zhu, Y., Zhang, Q., Niu, Z., & Zhu, J. (2008). On optimal QoS-aware physical carrier sensing for IEEE 802.11 based WLANs: Theoretical analysis and protocol design. *IEEE Transactions on Wireless Communications*, *7*(4), 1369–1378.

Mayur M. Vegad received his B.E. degree in electronics and communication engineering with distinction in 1995 from Dharmsinh Desai Institute of Technology, Gujarat University, India, and M.Tech. in Computer Technology from Indian Institute of Technology (IIT) Delhi, in 2004. He worked as an Engineer in the Quality Assurance department of M/s Videocon Intl Ltd., Gandhinagar, for more than three years. Since July 1998, Mr. Vegad is on the faculty of the department of Computer Engineering at the Birla Vishvakarma Mahavidyalaya (BVM) Engineering College, Gujarat. Since July 2007 he has been a PhD student in the Electrical Engineering department at IIT Delhi. His main research interests include wireless computer networks and artificial intelligence.

Swades De received his B.Tech. in Radiophysics and Electronics from the University of Calcutta, India, in 1993, M.Tech. in Optoelectronics and Optical Communication from the Indian Institute of Technology (IIT) Delhi, in 1998, and Ph.D. in Electrical Engineering from the State University of New York at Buffalo, in 2004. Before moving to IIT Delhi in 2007, he was an Assistant Professor of Electrical and Computer Engineering at NJIT (2004–2007). He also worked as a postdoctoral researcher at ISTI-CNR, Pisa, Italy (2004), and has nearly five years industry experience in India in telecommunication hardware and software development (1993–1997, 1999). His research interests include performance study, resource efficiency in multihop wireless and high-speed networks, broadband wireless access, and communication and systems issues in optical networks.

Brejesh Lall received B.E. degree in electronics and communication engineering from Delhi College of Engineering, Delhi, India in 1991, M.E. in electronics and communication engineering also from Delhi College of Engineering, Delhi, India in 1992 and Ph.D. degree from Indian Institute of Technology Delhi, India in 1999. He joined Hughes Software Systems, Gurgaon, India in 1997 and worked there in the Signal Processing group till 2005. In 2005 he joined Indian Institute of Technology Delhi as an Assistant Professor in the Electrical Engineering Department and is currently working there as an Associate Professor. His research interests include Multirate Signal Processing, Image Processing and Wireless communication.

APPLICATION OF GREEN CHEMISTRY PRICIPLES IN ORGANO-GRIGNARD REACTIONS

Parin D .Shah[1]
[1]*Chemical Engineering Department, Institute Of Technology Nirma University, Gujarat, (India)*

ABSTACT

2-Methyltetrahydrofuran (MTHF) is a commercially available solvent that is produced from renewable resources. The properties of MTHF place it between tetrahydrofuran (THF) and diethyl ether (DEE) in terms of solvent polarity and Lewis base strength. The formation and reaction of Grignard reagents in MTHF and THF are similar. MTHF is partially miscible in water, whilst THF is infinite miscible in water resulting in simple solvent recovery and drying. This paper is intended to show that MTHF is a green and cost- effective alternative to THF, based on actual application of the solvent in pharmaceutical industry for production of anti-hypertension drug. By comparing performance of MTHF with THF, it is concluded that in MTHF, the reaction yield improved significantly, stability of solvent to acid and base increased and the work-up is simplified. This paper demonstrates through the practical commercial example the economic and environmental advantages offered by MTHF with improved productivity.

Keywords: Green Solvent, Green Chemistry, 2-Methyltetrahydrofuran, THF, Organo-Grignard Reaction

I. INTRODUCTION

2-Methyltetrahydrofuran (MTHF) is an aprotic ether solvent, while being a strong Lewis base like THF. It is only partially miscible with water and is increasingly being used in organo-metallic and biphasic chemical processes because this interesting combination of properties leading to process simplification [1, 2]. THF is the primary ether solvent used in organo-metallic reactions because it strongly coordinates with many metals and has a moderate boiling point of 65.7 °C. However since THF is completely water miscible, it often causes problems in the water-quenching step that is used to remove the metal .Typically another solvent like toluene must be added to partition the desired product into the organic phase or to provide a clean phase separation of the organic and water phase. With MTHF, the product can be conveniently isolated without adding another solvent. MTHF provides very clean organic-water phase separations with little tendency to form emulsions or rag layers. Besides MTHF, diethyl ether (Et_2O) is the only other commercially available mono-dentate alkyl ether that is not water miscible and can be used in place of THF in organo-metallic reactions that require a strong Lewis base. However, the low boiling point (35.4 °C) of Et_2O makes it difficult to use in industrial processes. Available data rates MTHF between THF and Et_2O in solvent polarity and Lewis base strength. Organo-metallic reagents in MTHF have recently become available on industrial scale due to increasing demand for these products around the world [3]. Various organo-metalic reagents in MTHF as well as the solvent itself

are today a global emerging market in the fine chemical industry [4]. This paper demonstrates through examples from organo-grignard applications the advantages offered by MTHF.

II. FEATURES OF GREEN SOLVENT 2-MTHF

Available information suggests that MTHF can replace THF and DEE in organo-metallic reactions; the reaction yields are superior, the stability of the solvent to extreme pH is improved and the work-up is simplified. For example, it has been shown that the use of MTHF consistently *improves the yield* of benzyl and allyl organo-grignards generation (Table 1). Subsequent addition step results in comparable or better yield than in THF. The use of MTHF also allows for a much *higher concentration* of organo-grignard bromides as shown in Table 2.

Table 1 Yields of Organo-Grignard with THF and MTHF

Reagent	Solvent	Organo-magnesium Yield	Yield Difference MTHF/THF
Benzyl Chloride	THF MTHF	85 % 99 %	14 %
Benzyl Bromide	THF MTHF	83 % 98 %	15 %
O-Methylbenzyl Choride	THF MTHF	78 % 97 %	15 %
O-Chlorobenzyl Choride	THF MTHF	20 % 86 %	66 %
Allyl Chloride	THF MTHF	73 % 89 %	16 %

Table 2 Grignard Bromides Are Highly Soluble At Low Temperatures In MTHF

RMgBr	Solution in MTHF			Solution in THF		
	w/w %	Mol/L	Cryst. Temp.	w/w %	Mol/L	Cryst. Temp.
MethylMgBr	35	3.2	< -10 ^{0}C	15	1.2	< 15 ^{0}C
EthylMgBr	40	3.4	< -10 ^{0}C	8	0.6	< 5 ^{0}C
PhenylMgBr	45	2.9	< -10 ^{0}C	17	0.9	< 20 ^{0}C

Table 3 Comparison Of Magnesium Turnings Requirement

Reagent	Solvent	Mg moles used per moles subtract	Yield	Yield Difference MTHF/THF
Benzyl Chloride	THF MTHF	2 1.05	85 % 99 %	14 %
Benzyl Bromide	THF MTHF	2 1.2	83 % 98 %	15 %

As a rule of thumb organo-grignard bromides are three times more soluble in MTHF than THF. Moreover, the organo-grignard solutions in MTHF have the crystallization temperature under -10°C, much lower than the crystallization temperature in THF. This in turn simplifies greatly transportation and storage conditions and creates the opportunity to carry out the reaction at higher concentration. The organo-grignards generation in MTHF is close to stoichiometric consumption in magnesium turnings as shown in Table 3. By contrast THF requires excess Mg turnings in an effort to minimize the competitive dimerization to dibenzyl[5].

From the perspective of physical properties the product isolation is easier in MTHF because MTHF is not water-miscible (whilst THF is). The recovery and drying of the solvent is simpler since MTHF forms a water-rich azeotrope at atmospheric pressure. The extraction yields are improved (MTHF reduces the number of extraction steps) [6,7].

2.1 Opportunity To Increase Productivity

Based on the examples given above the use of MTHF organo-grignards provide the opportunity to increase productivity by reducing cycle time and increasing throughput. Reduction in cycle time will result both from reduced set up times (loading/unloading, heating/cooling times) and also from faster production (e.g. quick phase separation) For example, the possibility to work at three time higher concentration with organo-grignard bromides, reduces loading/unloading as well as heating and cooling times to one third due to reduced solvent volume. THF, a water soluble solvent, is often mixed with hydrophobic solvents such as toluene to achieve phase separation [8]. These mixtures form oftentimes persistent emulsions and rag layers which are time consuming to get separated on an industrial scale. MTHF was shown to be a more efficient extraction solvent and throughput could increase through reduction of the number of the extraction steps needed to recover the product [9]. Another source of reducing the total cycle time is the higher boiling point of MTHF; it boils more than 10°C higher than THF, therefore the reaction time should be reduced by 50 percent (from the Arrhenius equation).

2.2 Environmental Advantages

From environment point of view, MTHF is obtained from naturally occurring pentoses in agricultural wastes like corncobs or bagasse (sugar cane). The carbon dioxide generated through incineration of spent MTHF will simply return the carbon dioxide absorbed by the crop from the atmosphere. MTHF could also qualify for carbon emission credits. By contrast THF and DEE are commercially produced from oil therefore carbon emission credits are not an option. MTHF will also ensure a reduced carbon footprint by reducing waste. The higher boiling point of MTHF (80°C) compared to THF (64°C) will decrease the amount of solvent released in the air, reducing reported VOC emissions. THF is water miscible therefore effluents are by definition rich in solvent.

2.3 Quality Control And Work Place Safety

MTHF is more stable under acidic and basic conditions than THF. From a quality control perspective this translates into a stable impurity profile of the product which automatically translates in reduced cost of quality. In the case of organo-grignard reagents, excess magnesium is not needed in MTHF compared to THF. The excess, pyrophoric magnesium powder does not need to be filtered and disposed of after the reaction, a distinct advantage from a safety perspective. Both MTHF and THF organo-grignard solutions have comparable thermal stability. The start of exothermic thermal decomposition is observed around 180°-200°C for both solutions, demonstrating that MTHF solutions are safe even at much higher concentration than THF saturated solutions. Stability to peroxide formation is also comparable for THF and MTHF with a slightly increased propensity to form peroxides for the latter solvent. From a storage and transportation safety perspective, peroxide formation rate increases with the stirring. The difference between the two solvents is negligible if the solvent is not stirred while a 50 percent increase in peroxide formation is observed under intense stirring[3]. Normal safety precautions similar to THF handling are recommended.

III. EXPERIMENTAL WORK

Grignard reactions are frequently used in pharmaceutical and fine chemical processes, and THF is the most common solvent used for Grignard reactions. MTHF could be used in similar reactions using THF in the formation and reaction of alkyl and aryl Grignard reagents. Laboratory Reagent grade MTHF from Spectrochem Pvt. Ltd. Mumbai was used in the experiments. Other chemicals were obtained from Lab supply houses. Chemicals were used as obtained except the water level was checked to make sure it was below 500 ppm for the organo-metallic reactions. Product yields were determined by GC using standards of known purity.

Under nitrogen atmosphere, 145 ml MTHF was charged in an oven dried flask equipped with a nitrogen bubbler, a stirrer, condenser and addition funnel. Mg-turnings (19.3 g, 0.7942 moles) were added at 25-30 ^{0}C. The reaction mass was stirred and heated up-to 38 to 42 °C. Reaction assembly was insulated to prevent heat loss from the system. 3.5 gm Ethylene Di-Bromide (EDB) was added in reaction mass to activate Mg- tuning surface as well as to initiate the reaction. After that temperature was increased up to 50 °C. 1st lot (13 gm) of Phenyl Ethyl Chloride (PEC) was charged with dropping funnel and temperature was observed increase up-to 60 to 62 °C. 2nd lot (87 gm) of PEC dilution with 70 ml MTHF solvent was charged. With addition of PEC, exothermic reaction took place and reaction temperature was raised maximum up-to 102 °C. Reaction mass temperature was maintained at 97 to 102 °C for 60 min. and then reaction mass was cool to RT (30 – 35 °C). The yield of the Grignard reagent was checked by GC. The Grignard reagent was transferred to another nitrogen blanketed flask before reacting with an electrophile. 500 ml toluene and 105 ml Diethyl oxalate (DEO) were charged as an electrophile in three-neck flask and mixture was stirred under nitrogen. Reaction mass was chilled to –14 to –19 °C and stirred for 30 min. With maintaining the temperature under nitrogen, Grignard reagent solution was added drop by drop then temperature was raised to –5 to 0 °C. For hydrolysis of product with dilute acid, solution of 75 ml concentrated HCl and 232 ml water was charged at –5 to 13 °C and stirred for 15 min. Temperature was raised up-to 25 to 30 °C. From reaction mass, organic (toluene) and aqueous layers were separated and aqueous layer was discarded. Water wash (200 ml water) was given to toluene layer. Reaction mass was stirred and layers were separated. To neutralize the reaction mass, sodium bicarbonate washes were given (8 g sodium bicarbonate + 400 ml water) (three washing (100 ml + 100 ml + 200 ml)). Two water washes (200 ml + 200 ml) were given to toluene layer. pH of final aqueous layer was checked (pH = 6 to 7). Under high vacuum, Toluene layer was distilled out at 60 to 90 °C to get pure product in form of oily mass remaining in RBF. The product yields and % assay were determined by GC analysis.

Same reactions were performed using THF and MTHF solvent. In THF solvent, % Assay of Grignard reagent was observed 29.07 % by GC and same in MTHF was observed 37.21%. It is concluded that better quality of Grignard reagent can be prepared using MTHF solvent. In MTHF, % Assay of main product was noted 86.1 % with yield 1.18 compare to THF 86 % and 1.00 respectively. Approximately 18% improvement in yield is possible by using alternate MTHF solvent.

VI. CONCLUSION

2-Methyltetrahydrofuran can be used as a solvent for most organo-metallic reactions that require a strong Lewis base like THF. When MTHF is used to replace THF in organo-metallic reaction processes, it can conveniently be used to recover the reaction product because it is only partially water miscible. The MTHF/water azeotrope can be used to dry the reaction product for subsequent process steps and to recycle dry MTHF. MTHF can also

be used as an efficient replacement for dichloromethane in biphasic reactions and as a solvent for efficiently recovering water soluble compounds. Switching processes from THF-based to MTHF-based technologies provides a great opportunity to move innovative companies to greener technologies while simultaneously obtaining a sustainable competitive cost advantage.

REFERENCES

[1] Available from Penn Specialty Chemicals, Inc. in drum or bulk quantities. www.pschem.com
[2] Gutman, V. Coord. Chem. ReV. 1976, 18/2, 225-55
[3] Chemetall GmbH and Penn Specialty Chemicals Inc. have a joint marketing program for the development of theMTHF based organometallic market
[4] MTHF was selected among the CPhI Innovation Award Nominees (2006 Paris) and is nominated for The Presidential Green Chemistry Award (Washington DC, June 2007)
[5] R. Aul, B. Comanita, Manufacturing Chemist, May 2007, pp. 33-34. Experimental results obtained by Penn Specialty Chemicals, Inc.
[6] B. Comanita, D. Aycock, Industrie Pharma Magazine 17, pp. 54-58 (2005)
[7] B. Comanita, Industrie Pharma Magazine 22, pp. 1-4 (2006)
[8] R. Kotte, Furan & Derivatives, Kirk-Othmer Encyclopedia Chem. Technol.
[9] Kotte, Furan & Derivatives, Kirk-Othmer Encyclopedia Chem. Technol., S155 (1998)

MODELLING& SIMULATION OF SOLAR PV ARRAY FIELD INCORPORATED WITH SOLAR IRRADIANCE AND TEMPERATURE VARIATION TO ESTIMATE OUTPUT POWER OF SOLAR PV FIELD

Vishwesh Kamble[1], Milind Marathe[2], Rahul Rane[3]

[1]*Student, Dept. Of Electronics, K. J. Somaiya Collage of Engineering, Vidyavihar, Mumbai, India.*
[2]*Faculty, Dept. Of Electronics, K. J. Somaiya Collage of Engineering, Vidyavihar, Mumbai, India.*
[3]*Head, Technology Centre, E&A, L&T PVT. Limited, Mahape, Navi Mumbai, India.*

ABSTRACT

Photovoltaic systems are designed to feed either to grid or direct consumption. Due to global concerns, significant growth is being observed in Grid connected solar PV Plants. Since the PV module generates DC power, inverter is needed to interface it with grid. The power generated by a solar PV module depends on surrounding such as irradiance and temperature. This paper presents modelling of solar PV arrays connected to grid-connected plant incorporated with irradiance and temperature variation, to design simulator to study and analyse effect on output power of solar PV arrays with irradiance and temperature variation, also to estimate the output power generated by PV arrays. The mathematical model is designed implemented separately on simulator for each PV components connected in PV systems, which are PV cell, Module, sting, array and field of arrays. The results from simulation based on model are verified by the data collected from power plants and experiments done on solar PV cell.

Keywords: Photovoltaic, Irradiance, Temperature, Array, Model, Simulator.

I. INTRODUCTION

Photovoltaic power generation is gaining acceptance today as source of clean and pollution free energy. These power generators shows significant growth in grid connected as well as stand-alone applications. Our objective was to create mathematical model for solar PV array connected across these generators, incorporated with irradiance and temperature variation and implement the model using simulation for study and analyse the effect on output of field of solar PV arrays and also to estimate the power output of a solar PV arrays connected across power plants. We implemented our mathematical model using iVisionMax[1] PC suit to create simulation. We verified results from simulator based on our model by comparing it with data collected from power plants and results from experiment on solar cell.

II. LOGICAL THINKING

To create a model for solar PV system and implement it on simulation software we made some assumptions regarding atmospheric conditions effect on PV array. With the model for simulating PV arrays, we also wanted

simulator to implement graphical representation of Arrays, therefore we used some basic design models for graphical design of PV system in simulator. The assumptions we made for simulation are as follows:

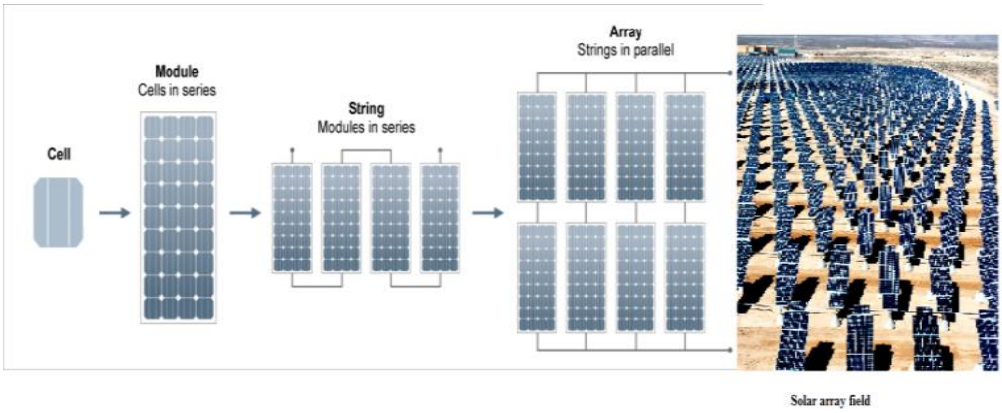

Fig. 1 Illustration of Solar Array Field

Figure 1 shows the illustration of solar array field which shows the order in which solar field is designed, we can see that field of arrays are made by solar array connected together, array is made up of strings connected in parallel, string is made up of modules connected in series and module is made up of cells connected in series. We designed software to simulate whole field, each array, each string and module connected in the field separately. We designed dedicated windows for every level.

2.1 Assumptions

2.1.1 Input

Inputs to simulator are as follows:

Climate conditions= Sunny and Cloudy, Solar irradiance= 0 W/m² to 1000 w/m², Module temperature = -5ºC to 80º, [10] Shadow density = 1% to 100%.

2.1.2 Effect of Other Atmospheric Conditions

All other atmospheric conditions such as humidity, wind speed, edging of sunrays, dust and snow are already imposing their effect on solar irradiance and module temperature as well.

Therefore,

$$Module\ Temperature = b0(ambiant\ temp.) + b1(wind\ temp.) + b2(irradiance) + b3(humidity) + b4(dust\ or\ snow) + b5(shadow) \quad (1)$$

Where, b0, b1, b2, b3, b4, b5 are regression coeff. Which are may vary according to location. It means that module temperature is already affected by other conditions and it's the same in case of irradiance.

2.1.3 Climatic Conditions

Climate conditions are depends upon the seasons of particular locations therefore we are assuming following conditions: Sunny Conditions: In sunny conditions, we are assuming that the location where the PV array is set up is free from all kinds of shadows including cloud shadow as well as other monumental shadows (clear sky). Solar PV modules are directly coming across Sun with no shadow effect and output of PV array is clearly dependent on solar irradiance and Module temperature. The tilt angle of Solar PV modules should be equal to latitude and the orientation of the Array should be always facing South (True south). Cloudy conditions: In cloudy conditions, we are introducing shadow over modules which will affect irradiance as well as module temperature. We are inputting shadow density of a cloud in simulator which will change the given irradiation and module temperature as input before and accordingly output will be changed.to simulate cloudy conditions we are assuming that cloud shadow is covering all the PV modules in PV array field with same amount of shadow density and whole sun is being covered by cloud (for Eg. Rainy day).

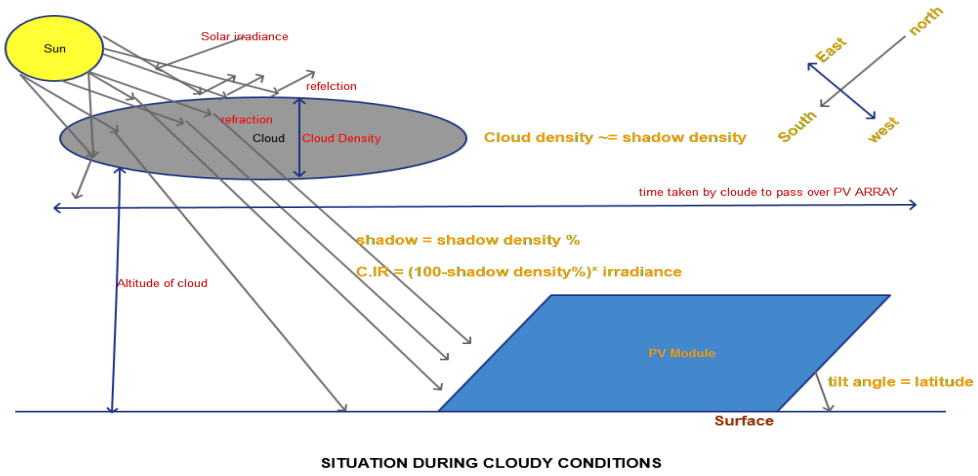

Fig. 2 Assumptionof Cloudy Condition for Simulator [4]

When shadow comes over PV module or an array, what happens is that shadow will resist solar insolation and irradiance. As much as the shadow density (SD)[10], darker the shadow hence, irradiation reaching to the module isreduced by amount of shadow present due to cloud as shown in figure 3(a). Similarly, module temperature also gets affected due to shadow over module, but it doesn't happen rapidly as irradiance, it will need some time to see reduction in temperature. Therefore we are considering time for shadow to remain over PV array, to give the change in Module temperature. To simulate or mimic change in module temperature we are using Newton's law of cooling, which we will enlighten in next sub-topic. From experimenting and studying we can say that change in irradiation due to shadow is linear in nature and change in module temperature is logarithmic and exponential. Studies show that module temperature is always 20 to 30% [5] more than ambient temperature. While designing the equations for simulation we are considering ambient temperature 80 % approx. of a module temperature. Which is calculated in cloudy condition after the module temperature is specified. [7][6]

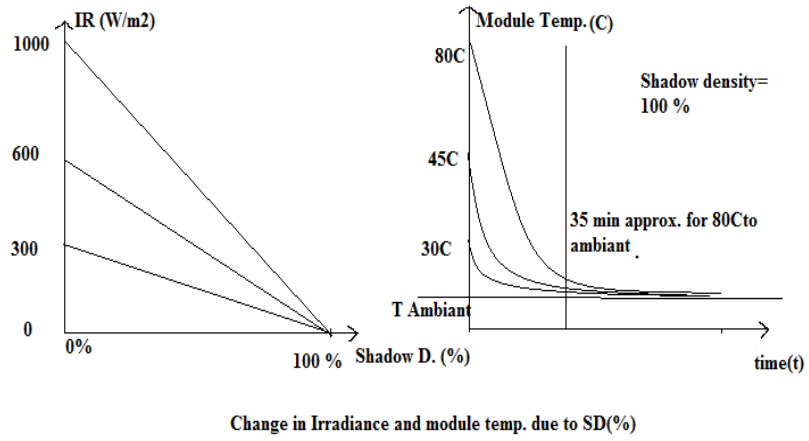

Fig. 3 Change in Irradiance and Module Temp Due to Shadow Density (Based On Experiments and Observation)

Since the purpose of designing the simulator is to study and analyse effect of atmospheric conditions on solar PV module and its fields of arrays therefore we are not considering any other effect on the output of module. We are just concerned about how much power required from solar Array field and how it will get affected by change in atmospheric conditions.

III. MATHEMATICAL MODELLING

3.1 PV Module Mathematical Modelling

Assumptions: the following terms we are using in the programming while designing the simulation software in iVisionMax.

Voltc = Vmax of a PV cell.
Crin = Imax of a PV cell.
Refchng = change in voltage due to irradiance variation.
I0 = Diode saturation current (f (i0) i.e. base value of I0 of a cell)
Ir = Solar irradiance.
M.Temp = Module Temperature in ºC.
Tambient= Ambient temperature in ºC.
Chngeintemp = change in ambient temperature.

Equation 2 derives the base value of diode saturation current which is denoted as i0, it is already present in silicon solar cell due to its material characteristics. but Base i0‘s presence can be neglected till module temperature is 25º C. if the module temperature is increased than diode saturation current will rise and gets added with output current. Equation 3 illustrates the change in diode saturation current.

$$io = \frac{qADnni^2}{LnNa}[8] \quad (2)$$

where,q is charge in a cell, A is surface area in mm²,Dn is Depletion width, ni is intrinsic concentration, Ln is length if n region, Na is Doping density.

$$I0 = i0.e^{0.09672\,(M.temp-25)}\ [2] \quad (3)$$

I0 is diode saturation current of a PV cell which increases with rise in temperature, it is negligible because it is too small to count but it does flows into PV cell, and it affects current as well as voltage generated in PV cell. Which will have accountable effect on output power of Solar array field connected to grid.

3.1.1 Application Of Newton's Law Of Cooling For Change In Module Temperature Due To Cloud:

Newton's Law makes a statement about an **instantaneous** rate of change of the temperature [9].

Newton's law of cooling

$$\frac{dT}{dt} = -k(T - T_a).$$
$$T(0) = T_o$$

Solution,

$$T(t) = T_a + (T_o - T_a)e^{-kt}$$

To apply newton's law of cooling we have to find value of k, which is the relation between change in temperature of module with respect to time. To find k, we have to perform experiment as shown in figure 4. For experiment what we did is we heated the solar PV cell module up to 60º C in laboratory with no sunlight spectrum, we can assume that with no irradiance. We forcefully heated the module and then we observed and recorded time taken by the module to cool down to ambient temperature the table below shows us reading of the experiment, initially module temperature is 26.5 ºC and ambient temperature is 25.5 ºC. We used hair dryer as heating source from which we heated the module to 60 ºC and we measured the temperature on multichannel RTD device as shown in figure 4. We used multichannel RTD for measuring ambient temperature as well as module temperature at same time so that we can measure exact time for cooling down of module, table 1 shows the results from the experiment:

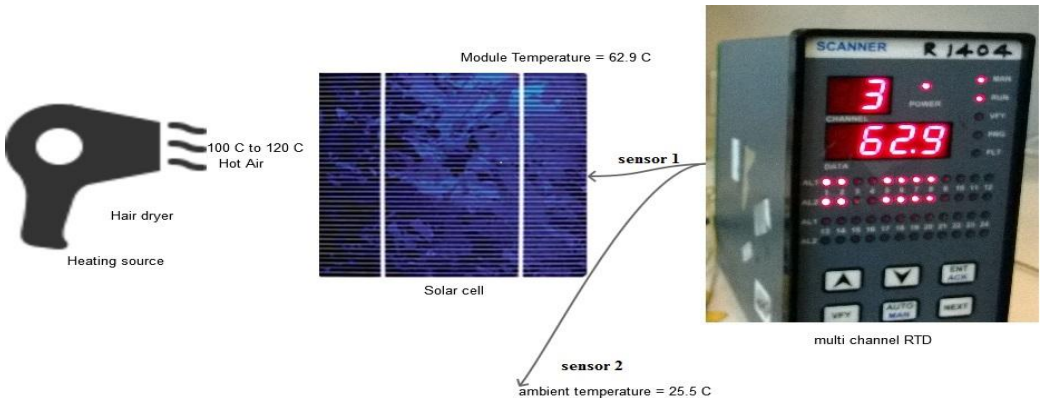

Fig. 4: Experiment Setup for Change in Module Temp Due To Cloud

TABLE I

CHANGE IN MODULE TEMPERATURE IN CLOUDYCONDITIONS

Date: 20/05/14 Time:	Ambient Temperature				
	Initial AT	After time(t)	Initial M.Temp.	M. Temp after time(t)	Time (min)
10.40 AM	25.5ºC	27.6 ºC	60 ºC	28.2 ºC	34.21 min
11.20 AM	28.0º C	27.2 ºC	60 ºC	27.6 ºC	36.47 min
12.02 PM	28.0 ºC	27.8 ºC	60 ºC	28.7 ºC	34.47 min

It is seen that module takes approximately 35.05 minutes to cool down to ambient temperature. We repeated the same procedure 3 times on same module to see the change in module temperature with reference to ambient temperature. To find out change in module temperature due to shadow of a cloud, we have to find change in ambient temperature due to shadow, which is illustrated by equation 6 and 7.

3.1.2 Newton's Law Of Cooling Regression Coefficient

Now let's see, how to find K? When shadow is over module, 1st we have to measure change in ambient temperature. Since we are feeding module temperature directly we are using property of relation between ambient temperature and module temperature. Ambient temp is always 75% to 80% of module temperature. [5]

$$Tambient = (M.temp).\left(\frac{80\ \%}{100}\right) \quad [5] \qquad (6)$$

$$Chngeintemp = Tambient - Tambient.\left(e^{\frac{-time\ (t)}{\tau=0.00995}}\right).\left(e^{\frac{-(shd_dnsity\ \%)}{100}}\right) \quad (7)$$

In equation 7, we are using heat transfer equation for calculating change in module temperature due to shadow and presence of shadow over module. Change in ambient temperature is function of shadow density in % and time of presence of shadow over module. Here, equation 8 is derived from solution of Newton's law of cooling. To find k we solved the equation and also did experiment on module to acquire the data for calculation, below equation 8 we can see the calculation for k using experiment results. We used the value of k as constant in equation 9.

$$k = \ln\left(\frac{M.Temp - Tambient\ /\Delta\ M.Temp - Tambient}{time\ (t)}\right) \quad (8)$$

k= 0.08124.

From table 1, we took values to solve the equation 8. Change in module temperature is function of change in ambient temperature and time required to cool down to ambient temperature with time and constant k . Equation 9 ,shows the calculation for changed module temperature based on change in ambient temperature. Here we are calculating effect of ambient temperature only not shadow effect because we have already calculated ambient

temperature over shadow. Equation 10, shows the changed irradiance due to shadow of a cloud over module. Figure 3 shows the relation of irradiance with shadow and module temperature with shadow.

$$\Delta M.temp = chnageintemp + (M.temp - changeintemp).\left(e^{-k.(time)}\right) \quad (9)$$

$$\Delta ir = \left(\frac{100 - shd_dnsity}{100}\right).ir[2] \quad (10)$$

3.1.3 Output Equations

As we explained mathematical modelling of the input side, now let's see equations and formulations from the output side. Equation 11, 12 and 11a are representing regression coefficients or factors which relets the change in input to change in output, *voltc* gives voltage of a cell from module specified by user. *Crin* is regression coefficient between current and solar irradiance and *refchnge* gives the relation between changes in irradiance to change in voltage.

$$voltc = \frac{Vmax}{No.of\ PV\ cells} \quad (11)$$

$$crin = \frac{Imax}{1000} \quad (12)$$

$$refchnge\ (ir\ coeff.) = \frac{11mv - voc\ of\ PV\ cell}{\ln(1000 - ir)} \quad (11a)$$

Where,

ir = 10 W/m2, VOC = 600mv, 11 mv [according to real diode characteristics].[3]

Equation 13 gives the voltage of a module dependent upon module temperature without effect of irradiance over it, for this equation we always assume that except change in temperature other parameters are at ideal state, but we are compensating effect of other conditions such as irradiance separately which we will see in the following conditions we made. The temperature coefficient we took is always specified in specification sheet provided by manufacturers. Here we are taking it as constant but it may vary with manufacturer to manufacturer. Module current equation 14 is based in the principle states that, current directly proportional to irradiance. Where, *crin* is regression coefficient which always gets changed with module to module.as illustrated in equation 12. Equation 15 is product of voltage and current obtained from 13 and 14 i.e. power of a module.

$$Vmodule = voltc.\left(1 + (M.temp - 25).\left(\frac{-0.34}{100}\right)\right).No.of\ PV\ cells \quad (13)$$

Where,

(-0.34 % is temperature coeff. provided by manufacturer.)

$$Imodule = (crin).(ir) \quad (14)$$

$$Pmodule = Vmodule.Imodule \quad (15)$$

Condition 1: Effect of module temperature on module current if > 25º C

As we seen earlier in equation 13 and 14 are independently related to voltage and current respectively. Here, we are relating module temperature with current. It states that if module temperature increased over 25º C, Carrier concentration is changed due to which band gap of PV module decreases, so I0 (i.e. Diode saturation current) increases, and eventually module voltage decreases.I0 gets introduced in Module output current. We are already defining decrease in voltage from equation 14 and we are also calculating I0 from equation 3. Therefore we add I0 with module current. As we can see in figure 5 Isc is slightly increase with decrease in VOC.Change in output current due to change in module temperature is shown in equation 16.

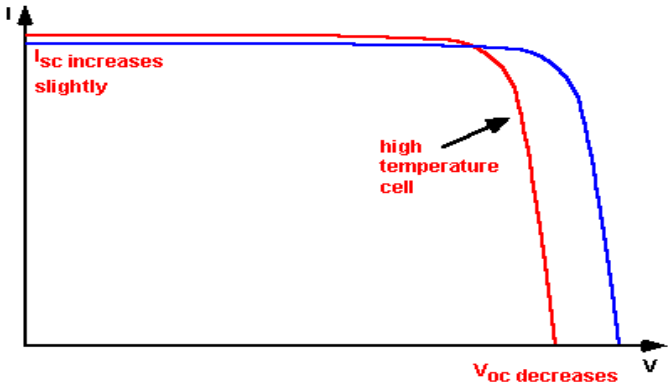

Fig. 5: The Effect Of Temperature On The IV Characteristics Of A Solar Cell.[3]

$$\Delta Imodule = \left(Imodule.\left(1 + (M.temp - 25)\right).\left(\frac{0.1}{100}\right)\right) - I0 \quad (16)$$

Condition 2- Effect of solar irradiance on module voltage if irradiance is < 1000 W/m²

As we know that, irradiance is not stable in nature and there are rapid variations. Solar irradiance does not reach to its maximum value every time i.e. 1000 W/m² throughout the day. The variations in irradiance not only will affect the current but also voltage of a module. To simulate change in module voltage we introduce regression coeff. refchnge (β) as we explained earlier in equation 11a. The module voltage will face exponential or logarithmic change due to change in solar irradiance. We illustrated this scenario by equation 17. It states that if solar irradiance is less than 1000 W/m² and varies with time then effect on module voltage will be deduction in module voltage with product of irradiance regression factor refchnge and natural log of 1000 - solar irradiance.

$$\Delta Vmodule = \left(Vmodule - (\ln(1000 - ir)).refchnge(\beta)\right) \quad (17)$$

3.2 PV String Mathematical Modelling

3.2.1 Design Formulation For String

String is nothing but No. of PV modules connected in series connection. The string in PV array decides output voltage of PV array field of a power plant. For example, if want to generate 70 V dc voltage and we are having 50 W PV module with Vmax of 35V so we have connect two PV module in series to make a string which will

generate 70 V at standard atmospheric conditions. In case of simulator, to design string it is important to find No. of modules needed in a string based on given estimated voltage and module specified. (for eg.290 w module.)

$$No.of\ modules\ in\ a\ string = \frac{Estimated\ voltage}{Vmax} \quad (18)$$

$$Vmax = (voltc).(No.of\ PV\ cells) \quad (18a)$$

Or

$$No.of\ modules\ in\ a\ string = \frac{Estimated\ power}{Pmax} \quad (19)$$

3.2.2 Simulation Formulas For String

All other simulation formulas used are same as module simulator except module voltage, module voltage will be multiplied by total number of modules connected in a string.

$$Vstring = Vmodule \times Total\ \ No.ofmodules\ in\ a\ string \quad (20)$$

3) PV Array mathematical modelling

3.2.3 Design Formulations For Array

Array is made by connecting strings of PV module in series or parallel connection to meet our power requirement from PV array field. Mostly in solar arrays all the strings are always connected in parallel. Array defines current output required from PV field. In case of Solar array now there are two factors are important Array voltage and array current. Array voltage is equal to String voltage i.e. string decides the voltage of array as well as field. Array current is defined by no of string connected in parallel mostly dependent on no. of channels in array junction box (AJB or SMB).

$$No.of\ PV\ modules = \frac{estimated\ power\ /_{Pmax}}{total\ No.of\ strings} \quad (21)$$

Or

$$No.of\ PV\ modules = \frac{Estimated\ voltage}{Vmax} \quad (22)$$

3.2.4 Simulation Formulas For Array

Simulation formulas are same as module and string simulation except array voltage and array current.

$$Varray = Vstring \quad (23)$$

$$Iarray = Istring \times Total\ No.of\ strings\ in\ PV\ array. \quad (24)$$

4) PV Field mathematical modelling

3.2.5 Design Formulation For Field

The term field is not used prominently in the industry because PV arrays are built for generating power in power plant but since it is type of energy harvesting therefore we use the term PV array field to pronounce solar power plant. Solar array field is nothing but No. of PV arrays connected together across solar inverter or to grid inverter to generate the power. In here Field voltage and Field Current are defined by No. of modules in a string and total No. of strings in a field respectively. No. of arrays are in a field are also important here while designing.

$$No.\,of\ PV\ modules\ in\ a\ string = \frac{Estimaed\ voltage}{Vmax\ of\ PV\ module}. \quad (25)$$

$$Total\ Pv\ modules\ in\ PV\ array = \frac{Estimaed\ power}{Pmax\ of\ PV\ module} (26)$$

$$Total\ Pv\ strings\ in\ PV\ field = \frac{Total\ modules}{No\ of\ PV\ module\ in\ a\ string} (27)$$

$$No\ of\ arrays\ in\ a\ PV\ field = \frac{Total\ PV\ strings}{No\ of\ PV\ strings\ in\ a\ single\ array} (28)$$

3.2.6 Simulation Formulas For Field

We are already calculating total number of modules and total number of strings connected in field of arrays, as we can see it in equation 26 and 27. Therefore, simulation formulas will remain same for field simulations.

5) Calculations for constants

3.2.7 For Time Constant (T)

Here we can see the solution for finding out the τ, which we have used in equation 7. τ is nothing but time constant for heat transfer in ambient temperature.

$$\Delta\, Tambient = Tambient - Tambient.\left(e^{\frac{-time(t)}{\tau}}\right)$$

Based on experiment:

Tambient = 60º C

Changed ambient T = 59.6ºC

Time = 3 sec (i.e. 0.05)

$$59.6°\,C = 60°\,C - 60°\,C.\left(e^{\frac{-(0.05)}{\tau}}\right)$$

$$\tau = 0.00995.$$

3.2.8 For Refchng:

We observed that for typical (156X156) Poly crystalline solar cell there is 11mv change in VOC per 10 W/m² [3]. Studies show that a cell generates 600 mv against the full sun spectrum. Using above information we can find *refchnge*coeff.

$$11\ mv = 600\ mv - \ln(1000 - ir).refchnge$$

Refchnge = 0.085776

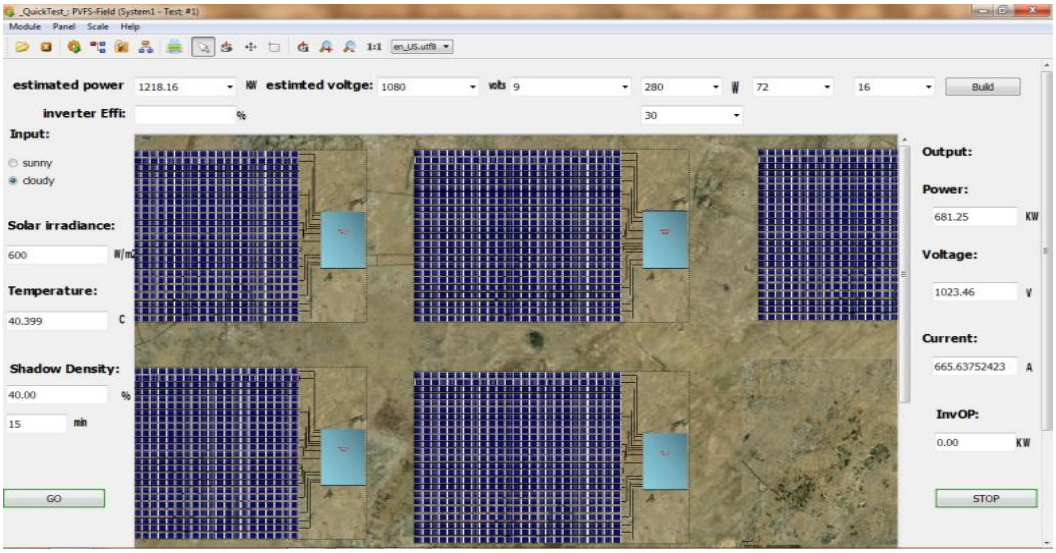

Fig. 6: PV Field Simulator Using Ivisionmax

IV. RESULTS AND VALIDATION

To verify the simulation and mathematical model, we studied couple of power plants and also we performed experiment on Solar cells, so that we can validate our model and simulation results by comparing them with the results from experiment and data collected from power plant.

4.1 Experiment Done Over Solar Cells

We performed experiment on 3 kinds of solar cells; all three solar cells are top end polycrystalline solar cells available in market. They differed from each other based on cell efficiency.

We used 16.10%, 17% and 18% efficiency solar cells and performed test on them with effect of solar irradiance and temperature variation. The set up for solar cell experiment is shown in figure 7.

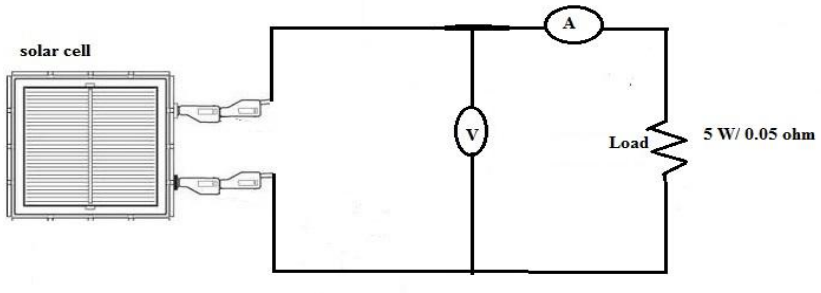

Fig 7: Setup For Solar Cell Experiment

Specifications:

Cell 1: 4.38 W (cell eff. 18 %) Vmax = 35 V, Imax = 9.01 A

Cell 2: 4.13W (cell eff. 17 %) Vmax = 35 V, Imax = 8.49 A

Cell 3: 3.91W (cell eff. 16.1 %) Vmax = 35 V, Imax = 8.04 A

TABLE II

Comaparision Results Between Experiment Results And Simulation Results

Time	Irradiance (W/m^2)	M. temp. (°C)	Actual power (W)	Simulated power (W)	Error (%)
Cell 1					
10:45	310 w/m^2	42 °C	1.19 W	1.26 W	-5.88%
10:59	252 w/m^2	53 °C	0.92 W	0.99W	-7.6%
11:53	296 w/m^2	55 °C	1.02 W	1.06W	-3.7%
Cell 2					
12:33	317 w/m^2	45.2 °C	1.14 W	1.19W	-4.3%
12:36	278 w/m^2	46 °C	0.97 W	1.04W	-7.2%
1:02	252 w/m^2	51.4 °C	0.91 W	0.93W	-2.1%
12:50	167 w/m^2	50.9 °C	0.60 W	0.61W	-1.6%
Cell 3					
13:18	287 w/m^2	51 °C	0.97W	1.00W	-3%
13:26	266 w/m^2	54 °C	0.92 W	0.92W	0%
13:45	272 w/m^2	56°C	0.88W	0.93W	-1.6%

From table II, we can see that, we got error within ± 10% which is allowable in case of simulator. Therefore we can say that our system is near to accurate and within the permissible range right from solar cell to solar array field, Which validates our simulator as we compared the simulated results with actual results from the field.

4.2 Case Study 1- 50 KW Power Plant (L&T)

Structural design:

Type of module: 180W (bp)

Pmax = 160 W

Vmax = 35.2 v

Imax = 4.7 A

No. of cells in module = 60 units.

Total No. of modules in Power plant = 300 units; Inverter efficiency = 96 %

In a Power Plant, it is observed that there are two types of Array boxes are used, they are all 5 channel Array boxes classified as “Array junction Box” (AJB’s) and “Main junction Box”. First small String are made of 4 No. of modules. 5 strings are connected to each(parallel) array junction box. And 3 AJB’s are connected to Main Junction Box so eventually 12 modules are making on big string connected to Main Junction box’s one channel. Therefore,

Total no of small strings: 75 units

Total no of big strings: 25 units

Modules in small string: 4 units

Modules in big string: 12 units

Main array Junction Box: 5 units

Table III shows comparison of results from simulator and L&T power plant, we can see the error of the comparison result is within the allowable range of error. We compared power generated by 50KW power plant with our simulated results for the same weather conditions as we can see it in table.

TABLE III

Comparision Results Of L&T P/W Plant And Simulation Result

Date & time	Solar irradiance	Module Temp.	Power (actual)	Power (Simulator)	Error (%)
10/06/14 2.15 PM	198.6 W/m²	63.2 ºC	9.49 KW	9.42 KW	0.73%
5/08/14 10.52 AM	126 W/ m²	31 ºC	6.687 KW	6.57 KW	1.7%
5/08/14 10.52 AM	147 W/m²	31 ºC	7.449 KW	7.66KW	-2.8%
5/08/14 10.53 AM	208 W/m²	31 ºC	10.14 KW	10.85KW	-7.00%
5/08/14 10.53 AM	201 W/m²	31 ºC	9.792 KW	10.48KW	-7.02%
5/08/14 10.53 AM	203 W/m²	31 ºC	9.887 KW	10.59KW	-7.1%
5/08/14 10.53	205 W/m²	31 ºC	9.918 KW	10.69KW	-7.7 %

4.3 Case Study 2- 1 MW Power Plant, Enrich Energies, Solapur.

We studied 1MW power plant situated in Solapur, from Enrich energies LTD. the comparison results of 1mw power plant and simulation results are shown in table IV. First two readings from the table are from same day dated 26/5/2014 time 13.43 pm and 16.14 pm respectively. Next three reading are of same power plant taken earlier dated 26/11/2013 time 16.41 pm, 29/11/2013 time 12.15 pm and time 12.15.33 pm respectively.

TABLE IV

Comparision Between 1 Mw Plant & Simulation Result

Irradiance (w/m²)	Ambient temp. (ºC)	Module temp. (ºC)	Actual Output (KW) (Enrich)	Simulator Output (KW)	Error (%)
804 W/m²	38.04 ºC	51.49ºC	703.00KW	704.39KW	-0.2%
190 W/m²	38.75 ºC	51.25ºC	173 KW	165.11KW	4.5%
142.2W/m²	31.50 ºC	42.00ºC	117.80KW	126.42KW	-7.3%
464.19W/m²	26.14 ºC	35.00ºC	395.60KW	422.93KW	-6.9%
469.97W/m²	26.24 ºC	35.20ºC	419.50KW	427.29KW	-1.1%

From table we can see that by comparing results from our simulator with actual Power plant output results, we achieved accuracy within ±10% error which is within the allowable margin of error. The error after comparison between experiment results, collected data from power plants and simulated results is varies from – 7.7 % to + 4.5 %. From these results we can say that our simulation model for studying the PV solar Array field incorporated with solar irradiation and temperature variation is near to accurate. Finally, based on the analyses performed for this work, we can help to inform one of the most problematic issues of project acceptance from a commercial perspective – that of the appropriate allowable Error margin to attach to a system rating result.

While a full uncertainty analysis is outside the scope of this paper, we can point out the largest source of error in this type of test. They include:

- Model uncertainty, which we estimate at -7.7 to 4.5%
- Solar Irradiance measurement uncertainty, which ranges between 2-5%
- Module temperature measurement uncertainty, which ranges between 2-4%

  Therefore, we estimate that total Error in the comparison results of power output of Solar array field studied and tests done on solar module with the simulated results will be -4.95 to 5 %.

V. CONCLUSIONS

From above study and research we can conclude that, change in atmospheric conditions such as humidity, wind, dust and edging will lend us on showing change in temperature of array and irradiance of sun. So if we consider effect of temperature and irradiance parameters, we can obtain power output solar cell of solar field, we can able to estimate and predict output power of whole solar field. Our main goal is to model and simulate the PV solar array field to study and analyse the output change in the PV Solar array according to solar irradiance and temperature variation. With solar irradiance and module temperature we also added shadow density as another input which will mimic cloudy condition effect with time of shadow present over module. We hope we validated our simulation model by comparing the results from PV Power plants and results from our PV simulator. Hence we achieved our objective of modelling and simulation of PV solar array which can helps us to study and analyse change in nature of PV array fields output with respect to change in atmospheric conditions.

REFERENCES

[1] L & T automation, Mahape, *iVisionPMSmaxTM Vision* A Complete Power Management System
[2] http://www.lapsys.co.jp/english/
[3] http://pveducation.org/pvcdrom/solar-cell-operation/
[4] http://homeguides.sfgate.com/effects-temperature-solar-panel-power-production-79764.html
[5] http://www.earthsolar.co.uk/page9.html
[6] https://www.grc.nasa.gov/www/K-12/problems/Jim_Naus/TEMPandALTITUDE_ans.html
[7] http://mentalfloss.com/article/49786/how-much-does-cloud-weigh
[8] "Introduction to semiconductor materials and devices", M.S.Tyagi. John Wiley & Sons.
[9]]http://www.ugrad.math.ubc.ca/coursedoc/math100/notes/diffeqs/cool.html
[10] "*Vue-7: from the ground up"* by Ami Chopine and VladmireChopine.

OFDM PAPR REDUCTION USING LINEAR BLOCK CODES WITH ERROR CORRECTION IN RAYLEIGH FADING CHANNEL

Varsha Muraleedharan[1], Vandna Bansal[2]

[1]*Department of Electronics And Communication Engineering, RPIIT, Karnal (India)*
[2]*Assistant Professor, Department Of Electronics and Communication Engineering, RPIIT, Karnal (India)*

ABSTRACT

The past decade has seen many radical changes and achievements in the field of wireless communication. Applications of wireless communication have grown swiftly in the recent past. This rigorous growth leads to more throughputs over wireless channels along with increased reliability. But still the bandwidth demands are endless and increasing day by day. Today we need to constantly work towards achieving reliable wireless communication with high spectral efficiency, low complexity and good error performance results. Orthogonal frequency division multiplexing (OFDM) technique is a promising technique in this regard as it offers high data rate and reliable communications over various fading channels. But the main drawback of OFDM is the high peak to average power ratio (PAPR). In this paper we present the technique to reduce the PAPR using linear block codes with error correction. Simulation results show that the bit error rate (BER) of proposed scheme considerably outperforms the conventional OFDM system.

Keywords: BER, OFDM, PAPR

I. INTRODUCTION

The basic principle of OFDM is to split input data stream into a number of lower rate streams that are transferred simultaneously over a number of subcarriers, the transmission rate is slower in parallel subcarriers, a frequency selective channel seems flat to each subcarrier. ISI is reduced almost completely by adding a guard interval at the beginning of each OFDM symbol. However, instead of using an empty guard time, this interval is filled with a cyclically extended version of the OFDM symbol. This method is used to avoid ICI. In MCM, input data stream is distributed into lower rate substreams, these are used to modulate few subcarriers. The spacing among these subcarriers is large enough such that individual spectrum of subcarriers do not overlap. Therefore the receiver uses a band pass filter tuned to that subcarrier frequency in order to demodulate the signal. In OFDM, subcarrier spacing is kept at minimum, while still preserving the time domain orthogonality between subcarriers, even though the individual frequency spectrum may overlap. The least subcarrier spacing should equal to 1/T, where T is the symbol period. An OFDM symbol in baseband is defined as:

$$x(t) = \sum_{i=-\frac{N}{2}}^{\frac{N}{2}-1} a_{i+\frac{N}{2}} \exp\left(j\frac{2\pi it}{T}\right) s(t) \qquad 0 \le t \le T$$

where, denotes the complex symbol modulating the i-th carrier, s(t) is the time window function defined in the interval [0,T], N is the number of subcarriers, and T is the OFDM symbol period. Subcarriers are spaced apart. The correlation coefficient between the subcarriers may be defined as:

$$\rho_{kn} = \frac{1}{T}\int_0^T \exp\left(j\frac{2\pi kt}{T}\right)\exp\left(-j\frac{2\pi nt}{T}\right)dt$$

As can be seen from (1)

Therefore, OFDM signal of the form (1) satisfies the condition of mutual orthogonality among subcarriers in the symbol interval. In order to obtain the data modulating the *k-th* subcarrier OFDM symbol should be down converted with a frequency of *k*/T, and then integrated over the symbol period [1]. Then above operation may be shown as:

$$\frac{1}{T}\int_0^T \exp \qquad (2)$$

(3)

Using (2) and (3) together

Resultant signal= considering the sequential transmission of symbols, the baseband signal at the OFDM modulator output can be expressed as:

$$x(t) = \sum_{n}\sum_{i=-\frac{N}{2}}^{\frac{N}{2}-1} a_{i+\frac{N}{2},n} \exp\left(j\frac{2\pi i(t-nT)}{T}\right) s(t-nT)$$

Where, represents the data modulating the *i-th* carrier of the n-th OFDM symbol. The n-th OFDM symbol is transmitted in the time interval [*n*T, *n*T+T]. Assuming that the windowing function *s(t)* is nonzero only in [0,T] interval, if N samples are taken from *x(t)* at time instants {*n*T+*k*T/N, *k*=0…N-1}, the result will be [1]:

$$y[k] = x(nT + \frac{kT}{N} = \sum_{n}\sum_{i=-N/2}^{N/2-1} a_{i+\frac{N}{2},n} \exp\left(j\frac{2\pi i(nT + kT/N - nT)}{T}\right) s(nT + kT/N - nT)$$

$$= \sum_{i=-N/2}^{N/2-1} a_{i+\frac{N}{2},} \quad (4)$$

It can be seen from (4) that, N samples reserved from n-th OFDM symbol at a rate of N/T can be achieved by taking N-point inverse Discrete Fourier Transform (IDFT) of the input data $a_{k,n}$, *k*=0…N-1, weighted by the window function *s(t)* at the sampling time instants.

But the major disadvantage of OFDM is the high peak to average power ratio. Our objective is to develop a technique to reduce the PAPR using linear block codes. We will use linear block codes for reducing PAPR and try and evaluate the resultant system performance with and without error correction capability of linear block codes, on slow Rayleigh fading channel with additive white Gaussian noise added at the receiver.

II. GENERAL OFDM SYSTEM

Fig. 1 and 2 shows a general OFDM system. The transmitter first converts the input data from a serial stream to parallel sets. Each set of data contains one information bit for each carrier frequency. Then, parallel data are modulated to the orthogonal carrier frequencies. The IFFT (Inverse Fast Fourier Transform) converts the parallel data into time domain waveforms. Finally, these waveforms are combined to create a single time domain signal for transmission. The receiver basically performs the inverse of the transmitter by first separating the data into parallel streams. Then, the FFT (Fast Fourier Transform) converts these parallel data streams into frequency domain data. The data are now available in modulated form on the orthogonal carriers. Demodulation down-converts this information back to the baseband. Finally, this parallel data are converted back into a serial stream to recover the original signal. OFDM faces several challenges. The key challenges are ISI due to multipath-use guard interval, large peak to average ratio due to non-linearity of amplifier; phase noise problems of oscillator, need frequency offset correction in the receiver. Inter-symbol interference (ISI) is eliminated almost completely by introducing a guard time in every OFDM symbol. Large peak-to-average power ratio (PAPR) which distorts the signal if the transmitter contains nonlinear components such as power amplifiers (PAs). The nonlinear effects on the transmitted OFDM symbols are spectral spreading, inter modulation and changing the signal constellation. In other words, the nonlinear distortion causes both in-band and out-of-band interference to signals. Therefore the PAs requires a back off which is approximately equal to the PAPR for distortion-less transmission. This decreases the efficiency for amplifiers. Therefore, reducing the PAPR is of practical interest. The serial input data stream is distributed into frames of N_f bits. These N_f bits are arranged into N groups, where N is the number of subcarriers. The number of bits in each of the N groups determines the constellation size for that particular subcarrier. For example, if all the subcarriers are modulated by QPSK then each of the groups consists of 2 bits, if 16-QAM modulation is used each group holds 4 bits. This scheme is called as fixed loading. However, this is not the only way of distributing input bits among the subchannels. N_f bits could be distributed among subcarriers according to the channel states. Therefore, one of the subcarriers can be modulated with 16-QAM whereas another one can be modulated with 32-QAM, etc. The former subcarrier consists of 4 bits and the latter subcarrier resides of 5 bits. This scheme is named as adaptive loading. OFDM can be considered as N independent QAM channels, each having a different QAM constellation but each operating at the same symbol rate 1/T. After signal mapping, N complex points are obtained. These multiple points are passed over an IDFT block. Cyclic prefix of length v is added to the IDFT output in order to combat with ICI and ISI. After Parallel–to- Serial conversion, windowing function is applied. The output is fed into a Digital-to-Analog converter efficient at a frequency of N/T. Finally transfer filter is applied in order to deliver necessary spectrum shaping before power enlargement.

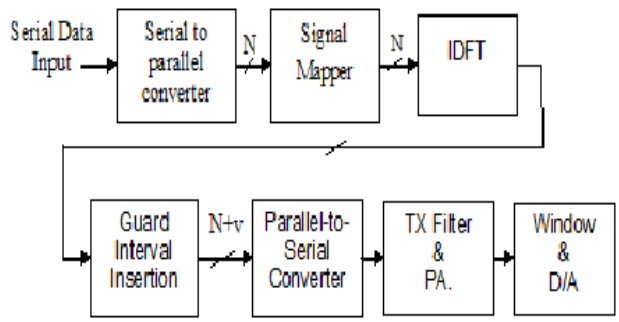

Fig. 1 Block Diagram Of An OFDM Transmitter

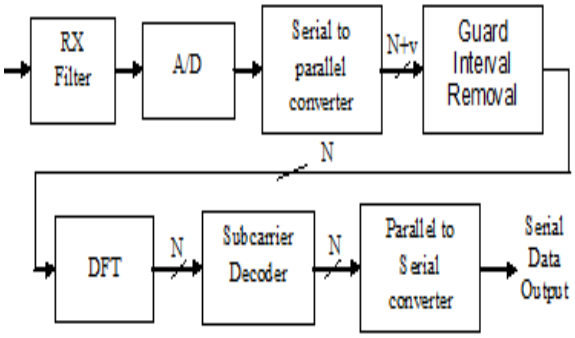

Fig. 2 Block Diagram Of An OFDM Receiver

The receiver implements inverse processes of the transmitter. Received signal is delivered through a receive filter and an Analog-to-Digital converter operating at a frequency of N/T. After these down converting and sampling processes, cyclic prefix is detached from the signal and a DFT operation is achieved on the resultant complex points in order to demodulate the subcarriers. Subcarrier decoder translates obtained complex points to the corresponding bit stream. Due to the major disadvantage of OFDM which is the high peak to average power ratio, our objective is to develop a technique to reduce the PAPR using linear block codes with error detection and correction capabilities. Linear Block Codes perform up to mark in case error detection and correction problems. If we can use this capability of error detection and correction of the linear block codes in an OFDM environment then we can control PAPR and thus get higher throughput along with a reliable and less error prone wireless communication. Also we can compare the performance of the linear block codes with and without error detection and error correction capability and accordingly deduce the results.

III. PROPOSED OFDM SYSTEM

The OFDM transmitter used in our result simulations is shown in fig.3. The probability that, the PAPR of the OFDM signal exceeds a certain threshold λ is given by:

$$Pr\{PAPR > \lambda\} = 1 - \left(1 - e^{-\lambda}\right)^{N}$$

The probability that, the lowest PAPR λ_l exceeds a certain threshold λ is given by:

$$Pr\{\lambda_l > \lambda\} = Pr\{PAPR > \lambda\}$$

To generate the sequences that would result in lower PAPR, linear block coding is used at the start of the OFDM system as shown in figure 3.3. The Linear Block Coder transform the serial data before it is mapped to the orthogonal channels. Different sequences are generated by encoding the raw data bits at the beginning of the system. This transformation leads to a lower PAPR value as illustrated in the above equations. The linear block code transforms *k* data bits to *n* serial data bits. These *n* serial data bits consist of enough redundancy to lower the PAPR value as compared to the one generated with raw *k* data bits. The OFDM receiver used in our result simulations is shown in fig. 4. It is similar to the one described earlier, the only difference being the use of a linear block coder at the end of the receiver system.

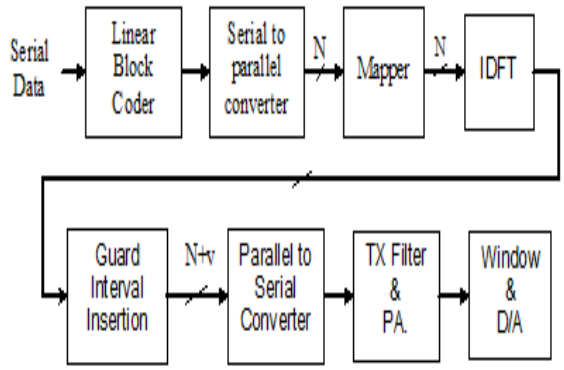

Fig. 3 New OFDM Transmitter

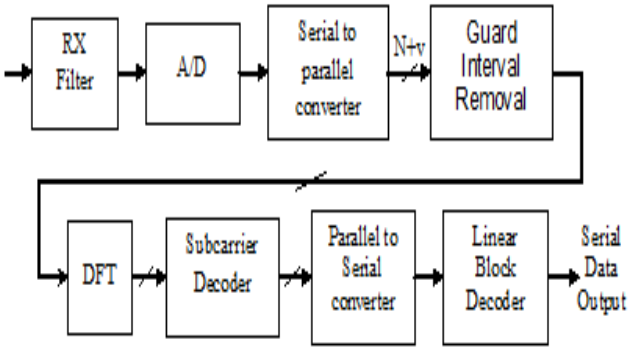

Fig. 4 New OFDM Receiver

The linear block decoder is used to recover the data encoded firstly at the transmitter side. It works in a reverse manner by transforming *n* encoded data bits to *k* message bits, thereby removing any added redundancy from the final serial data output.

IV. SIMULATION RESULTS

TABLE. 1 lists the required OFDM system specifications used while simulation. Fig. 5 illustrates the bit error rate (BER) performance of an OFDM system combined with a (4, 7) Linear Block Codes (LBCs). BER performance is measured over Rayleigh channel. The Rayleigh channel is considered to be a quasi-static or slow Rayleigh fading channel with additive white Gaussian noise added at the receiver.

Table. 1 OFDM System Specifications.

Parameter	**Value**
FFT size	64
Number of subcarriers	52
Subcarrier spacing	312.5 kHz
FFT Sampling frequency	20 MHz
Used subcarrier index	{-26 to -1, +1 to +26}
Cyclic prefix duration	0.8 us
Data symbol duration	3.2 us
Total Symbol duration	4 us

Similarly, from fig. 5, we can see that there is significant improvement in the BER performance with LBCs, both with and without error correction on Rayleigh channel. The system using LBCs with error correction outperforms the system using LBCs without error correction. The former system is superior by about 7 dB at BER of 10^{-3}. The former system outperforms the OFDM system without LBCs by about 9 dB at BER of 10^{-3}.

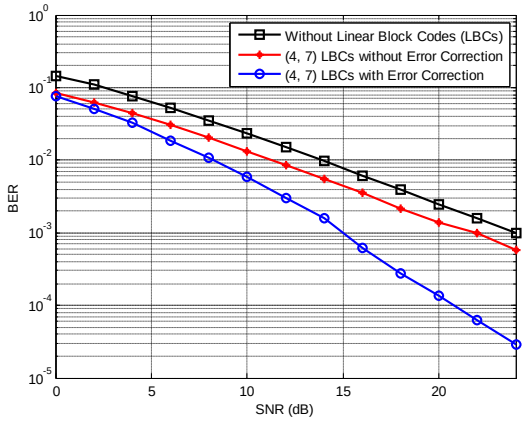

Fig. 5 BER Performance Of An OFDM System With (4, 7) Lbcs Over Rayleigh

V. CONCLUSION

In this paper we presented a technique to reduce the PAPR of an OFDM system using linear block codes with error correction on AWGN and Rayleigh fading channel. Here we gave an overview of an OFDM system and discussed how an orthogonal frequency division multiplexing (OFDM) system offers high data rate and reliable communications over fading channels. We also discussed about the advantages and disadvantages of an OFDM system. The major disadvantage of OFDM is the high peak to average power ratio. To mitigate the effect of PAPR or rather somewhat reduce PAPR to certain mean value we used linear block codes. Linear Block Codes perform up to mark in case error detection and correction problems. If we can use this capability of error detection and correction of the linear block codes in an OFDM system then we can achieve higher throughput along with a reliable and less error prone communication. We discussed the OFDM transmitter and OFDM receiver system model that we have used in our simulations. We evaluated the resultant system performance with and without error correction capability of linear block codes, on slow Rayleigh fading channel with additive white Gaussian noise added at the receiver. As expected, when we can compared the performance of the linear block codes with and without error detection and error correction capability, we found that BER decreased and thus we can say that PAPR also reduced by the use of linear block codes. There are various techniques to reduce PAPR cum BER and we are using linear block coding technique since it helps to do the same in more effective way. But if we combine some techniques which are advantageous compared to others, there is a scope of even more reduction of PAPR on which we need to research more.

REFERENCES

[1] Y. Kyeongcheol and S. Chang, "Peak-to-average power control in OFDM using standard arrays of linear block codes," in IEEE Journals, Vol. 7, Issue: 4, pp. 174-176, 2003.

[2] L. Yingshan, L. Jun-Seo, L. Kang-Me and Heung-Gyoon Ryu, "STFBC method for the ICI reduction in OFDM communication system," in 5th IEEE International Symposium on Multi-Dimensional Mobile Communications, Vol. 2, pp. 927-931, 2004.

[3] J. Yuwen, Z. Zhuquan and W.Yan, "PAPR Distribution Analysis of OFDM signals with Pulse Shaping," In IEEE Asia-Pacific Conference, pp. 473-477, 2005.

[4] T.T.T. Ngo, H. Taeyoungand K. Nam, "Power efficiency improvement by PAPR reduction and predistorter in MIMO-OFDM system," In 7th IEEE International Conference, Vol. 2, pp. 1381-1386, 2005.

[5] C. Houshou and L. Hsinying, "PAPR Reduction of OFDM Signals Using Partial Transmit Sequences and Reed-Muller Codes," in IEEE, Vol. 1, Issue: 6, pp. 528-530, 2007.

MANAGING INTRUSION DETECTION AND DIAGNOSIS AS A SERVICE IN CLOUD COMPUTING

Prakash Kumar Pathak
Computer Science, Research Scholar, Singhania University, (India)

ABSTRACT

The Cloud computing is an internet based distributed network technology which refer to application and services that run on a distributed network. The cloud Computing service provide flexibility scalability and Economics of Scale .Security is main concern for this feature .As more data moves from centrally located on cloud server .The personal and private data storage on cloud server. Confidential data or information which is stored on the cloud server is on the risk. If we do not appropriate measure the hacker can hake the data .Because cloud computing provides services as flexibility, scalability and cloud computing also provide virtual resource to the cloud user.

The cloud computing has a three types of service.

1) *SaaS (Software As A Service.)*
2) *PaaS (Plateform As A Service)*
3) *IaaS (Infrastructure As A Service)*

Each service level security concerns that need to address. The Cloud computing are important Vulnerable targets for intruder attacks. The reason behind that distributed network environment. For the distributed environment, Intrusion Detection System we are using to enhance the security system. Because the privacy of data even from the administrator of data at Service Provider we cannot be hidden or cannot be secure. Along with the gains achieved in cloud computing there are inherent risks.

Keywords: - Distributed Network Privacy Of Data, Data Administrator, Service Provider, Security Service.

I. INTRODUCTION

In the last decade, most people were concerned about obtaining computers in their offices, schools and homes. The main reason behind that was to get close to the world and communicate and exchange data via these devices. In contrast, today people are concerned about the Internet and its speed for effective and efficient communication. In addition, often they need extra services to the existing legacy service provided by the Internet. These services are known as some kinds of computing tasks that are delivered by the Internet Service Providers (ISP). While getting required service is the users' demand, with the advanced development of the Internet tools around the world, attackers also aim to identify various loopholes in the operating system and networks. When we talk about Clouds, The main target of the attackers is to make illegitimate and unlawful attack to the available resources in the Cloud computing settings. In order to overcome these obstacles, some actions need be taken in the host based (HB) and Network based (NB) level. Even though the use of intrusion detection system (IDS) is

not guaranteed and cannot be considered as complete defense, we believe it can play a significant role in the Cloud security architecture [1]. Some organizations are using the intrusion detection system (IDS) for both Host Based and Network Based in the Cloud computing [2]. Intrusion detection systems (IDS) which are hardware and/or software mechanisms that detect and log inappropriate, incorrect, or anomalous activities and report these for further investigations [3]. Intrusion Prevention Systems (IPS), which contain IDS functionality but more sophisticated systems that are capable of taking immediate action in order to prevent or reduce the malicious behavior [4]. Thus, this work utilizes both systems: (IDS) and (IPS) and refers to it as Intrusion Detection and Prevention System (IDPS). Furthermore, many works have been done in using one of the (IDS) techniques; either Anomaly Detection (AD) or Signature based Detection or hybrid of both. The ADS (Anomaly Detection System) can be used to detect unknown attacks in the networks which come from rogue nodes. In fact, such system is designed for the offline analysis due to their expensive. Processing and memory storage. On the other hand, the SD is used in this system to detect and identify manually the attack signature which is known as attacks in the real time traffic [5]. Therefore, both methods are essential in detecting the intrusions. So, we propose an integrated scheme which makes use of both methods to detect the attacks as soon as possible and prevent the attackers from generating the malicious activities inside the Cloud.

1.1 About Cloud Computing

Cloud computing refers to the provision of computational resources on demand via a computer network. Users or clients can submit a task, such as word processing, to the service provider, such as Google, without actually possessing the required Software or hardware. The consumer's computer may contain very little software or data (perhaps a minimal operating system and web browser only), serving as little more than a display terminal connected to the Internet. Since the Cloud is the underlying delivery mechanism, Cloud based applications and services may support. Any type of software application or service in use today [6]. The essential characteristics of Cloud Computing include [7]: 1.On-demand self-service that enables users to consume computing capabilities (e.g., applications, server time, and network storage) as and when required. 2. Resource pooling that allows combining computing resources (e.g., hardware, software, processing, Network bandwidth) to serve multiple consumers - such resources being dynamically assigned. 3. Rapid elasticity and scalability that allow functionalities and resources to be rapidly and automatically provisioned and scaled. 4. Measured provision to optimize resource allocation and to provide a metering capability to determine usage for billing purposes Extension to existing hardware and application resources, thus, reducing the cost of additional resource provisioning.

1.2 Cloud Computing Architecture

Cloud computing comprises of two different services components for the users namely as software and hardware over the Internet .However , there are various Cloud service delivery models that are developed, which can be divided into three layers [8] depending on the type of resources provided by the Cloud, distinct layers can be defined (see Figure 2). The bottom-most layer provides basic infrastructure components such as CPUs, memory, and storage, and is henceforth often denoted as Infrastructure as a Service (**IaaS**). Amazon's Elastic Compute Cloud (EC2) is a prominent example for an IaaS offer. On top of IaaS, more platform-oriented services allow the usage of hosting environments tailored to a specific need. Google App Engine is an example for a Web platform as a service (**PaaS**) which enables to deploy and dynamically scale Python and Java based Web applications.

Finally, the top-most layer provides the users with ready to use applications also known as Software as a Service (**SaaS**) [8] [9]. In addition, it is possible to observe the significant interaction between the services model in the Cloud computing which are Software as a service (SaaS), Platform as a service (PaaS) and Infrastructure as a Service (IaaS) as shown in Figure 3. Each one of these models provides unique service to the users in the Cloud computing environment.

1.3 About Intrusion Detection System

Intrusion detection systems (IDS) are an essential component of defensive measures protecting computer systems and network against harm abuse [1]. It becomes crucial part in the Cloud computing environment. The main aim of IDS is to detect computer attacks and provide the proper response [10]. An IDS is defined as the technique that is used to detect and respond to intrusion activities from malicious host or network [2]. There are mainly two categories of IDSs

1.4 Intrusion Detection System In Cloud Computing

As mentioned before, Intrusion detection is the process of monitoring the events occurring in a computer system or network and analyzing them for signs of intrusions, defined as attempts to compromise the confidentiality, integrity, availability, or to bypass the security mechanisms of a computer or network. Intrusions are caused by attackers accessing the Systems from the Internet or by Authorized users of the systems who attempt to gain additional privileges for which they are not authorized or by authorized users who misuse the privileges given to them. Intrusion Detection Systems (IDSs) are software or hardware products that automate this monitoring and analysis process [11]. The Intrusion Detection Service (IDS) service increases a Cloud's security level by providing two methods of intrusion detection. First method is behavior-based method which dictates how to compare recent user actions to the usual behavior. The second approach is knowledge-based method that detects known trails left by attacks or certain sequences of actions from a user who might represent an attack. The audited data is sent to the IDS service core, which analyzes the behavior using artificial intelligence to detect deviations. This has two subsystems namely analyzer system and alert system.

In order to detect the intruders the following techniques should be implemented in either HIDS or NIDS [12] [2].

II. ANOMALY DETECTION (AD)

Basically, Anomaly Detection was introduced in the late of 1980's with Intrusion detection expert system (IDES) [12]. Anomaly detectors identify abnormal unusual behavior (anomalies) on a host or network. They function on the assumption that attacks are different from "normal" (legitimate) activity and can therefore be detected by systems that identify these differences. Anomaly detectors construct profiles representing normal behavior of users, hosts, or network connections. These profiles are constructed from historical data collected over a period of normal operation. The detectors then collect event data and use a variety of measures to determine when monitored activity deviates from the norm. There are many measures and techniques that are used in anomaly detection including; Threshold detection, Statistical measures, Rule-based measures, other measures, including neural networks, genetic algorithms, and immune system models

III. SIGNATURE DETECTION (SD)

Misuse detectors analyze system activity, looking for events or sets of events that match a predefined pattern of events that describe a known attack. As the patterns corresponding to known attacks are called signatures, misuse detection is sometimes called "signature-based detection". The most common form of misuse detection used in commercial products specifies each pattern of events corresponding to an attack as a separate signature. However, there are more sophisticated approaches to doing misuse detection (called "state-based" analysis techniques) that can leverage a single signature to detect groups of attacks Misuse detection techniques, in general, are not effective against the latest attacks that have no matched rules or pattern yet. In this work, we will focus on applying IDS on IaaS which is the most flexible model for ID deployment. So, we need to identify the locations that should be considered when thinking about ID in the IaaS Cloud. There are four primary "spots" [13]:

• In the virtual machine (VM) itself: Deploying ID in the VM allows monitoring the activity of the system, and detecting and alerting on issues that may arise. • In the hypervisor or host system: Deploying ID in the hypervisor allows to not only monitor the hypervisor but anything traveling between the VMs on that hypervisor. It is a more centralized location for ID, but there may be issues in keeping up with performance or dropping some information if the amount of data is too large. • In the virtual network: Deploying ID to monitor the virtual network (i.e., the network Established within the host itself) allows monitoring the network traffic between the VMs on the host, as well as the traffic between the VMs and the host. This "network" traffic never hits the traditional network.

• In the traditional network: Deploying ID here allows monitoring, detecting, and alerting on traffic that passes over the traditional network infrastructure.

REFERENCES

[1] J. Mchugh, A. Christie, and J. Allen, "Defending Yourself: The Role of Intrusion Detection Systems", IEEE Software, Volume 17, Issue 5, Sep.-Oct., pp. 42-51, 2000.

[2] K. V. S. N. R. Rao, A. Pal, and M. R. Patra, "A Service Oriented Architectural Design for Building Intrusion Detection Systems", International Journal of Recent Trends in Engineering, vol. 1, no. 2, pp. 11-14, 2009.

[3] E-Banking Appendix B: Glossary, http://www.ffiec.gov/ffiecinfobase/booklets/e_banking/ebanking_04_appx_b_glossary.html, Accessed on: 23/02/2012

[4] Information Technology at Johns Hopkins-Glossary G-I, http://www.it.jhmi.edu/glossary/ghi.html Accessed on: 23/02/2012

[5] K. Hwang, M. Cai, Y. Chen, S. Member, and M. Qin, "Hybrid Intrusion Detection with Weighted Signature Generation over Anomalous Internet Episodes", IEEE transactions on dependable and secure Computing, vol. 4, no. 1, pp. 1-15, 2007.

[6] P. Jain, D. Rane, and S. Patidar, "A Survey and Analysis of Cloud Model-Based Security for Computing Secure Cloud Bursting and Aggregation in Renal Environment", IEEE 2011 World Congress on Information and Communication Technologies, pp. 456-461, 2011.

[7] Z. Mahmood, "Cloud Computing: Characteristics and Deployment Approaches", 11th IEEE International Conference on Computer and Information Technology, pp. 121-126, 2011.

[8] M. Jensen, N. Gruschka, L. L. Iacono, and G. Horst, "On Technical Security Issues in Cloud Computing", 2009 IEEE International Conference on Cloud Computing, pp. 109-116, 2009.

[9] R. Wu, G.-joon Ahnl, and H. Hul, "Information Flow Control in Cloud Computing", IEEE Collaborative Computing: Networking, Applications and Worksharing (CollaborateCom), pp. 1-7, 2010.

[10] U. Thakar, "HoneyAnalyzer – Analysis and Extraction of Intrusion Detection Patterns & Signatures Using Honeypot", The second International Conference on Innovations in Information Technology, Dubai, UAE September 26-28, 2005.

[11] R. Bace and P. Mell, "NIST Special Publication on Intrusion Detection Systems", National Institute of StandTechnology.

[12] E-Cooke Examination of a DIDS available at:Http://csc.columbusstate.edu/Bosworth/CIAE/student Papers/cooke.edgar.pdf

DEVELOPING A LOW COST MICROCONTROLLER BASED DATA ACQUISITION SYSTEM TO MONITOR CIVIL STRUCTURES

Anirban Patra

Assistant Professor, Dept. of ECE, JIS College of Engineering [An Autonomous Institution], Kalyani, West Bengal, (India)

ABSTRACT

Ultrasonic measurements are used in structural engineering to determine material properties, detect defects and assess deterioration. Ultrasonic wave propagation characteristics that can be used for these purposes are: velocity, attenuation, frequency, and energy. Rapid growth in demand for value-added techniques for health monitoring of structures has focused worldwide interest on sensors as the provider of an effective solution to measurement problems. Recent advances in measurement technology have demonstrated that ultrasonic sensors are suitable for the monitoring of civil structures. Nowadays engineers of civil department are inventing new sophisticated measuring instruments regularly. Unfortunately due to high cost, these instruments are procured only by large companies. Most of the small and medium size companies can't afford this due to economic problem. So our main target should be to develop or invent some good measuring instruments at low cost for the sake of these companies. In this project we have tried something to do this. The aim of our project is to design a microcontroller based circuit to detect any defects in a concrete structure that is easy to handle & pocket friendly.

Keywords: ***Ultrasonic Transducer, Pulse Velocity Test, 8051 Microcontroller, LCD Display***

I. INTRODUCTION

It is now well established that by propagating ultrasound in a given medium, useful information about the medium can be generated by analyzing the transmitted signals. This is analogous to all other methods of characterization and analysis also founded upon wave-material interaction phenomena. These are: Optics, X-ray, IR, Raman Spectroscopy, NMR, neutron, g-ray, mass spectrometry, etc. Ultrasound differs from these methods because it does not require sample preparation, is non-hazardous, provides the means to determine mechanical properties, microstructure, imaging, & microscopy, is portable, and is cost-effective. Furthermore, ultrasound is applicable to all states of matter, with the exceptions of plasma and vacuum. Propagation of ultrasound in a medium is not affected by its optical opacity.

1.1 Introduction To Pulse Propagation Through Concrete

Three types of waves are generated by an impulse applied to a solid mass. Surface waves having an elliptical particle displacement are the slowest, whereas shear or transverse waves with particle displacement at right

angles to the direction of travel are faster. Longitudinal waves with particle displacement in the direction of travel (sometimes known as compression waves) are the most important since these are the fastest and generally provide more useful information. Electro acoustical transducers produce waves primarily of this type; other types generally cause little interference because of their lower speed. The wave velocity depends upon the elastic properties and mass of the medium, and hence if the mass and velocity of wave propagation are known it is possible to assess the elastic properties. For an infinite, homogeneous, isotropic elastic medium, the compression wave velocity is given by:

$$V = \sqrt{\frac{K \cdot E_d}{\rho}}$$

where V = compression wave velocity (km/s)

$$K = \frac{(1 - v)}{(1 + v)(1 - 2v)}$$

Ed = Dynamic Modulus of Elasticity (kN/mm^2) ; ρ = Density (kg/m^3) and v = Dynamic Poisson's Ratio

In this expression the value of K is relatively insensitive to variations of the dynamic Poisson's ratio v, and hence, provided that a reasonable estimate of this value and the density can be made, it is possible to compute E_d using a measured value of wave velocity V. Since v and p will vary little for mixes with natural aggregates, the relationship between velocity and dynamic elastic modulus may be expected to be reasonably consistent despite the fact that concrete is not necessarily the 'ideal' medium to which the mathematical relationship is applied.

1.2 Pulse Velocity Method

This can be sub divided into two parts

1) Mechanical sonic pulse velocity method, which involves measurement of the time of travel of longitudinal or compressional waves by a single impact hammer blow or repeated blows.
2) Ultrasonic pulse velocity method, which involves measurement of the time of travel of electronically generated mechanical pulses through the concrete.

Out of this two, Ultrasonic pulse velocity method is the most popular method all over the world. When mechanical impulses are applied to a solid mass, three different kinds of waves are generated. These waves are known as longitudinal waves, shear waves and surface waves. These three waves travel at different speed. The longitudinal wave travels as twice fast as other two types. The shear wave is not so fast, the surface wave is the slowest among all waves. The pulses can be generated either by hammer blows or by the use of electroacoustic transducer. Electroacoustic transducers are preferred as they provide better control on the type and frequency of pulses generated. Ultrasonic pulse velocity method consists of measuring the time of travel of ultrasonic pulse, passing through the concrete to be tested. The pulse generator circuit consists of ultrasonic circuit for generating ultrasonic pulses and a transducer for transforming these electronic pulses into mechanical energy having vibration frequencies in the range of 15 to 50 KHz. The time of travel between initial onset and the reception of

the pulse is measured electronically. The entire length between the transducer divided by the time of travel gives the average velocity of the propagation.

II. BASIC OF THE MICROCONTROLLER BASED MEASUREMENT SYSTEM

Fault detection is a crucial step in implementing energy efficient changes to building and industrial systems. Fault detection is utilized to determine that a problem has occurred within in a certain channel or area of operation. Now all this techniques are effective but very much difficult to handle and costly. Our aim is to design a fault detection system so that the software application identifies the reason for the sub-optimal performance, or fault, so that the business or organization can pinpoint the fault, and fix it. But already there is many more fault detecting process is available in the markets that are effective to a great extent. So we aim to develop a system that is easy to implement and also cost effective. The aim of our project is to design a microcontroller based circuit to detect any defects in a concrete structure that is easy to handle & pocket friendly. To achieve our aim we have designed a transmitter circuit with the help of IC 4013, IC4017 & some discrete components. The receiver circuit is designed with the help of IC4017 and some discrete components like resister capacitor etc, and last of all the microcontroller circuit is designed with the help of AT89C52 and several capacitors and resistors. To display the results of the microcontroller output one LCD is connected with it. The signal that can successfully penetrate the concrete block to see whether there is any fault in the concrete block is of the order of 54 kHz. But here to accomplish our project we are using a signal of 40 kHz to test our hardware setup. The signal of the range of 40 kHz generally detects the concrete as an obstacle and deals with a problem of penetrating the concrete block. The reason behind the use of less compatible signal is because of the limitation of the cost and availability of the transducer generating the signal in the range of 54 kHz.

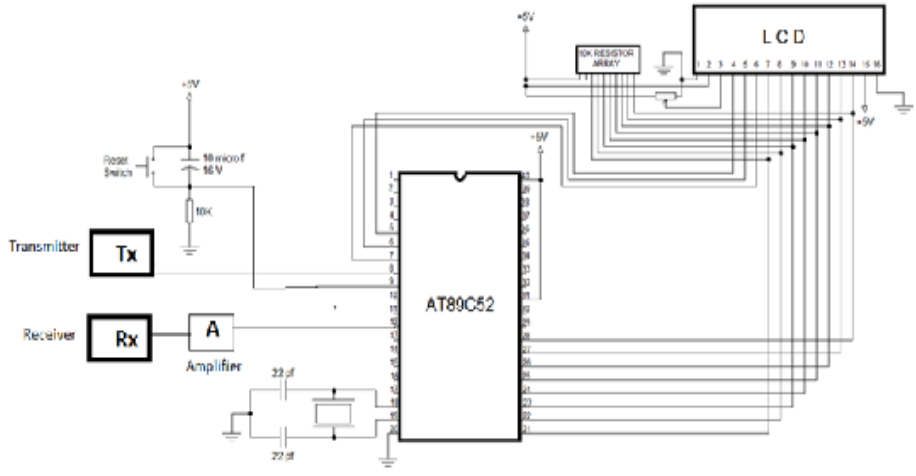

In our project we are using the microcontroller AT89C52, The AT89C52 is a low-power, high-performance CMOS 8-bit microcomputer with 8K bytes of Flash programmable and erasable read only memory (PEROM). The device is manufactured using Atmel's high-density non-volatile memory technology and is compatible with the industry-standard 80C51 and 80C52 instruction set and pin out. The on-chip Flash allows the program memory to be reprogrammed in-system or by a conventional non-volatile memory programmer. By combining a versatile 8-bit CPU with Flash on a monolithic chip, the Atmel AT89C52 is a powerful microcomputer which provides a highly-flexible and cost-effective solution to many embedded control application. For the calculation

of the delay of the signal when it passes through the concrete block, we have used the microcontroller. We used the micro controller more of as a practical clock which counts the time delay in mille seconds with the help of its counter mode. In the veroboard we have connected a chip holder to hold the microcontroller so that it is easy for us to change the microcontroller chip if it is damaged or not functioning properly. As it can be seen in the circuit diagram we have used the port 1 pins to receive the signals from transmitter and receiver. The transmitter when transmits the 40 KHz signal the corresponding pin say pin 1 of port 1 gets a signal, and when the receiver receives the signal the corresponding port of microcontroller sat pin 2 of port 1 is at high. When microcontroller detects that the pin 1 of port 1 is at high (i.e. 1) then it loads a value in the TMOD special function resister so that the timer is on and the microcontroller acts as a 16 bit auto reload counter. There is a delay subroutine in the memory which provides a delay of 1 mille seconds. Microcontroller after executing the delay subroutine checks if the corresponding bit of the receiver is high or not. If the pin is high then it stops the counting and shows the result in the LCD display. But if the pin is not high then it resumes its counting with one mille seconds delay each. The LCD circuit is connected to the microcontroller circuit as the display unit. When the microcontroller is done counting it displays the result in the LCD display screen. The pins 4 ,5, 6 are connected to the microcontroller port 1, and pins 7 to 14 are connected to the port 2 of the microcontroller, as well as to the 10K register array.

III. TABLE AND GRAPH

Suggested Pulse Velocity in Concrete

Pulse Velocity (m/s)	General Conditions
4575	Excellent
3660- 4575	Good
3050 - 3660	Questionable
2135 - 3050	Poor
2135	Very Poor

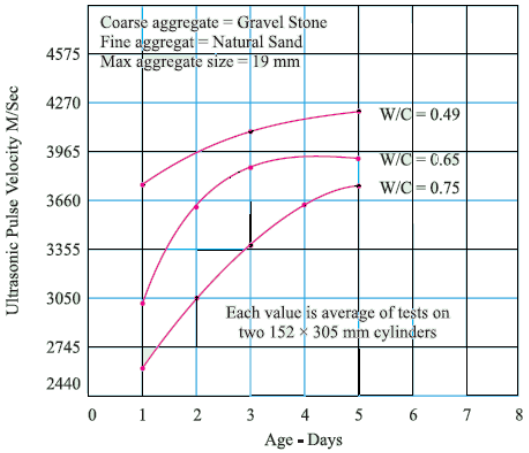

IV. CONCLUSION

Ultrasonic pulse velocity measurement has been found to be a valuable and reliable method of examining the interior of a body of concrete in a truly nondestructive manner. Modern equipment is robust, reasonably cheap and easy to operate, and reliable even under site conditions; however, it cannot be overemphasized that operators must be well trained and aware of the factors affecting the readings. It is similarly essential that results are properly evaluated and interpreted by experienced engineers who are familiar with the technique. For comparative purposes the method has few limitations, other than when two opposite faces of a member are not available. The method provides the only readily available method of determining the extent of cracking within concrete; however, the use for detection of flaws within the concrete is not reliable when the concrete is wet. The aim of this project is to design a microcontroller based circuit to detect any defects in a concrete structure

that is easy to handle & pocket friendly. So the main part of this project is to design Microcontroller Based circuit. It is mainly our R&D project and we have tried to use the transmitter circuit which generates 40 kHz ultrasonic frequency. So it was our hope that it will penetrate the plasma state of concrete structure. But later we have studied that only 54 KHz transducer can penetrate concrete. The price of this transducer is more than one lakh which exceed total project cost. So we could not forward our R and D work after a certain level. In this project we made the transmitter circuit and checked by the CRO which generates the 40 kHz frequency. Here in this project we use many of components for transmitter like capacitor, inductor, resistor, crystal oscillator, IC4017, IC4013 etc. Then we have burned the program in the microcontroller chip. We have not tested the setup practically because it is partially completed. But if 54 KHz will be transducer in place of 40 KHz, then the system may work fine.

V. REFERRENCE

Journal Paper:

[1] Combined static and dynamic monitoring of civil structures with long-gauge fiber optic sensors: Daniele Inaudi, Daniele Posenato, Branko Glisic SMARTEC SA, Jeff Miller, Tom Graver.

[2] Ultrasonic Pulse Velocity in Concrete Using Direct and Indirect Transmission: Ismail Ozgur Yaman, Gokhan Inei, Nazli Yesiller, and Haluk . Aktan.

Conference Paper:

[1] Microcontroller-based Ultrasonic Distance Meter: K. Padmaanavan

[2] Non Destructive Testing of Concrete - History and Challenges: N. J. Cario

Book:

[1] Concrete Technology - : Theory and Pactice: - M. S. Shetty

[2] Non Destructive Testing of Concrete – R. Jones, Cambridge University

[3] Strength in Concrete Structure – U. Bellander

[4] 8051 Microcontroller – Kenneth J Ayala

[5] 8051 Microcontroller and Embedded System – Mazidi and Mazidi

PREVENTNG DEFENSES AGAINST ONLINE PASSWORD GUESSING ATTACKS

[1]C.P Dhanakarna, [2]S.Jayalakshmi

[1]Research Scholar, Department of Computer Science, [2]Asst. Prof, Department of IT,
VELS University, Pallavaram, Chennai – 117, Tamil Nadu, (India)

ABSTRACT

Brute force and dictionary attacks on password-only remote login services are now widespread and ever increasing. Enabling convenient login for licensed users while preventing such attacks is a difficult problem. Automated Turing Tests (ATTs) continue to be an effective, easy-to-deploy approach to identify automated malicious login attempts with reasonable cost of inconvenience to users. In this paper we discuss the deficiency of existing and proposed login protocols designed to address large-scale online dictionary attacks (e.g., from a botnet of hundreds of thousands of nodes). We propose a new Password Guessing Resistant Protocol (PGRP), derived upon revisiting prior proposals designed to restrict such attacks. While PGRP limits the total number of login attempts from unknown remote hosts to as low as a single attempt per username, licensed users in most cases (e.g., When attempts are made from known, frequently-used machines) can make several failed login attempts before being challenged with an ATT. We analyze the performance of PGRP with two real-world datasets and find it more promising than existing proposals.

I INTRODUCTION

Online guessing attacks on password-based systems are unavoidable and commonly observed against web applications and SSH logins. However, online attacks have some inherent disadvantages compared to offline attacks: attacking machines must engage in an interactive protocol, thus allowing easier detection; and in most cases, attackers can try only limited number of guesses from a single machine before being locked out, delayed, or challenged to answer Automated Turing Tests (ATTs, e.g., CAPTCHAs). Consequently, attackers often must employ a large number of machines to avoid detection or lock-out. On the other hand, as users generally choose common and relatively weak passwords (thus allowing effective password dictionaries and attackers currently control large botnets (e.g., Conficker), online attacks are much easier than before.

II PASSWORD GUESSING RESISTANT PROTOCOL (PGRP)

Goals, Operational Assumptions

2.1 Protocol goals

Our objectives for PGRP include the Following:

1) The login protocol should make brute-force and dictionary attacks ineffective even for rival with access to large botnets (i.e., capable of launching the attack from many remote hosts).

2) The protocol should not have any significant impact on usability (user convenience). For example: for licensed users, any additional steps besides entering login credentials should be minimum. Increasing the security of the protocol must have minimum effect in decreasing the login usability.

3) The protocol should be easy to deploy and scalable, requiring minimum computational resources in terms of memory, processing time, and disk space.

2.2 Assumptions

We assume that rival can solve a small percentage of ATTs, e.g., through automated programs, brute force mechanisms, and low paid workers (e.g., Amazon Mechanical Turk . Incidents of attackers using IP addresses of known machines and cookie theft for targeted password guessing are also assumed to be minimum. Traditional password-based authentication is not suitable for any untrusted environment (e.g., a key logger may record all keystrokes, including passwords in a system, and forward those to a remote attacker). We do not prevent existing such attacks in untrusted environments, and thus essentially assume any chiness that licensed users use for login are trustworthy. The data integrity of cookies must be protected (e.g., by a MAC using a key known only to the login server).

Our method of protection against online password-guessing attacks and related denial-of-service attacks, the owner and the users granted administrative privileges are referred to administrators. Only the owner registers with the application provider other user accounts are created by admin using a Web interface. Each user logs in with three credentials rather than the usual two: The application instance name, which is considered a secret shared by the users of the application instance. The instance name can be changed by the owner. A user ID, which is known only to the user and the administrators.

The user ID is chosen by the admin who creates the user account, and can be changed by an admin (by any administrator if the user has no administrative privileges, by the owner if the user is herself an admin). A password, known only to the user. After a certain number of consecutive bad guesses against a password, the user is locked out. Bad guesses are considered to be consecutive if there is no intervening successfully completed login to the user's account. All the consecutive bad guesses must be against the same password; counting starts over if the password is changed. A user who has been locked out was allowed to log in again once her password has been reset.

When the user changes her password, she is not allowed to select as the new password a password that has previously been used as a permanent or temporary password on her user account. This method provides protection against online guessing attacks and related denial-of-service attacks, including attacks by ex-users, and other security benefits.

III THE REMOTE NETWORK MONITORING (RMON)

Remote Monitoring (RMON) is a standard monitoring specification that enables various network monitors and console systems to exchange network-monitoring data. RMON provides network administrators with more freedom in selecting network-monitoring probes and consoles with features that meet their particular networking needs. An RMON implementation typically operates in a client/server model. Monitoring devices (commonly called "probes" in this context) contain RMON software agents that collect information and analyze packets. These probes act as servers and the Network Management applications that communicate with them act as clients.

In our research work the Remote Monitoring is achieved by the use of Android Mobile device . Android Mobile device acts as remote. Others are clients.

Advantages:

- The user ID is chosen by the admin who creates the user account, and can be changed by an admin.
- Hackers trying to attempt more time to lock the particular account.

3.1 Data Structure and Function Description

PGRP maintains three data structures:

1) W: A list of fsource IP address, usernameg pairs such that for each pair, a successful login from the source IP address has been initiated for the username previously.

2) FT: Each entry in this table represents the number of failed login attempts for a valid username, UN. A maximum of failed login attempts are recorded. Accessing a non-existing index returns 0.

3) FS: Each entry in this table represents the number of failed login attempts for each pair of (srcIP, UN). Here, srcIP is the IP address for a host in W or a host with a valid cookie, and UN is a valid username attempted from srcIP. A maximum of k1 failed login attempts are recorded; crossing this threshold may mandate passing an ATT. An entry is set to 0 after a successful login attempt. Accessing a non-existing index returns 0. Each entry in W, FT, and FS has a "write-expiry" interval such that the entry is deleted when the given Period of time has lapsed since the last time the entry was inserted or modified. There are different ways to implement write-expiry intervals (e.g., hash belt. A simple approach is to store a timestamp of the insertion time with each entry such that the timestamp is updated whenever the entry is modified. At anytime the entry is accessed, if the delta between the access time and the entry timestamp is greater than the data structure write-expiry interval, the entry is deleted.

IV CONCLUDING

Online password guessing attacks on password-only systems have been observed for decades. Present-day attackers targeting such systems were empowered by having control of thousand to million node botnets. PGRP appears suitable for organizations of both small and large number of user accounts.

The required system resources (e.g., memory space) are linearly proportional to the number of users in a system. PGRP can also be used with remote login services where cookies are not applicable (e.g., SSH and FTP).

REFERENCES

[1] Amazon Mechanical Turk. Accessed: June 2010. https://www. mturk.com/mturk/.

[2] S. M. Bellovin. A technique for counting natted hosts. In ACM SIGCOMM Workshop on Internet measurement, pages 267–272, New York, NY, USA, 2002. ACM.

[3] E. Bursztein, S. Bethard, J. C. Mitchell, D. Jurafsky, and C. Fabry. How good are humans at solving CAPTCHAs? A large scale evaluation. In IEEE Symposium on Security and Privacy, Oakland, CA, USA, May 2010.

[4] M. Casado and M. J. Freedman. Peering through the shroud: The effect of edge opacity on ip-based client identification. In 4th USENIX Symposium on Networked Systems Design and Implementation (NDSS'07), 2007.

[5] S. Chiasson, P. C. van Oorschot, and R. Biddle. A usability studyand critique of two password managers. In USENIX Security Symposium, pages 1–16, Vancouver, B.C., Canada, 2006.

[6] D. Florˆencio, C. Herley, and B. Coskun. Do strong web passwords accomplish anything? In USENIX workshop on Hot topics in security (HotSec'07), pages 1–6, Berkeley, CA, USA, 2007.

[7] K. Fu, E. Sit, K. Smith, and N. Feamster. Dos and don'ts of client authentication on the web. In USENIX Security Symposium, pages 251–268, Washington, DC, USA, 2001.

[8] P. Hansteen. Rickrolled? Get Ready for the Hail Mary Cloud! http://bsdly.blogspot.com/2009/11/ rickrolled-get-ready-for-hail-mary.html. Accessed: Feb. 2010.

[9] Y. He and Z. Han. User authentication with provable security against online dictionary attacks. Journal of Networks (JNW), 4(3):200–207, May 2009.

[10] T. Kohno, A. Broido, and K. C. Claffy. Remote physical device fingerprinting. In IEEE Symposium on Security and Privacy, pages 211–225, Washington, DC, USA, 2005. IEEE Computer Society.

[11] M. Motoyama, K. Levchenko, C. Kanich, D. Mccoy, G. M. Voelker, and S. Savage. Re: CAPTCHAs understanding CAPTCHAsolving services in an economic context. In USENIX Security Symposium, Washington, DC, USA, Aug. 2010.

INVESTIGATION OF FREQUENCY DEPENDENCE ON THE NOISE RESPONSE OF A NOVEL TRANSPARENT GATE RECESSED CHANNEL MOSFET

Ajay Kumar[1], Neha Gupta[2] and Rishu Chaujar[3]

[1]*Department of Engineering Physics, DTU, Delhi (India)*

[2]*Department of Engineering Physics, DTU, Delhi (India)*

[3] *Assistant Professor, Department of Engineering Physics, DTU, Delhi (India)*

ABSTRACT

The noise assessment of Novel Transparent Gate Recessed Channel MOSFET has been investigated based on the simulated result from ATLAS device simulation. TCAD simulation results show TGRC-MOSFET divulges Conventional Recessed Channel (CRC)-MOSFET in terms of reduction in noise figure, cross correlation, noise conductance and parasitic capacitances. It also achieves higher optimum source impedance for high performance applications where noise immunity is a key factor.

Keywords: ATLAS, CRC-MOSFET, noise, optimum impedance, paracitic capacitance, TGRC MOSFET.

I. INTRODUCTION

Field Effect Transistor (MOSFET) sizes close to their physical limits. CMOS technology is being used for the designing Linearity of RF amplifier is an important factor for use in digital communication. Application of RF circuits need transistor with minimum intermodulation distortion and noise [1]. Advancements in semiconductor manufacturing techniques and to achieve high speed and more packing density, complicated Integrated Circuits (ICs) have driven the associated Metal Oxide Semiconductor of circuits for super high frequencies communication. Scaling-down of MOS devices improves RF performance characterstics. On the other hand, it is difficult to scale-down the supply voltage used to perform these ICs consistently due to compatibility problem with earlier generation circuits, noise margin, power and delay requirements, but not scaling of subthresold slope and threshold voltage. While the successive increase in internal electric fields in aggressively scaled MOSFETs comes with the additional ameliorate of increased carrier velocities, and hence increased switching speed, it also presents higher reliability complications for the long period of operation of these devices [2]. As the size and signal levels of a MOSFET is scaled-down, the low frequency noise (LFN) properties become more important as the LFN is higher than the signals [3-4].

To abate the noise effects in CRC-MOSFET, instead of metallic gate, Indium Tin Oxide has been used. Indium tin oxide (ITO or tin-doped indium oxide) is a solid solution of indium oxide (In_2O_3) and tin oxide (SnO_2). It is

colorless and transparent in thin layers. Indium tin oxide is one of the most widely used transparent conducting oxides because of its two leading properties, its optical transparency and electrical conductivity , as well as the ease with which it can be deposited as a thin film [5]. The In_2O_3 phase itself contributes free electron for electrical conductivity [6-8]. When Tin (Sn) is diffused, then some of the oxygen vacancies may be created by SnO_2 which creates free electrons to enhance the concentration of carriers and hence increase conductivity and decrease the resistivity with temperature. As the device scales-down, parasitic capacitances arises. These parasitic capacitances degrade the device performance. By using TGRC-MOSFET, parasitic capacitances can be reduced significantly.

II. DEVICE STRUCTURE AND ITS PARAMETERS

The simulation device structure i.e. Transparent Gate Recessed Channel MOSFET consists of gate which is made by transparent conducting material Indium Tin Oxide (ITO) as shown in Fig 1. The total gate length is 30 nm and thickness of oxide is 2.0 nm. Groove depth is 38 nm and source/drain junction depth is 30 nm. Here we have taken negative junction depth 10 nm.

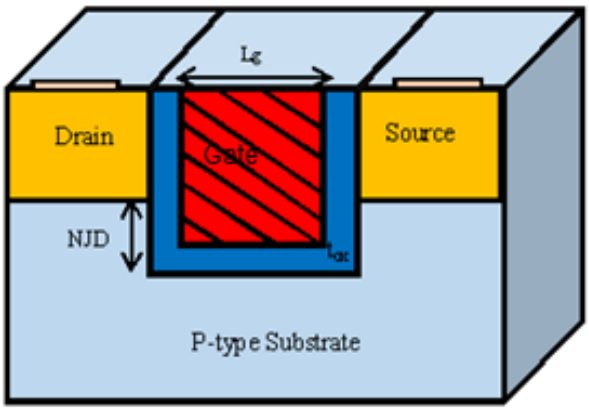

Fig. 1: Structure of Transparent Gate Recessed Channel MOSFET.

Gate to source and drain to source voltage is 0.7 V. Workfuntion taken for transparent material is 4.7 eV in TGRC-MOSFET and 4.1 eV for metal in CRC-MOSFET. All simulations have been performed using ATLAS device simulator. The simulations are based on the inversion layer Lombardi CVT mobility model with the Auger recombination model and Shockley-Read –Hall (SRH) for minority carrier recombination. Further the hydrodynamic energy transport model comprising of the continuity equations, energy balance equations of the carriers, momentum transport equations and Poisson's equation have also been enabled [9].

III. TCAD SIMULATION RESULTS OF TRANSPARENT GATE RECESSED CHANNEL MOSFET

The present analysis is carried out for a channel length, L_G=30nm, uniformly doped source/drain, N_D with doping density of $1x10^{19}$ cm^{-3}, p type substrate doping, N_A with a doping density of $1x10^{17}$ cm^{-3}, SiO_2 thickness, t_{ox}=2.0 nm. The gate work function (Φ_{ITO}) is 4.7 eV.

3.1 Minimum Noise Figure

Noise figure is generally used as a measure of an amplifer's RF performance. Fig.2. shows the minimum noise figure for CRC-MOSFET and TGRC-MOSFET at different frequencies. When frequency increases from 100 Hz to 10 GHz, minimum noise figure decreases in TGRC-MOSEFT compared to CRC-MOSFET.

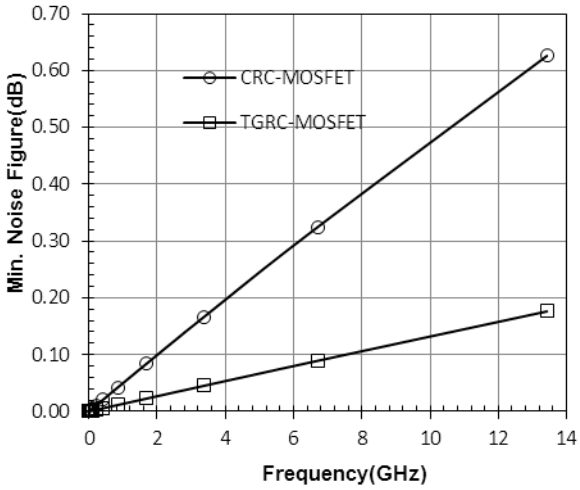

Fig. 2: Minimum noise figure for CRC- MOSFET and TGRC-MOSFET.

The observation is mainly attributed to the transparent conducting material in the TGRC-MOSFET architecture because in transparent material, random motion of free electrons decreases. In transparent conducting material, the temperature rise is not much significant when concentration of charge carriers is increased, due to which noise figure decreases.

3.2 Optimum Source Impedance

Fig.3. predicts the behavior of optimum source impedance ($Z_{OPT}=R_{OPT}+jX_{OPT}$) with respect to frequency. When the frequency increases, optimum impedance decreases in CRC-MOSFET while it is maximum at low frequencies.

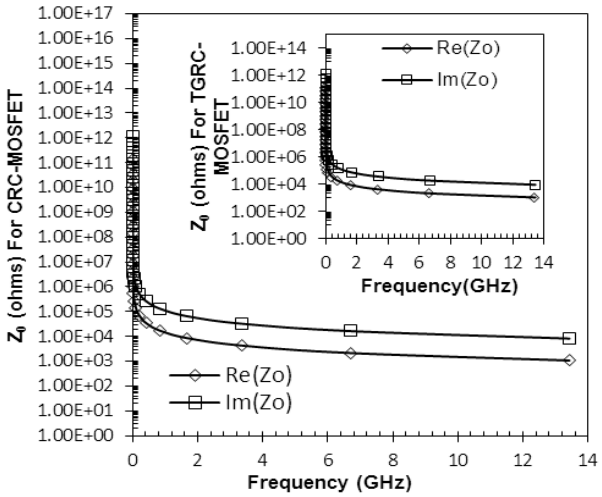

Fig. 3: Optimum source impedance Z_0 for CRC-MOSFET. Inset- Optimum source impedance Z_0 for TGRC- MOSFET.

As evident from Fig.3, the optimum source impedance in TGRC-MOSFET is slightly higher than CRC-MOSFET because of the presence of indium tin oxide in TGRC-MOSFET which is effectively acting as a parallel oxide with SiO_2 and hence effective permittivity is increased which eventually leads to increase in input impedance. This high impedance of TGRC-MOSFET also helps in reduction of electrostatic charges, which basically comes in to existence with scale-down of oxide [10].

3.3 Parasitic Capacitance

In addition, for better performance of a device in microwave-communication, parasitic capacitances should be as small as possible. Local stress on the radio-frequency (RF) performance of the transistor and parasitic capacitances are investigated in 30-nm CMOS technology [11]. Parasitic capacitances and resistance put upper limit on the speed of a transistor [12].

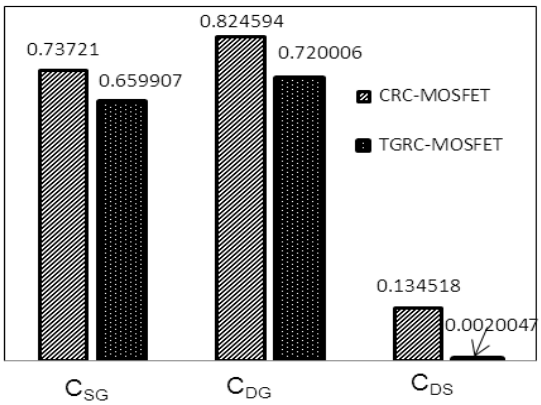

Fig. 4: Parasitic capacitance (femto-Farad) for CRC- MOSFET and TGRC-MOSFET.

Parasitic capacitance is the cause of delay in logic-cell. When one logic cell drives another, the parasitic input capacitance of the driven cell becomes the load capacitance of the driven cell [13]. Fig.4 shows that the parasitic capacitances in TGRC-MOSFET are less than the CRC-MOSFET. The ITO-SiO_2 forms a MOS capacitor with ITO serving as metallic gate electrode at GHz frequencies and SiO_2 forming the gate insulator [14].

3.4 Noise Conductance

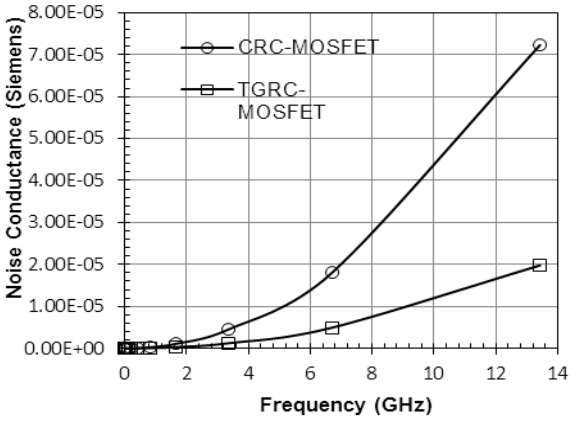

Fig. 5: Noise conductance for CRC- MOSFET and TGRC-MOSFET.

Further, in the RF applications of a MOS device, noise conductance should be as low as possible. In a MOS device, noise conductance increases due to thermally generated charge carriers. In TGRC-MOSFET, noise conductance is low because in transparent conducting material, oxygen vacancies created by oxides give more free electrons and hence, mobility decreases with increase in the concentration of charge carriers, leading to lesser number of thermally generated charge carriers as is shown in Fig.5.

3.5 Cross Correlation

Here, MOSFET is considered as a two port device as shown in Fig.6 i.e. the noise induced at the gate terminal is separated from the MOSFET and is represented by V1 and the noise received at the output is replaced by a voltage V2 [15]. Some statistical analysis is obligatory for this research since noise is a random phenomenon. Thus, cross correlation of the voltages at the two port of the device is compared. It is clearly evident from Fig.7 that cross correlation in TGRC-MOSFET is lower as compared to CRC-MOSFET at GHz frequencies.

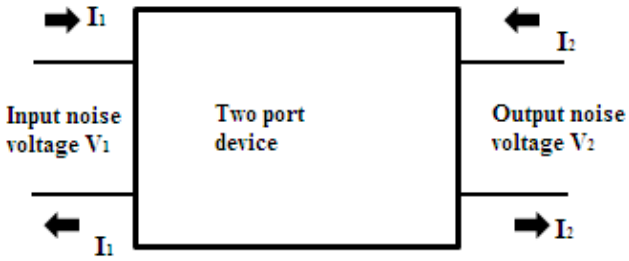

Fig. 6: MOSFET as a two port device where the input noise is replaced by a voltage V1 and the noise received at output is replaced by V2.

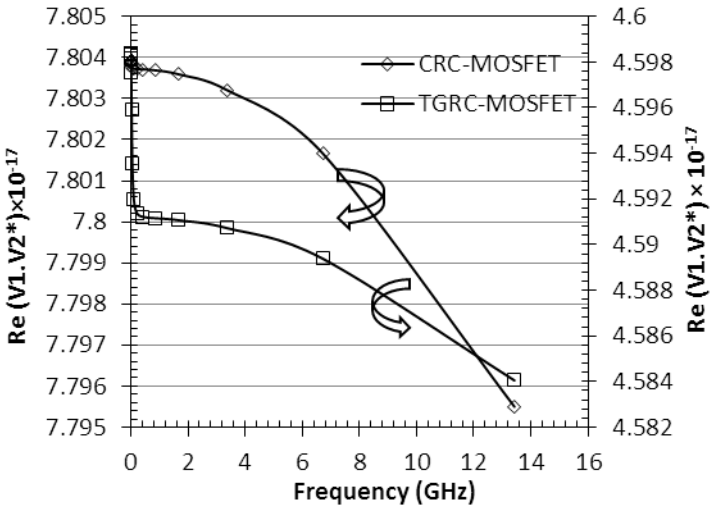

Fig. 7: Cross correlation for CRC- MOSFET and TGRC-MOSFET.

In TGRC-MOSFET electric field is lower at the drain side. Therefore, isotropic scattering reduces and mean free path (λ) of carriers crossing the channel (as a function of frequency) is much larger than CRC-MOSFET [6] due to transparent gate and reduced surface scattering at the Si-SiO_2 interface. Due to this reduced isotropic

scattering, the scattering mechanism is not so effective in breaking the correlation between gate current and drain current [15]. Thus, cross correlation (i.e. V1.V2*) reduces in TGRC-MOSFET at higher frequencies.

IV CONCLUSION

In this work, we focused on Transparent Gate incorporation onto the Conventional Recessed Channel MOSFET for superior noise performance of scaled MOS devices. TCAD simulation reveals reduction in minimum noise figure, noise conductance and parasitic capacitances for TGRC-MOSFET. It also achieves higher optimum source impedance. Hence TGRC-MOSFET is a reliable solution for RF applications and CMOS technology for the designing of multi-gigahertz communication circuits.

V. ACKNOWLEDGMENT

The authors would like to gratitude to Microelectronics Research Lab, Department of Engineering Physics, Delhi Technological University to carry out this work

REFERENCES

[1] Chaujar. R., Kaur. R., Saxena. M., Gupta. M. and Gupta. R.S., "GEWE-RCMOSFET: A Solution to CMOS Technology for RFIC Design Based on the Concept of Intercept Point", IEEE Interactional Conference on Recent Advances in Microwave Theory and Applications, 2008, Jaipur, India, 661-662.

[2] Arora. N., "MOSFET models for VLSI circuit simulation theory and practice", Springer Verlag Wien New York, 1993, 87-89.

[3] Brederlow. R., Weber. W., Schmitt-Landsidel. D. and Thewes. R., "Fluctuations of the low frequency noise of MOS transistors and their modeling in analog and RF-circuit", International Electron Device Meeting, Tech. Dig., 1999, Washington, DC, USA, 159-162.

[4] Sánden. M., Marinov. O., Deen. M. J. and Ostling. M., "A new model for the low-frequency noise and the noise level variation in polysilicon emitter BJTs", IEEE Trans. Electron Devices 49(3), 2002, 514-520.

[5] Kim. H., Gilmore. C. M., Piqué. V, Horwitz. J. S., Mattoussi. H., Murata. H., Kafafi. Z. H. and Chrisey. D. B., "Electrical, optical, and structural properties of indium–tin–oxide thin films for organic light-emitting devices", Journal of Applied Physics, 86 (11), 1999, 6451.

[6] Chaujar. R., Kaur. R., Saxena. M., Gupta. M. and Gupta. R. S., "TCAD Assessment of Gate Electrode Workfunction Engineered Recessed Channel (GEWE-RC) MOSFET and Its Multilayered Gate Architecture—Part I: Hot-Carrier-Reliability Evaluation", IEEE Trans. Electron Devices 55(10), 2008, 2602-2613.

[7] Pammi. S. V. N., Jung. H. J. and Yoon. S. G., "Low-Temperature Nanocluster Deposition (NCD) for Improvement of the Structural, Electrical, and Optical Properties of ITO Thin Films", IEEE Transactions on Nanotechnology 10(5), 2011, 1059-1065.

[8] Chaujar. R., Kaur. R., Saxena. M., Gupta. M. and Gupta. R.S., "Solution to CMOS Technology for high Performance Analog Applications: GEWE-RCMOSFET", IEEE 2nd National Workshop on Advanced Optoelectronic Materials and Devices, 2008, Varanasi, India, 201-205.

[9] ATLAS User's Manual, SILVACO Int., Santa Clara, 2011, CA.

[10] Agarwal. A. and Chaujar. R., "Noise Analysis of Gate Electrode Work function Engineered Recessed Channel (GEWE-RC) MOSFET", Journal of Physics Conference Series 367, 2012, 012013(1-8).

[11] Kim. H. S., Kim. J., Chung. C., Lim. J., Jeong. J., Joe, J. H., Park. J., Park. K. W., Oh. H. and Yoon. J. S., "Effects of Parasitic Capacitance, External Resistance, and Local Stress on the RF Performance of the Transistors Fabricated by Standard 65-nm CMOS Technologies", IEEE Transactions on Electron Devices 55(10), 2008, 2712-2717.

[12] Whitaker. J. C., The Electronics Handbook, Second Edition, CRC Press, 2005.

[13] Smith. M. J. S., Application-specific Integrated Circuits, Pearson, 1997.

[14] Vasudev. A. P., Kang. J. H., Park. J., Liu. X. and Brongersma. M. L., "Electro-optical modulation of a silicon waveguide with an epsilon-near-zero material", Electro-optical materials 21(22), 2013, 26387-26397.

[15] Belostotski. L. and Haslett. J. W., "Two-port noise figure optimization of source-degenerated cascode CMOS LNAs", Analog Integer. Circuits Signal Process 55(2), 2008, 125–137.

Biographical Notes

Mr. Ajay Kumar is presently working as Ph. D Research Scholar in Engineering Physics Department from Delhi Technological University (DTU), Delhi, India.

Mrs. Neha Gupta is presently working as a Ph. D Research Scholar in Engineering Physics Department from Delhi Technological University (DTU), Delhi, India.

Dr. Rishu Chaujar is working as an Assistant Professor in Engineering Physics Department from Delhi Technological University (DTU), Delhi, India.

ADVANCE TECHNIQUE FOR WEBSITE NAVIGATION IMPROVEMENT USING MACHINE LEARNING

[1]Leelashankar Salitra, [2]Prof. Namrata Tapaswi

IES-IPS Academy, Indore (India)

ABSTRACT

Web searching and information retrieval in a website is a extremely recurrent activity in web browsing. When a customer again finding a website particularly after a long time, he comes across some problems between which beings ignorant regarding the information structure of the site is extremely prominent a different problem is that in a website, customer have no technique to systematize the information space or the navigational structure of the website. Our aim is to improve Web navigation efficiency by reorganizing Web structure. To avoid customer to lose their orientation, structure stability is taken into consideration. We are proposing a technique to progress the navigation effectiveness of a website while minimizing changes to its existing structure we present a survey of the use of Web mining for Web transformation approaches.

Keywords: Clustering, Navigability, Web Mining, Web Personalization, Web Transformation.

I INTRODUCTION

Website navigation has been appear as one of the mainly significant design features transversely many domains with finance, e-commerce, activity, learning, administration, and medical. A major reason is that the web developers lenient of how a website must be structured can be considerably dissimilar from that of the customer.web site moreover enclose a lot of links and pages each user need dissimilar pages at similar time or identical user might access dissimilar pages at different time. As customer increase over internet we require to build web intelligent we apprehension here concerning intelligent website. To build web site intellectual we have to identify what is content of website, which are customer and how website structured every one this identified as web mining. Now as data mining plan at discover expensive information that is hidden in conservative databases, the promising field of Web mining plan at verdict and extract appropriate information that is hidden in Web associated data. Web mining is a multi-disciplinary attempt that draw method from field similar to information retrieval, statistics, machine learning, natural language dispensation, and others. Basically a Web mining deal among three main areas web content mining, web usage mining and web structure mining. for prefer web structure mining is because web site is huge source of information, except users frequently browsing ineffective page which irritate customer and customer lost attention from searching data over website. A most important cause of poor web design is to the web developers considerate of how a website must be structured can be significantly dissimilar from those of the customer however, the determine of website efficiency should be the approval of the users somewhat than that of the developers. Thus,

Web pages must be prearranged in a method that usually matches the user's replica of how pages be supposed to be prepared. There are two conduct to advance customer navigability web personalization and web conversion. Web personalization deal with customer behavior and customer profile, sessions and history of data moreover called as web logs which is formed by user's action on web site, but alteration come up to mostly focus on increasing technique to totally rearrange the link structure of a website. We accept web transformation method to help user navigation. Proposed approach are links based clustering to modify structure of website as we recognize clustering is one method of data reduction so lager web usage data is utilize as compacted and time of reorganize web site structure is concentrated. In later section we provide details of some popular clustering algorithm and comparison between clustering algorithm with respect to time. Our propose technique addresses how to improve a website without introducing substantial changes.

II RELATED WORK

In this research, we have distinguished a method that discovers the gap among Web site designer prospect and customer behavior. The previous are assessed by measure the inter-page intangible significance and the final by measure the inter-page entrance co-occurrence.

Chen and Young [1] examine the questions of how to get better user navigation in a website with minimal modify to its structure. It complements the literature of alteration approach that focuses on reconstruct the link structure of a website. Their proposed model is appropriate for website continuation and can be functional in a regular manner.

Biswas et al. [2] propose a narrative approach named Dashboard which supports structure custom navigational menus system and permit each user construct her own hierarchical information structure. They was demonstrated how this innovative approach help rapidly re-finding information on re-visitation of a website.

Wang and Yen [3] improves navigation efficiency precisely and relieve the expensive of tedious chore to adapt the structure in transformation. If several constraints, e.g. structural constancy constraint, is relaxed, there is still room for development. Some improvements are important but will saturate or even reduce as after addition a positive number of links.

Lin and Tseng [4] proposed model decreases the information excess and search depth for user surfing the web. A heuristic approach has as well been planned to decrease the necessary computation time. Though, the heuristic approach connecting two successive 0-1 programming models immobile require a extremely long computation time to discover the optimal solution, particularly when the website contains a lot of hyperlinks. To determine the effectiveness problem, proposes an ant colony system to reorder website structure. The proposed algorithm is experienced lengthily with numerical examples. Moreover, an experiential study with a real-world website is conduct to confirm the algorithm applicability.

Martın-Guerrero et al. [5] estimate the feasibility of implementing a recommender in Web portal is proposed. The primary step of the proposed method is to cluster user data based on simulation in order to make sure that the

collaborative filter is robust crosswise a range of user models. These consequences demonstrated the predictive accuracy of cluster based recommender systems with the ART2 neural network algorithm practical to profiles of replicated user data. This predictive accuracy then supports the present of services that are novel to the user.

Kim and Shim [6] present narrative algorithms for extract templates from a huge number of web documents which are generate from heterogeneous templates. We cluster the web credentials based on the resemblance of essential template structures in the documents so that the template for each cluster is extract concurrently. They have developed a novel goodness compute with its quick estimate for clustering and present comprehensive investigation of their algorithm. With real-life data sets corroborate the efficiency and strength of their algorithm compare to the state of the art for template detection algorithms.

III PROPOSED METHODOLOGY

The confront for web structure mining is to arrangement with the configuration of the hyperlinks inside the web itself. Link study is an getting on region of research. However, through the rising attention in web mining, the investigate of structure investigation had improved and these efforts had resulted in a recently rising research region called link mining [1][7], which is situated at the connection of the effort in link analysis, hypertext and web mining, relational knowledge and inductive logic encoding, and graph mining. There is a potentially broad range of function area for this novel area of research, with WWW. The web contain a diversity of objects with about no unite structure, with difference in the authoring style and content a group improved than in normal collection of text documents.

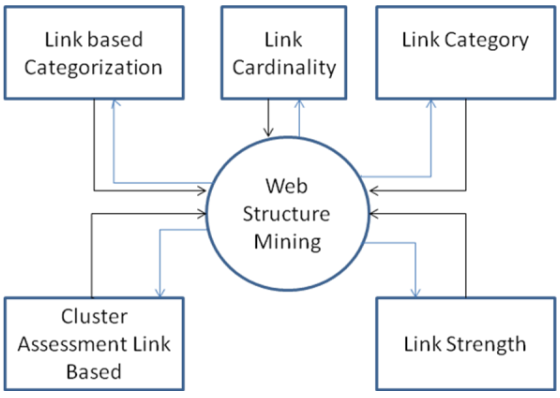

Fig.1 Website Navigation Improvement

The objects in the internet are web pages, and links are in-, out- and co-citation. Attributes contain html tags, word manifestation and anchor texts [2][7]. this variety of objects create novel problems and challenge, since is not probable to directly complete use of obtainable method such as from database supervision or in succession retrieval. Link mining had created a few protests on several of the traditional data mining tasks. as follow link-based categorization is the nearly all new improve of a typical data mining task to connected domains [7]. the task is to focal point on the prediction of the group of a web page, support on words that happen on the page, links among pages, anchor text, html tags and other likely attributes establish on the webpage.

The objective in cluster study is to discover obviously happening sub-classes. the data is segmented into group, where alike substance are group jointly, and different objects are group into dissimilar groups preceding task, link-based cluster study is unverified and can be use to find out hidden patterns beginning data. There are a extensive range of odd jobs about the prediction of the continuation of links, such as predicting the style of link among two entities, or predicting the rationale of a link.

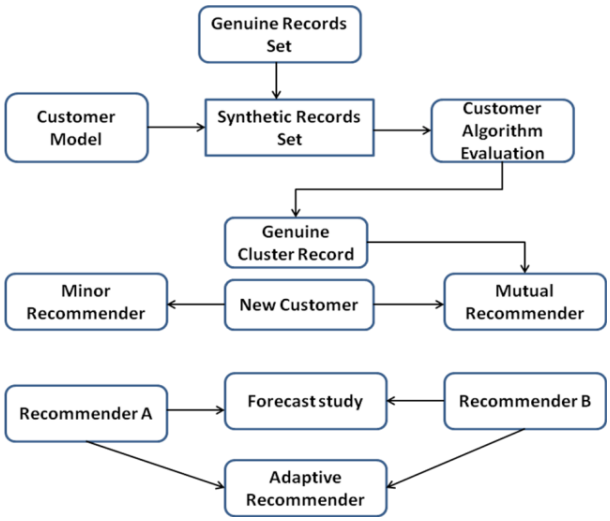

Fig.2 Technique for clustering web page

Links could be connected with weights. The foremost task here is to calculate the quantity of links among objects. There is a lot of conduct to use the link structure of the web to make notions of authority. The major goal in increasing function for link mining is to complete superior use of the accepting of these

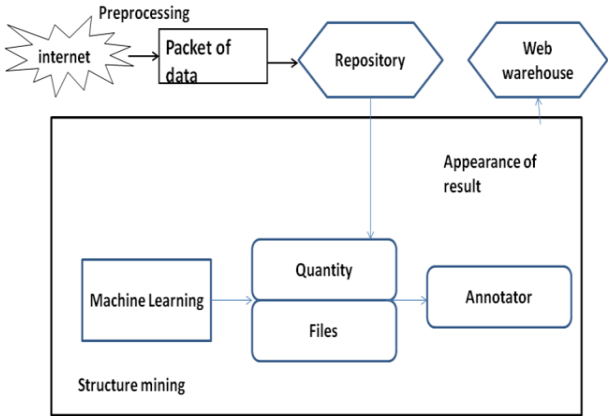

Fig.3 Link Extraction Technique

Intrinsic social association of the web) pages can't be complex in regulate to adjust the construction. Real-world data lean to be dirty, partial and incompatible. Data preprocessing techniques in machine learning can get improved the quality of the data, thereby segment to recover the precision and capability of the subsequent mining process. Data preprocessing is an important walk in the knowledge ruling process, since superiority decisions be necessary to

be base on advantage data. Data used in preprocessing cover server log files, web page content, web site construction and hit count of pages in the web site. Amalgamation of web usage and web structure mining. Data crackdown removes entries unsupportive to data analyzing and mining. It has to eliminate log entries that have status code as failure or error. Secondly some routine search engines make some access report, those have to be identified and detached from the log file. Some of other frequent indicator such as the frequent request for the similar URL from the similar host. a time period among needs too small to detain the contents of a page and a series of needs from one host every one of whose referrer URLs are empty .The dynamic performance of web users below a exacting session can be some of the next These behaviors can be use to make more multifarious navigation behaviors in a single session. the basic behaviors build complex navigations are specified below: A Web customer can initiate session with several single of the probable entry pages of a web site. This performance contain new page which is not request by some other previous page access from the similar domain in near-time A Web customer can choose the next page have a link from the nearly everyone recently accessed page. A Web customer can press the back button one additional time and thus select as the next page a page have a link as of some one of the before browse pages. The information composed from the web site can facilitate discover the knowledge. This information composed can be used to obtain decision on various factors like the web pages with maximum hit counts will be the accepted pages. What is probable the navigation patterns of users. The time done in on each web page which tells about consequence of the web page. If time used up on challenging web page is irrelevant it identify that the web page does not enclose significant information. The web pages for which no consumer be relevant for is there, identify that page have to be customized. If log file entry says frequently for exacting web page redirect, it should be notify to web site designer owner. following the pattern study is done on web pages, the significant decision can be done concerning structure of the website. The exceptional web pages will be stimulated extremely near to the home page, at next level medium class web pages moved and so on. The pages with extra hit count can be known the preference to be bring closer to the home page provide web site owner designer agrees. We will heap tree can be generated based on hit counts obtainable in the log file throughout exacting session. This heap tree generate will assist us create decision about topology of web site throughout next interval so that the web pages which are extra popular can be brought extremely near to the home parent web page. With this reformation, the web users can gain rapid access to the web pages down with best consumption of bandwidth and server's memory space as every HTTP request will be go into the log file of the server. Access earlier to the almost everybody recently accessed one. A Web customer can conclude his/her session. Adding, deleting and modify links should be careful at the sometime. it's tricky to find out user's require on web site.

IV WEB EFFICIENCY MODELING AND IMPROVEMENT

In this analysis, we limit our analysis scope by bearing in mind two considerations for webmaster and users.

(1) Minimize additional work for web users. to protect the site's original design from destructive changes. Limited number of links can be added or removed, and also limited number of pages can be created or destroyed.

(2) Make the website transformation for everyone, especially first-time users and casual users. Customization is very useful for experienced users, but does not benefit first-time users.

(3) To propose a model who find out the instruct of user.

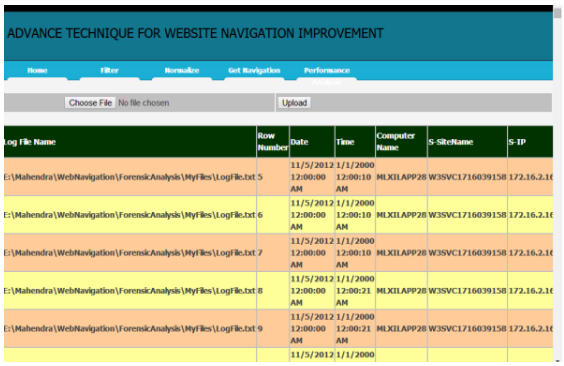

Fig.4 Finding Web Navigation

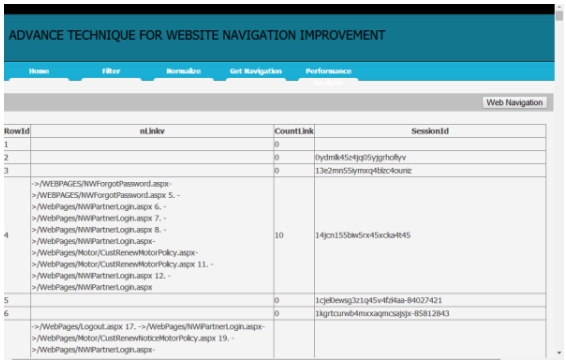

Fig.5 Web Site Navigation Using Clustering

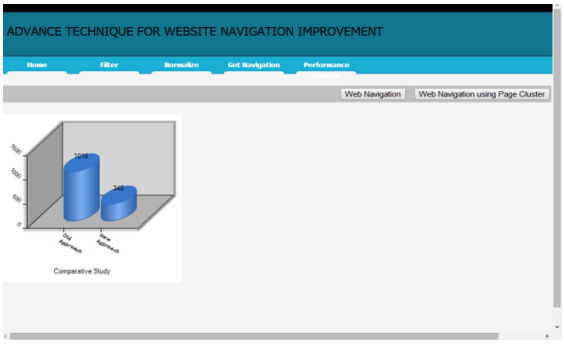

Fig.6 Web Navigation Using Page Clustering

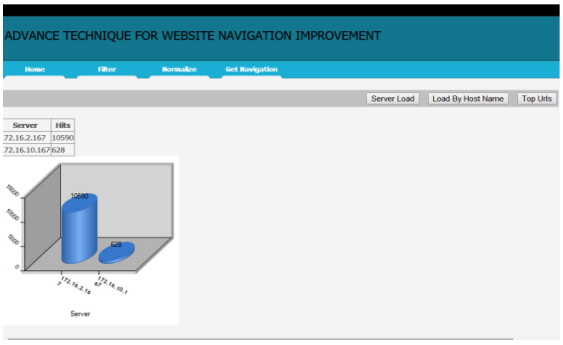

Fig.7 Finding Server Load And Top URL

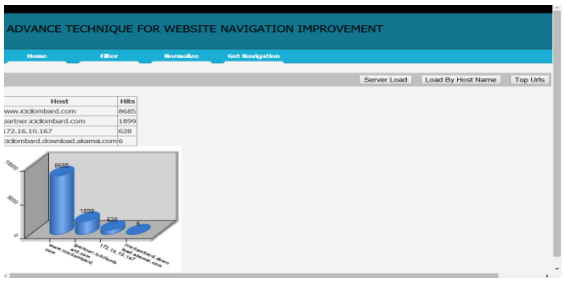

Fig.8 Load on Server for Top Url Hits

V CONCLUSION

Our aim is to improve Web navigation efficiency by reorganizing Web structure. To avoid users to lose their orientation, structure stability is taken into consideration. This analysis proposes a mathematical programming

method to reorganize Web structure in order to achieve better navigation efficiency and also increase our three features which help to improve the user navigation. This analysis has the advantage of improving navigation efficiency mathematically and relieving the designer to modify the structure in transformation. If some constraint, e.g. structural stability constraint, is relaxed, there is still room for improvement. Some improvements are significant but will saturate or even decrease as after adding a certain number of links. To propose a mathematical programming model to improve the navigation effectiveness of a website while minimizing changes to its current structure, a critical issue that has not been examined in the literature.

REFERENCES

[1] Min Chen and Young U. Ryu," Facilitating Effective User Navigation through Website Structure Improvement" IEEE TRANSACTIONS ON KNOWLEDGE AND DATA ENGINEERING, VOL. 25, NO. 3, MARCH 2013

[2] Biswas, P , Debnath, M. ; Ghosh, S. ; Rahim, S. ; Mahamud, A.;Chowdhury, N." Dashboard - a novel approach to re-find information in a website through building personalized navigationnal menus" Computer and Information Technology (ICCIT), 2011 IEEE 14th International Conference.

[3] May Wang , Benjamin Yen ," Web Structure Reorganization to Improve Web Navigation Efficiency" 11th Pacific-Asia Conference on Information Systems.

[4] C.C. Lin and L. Tseng, "Website Reorganization Using an Ant Colony System," Expert Systems with Applications, vol. 37, no. 12, pp. 7598-7605, 2010.

[5] Jose´ D. Martı´n-Guerrero a,*, Paulo J.G. Lisboa b, Emilio Soria-Olivas a, Alberto Palomares c, Emili Balaguer c ," An approach based on the Adaptive Resonance Theory for analysing the viability of recommender systems in a citizen Web porta" Expert Systems with Applications 33 (2007) 743–753.

[6] C. Kim and K. Shim, "TEXT: Automatic Template Extraction from Heterogeneous Web Pages," IEEE Trans. Knowledge and Data Eng., vol. 23, no. 4, pp. 612-626, Apr. 2011.

[7] L. Getoor, Link Mining: A New Data Mining Challenge. SIGKDD Explorations, vol. 4, issue 2, 2003.

[8] Marcio dos Santos Galli, Eduardo Pezutti Beletato dos Santos," TagVisor: Extending Web Pages with Interaction Events to Support Presentation in Digital Signage " WWW 2013 Companion, May 13–17, 2013, Rio de Janeiro, Brazil. ACM 978-1-4503-2038-2/13/05.

[9] Jennifer Pearson," Supporting Effective User Navigation in Digital Documents" CHI 2010, April 10-15, 2010, Atlanta, Georgia, USA. ACM 978-1-60558-930-5/10/04.

[10] T.L.N.Divya, G.Loshma, Dr. Nagaratna P Hegde," Template Extraction from Heterogeneous Web Pages Using Text Clustering" International Journal of Computer Trends and Technology- volume3Issue3- 2012.

[11] C. Kim and K. Shim, "TEXT: Automatic Template Extraction from Heterogeneous Web Pages," IEEE Trans. Knowledge and Data Eng., vol. 23, no. 4, pp. 612-626, Apr. 2011.

[12] Y. Yang, Y. Cao, Z. Nie, J. Zhou, and J. Wen, "Closing the Loop in Webpage Understanding," IEEE Trans. Knowledge and Data Eng., vol. 22, no. 5, pp. 639-650, May 2010.

RECOGNITION AND DESCRIPTION OF TOPONYM IN KANNADA CARTOGRAPHIC MAPS

[1]Jagadishappa B Akkimaradi , [2]Jagadish S Kallimani

[1,2] Department of Computer Science and Engineering

M S Ramaiah Institute of Technology, Bangalore, (India)

ABSTRACT

Graphical documents such as cartographic maps contain great variety of textual elements appearing in different spatial positions, in different sizes and colors and overlapping graphical symbols. This greatly complicates automatic optical recognition of textual elements in the process of raster-to-vector conversion of graphical documents. At present a lot of methods and programs for automatic text recognition exist. However there are no effective text recognition systems for graphic documents. Graphic documents usually contain a great variety of textual information. There are no sufficient number of works on Indian language character recognition especially Kannada script among twelve major scripts in India. The goal is to present a review of existing work on printed Kannada script and their results. The characteristics of Kannada script and Kannada Character Recognition System KCR are discussed in detail. Finally fusion at the classifier level is proposed to increase the recognition accuracy. This dissertation work is an effort to toponym recognition in cartographic maps of Kannada language.

Keywords: Cartography, Toponyms, Segmentation, Template Matching

I INTRODUCTION

A huge amount of geographic information collected in the last centuries is available in the form of maps printed or drawn on paper. Currently, Google maps serves as an excellent tool in retrieving almost every details from different types of maps. To store, search, distribute, and view these maps in the electronic form they are to be converted in one of the digital format developed for this purpose. The simplest way of such a conversion is scanning the paper map to obtain an image (a picture) stored in any of the raster graphical formats such as TIFF, GIF, etc. After that, a raster-to-vector conversion may be applied to include obtained vector maps into Geographic Information Systems (GIS).

Cartography is the study and practice of making maps. Combining science and technique, cartography builds on the premise that reality can be modelled in ways that communicate spatial information effectively.

The fundamental problems of traditional cartography are to

- Set the map's agenda and select traits of the object to be mapped. This is the concern of map editing. Traits may be physical, such as roads or land masses, or may be abstract, such as toponyms or political boundaries.
- Represent the terrain of the mapped object on flat media. This is the concern of map projections.
- Eliminate characteristics of the mapped object that are not relevant to the map's purpose. This is the concern of generalization.
- Reduce the complexity of the characteristics that will be mapped. This is also the concern of generalization.

- Orchestrate the elements of the map to best convey its message to its audience. This is the concern of map design.

Modern cartography is largely integrated with geographic information science (GIScience) and constitutes many theoretical and practical foundations of geographic information systems.

The earliest known map is a matter of some debate, both because the definition of "map" is not sharp and because some artifacts speculated to be maps might actually be something else. In cartography, technology has continually changed in order to meet the demands of new generations of mapmakers and map users. The first maps were manually constructed with brushes and parchment; therefore, varied in quality and were limited in distribution. The advent of magnetic devices, such as the compass and much later, magnetic storage devices allowed for the creation of far more accurate maps and the ability to store and manipulate them digitally.

The separation of overlapping text and graphics is a challenging problem in document image analysis. This problem is found in many applications, including forms processing, maps interpretation and engineering drawings interpretation, where text and graphics are processed in fundamentally different ways. [1]

The problem of text extraction from an imaged document still remains an important issue in the field of image processing. Applications such as map interpretation, referencing system for digitized manuscripts, and news article search from microfilms require some form of text extraction and categorizing of text images into logical groups.

Document Processing in the Indian environment has special significance, since eighteen official languages are in use in the country. Throughout the country, every government office uses at least two languages, English and the official language of the corresponding state. The state of Karnataka has an official language as Kannada, however many national organizations such as Banks, use English and Kannada. Even all the documents in the government offices of Karnataka state usually appear in two languages, Kannada and English. The aim of the automation of document processing is to convert the scanned paper document to the machine readable codes such as ASCII.

Computer vision research today is still facing greater difficulties in understanding graphical objects than character strings which can be handled using OCR with reasonable success. Any words that can be found in a document image by the computer will certainly assist in the understanding of the image. One major technique reported in the literature for text/graphics separation relies on connected component analysis through examination of the relationships among neighbouring components.

Advances in mechanical devices such as the printing press, quadrant and vernier, allowed for the mass production of maps and the ability to make accurate reproductions from more accurate data. Optical technology, such as the telescope, sextant and other devices that use telescopes, allowed for accurate surveying of land and the ability of mapmakers and navigators to find their latitude by measuring angles to the North Star at night or the sun at noon.

Advances in photochemical technology, such as the lithographic and photochemical processes, have allowed for the creation of maps that have fine details, do not distort in shape and resist moisture and wear. This also eliminated the need for engraving, which further shortened the time it takes to make and reproduce maps.

Advancements in electronic technology in the 20th century ushered in another revolution in cartography. Ready availability of computers and peripherals such as monitors, plotters, printers, scanners (remote and document) and analytic stereo plotters, along with computer programs for visualization, image processing, spatial analysis,

and database management, have democratized and greatly expanded the making of maps. The ability to superimpose spatially located variables onto existing maps created new uses for maps and new industries to explore and exploit these potentials.

These days most commercial-quality maps are made using software that falls into one of three main types: CAD, GIS and specialized illustration software. Spatial information can be stored in a database, from which it can be extracted on demand. These tools lead to increasingly dynamic, interactive maps that can be manipulated digitally.

With the field rugged computers, GPS and laser rangefinders, it is possible to perform mapping directly in the terrain. Construction of a map in real time, for example by using Field-Map technology, improves productivity and quality of the result.

The source maps are from a local Street Directory. The maps are printed in color. The focus here is on the black layer, which includes text, small icons, road lines, outlines of buildings and parks, and so on. Some icons in the maps are solid components, such as solid arrowheads, solid overhead pedestrian bridge. The road lines are either thick or thin lines, mostly curves. Some tracks and outlines of parks are dashed lines. Most outlines of buildings and parks are polygons.

The text strings in the maps are mainly road names, names of buildings and parks, and so on. The road names are labeled along the roads. That means the labels may be along curved lines. The touching of road names with road lines is somewhat similar to the case of strings touching the underlines or upper lines. On the other hand, the connection of the names and the outlines of the buildings are much more complicated. The reason is that the outlines of the buildings can be of any shapes.

II RELATED WORKS

Text detection and recognition are very difficult problems which have generated a lot of research work. The main difficulty lies in the graphics that surround or intersect the text. The main feature of a good text detection algorithm is to be independent in respect to text font, size and orientation. One can distinguish two main families of methods: (i) methods devoted to detect text in paper-based documents, (ii) methods developed for text detection in videos or textured images. The later methods are mostly based on texture analysis. [3]

An early approach in [4] introduced an algorithm which permits to extract text on binary images such as electronic circuits. Using connected components, a selection of possible characters is performed using the components' characteristics. The characters are merged into words using Hough Transform. This method, which inspired our paper, gives good results and has the advantage to be usable for various orientations and sizes of texts.

In [5], authors develop a model to extract black characters in urban maps. They use street lines data to recover the characters composing street names. Due to the possible overlapping between street names and street lines describing the street, they develop a specific OCR algorithm to produce an efficient text file of street names.

The move from paper-based documentation towards computerized storage and retrieval systems has been prompted by the many advantages to be gained from the ‘‘electronic document” environment. Document update and revision is efficiently achieved in the computerized form. For efficient processing and storage of documents, however, it is necessary to generate a description of graphical elements in the document rather than a bit-map in order to decrease the storage and processing time. Thus, increasing emphasis is being placed on the need for the

realization of computer-based systems which are capable of providing automated analysis and interpretation of paper-based documents**.** Much of the attention paid to automated document analysis systems in the literature has been in relation to engineering drawings and diagrams**.** Such systems provide a means for originating technical information (text and graphics) in a digital form suitable for interactive graphics editing, reproduction, and distribution. [4]

The initial processing stage in an automated document analysis system requires conversion of paper-based graphics/text to a digital bit-map representation. Wherever the primary goal of the automated document analysis system is interpretation of graphic data, text strings present within the digitized document must first be separated from the graphics in order that subsequent processing stages may operate exclusively on the graphic information. The extracted text may be stored separately for input to a character recognition system for later retrieval or revision. Since document types vary widely in style and content of both graphic and text data, an algorithm to perform text string removal must be able to accommodate documents containing text of various font styles and sizes.Further, the documents may contain text strings which are intermingled with graphics, and text characters which are similar in size or shape to graphics. In general, text strings may be of any orientation in the image; not simply horizontal or vertical but possibly diagonally aligned.

Several algorithms for text string separation have been reported in the literature [6][7]. However, many of these algorithms are very restrictive in the type of documents they can process and are therefore not useful in a general automated document analysis system. The Bley algorithm [7] is also sensitive to variations in text font style and size; the algorithm breaks connected components into subcomponents, which makes it difficult to process the components for graphics recognition. Thus there is no single algorithm which is robust enough to segment images containing mixed graphics and text, with multiple font styles and sizes and strings of arbitrary orientation.

In [8], proposed a fast algorithm for speeding up the process of template matching that uses M-estimators for dealing with outliers. In this a particular image hierarchy called the -pyramid that can be exploited to generate a list of ascending lower bounds of the minimal matching errors when a non decreasing robust error measure is adopted. Then, the set of lower bounds can be used to prune the search of the -pyramid, and a fast algorithm is thereby developed in this paper. This fast algorithm ensures finding the global minimum of the robust template matching problem in which a non decreasing M-estimator serves as an error measure. Experimental results demonstrate the effectiveness of our method. The basic idea of the M-estimator technique is to limit the influence of outliers in the matching error. In principle, the effects of the outlier can be suppressed with the M-estimator technique and therefore better estimations are obtained.

Text recognition from documents that contain non homogeneous text, such as from raster maps [6], is a difficult task, and hence much of the previous research only works on specific cases. Fletcher and Kasturi [4] utilize the Hough transformation to group characters and identify text strings. Since the Hough transformation detects straight lines, their method cannot be applied on curved strings. Moreover, their work does not handle multi-sized characters.

Vel´azquez and Levachkine [2] and Pal et al. [9] present text recognition techniques to handle characters in various font sizes, font types, and orientations. Their techniques are based on detecting straight string baselines for identifying individual text strings. These techniques cannot work on curved strings.

In our previous work [10], a text recognition approach that locates individual multi-oriented text labels in raster maps and detects the label orientations to then leverage the horizontal text recognition capability of commercial OCR software. The previous work requires manually specified character spacing for identifying individual text labels and does not consider multi-sized characters. In this paper, we present a text recognition technique to dynamically group characters from non-homogeneous text into text strings based on the character sizes and maximum desired string curvature. The hypothesis is that characters in a text string are similar in size and are spatially closer than the characters in two separated strings. Our text recognition technique does not require training for specific fonts and can be easily integrated with a commercial OCR product for processing documents that contain non-homogeneous text. [10]

III METHODOLOGY

The main objective of our method is to generate a set of images containing potential strings by detecting them on the map and to match the templates in order to obtain a consistent vectorized toponyms data file. We discuss how such additional information can be used to work around the problems arising in recognition of the inscriptions in the maps, associating them with specific cartographic objects, and importing information on these objects from available databases.

The following are the list of responsibilities involved in this dissertation work:

- A detailed survey and study on various types of cartographic maps in Kannada language.
- Develop a dictionary of all places, rivers, mountains, etc, for a limited geographical area maps.
- Develop an algorithm to recognize and describe the various features of the identified regions.
- Conduct subjective and objective test result analysis.

3.1 Segmentation

Segmentation is the process of extracting objects of interest from an image. The first step in segmentation is detecting lines.The first step of our technique consists in a binary classification of each pixel in order to eliminate pixel values that can definitively not be a part of a character.

A raster map has to be segmented first. All its elements should be retrieved with their coordinates and features, and then sent to the corresponding thematic layers. The layers can be symbols, landmarks, isolines, natural and artificial surroundings, words and numbers, lakes and other “punctual”, “linear” and polygonal bodies. Cartographic maps are the most complex graphic documents due to the high density of information that they contain. [2]

3.2 Template Matching Approach

Template matching is one of the Character Recognition techniques. It is the process of finding the location of a sub image called a template inside an image. Once a number of corresponding templates is found, their centers are used as corresponding points to determine the registration parameters. Template matching involves determining similarities between a given template and windows of the same size in an image and identifying the window that produces the highest similarity measure. It works by comparing derived image features of the

image and the template for each possible displacement of the template. This process involves the use of a database of characters or templates. There exists a template for all possible input characters.

In this method the dictionary is created for storing the Kannada toponyms. And this is used to compare with recognized toponym. The dictionary contains toponyms with their description that contains the information like name of river, city, etc

Template of all the characters to be recognized by the system is formed. A type of similarity measure is performed between the test character and the templates. At present, template matching is popularly used algorithm in character recognition. This method is efficient and has high speed when dealing with character identification. In the proposed method, recognition is done using template matching.

IV RESULTS

The accuracy of segmentation module of the proposed method has been checked and the results are obtained as per the below table and figure. It is evident that majority of the names are identified correctly. This shows that the method adopted is reliable and can be enhanced in future.

Table 1: Detection percentage of samples

SI No	Districts Names	Segmentation Accuracy
1	ಬೀದರ (Bidar)	100%
2	ಬೆಂಗಳೂರು (Bangalore)	100%
3	ಬೆಂಗಳೂರು ಗ್ರಾಮಾಂತರ (Bangalore Rural)	100%
4	ಕೋಲಾರ (Kolar)	100%
5	ಚಿಕ್ಕಬಳ್ಳಾಪುರ (Chikkaballapur)	85%
6	ರಾಮನಗರ (Ramnagar)	100%
7	ಗದಗ (Gadag)	100%
8	ಬೆಳಗಾವಿ (Belgaum)	100%
9	ಬಿಜಾಪುರ (Bijapur)	100%
10	ಹಾವೇರಿ (Haveri)	100%
11	ಧಾರವಾಡ (Dharwad)	100%
12	ಬಾಗಲಕೋಟ (Bagalkot)	100%s
13	ಉತ್ತರ ಕನ್ನಡ (Uttar Kannada)	98%
14	ಶಿವಮೊಗ್ಗ (Shimoga)	100%
15	ಬಳ್ಳಾರಿ (Bellary)	100%
16	ಗುಲ್ಬರ್ಗ (Gulbarga)	100%
17	ಕೊಪ್ಪಳ (Koppal)	100%
18	ರಾಯಚೂರು (Raichur)	100%
19	ಯಾದಗಿರಿ (Yadgir)	100%
20	ಚಾಮರಾಜನಗರ (Chamarajnagar)	85%
21	ಚಿಕ್ಕಮಗಳೂರು (Chikmagalur)	100%
22	ದಕ್ಷಿಣ ಕನ್ನಡ (Dakshin Kannada)	100%

23	ಹಾಸನ (Hassan)	100%
24	ಕೊಡಗು (Kodagu)	100%
25	ಮಂಡ್ಯ (Mandya)	100%
26	ಮೈಸೂರು (Mysore)	100%
27	ಉಡುಪಿ (Udupi)	100%
28	ಚಿತ್ರದುರ್ಗ (Chitradurga)	100%
29	ದಾವಣಗೆರೆ (Davangere)	98%
30	ತುಮಕೂರು (Tumkur)	100%

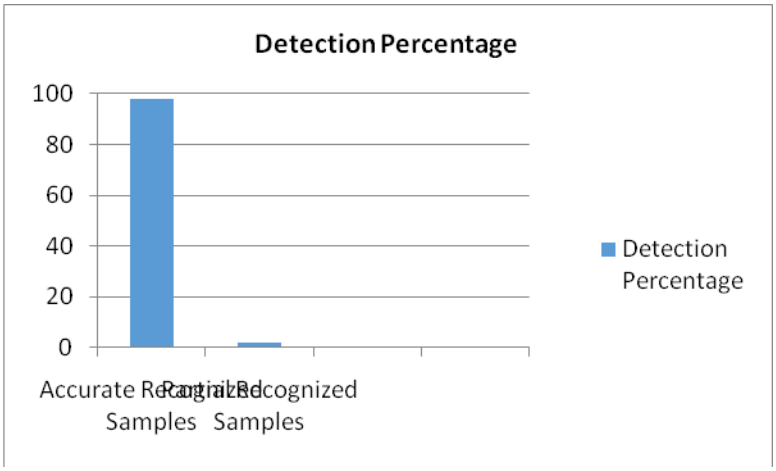

Figure 1: Graph of Detection Results.

V CONCLUSION

An automatic method to extract and recognize the textual layer of scanned color topographic maps has been described. The proposed method is mainly based on image segmentation and connected component processing. At each step, pruning or corrections are done using empirical filtering. A new algorithm for text string separation from mixed text/graphics images has been presented. The algorithm is robust to changes in text font style and size within an image. The algorithm presented has several advantages over previously applied techniques. With improvements made to the algorithm in terms of processing speed and efficiency of data representation, the application of the algorithm will become highly appropriate for use in document analysis systems.

REFERENCES

[1]. Detection and Extraction of Text Connected to Graphics in Maps

[2]. Vel´azquez, A. and Levachkine, S. (2004). Text/graphics separation and recognition in raster-scanned color cartographic maps. In GREC, vol 3088 of LNCS, pages 63–74.

[3]. Pouderoux, J., Gonzato, J. C., Pereira, A., and Guitton, P. (2007). Toponym recognition in scanned color topographic maps. In Proceedings of the 9th ICDAR, volume 1, pages 531 -535.

[4]. L. Fletcher and R. Kasturi. A robust algorithm for text string separation from mixed text/graphics images. IEEE Trans Pattern Anal. Mach. Intell., 10(6):910–918, 1988.

[5]. L. Li, G. Nagy, A. Samal, S. Seth, and Y. Xu. Cooperative text and line-art extraction from a topographic map. In Proceedings of ICDAR '99, pages 467–470, 1999.

[6]. L. T. Watson, K. Arvind, A. W. Ehrich, and R. M. Haralick, "Extraction of lines and regions from grey tone line drawing images," Pattern Recognition, vol. 17, pp. 493-506, 1984.

[7]. H. Bley, "Segmentation and pre-processing of electrical schematics using picture graphs," Cornput. Vision, Graphics, Image Processing, vol. 28, pp. 271-288, 1984.

[8]. Fast Algorithm for Robust Template Matching With M-Estimators Jiun-Hung Chen, Chu-Song Chen, and Yong-Sheng Chen IEEE TRANSACTIONS ON SIGNAL PROCESSING, VOL. 51, NO. 1, JANUARY 2003

[9]. Pal, U., Sinha, S., and Chaudhuri, B. B. (2003). Multioriented english text line identification. In Proceedings of the 13th Scandinavian conference on Image analysis, pages 1146–1153.

[10]. Chiang, Y.-Y. and Knoblock, C. A. (2010). An approach for recognizing text labels in raster maps. In Proceedings of the 20th ICPR, pages 3199–3202.

INVESTIGATION OF FREQUENCY DEPENDENT PARAMETER OF GEWE-SiNW MOSFET FOR MICROWAVE AND RF APPLICATIONS

Neha Gupta[1], Ajay Kumar[2] and Rishu Chaujar[3]
[1]Department of Engineering Physics, DTU, Delhi (India)
[2]Department of Engineering Physics, DTU, Delhi (India)
[3] Assistant Professor, Department of Engineering Physics, DTU, Delhi (India)

ABSTRACT

This paper presents the RF and high frequency performance of Gate Electrode Workfunction Engineered-Silicon Nanowire (GEWE-SiNW) MOSFET and the results so obtained are compared with Silicon Nanowire (SiNW) and Conventional MOSFET by using DEVEDIT-3D and ATLAS device simulator. The simulation results unfold the reduction in parasitic capacitances and lowering of intrinsic delay in GEWE-SiNW MOSFET. Furthermore, significant improvement in stern stability factor (K) has also been observed for GEWE-SiNW MOSFET as compared to conventional and SiNW MOSFETs, thus, reinforcing its use for high frequency wireless applications.

Keywords: Cut-Off Frequency (F_t), GEWE, Maximum Frequency (F_{max}), RF, Stability.

I. INTRODUCTION

The rapid growth of the mobile telecommunication markets emphasizes the need for reliable analog IC design at high frequencies. The RF performance of the Silicon MOSFET has been improved considerably during the late 1990s and early 2000s due to scaling of MOSFET. The reduction of the channel length in CMOS technologies has significantly improved the high frequency properties of the MOSFETs, making CMOS technology suitable for wireless communications and other RF applications [1-2]. Although, scaled technologies leads to undesirable effects such as short channel effects, leakage current, hot carrier effects (HCE), parasitic capacitances which results in degradation of device characteristics such as transconductance, voltage gains, subthreshold slope etc., which is unsuitable for RF/wireless applications [3]. GAA SiNW MOSET [4] is getting more attention for its advantages of small DIBL, small subthreshold swing etc. Also, it has found that their cut-off frequency can be much larger than that of planar Si-MOSFET [5]. Further, to enhance the carrier efficiency of a device, Zhou and Long [6] in 1999 proposed the concept of GEWE. With this scheme there is appreciable reduction in short channel effects and improvement in on-current due to step potential profile at the interface of metal gates owing to difference in metal workfunctions which results in enhanced lateral electric field allowing the carriers to travel faster hence improving the gate transport efficiency. Moreover, integration of GEWE scheme onto SiNW MOSFET ameliorates device efficiency, enhanced driving capability, minimizes short channel effects etc. [7-8]. Also, due to the increased demand for high-speed electronics products, the accurate analysis of the MOSFET at high frequencies (HF) is requisite to represent the behavior of device in microwave circuits and systems [9]. In

this work, TCAD simulation tool is used to evaluate RF figure of merits of GEWE-SiNW MOSFET in terms of enhanced digital and RF performance of scaled devices in comparison to its conventional counterparts.

II. DEVICE STRUCTURE AND SIMULATION

Fig.1 shows a schematic cross-sectional view of GEWE-SiNW MOSFET where L1 and L2 are lengths of two different gate materials with workfunction Φ_{M1}=4.8eV and Φ_{M2}=4.4eV respectively. For n-channel MOSFET, we select two gate materials in such a way that the gate material having highest work function is placed near the source end and the gate material having lowest workfunction is placed near the drain end.

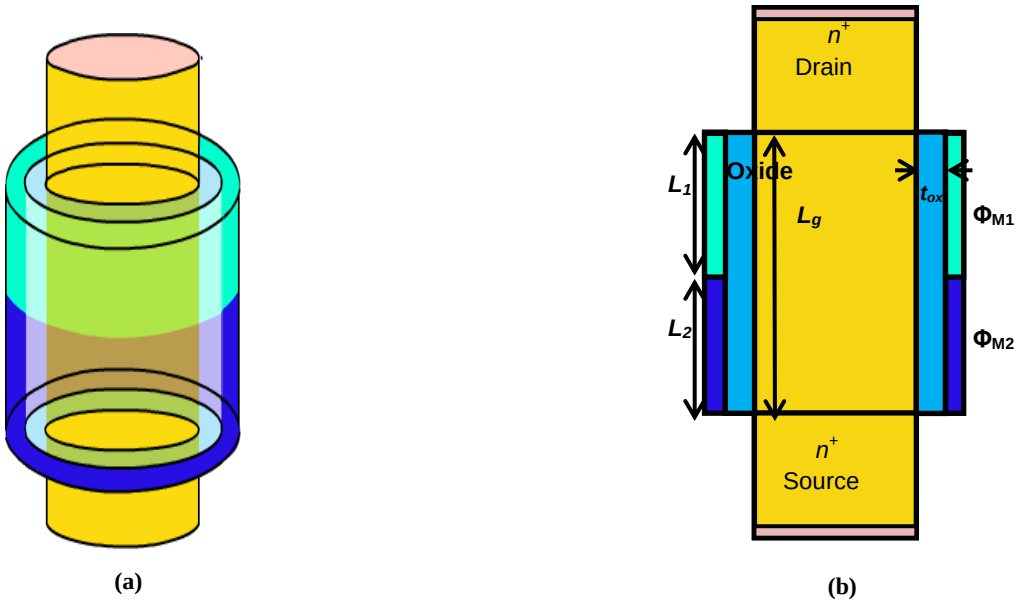

Fig. 1(a-b): Simulated structure and cross section of GEWE-SiNW MOSFET respectively

All the simulations have been performed using physical models accounting for the electric field-dependent and concentration-dependent carrier mobilities, Shockley–Read–Hall recombination/generation with doping dependent carrier lifetime, inversion layer Lombardi CVT mobility model, wherein concentration-dependent mobility, high field saturation model are all included [10]. In our simulation, we have adopted the hydrodynamic energy transport model which includes all nonlocal effects and is more accurate than the drift-diffusion method.

III. RESULTS AND DISCUSSION

In this paper, we compare GEWE-SiNW MOSFET with its conventional counterparts. The present analysis is carried out for a channel length, L_g=30 nm, radius of NW, R=5nm and thickness of oxide, t_{ox}= 1.5 nm, substrate doping concentration is $1\times10^{16}cm^{-3}$. It is evident from Fig. 2(a-c) that GEWE-SiNW exhibits smaller C_{SG}, C_{DG} and C_{DS} in comparison to its conventional MOSFET at 240 GHz due to metal gate workfunction difference which results in improved screening of conducting channel from drain variations. In addition, due to Silicon nanowire carrier mobility across the channel is enhanced [11-12], thereby reducing the parasitic capacitances. The higher value of these capacitances acts as an obstruction in device switching performance due to increase in the turn-on delay time.

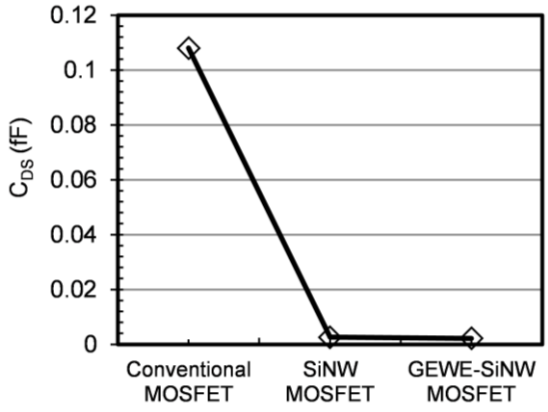

2(a)

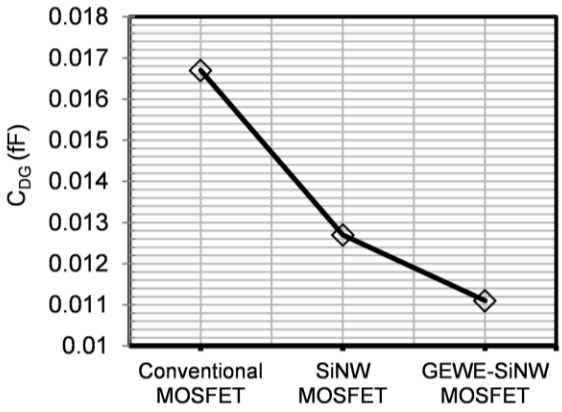

2(b)

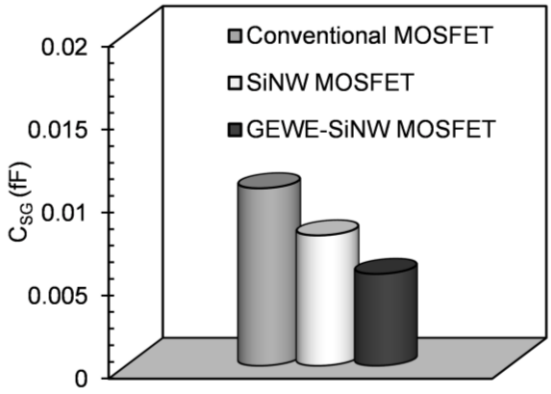

2(c)

Fig. 2 (a-c): Parasitic capacitance (femto farad) of Drain to source, Drain to Gate and Source to gate for Conventional, SiNW and GEWE-SiNW MOSFET respectively at 240 GHz.

The stern stability factor (K) determines the stability of a device. This factor estimates whether the device is conditionally/unconditionally stable. It must satisfy the condition K>1 for a device to be unconditionally stable [13-15].

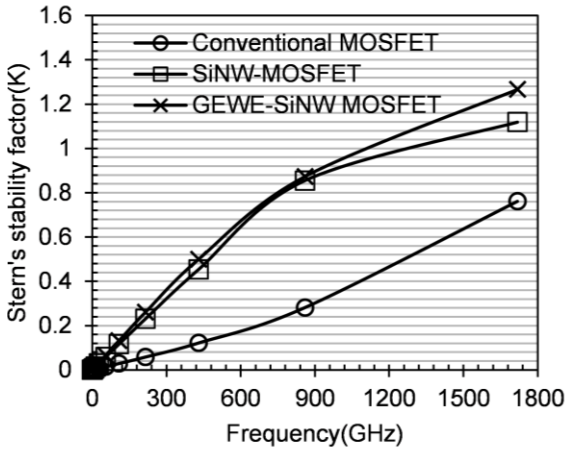

Fig. 3: Variation of Stern's stability (K) factor for Conventional, SiNW and GEWE-SiNW MOSFET

Fig. 3 shows the variation of stern's stability factor at higher frequencies. As is clear from the figure, K is significantly larger (greater than 1) as frequency increases, for GEWE-SiNW MOSFET in comparison to its counterpart where K is approaching 1.1 in SiNW MOSFET and 0.76 in conventional MOSFET. This is due to increased control of gate, which causes maximum power transfer from source to load. Hence, GEWE-SiNW is suitable for Low noise amplifier and RF applications.

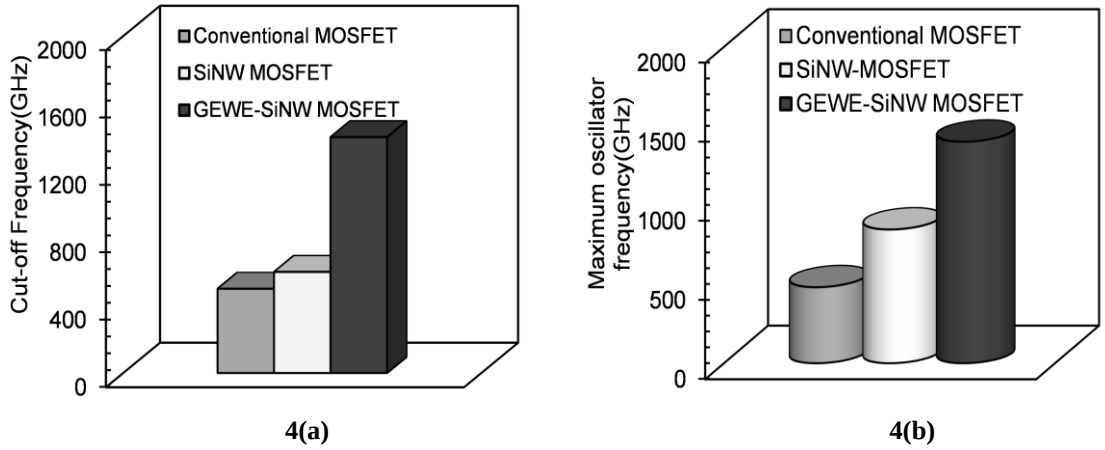

4(a) **4(b)**

Fig. 4: (a-b) Maximum oscillator frequency and Cut-off frequency for Conventional, SiNW and GEWE-SiNW MOSFET respectively

Further, the cut-off frequency f_T is the frequency when the current gain is unity, whereas f_{MAX} is the frequency when the power gain is unity [16-17]. f_T is a specification for high-speed digital applications (speed and high swing) while f_{MAX} analogous to the transit frequency of the maximum available power gain that is a realistic parameter of the optimization of microwave amplifiers. The f_{MAX}, as is seen from Fig.4 (a), for GEWE-SiNW MOSFET, is higher than for SiNW and Conventional MOSFET, which shows large parasitic capacitance in the conventional and SiNW MOSFET, thereby giving the GEWE-SiNW design a new strength for switching applications and wireless communication. Also, the use of metal gates results in reduced gate resistance, and hence increases in f_{MAX}. Fig. 4(b) shows the cut-off frequency of GEWE-SiNW MOSFET is greater than the cut-off frequency for bulk MOSFET. Due to the enhanced gate control over channel and screening of potential from drain side, it reduces the short channel effects and enhances the transconductance, leading to increase the cut-off frequency and packing density, thereby making the device suitable for CMOS wireless applications.

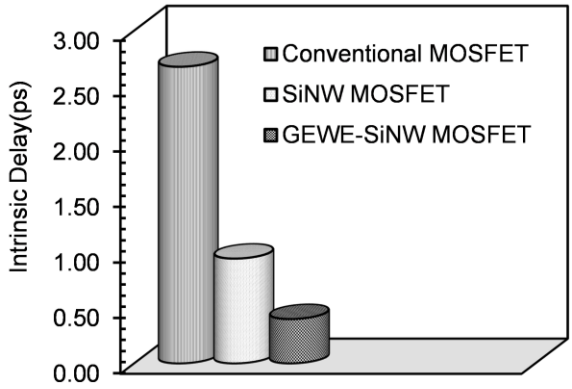

Fig. 5: Intrinsic Delay for Conventional, SiNW and GEWE-SiNW MOSFET

The increasing capacitance between the gate and the overlapped S/D region degrades the intrinsic gate delay. Fig. 5 shows the comparison of GEWE-SiNW with SiNW and conventional MOSFET in terms of intrinsic delay parameter. As is evident from the figure, there is notable reduction in intrinsic delay of GEWE-SiNW MOSFET than its conventional counterparts due to cylindrical gate which increases on-current, reduces parasitic capacitances and incorporation of two dissimilar metal gates, which leads to considerable reduction of intrinsic delay by 55.5%.

IV. CONCLUSION

In this work, we have investigated the improved RF performance of GEWE-SiNW MOSFET and compared it with conventional and SiNW MOSFET, it has been scrutinized that GEWE SiNW MOSFET exhibit lower parasitic capacitances, enhanced cut-off and maximum frequency with an appreciably low intrinsic delay, hence suitable for RF/wireless applications. Furthermore, GEWE-SiNW is found to be more stable than its conventional counterparts, thereby providing its efficacy for high-performance RF applications.

V. ACKNOWLEDGMENT

The authors would like to thank the Microelectronics Research Lab, Department of Engineering Physics, Delhi Technological University (formerly DCE) and one of the authors (Neha Gupta) is grateful to the University Grant Commission (UGC) for providing the necessary financial assistance to carry out this research work.

REFERENCES

[1] Larson, L. E., "Silicon technology tradeoffs for radio-frequency/mixed-signal system-on-a-chip", IEEE Trans Electron Devices 50(3), 2003, 683–99.

[2] Saijets. J., Andersson. M. and Berg. M. A., "A Comparative Study of Various MOSFET Models at Radio Frequencies", Analog Integrated Circuits and Signal Processing 33(1), 2002, 5–17

[3] Chen. Q., "Compact Modeling of Multi-Gate MOSFETs for RF Designs", IEEE International Wireless Symposium, Bejing , 2013, 1-4

[4] Kim. D. W., Yeo. K. H., Suk. S. D., Li. M., Yeoh. Y. Y., Kyun. S. D. and Chung. C., "Fabrication and electrical characteristics of self-aligned (SA) gate-all-around (GAA) Si nanowire MOSFETs (SNWFET)", IC Design and Technology (ICICDT), IEEE International Conference, 2010, Grenoble, 63-66.

[5] Wang. C., Zhuge. C., Huang. R., Tian. Y., Xiao. H., Zhang. L., Li. C., Zhang. X. and Wang. Y., "Analog/RF performance of Si nanowire MOSFETs and the impact of process variation", IEEE Trans. Electron Devices 54(6), 2007, 1288–1294.

[6] Long. W. and Chin. K. K., **"**Dual Material Gate Field Effect Transistor (DMGFET)", Electron Devices Meeting Tech Dig., 1999, Washington, DC, USA, 549-552.

[7] Gupta. N and Chaujar. R, "Implications of Transport models on the analog performance of gate electrode workfunction engineered (GEWE) SiNW MOSFET", IEEE Second International conference on Devices, Circuits and Systems (ICDCS'2014), 2014, Coimbatore, India, 278-282.

[8] Gupta. N, Chaujar. R and Kumar. A, "Simulation analysis of Gate Electrode Workfunction Engineered (GEWE) Silicon Nanowire MOSFET for hot carrier reliability", IEEE 1st International conference on Microelectronics, Circuits and Systems, 2014, Kolkata, India, 150-153

[9] Doan. C.H., Emami. S., Niknejad. A.M. and Brodersen. R.W., "Millimeter-wave CMOS design", IEEE J. Solid-State Circuits 40(1), 2005, 144–155.

[10] ATLAS User's Manual, SILVACO Int., Santa Clara, 2011, CA.

[11] Frey. M., Esposito. A. and Schenk. A., "Computational comparison of conductivity and mobility models for silicon nanowire devices", J. Appl. Phys. 109(8), 2011, 083707 - 083707-6

[12] Ramayya. E. B., Vasileska. D., Goodnick. R.W. and Knezevic. I., "Electron Mobility in Silicon Nanowires", IEEE Transactions on Nanotechnology, 6(1), 2008, 113-116.

[13] Voldman. S. H., (ESD: RF technology and circuits, Wiley, 2006)

[14] Cho. S., Kim. K. R., Park. B. G. and Kang. I. M., "RF performance and small-signal parameter extraction of junctionless silicon nanowire MOSFETs", IEEE Trans. Electron Devices 58(5), 2011, 1388–1396.

[15] Oh. Y. and Rieh. J. S., "Effect of Device Layout on the Stability of RF MOSFETs", IEEE Transactions on Microwave Theory and Techniques 61(5), 2013, 1861-1869.

[16] Nae. B., Lazaro. A. and Iniguez. B., "High Frequency and Noise Model of Gate-All-Around MOSFETs, Spanish Conference on Electron Devices", 2009, Santiago de Compostela, 112-115.

[17] Sarkar. A., De. S., Dey. A. and Sarkar. C. K., "Analog and RF performance investigation of cylindrical surrounding-gate MOSFET with an analytical pseudo-2D model", Journal of Computational Electronics, 2012, 11(2), 182-185.

Biographical Notes

Mrs. Neha Gupta is presently working as a Ph. D Research Scholar in Engineering Physics Department from Delhi Technological University (DTU), Delhi, India.

Mr. Ajay Kumar is presently working as Ph. D Research Scholar in Engineering Physics Department from Delhi Technological University (DTU), Delhi, India.

Dr. Rishu Chaujar is working as an Assistant Professor in Engineering Physics Department from Delhi Technological University (DTU), Delhi, India.

CDTA BASED CURRENT MODE ADC

Neeta Pandey[1], Rajeshwari Pandey[2], Ranjana Sridhar[3], Veepsa Bhatia[4], Alok Kumar Singh[5], Pradeep Kumar[6]

[1,2,3,4,5,6] *Department of Electronics and Communication Engineering*
Delhi Technological University, Delhi, (India)

ABSTRACT

This paper presents a CDTA based current mode analog to digital converter which shows the usefulness of CDTA as a building block in ADC design. The circuit is simple and is suitable for IC implementation as no external resistors or capacitors are required. The functionality of the circuit is verified with SPICE simulation using 0.35 μm CMOS technology parameters.

Keywords:Active Block; CDTA; Current Mode; Comparator; Flash ADC

I INTRODUCTION

Signal processing is an important part of myriad systems around us. The input signals be they speech, temperature, voltage, current etc. are in analog form and can be processed directly. But with the advent of digital signal processing two main advantages could be had: higher accuracy and faster processing of complex manipulations. Digital signal processing is a critical part diverse system like telecommunication, audio processing, medical diagnostic imaging, function generation etc.

In digital signal processing or other digital instruments, sensors measure process variables which are in the form of analog signals. Then an electronic circuit, termed the analog-to-digital converter (ADC), converts the analog signals into equivalent digital representation of required accuracy that can be stored and processed. The overall speed and accuracy of the digital signal processing system is influenced by the speed and accuracy of analog to digital conversion as processing is carried generally on high speed special purpose microprocessor or microcontroller. Thus, the design of an ADC is very crucial as it determines the speed, accuracy, power dissipation of the digital signal processing system.

These days, current mode circuits are gaining popularity because of the advantages offered such as wider bandwidth and the capability for working under low voltage [1]. Most modern designs employ voltage mode elements like op-amps for implementation of various electronic circuits. These elements are used widely due to their small sizes and good performance. With the demand for portable battery powered equipment increasing, designers have begun to look into different architectures to fit these demanding designs. This issue is not easily solved with voltage mode elements since the voltage supply if reduced will cause problems with realizing good, fully-functional circuits. Instead, current mode (CM) elements are now being considered for the same circuits and these issues can then be addressed.

IJARSE

In this paper we present the design of a current mode ADC using the recently introduced active building block (ABB) current differencing transconductance amplifier (CDTA). The CDTA is characterized by large bandwidth and close-to-ideal terminal impedances. CDTA is a versatile sub circuit like the op-amp whose use in variety of applications in current mode signal processing, sinusoidal oscillators [2-13] has been explored. But, CDTA has not been used in applications like current mode ADCs and hence to check its viability, the paper focuses on this aspect. Section II discusses the basics of CDTA followed by Section III which enumerates the concept of CDTA based ADC. In Section IV, simulation results are presented followed by conclusion.

II CDTA BASICS

The circuit symbol of the CDTA is shown in Fig. 1 and the corresponding CMOS implementation in Fig. 2 [14] respectively. For Fig. 1, the terminal relationships can be described as $V_p=V_n=0$, $I_z = I_p - I_n$, $I_{x+} = g_m V_z$, $I_{x-} = -g_m V_z$, where V_p, V_n, V_x and V_z are the voltages at p , n, x and z terminals respectively, I_x is the output current at x terminal, I_0 is the input bias current and g_m represents transconductance. Here, from output terminal x, currents are equal in magnitude, but they flow in opposite directions, and the product of transconductance (g_m) and the voltage at the z terminal gives their magnitudes.

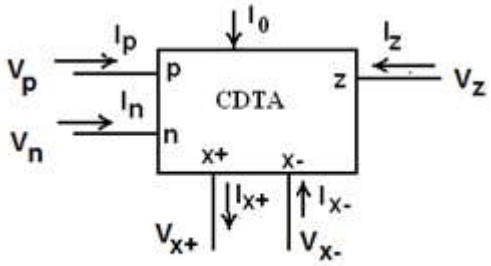

Fig. 1 Circuit symbol for CDTA

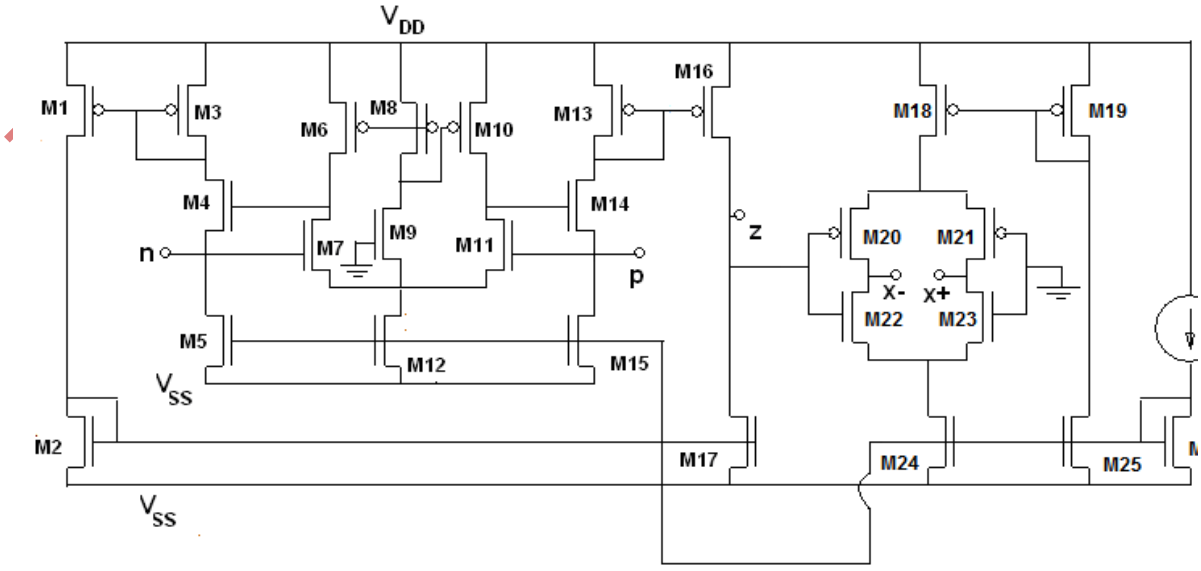

Fig. 2 CMOS CDTA implementation [14]

The p and n terminals are a pair of low-impedance current inputs and auxiliary terminal z has outgoing current which is the difference of input currents. Therefore, CDTA can be thought of as a combination of a current differencing unit followed by a dual-output operational transconductance amplifier, DO-OTA.

III CDTA BASED ADC

Current mode ADC plays an important role in front end signal processing and the design of a current mode ADC using CDTA is presented in this section. A current mode comparator performs comparison between two input currents and gives binary output voltage depending on which input current is greater. Generally, one of the two input currents is a constant, known as the reference current. The output equation of current comparator can be represented as in (1) where Ip(t) and In(t) are input currents and v_{out} is the output voltage.

$$v_{out}(t)=1, \text{ for } Ip(t)>In(t) \quad (1)$$

$$0, \text{ for } In(t)>Ip(t)$$

The input current and the reference current is supplied to p and n terminals of CDTA. The z terminal is left open therefore the voltage at X+ and X- terminals i.e. V_{X+} and V_X saturate at V_{DD} or V_{SS} [7]. The output of the CDTA is taken from X+ terminal and two cascaded CMOS inverters are used to bring the output voltage to 0-V_{DD} range.

The general schematic of a 2-bit current mode flash ADC is shown in Fig. 3. A flash ADC has the highest speed of any type of ADC [15]. It uses one comparator per quantization level and the 2^N -1 reference currents are generated and fed to each comparator. The input signal is compared to the reference level and the output of each comparator is a binary 1 or 0. The output of all the comparators together forms a thermometer code which is converted into binary code using a code converter circuit. The thermometer to binary encoder was designed using transmission gates and the implementation is shown in Fig. 4 with thermometer code (C1, C2 and C3) and the binary output (B0 and B1). The Boolean expression for the thermometer to binary code conversion is represented by (2) and (3).

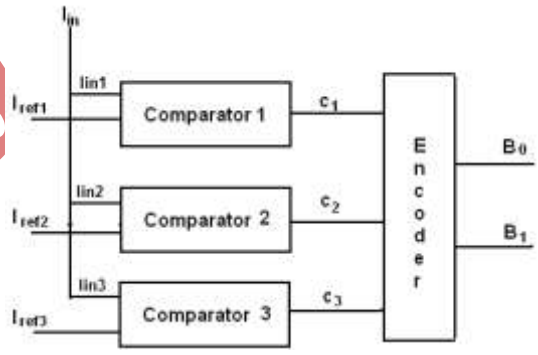

Fig. 3 2 bit Flash ADC

$$B_0 = C_1 * C_2 + C_3 * \overline{C_2} \quad (2)$$

$$B_1 = C_2 \quad (3)$$

IJARSE

The ADC was designed to work in the current range 0-40µA with a step size of 10µA. The reference currents I_{ref1}, I_{ref2}, I_{ref3} were accordingly set at 5µA, 15µA and 25µA respectively. The input current was mirrored into I_{in1}, I_{in2} and I_{in3} using a regulated cascode current mirror. The performance of the ADC is generally characterized by the parameters resolution, sampling rate, INL, DNL, offset and gain error. These parameters were measured through simulations and are presented in the simulation section.

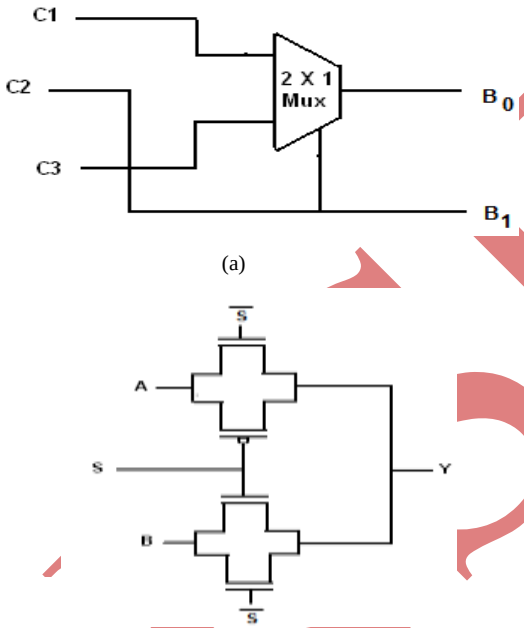

Fig. 4 (a) Encoder using multiplexer (b) TG based multiplexer implementation

IV SIMULATION RESULTS

The 2-bit flash current mode ADC using CDTA was implemented in 0.35µm CMOS technology in ORCAD PSIPCE and the corresponding transistor widths are reported in Table I. All the transistor lengths were set at 0.7 µm . The simulation conditions are reported in Table II.

TABLE I. TRANSISTOR DIMENSIONS FOR CMOS CDTA-ADC

Transistor No.	W(µm)
M1	9.8
M2-3,M13, M16-17	10.5
M4, M14	42
M5,M12,M15	35
M6,M8,M10, M21	28
M7,M9,M11	70
M18, M24-25	56
M19	58.8
M20	28.7
M22-23	16.1
M26	7

TABLE II. SIMULATION CONDITION FOR CDTA BASED CURRENT MODE ADC

Temperature	27°C
Technology	0.35µm CMOS
Power Supply	1.8 V
Iref$_{i=1,2,3}$	5µA,15µA, 25µA

The CDTA based ADC was fed with input current in the range of 0-40µA and DC analysis was carried out. The corresponding output for is shown in Fig. 5. The input currents at which the ADC output transitions occurred were noted and these were used to construct the actual ADC transfer characteristic. This is shown in Fig. 6 along with the ideal ADC transfer characteristic and it is seen that the ADC doesn't suffer from missing codes. The DNL and the INL were calculated from Fig. 6 and are plotted in Fig. 7 and Fig. 8 respectively. The DNL is -0.45LSB and the INL is -0.000225LSB and both are much lower than the maximum value of half of least significant bit (LSB), with LSB/2= 5 µA. The offset and the gain error were calculated as 0.5µA and 0.98 respectively. To characterize the speed of the CDTA based ADC, transient analysis was performed by feeding input pulse of 0-40 µA amplitude and frequency 500 KHz. The maximum delay under the above input conditions was found to be 81.332ns. The ADC was also subjected to sine input of frequency 6 MHz and it showed correct output as demonstrated by Fig. 9.

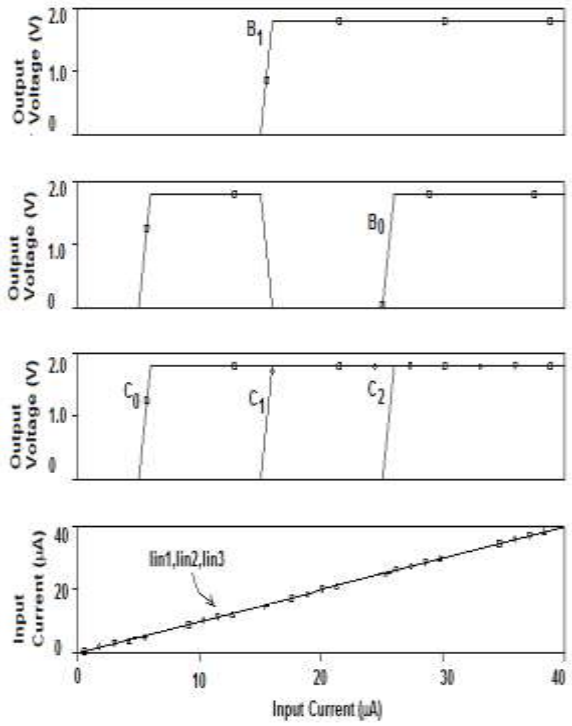

Fig. 5 ADC output for ramp input

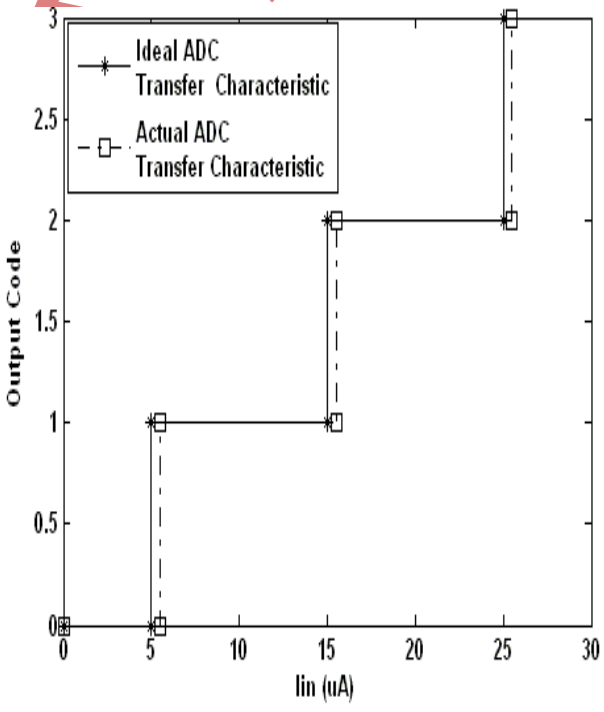

Fig. 6. Ideal and simulated ADC characteristics

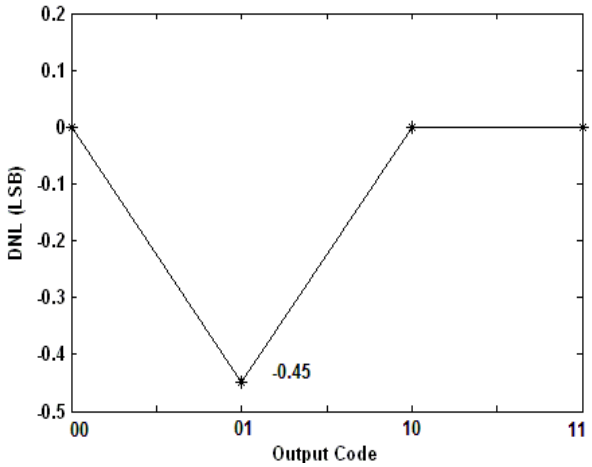

Fig. 7DNL versus Otput Code

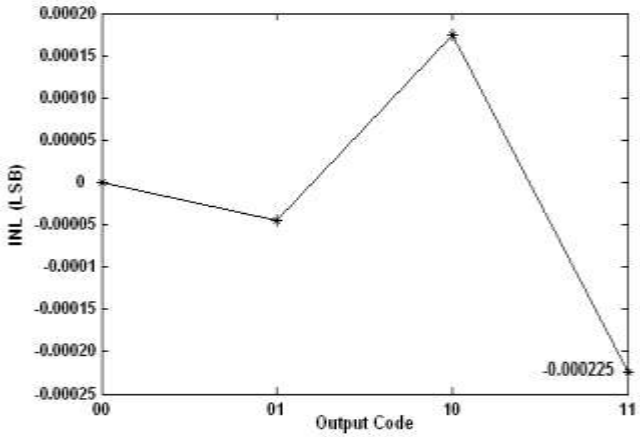

Fig. 8 INL versus Output Code

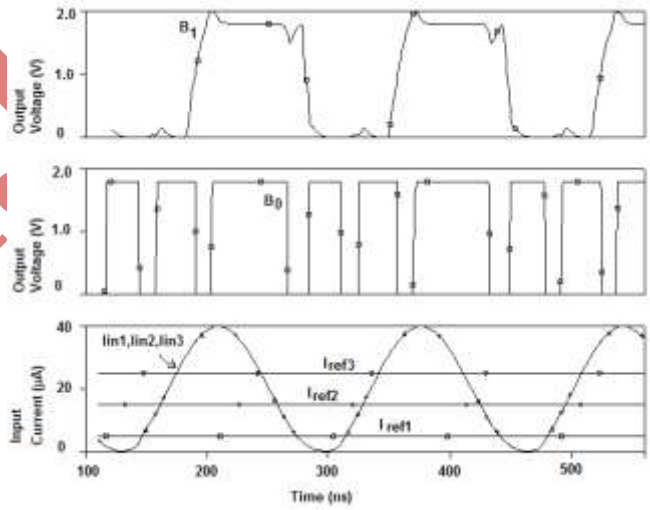

Fig. 9 ADC Output For Input Sine of Frequency 6 Mhz

V CONCLUSION

In this paper, a newly introduced active building block the current differencing transconductance amplifier (CDTA) is used for implementation of a current mode ADC. This application of CDTA has not yet been enumerated elsewhere and the results from the simulation section are promising. The INL and DNL of the CDTA based ADC is much lower than the maximum value of half of least significant bit (LSB). It also shows a delay of around 80ns at an input pulse of 500 KHz.

REFERENCES

[1] F. Yuan, "CMOS Current-Mode Circuits for Data Communications", Springer, 2007.

[2] D. Biolek, "CDTA- Building block for current-mode analog signal processing", Proceedings of ECCTD 03, Poland, Vol. III, pp. 397-400, 2003.

[3] A.U. Keskin, D. Biolek, E. Hancioglu and V. Biolkova, "Current-mode KHN filter employing current differencing transconductance amplifier", AEU- International Journal of Electronics and Communications, 60 (6), 2006, 443-446.

[4] A. Uygur, H. Kuntman and A. Zeki, "Multi-input multi-output CDTA-based KHN filter", Proc. of ELECO: The 4th International Conference on Electrical and Electronics, pp. 46-50, 2005.

[5] W. Tangsrirat, T. Dumawipata and W. Surakampontorn, "Multiple input single-output current-mode multifunction filter using current of Electronics and Communications, 61, 2006, 209-214.

[6] A. Uygur and H. Kuntman, "Seventh order elliptic video filter with 0.1dB pass band ripple employed CMOS CDTAs", AEU- International Journal of Electronics and Communications, 61, 2007, 320-328.

[7] N. Pandey and R. Pandey, "Current Mode Full-Wave Rectifier Based on a Single MZC-CDTA", Active and Passive Electronic Components, Volume 2013 (2013), Article ID 967057, 5 pages.

[8] A.U. Keskin and D. Biolek, "Current mode quadrature oscillator using current differencing transconductance amplifiers (CDTA)", IEE Proc.-Circuits Devices and Systems, 153(3), 2006, 214-218.

[9] D. Prasad, D.R. Bhaskar and A.K. Singh, "Realisation of Single-Resistance-Controlled Sinusoidal Oscillator: A new application of the CDTA", WSEAS Transactions on Electronics, 5(6), 2008, 257-259.

[10] W. Jaikla, M. Siripruchyanun, J. Bajer and D. Biolek, "A Simple Current-Mode Quadrature Oscillator Using Single CDTA", Radio engineering, 17(4), 2008, 33-40.

[11] A. Lahiri, "New current-mode quadrature oscillators using CDTA", IEICE Electronics Express, 6(3), 2009, 135-140.

[12] A. Lahiri, "Novel voltage/current-mode quadrature oscillator using current differencing transconductance amplifier", Analog Integrated Circuits and Signal Processing, 61(2), 2009, 199-203.

[13] W. Tangsrirat, "Current differencing transconductance amplifier-based current-mode four-phase quadrature oscillator", Indian Journal of Engineering and Materials Sciences, 14(7), 2007, 289-294.

[14] D. Biolek, E. Hancioglu, A. Ü. Keskin, High-performance current differencing transconductance amplifier and its application in precision current-mode rectification, International Journal of Electronics Communication (AEÜ), 62, 2008, 92 – 96.

[15] R.J.Baker, CMOS Circuit Design,Layout and Simulation, IEEE Press Series on Microelectronics, Second Edition.

IJARSE

This article has been accepted for publication in a future issue of this journal, but has not been fully edited. Content may change prior to final publication. Citation information: DOI 10.1109/TIE.2014.2371431, IEEE Transactions on Industrial Electronics

Control of DC-Fault-Resilient Voltage Source Converter Based HVDC Transmission System under DC Fault Operating Condition

Nima Yousefpoor, *Student Member, IEEE,* Ajit Narwal, and Subhashish Bhattacharya, *Senior Member, IEEE*

***Abstract*—Voltage source converter (VSC) based High Voltage Direct Current (HVDC) transmission systems have attractive advantages compared to classical thyristor based HVDC transmission systems. However, VSC based HVDC transmission systems are vulnerable to DC side fault, and expensive DC circuit breakers are required to protect them against DC fault. This paper proposes a control method of a DC fault resilient voltage source converter which can be protected against DC fault without using expensive DC circuit breakers. In the VSC configuration, several H-bridge modules are connected in cascade, so the voltage balancing control of several floating DC capacitors is required. In this paper, an appropriate control structure with the capacitor voltage balancing controller is proposed. The appropriate control algorithm for DC fault operation and recovery after DC fault is also proposed. PSCAD simulation results are presented to validate the proposed control structure under normal and DC fault operating conditions. Real Time Digital Simulator (RTDS) results are also presented to verify the control structure.**

***Index Terms*— Voltage Source Converter (VSC), HVDC transmission systems, Capacitor Voltage Balancing Controller, DC Fault, Recovery after DC Fault.**

I. Introduction

Voltage Source Converter (VSC) based High Voltage Direct Current (HVDC) transmission systems have attractive features compared to classical thyristor based HVDC transmission systems. Flexibility in bidirectional power flow control is the main advantage of VSC based HVDC transmission systems [1-2]. However, the VSC based HVDC transmission system is susceptible to DC side fault, and expensive DC circuit breakers are necessary to protect the converter against DC fault [3-4].

DC circuit breakers can be used to achieve DC fault clearance, but the availability of DC circuit breakers with High voltage and large current is so limited [5]. Recently, several topologies with dc fault ride through capability have been proposed. Full bridge Modular Multi-level Converter (MMC) [6] can clear dc-link fault current. However, in this topology, the galvanic isolation is not provided in the VSC configuration. In HVDC transmission systems, the proposed structure should be able to provide the isolation between two different high voltage sources. This paper proposes a control method of a DC fault resilient converter with high frequency isolation and ultra-fast electronic isolation capability following DC fault which can be protected against DC fault without using expensive DC circuit breakers. In this topology, the high frequency isolation is also provided [7].

In the VSC configuration proposed by [7], several AC/DC modules in all three phases are connected in series, so the voltage balancing control of multiple floating dc capacitors is required. In this paper, the phase voltage balancing controller is proposed to ensure that the sum of capacitor voltages of A-phase is equal to the sum of capacitor voltages of B-phase and C-phase. The common mode point voltage is used to perform phase voltage balancing control. The module voltage balancing controller [8-9] is also used to guarantee that the capacitor voltage of each module in each phase is similar to the capacitor voltage of other modules in that phase.

Both DC cables and overhead transmission lines can be used for the HVDC transmission systems. Although DC cables are mostly used, but the application of DC cables in some mountainous areas is limited. In these areas, DC overhead lines are used. In DC overhead lines, DC-link short circuit is so common because of insulation breakdown following lightning strikes [10-11]. In this paper, the detailed control algorithm is proposed to protect the VSC based HVDC transmission systems against DC faults on DC overhead lines.

In the following, this paper is organized as follows. In section II, the VSC based HVDC transmission system configuration is briefly explained. In section III, the control structure of VSC configuration under normal operating condition is proposed. In section IV, the appropriate control algorithm for DC fault operating condition and recovery after DC fault is presented. Section V explores the dynamic performance of VSC based HVDC system under DC fault operating condition through PSCAD simulation. In section VI, Real Time Digital Simulator (RTDS) simulation results are

Manuscript received April 30, 2014; revised August 20, 2014 and September 29, 2014; accepted October 24, 2014.

Copyright (c) 2014 IEEE. Personal use of this material is permitted. However, permission to use this material for any other purposes must be obtained from the IEEE by sending a request to pubs-permissions@ieee.org.

N. Yousefpoor, A. Narwal, and S. Bhattacharya are with the North Carolina State University, Raleigh, NC, USA (e-mail: nyousef@ncsu.edu; anarwal@ncsu.edu; sbhattacharya@ncsu.edu).

0278-0046 (c) 2013 IEEE. Personal use is permitted, but republication/redistribution requires IEEE permission. See http://www.ieee.org/publications_standards/publications/rights/index.html for more information.

This article has been accepted for publication in a future issue of this journal, but has not been fully edited. Content may change prior to final publication. Citation information: DOI 10.1109/TIE.2014.2371431, IEEE Transactions on Industrial Electronics

presented to verify the proposed control algorithms. Finally, Section VII presents the concluding remarks.

II. Voltage Source Converter Based HVDC Transmission System Configuration

In this section, the configuration of Voltage Source Converter (VSC) based HVDC transmission system is explained. The configuration of VSC based HVDC transmission system is shown in Fig. 1. Every power conversion module consists of two stages: AC/DC converter and High frequency link DC/DC converter as shown in Fig. 2. As can be seen, the isolation is also provided by the high frequency transformer in DC/DC converter.

III. Control Structure of Voltage Source Converter Based HVDC Transmission System

In this section, the control scheme of VSC based HVDC transmission system is presented. In this configuration, several floating DC capacitors in all three phases are connected in series. So, the voltage balancing algorithm is required to match the DC capacitor voltages in all power electronic building blocks. The voltage balancing algorithm is implemented in AC/DC sub-module. The control scheme for AC/DC sub-module has four layers including power flow controller, DC bus voltage controller, phase voltage balancing controller, and module voltage balancing controller. The detailed control scheme of each layer is shown in Fig. 3. In the following, each part of the proposed controller will be explained in detail.

A. Power Flow Controller

Power flow controller determines the reference value of DC bus voltage of each terminal. For power flow control, DC overhead line can be simply modeled with inductor and resistor as shown in Fig. 4. The DC bus voltage at the sending-end and receiving-end terminal can be defined as (1) and (2) respectively. The transferred power is defined as the average power of the sending-end and the receiving-end power as (3).

$$V_{dcT1} = V_{dcave} + 0.5\Delta V \tag{1}$$

$$V_{dcT2} = V_{dcave} - 0.5\Delta V \tag{2}$$

$$P = V_{dcave} I_{dc} = \frac{V_{dcT1} + V_{dcT2}}{2} I_{dc} \tag{3}$$

The DC current can be determined with the DC grid resistance and the voltage difference between two terminals as (4). So, the transferred power can be rewritten with the DC grid resistance and the voltage difference between two terminals as (5). Power flow controller can be implemented as shown in Fig. (3a). As can be seen, the reference values of DC bus voltage for both terminals can be determined according to the reference value of active power flow.

$$I_{dc} = \frac{\Delta V}{R_{dc}} \tag{4}$$

$$P = V_{dcave} \frac{\Delta V}{R_{dc}} = \frac{V_{dcT1} + V_{dcT2}}{2} \frac{\Delta V}{R_{dc}} \tag{5}$$

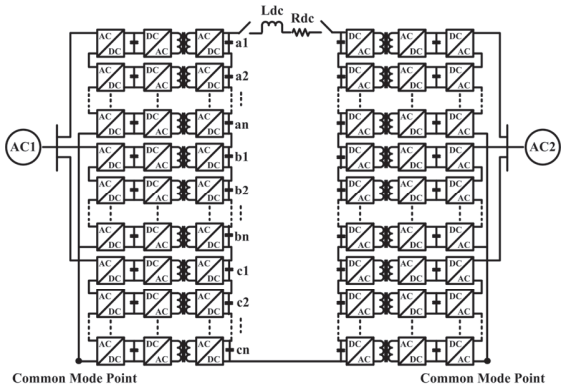

Fig. 1. Voltage source converter based HVDC transmission system.

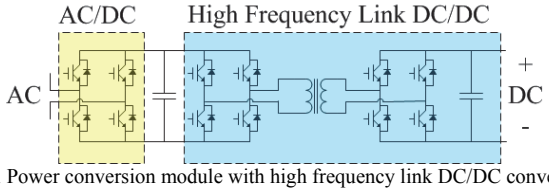

Fig. 2. Power conversion module with high frequency link DC/DC converter.

B. Terminal DC Bus Voltage Controller

Terminal DC bus voltage controller generates the dq-axis current references in the synchronous reference frame. Fig. (3b) shows terminal DC bus voltage controller with the AC current controller in detail.

C. Phase Voltage Balancing Controller

If each phase has *N* power conversion modules, the sum of *N* capacitor voltages of A-phase should be balanced with the sum of *N* capacitor voltages of phase-B and phase-C. The phase voltage balancing can be achieved by controlling the common-mode voltage. Each phase power can be calculated by multiplication of phase voltage and phase current as (6). Based on (6), the phase power can be written as (7)-(9). When the common-mode voltage is considered as (10), the phase power can be expressed as (11)-(13). Each phase power has an average value and a second order harmonic component. The average value of each phase power can be written as (14)-(16). The average value of each phase power with the common-mode voltage can be written in the stationary reference frame as (17).

$$\begin{aligned} &v_a = V_m \cos(\omega t); i_a = I_m \cos(\omega t + \theta_i) \\ &v_b = V_m \cos(\omega t - 2\pi/3); i_b = I_m \cos(\omega t + \theta_i - 2\pi/3) \\ &v_c = V_m \cos(\omega t + 2\pi/3); i_c = I_m \cos(\omega t + \theta_i + 2\pi/3) \end{aligned} \tag{6}$$

$$\begin{aligned} P_a &= v_a i_a = 0.5 V_m I_m \cos(\theta_i) \\ &\quad + 0.5 V_m I_m \cos(2\omega t + \theta_i) \end{aligned} \tag{7}$$

$$\begin{aligned} P_b &= v_b i_b = 0.5 V_m I_m \cos(\theta_i) \\ &\quad + 0.5 V_m I_m \cos(2\omega t + \theta_i + 2\pi/3) \end{aligned} \tag{8}$$

$$\begin{aligned} P_c &= v_c i_c = 0.5 V_m I_m \cos(\theta_i) \\ &\quad + 0.5 V_m I_m \cos(2\omega t + \theta_i - 2\pi/3) \end{aligned} \tag{9}$$

0278-0046 (c) 2013 IEEE. Personal use is permitted, but republication/redistribution requires IEEE permission. See http://www.ieee.org/publications_standards/publications/rights/index.html for more information.

This article has been accepted for publication in a future issue of this journal, but has not been fully edited. Content may change prior to final publication. Citation information: DOI 10.1109/TIE.2014.2371431, IEEE Transactions on Industrial Electronics

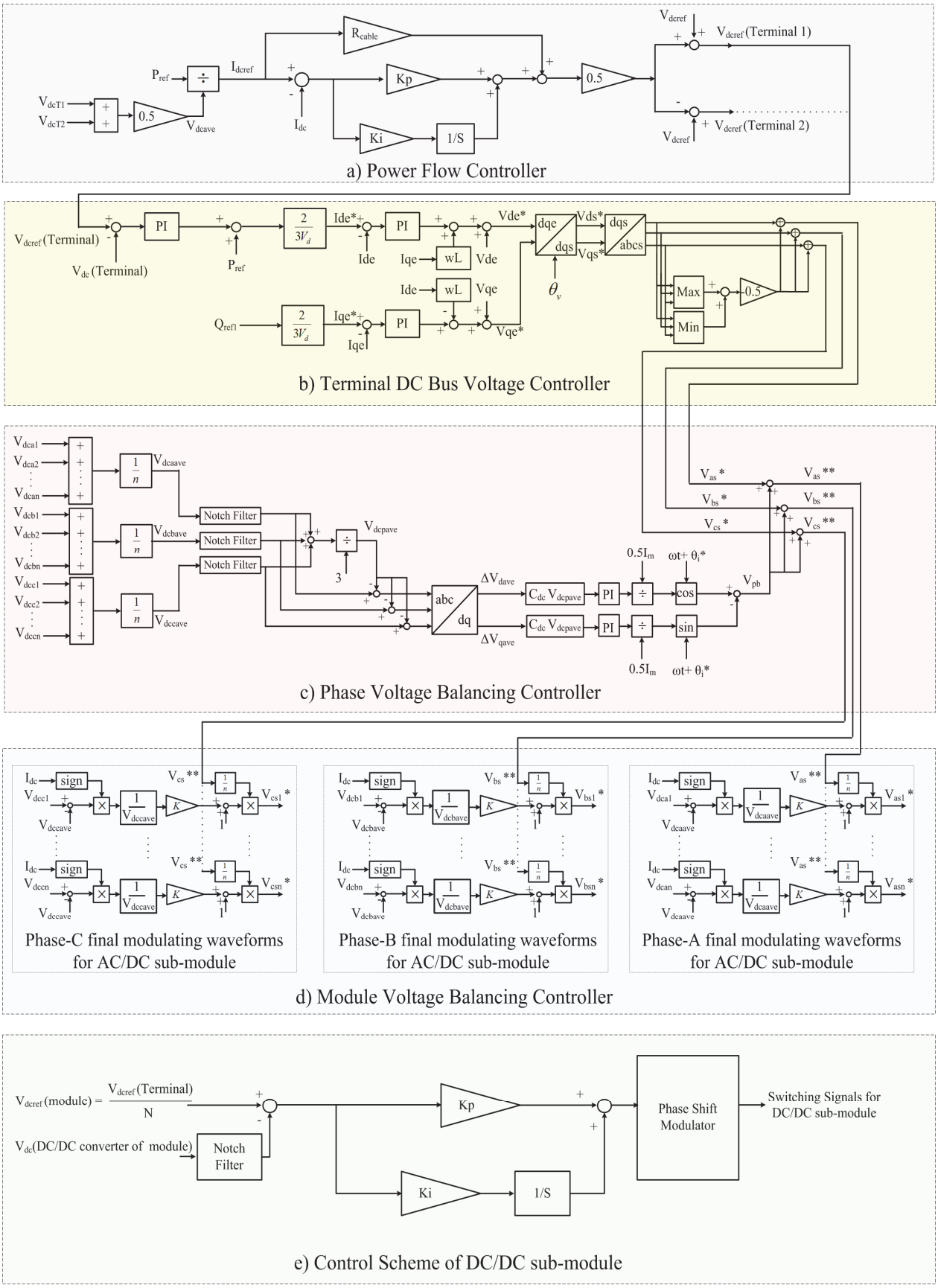

Fig. 3. Detailed proposed control scheme of VSC based HVDC transmission system.

0278-0046 (c) 2013 IEEE. Personal use is permitted, but republication/redistribution requires IEEE permission. See http://www.ieee.org/publications_standards/publications/rights/index.html for more information.

This article has been accepted for publication in a future issue of this journal, but has not been fully edited. Content may change prior to final publication. Citation information: DOI 10.1109/TIE.2014.2371431, IEEE Transactions on Industrial Electronics

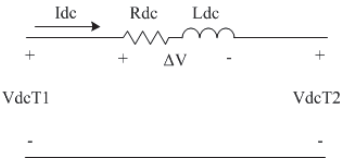

Fig. 4. Two-terminal HVDC transmission system with DC overhead line.

The energy balance in the capacitors for all three phases can be written as (18). This three-phase energy can be expressed in the stationary reference frame as (19). This dq-axis energy variation can be compensated with the common-mode voltage. These energy variations are fed to the PI-controller. The outputs of the PI-controller should be the added power reference to compensate the energy variation as (20). Using (17), the dq-axis power references are transformed to the stationary common-mode voltage as (21). Fig. (3c) shows the phase voltage balancing controller in detail.

$$V_{pb} = V_{cm}\cos(\omega t + \phi) \tag{10}$$

$$P'_a = P_a + 0.5V_{cm}I_m\cos(\phi - \theta_i) + 0.5V_{cm}I_m\cos(2\omega t + \theta_i + \phi) \tag{11}$$

$$P'_b = P_b + 0.5V_{cm}I_m\cos(\phi - \theta_i + 2\pi/3) + 0.5V_{cm}I_m\cos(2\omega t + \theta_i + \phi - 2\pi/3) \tag{12}$$

$$P'_c = P_c + 0.5V_{cm}I_m\cos(\phi - \theta_i - 2\pi/3) + 0.5V_{cm}I_m\cos(2\omega t + \theta_i + \phi + 2\pi/3) \tag{13}$$

$$P'_{aavg} = 0.5V_mI_m\cos(\theta_i) + 0.5V_{cm}I_m\cos(\phi - \theta_i) \tag{14}$$

$$P'_{bavg} = 0.5V_mI_m\cos(\theta_i) + 0.5V_{cm}I_m\cos(\phi - \theta_i + 2\pi/3) \tag{15}$$

$$P'_{cavg} = 0.5V_mI_m\cos(\theta_i) + 0.5V_{cm}I_m\cos(\phi - \theta_i - 2\pi/3) \tag{16}$$

$$\begin{bmatrix} P'_{davg} \\ P'_{qavg} \end{bmatrix} = \frac{1}{2}V_{cm}I_m\begin{bmatrix} \cos(\phi - \theta_i) \\ \sin(\phi - \theta_i) \end{bmatrix} \tag{17}$$

$$\begin{bmatrix} \Delta E_{aavg} \\ \Delta E_{bavg} \\ \Delta E_{cavg} \end{bmatrix} = C_{dc}V_{pavg}\begin{bmatrix} \Delta V_{aavg} \\ \Delta V_{bavg} \\ \Delta V_{cavg} \end{bmatrix} \tag{18}$$

$$\begin{bmatrix} \Delta E_{davg} \\ \Delta E_{qavg} \end{bmatrix} = \frac{2}{3}\begin{bmatrix} 1 & -\frac{1}{2} & -\frac{1}{2} \\ 0 & \frac{\sqrt{3}}{2} & -\frac{\sqrt{3}}{2} \end{bmatrix}\begin{bmatrix} \Delta E_{aavg} \\ \Delta E_{bavg} \\ \Delta E_{cavg} \end{bmatrix} \tag{19}$$

$$\begin{bmatrix} P^*_{dpavg} \\ P^*_{qpavg} \end{bmatrix} = \frac{K_p + K_i s}{s}\begin{bmatrix} -\Delta E_{davg} \\ -\Delta E_{qavg} \end{bmatrix} \tag{20}$$

$$V_{pb} = \frac{\cos(\omega t + \theta_i^*)P^*_{dpavg} - \sin(\omega t + \theta_i^*)P^*_{qpavg}}{0.5I_m} \tag{21}$$

D. Module Voltage Balancing Controller

Fig. (3d) shows module voltage balancing controller. The module voltage balancing can be accomplished by dividing the phase voltage references into the module voltage references [8-9] as can be seen in Fig. (3d).

E. Control Scheme of DC/DC sub-module

The control scheme of DC/DC sub- module is similar to the control structue used in [12] shown in Fig. (3e). As can be seen, notch filter is used to remove 120 Hz oscillation of the measured value of DC/DC converter capacitor voltage.

IV. Control Algorithm of VSC based HVDC Transmission System under DC Fault Operating Condition and Recovery After DC Fault

Generally, the VSC based HVDC transmission system is vulnerable to DC side fault, but the VSC based HVDC system configuration considered in this paper has the feature to be protected against DC fault with the appropriate control algorithm without using DC circuit breakers. In fact, this advantage allows us to use AC circuit breakers instead of DC circuit breakers for DC fault protection.

The proposed control algorithm of VSC based HVDC transmission system for DC fault operation is shown in Fig. 5. According to the control scheme for DC fault operation, DC fault is detected when the measured value of DC side current is twice the rated value of DC side current. Once DC fault is detected at time t_0, the reference value of active power flow is changed to zero. Also, once fault is detected, all switches of DC/DC converters are turned off. As a result, the total energy of all DC capacitor voltages is discharged in DC side inductor *(L)* and DC overhead line resistance *(R)* as can be shown in Fig. 6. The inductor current has an initial value $i_L(t_0)=I_0$, and each capacitor voltage has an initial value $V_{cm}(t_0)=V_{c0}$. So, the total initial value of capacitor voltage for all n modules is $V_0=n\times V_{c0}$. The DC side current can be expressed as (22) if $R < 2\sqrt{L/C}$. The DC bus voltage is also written as (23).

$$i_{dc}(t) = I_0e^{-\alpha t}\cos(\sqrt{\omega_0^2 - \alpha^2}\,t) + \left[\left(\frac{V_0}{L} - I_0\alpha\right)\Big/\sqrt{\omega_0^2 - \alpha^2}\right]e^{-\alpha t}\sin(\sqrt{\omega_0^2 - \alpha^2}\,t) \tag{22}$$

$$V_c(t) = V_0e^{-\alpha t}\cos(\sqrt{\omega_0^2 - \alpha^2}\,t) + \left[\left(V_0\alpha - \frac{I_0}{C}\right)\Big/\sqrt{\omega_0^2 - \alpha^2}\right]e^{-\alpha t}\sin(\sqrt{\omega_0^2 - \alpha^2}\,t) \tag{23}$$

Where $\alpha = R/2L; \omega_0 = 1/\sqrt{LC}; C = C_m/n$. The time when the capacitor voltage becomes zero can be computed by (24).

$$t_1 = t_0 + \frac{\arctan\left[\dfrac{V_0C\sqrt{\omega_0^2 - \alpha^2}}{I_0 - V_0\alpha C}\right]}{\sqrt{\omega_0^2 - \alpha^2}} \tag{24}$$

0278-0046 (c) 2013 IEEE. Personal use is permitted, but republication/redistribution requires IEEE permission. See http://www.ieee.org/publications_standards/publications/rights/index.html for more information.

This article has been accepted for publication in a future issue of this journal, but has not been fully edited. Content may change prior to final publication. Citation information: DOI 10.1109/TIE.2014.2371431, IEEE Transactions on Industrial Electronics

When DC bus voltage becomes zero at time t_1, the total energy of DC side inductor is discharged in DC overhead line resistance and anti-parallel diodes as can be shown in Fig. 7. At time t_1, the inductor current has an initial value of $i_L(t_1)=I_1$. So, the DC side current can be written as (25).

$$i_{dc}(t) = I_1 e^{\frac{-R}{L}t}; T = \frac{L}{R} \quad (25)$$

According to (25), the DC current is reduced, and the time when the inductor current becomes zero is obtained by (26).

$$t_2 = t_1 + \frac{5L}{R} \quad (26)$$

When the magnitude of DC current becomes zero, circuit breakers are opened to disconnect terminal 1 from terminal 2.

The control strategy for recovery after DC fault is shown in Fig. 8. When DC fault is cleared, all switching signals of DC/DC converters are enabled to charge DC/DC capacitor voltages. Once DC bus voltage is regulated at its reference value, terminal 1 is connected to terminal 2, and the reference active power flow is ramped up from zero to the rated value.

V. Dynamic Performance Evaluation of VSC based HVDC Transmission System under DC Fault Operating Condition and Recovery After DC Fault

In this section, the dynamic performance of the VSC based HVDC transmission system under DC fault operating condition is evaluated through PSCAD simulation. For DC fault simulation, the positive DC line is connected into the ground as shown in Fig. 9, and the system parameters are summarized in table I. DC fault happens at t=0.9s, and it is cleared at t=1s. An overhead line with the length of 480 (km) is used in the simulation.

Fig. 10 shows the dynamic performance of VSC based HVDC system under DC fault operating condition. Initially, the switching signals of AC/DC and DC/DC converters are off, and they are enabled at t=0.1s. Therefore, terminal DC bus voltage is adjusted at 320 kV at this time. The reference value of active power is also ramped up from 0 at t=0.4s to 320 MW at t=0.7s. DC fault happens at t=0.9s when the rated power is transferred from terminal 1 to terminal 2 as shown in Fig. 10. When DC fault is detected, the reference value of active power is reduced from 320 MW to 0 MW, and all the switching signals of DC/DC converter switches will be turned off. As a result, the total energy of all DC capacitor voltages is discharged in DC side inductor and DC overhead line resistance as explained in the previous section. When DC bus voltage becomes zero, the total energy of DC side inductor is discharged, and as a result the magnitude of DC current is reduced as can be seen in Fig. 10. When the magnitude of DC current becomes zero, the circuit breaker will be opened to disconnect terminal 1 from terminal 2. Three-phase ac current in both terminals is also shown in Fig. 10. DC fault is cleared at t=1s, and the control algorithm for recovery after DC fault is implemented. First, the switching signals of DC/DC converters are enabled at t=1s. At this time, DC bus voltage is regulated at 320 kV. At t=1.15s, terminal 1 is connected to terminal 2. Then, the reference value of active power is increased from zero at t=1.2s to 320 MW at t=1.5s.

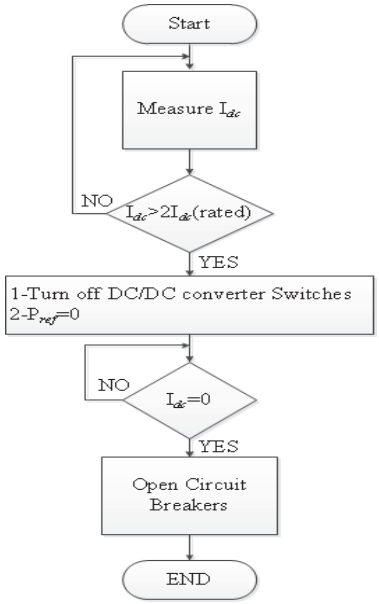

Fig. 5. Control algorithm of VSC based HVDC transmission system under DC fault operating condition.

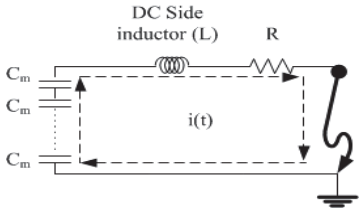

Fig. 6. Equivalent circuit of VSC based HVDC transmission system when DC fault is detected (capacitor discharging mode).

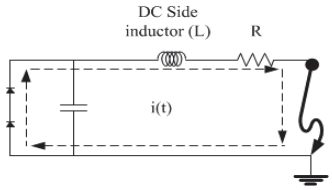

Fig. 7. Equivalent circuit of VSC based HVDC transmission system when DC bus voltage becomes zero (inductor discharging mode).

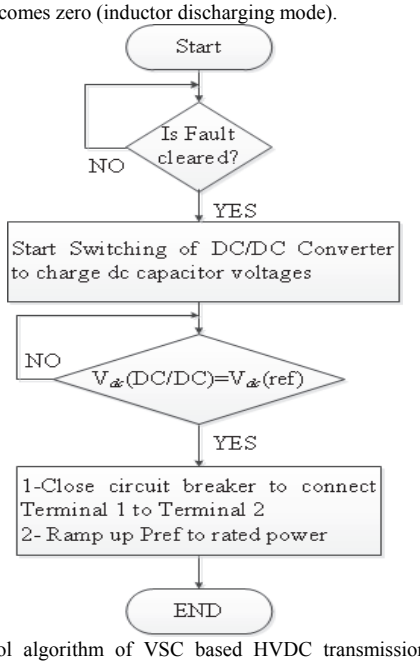

Fig. 8. Control algorithm of VSC based HVDC transmission system for recovery after DC fault.

0278-0046 (c) 2013 IEEE. Personal use is permitted, but republication/redistribution requires IEEE permission. See http://www.ieee.org/publications_standards/publications/rights/index.html for more information.

This article has been accepted for publication in a future issue of this journal, but has not been fully edited. Content may change prior to final publication. Citation information: DOI 10.1109/TIE.2014.2371431, IEEE Transactions on Industrial Electronics

During fault duration, the AC/DC converters are controlled to regulate capacitor DC voltages of each AC/DC module at 106.67 kV as shown in Figs. 11, and 12. Capacitor DC bus voltages of DC/DC converters for terminal 1 and 2 are also shown in Figs. 13, and 14 respectively. When DC fault is detected at t=0.9s, the switching signals of DC/DC converters are disabled. So, the capacitor voltages of DC/DC converters become zero. When DC fault is cleared at t=1s, the switching signals of DC/DC converters are enabled, and the capacitor voltages of DC/DC converters are regulated at 106.67 kV again.

Fig. 15 shows the zero crossing time of DC current versus fault location and DC side inductor based on the theoretical results obtained by Eq. (26). As can be seen, DC current zero crossing time increases as DC side inductor increases. Also, as fault location increases, R value increases, and as a result zero crossing time decreases. Fig. 16 also shows the zero crossing time of DC current versus fault location and DC side inductor based on the obtained simulation results. Comparison of simulation and theoretical results shows that Eq. (26) is accurate enough to find the zero crossing time of DC current.

VI. Real Time Digital Simulation of VSC based HVDC System under DC Fault Operating Condition

This section presents the dynamic performance of VSC based HVDC transmission system through RTDS simulation. The hardware in the loop implementation of VSC based HVDC transmission system is performed by Real Time Digital Simulator (RTDS), shown in Fig. 17, and the system parameters are same as the parameters tabulated in table I. The VSC based HVDC transmission system is simulated by the real time digital simulator. The *Concerto control board* is used as the main controller.

Fig. 18 shows the RTDS results for DC fault operating condition. At t=13s, the reference value of active power is changed to 320 MW. DC fault happens at t=30s. When DC fault is detected, the reference value of active power is reduced to zero, and all the switching signals of DC/DC converter switches will be turned off. As a result, the total energy of all DC capacitor voltages is discharged. When DC bus voltage becomes zero, the magnitude of DC current is reduced. When the magnitude of DC current becomes zero, the circuit breaker will be opened to disconnect terminal 1 from terminal 2. Three-phase ac current in both terminals is also shown in Fig. 18. DC fault is cleared at t=33s, and the control algorithm for recovery after DC fault is implemented. First, the switching signals of DC/DC converters are enabled at t=33s. At this time, DC bus voltage is regulated at 320 kV. At t=38s, terminal 1 is connected to terminal 2. Then, the reference value of active power is increased to 320 MW at t=40s.

Capacitor DC bus voltages of DC/DC converters for terminal 1 and 2 are shown in Figs. 19, and 20 respectively. When DC fault is detected at t=30s, the switching signals of DC/DC converters are disabled. So, the capacitor voltages of DC/DC converters become zero. When DC fault is cleared at t=33s, the switching signals of DC/DC converters are enabled, and the capacitor voltages of DC/DC converters are regulated at 106.67 kV.

TABLE I. VSC BASED HVDC SYSTEM PARAMETERS

Terminal rated power	P	320 MVA
Terminal voltage reference	V_{dc}	320 kV
DC grid side inductance	L_{dc}	100 mH
Overhead line resistance	R_{dc}	11.5 Ω
Module number (per terminal)	N	3
AC/DC capacitor voltage	$V_{(AC/DC)}$	106.67 kV
DC/DC capacitor voltage	$V_{(DC/DC)}$	106.67 kV
Capacitor value	C	100 uF
AC/DC PWM switching frequency	f_{sw} *(AC/DC)*	2 kHz
DC/DC PWM switching frequency	f_{sw} *(DC/DC)*	20 kHz

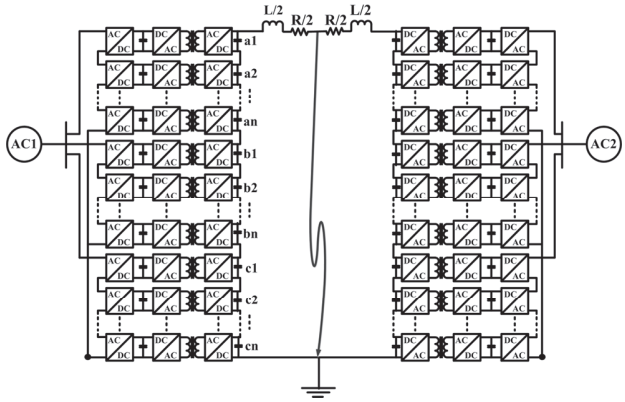

Fig. 9. VSC based HVDC system under DC fault operating condition.

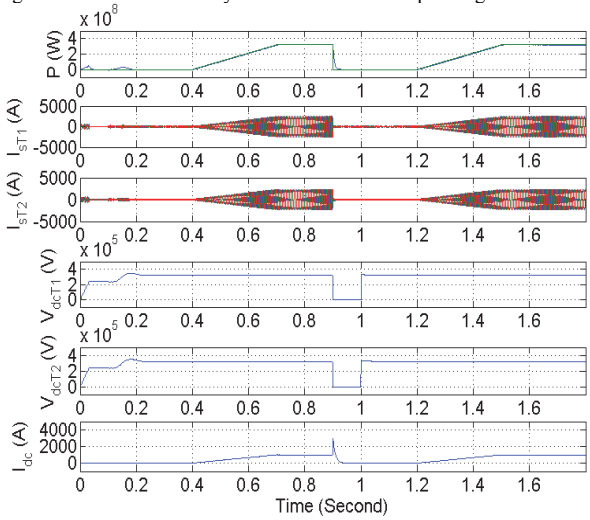

Fig. 10. Dynamic performance of VSC based HVDC system under DC fault - PSCAD result.

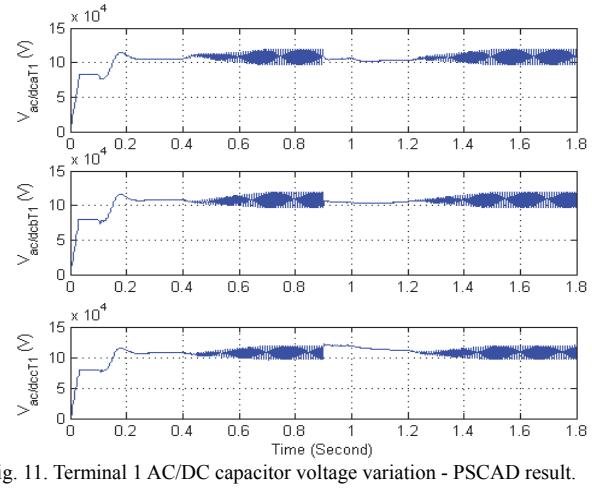

Fig. 11. Terminal 1 AC/DC capacitor voltage variation - PSCAD result.

0278-0046 (c) 2013 IEEE. Personal use is permitted, but republication/redistribution requires IEEE permission. See http://www.ieee.org/publications_standards/publications/rights/index.html for more information.

This article has been accepted for publication in a future issue of this journal, but has not been fully edited. Content may change prior to final publication. Citation information: DOI 10.1109/TIE.2014.2371431, IEEE Transactions on Industrial Electronics

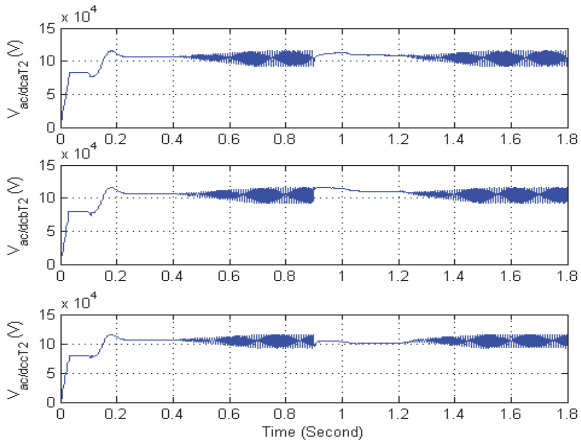

Fig. 12. Terminal 2 AC/DC capacitor voltage variation - PSCAD result.

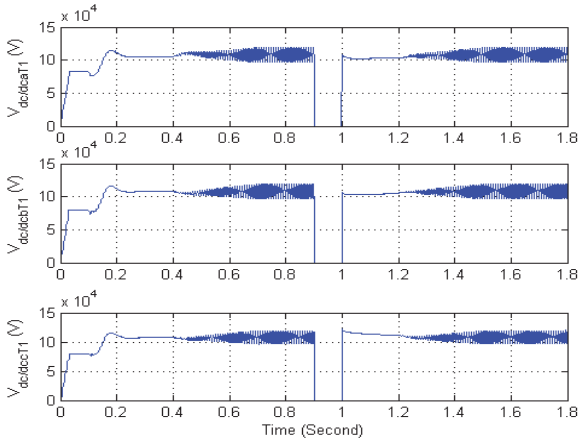

Fig. 13. Terminal 1 DC/DC capacitor voltage variation - PSCAD result.

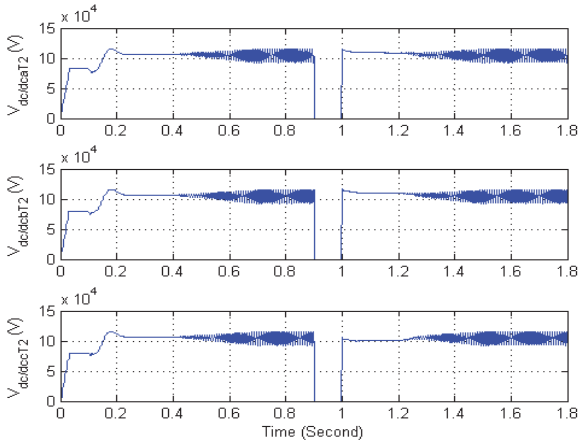

Fig. 14. Terminal 2 DC/DC capacitor voltage variation - PSCAD result.

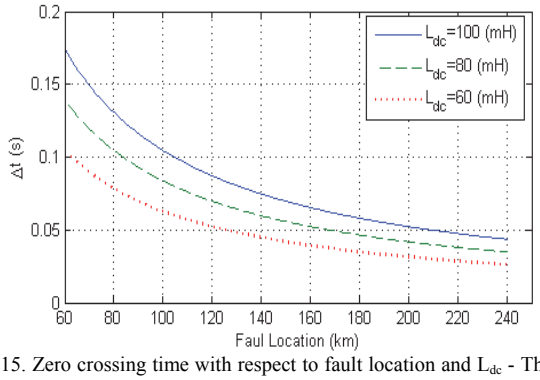

Fig. 15. Zero crossing time with respect to fault location and L_{dc} - Theoretical results.

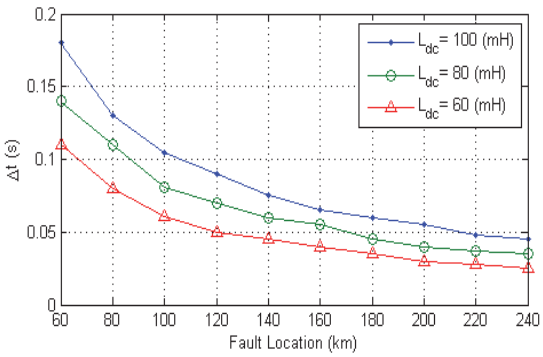

Fig. 16. Zero crossing time with respect to fault location and L_{dc} – PSCAD simulation results.

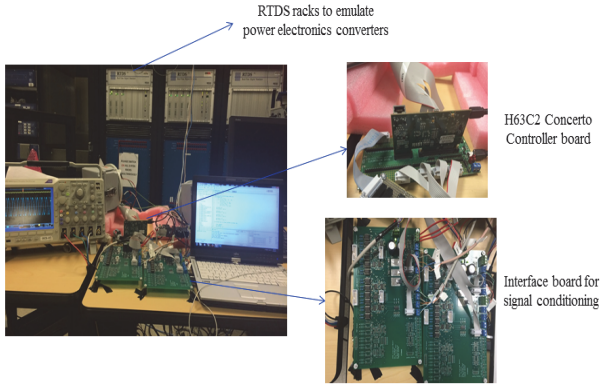

Fig. 17. The Real Time Digital Simulator (RTDS) setup.

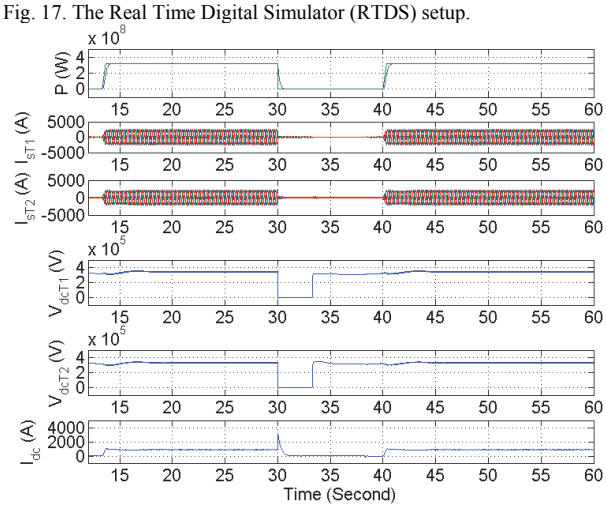

Fig. 18. Dynamic performance of VSC based HVDC system - RTDS result.

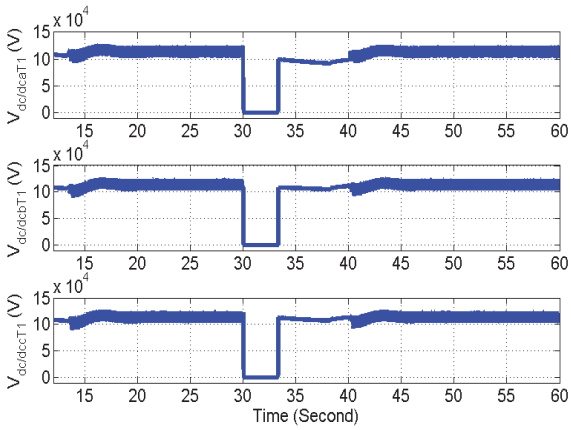

Fig. 19. Terminal 1 DC/DC capacitor voltage variation - RTDS result.

0278-0046 (c) 2013 IEEE. Personal use is permitted, but republication/redistribution requires IEEE permission. See http://www.ieee.org/publications_standards/publications/rights/index.html for more information.

This article has been accepted for publication in a future issue of this journal, but has not been fully edited. Content may change prior to final publication. Citation information: DOI 10.1109/TIE.2014.2371431, IEEE Transactions on Industrial Electronics

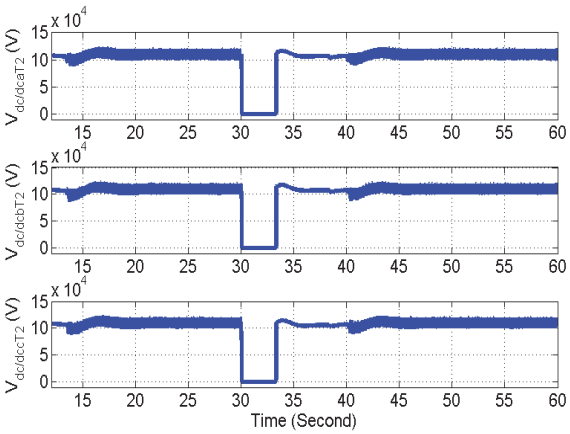

Fig. 20. Terminal 2 DC/DC capacitor voltage variation - RTDS result.

VII. Conclusion

This paper proposed a control method of a DC fault resilient converter which can be protected against DC fault without using expensive DC circuit breakers. In this paper, an appropriate control structure with the capacitor voltage balancing controller was proposed. The proposed control scheme consists of four layers to control power flow and terminal DC bus voltage as well as DC capacitor voltages of each module. The control algorithm for DC fault operation and recovery after DC fault was proposed. The performance of converter was thoroughly analyzed under DC fault operating condition, and PSCAD simulation results were presented to validate the control structures. The feasibility of the VSC based HVDC transmission system operation via controller hardware-in-the-loop simulation with RTDS was demonstrated, and RTDS simulation results verified the controller performance under DC fault operating conditions.

References

[1] A. Egea-Alvarez, F. Bianchi, A. Junyent-Ferre, G. Gross, and O. Gomis-Bellmunt, "Voltage Control of Multi-terminal VSC-HVDC Transmission Systems for Offshore Wind Power Plants: Design and Implementation in a Scaled Platform ," *IEEE Trans. Ind. Electron.,* vol. 60, no. 6, pp. 2381-2391 , Jun 2013.

[2] R.T. Pinto, P. Bauer, S.F. Rodrigues, E.J. Wiggelinkhuizen, J. Pierik, and B. Ferreira, "A Novel Distributed Direct-Voltage Control Strategy for Grid Integration of Offshore Wind Energy Systems Through MTDC Network ," *IEEE Trans. Ind. Electron.,* vol. 60, no. 6, pp. 2429-2441 , Jun 2013.

[3] L. Tang and B.T. Ooi, "Locating and Isolating DC Faults in Multi-Terminal DC Systems," *IEEE Trans. Power Del.*, vol.22, no.3, pp.1877, 1884, July 2007.

[4] L. Tang and B.T. Ooi, "Protection of VSC-multi-terminal HVDC against DC faults," *Power Electronics Specialists Conference, 2002. pesc 02. 2002 IEEE 33rd Annual*, pp.719, 724 vol.2, 2002.

[5] N. Flourentzou, V.G. Agelidis, G.D. Demetriades, "VSC-Based HVDC Power Transmission Systems: An Overview," *IEEE Trans. Power Electron.*, vol.24, no.3, pp.592, 602, March 2009.

[6] H. Akagi, "Classification, Terminology, and Application of the Modular Multilevel Cascade Converter (MMCC)," *IEEE Trans. Power Electron.*, vol.26, no.11, pp.3119-3130, Nov. 2011.

[7] R. Gupta, "Resilient Multi-Terminal HVDC Networks with High-Voltage High-Frequency Electronics" – GE Global Research – Arpa-e project award# DE-AR0000224.

[8] M. Hagiwara and H. Akagi, "Control and experiment of pulse width modulated modular multilevel converters," *IEEE Trans. Power Electron.*, vol. 24, no. 7, July 2009, pp. 1737-1746.

[9] M. Hagiwara and H. Akagi, "PWM control and experiment of modular multilevel converters," in Power Electronics Specialists Conference, PESC IEEE, pp. 154-161, 2008.

[10] J. Yang, J.E. Fletcher, and J. O'Reilly, "Short-Circuit and Ground Fault Analyses and Location in VSC-Based DC Network Cables," *IEEE Trans. Ind. Electron.*, vol.59, no.10, pp.3827-3837, Oct. 2012.

[11] X. Li, Q. Song, W. Liu, H. Rao, S. Xu, and L. Li, "Protection of Nonpermanent Faults on DC Overhead Lines in MMC-Based HVDC Systems," *IEEE Trans. Power Del.*, vol.28, no.1, pp.483,490, Jan. 2013.

[12] D.Costinett, D. Maksimovic, and R. Zane, "Design and Control for High Efficiency in High Step-Down Dual Active Bridge Converters Operating at High Switching Frequency," *IEEE Trans. Power Electron.* , vol.28, no.8, pp.3931,3940, Aug. 2013.

Nima Yousefpoor (S'12) received the B.Sc. and M.Sc. degrees in electrical engineering from Amirkabir University of Technology, Tehran, Iran, in 2008 and 2010, respectively. He received his Ph.D. degree from Electrical and Computer Engineering Department of North Carolina State University, Raleigh, NC in 2014. His research interests include HVDC transmission systems, multi-level inverters, Flexible AC Transmission System (FACTS) devices, and renewable energy systems.

Ajit Narwal received the B.E. degree in electrical engineering from Delhi College of Engineering, University of Delhi, India, in 2009 and thereafter joined National Thermal Power Corp., and worked with the turbo-generator and auxiliary design section till August 2011. He received the M.S. degree in electrical engineering from North Carolina State University, Raleigh, NC in August 2014. His research interests include multi-level converters, low voltage DC-DC converters, analog design, and renewable energy systems.

Subhashish Bhattacharya (M'85-SM'12) received the B.E. (Hons.) degree from the Indian Institute of Technology Roorkee (formerly University of Roorkee), Roorkee, India, in 1986, the M.E. degree from the Indian Institute of Science, Bangalore, India, in 1988, and the Ph.D. degree from the University of Wisconsin-Madison, Madison, in 2003, all in electrical engineering. He has worked in the Flexible AC Transmission Systems (FACTS) and Power Quality Group at Westinghouse R&D Center in Pittsburgh, PA, which was later part of Siemens Power Transmission & Distribution, from 1998 to 2005. He joined the Department of Electrical and Computer Engineering, North Carolina State University (NCSU) as an Assistant Professor in August 2005, where he has been the ABB Term Associate Professor since August 2011 and also a Faculty Member of the NSF Engineering Research Center for Future Renewable Electric Energy Delivery and Management Systems Center (www.freedm.ncsu.edu) and Advanced Transportation Energy Center (www.atec.ncsu.edu) at NCSU. His research interests include FACTS, utility applications of power electronics and power quality issues, solid-state transformer, high-frequency magnetics, active filters, high-power converters, converter control techniques, integration of energy storage to the grid, and application of new power semiconductor devices such as SiC for converter topologies.

0278-0046 (c) 2013 IEEE. Personal use is permitted, but republication/redistribution requires IEEE permission. See http://www.ieee.org/publications_standards/publications/rights/index.html for more information.

Defect Collection and Reporting System for Git based Open Source Software

Ruchika Malhotra[#1], Nakul Pritam[*2], Kanishk Nagpal[#3], Prakarsh Upmanyu[*4]

Department of Computer Engineering, Delhi Technological University
Bawana Road, Shahbad, Daulatpur, Delhi-110042, India

[1]ruchikamalhotra2004@yahoo.com
[2]nakul.pritam@gmail.com
[3]kanishk0001@gmail.com
[4]prakarsh.upmanyu23@gmail.com

***Abstract*— This paper describes Defect Collection and Reporting System which is an automated tool that aids in generating various reports to provide useful information regarding the defects which were present in a given version of a Git Version Control System based Open Source Software and were fixed in the subsequent version. The generated reports contain information such as the total number of defects, class wise and the corresponding values of different OO metrics for each class in the source code. Such kind of defect data can be readily used for defect prediction hypothesis pertaining to Git based Open Source Software. Some potential fields of application could be analysis and validation of the effect of a given metric suite on fault proneness; to predict fault proneness models for Defect Prediction, etc. In addition to the core functionalities and overall functioning of the above stated tool, this paper also gives an overview of some of the functionalities which might be useful for the end user, namely- cloning of Git Repositories, and self-logging data of the tool.**

***Keywords*— Open Source, Defect Collection, Metrics, Git, Cloning, Self-logging.**

I. INTRODUCTION

Today's world is characterized by rapidly evolving technologies and the role of Open Source Software has increased manifold. Open Source Software has truly become the most prominent feature of Open Source Development. As compared to Closed Source or Proprietary Software, Open Source Software is characterized by lower costs, better security, no vendor or copyright issues and higher quality. Also, Open Source Software is developed with a different approach and methodology. Users are generally treated as co-developers and development is accomplished through collaborative effort of programmers. The working product is released much earlier and is usually followed by various versions which offer fewer functionalities but more stability. High Modularization and Dynamic Decision Making are commonly employed. Version Control Systems (such as Git) for Open Source Software ensure much easier and structured maintenance, especially for the changes incurred. Owing to these reasons, Open Source Software is increasingly being adopted by individuals and many organizations across the globe. Perhaps the best example that clearly depicts the capabilities of an Open Source Software is Android OS. It is a Linux-based Operating System which has been designed primarily for touch screen devices, including smart phones and tablets. Unveiled in 2007, Android today has become the most widely used operating system for mobile devices throughout the world, completely outwitting Proprietary Software for mobile devices, such as Symbian OS. Android's source code is available at Google's Git Repository; and a vast developer community caters to the development of applications ("apps") that extend the functionality of devices.

Open source software repositories provide rich data that can be extracted and employed in various empirical studies. Primary focus is on defect and change data which can be obtained from version control repositories of open source software systems. For instance, previous studies have shown that defect data collected from open source projects can be used in research areas such as defect prediction [1]. Some commonly traversed areas of defect prediction include Analysis and Validation of the effect of given metric suite, (such as CKJM and QMOOD) on fault proneness [2]; and evaluating the performance of fault proneness models, such as Artificial Neural Networks [3]. However, an important question here is that what kind of software repositories may be potentially mined for extracting such kind of data. After a rigorous study and analysis, we came across software repositories which employ 'Git' as the Version Control System and these can be appropriate candidates for evaluation and selection so as to be employed in research and empirical studies. The reasons for selecting Git based Software systems are:

- Git is the most popular distributed version control system and the defect and change data can be extracted in relatively easier ways through the change logs maintained by Git.
- A large number of open source software systems are maintained through Git, including Google's Android OS and a vast range of Apache's Software applications.

But at present, most of the empirical data collection process is carried out manually. There exists no mechanism which can employ an automated process to collect the defect data for Git based Open Source Software, and provide information useful enough to be used in research areas mentioned above.

978-1-4799-4674-7/14/$31.00 ©2014 IEEE

Therefore, a system is required which can efficiently collect defect data for a Git-based open source software, which might be used in the above mentioned research areas and other applications.

Such kind of a system is expected to perform the following operations: First, obtain the 'git change logs' for a given software and process them to obtain the defects which were reported in a specific version of that software and were fixed in the subsequent version. Then, the system should extract vital defect information such as unique bug or defect identifier and the defect description, if provided. Next, we require the association of defects to their corresponding source files (java code files, or class files contained in the source code). Then the system should perform the computation of total number of defects fixed corresponding to each class, i.e., the number of defects associated with that class. Finally, the corresponding values of different metrics should be calculated by the system for each source code file for previous version of the open source software.

In this work, we have developed a tool named Defect Collection and Reporting System (here onwards, referred to as DCRS), which incorporates each and every functionality stated above and consequently generates various reports that present the collected data in a more processed, meaningful and useful form.

Rest of the paper is organized as follows: Overall functioning of the DCRS for collection of defect data and report generation is summarized in Section II. Section III describes different types of reports that are generated by the DCRS from the collected defect data. Section IV summarizes some additional functionalities of the DCRS. Demonstration of the DCRS, including data source, preliminary analysis and results, is presented in Section V. Section VI gives an overview of some potential applications of the DCRS. Section VII presents the conclusions and future work.

II. Working Mechanism

The DCRS sequentially carries out a series of well-defined operations to collect and process the Defect Data of Git based Open Source Software and then finally generate various types of reports for the same. These operations are described as follows:

First, the DCRS processes an open source software's source code (obtained from Git repository) for each of the two predetermined consecutive versions, to retrieve what are known as Git Change-Logs, or simply change logs. A Change Log provides information about the changes or modifications that have been incurred from time to time in the software's source code. These changes could have been made for various purposes, such as bug or defect fixing, feature addition, refactoring, enhancements, etc. Each and every change incurred, no matter how big (significant) or small, is recorded in the change logs and thus constitutes an individual change record. An individual change record provides various kinds of information such as-

- The Timestamp of committing (i.e., recording) the incurred change with the Git Repository.
- Unique change identifier
- If the change has been made for defect fixing, a unique defect identifier is provided in most of the cases.
- An optional change description or information.
- List of the changed or modified source code files, along with the LOC changes for each of the changed files.

Source code for both of the versions is necessary for processing because a change log provides the change information since the beginning of time (i.e., when the initial release of the software was made available), but we're interested only in the changes which were incurred during the transition from a given previous version to the subsequent one.

Here, we have applied the 'git whatchanged' command with a 'stat' flag to get the change records along with the LOC changes. Fig. 1 depicts the general format of a change log file (along with an individual change record) for Open Source Software hosted at Git Repository, obtained by applying the above command.

<Change Log Record-1>
    <Timestamp>
    <Change-Id>
    <Defect-Id>*
    <Change Description>*
    <Changed Source File 1> +++...+---...- **
    <Changed Source File 2> +++...+---...- **
        .
        .
        .
<Change Log Record-2>
        .
        .
        .
<Change Log Record-N>

* May or may not be present
** + : 1 LOC Insertion; - : 1 LOC Deletion

Fig. 1 General format of Git change log file

In the next operation, Git change logs are further processed, an individual change record at a time, to obtain Defect-Records (i.e. changes which were incurred for defect-fixing, not for other any other reason such as refactoring, enhancement, etc.). Bug or Defect-Ids and the Defect Description, if any, are retrieved from the Defect-Logs. If there's no Defect-Id but only a change description, then we look for various keywords such as 'bug', 'issue', 'defect', etc. in the provided description, and treat the change record as a defect record. In such a case, a default value is stored for the Defect-Id.

The collected defects (with or without any Defect-Id) are finally mapped to Classes in the source code. We have considered only class files or java source code files and other types of files are ignored. The data collected is consequently employed to generate various reports in .csv format. These reports are described later in the paper. Fig. 2 presents the format of Defect information stored by DCRS.

<Defect ID 1> <Defect ID 2> ... <Defect ID N>

<Defect Description>

<Java Source File 2 Changed For Defect Fixing>
<LOC Inserted, Deleted>

<Java Source File 2 Changed For Defect Fixing >
.
.
.
<Java Source File Changed M For Defect Fixing >

Fig. 2: Defect information Stored by DCRS

The entire DCRS system has been implemented in the Java Programming Language (Java SE 1.7). The data for required Metrics for the class files of previous version for a given open source software has been obtained by embedding an open source software in the DCRS, which is available at http://gromit.iiar.pwr.wroc.pl/p_inf/ckjm/metric.html and covers a wide range of metrics [4]-[7]. The procedure for defect collection and reporting is presented in Fig. 3.

III. Reports Generated by the DCRS

From the defect data collected as stated in the above section, the tool generates following primary reports:

A. *Defect Details Report*

This report provides descriptive and statistical information corresponding to each defect: The Defect-Id (if any), description (if any), and the source code file(s) (specifically the Java files) which have been changed for fixing that particular defect. The report also contains data for the LOC changes for each class which was modified in order to fix any reported defect.

The fields which are contained in this report, corresponding to each defect, are:

- Java source code file name or simply the class file name
- Unique defect identifier, if any
- Defect description, if any
- LOC inserted and deleted to fix the defect (modification data was not provided in the change logs).

B. *Defect Count and Metrics Report*

This report provides the total number of defects fixed source-file wise (i.e. total number of times a source-file was modified to fix defects), along with total LOC changes, with the data for the following metrics [4]-[7]:

- CKJM Suite (CBO, NPM, RFC, LCOM, DIT, WMC)
- QMOOD Suite (NPM, DAM, MOA, CAM, MFA)
- Martin's Metrics (Ca, Ce)
- Miscellaneous (LOC, LCOM3, AMC, IC, CBM).

More information regarding these metrics may be obtained from [4]-[7]. The fields which are contained in this report are given below:

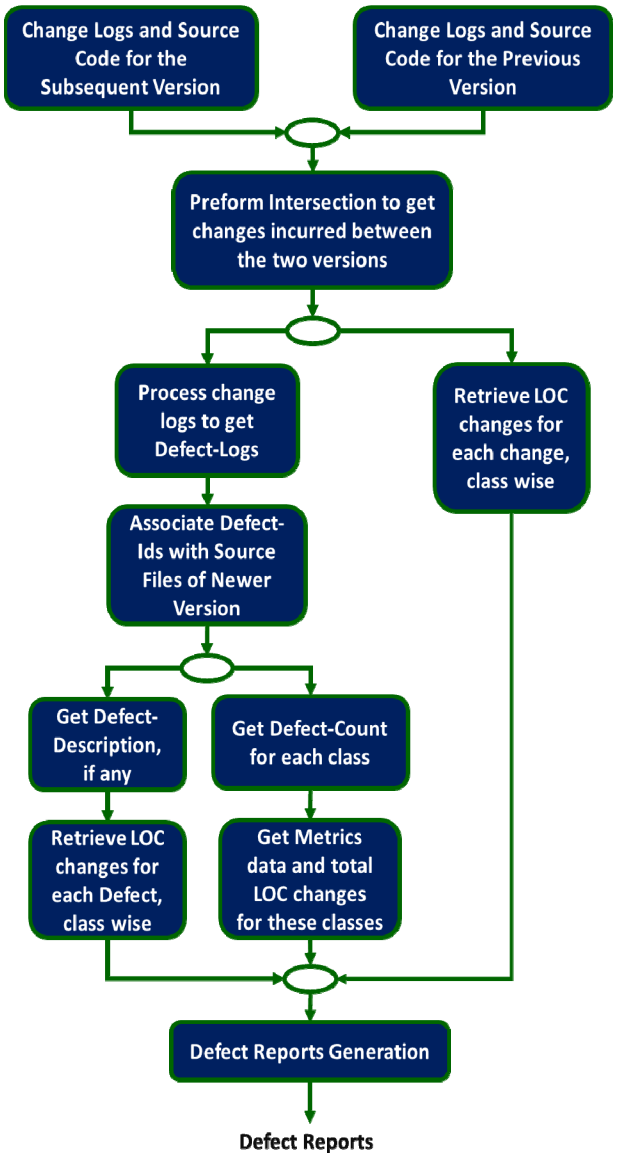

Fig. 3 Flowchart for Defect collection and reporting mechanism

- Java source file name
- Total number of defects mapped to the above class.
- Total LOC inserted and deleted for all of the defects mapped to this class.
- List of metric values, corresponding to the above class.

C. *LOC Changes Report*

This report contains the total number of LOC changes incurred in the source code files, corresponding to each change (irrespective of the purpose of that change, i.e. enhancement, defect-fixing, refactoring, etc.).

The fields which are contained in this report are as follows:

- Java source file name
- Total LOC inserted and deleted for all the changes (including defect fixes, enhancement, etc.) mapped to the above class.

In addition to the above primary reports, the following auxiliary reports are also generated by the DCRS:

D. Newly Added Source Files

This reports contains the list of source code files which were not present in the previous version of the considered open source software, but were introduced or added during the transition to subsequent version. The total number of Defects reported for each class file, and the corresponding LOC changes are also included in the report.

The fields which are contained in this report are as follows:

- Java source file name added in the subsequent version
- Total number of defects for which the above source file has been modified
- Total LOC inserted and deleted for all of the defects mapped to this class file

E. Deleted Source Files

This reports contains the list of source-files which were present in the previous version of an open source software, but have been deleted or removed during the transition to the subsequent version. The total number of Defects reported and corresponding LOC changes are also included, considering the probability of deleting a source file in the latest version after fixing some defects.

The fields which are contained in this report are as follows:

- Java source file name removed from the subsequent version
- Total number of defects for which the above source file has been modified
- Total LOC inserted and deleted for all of the defects mapped to this class file.

F. Consolidated Defect and Change Report

This report is similar to the defect or bug-count report described in B., but the only difference here is that instead of reporting the LOC Changes corresponding to all the defects mapped to a particular class, we report total LOC changes which are incurred in that class. These changes may not only be incurred for issue, defect or bug fixing, but for any other purpose, such as enhancement, refactoring, etc. In other words, this report can be considered as the combination of Bug-Count report and LOC changes report (described in B and C respectively), wherein we report the bug-data from bug-count report, but LOC Changes incurred for each class are reported from the LOC Changes report.

G. Descriptive Statistics Report

This reports gives various statistical measures for each and every metric incorporated in the tool. The various statistical measures for a metric are summarized in Table I.

TABLE I
STATISTICAL MEASURES

Characteristic	Definition
Mean	The arithmetic mean
Median	Middle value when the values for are sorted
Mode	The most frequently occurring value
Harmonic Mean	Reciprocal or inverse of the arithmetic mean
Minimum	The lowest value
Maximum	The highest value
Range	The difference between maximum and minimum values
First Quartile	The value above 25% of the minimum values
Third Quartile	The value above 75% of the minimum values
Interquartile Range	The difference between Third and First Quartiles.
Variance	Arithmetic mean of the square of difference between mean and the individual values
Standard Deviation	Square root of variance
Coefficient of Variation	The ratio of standard deviation to the mean
Variation Ratio	Proportion of values that are not mode
Skewness	It is a measure of the asymmetry of the given values.
Kurtosis	It is a measure of the peakedness of the given values.

IV. Additional Functionalities

Apart from the core functionalities of defect collection and report generation, the DCRS also incorporates some additional features or functionalities which might prove to be useful for the end user. These are grouped into two broad categories-

A. Cloning of Git based Software Repositories

The system provides full support for “cloning” software repositories which employ Git as the Version Control System. “Cloning” implies ‘copying and pasting’ the entire software repository from a local or remote hosting server to the end-user machine. Software Repositories may be generally classified as [8]:

- *Source Control Repositories,* such as Git and CVS, which record the development track or history of a software project and track all the changes incurred in the project along with the meta-data for each change (timestamp, developer information, etc.).
- *Bug Repositories,* which maintain the history of defect reports and/or feature requests that may be reported by the users and as well as developers of medium to large software. Bugzilla and Jira are popular bug repositories.
- Discussions about various aspects during the lifetime of a software project are maintained in *Archived Repositories* such as Mailing lists, emails, instant messages, etc.
- *Deployment Logs*, that record the execution information of single or multiple deployments of a software application. We can detect execution anomalies by studying the usage patterns across various deployments, and then deviations from these patterns may be recorded
- *Code Repositories*, which archive the source code for a huge number of software projects. Google code and Sourceforge.net are two large source code repositories.

Different types of artefacts may be obtained from a software repository depending upon the type of that repository. For example, source control repositories provide change-logs. Source code may be obtained through code repositories.

In our case, the DCRS supports cloning of Code Repositories which employ Git as the Source Control Repository or Version Control System. The user can thus obtain the source code and as well as Git change logs, which were described earlier. These two artefacts may be then employed for various purposes. For instance, the DCRS employs these artefacts for generating various types of defect reports we have stated earlier. Two crucial areas of application include research related to fault-proneness or defect-prediction, and change proneness. These are discussed later in Section VI.

B. *Self-Logging*

Self-Logging or simply logging may be defined as the process of automatically recording events, data and/or data structures about a tool's execution to provide an audit trail. The recorded information can be employed by developers, testers and support personal for identifying software problems, monitoring live systems and for other purposes such as auditing and post-deployment debugging. Logging process generally involves the transfer of recorded data to monitoring applications and/or writing the recorded information and appropriate messages, if any, to files.

We've also provided the user with the functionality to view the operational logs of the tool. These self-logs are stored as text file(s), indicating the different events, and/or operations which have occurred during the tool's working along with their timestamp. These are ordered by the sequence and hence, the timestamp. The self-log file follows a daily rolling append policy, i.e. logs for a given day are appended to the same file, and a new file is created after every 24 hours. The previous day's file is stored with a name that indicates the time of creation. Java Libraries of LogBack and SLF4J have been employed to implement self-logging in the DCRS. They can be downloaded from http://www.slf4j.org/download.html.

V. Demonstration of the DCRS

In this section, we present our demonstration of the DCRS by operating it on a Git based open source software, and then discuss the results obtained for the same.

A. *Data Source*

For our demonstration of the DCRS, we've selected the open source Android OS with Git as its Version Control System. The two versions of Android OS, namely – Ice Cream Sandwich (v4.0) and Jelly Bean (v4.1) have been considered for data collection. The source code has been obtained from Google's Git Repository (https://android.googlesource.com.

It was noted that the source code for Android was unevenly distributed in as many as 379 application packages. These include the packages for kernel, compilation headers, build libraries, linker code, and the native applications which are included in the Android OS, such as Web browser, Gallery, E- mail, Contacts, Music Player, Calendar, Telephony, etc.

Since we want to consider only the java source code or class files in the source code, we have analysed a few of the available Android application packages in order to determine the percentage of java source code files in every package. It was observed that there were significantly less number of java source code files as compared to other files formats, such as interface or activity layout files, resource files such as media, string values, etc. in each and every application package we had analysed. Table II presents the summary of Java source files contained in a few Android Application Packages for Android v4.0.

TABLE II
DISTRIBUTION OF JAVA FILES IN APPLICATION PACKAGES

Android Source Package	Total Number of Source Files	Number of Java Files	Percentage of Java files (%)
Email	1070	402	37.62
Contacts	1071	331	31.00
Telephony	707	200	28.61
Gallery	87	22	25.29
Bluetooth	207	38	18.47
Calculator	121	13	10.72
Desk Clock	301	31	10.33
Music Player	516	48	9.32
NFC	243	22	9.13
Calendar	398	11	2.81
Total	**4721**	**1154**	**18.66**

Fig. 4 gives the distribution percentage of Java source files for the same data in Android v4.0. However, the Android Application Packages were "cloned" (downloaded) by the DCRS itself from the git repository: https://android.googlsesource.com. This functionality has already been discussed in detail in Section IV.

We now discuss the results obtained for the Android 'Contacts' Application Package.

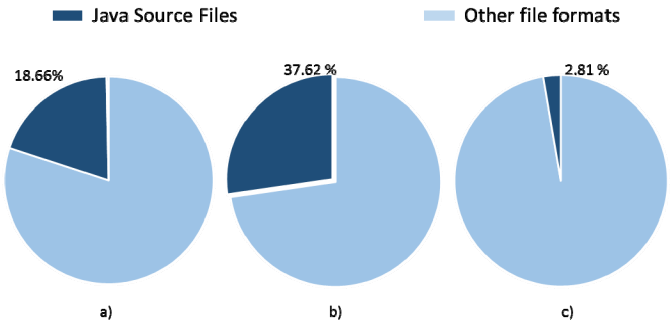

Fig. 4. Distribution of Java Files in Android Application Packages – Mean Percentage in a, Maximum in b and Minimum in c.

B. *Analysis of Results*

We have operated the DCRS on Android's 'Contacts' Application Package (v4.0 and v4.1) to first obtain the change-logs and finally various defect reports as stated in Section III. Fig. 5 presents a sample change record from the change-log of the Contacts application.

```
TIMESTAMP 1354144296

BEGINNING OF THE COMMIT RECORD

Prevent going into single contact mode un-necessarily. On a
tablet, after creating a new contact, the contact list
would enter "single contact mode". This mode is intended
for the case where you may have an account filter set and
you want to see a contact in a different account.  Combined
with a stale contact list, this caused the app to go into
single mode when it was not necessary.
This will fix the most common case where all accounts are
shown and a new contact is added. The new contact will be
displayed in the normal list. This will not fix the case
where an account filter is active and a new contact is
created.  In this case, the new contact is still displayed
in single contact mode.

Also tested was the test cases in:
I233162572e25acb737c9eae787dfc146879a0dc2

Bug: 7621855
Change-Id: I6f323c4003677cec9db63cae347f4532071037b9

ENDING OF THE COMMIT RECORD BODY
src/com/android/contacts/list/ContactBrowseListFragment.jav
a | 9 ++++++++-
1 file changed, 8 insertions(+), 1 deletion(-)
```

Fig. 5. Sample change record in the change-log of Contacts Application

1) Defect Data Analysis: From the Defect count and metrics report, we were able to obtain the data for the total number of defects reported in the classes for v4.0, during the transition from v4.0 to v4.1. Table III presents the distribution of defects in the classes of Contacts application in v4.0. Fig. 6 depicts a diagrammatic representation of the defect distribution in the considered software. Majority of the classes (67.8%) were found to have no defect during the transition from v4.0 to v4.2. 29% of the classes were found to be having a defect count in the range of 1-5. Classes with the defect count of 6 and above were merely 3.2%.

TABLE III
DISTRIBUTION OF DEFECTS IN THE CLASSES

Number of Defects	0	1-5	6-10	11-15	>15
No of classes	224	96	4	4	3

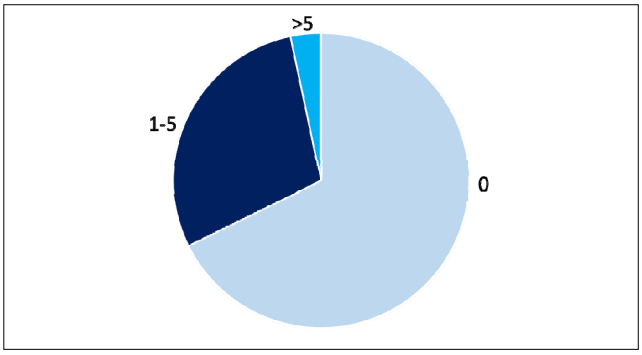

Fig. 6. Distribution of Defects

2) Change Data Analysis: From the consolidated defect and change report, we were able to obtain the data for the total number of changes incurred in the classes for v4.0, during the transition from v4.0 to v4.1. Table IV presents the distribution of changes in the classes of Contacts application in v4.0. Fig. 7 depicts a diagrammatic representation of the change distribution in the considered software. Majority of the classes (64%) were found to have no change incurred during the transition from v4.0 to v4.2. 33% of the classes were found to be having a change count in the range of 1-5. Classes with the total number of incurred changes more than 5 were only 3%.

TABLE IV
DISTRIBUTION OF CHANGES IN THE CLASSES

Number of Changes	0	1-5	6-10	11-15	>15
No of classes	212	109	4	2	4

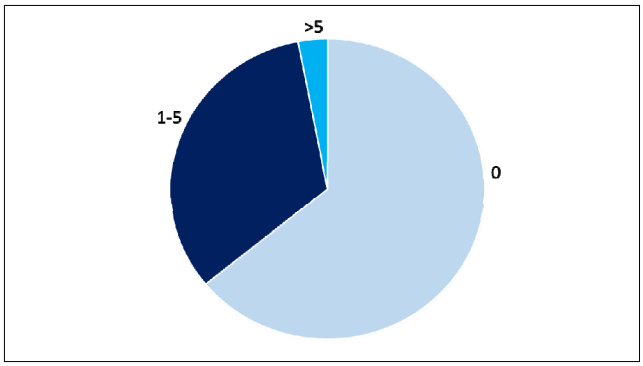

Fig. 7. Distribution of Changes

3) Statistical Comparison: From the analysis of newly added and deleted source code file reports, we can perform a statistical comparison of the two different versions (v4.0 and v4.1) of the Android Contacts application in the terms of, for example, the total number of added java files, total number of deleted java files, etc. Table V summarizes the various parameters we have computed for comparing the two versions of the application under consideration.

TABLE V
PARAMETERS FOR COMPARISON

Parameter	Value
Number of new source code files	31
Number of defects reported in new files	64
Number of deleted source code files	8
Number of defects reported in deleted files	10
Number of files added and then deleted from v4.1	0
Total number of file changes	23

VI. APPLICATION OF THE DATA COLLECTED THROUGH DCRS

In the previous section, we presented a demonstration of the DCRS for a sample Android OS application and analysed the data and results obtained from the various generated reports. On the basis of this discussion, we can state that the data collected from DCRS can be potentially employed in the following applications:

A. Defect Prediction Studies

Fault proneness or defect prediction is a useful technique for predicting the fault prone classes in a given software.

Simply, it can be stated as the method to predict the occurrence and/or number of defects in the software under consideration. For the past many years, defect prediction has been recognized as an important research field so as to organize a software project's testing resources and facilities. For example, consider a scenario wherein we have limited time and/or resources available for software testing procedure and activities. In such a situation, appropriate defect prediction models can aid the testing personnel to focus more attentively on those classes which are highly probable to be defective in the later releases of the software. Various studies have been conducted in the past for predicting effective fault proneness models, and also for validating the impact of OO Metrics on fault proneness ([1]-[3], [9], [10]).

It can be observed form Section V B. that the defect reports generated by the DCRS can be effectively employed for such studies.

B. Change Proneness Studies

Change proneness may be defined as the probability that a given component of the software would change. Along with defect prediction or fault proneness, change proneness is also very crucial and needs to be evaluated accurately. Prediction of change prone classes may aid substantially in maintenance and testing. A class that is highly probable to change in the later releases of a software needs to be tested rigorously, and proper tracking is required for that class while modifying and maintaining the software. Therefore, various studies have also been carried out in the past for predicting effective change proneness models, and to validate the impact of OO Metrics on change proneness [11]-[14].

As we have already described in Section V B., the DCRS reports can also be used in Change analysis and therefore for change proneness studies as well.

C. Statistical Comparison

We have already demonstrated the statistical comparison of the two versions (v4.0 and v4.1) of the Android OS Contacts Application Package in Section V B. Such kind of comparison can also be extended or generalized for a large number of Git based open source software systems and applications. We may also identify some additional parameters for the comparison through defect and change data analysis, such as the total number of defects reported and total number of changes incurred in the previous version of the considered software.

VII. CONCLUSIONS AND FUTURE WORK

Giving a description of the Defect Collection and Reporting System, this paper concludes that the developed system can be potentially employed for the collection of Defect Data pertaining to Open Source Software (which employ Git as the Version Control System) and generating useful reports for the same.

The gathered information can be effectively used for various purposes, including the following applications:

- Defect prediction, change prediction and related research work or studies, including analysis and validation of the effect of given metric suite on fault and/or change proneness (CKJM, QMOOD, etc.) and the evaluation and comparison of various techniques in predicting fault and/or change proneness models, such as statistical and machine learning methods.
- Statistical Comparison of any two versions of a given Open Source Software (which is based on Git version control system), in terms of various parameters, including the number of source files which have been added in the newer version, the number of source files which were present in the previous version but have been deleted in the newer version, and the number of defects which have been reported in the previous version of the software under consideration.

We have planned to carry out similar studies and work which would not be limited to only Git Version Control System based Open Source Software, but also for other widely used open source applications that are made available through various software repositories.

REFERENCES

[1] R. Malhotra, "A Defect Prediction Model for Open Source Software", *Proceedings of the World Congress on Engineering* (2012) Vol II, London, U.K, 2012.

[2] K.K. Aggarwal, Y. Singh, A. Kaur and R. Malhotra, "Empirical Analysis for Investigating the Effect of Object- Oriented Metrics on Fault Proneness: A Replicated Case Study", *Softw. Process Improve. Pract.* , 389-412, 2008.

[3] I. Gondra, "Applying machine learning to software fault-proneness prediction", *Journal of Systems and Software 81*, 186–195, 2008.

[4] B. Handerson and Selleres, "Object-Oriented Metrics, Measures of Complexity", *Pentice Hall,* 1996.

[5] S. Chidamber and C. Kemerer, "A metrics Suite for Object-Oriented Design", *IEEE Trans. Software Engineering*, vol. SE-20, no.6, 476-493, 1994.

[6] J. Bansiya and C. Davis, "A Hierarchical Model for Object-Oriented Design Quality Assessment", *IEEE Transactions on Software Engineering*, vol. 28, no. 1, 4-17, 2002.

[7] T. McCabe, "A Complexity Measure", *IEEE Transactions on Software Engineering*, vol. 2, no. 4, 1996.

[8] A. Hassan, "The Road Ahead for Mining Software Repositories", *Frontiers of Software Maintenance,* 48-57, 2008.

[9] Y. Kaur and R. Malhotra, "Application of Random Forest in Predicting Fault-Prone Classes", *International Conference on Advanced Computer Theory and Engineering,* 37-43, 2008.

[10] F. Peters, T. Menzies and A. Marcus, "Better Cross Company Defect Prediction", *MSR 2013,* San Francisco, CA, US, 409-418, 2013.

[11] P. Liang and J. Li, "A Change-Oriented Conceptual Framework of Software Configuration Management", IEEE.

[12] R. Malhotra and M. Khanna, "Investigation of relationship between object-oriented metrics and change proneness", *International Journal of Machine Learning and Cyber*netics, Vol. 137, Number 1(January 2010), 2012.

[13] X. Tao, "Software Configuration Management of Change Control Study Based on Baseline", *International Conference on Intelligent Control and Information Processing*, August 13-15, 2010 - Dalian, China.

[14] Z. Yuming, L. Hareton and X. Baowen, "Examining the Potentially Confounding Effect of Class Size on the Associations between Object-Oriented Metrics and Change-Proneness", *IEEE Transactions on Software Engineering*, Vol. 35, No. 5, September/October 2009.

Available online at www.sciencedirect.com

ScienceDirect

Procedia Technology 17 (2014) 289 – 294

Procedia Technology

Conference on Electronics, Telecommunications and Computers – CETC 2013

Design and analyze the Refractive Index sensor having the discontinuity between sensing region and cladding area by large core diameter

Himanshu Mohan[a], Gopal[b], Ajeet Kumar[c]

[a]*Delhi Technological University, Delhi, India*
[b]*Netaji Subhas Institute Of Technology,New Delhi, India*
[c]*Delhi Technological University, Delhi, India*

Abstract

We present the design and analysis of the Refractive Index sensor having the discontinuity between sensing region and cladding area by large core diameter. If sensing region is placed in different refractive index medium then the cladding, the modal field distribution changes. The overlap of modal fields in the cladded region and the sensing region gives an estimate of fractional power transfer from the input end to output end. This fractional power transfer gives us the refractive index of the medium.
© 2014 The Authors. Published by Elsevier Ltd. This is an open access article under the CC BY-NC-ND license (http://creativecommons.org/licenses/by-nc-nd/3.0/).
Peer-review under responsibility of ISEL – Instituto Superior de Engenharia de Lisboa, Lisbon, PORTUGAL.
Keywords: Core diameter mismatch; large-mode-area-fibre; leakage loss; optical communication; refractive index sensor; single-mode fibre; speciality fiber.

1. Introduction

Optical fiber has numerous applications [1], [2]. One of them is as a refractive index (RI) sensor. Optical refractive index (RI) sensors are widely researched for a number of applications and are prominent among the commercial landscape of current sensing technologies. This sensing epitome promises a real time and accurate result with minimum sample preparation. Also this fiber based sensor can be very compact in size and be made suitable for remote sensing. Metal coated fiber has also been used as a sensor of absorption [3–6]. Metal coated fibers using surface plasmon resonance [7], [8] and in fiber bragg grating [9], [10] have been used as a highly sensitive RI sensing devices. Tapering of fiber and stripping of the fiber cladding have been used to make optical fiber a sensitive sensor of RI [11–15]. Untapered, fully cladded fibers with thin films deposited on them have also been used as RI sensors [16]. Optical fiber can be used as sensors [17], [1] to measure refractive index, strain, temperature, pressure and other quantities by

* Himanshu mohan. Tel.: +91-9540362077 .
E-mail address: himanshumohan.dtu@gmail.com

2212-0173 © 2014 The Authors. Published by Elsevier Ltd. This is an open access article under the CC BY-NC-ND license (http://creativecommons.org/licenses/by-nc-nd/3.0/).
Peer-review under responsibility of ISEL – Instituto Superior de Engenharia de Lisboa, Lisbon, PORTUGAL.
doi:10.1016/j.protcy.2014.10.239

modifying a fiber so that the property to be measured modulates the power transferred, intensity, phase, polarization, wavelength, or transit time of light in the fiber. Sensors that vary the intensity of light are the simplest, since only a simple source and detector are required. A particularly useful feature of such fiber optic sensors is that they can, if required, provide distributed sensing over distances of up to one meter.

2. Refractive Index Sensor

Different chemical substances as well as several physical and biological parameters can be detected through measurements of the refractive index (RI). For this reason, RI sensors [18], [19] have gained considerable attention by the sensor community. Fiber-based refractometric devices [20] are attractive, owing to the inherent advantages over their counterparts based on other techniques. For example, they can be multiplexed on a single fiber network and are suitable for in situ and remote RI measurements. Moreover, they are compact and lightweight. In addition, the amount of sample needed to carry out the measurements can be very small. So far, different alternatives have been proposed to design RI sensors with conventional optical fibers. These include core-exposed or tapered fibers, fiber Bragg gratings (FBGs) [21], long period gratings (LPGs) [19], [22] interferometers made with FBGs or LPGs, refractive index sensors based on core diameter mismatch etc. The advent of micro structured optical fibers has also opened new possibilities for RI sensing.

3. Basic Principle of Sensing

The basic principle of sensing is to have a mismatch between the diameter of core of uncladded region (sensing region) and core of cladded region. So not all of the light couples with uncladded region, i.e, some portion of light radiate out when it goes from the cladded region to the sensing region. Hence the modal field is modulated in the sensing region. Hence total power at output is also modulated and become sensitive to the refractive index of the external medium. By measuring the output power and input power we can find out the refractive index of the external medium.

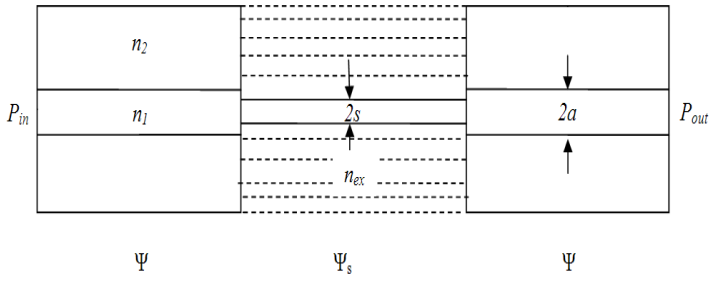

Fig. 1. Schematic diagram for the core diameter mismatch sensor

Schematic of core diameter mismatch sensor is shown in Fig. 1. n_1, n_2, n_{ex} are refractive indices of core, cladding and external medium. Here a and s defines the core radii in cladded and sensing region respectively. The modal fields in the cladded and the sensing regions are represented by ψ and ψ_s respectively. If the sensing region of the fiber is placed into a medium having refractive index different from that of cladding, the modal field distribution changes. The overlap of modal fields in cladded region and sensing region gives estimate of fractional power transfer from the input end to output end. The fractional power transfer is given by

$$T = \frac{P_{out}}{P_{in}} \tag{1}$$

$$T = \frac{|\int\int \psi^* \psi_s r dr d|^2}{(\int\int |\psi|^2 r dr d \int\int |\psi_s|^2 r dr d\varphi)} \tag{2}$$

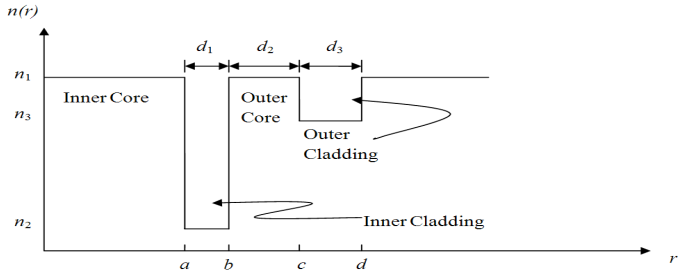

Fig. 2. Schematic of the refractive index profile of a co-axial duel core leaky fiber

When $n_{ex} = 1$, there is strong confinement of modal field in the core of the sensing region and the overlap between ψ and ψ_s is small. As the value of n_{ex} increases, the field spreads into the sensing region and the overlap increases. This will change the transmitted optical power.

4. Large Core Area Refractive Index Sensor

It is impossible to achieve single mode operation by a large core conventional fiber. So we have used a specialty fiber that is co-axial dual core leaky fiber. The fiber works on the principle of mode filtering. By using the concept of core-diameter mismatch such a large core single mode fiber can be used to design a single single-mode refractive index sensor for wide refractive index.

4.1. Co-axial Dual Core Leaky Fiber

The refractive index profile of the proposed design is shown in the Fig. 2 and is defined as

$$n(r) = \begin{cases} n_1; & 0 < r < a \\ n_2; & a < r < b \\ n_1; & b < r < c \\ n_3; & c < r < d \end{cases} \tag{3}$$

where $n_1 > n_3 > n_2$.

The high index regions $0 < r < a$ and $b < r < c$ define inner and outer cores of the fiber, respectively. The regions $a < r < b$ and $c < r < d$ are depressed cladding regions and can be defined as inner and outer cladding respectively. The outermost high index region ($r > d$) makes the overall design leaky, and all the modes suffer from finite leakage loss. The width of different layers are defined as $d_1 = b - a$, $d_2 = c - b$ and $d_3 = d - c$.

5. Results and Discussions

For the fiber structure proposed in Fig. 1 and having profile parameter in eq. 3, following results are obtained which are responsible for single mode operation and large core area refractive index sensor. We define the inner core of the fiber by the following parameters: $n_1 = 1.444388$, $\triangle = 0.006$, $a = 15\mu m$. The wavelength of operation used is $1.55\mu m$. We choose the outer core width $d_2 = 8\mu m$, and the separation between the two cores is $d_1 = 4\mu m$. The fiber works on the principle of mode filtering. A high differential leakage loss between the fundamental and the higher-order modes with a nominal loss to the fundamental mode ensures effective single-mode (SM) behavior of the fiber. We use the outer cladding parameters n_3 and d_3 to primarily control the leakage losses of the modes.

In Fig. 3, the variation of leakage loss with refractive index is shown for first three modes. The leakage losses of the modes increase with the outer cladding index n_3. A peak appearing in the loss curve of the LP_{11} mode around $n_3 = 1.4425$ reflects the resonant coupling of power from the LP_{11} mode to the outer core, which is highly leaky. Such a coupling of power facilitates the stripping of the LP_{11} mode quickly, even before the LP_{02} mode. At this resonance

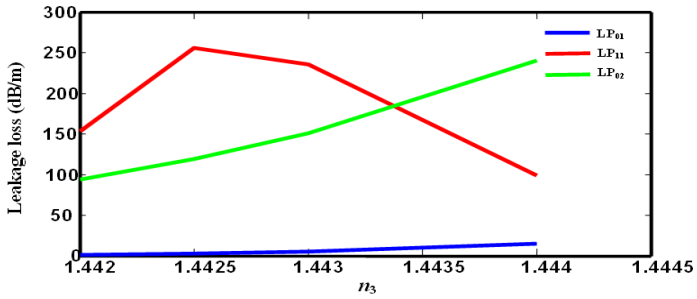

Fig. 3. Variation of leakage losses of first three modes of a fiber with outer index n_3

cladding index it is the differential leakage loss of the LP_{02} mode which now determines the single-mode operation of the fiber. The variation of outer cladding width with leakage loss is also studied and significantly decreases with d_3.

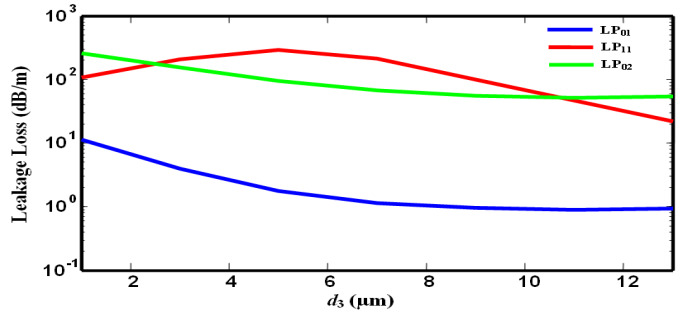

Fig. 4. Variation of leakage losses of first three modes of a fiber with outer cladding width d_3

For higher-order modes, one can note that in the range $2.4\mu m < d_3 < 11.3\mu m$, the leakage loss of the LP_{11} mode surpasses that of the LP_{02} mode and reflects a resonant coupling effect. This range of d_3 can be used to design a large mode area leaky fiber. Figure 4 can, thus, help us in choosing the efficient design parameters. At the first crossing point ($d_3 = 2.4\mu m$) the leakage loss of the LP_{11} and LP_{02} modes is 186 dB m^{-1} and that of the LP_{01} mode is 5 dBm^{-1}. In a design corresponding to this point, the higher-order modes would strip off in just 10 cm propagating distance. However, the fundamental mode would suffer from quite a large loss. When we increase the value of d_3, the differential leakage loss increases, and also the loss of the LP_{01} mode goes down considerably. At the second crossing point ($d_3 = 11.3\mu m$) the leakage loss of the LP_{11} and LP_{02} modes is 55 dB m^{-1} and that of the fundamental mode is 0.04 dB m^{-1}. The higher-order modes, thus, strip off only after 36 cm propagation distance and the fundamental mode suffers from a nominal loss. The fiber, thus, shows an effective SM operation. To analyze the performance of proposed LMA sensor we have studied the effect of ambient medium on the fractional power output for different etched core radius.

5.1. Same Core Diameter

The given graph tells us, how the fractional power transfer varies with different external refractive index. The total power transfer varies from 98.6 % to 99.8% for the variation in external refractive index from 1.32 to 1.44. This shows a small sensitivity for such a large range of refractive index. Hence sensing radius equal to the core radius gives less sensitivity. This is due to the approximately 100% power transfer from the cladded region to the sensing region.

5.2. Core Diameter Mismatch

Figure 6 shows that the Fractional Power Transfer changes with the change in the Refractive Index of the external medium. This shows that the power transfer from the input to the output varies from 25% to 65% as the refractive

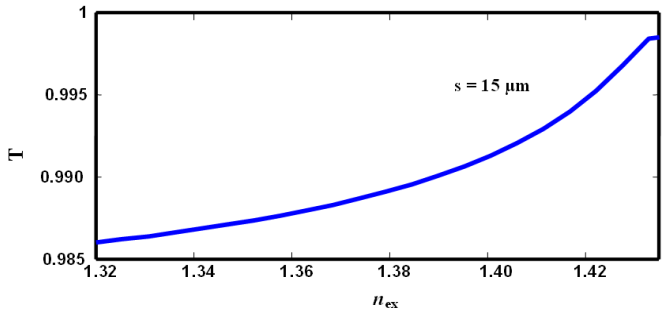

Fig. 5. Fractional power transfer (T) versus the refractive index of the external medium for sensing radius of 15μm

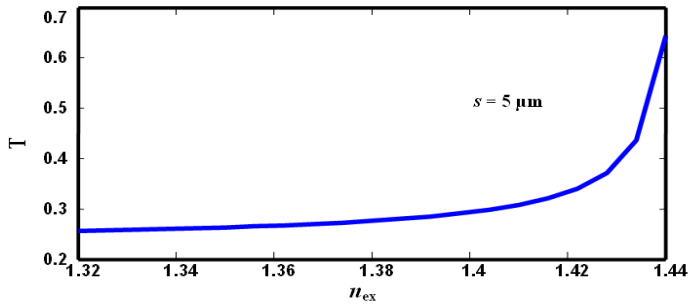

Fig. 6. Fractional power transfer (T) versus the refractive index of the external medium for sensing radius of 5μm

index of the external medium varies from 1.32 to 1.44. In this case, As core diameter mismatch is very high, The sensitivity is very large. Such a large variation in the T is due to the fact that field in the sensing region resembles the cladded region field on increasing the n_{ex}.

This plot gives the variation of Fractional Power Transfer with the External Refractive Index. The power transfer is from 48% to 76% as refractive index varies from 1.32 to 1.44. In this case the power transfer is more than the $s = 5\mu m$ case. As the sensing radius is increased more power can propagate.

The total power transfer for the different sensing radius is plotted on the same graph and shown below.

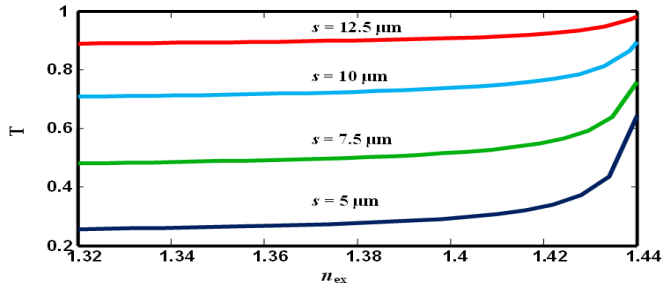

Fig. 7. Fractional power transfer (T) versus the refractive index of the external medium for different sensing radius

As it can be seen from the above plot that as the core diameter mismatch increases, the range of total power transfer increases. Hence this shows that sensitivity is increased as the core diameter mismatch increases.

6. Conclusion and Scope for Future Work

A refractive index sensor is proposed with a large core area with a single fiber having effective single mode operation. Single mode operation is made possible with the help of certain design parameters due to which higher order

modes are leaked out. Due to large core area it can support large power and is also less fragile. This is a great advantage. Apart from this, T varies from approximately 25% to 65% for $s = 5\mu m$ when n_{ex} is increased from 1.32 to 1.44. In comparison, in single mode optical fiber refractive index sensor configuration of Ref. [18] change is from 50% to 78% for $s = 0.7\mu m$. Again in comparison to the multimode-single-mode-multimode configuration of Ref. [23], change is from 86% to 97% for same s. The results indicate that the core diameter mismatch sensor, in which a part of the core has also been removed, is more sensitive to the same core diameter sensor. Also as we increase the core diameter mismatch the sensitivity also increases. The proposed sensor can be used as a compact refractometer. It can also be used for other wavelengths for which sensitivity may be more.

References

[1] Ghatak, A., Thyagarajan, K.. An introduction to fiber optics. Cambridge university press; 1998.
[2] Senior, J.M., Jamro, M.Y.. Optical fiber communications: principles and practice. Pearson College Division; 2008.
[3] Paul, P.H., Kychakoff, G.. Fiber-optic evanescent field absorption sensor. Applied physics letters 1987;51(1):12–14.
[4] Gupta, B.D., Singh, C.D., Sharma, A.. Fiber optic evanescent field absorption sensor: effect of launching condition and the geometry of the sensing region. Optical Engineering 1994;33(6):1864–1868.
[5] Ruddy, V., MacCraith, B., Murphy, J.. Evanescent wave absorption spectroscopy using multimode fibers. Journal of Applied Physics 1990;67(10):6070–6074.
[6] Ruddy, V.. An effective attenuation coefficient for evanescent wave spectroscopy using multimode fiber. Fiber & Integrated Optics 1990;9(2):143–151.
[7] Iga, M., Seki, A., Watanabe, K.. Hetero-core structured fiber optic surface plasmon resonance sensor with silver film. Sensors and Actuators B: Chemical 2004;101(3):368–372.
[8] Monzón-Hernández, D., Villatoro, J., Talavera, D., Luna-Moreno, D.. Optical-fiber surface-plasmon resonance sensor with multiple resonance peaks. Applied optics 2004;43(6):1216–1220.
[9] Shu, X., Gwandu, B.A., Liu, Y., Zhang, L., Bennion, I.. Sampled fiber bragg grating for simultaneous refractive-index and temperature measurement. Optics letters 2001;26(11):774–776.
[10] Schroeder, K., Ecke, W., Mueller, R., Willsch, R., Andreev, A.. A fibre bragg grating refractometer. Measurement Science and technology 2001;12(7):757.
[11] Wong, Y., Scully, P., Kadim, H., Alexiou, V., Bartlett, R.. Automation and dynamic characterization of light intensity with applications to tapered plastic optical fibre. Journal of Optics A: Pure and Applied Optics 2003;5(4):S51.
[12] Kumar, A., Subrahmanyam, T., Sharma, A., Thyagarajan, K., Pal, B., Goyal, I.. Novel refractometer using a tapered optical fibre. Electronics Letters 1984;20(13):534–535.
[13] Villatoro, J., Monzón-Hernández, D., Talavera, D.. High resolution refractive index sensing with cladded multimode tapered optical fibre. Electronics letters 2004;40(2):106–107.
[14] Afromowitz, M.A., Lam, K.Y.. Fiber optic cure sensor for thermoset composites. In: OE/Fiber LASE'88. International Society for Optics and Photonics; 1989, p. 135–139.
[15] Lam, K.Y., Afromowitz, M.A.. Fiber-optic epoxy composite cure sensor. ii. performance characteristics. Applied optics 1995;34(25):5639–5644.
[16] Cusano, A., Cutolo, A., Giordano, M., Nicolais, L.. Optoelectronic refractive index measurements: application to smart processing. Sensors Journal, IEEE 2003;3(6):781–787.
[17] Agrawal, G.P.. Nonlinear fiber optics. Springer; 2000.
[18] Kamakshi, K., Rastogi, V., Kumar, A., Rai, J.. Design and fabrication of a single-mode optical fiber based refractive-index sensor. Microwave and Optical Technology Letters 2010;52(6):1408–1411.
[19] Tsuchida, Y., Saitoh, K., Koshiba, M.. A design method for single-polarization holey fibers with improved beam quality factor. Journal of Lightwave Technology 2008;26(14):2162–2167.
[20] Rastogi, V., Kamakshi, K., Patra, R., Kumar, A., Rai, J.. Design and fabrication of single mode fibre optic refractive index sensor ????;.
[21] Stegall, D., Erdogan, T.. Leaky cladding mode propagation in long-period fiber grating devices. Photonics Technology Letters, IEEE 1999;11(3):343–345.
[22] Mukherjee, A., Munsi, D., Saxena, V., Rajput, R., Tewari, P., Singh, V., et al. Characterization of a fiber optic liquid refractive index sensor. Sensors and Actuators B: Chemical 2010;145(1):265–271.
[23] Villatoro, J., Monzón-Hernández, D.. Low-cost optical fiber refractive-index sensor based on core diameter mismatch. Lightwave Technology, Journal of 2006;24(3):1409–1413.

DESIGN AND STUDY OF A SOLAR THERMAL SYPHON PUMP

Md. Zishan Akhter[1], Md. Sarwar Khan[2], Md Sameer Farooque[3], Kaushalendra K. Dubey[4], Gopal P. Sinha[5]

[1,2,3]U.G.Student,Dept of M & AE, School of Engg & Tech, Sharda University,Gr Noida,U.P. India
[4] Research Scholar, Dept of Mechanical, Production, Industrial & Automobile Engg, Delhi Technological University, New Delhi, India
[5]Professor,Dept of M & AE, School of Engg & Tech, Sharda University,Gr Noida,U.P. India

ABSTRACT

This paper describes the idea and the development of a solar thermal energy driven pump for lifting of ground water for irrigation as well as for meeting urban supply system. This has the potential of saving over 93billion kWh of electrical energy and 3.3 billion litres of diesel (fossil fuel) per year, for India. The invention has been patented. The most attractive feature of the pump is the absence of any moving part, which makes it almost maintenance-free. Solar thermal energy is used to create a pressure higher than the atmospheric pressure, over the surface of liquid to be pumped to height H. The estimated thermal efficiency of solar thermal syphon pumping is four times of photovoltaic pumping system.

Keywords - Solar Thermal Energy, Syphon Pump, Overall Efficiency.

NOMENCLATURE

Aa = aperture area of PTC in m^2
Sc = solar constant in KW/m^2
Pc = pressure created by solar energy in Pascal,
P_A = Atmospheric pressure in Pascal
Ƥ = Mass density of liquid in kg /m^3.
g = acceleration due to gravity in m/s^2.
h = Enthalpy of steam.
H = Discharge height.
m_w = mass flow rate of water in m^3/s.
m_s = mass flow of steam in m^3/s.
V = flow velocity of water in m/s
Hs = friction loss in pipe.

ϕ = Latitude angle of location where system is installed in degree

β = Inclination angle of PTC system from horizontal in degree.

r_r = Rim Radius in meter.

ϕ_r = Rim Angle in degree

f = Focal Distance in meter.

h_p = Parabolic Height in meter.

D = Receiver or Boiler Diameter in meter.

C_R = Concentration Ratio

Θ = Incidence Angle in degree.

ω = Hour angle

γ = System Azimuth angle in degree

δ = Solar Incidence angle in degree.

n = Total no of day in month measured from 1st January.

$\eta_{opto\text{-}thermal}$ = Opto-Thermal efficiency of Syphon system

Ib = Solar Irradiation

q_u = Rate of use full energy in joule

U_L = heat loss co-efficient (W / m^2k)

Tc = Receiver Temperature in ^0C

Tr = Mean Receiver Temperature in ^0C

Ta = Ambient Temperature in ^0C

Rk = Thermal Resistance of Receiver or Boiler Tube

Acond = Effective area of conduction in m^2

ϵr = Non selective absorber parameter.

$\tau\alpha$ = Effective Transmission.

Qgen = Heat generated from PTC.

Qreq = Required Heat for steam generation.

$\eta_{thermo\text{-}syphon}$ = Thermal Efficiency of system.

ηo = Overall Efficiency.

η_{SPV} =Solar Photovoltaic panel Efficiency.

η_{pump} = Irrigation pump Efficiency.

η_{CC} = Charge-Controller Efficiency.

η_B = Battery Efficiency.

l = Length

b = Width

t = Thickness

PTC=Parabolic Through Collector.

STSP= Solar Thermal Syphon Pump.

SPVP= Solar Photovoltaic Pump System.

IJARSE

I. INTRODUCTION.

Most of the developing countries have large needs of irrigation for meeting their agricultural requirements for food-security. The drinking water requirement also necessitates lifting of ground water to a height ranging from 50 to 200 feet. This requires huge amount of energy which is currently supplied through electricity and fossil fuel based engines. For a country like India the energy consumed for lift irrigation has been 93225.28MU, (in the year 2011),1MU= 1M kWhr [6].In most of the cases the developing countries are endowed with rich solar energy. Some of it has been used for lift irrigation using photovoltaic panels electrically coupled to a conventional motor pump system, or Stirling cycle based engine coupled through a conventional pump. The potential number of SPV pumps is estimated at 70 million, with extending irrigation support to untapped markets [7]. This work reports the use of direct solar thermal energy for creating pumping action. The uniqueness of this development is that the pumping action requires no moving parts-reciprocating, rotating or expander action. Therefore there is no possibility of wear and tear or lubrication requirement or loss of energy due to friction between moving parts. Syphon action created by water vapour picked-up from the source, lifts the water from the reservoir through the delivery head. This is being demonstrated for the first time. The efficiency of the entire system is also high on account of no moving parts. An excellent review of the development of solar energy based pumps have been carried out by Y.Wong et al [11].The proposed thermo-syphon pump is a high pressure steam forced pump where there is no limitation of a suction head of less than 34 feet of water, the delivery head is unlimited based on the concentration of solar energy and the aperture area requirement of the solar collector has been worked out in subsequent paragraphs.

A model has been fabricated for proving the concept. This model demonstrates lifting of water through a head of nearly 5 to 10 feet Fig.2, shows a sketch of the parabolic trough collector (PTC) used for concentrating the solar thermal energy.

In most of the developing countries are endowed with rich solar energy. Some of it has been used for lift irrigation using photovoltaic panels electrically coupled to a conventional pump, or Stirling cycle based engine coupled through a conventional pump. The potential number of SPV pumps is estimated at 70 million, with extending irrigation support to untapped markets [7]. Total cost (before subsidy) for installation and commissioning of SPV water pump system varies from Rs. 190,000 to 290,000 or even Rs. 450,000/- [8][9].Capital cost of a 1.8 kWp solar PV pump is about Rs. 0.3 million. The payback period of solar PV pump (without subsidy) replacing a diesel pump is about 9 years (at a cost of diesel is Rs. 32/litre) [12].Purohit evaluated the financial attractiveness of different renewable energy technologies for irrigation water pumping in India. He calculated the following unit costs for water for SVP pumping systems [10]. The unique part of this development is that the pumping action requires no moving parts, reciprocating or rotating and therefore there is no possibility of wear and tear or lubrication requirement. A model has been fabricated for proving the concept as shown in Fig.1a and Fig.1b. This model demonstrates lifting of water through a head of nearly 5 to 10 feet.

II. WORKING OF SOLAR THERMAL SYPHON PUMP.

Solar Thermal Syphon pumping system (STSP) may be used to lift water from the ground or any liquid to a height without using any moving mechanical-part by pressurized steam through syphon action. The steam is generated by solar energy concentrator on a tube filled with the liquid. The concentration of solar energy can be

achieved by parabolic trough collector (PTC) / concave / plane mirrors type solar concentrator or through Fresnel lenses based solar thermal system.

Water liquid enters into a boiler cell, through an inlet regulated by a float valve action, for maintaining a uniform level. Steam generated in the boiler flows through a perfectly insulated and sealed pipe into an enclosures connected to ground water to be pumped. The discharge pipe is dipped below the ground water. The pressurized steam lifts the water to the delivery head H, through a syphon action. The conversion of water in to steam at boiling temperature of water depends upon the thermal energy obtained from the area of PTC (Aperture Area of concentrator).The heat raise the temperature of boiler and water gets converts into steam. The water feeding pipe use some amount of steam pressure feeding water to the boiler [8]. Fig.1a and Fig.1b, show the model and working set up of the thermo-syphon pump. This system has been developed in mechanical

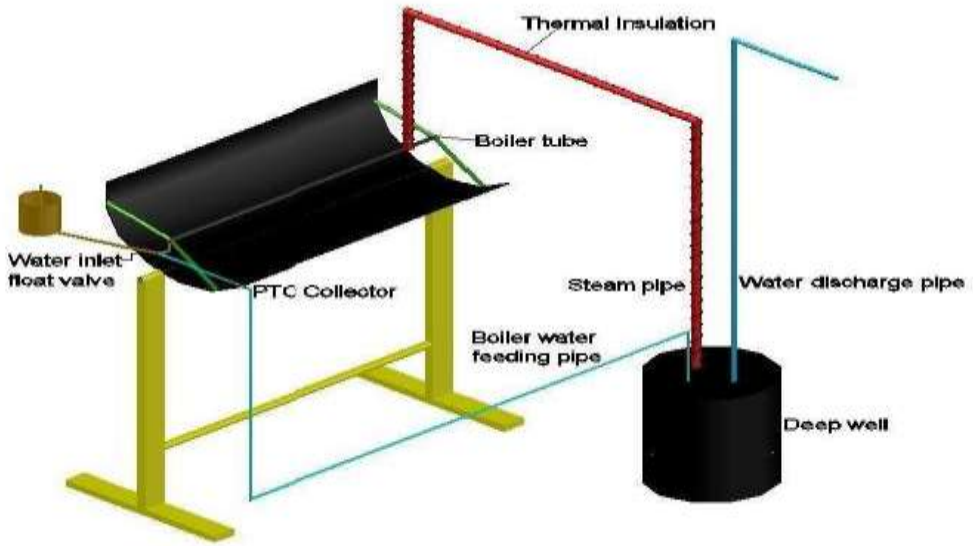

engineering department sharda university greater noida,u.p. state, India. Dimension of all parts of STSP listed in Table-1

Fig. 1a: Schematic of Solar thermal Syphon Pump.

Fig. 1b: Working set up of Solar thermal Syphon Pump at Sharda University Greater Noida campus.

III. PRINCIPLES OF THE SOLAR THERMAL SYPHON SYSTEM.

The solar thermal syphon pump derives its pumping action by putting additional pressure on the surface of the liquid, to be lifted. This additional pressure is obtained using solar thermal energy in concentrated form. The concentrated solar thermal energy obtained by a parabolic trough collector (PTC) is given by

[2]

Q_{gen} = Aa Ib W……..(1)

The useful solar gain by the collector Qu = Aa (τα) Ib W

τα = Effective Transmission

The head of lifted water or liquid is given by

H = (Pc - P_A)/ βg meters .Where Pc is pressure created by solar energy in Pascal, P_A is Atmospheric pressure in Pascal ,β is Mass density of liquid in kg /m^3 and g is acceleration due to gravity in m/s^2.

3.1 Collection and concentration of solar thermal energy using PTC.

For generating steam, whose pressure is used for pumping of liquid to a height, we require concentrated solar thermal energy for super heated high pressure steam at a high pressure. This is achieved by a PTC or a Fresnel lens or a combination of the two. The concentrated thermal energy obtained through PTC is given by Heat required for steam generation [4],

$Q_{reqired}$ = m_{water} [Cp_{water} ($T_{boiling}$ - $T_{ambient}$) + LH_{water}]+

m_{steam} [Cp_{steam} (T_{sup} –$T_{boiling}$) + $LH_{vaporisation}$] KJ……..(2)

For system to work continuously

Qgen >_ Qreq……..(3)

Boiling Temperature of water for the exerting the required steam pressure ($T_{boiling}$) is directly taken from steam table corresponding to the pressure Pc.This heat can generate steam at a pressure Pc is given by

Pressure required on water table for achieving the discharge head

Pc = 10^5 + 10^4 H Pa……..(4)

This pressure on the surface of the liquid can lift it by 'H' meter through syphon action is given by

H = (Pc - Pa)/ βg meter……..(5)

3.2 Estimation of specified head H and flow rate Q.

Heat from PTC is mainly required to meet the heat loss occurring due to imperfect insulation and the temperature difference between the superheated steam and the ambient. It is given by,

Total energy in steam = Energy given to discharge

m_s h = m_w g H + ½ $m_w v^2$ + hs……..(6)

Conduction loss in pipe = Effective surface area for conduction (Acond) / thermal resistance (R_k).

$$\left[\frac{(Tr-Ta)}{Rk} \times \frac{Acond}{Aa}\right] \ldots\ldots\ldots\

3.4 Dimensions of STSP parts.

Table-1 Dimensions of STSP

STSP Parts	Dimensions
Reflector	l = 2.44 m, b= 1.25 m, t= 0.4 m. Aperture Area = 2.44 m^2
G.I Sheet for reflector support.	l = 2.44 m, b= 1.25 m, t= 0.36 m.
Copper Water Tube	L = 2.44m,Diameter = 20mm, Volume = 7.6 ×10 $^{-5}$ m^3
PVC Steam Tube	Diameter =14mm, Thermally insulated with glass wool.
Supporting Iron Frame **Arc** **Rods** **Rivets** **Mounting Nut**	No. Of Arc = 5, No of Rods = 3 t = 3 mm, Arc length = 1.25 m t = 3mm, l = 2.44 m 10 (Aluminium with head), l = 10mm, diameter = 4mm. Diameter = 9mm (5mm from top and each side)
Iron Stand	l = 1.17 m, t = 5mm.

IV. EFFICIENCY INVOLVED.

4.1 Opto-Thermal Efficiency ($\eta_{opto\text{-}thermal}$)

$\eta_{opto\text{-}thermal}$ =qu / Ib Aa = η_O - $\frac{1}{Ib}[\frac{(Tr-Ta)}{Rk} \times \frac{Acond}{Aa}] + €r\,[\frac{Tr4-Tc4}{CR}]$……..(14)

Rate of use full energy = $q_u = \eta o\, I_b\, Aa - U_L(Tr - Ta)Aa$ ……..(15)

Rk = Thermal Resistance of Receiver or Boiler Tube =

$$\frac{\text{Distence Travel by conductive heat in boiler tube or recevier } (x)}{\text{Thermal conductivity of recevier metal } (K) \times \text{Condution Area } (A)}$$

4.2 Thermal Efficiency ($\eta_{thermo\text{-}syphon}$)

$\eta_{thermo\text{-}siphon}$ or η_I = $Q_{required} / Q_{gen}$ ……(16)

4.3 Over All Efficiency (ηo)

$\eta o = \eta_{opto\text{-}thermal} \times \eta_{thermo\text{-}syphon}$ ……(17)

V. ESTIMATION OF STSP EFFICIENCY WITH PHOTOVOLTAIC PUMP EFFICIENCY.

Efficiency of Solar Photovoltaic Pump (η_{SPVP})

$$\eta_{SPVP} = \eta_{SPV} * \eta_B * \eta_{CC} * \eta_{pump}$$

η_{SPV} = 15%

η_{pump} = 50%

η_{CC} = 90%

η_B = 85%

Lead-acid batteries typically have columbic efficiency of 85% and energy efficiencies in order of 70 % [9]. Columbic efficiency is the ratio of number of charges that enter the battery during charging compared to the number that can be extracted from the battery during discharging [9].

η_{CC} depend on the input-output level of voltage-current. DC-AC conversion efficiency as 100% but practically it is not possible because some account of heat dissipated by the passive components. Therefore, there is no way to simulate 100% charge-controller efficiency. We can assume more than 90%.

Farm irrigation pumping is around 70 to 80% of total farm electricity usage [10].

η_{SPVP} = 15% * 85% * 90% * 70% = 8.08 %

VI. RESULTS AND DISCUSSION.

An experiment with the fabricated model was carried out in the month of April-May. In a mid day when the sun rays were focused on the copper boiler, the pump lifted the water from the down reservoir and sprayed a stream up to a height of 10 feet. This gave a feel that about 50% of energy was lost in reflector. A more reflective surface with better focussing power is recommended. The concept was clearly demonstrated.

The result of energy and exergy analysis of STSP shown in Table 2:

Table-2, STSP Efficiency results

System/Efficiency (%) → ↓	$\eta_{optical}$	$\eta_{thermal}$ or η_I	$\eta_{overall} = \eta_{optical} \times \eta_{thermal}$
STSP	75	46.6	34.9
SPV Pump			8.08

VII. CONCLUSION.

It is possible to use direct solar thermal energy for pumping action instead of going through the photovoltaic electrical route, where the SPV pumpinjg system overall efficiency comes to 8% against 35 % (η_{opt} and η_I comes 75% and 46% respectively) of solar thermal syphon pump system. Apart from this significant gain in utilisation of solar energy, there is further indirect savings in energy required for production of solar photovoltaic panel. The solar thermal syphon pump would be a significant environment friendly attempt for harnessing solar energy.

The unique part of this development is that the solar thermal syphon pump has no moving parts and it is thus maintenance free.

VIII. ACKNOWLEDGMENT

This project has been funded by Sharda University and we are very thankful for this.

REFERENCES.

[1] Principles of solar engineering by Frank Kreith, Jan F. Kreider, McGraw-Hill, 1981.

[2] Solar Energy: Principles of Thermal Collection and Storage By S.P. Sukhatme.Tata McGraw-Hill,2008.

[3] Introduction to Fluid Mechanics by Fox & McDonald,John Wiley & Sons,2008

[4] Basic and applied Thermodynamics by P.K.Nag,Tata McGraw-Hill, 2004

[5] Kalogirou, S.; and Lloyd, S.Use of solar parabolic trough collectors for hot water production in Cyprus. A feasibility study. Renewable Energy 2(2): 117-124.1992.

[6] State-wise Electricity Consumption & Conservation Potential in India. Bureau Of Energy Efficiency (BEE) Ministry of Power, Government of India, Report2009, www.emt india.net/eca2009/14Dec2009/CombinedSummaryReport.pdf.

[7] HWWI (2005): CDM potential of SPV pumps India. http://www.hwwi.org/uploads/tx_wilpubdb/HWWI_Research_Paper_4.pdf.

[8] "Solar Thermal Syphon pump System for Irrigation",Gopal P Sinha,Kaushalendra Kr Dubey, India Patent,Patent Docket No- 9684,Application No-1626/DEL/2013,Reference No- E-2/5773/2013-DEL, E-3/5571/2013-DEL, E-5/5240/2013-DEL,Date of Patent filied-30/05/2013.

[9] Cral John Rydh, BjornA. Sanden, Energy Analysis of batteries in photovoltaic syste,Part-ll, Energy return factors and overall efficiencies, Journal of energy conversion and management,Elsevier,46 (2005),1980-2000.

[10] Jamse Curaan, Agricultural Resource Management. Irrigation Pump Efficiency, www.farmpoint.tas.gov.au.

[11] Solar thermal water pumping systems-a review Y.W. Wong,K.Sumathy_ Department of Mechanical Engineering\ University of Hong Kong\ Hong Kong, August 1998.

IJARSE

Design of CDTA and VDTA Based Frequency Agile Filters

Neeta Pandey[1], Aseem Sayal[2], Richa Choudhary[3], Rajeshwari Pandey[4]
[1,4]Deptartment of Electronics and Communication Engineering, [2,3]Deptartment of Electrical Engineering
Delhi Technological University, Delhi, INDIA
[1]n66pandey@rediffmail.com, [2]aseem.sayal@gmail.com, [3] dce.richa@gmail.com, [4]rajeshwaripandey@gmail.com

Abstract

This paper presents frequency agile filters based on current difference transconductance amplifier (CDTA) and voltage difference transconductance amplifier (VDTA). The proposed agile filter configurations are suitable for integration as it employs grounded passive components. Extensive SPICE simulationsusing 0.25µm TSMC CMOS technology model parameters are carried out for functional verification. The performance of proposed configurations is compared in terms of power dissipation, signal to noise ratio (SNR) and maximum output noise voltage. The VDTA based filtersshow optimum performance concerning the power dissipation and Signal to Noise ratio. The maximum output noise voltage is better in CDTA based FAF for *Class0* whereas VDTA based *Class1* and *Class2* FAF have lesser noise in compared to CDTA configurations.

Keywords - Current Difference transconductance amplifier (CDTA), Frequency agile filter (FAF), Signal to Noise Ratio (SNR), Voltage Difference transconductance amplifier (VDTA).

1. Introduction

The rapid evolution of wireless services has led to demand for one-fits-all "analog" front end solution. These services use different standards and therefore necessitate development of integrated multi-standard transceivers as it results in reduction of size, price, complexity and power consumption. The parameters of integrated transceiver can be modified in order to be able to adapt to the specifications of each standard [1]. Practically, the designs employ either element handling various standards in parallel or reconfigurable elements. The frequency agile filter (FAF) [1]-[10] characterized by adjustment range, re-configurability, and agility may be used in transceivers. The term shadow filters is sometimes used in literature to refer FAF.The literature survey shows that a limited number of topologies of active FAF are available and are based on op-amp [1] and current mode active block [2]-[3] and CMOS [4].

There is a wide range of current mode building blocks available in open literature. Among these blocks current difference transconductance amplifier (CDTA) [11] has received considerable interest as it presents low input impedance and therefore is free from input capacitance. Many applications such as filters and oscillators based on CDTA and VDTA are available have been reported in the literature [11]-[25] and references cited therein. A new class of 2nd order filters, namely shadow filter [26]-[27] has been reported recently in which center frequency, bandwidth, gain and quality factor can be varied by controlling the gain of external amplifier connected in feedback loop. The proposed FAF circuit can be implemented for any order, therefore can be employed for various industrial applications.

The main intention of this paper is to present a CDTA and VDTA based frequency agile filter topologies. The proposed filters are suitable for integration as it uses grounded capacitors and a resistor. FAF implementation scheme is briefly reviewed in Section 2. The proposed CDTA based implementation of *Class0*, *Class1* and *Class 2* FAF is presented in Section 3. Section 4 deals with the realization of proposed VDTA based *Class0*, *Class1* and *Class 2* FAF. Simulation results are provided in Section 5 to substantiate the proposed FAF topologies. The performance characteristics of filter topologies are described in section 6. The paper is concluded in section 7.

2. Implementation Scheme of FAF

The implementation scheme of frequency agile filter (FAF) [3] isbriefly reviewed in this section.

2.1 Class *0* FAF

A classical second order filter with band pass (I_{BP}) and low pass (I_{LP}) outputs of Fig. 1 is designated as *Class0* FAF [3]. The transfer functions of class *0* FAF are given by (1)-(2).

Fig. 1. Class *0* FAF [3]

$$T_{BP}(s) = \frac{I_{BP}}{I_{IN}} = \frac{ks}{1+\alpha s+\beta s^2} \tag{1}$$

$$T_{LP}(s) = \frac{I_{LP}}{I_{IN}} = \frac{p}{1+\alpha s+\beta s^2} \tag{2}$$

The center frequency (f_0) and quality factor (Q) of the filter are represented by (3)-(4) respectively.

$$f_0 = \frac{1}{2\pi\sqrt{\beta}} \tag{3}$$

$$Q = \frac{\sqrt{\beta}}{\alpha} \tag{4}$$

2.2 Class *1* FAF

The basic block diagram of class *1* FAF is shown in Fig. 2 wherein the low pass output of the class *0* FAF is amplified (with variable gain *A*) and fed back to the input. The characteristic frequency (f_{0A}) and quality factor (Q_A) of Class *1* FAF are given by (5) and (6) respectively.

$$f_{0A} = f_0\sqrt{(1+Ap)} \tag{5}$$

$$Q_A = Q\sqrt{(1+Ap)} \tag{6}$$

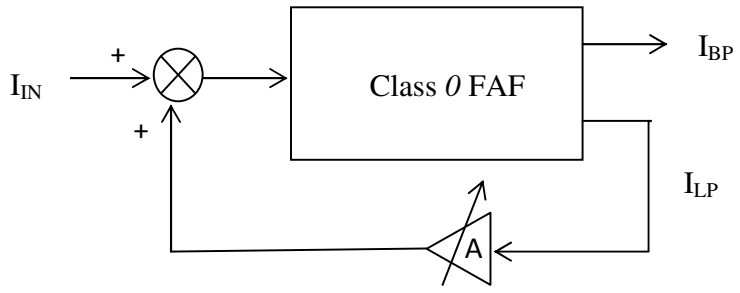

Fig. 2. Class *1* FAF.

2.3 Class n FAF

The method outlined for class *1* FAF realization can be extended for class *n* FAF implementation as shown in Fig. 3. This requires *n* amplifiers to be placed in *n* feedback paths obtained in the same way as done in class *1* implementation. It is noticeable that only adjustable-gain amplifiers with gain *A* ($A_1 = A_2 = \ldots = A_{n-1} = A_n$) are required along with class *0 FAF*. The characteristic parameters of class *n* FAF are given by (7)-(8).

$$f_{0An} = f_0(1+Ap)^{\frac{n}{2}} \tag{7}$$

$$Q_{An} = Q(1+Ap)^{\frac{n}{2}} \tag{8}$$

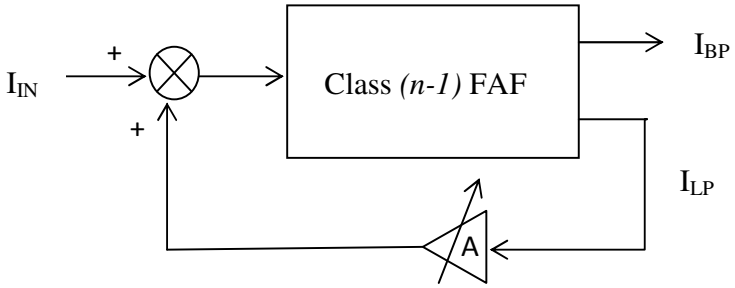

Fig. 3.Class *n* FAF.

3. CDTA based FAF

The CDTA [11]-[18] consists of a unity-gain current source controlled by the difference of the input currents and a transconductance amplifier providing electronic tunability through its transconductance gain. The CDTA symbol is shown in Fig. 4 and its terminal characteristic in matrix form are given by (9).

$$\begin{bmatrix} V_p \\ V_n \\ I_z \\ I_{x+} \\ I_{x-} \end{bmatrix} = \begin{bmatrix} 0 & 0 & 0 & 0 & 0 \\ 0 & 0 & 0 & 0 & 0 \\ 1 & -1 & 0 & 0 & 0 \\ 0 & 0 & g & 0 & 0 \\ 0 & 0 & g & 0 & 0 \end{bmatrix} \begin{bmatrix} I_p \\ I_n \\ V_z \\ V_{x+} \\ V_{x-} \end{bmatrix} \tag{9}$$

where, *g*is transconductance of the CDTA. The CMOS implementation of CDTA [16] is given in Fig. 5 consisting of a current differencing block (Mc1–Mc17) [16] followed by transconductance amplifier (TA) block (Mc18–Mc26). The value of transconductance (*g*)is expressed as

$$g = \sqrt{2\mu C_{ox}(W/L)_{19,21} I_{Bias}} \tag{10}$$

which can be adjusted by bias current I_{Bias} of CDTA.

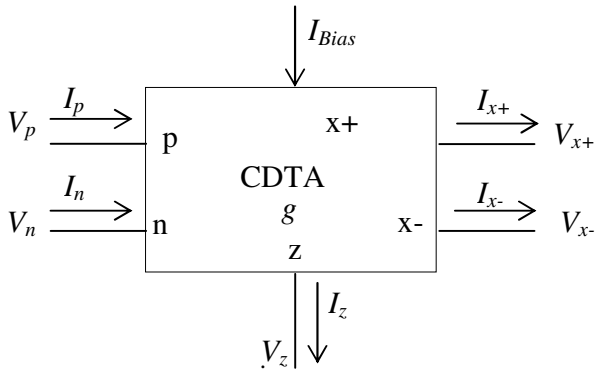

Fig. 4.Symbol of CDTA.

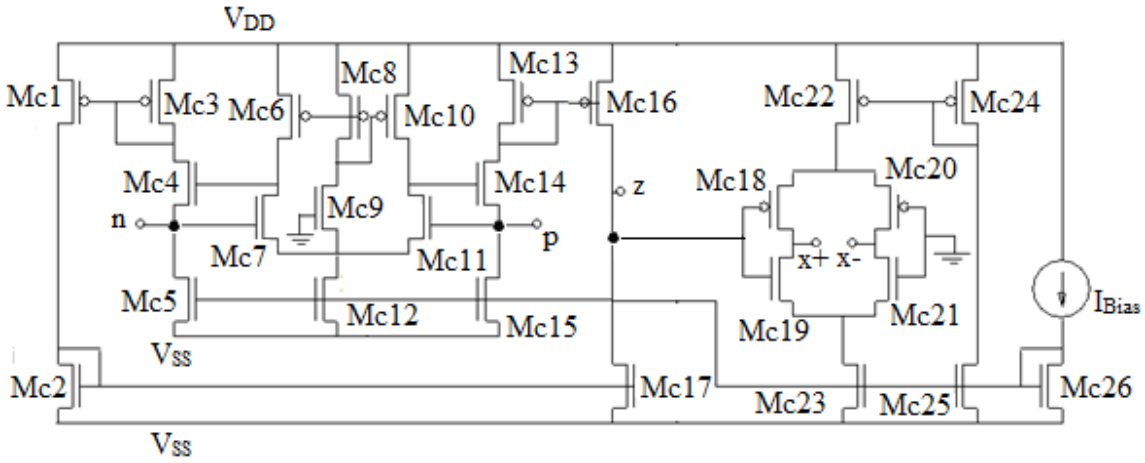

Fig. 5.CMOS implementation of CDTA [16].

3.1CDTA based class *0* FAF

The CDTA based second order filter employing two CDTA blocks and two grounded capacitors is shown in Fig. 6. The second CDTA block uses additional TA block. It provides both low pass and band pass responses at high output impedance and can be used as *Class 0* FAF. The current flowing through x+ and x-are controlled through transcoundance g_2 whereas current flowing through terminals x_c+ and x_c- are controlled through g_3. The low pass and band pass transfer functions of CDTA based *Class0* FAF are given by (11) and (12) respectively. The *Q* of the *Class0* FAF can be controlled independent of f_0 by varying g_3.

$$\frac{I_{LP}}{I_{IN}} = \frac{g_1 g_2}{C_1 C_2 s^2 + s C_1 g_3 + g_1 g_2} \tag{11}$$

$$\frac{I_{BP}}{I_{IN}} = \frac{s C_2 g_1}{C_1 C_2 s^2 + s C_1 g_3 + g_1 g_2} \tag{12}$$

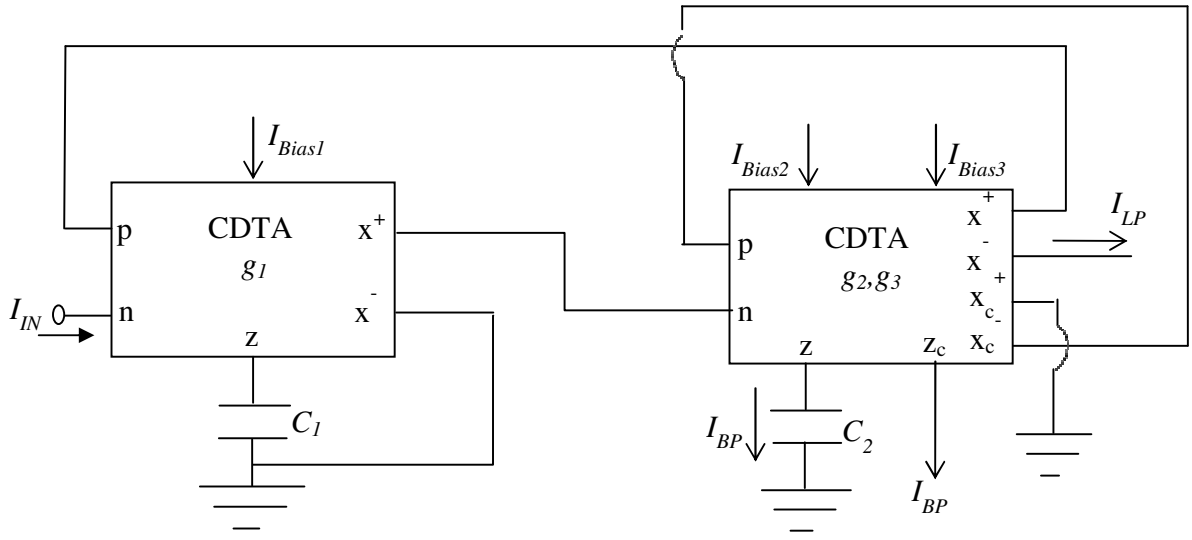

Fig. 6. CDTA based Class *0* FAF.

The center frequency and quality factor of *Class0* FAF are expressed as

$$f_0 = \frac{1}{2\pi}\sqrt{\frac{g_1 g_2}{C_1 C_2}} \tag{13}$$

$$Q = \frac{1}{g_3}\sqrt{\frac{g_1 g_2 C_2}{C_1}} \tag{14}$$

3.2CDTA based Class *1* FAF

The CDTA based class *1* FAF is shown in Fig. 7. It employs class *0* FAF of Fig. 6 alongwith an additional TA block and one grounded resistor. The TA block in the feedback path functions as an amplifier with tunable gain *A* as given in (15).

$$A = g_4 R \tag{15}$$

where g4 is TA block transconductance of value equal to $\sqrt{2\mu C_{ox}(W/L)_{19,21} I_{Bias4}}$.

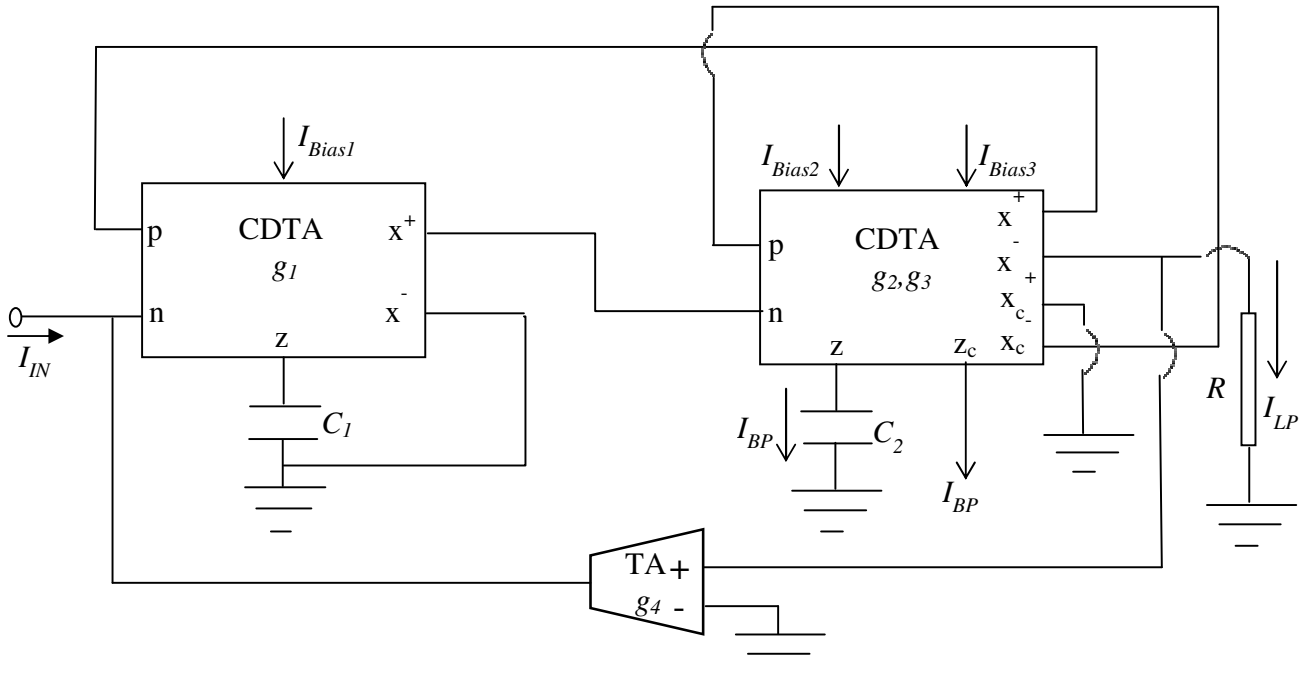

Fig. 7. CDTA based Class *1* FAF.

The low pass and band pass transfer functions of CDTA based *Class 1* FAF are given by (16)-(17) respectively.

$$\frac{I_{LP}}{I_{IN}} = \frac{g_1 g_2}{C_1 C_2 s^2 + s C_1 g_3 + g_1 g_2 (1 + R g_4)} \tag{16}$$

$$\frac{I_{BP}}{I_{IN}} = \frac{s g_1 C_2}{C_1 C_2 s^2 + s C_1 g_3 + g_1 g_2 (1 + R g_4)} \tag{17}$$

The center frequency and quality factor of the CDTA based *Class1* FAF are expressed by (18)-(19) respectively.

$$f_{0A} = \frac{1}{2\pi}\sqrt{\frac{g_1 g_2}{C_1 C_2}}\sqrt{(1 + g_4 R)} \tag{18}$$

$$Q_A = \frac{1}{g_3}\sqrt{\frac{g_1 g_2 C_2}{C_1}}\sqrt{(1+g_4 R)} \tag{19}$$

3.3CDTA based Class *2* FAF

The CDTA based *Class2* FAF is shown in Fig. 8. It employs two CDTA blocks, two grounded capacitors, three TA blocks and two grounded resistors. The TA blocks in the feedback path is used as amplifier with tunable gain A. The gain A of TA based amplifier is given by (20).The second CDTA block uses two additional TA blocks. It provides both low pass and band pass responses at high output impedance and can be used as *Class 0* FAF. The current flowing through x+,x-, x_{cc}+,x_{cc}- are controlled through transcoundance g_2 whereas current flowing through terminals x_c+ and x_c- are controlled through g_3.

$$A = g_4 R \tag{20}$$

The low pass and band pass transfer functions of CDTA based class *1* FAF are given by (21)-(22) respectively.

$$\frac{I_{LP}}{I_{IN}} = \frac{g_1 g_2}{C_1 C_2 s^2 + s C_1 g_3 + g_1 g_2 (1+Rg_4)^2} \tag{21}$$

$$\frac{I_{BP}}{I_{IN}} = \frac{s g_1 C_2}{C_1 C_2 s^2 + s C_1 g_3 + g_1 g_2 (1+Rg_4)^2} \tag{22}$$

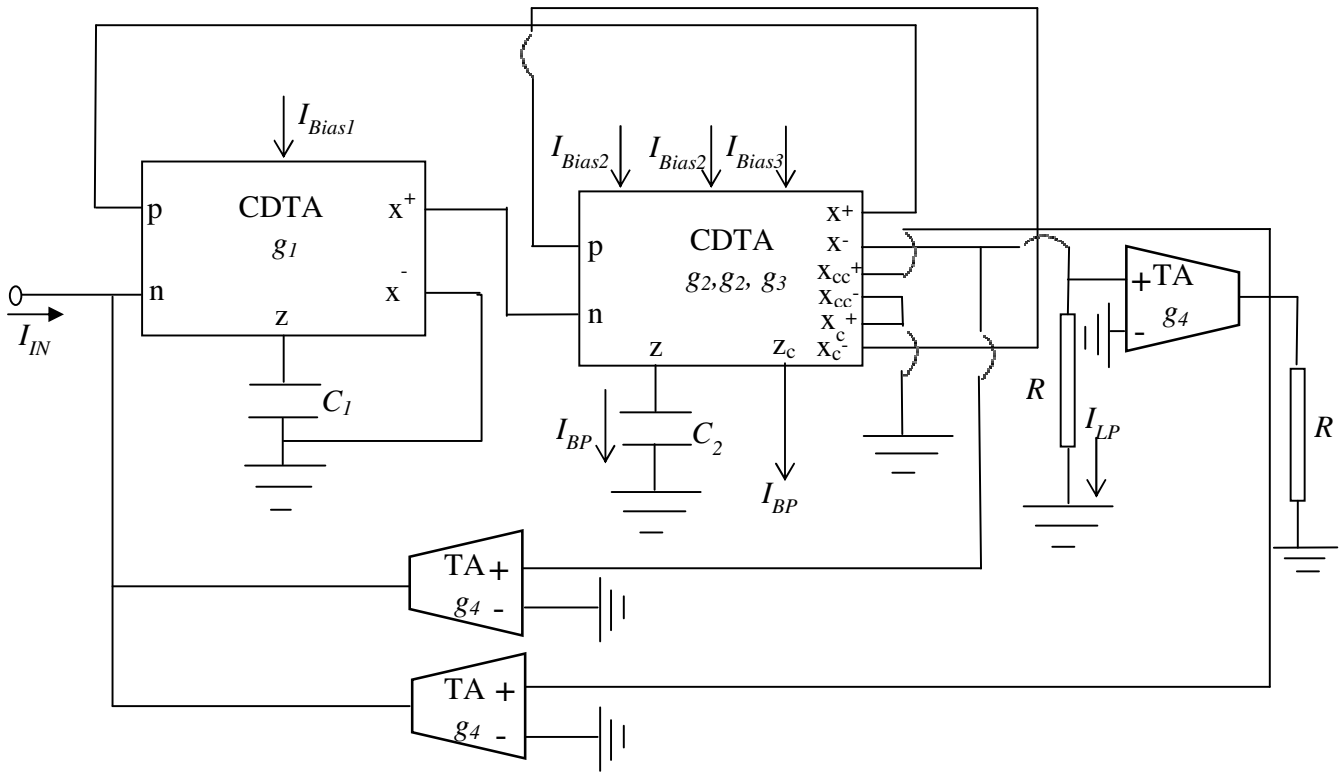

Fig. 8. CDTA based Class *2* FAF.

The center frequency and quality factor of the CDTA based class *1* FAF are expressed by (23)-(24) respectively.

$$f_{0A} = \frac{1}{2\pi}\sqrt{\frac{g_1 g_2}{C_1 C_2}}(1+g_4 R) \tag{23}$$

$$Q_A = \frac{1}{g_3}\sqrt{\frac{g_1 g_2 C_2}{C_1}}(1+g_4 R) \tag{24}$$

The proposed filter uses grounded resistor of value R (= $1/g$) can easily be implemented using the TA based structure given in Fig. 9.

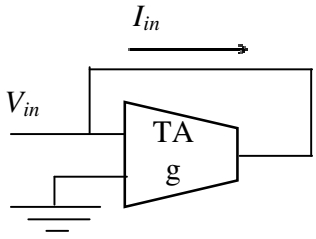

Fig. 9. TA Realization of a grounded resistor.

4. VDTA based FAF

VDTA (Voltage Differencing Transconductance Amplifier) is composed of the current source controlled by the difference of two input voltages and a single-output transconductance amplifier, providing electronic tuning ability through its transconductance gains [20]-[21]. The terminal characteristics of VDTA are given by (25) where, g_1 and g_2 are transconductance of the OTAs in VDTA. The VDTA symbol is shown in Fig. 10. Fig. 11 describes the OTA based realization of VDTA.

$$\begin{bmatrix} i_z \\ i_{zc} \\ i_{x+} \end{bmatrix} = \begin{bmatrix} g_1 & -g_1 & 0 \\ -g_1 & g_1 & 0 \\ 0 & 0 & g_2 \end{bmatrix} \begin{bmatrix} v_p \\ v_n \\ v_z \end{bmatrix} \tag{25}$$

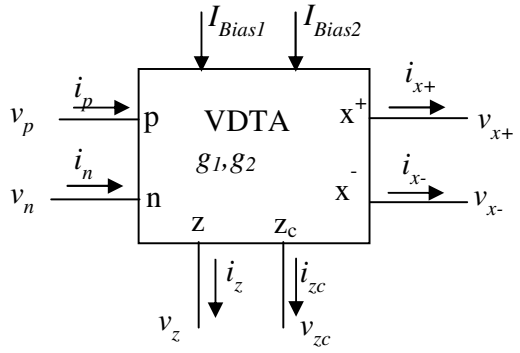

Fig.10.Symbol of VDTA.

The CMOS implementation of VDTA [16] is given in Fig. 11 consisting of cascaded transconductance amplifiers (TA) blocks. The value of transconductance $g_1$and$g_2$is expressed by (26)-(27) which can be adjusted by bias current I_{Bias1} andI_{Bias2} respectively.

$$g_1 = \sqrt{2\mu C_{ox}(W/L)_{1,2} I_{Bias1}} \tag{26}$$

$$g_2 = \sqrt{2\mu C_{ox}(W/L)_{5,6} I_{Bias2}} \tag{27}$$

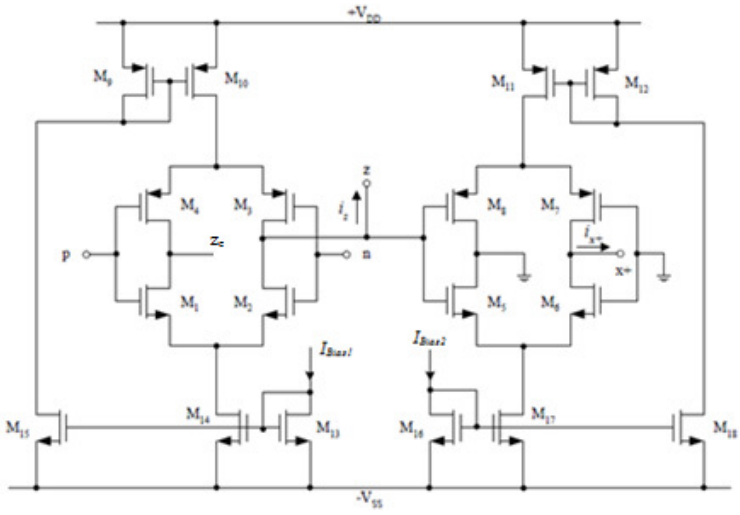

Fig. 11. CMOS implementation of VDTA[21].

4.1VDTA based class *0* FAF

The VDTA based second order filteremploying one VDTAbock and two grounded capacitors are shown in Fig. 12. The circuit configuration is based on second order filter presented in [21] but allows independent control of quality factor and center frequency. The VDTA block employs one additional TA block. The current flowing through z terminal is controlled by transconductance g_1 whereas current flowing through $z_c$terminal is controlled by g_2.The terminal characteristics of VDTA block is given by (28). It provides both low pass and band pass responses at high output impedance and can be used as *Class 0* FAF. The low pass and band pass transfer functions of VDTA based *Class0* FAF are given by (29) and (30) respectively.

$$\begin{bmatrix} i_z \\ i_{zc} \\ i_z^{'} \\ i_{zc}^{'} \\ i_{x+} \end{bmatrix} = \begin{bmatrix} g_1 & -g_1 & 0 \\ -g_1 & g_1 & 0 \\ g_2 & -g_2 & 0 \\ -g_2 & g_2 & 0 \\ 0 & 0 & g_3 \end{bmatrix} \begin{bmatrix} v_p \\ v_n \\ v_z \end{bmatrix} \tag{28}$$

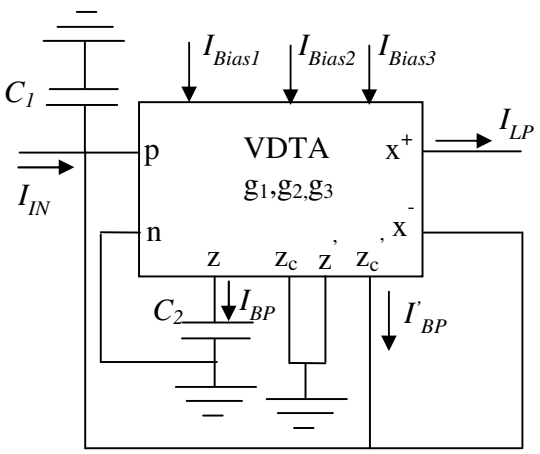

Fig. 12.VDTA based Class *0* FAF.

$$\frac{I_{LP}}{I_{IN}} = \frac{g_1 g_3}{C_1 C_2 s^2 + s C_2 g_2 + g_1 g_3} \tag{29}$$

$$\frac{I_{BP}}{I_{IN}} = \frac{sC_2 g_1}{C_1 C_2 s^2 + sC_2 g_2 + g_1 g_3} \tag{30}$$

The center frequency and quality factor of *Class0* FAF are expressed by (31)-(32). The center frequency can be controlled by I_{Bias1} and I_{Bias3} whereas quality factor can be independently controlled by I_{Bias2}.

$$f_0 = \frac{1}{2\pi}\sqrt{\frac{g_1 g_3}{C_1 C_2}} \tag{31}$$

$$Q = \frac{1}{g_2}\sqrt{\frac{g_1 g_3 C_1}{C_2}} \tag{32}$$

4.2VDTA based Class *1* FAF

The VDTA based class *1* FAF is shown in Fig. 13. It employs twoVDTA blocks and two grounded capacitors. The first VDTA block employs one additional TA block. The current flowing through z terminal is controlled by transconductance g_1 whereas current flowing through $z_c$terminal is controlled by g_2. The terminal characteristics of first VDTA block is given by (28). The second VDTA block is used as amplifier with tunable gain *A*. The gain *A* of VDTA based amplifier is given by (33)

$$A = \frac{g_4}{g_3} \tag{33}$$

and can be adjusted by varying $I_{Bias3}$and I_{Bias2}.

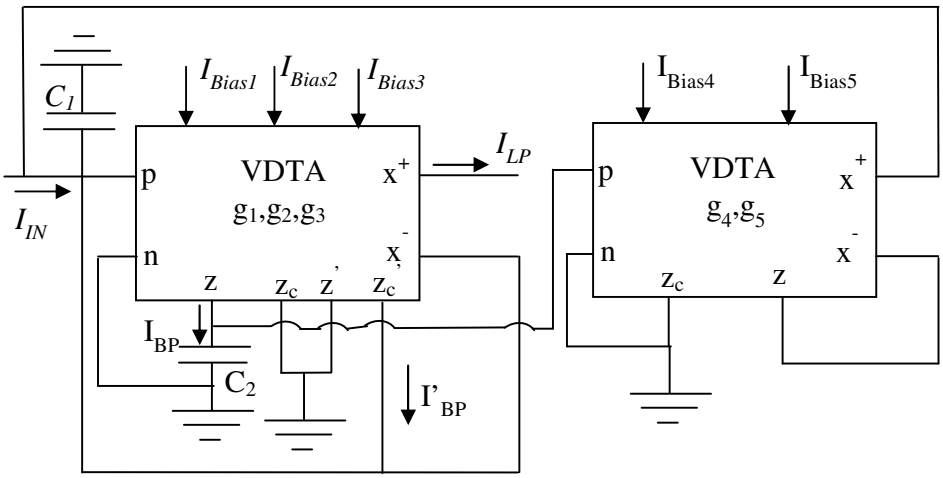

Fig. 13.VDTA based Class *1* FAF

The low pass and band pass transfer functions of VDTA based *Class 1* FAF are given by (34)-(35) respectively

$$\frac{I_{LP}}{I_{IN}} = \frac{g_1 g_3}{C_1 C_2 s^2 + sC_2 g_2 + g_1 g_3\left(1 + \frac{g_4}{g_3}\right)} \tag{34}$$

$$\frac{I_{BP}}{I_{IN}} = \frac{sg_1 C_2}{C_1 C_2 s^2 + sC_2 g_2 + g_1 g_3\left(1 + \frac{g_4}{g_3}\right)} \tag{35}$$

The center frequency and quality factor of the CDTA based *Class1* FAF is expressed by (36)-(37) respectively. The center frequency can be independently controlled by varying I_{Bias2} without changing center frequency.

$$f_{0A} = \frac{1}{2\pi}\sqrt{\frac{g_1 g_3}{C_1 C_2}}\left(\sqrt{1+\frac{g_4}{g_3}}\right) \tag{36}$$

$$Q_A = \frac{1}{g_2}\sqrt{\frac{g_1 g_3 C_1}{C_2}}\left(\sqrt{1+\frac{g_4}{g_3}}\right) \tag{37}$$

4.3VDTA based Class *2* FAF

The VDTA based *Class2* FAF is shown in Fig. 14. It employs three VDTA blocks, two grounded capacitors and one grounded resistor. The first VDTA block employs one additional TA block. The current flowing through z terminal is controlled by transconductance g_1 whereas current flowing through z_c terminal is controlled by g_2.The terminal characteristics of first VDTA block is given by (28). The second VDTA block is used as amplifier with tunable gain A. The gain A of VDTA based amplifier is given by (38). The proposed filter uses grounded resistor which can easily be implemented using the TA with transconductance equal to $g_3$based structure given in Fig. 9. To realize second order filter, I_{Bias7} is set to value of I_{Bias4} such that g_7 is equal to g_4 and I_{Bias6} is set to value such that g_6 is equal to sum of g_3 and g_4, i.e. $g_6 = g_3 + g_4$.

$$A = \frac{g_4}{g_3} \tag{38}$$

and can be adjusted by varying I_{Bias3} and I_{Bias2}, thereby making f_{0A} tunable.

The low pass and band pass transfer functions of CDTA based class *1* FAF are given by (39)-(40) respectively.

$$\frac{I_{LP}}{I_{IN}} = \frac{g_1 g_3}{C_1 C_2 s^2 + s C_2 g_2 + g_1 g_3\left(1+\frac{g_4}{g_3}\right)^2} \tag{39}$$

$$\frac{I_{BP}}{I_{IN}} = \frac{s g_1 C_2}{C_1 C_2 s^2 + s C_2 g_2 + g_1 g_3\left(1+\frac{g_4}{g_3}\right)^2} \tag{40}$$

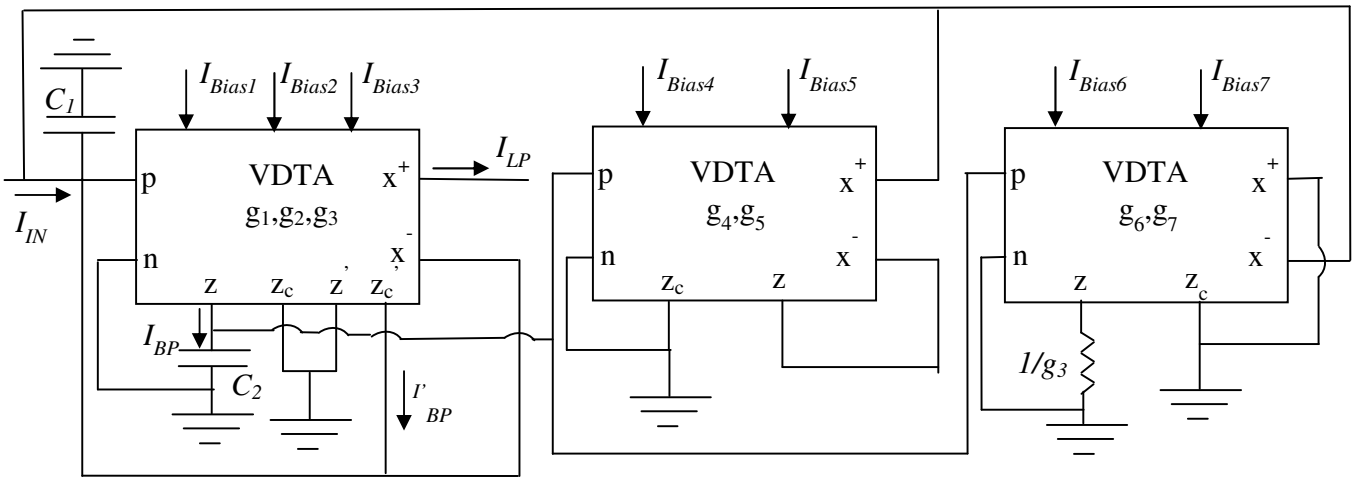

Fig. 14.VDTA based Class *2* FAF.

The center frequency and quality factor of the CDTA based class *1* FAF are expressed by (41)-(42) respectively.

$$f_{0A} = \frac{1}{2\pi}\sqrt{\frac{g_1 g_3}{C_1 C_2}}\left(1+\frac{g_4}{g_3}\right) \tag{41}$$

$$Q_A = \frac{1}{g_2}\sqrt{\frac{g_1 g_3 C_1}{C_2}}\left(1+\frac{g_4}{g_3}\right) \tag{42}$$

5 Simulation Results

In this section, the functionality of the proposed filters has been verified. The SPICE simulations results for CDTA and VDTA based filters have been presented using TSMC 0.25µm CMOS process model parameters and supply voltages of V_{DD} = -V_{SS} = *1.8 V.*

5.1 Simulation of CDTA Based FAF

The CMOS schematic of Fig. 5 is used for verifying CDTA based FAF and the aspect ratio of the MOS transistors is given in Table 1. The aspect ratios of MOS transistors for additional TA blocks ports (x_{C+} ,x_{C-},x_{cc}+ and x_{cc}-) aresame as that for x_+ and x_-. The two grounded capacitors C_1 and C_2 are taken as 50pF each. The grounded resistor of 10kΩ is realized by TA block by setting bias current value to 0.85µA. The frequency response of CDTA based Class *0*, Class *1* and Class *2* FAF topologies is depicted in Figs. 15, 16 and 17 respectively. The responses are obtained by varying bias currents I_{Bias1} and I_{Bias2} (I_{Bias}=I_{Bias1}=I_{Bias2}) to 1µA, 10µA, 30µA and 60µA while keeping I_{Bias3} *and* I_{Bias4} respectively at 0.5µA and10µA. It can be clearly noticed that center frequency f_0 increases on increasing the bias current.

Table 1.Aspect ratios of MOS transistors used in CDTA.

MOSFETs	***W(µm)/L(µm)***
Mc26	7.0/0.7
Mc1	9.8/0.7
Mc2, Mc3, Mc13,Mc16, Mc17	10.5/0.7
Mc19, Mc21	16.1/0.7
Mc6, Mc20	28.0/0.7
Mc8, Mc10, Mc18	28.7/0.7
Mc15, Mc12, Mc5	35.0/0.7
Mc4, Mc14	42.0/0.7
Mc22, Mc23, Mc25	56.0/0.7
Mc24	58.8/0.7
Mc7, Mc9, Mc11	70.0/0.7

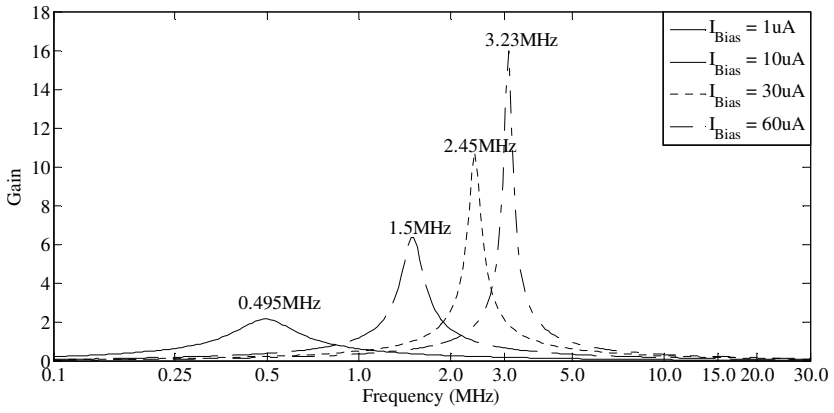

Fig. 15. Frequency response of CDTA based class *0* FAF with I_{Bias1}=I_{Bias2}=$I_{Bias.}$

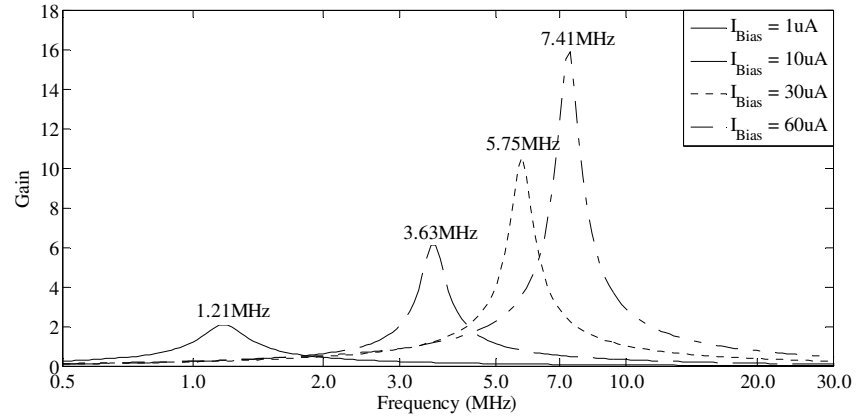

Fig. 16. Frequency response of CDTA based class *1* FAF with $I_{Bias1}=I_{Bias2}=I_{Bias.}$

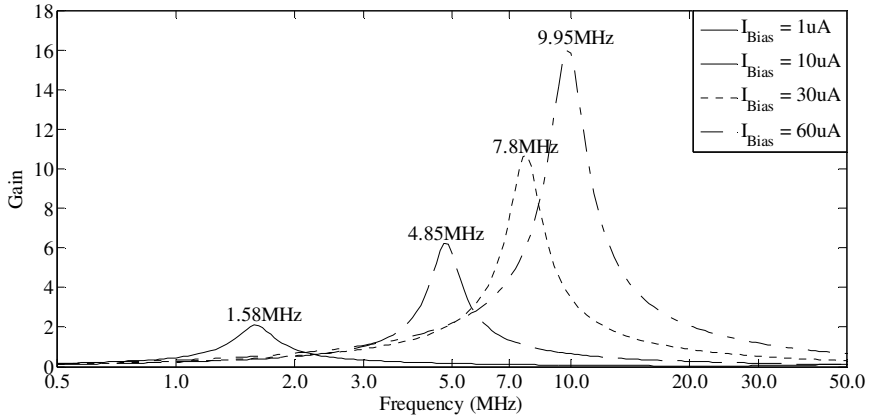

Fig. 17. Frequency response of CDTA based class *1* FAF with $I_{Bias1}=I_{Bias2}=I_{Bias}$

The electronic tunability of quality factor and center frequency for proposed *Class0*, *Class1* and *Class 2* FAF is plotted in Figs. 18 and 19 respectively. The analytical and simulated responses describing variation of quality factor are shown in Fig. 18 for different values of I_{Bias3} while setting I_{Bias1} and I_{Bias2} to 30µA. Fig. 19 depicts the analytical and simulated responses for center frequency variation for different values of $I_{Bias1}$and I_{Bias2} ($I_{Bias1}=I_{Bias2}$) while setting I_{Bias3} to 0.5µA. To plot responses for *Class 1*and *Class 2*FAF the bias current I_{Bias4} is taken as 10µA.

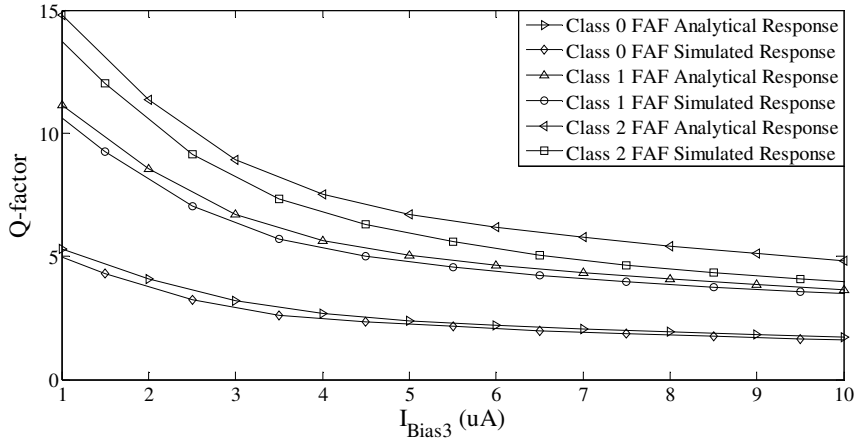

Fig. 18.Electronic Q-factor control of CDTA based FAF.

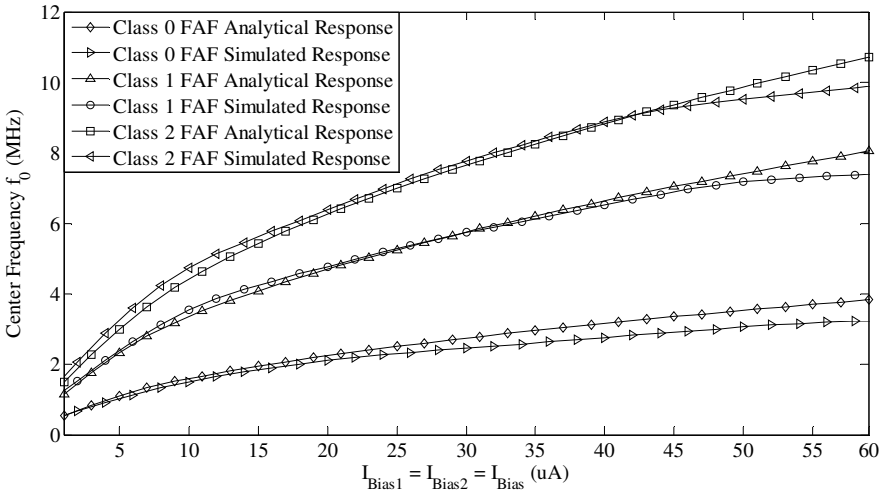

Fig. 19.Electronic center frequency control of CDTA based FAF.

The transient behaviour of proposed agile filter is also studied by applying input signals of frequencies 100KHz, 500KHz, 1MHz and 10MHz, each having an amplitude of 10µA each. . The responses for *Class 0* FAF are obtained by setting bias currents I_{Bias1} and I_{Bias2} each to 10µA and I_{Bias3} to 0.5 µA. Fig. 20 shows the input and output waveform along with their frequency spectrum for CDTA based *Class 0* FAF. It may clearly be noted that the CDTA based *Class 0* FAF allows only 1MHz signal to pass and significantly attenuates signals of frequencies 100KHz, 500KHz and 10MHz. Similar responses for *Class 1* and *Class 2* FAF were also obtained.

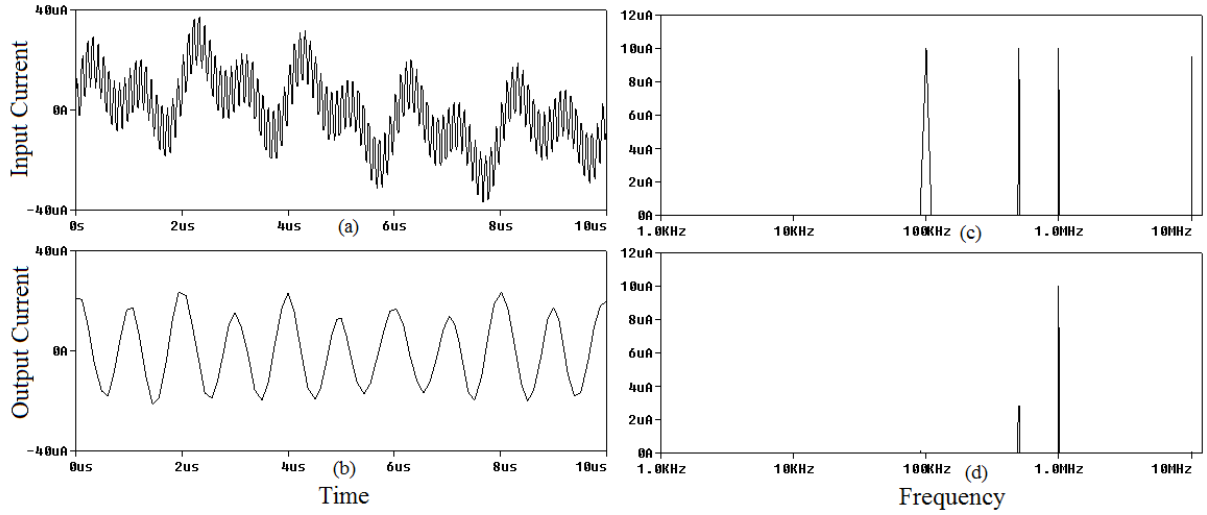

Fig. 20. (a) and (c) Input and its frequency spectrum (b) and (d) Output and its frequency spectrum for Class 0 FAF.

5.2 Simulation of VDTA based FAF

The CMOS schematic of Fig. 12 is used for verifying VDTA based FAF and the aspect ratio of the MOS transistors is given in Table 2. The two grounded capacitors C_1 and C_2 are taken as 50pF each. In the realization of Class *2* FAF, the grounded resistor is implemented by TA block by setting bias current value equal to I_{Bias3}. The frequency response of VDTA based *Class0*,*Class 1* and *Class2* FAF topologies are shown in Figs. 21, 22 and 23 respectively. The responses are obtained by keeping I_{Bias2} to 5µA and varying bias currents I_{Bias1} and I_{Bias3} (I_{Bias}=I_{Bias1}=I_{Bias3}) to 5µA, 10µA, 30µA and 60µA. In realization of Class *1* FAF, I_{Bias4}

is set to a value in such a manner that $g_4/g_3 = 3$ whereas I_{Bias5} is set equal to I_{Bias1}. In realization of Class *2* FAF, I_{Bias6} is set to value such that $g_6 = g_3+g_4$ whereas I_{Bias7} is equal to I_{Bias4}.

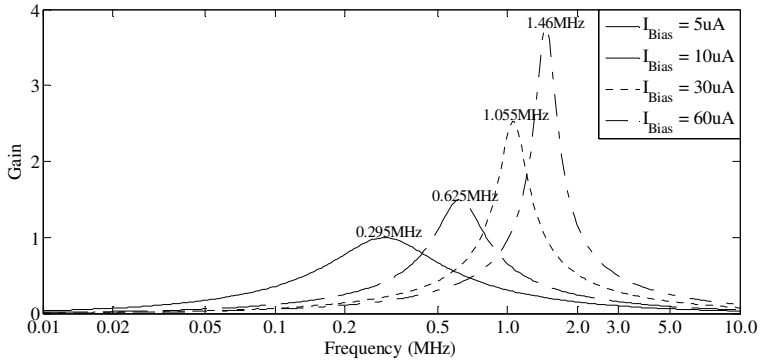

Fig. 21 Frequency response of VDTA based class *0* FAF with $I_{Bias1}=I_{Bias3}=I_{Bias}$

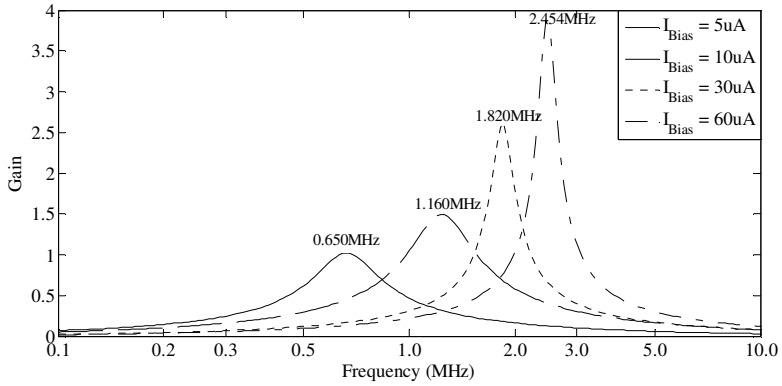

Fig. 22 Frequency response of VDTA based class *1* FAF with $I_{Bias1}=I_{Bias3}=I_{Bias}$

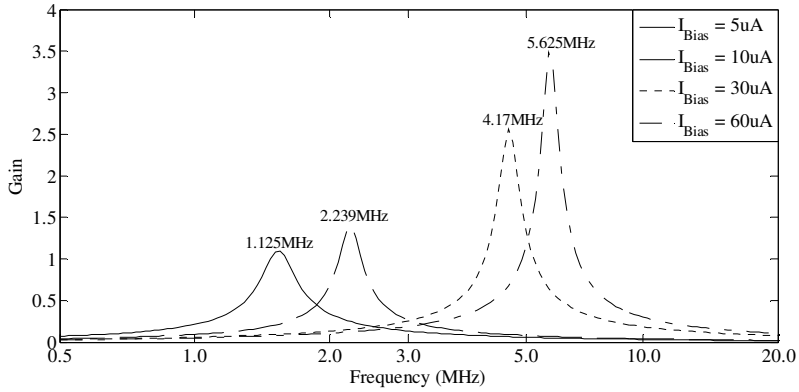

Fig. 23 Frequency response of VDTA based class *2* FAF with $I_{Bias1}=I_{Bias3}=I_{Bias}$

Table 2.Aspect ratio of MOS transistors used in VDTA.

MOSFETs	***W(μm)/L(μm)***
M1,M2,M5,M6	16.1/0.7
M3,M4,M7,M8	28/0.7
M9-M12	21/0.7
M13-M16	7/0.7
M14,M15,M17,M18	8.5/0.7

The electronic tunability of quality factor and center frequency for proposed *Class0*,*Class 1*and *Class 2* FAF is plotted in Figs. 24 and 25 respectively. The analytical and simulated responses describing variation of quality factor are shown in Fig. 24 for different values of I_{Bias2} while setting $I_{Bias1}$and I_{Bias3} to 30µA in *Class 0*. To plot responses for *Class 1*, I_{Bias4} is set to a value in such a manner that $g_4/g_3 = 3$ whereas I_{Bias5} is set equal to I_{Bias1}. *Class 2* FAF responses are plotted by setting I_{Bias6} to value such that $g_6 = g_3+g_4$ whereas I_{Bias7} is equal to I_{Bias4}.Fig. 25 depicts the analytical and simulated responses for center frequency variation for different values of $I_{Bias1}$and I_{Bias3} ($I_{Bias1}=I_{Bias3}$) and keeping I_{Bias2} to value of 5µA.To plot responsesfor *Class 1*, I_{Bias4} is set to a value in such a manner that $g_4/g_3 = 3$ whereas I_{Bias5} is set equal to I_{Bias1}. *Class 2* FAF responses are plotted by setting I_{Bias6} to value such that $g_6 = g_3+g_4$ whereas I_{Bias7} is equal to I_{Bias4}.

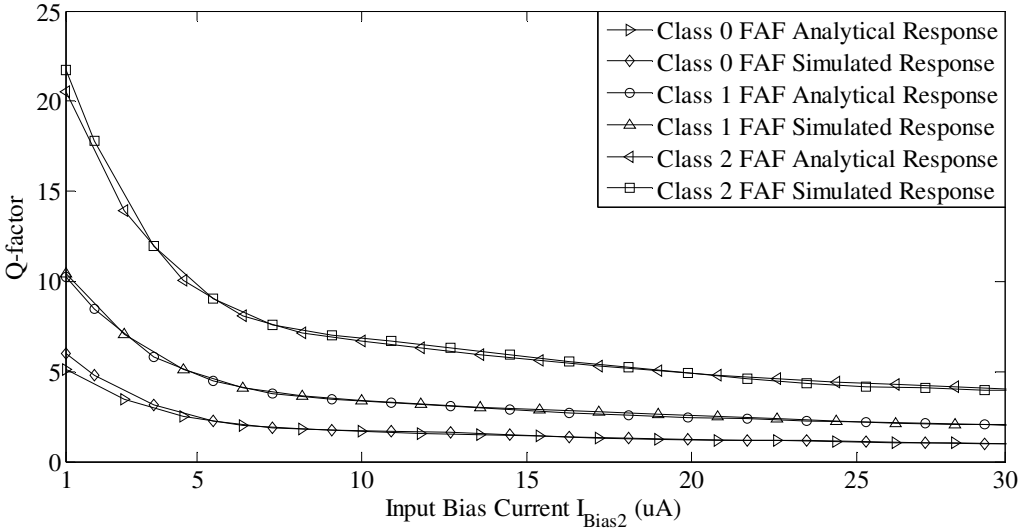

Fig. 24.Electronic Q-factor control of VDTA based FAF.

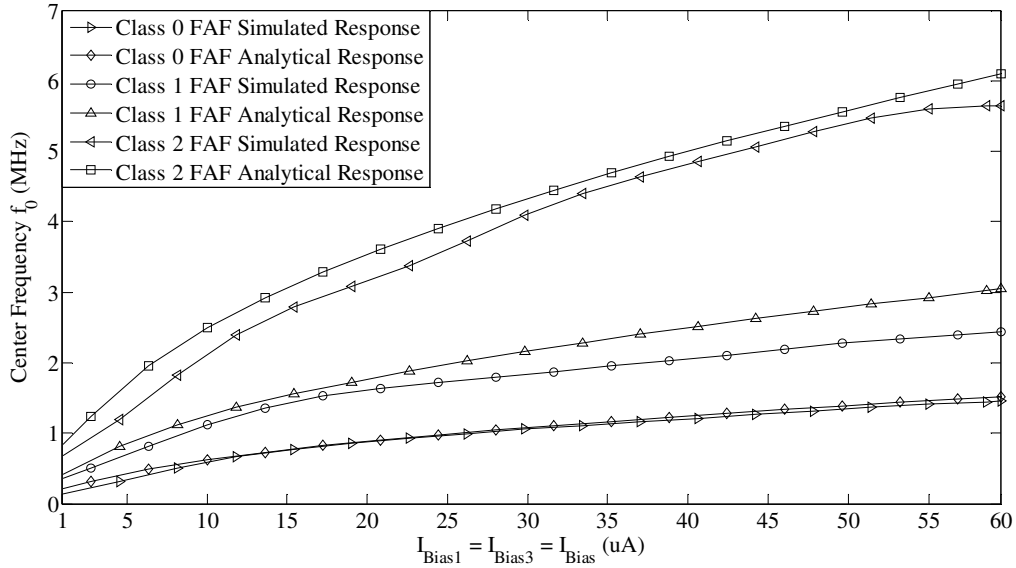

Fig. 25.Electronic center frequency control of VDTA based FAF.

The transient behaviour of proposed agile filter is also studied by applying input signals of frequencies 100KHz, 500KHz, 1MHz and 10MHz each having an amplitude of 10µA each. . The responses for *Class 0* FAF are obtained by setting bias currents I_{Bias1},I_{Bias2} and I_{Bias3} each to 30µA. Fig. 26 shows the input and output waveform along with their frequency spectrum for VDTA based *Class 0* FAF. It may clearly be noted that the VDTA based *Class 0* FAF allows only 1MHz signal to pass, partially attenuates signal of frequency 500KHz and significantly attenuates signals of frequencies 100KHz and 10MHz. Similar responses for *Class 1* and *Class 2* FAF were also obtained.

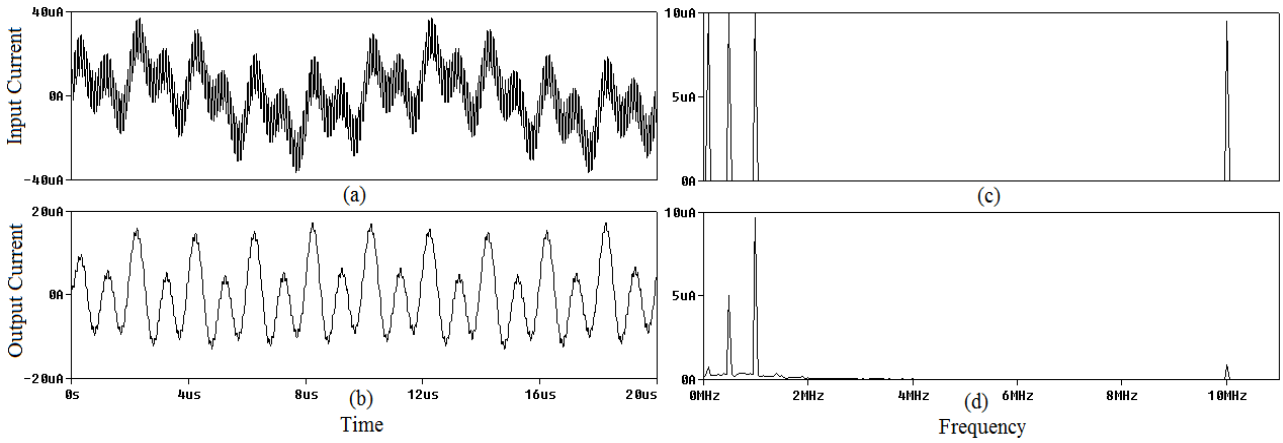

Fig. 26. (a) and (c) Input and its frequency spectrum (b) and (d) Output and its frequency spectrum for Class 0 FAF.

6 Performance Evaluation

The performance of proposed CDTA and VDTA based FAF circuits is studied in terms of power dissipation, output noise voltage and SNR. The overall performance characteristics are summarized in Table 3. Fig. 27and 28depicts the signal to noise ratio (SNR) for the proposed CDTA and VDTA based filter topologies for Class *0*, Class *1* and Class *2* respectively.

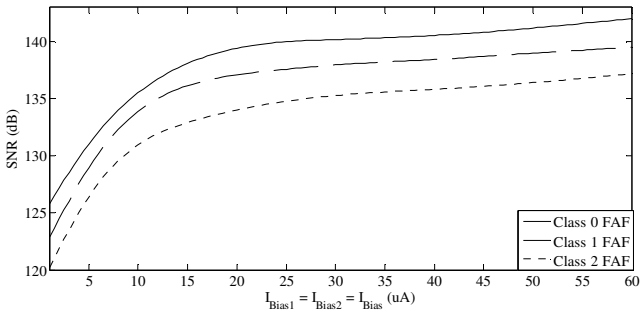

Fig. 27.SNR of CDTA based FAF.

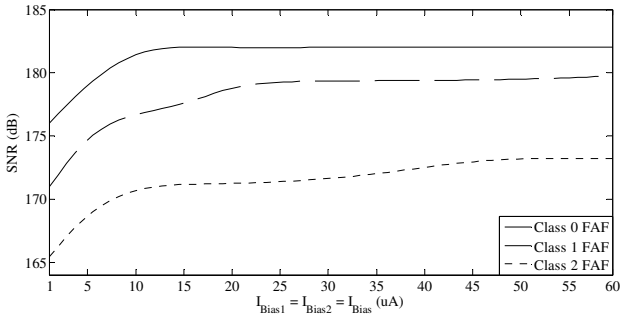

Fig. 28.SNR of VDTA based FAF.

Table 3. Performance Characteristics of CDTA and VDTA based *Class 0, Class 1* and *Class 2* FAF.

Performance Characteristics	**Type of FAF**	**I_{Bias}= 1µA**			**I_{Bias} = 10µA**			**I_{Bias} = 30µA**			**I_{Bias} = 60µA**		
		Class 0	***Class 1***	***Class 2***	***Class 0***	***Class 1***	***Class 2***	***Class 0***	***Class 1***	***Class 2***	***Class 0***	***Class 1***	***Class 2***
Power Dissipation (mW)	CDTA	0.359	0.997	1.63	3.34	3.99	4.63	9.98	10.7	11.3	19.9	20.6	21.2
	VDTA	0.089	0.177	0.405	0.32	1.19	3.45	0.835	3.34	9.57	1.60	6.28	17.4
SNR (dB)	CDTA	124.9	122.1	119.2	135.5	134.2	131.3	140.2	137.9	135.3	142.1	139.5	137.2
	VDTA	175.82	170.4	165.0	181.7	180.5	170.96	182.0	179.3	171.6	182.0	179.75	173.2
Max. output noise voltage (nV)	CDTA	79.37	74.92	75.49	155.02	82.99	58.97	210.46	70.69	40.85	290.59	60.56	31.92
	VDTA	82.5	28.85	28.1	38.92	37.43	51.3	46.10	44.4	38.1	51.62	52.63	25.6

The VDTA based FAF proved to be optimum concerning the power dissipation and Signal to Noise ratio. The maximum output noise voltage is better in CDTA based FAF for class 0 whereas VDTA based *Class 1* and *Class2* FAF have lesser noise in compared to CDTA configurations.

7 Conclusion

In this paper CDTA and VDTA based frequency agile filters are presented. The proposed FAF configurations employ grounded passive components and are suitable for integration. The filter configurations are designed in such a way that quality factor can be independently controlled without changing the center frequency. The simulation results are included to demonstrate the workability of the circuits. The performance of the proposed FAF is evaluated in terms of power dissipation, SNR and noise performance. The VDTA based FAF proved to be optimum concerning the power dissipation and Signal to Noise ratio. The maximum output noise voltage is better in CDTA based FAF for class 0 whereas VDTA based class 1 and class2 FAF have lesser noise in compared to CDTA configurations.

References

[1] P. I. Mak, Seng-Pan U, R. P. Martins, "Analog – baseband architecture and circuits for multistandard and low voltage wireless transceivers", Analog Integrated Circuits and Signal Processing, 2007.

[2] Y. Lakys, A. Fabre, "Multistandard transceivers: state of the art and a new versatile implementation for fully active frequency agile filters", Analog Integrated Circuits and Signal Processing, pp. 63-78, 2013.

[3] Y. Lakys, A. Fabre , "A fully active frequency agile filter for multi standard transceivers", International Conference on Applied Electronics, pp. 1-7, 2011.

[4] S. Kaehlert, D. Bormann, Tobias D. Werth, Muh-Dey Wei, Lei Liao, Stefan Heinen, "Design of frequency agile filters in RF frontend circuits", IEEE Radio and Wireless Symposium (RWS), pp. 13-16, 2012.

[5] A. J. X. Chen, Y. Wu, J. Hodiak, P. K. L.Yu, "Frequency Agile Digitally Tunable Microwave Photonic Filter", IEEE International Topical Meeting on Microwave Photonics, pp. 89-92, 2003.

[6] G. Subramanyam, F. W. Van Keuls, F. A. Miranda, "A K-Band-Frequency Agile Microstrip Bandpass Filter Using a Thin-Film HTS/Ferroelectric/Dielectric Multilayer Configuration", IEEE Transactions on Microwave Theory and Techniques, pp. 525 - 530, 2000.

[7] H. Chandrahalim, S. A. Bhave, R.G. Polcawich, J. Pulskamp, R. Kaul, "A Pb(Zr0.55Ti0.45)O3-Transduced Fully Differential Mechanically Coupled Frequency Agile Filter", IEEE Electron Device Letters, pp. 1296 – 1298, 2009.

[8] M. W. Wyville, R. C. Smiley, J. S. Wight, "Frequency Agile RF Filter for Interference Attenuation", IEEE Radio and Wireless Symposium (RWS), pp 399- 402, 2012.

[9] H. H. Sigmarsson, Juseop Lee, D. Peroulis, W. J. Chappell, "Reconfigurable-Order Bandpass Filter for Frequency Agile Systems", IEEE International Microwave Symposium Digest, pp. 1756-1759 , 2010.

[10] Y. Lakys, B. Godara, A. Fabre, "Cognitive and Encrypted Communications, Part 2: A New Approach to Active Frequency-Agile Filters and Validation Results for an Agile Bandpass Topology in SiGe-BiCMOS", International Conference on Electrical and Electronics Engineering, pp. II-16 –II-29, 2009.

[11] D. Biolek, "CDTA-building block for current-mode analog signal processing", Proceedings of the ECCTD'03, vol. III, Krakow, Poland, pp. 397–400, 2003.

[12] D. Biolek, V. Biolkova, Z. Kolka, "Current-mode biquad employing single CDTA", Indian Journal of Pure & Applied Physics, pp. 535-537, 2009.

[13] M. Kumngern, P. Phatsornsiri, K. Dejhan, "Four Inputs and One Output Current-Mode Multifunction Filter Using CDTAs and All-Grounded Passive Components", IEEE Tenth International Conference on ICT and Knowledge Engineering, pp. 59-62, 2012.

[14] S. K. Pandey, A. P. Singh, M. Kumar, S. Dubey, P. Tyagi, “A Current Mode Second Order Filter Using Dual Output CDTA”, International Journal of Computer Science & Communication Networks, pp. 210-213, 2012.

[15] F. Kacar, H. Kuntman, “A new CMOS current differencing transconductance amplifier (CDTA) and its biquad filter application”, IEEE EUROCON’09, pp. 189-196, 2009.

[16] D. Biolek, E. Hancioglu, A. U. Keskin, “High-performance current differencing transconductance amplifier and its application in precision current-mode rectification”, International Journal on Electronics and Communications, (AEU), pp. 92 – 96, 2008.

[17] A. Uygur, H. Kuntman, A. Zeki, “Multi-Input Multi-Output CDTA-Based KHN Filter”, IEEE International Microwave Symposium Digest, pp. 1756-1759, 2010.

[18] W. Chiu, S. I. Liu, H. W. Tsao, J. J. Chen, “CMOS differential difference current conveyor and their applications”, IEE Proceedings - Circuits Devices Systems, 143, pp. 91- 96, 1996.

[19] Z. Wang, “2-MOSFET Trans-resistor with extremely low distortion for output reaching supply voltages”, Electronics letters, vol. 26, no. 13, pp. 951-952, 1990.

[20] D. Biolek, M. Shaktour, V. Biolkova, Z. Kolka, “Current input current output universal biquad employing two bulk-driven VDTAs”, IEEE International Congress on Ultra Modern Telecommunications and Control Systems, pp. 484-489, 2012.

[21] J. Satansupa, W. Tangsrirata, “Single VDTA based current mode electronically tunable multifunction filter”, 4th International Science, Social Science, Engineering and Energy Conference, ISEEC, pp. 1 – 8, 2012

[22] P. Phatsornsiri, P. Lamun, M. Kumngern, U. Torteanchai, “Current mode third order quadrature oscillator using VDTAs and grounded capacitors”, Joint International Conference on Information and Communication Technology, Electronic and Electrical Engineering (JICTEE-2014), pp. 1 – 4, 2014.

[23] T. Pourak, P. Suwanjan, W. Jaikla, S. Maneewan, “Simple quadrature sinusoidal oscillator with orthogonal control using single active element”, International Conference on Signal Processing and Integrated Networks (SPIN), pp. 1 – 4, 2014.

[24] M. Srivastava, D. Prasad and D. R. Bhaskar, “New Parallel R-L impedance using single VDTA and its high pass filter application”, International Conference on Signal Processing and Integrated Networks (SPIN), pp. 535 – 537, 2014.

[25] K. Chumwangwapee, W. Jaikla, W. Sunthonkanokpong, W. Jaikhang, S. Maneewan, B. Sreewirote, “High input impedance mixed-mode biquad filter with orthogonal tune of natural frequency and quality factor”, International Conference on Information and Communication Technology, Electronic and Electrical Engineering (JICTEE-2014), pp. 1 – 4, 2014.

[26] V. Biolkova and D. Biolek, “Shadow filters for orthogonal modification of characteristic frequency and bandwidth”, Electronics letters, vol. 46, no. 12, pp. 511-512, 2010.

[27] Y. Lakys and A. Fabre, “Shadow filters – new family of second-order filters”, Electronics letters, vol. 46, no. 4, pp. 761-762, 2010.

DETECTION CLASSIFICATION AND LOCATION OF FAULTS ON 220 KV TRANSMISSION LINE WITH STATCOM USING WAVELET TRANSFORM AND NEURAL NETWORK

R.P. Hasabe[1], A. P. Vaidya[2]

[1, 2] *Electrical Engineering Department, Walchand College of Engineering Sangli, Maharashtra. (India)*

ABSTRACT

A new scheme to enhance the solution of the problems associated with Transmission line protection with Statcom connected is presented in this paper. The fault detection is carried out by using energy of the detail coefficients of the phase signals and artificial neutral network algorithm used for fault type classification and fault distance location for all the types of faults for 220 KV transmission line. The energies of the all three phases A, B, C and ground phase are given input to the neural network for the fault classification. For each type of fault separate neural network is prepared for finding out the fault location. An improved performance is obtained once the neutral network is trained suitably, thus performance correctly when faced with different system parameters and conditions.

Keywords — Discrete Wavelet Transform, Fault Detection, Fault Classification, Statcom, Wavelet Transform.

I. INTRODUCTION

Protecting of transmission lines is one of the important tasks to safeguard electric power systems. Wavelet transform has the advantage of fast response and increased accuracy as compared to conventional techniques. The wavelet transformation is a tool which helps the signal to be analyzed in time as well as frequency domain effectively. The detection of fault is carried out by the analysis of the wavelets coefficients energy related to phase currents. ANN based techniques have been used in power system protection and encouraging results are obtained [1], [2],[3]. In classification, the objective is to assign the input patterns to one of the different classes [4], [5]. Fault location in a transmission line using synchronized phasor measurements has been studied for a long time. Some selected papers are listed as [6]–[10]. When a fault occurs, the presence of a shunt compensator in the line creates new problems for fault location algorithms and since the control system of shunt compensator reacts to the fault, the voltages and currents at the fault locator point will be affected in the transient state. In this paper a scheme is propose for 220KV Statcom connected transmission line for fast and reliable fault detection using energy of the detail coefficients of the phase signals, classification and location using neural network. For fault classification current signals (Ia2, Ib2, Ic2, and IG) detail coefficients energy values are given as input to the neural network. For each type of fault location separate neural network with

different combination of input signals are prepared. In each of these cases, the current, voltage and ground phase current signals detail coefficients energies values of only phase involving in the fault signals are given as input to the neural network. For fault location of line with Statcom, impedance of line up to the fault point is calculated and as per value of line impedance fault is located. The MATLAB 7.10 version is used to generate the fault signals and verify the correctness of the algorithm. The proposed scheme is insensitive to variation of different parameters such as fault type, fault resistance etc.

II. DISCRETE WAVELET TRANSFORM

Discrete Wavelet Transform is found to be useful in analyzing transient phenomenon such as that associated with faults on the transmission lines. The fault signals are generally non stationary signals, any change may spread all over the frequency axis. The wavelet transform technique is well suited to wide band signals that may not be periodic and may contain both sinusoidal and non-sinusoidal components. Multi-Resolution Analysis (MRA) is one of the tools of Discrete Wavelet Transform (D.W.T), which decomposes original, typically non-stationary signal into low frequency signals called approximations and high frequency signals called details, with different levels or scales of resolution. The use of detail coefficients for fault detection is discussed in this paper. Detail coefficients contain information about the fault, which is required for fault detection.

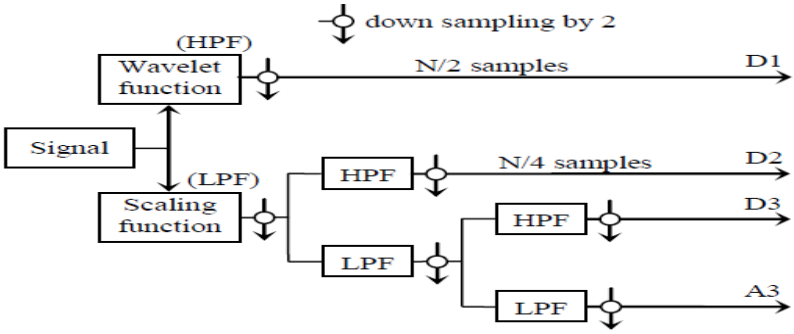

Fig.1. Wavelet Filter Bank

The signal of desired frequency component can be obtained from repetitive decompositions as shown by Fig.1. The mother wavelet determines the filters used to analyze signals. In this paper Db4 (Daubechies 4) wavelet was chosen because of its success in detecting faults [4], [5].

III. ARTIFICIAL NEURAL NETWORK

Artificial Neural Networks simulate the natural systems behavior by means of the interconnection of basic processing units called neurons. ANNs have a high degree of robustness and ability to learn [8]. Once the network is trained, it is able to properly resolve the different situations that are different from those presented in the learning process. The multilayered feed forward network has the ability of handling complex and nonlinear input-output relationship with hidden layers. In this method, errors are propagated backwards; the idea of back-propagation algorithm is to reduce errors until the ANN learns the training data [13] [14]. The multilayered feed forward network has been chosen to process the prepared input data obtained from the W.T.

VI. Transmission Line Model

In Fig.2, model of 220kv, 90 km transmission line from A to B is chosen. Generator of 500MW is connected at one end and loads are connected at 220kv.

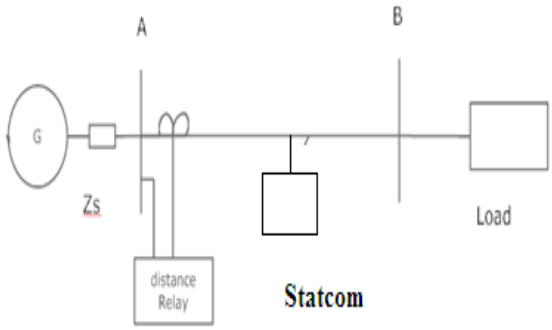

Fig.2. Transmission Line Single Line Mode

Various faults are simulated on that line by varying various parameters. Ratings of power system model are shown in Table I. As shown in Fig.2 a transmission line model is prepared in MATLAB7.10. The transmission line positive and zero sequence parameters are R1=0.10809Ω/km, R0=0.2188Ω/km, L1=0.00092H/km, L0=0.0032H/km, C1=1.25*10^{-8} f/km,0=7.85*10^{-9} f/km. The distributed parameter model of transmission line is considered for analysis. The current signals are sampled at sampling frequency of 20 kHz.

Table I . Model Parameters

1.	Generator	500MVA, 13.8kv, 50Hz, synchronous generator pu model
2.	Transformer1	13.8kv/220kv, 500MVA.
3.	Transfomer2	220kv/13.8kv, 500MVA.
4.	Load1	50MW, 220kv, 1Mvar, RL load.
5.	Load2	150MW, 220kv, , 1MVar, RL load
6	Load3	100MW, 220kv, , 1MVar, RL load
7	Transmission line	Length=90 km.

V. DESIGN OF FAULT DETECTION, CLASSIFICATION AND LOCATION

The design process of proposed fault detection, classification and location approach is as above. Combination of different fault conditions are to be considered and training patterns are required to be generated by simulating different kinds of faults on the power system. The fault resistance, fault location, and fault type are changed to generate different training patterns.

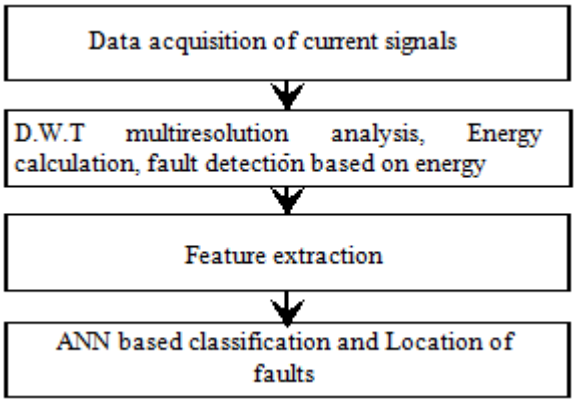

Fig.3. Process Of Fault Detection, Classification And Location.

VI. FAULT DETECTION

The signals taken from the scope are filtered, sampled at 20 kHz sampling frequency. Then DWT is applied up to level 5, and detail coefficients and approximate coefficients are calculated and detail coefficients energy is calculated. Then, we come to know that detail level 5 contains highest amount of energy than the level 4 [11], [12]. A moving data window of one cycle (400 samples) is taken and decomposition is done and energy of the details coefficients at level 5 is obtained for each data window. As the fault signals contain the high amount of harmonic components, the energy of the signal increases at the occurrence of fault as shown in Fig.4 Here, for detecting the fault, difference of energies between two adjacent windows has been considered. The energy of detail coefficients for a k^{th} window is given by equation (1),

$$E_d = \sum_{i=1}^{N} D_l^2(i) \qquad (1)$$

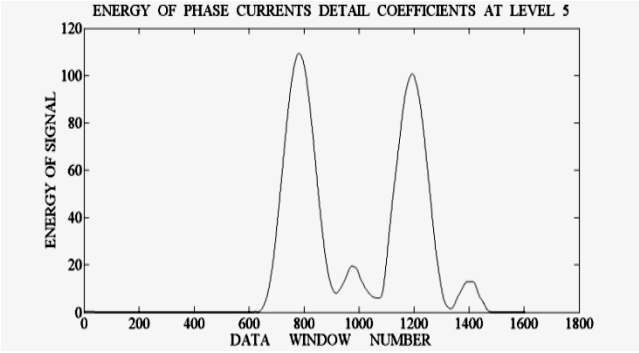

Fig. 4.Energy Of The Detail Level 5 Vs. Window Number

Where, k=window number, l=level of the DWT, N=length of Detail coefficients at level l. For accurately detecting the presence of faults, the difference between the two consecutive energies of the moving windows is calculated by (2) and shown in Fig.5.

$$F.D(k) = F.D(k-1) + [E_d(k) - E_d(k-400)] \qquad (2)$$

In this sampling frequency of 20 kHz gives 400 samples for each cycle of 20ms. Here, moving window slides taking only1 new sample at each move and keeping 399 previous samples. So one cycle corresponds to nearly 400 data samples.

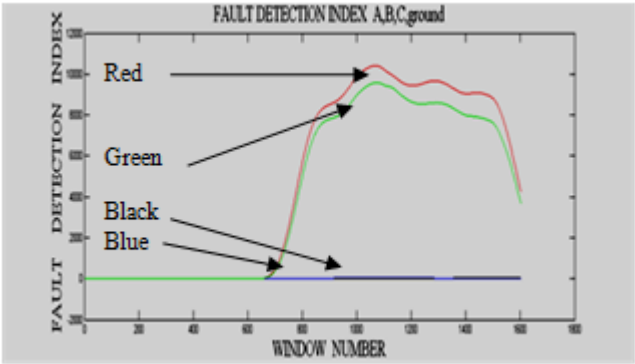

Fig. 5.F.D Index For Single Line To Ground Fault Vs. Window Number

The fault is present on R-phase and ground (G) for the present case. Red colour shows the R phase, green colour shows the ground (G) phase, black colour represents the Y phase and blue colour shows the B phase.The Fault Detection value is compared with threshold value for consecutive 10 data windows, and then decision is made whether fault is permanent or temporary. By using these Fault Detection values the faults can be accurately detected [7].

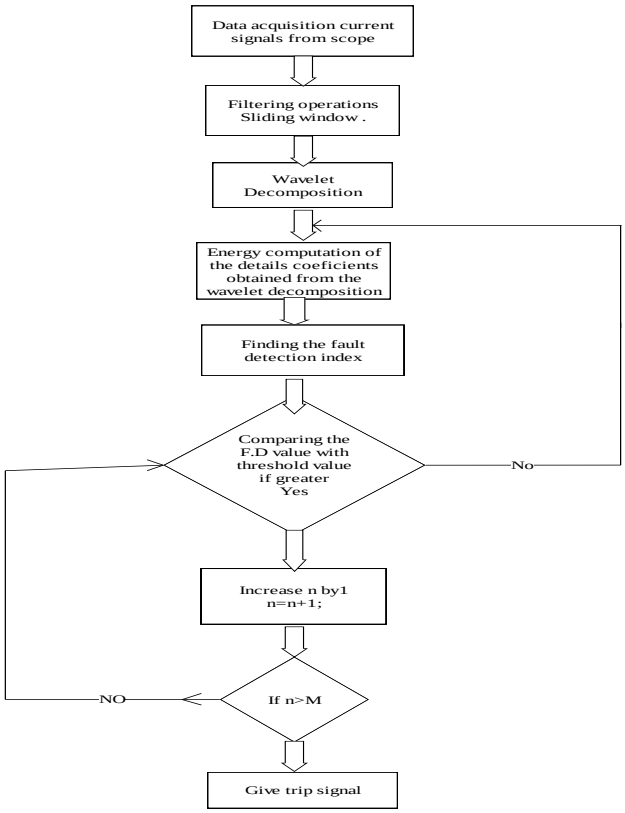

Fig. 6. Flow Chart Of Proposed Algorithm.

Fig. 6 Shows The Flow Chart Of Algorithm Of The Distance Relay For The Proposed Scheme. The Voltage And Current Phasors Are Estimated Using Discrete Wavelet Transform (DWT) At The Relaying Bus And At The

Terminal Of The Compensator. The Estimated Voltage And Current Phasors Of The Compensated Terminal Is Communicated At The Relaying Bus Using Fast Data Communication Link Like Fiber Optics, Etc. The Apparent Impedance Zappnew Is Then Calculated And Compared With The Relay Setting Zset For The Zones Of Protection Of The Transmission Line. If The Measured Impedance Is Less Than Or Equal To The Zset Value Then The Uncompensated Line Algorithm Is Running While Measured Impedance Is Greater Than Set Value Then Compensated Line Algorithm Is Running .

VII. NEURAL NETWORK BASED FAULT CLASSIFICATION

All different faults are simulated for different conditions and training patterns are generated from the energy values of the detail coefficients. The 4 input neurons and 4 output neurons are selected. Feed forward multilayer back propagation neural network is selected. The average values of energies of current signals, half cycle after the occurrence of fault are given as input to the neural network, along with the three lines energies, zero sequence current energy is also given as fourth input to the neural network. Three outputs show the statuses of the three phases, if fault is present it is shown by the presence of '1', otherwise with presence of '0'. Similarly fourth output indicates the ground fault. If ground is involved in the fault will be indicated by the presence of '1', otherwise it is presented by '0'. Generation of different training patterns is done as shown in Table II.

Table II. Training Patterns

Type of fault	LG, LLG, LL, LLL.
Location of fault (%) from busbar P.	20,30,40,50,60,70,80
Fault resistance	5,10,15,20 Ω.

For training neural network different fault conditions are simulated, features are extracted and network is trained. At 7 different locations on the transmission line fault is created, at 20, 30, 40, 50, 60, 70, 80% of the transmission line length from the sending end, 4 different values of fault resistances can be used and total 10 different faults are created, and this gives 7*4*10=280 cases for training neural network.

The different training algorithms are presented to train the neural network; they use the gradient of the performance function to determine how to adjust the weights to minimize a performance function. The gradient is determined using back propagation technique, which involves performing computations backwards through the network. A variation of back propagation algorithm called Levenberg-Marquardt (LM) algorithm was used for neural network training, since it is one of the fastest methods for training moderate-sized feed forward neural networks [15].

LM algorithm to weight update is given by (3),

$$X_{k+1} = X_k - [J^T J + \mu I]^{-1} * J^T * e \qquad (3)$$

Where J is Jacobean matrix that contains first derivatives of the network error with respect to the weights and biases, e is a vector of network errors. $J^T J$ is an approximation of the Hessian Matrix, $J^T e$ is the gradient and μ is the scalar affecting performance function. LM algorithm based method for training neural network is much faster than the other methods. Fig.7 shows the Multilayered Feed forward Neural Network (M.F.N.N.)

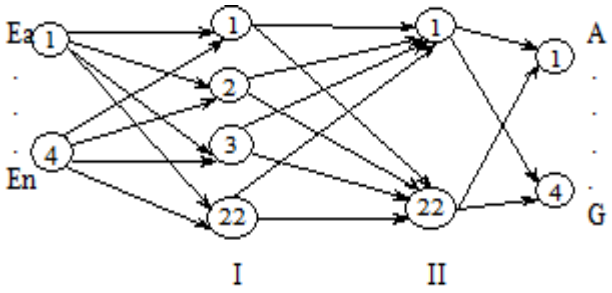

Fig.7. Multilayer Feed Forward Network For Fault Classification

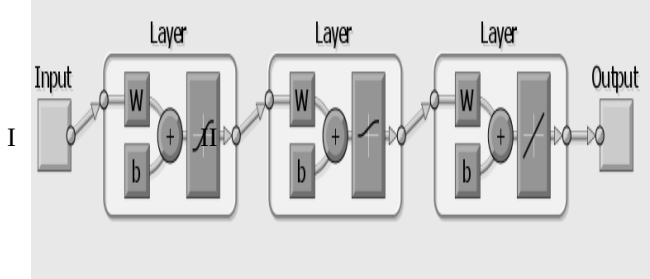

Fig.8. 4-22-22-4 'Tansig', 'Logsig', 'Purelin' Configuration.

Network with 2 hidden layers worked out to be better than the 1 hidden layer network.4-22-22-4 configuration give better results than the 4-22-4, 4-10-4 configurations. Activation functions used for the hidden layers I, II and output layer are 'tansig', 'logsig' and 'purelin' respectively. The Fig.8 shows the neural network.

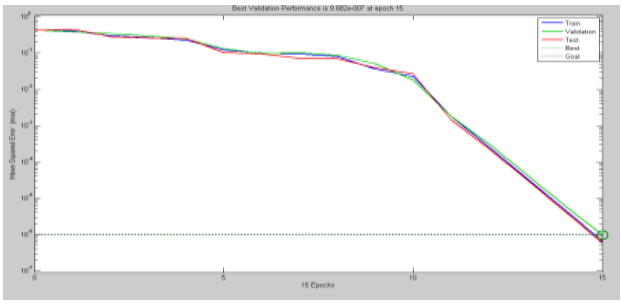

Fig.9. Performance Curve

The data used for training data division is done randomly; training function used is LM algorithm. Performance function used is Mean least square error method. The performance goal chosen is 10^{-6} . Fig.9 shows the performance curve.

VIII. TEST RESULTS

A validation data set consisting of different fault types was generated using the transmission line model shown in Fig.2. The validation test patterns were different than they were used for the training of the neural network .For different faults on the model system, fault type; fault location and fault resistance values are changed to investigate the effects of these factors on the performance of the proposed algorithm. Test results are as shown in

Table III. These results show the accuracy of neural network for varying fault location values and varying fault resistance value.

The output layer activation function used is 'Purelin', because of its success in the classification of faults correctly. The tansig and logsig transfer functions did not show a good classification capability. The output layer transfer function is fixed at 'Purelin' and the hidden layer transfer function was changed.

If the transfer functions of the hidden layers I and II are chosen as 1) Tansig-Tansig. 2) Logsig-Logsig. 3) Tansig-Logsig, the Table IV test result shows that the accuracy obtained with the Tansig-Logsig type of neural network is more and it is having good generalization capability. The classification results for almost all types of faults are satisfactory.

Table III. Testing Results

Fault type	Fault location from P(%)	Fault resistance Ω.	Output of neurons			
			A	B	C	G
AG	30%	10	1.0001	2*10^-3	4*10^-3	1.00
BCG	50%	15	0	1.00	0.9989	1.00
CAG	50%	10	1	0	1.00	0.998
CG	50%	10	1*10^-3	0.000	1.00	1.00
ABC	30%	10	1.00	1.00	0.999	0.00
ACG	70%	5	0.9996	-3*10^-4	0.997	1.000
AB	70%	5	1.018	1.0847	0.1587	0.052

Table IV. Comparison Of Transfer Functions

Transfer Functions for hidden layers. No. neurons in hidden layers.	Tansig-tansig. 22-22	Logsig-logsig. 22-22	Tansig-logsig. 22-22.
Performance error of test results	2.9*10^(-7)	5.5*10^(-7)	5.39*10^ (-8).

IX. ANN BASED FAULT DISTANCE LOCATOR

In this paper single line to Ground fault locator explains in detail.

Single Line to Ground Faults Locator

9.1. Selecting The Right Architecture

The network inputs chosen here are the magnitudes of the detail coefficients energies fundamental components (50 Hz) of phase voltages and currents measured at the relay location. As the basic task of fault location is to determine the distance to the fault, the distance to the fault, in km with regard to the total length of the line, should be the only output provided by the fault location network. Thus the input and the output for the fault location network are:

Input = different combinations of Va2, Vb2, Vc2, Ia2, Ib2, Ic2 and IG as per faults. (1)

Output Lf = Fault distance in KM. (2)

For each type of fault separate neural network is prepared for finding out the fault location. Through a series of trial and error, and modifications of the ANN architecture, the best performance is achieved by using a four layer neural network with 3 inputs and 1 output as shown in Fig. 10. After analysing the various possible combinations

of transfer functions normally used, such as logsig, tansig and linear functions, the tansig function was chosen as transfer function for the hidden layer, and pure linear function "purelin" in the output layer.

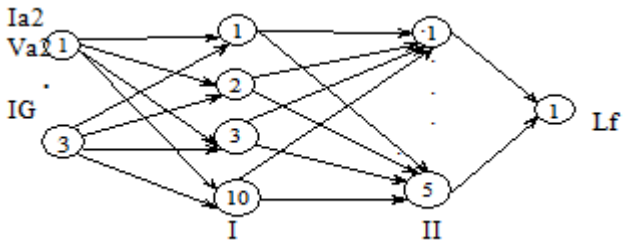

Fig.10 Structure Of The Chosen Ann With Configuration For Lg Fault

9.2. Learning Rule Selection

The back-propagation learning rule can be used to adjust the weights and biases of networks to minimize the sum-squared error of the network. The simple back-propagation method is slow because it requires small learning rates for stable learning, improvement techniques such as momentum and adaptive learning rate or an alternative method to gradient descent, Levenberg–Marquardt optimisation, can be used. Various techniques were applied to the different network architectures, and it was concluded that the most suitable training method for the architecture selected was based on the Levenberg–Marquardt (Trainlm) optimization technique.

9.3. Training Process

Using SIMULINK & SIMPOWERSYSTEM toolbox of MATLAB all the ten types of fault at different fault locations between 0-100% of line length and different fault resistance have been simulated as shown below in Table V. Feed forward back-propagation network have been surveyed for the purpose of single line-ground fault location, mainly because of the availability of the sufficient relevant data for training. In order to train the neural network, several single phase faults have been simulated on transmission line model. For each of the three phases, faults have been simulated at every 10 km on a 90 km transmission line. Total of 648 cases have been simulated with different fault resistances 1, 2, 3 ohms respectively. In each of these cases, the current and voltage signals detail coefficients energies of only phase involving in the fault and ground phase current signals given as input to the neural network such as Ia2, Ib2, Ic2,Va2 ,Vb2, Vc2 and IG. The output of the neural network is the distance to the fault from the sending end of the transmission line. The ANN based fault distance locator was trained using Levenberg–Marquardt training algorithm using neural network toolbox of Matlab as shown in Fig. 11

Table V. Training Patterns Generation

Sr. No.	Parameter	Set value
1	Fault type	LG: AG-Ia2, Va2, IG BG- Ib2, Vb2, IG CG -Ic2, Vc2, IG LL: AB- Ia2, Va2, Ib2, Vb2, LLG: ABG -Ia2, Va2, Ib2, Vb2, IG LLL: ABC- Ia2, Va2, Ib2, Vb2, Ic2, Vc2 LLLG:ABCG- Ia2, Va2, Ib2, Vb2, Ic2, Vc2, IG
2	Fault location (Lf in KM)	10, 20, 30, …80 and 90 km
3	Fault resistance (Rf)	1, 2, 3 ohm

Once the network is trained sufficiently and suitably with large training data sets, the network gives the correct output after one cycle from the inception of fault.

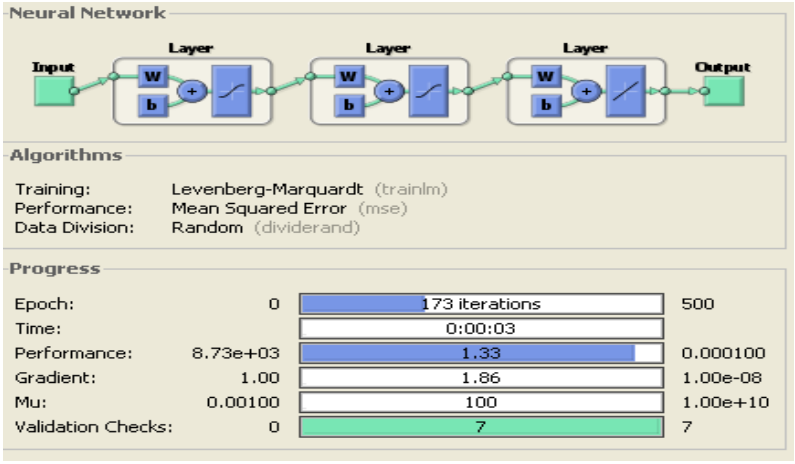

Fig. 11 Overview Of The Chosen Ann (3-10-5-1).

Fig. 11 plots the mean square error as a function of time during the learning process and it can be seen that the achieved MSE is about 2.61.

9.4 Test Result Of Ann Based Fault Distance Locator

Once training was completed, ANN based Fault distance locator was then extensively tested using independent data sets consisting of fault scenarios never used previously in training. For different faults of the validation/test data set, fault type, fault location, and fault resistance were changed to investigate the effects of these factors on the performance of the proposed algorithm. The network was tested and performance was validated by presenting all the ten types of fault cases with varying fault locations (Lf=0-90KM), fault resistances (Rf=1,2,3 etc) Table VI shows some of the test results of ANN based fault locator under different fault conditions. It can be seen that all results are correct with reasonable accuracy. At various locations different types of LG faults were tested to find out the maximum deviation of the estimated distance Lf measured from the relay location, from the actual fault location. Table VI. Percentage errors as a function of fault distance and fault resistance for the ANN chosen for single phase fault location.

Table VI. Result

Fault Distance (Km)		Measured Fault Location (Km)		Percentage Error (%)	
RF=1Ω	RF=4Ω	RF=1Ω	RF=4Ω	RF=1Ω	RF=4Ω
9	9	8.5	8	0.55	1.1
18	18	16	15.5	2	2.7
54	54	52	51	2.22	3
63	63	62	60	1	3.33
72	72	70.5	71	1.6	1.6

Then the resulted estimated error "e" is expressed as a percentage of total line length L In all the fault cases, the results have shown that the errors in locating the fault are less than 0.55% to +3.33%.

Table VI can show the percentage errors in fault location as a function of Fault Distance and Fault resistance. Different cases are shown with different fault resistances. Thus, the neural network performance is considered satisfactory and can be used for the purpose of single line- ground fault location.

X. CONCLUSION

In this paper accurate fault detection, classification and location technique is discussed. This technique depends upon the current and voltage signals. The features are extracted from the current and voltage signals by using wavelet transform. The feature vector is then given as input to the neural network. The capabilities of neural network in pattern classification were utilized. Simulation studies were performed and the performance of the scheme with different system parameters and conditions was investigated. The test result shows that the accuracy obtained for fault classification with the "tansig-logsig" transfer function for hidden layers I and II is satisfactory. For fault location after analysing the various possible combinations of transfer functions normally used, such as logsig, tansig and linear functions, the tansig function was chosen as transfer function for the hidden layer I and II, and pure linear function "Purelin" in the output layer gives satisfactory results.

REFERENCES

[1] K. Gayathri and N. Kumarapan, "Comparative Study of Fault Identification and Classification on EHV Lines Using Discrete Wavelet Transform and Fourier Transform Based ANN", World Academy of Science, Engineering and Technology, pp.822-831.2008.

[2] D. V. Coury, D. C. Jorge, "Artificial Neural Network Approach To Distance Protection Of Transmission Lines." IEEE Transactions on Power Delivery, Vol. 13, No. 1, January 1998.

[3] H. Khorashadi-Zadeh, M. R. Aghaebrahimi, "A Novel Approach to Fault Classification and Fault Location for Medium Voltage Cables Based on Artificial Neural Network", World Academy of Science, Engineering and Technology, pp.1100-1103.2008.

[4] V. S. Kale, S. R. Bhide, P. P. Bedekar, "Faulted Phase Selection on Double circuit Transmission Line using Wavelet Transform and Neural Network", Third International Conference On Power Systems, Kharagpur, INDIA, December 27-29.

[5] A. Abdollahi, S. Seyedtabaii, "Comparison of Fourier & Wavelet Transform Methods for Transmission Line Fault Classification", The 4th International Power Engineering and Optimization Conf. (PEOC2010), Shah Alam, Selangor, MALAYSIA: 23-24 June 2010.

[6] K. Takagi, Y. Yomakoshi, M. Yamaura, R. Kondow, and T. Matsushima, "Development of a new type fault locator using the one terminal voltage and current data," IEEE Trans. Power App. Syst., vol. PAS-101, pp. 2892–2898, Aug. 1982.

[7] A. Girgis, D. Hart, andW. Peterson, "A new fault location technique for two- and three-terminal lines," IEEE Trans. Power Delivery, vol. 7, pp. 98–107, Jan. 1992.

[8] M. Abe, T. Emura, N. Otsuzuki, and M. Takeuchi, "Development of a new fault location system for multi-terminal single transmission lines," IEEE Trans. Power Delivery, vol. 10, pp. 159–168, Jan. 1995.

[9] J.-A. Jiang, J.-Z. Yang, Y.-H. Lin, C.-W. Liu, and J.-C. Ma, "An adaptive PMU based fault detection/location technique for transmission lines part I: Theory and algorithms," IEEE Trans. Power Delivery, vol. 15, pp. 486–493, Apr. 2000.

[10] A. Gopalakrishnan, D. Hamai, M. Kezunovic, and S. McKenna, "Fault location using the distributed parameter transmission line model," IEEE Trans. Power Delivery, vol. 15, pp. 1169–1174, Oct. 2000.x

[11] V. S. Kale, S. R. Bhide, P. P. Bedekar, G. V. K. Mohan, "Detection and Classification of Faults on Parallel Transmission Lines using Wavelet Transform and Neural Network", International Journal of Electrical and Computer Engineering, pp.1063-1067, 16, 2008.

[12] N. Zamanan, M. Gilany, "A Sensitive Wavelet-Based Algorithm for Fault Detection in Power Distribution Networks" ACEEE Int. J. on Communication, Vol. 02, No. 01, Mar 2011.pp.46-50.

[13] S. Haykin, Neural Networks, IEEE Press, New York, 1994.

[14] H. Demuth and M. Beale, "Neural Network Toolbox Matlab" 1992.

[15] Mamta Patel, R. N. Patel, "Fault Detection and Classification on a Transmission Line using Wavelet Multi Resolution Analysis and Neural.

[16] Albasri F.A., Sidhu T.S., Varma R.K., "Mitigation of Adverse Effects of Midpoint Shunt- FACTS Compensated Transmission Lines on Distance Protection Schemes," Power Engineering Society General Meeting Rep. pp 1-8, 2007

[17] R. P. Hasabe received the B.E. degree in electrical engineering and the M.E. degree in electrical power systems from Shivaji University, Kolhapur, India in 2001 and 2006, respectively, and is currently pursuing the Ph.D. degree in Electrical engineering at Shivaji University Kolhapur.

[18] Currently, he is an Assistant Professor in the Department of Electrical Engineering, Walchand College of Engineering, Sangli. His research interests include power system protection, planning and design, system modeling, and simulation.

[19] A. P. Vaidya received the B.E. in electrical engineering and the M.E. in electrical power systems from Shivaji University, Kolhapur, India, in 1983 and 1993 respectively, and the Ph.D. degree from the IISc, Bangalore in 2005.

[20] Currently, he is Professor in the Department of Electrical Engineering, Walchand College of Engineering, Sangli. He has published more than 10 papers in journals and conferences at international and national levels.

[21] His research interests include power system protection, automation, planning and design, system modeling and simulation, and artificial intelligence.

A BASIS OF ONTOLOGY FOR ASPECT ORIENTED METRICS

Dr. Ananthi Sheshasaayee [1], Roby Jose [2]

[1]*Associate Professor And Head , Department Of Computer Science, QMGCW (India)*
[2] *Research Scholar, Department Of Computer Science, QMGCW (India)*

ABSTRACT

The feature modularization has paved the way for the growth of aspect oriented software development. Aspect Oriented paradigm supports the separation of concerns that are scattered over the system which helps in achieving modularity. Aspect Oriented Software Development encompass software engineering abstractions and complexity at new and different dimensions. As aspect orientation is a comparatively new paradigm, it lacks philosophical basis, as compared to object orientation. Since aspect orientation lacks a theoretical basis as enjoyed by object orientation, there is no clarity over what constitutes an aspect and the best approach to measure and assess the properties of an aspect oriented program. This paper looks at information necessitated to build ontology for aspect oriented quality measurement.

Keywords: Aspect Oriented Software Development, Concerns, Ontology, Separation Of Concerns, Software Measurement.

I. INTRODUCTION

These days' business and internet applications have to tackle features like logging, security et al that cut across multiple modules of a system. These features which are termed as concerns are identified in softwares developed of traditional approaches and isolated resulting in aspect oriented systems. Aspect oriented approach is not a replacement for object oriented approach, but complements object oriented approach. The work instigated by Chidamber and Kemerer [11] based on Wand and Weber [13] interpretation of the ontology for information systems had given elementary theoretical basis for object oriented measurement. The generalized concepts of Bunge [15] form the basis for the concept of objects. Even though Bunge's ontology did not provide an exact ontological definition for concepts in object oriented paradigm, Wand and Weber took up the concepts and changed to suit for object oriented domain. Many of the OO researchers applied the general concepts of Bunge to the object oriented domain. Bunge's ontology had significant followers in object oriented research as it had dealt with meaning and description of representations from real world. Consistent with this ontology, objects are defined independent of implementation considerations and include the concepts of encapsulation and inheritance. Wand and Weber's ontology for object orientation can be summarized as follows. The world is crafted of things: individuals and concepts. Individual possess properties and an onlooker can assign features to an individual but these are attributes and not properties. An individual and its properties constitute an object; therefore an object is a representation of the application domain that takes account of the methods and instance variables that a designer assigns to that object. The Chidamber and Kemerer [11] suite of object oriented metrics was formed on the basis of Wand and Weber's interpretation of Bunge's ontology. Chidamber and Kemerer used ontological model for measuring code and analyzing properties than a graph theory or structural attribute approach. Aspect Oriented Software Development (AOSD) Europe EU network of excellence has produced an ontology for aspect oriented paradigm. This paper aims at shaping guidance for building ontology for aspect oriented maintenance

metrics using the Public ontology for aspect orientation [2]. The rest of the paper is organized as follows. Section 2 presents some basic concepts of aspect orientation and the applicability of Dooyeweerd's theory of aspects to aspect oriented software development. Section 3 discusses a few of the related works. Section 4 provides an overview of public ontology for aspect orientation. The paper is concluded in Section 5.

II. ASPECT ORIENTATION

This section is divided into two subsections. The first subsection provides an overview of basic concepts of aspect oriented paradigm from the view of software architecture. The second subsection shows how Dooyeweerd's theory can be related to aspect oriented software development.

2.1 Basic Terminology

AOSD is a promising paradigm that allows separation of concerns. A concern is a part of the problem that is to be treated as only conceptual unit [9]. These concerns are termed crosscutting concerns as they cut across modularity of other concerns. Aspect Orientation has been proposed as a method for improving separation of concerns [9, 10] in the structure of OO software. AOSD uses aspects as new abstraction and make available mechanisms for creating aspects and components at joinpoints. Based on [3, 7] the concepts in Aspect Oriented programming are summarized below: Separation of Concern: Separation of concerns simplifies system development by allowing the development of specialized expertise by producing, by and large more comprehensible arrangement of elements Composition: Composition is bringing together separately created software elements. In other words composition integrates several modular artifacts into a logical whole.

Weaving: Weaving is the process of composing base modules of the system with aspects, thereby yielding a working system. Crosscutting Concern: A crosscutting concern is a concern for which the implementation is scattered throughout the rest of an implementation. Scattering: Scattering is the occurrence of elements that belong to one concern in modules encapsulating other concerns. Tangling: The intermixing of the code for the implementation of concerns give rise to tangling. Aspect: A modular unit designed to implement a concern is referred as aspect. Join Point: A join point is a point of interest in some object of the software lifecycle through which two or more concerns may be composed. Join Point Model: A Join Point Model provides the common frame of reference to enable the definition of the structure of aspects. Pointcut: A Pointcut designator describes a set of join points Advice: Advice is an aspect element, which augments or constrains other concerns at join points matched by a pointcut expression. The above given terms and their definitions are as per the book by Filman et al[3] and Kiczales[7] works. The Kiczales[7] definition are based on AspectJ language, the aspect oriented extension for Java.

2.2 Dooyeweerd's Theory And Aspect Orientation

Herman Dooyeweerd was a Christian philosopher whose work [8] Dooyeweerd theory of aspects, tells that the behavior of parts is determined by the behavior of whole. These parts or aspects enable human beings and every other thing to do their jobs and each aspect has its very own interrelated laws. Dooyeweerd's aspectual suit for human beings introduces fifteen aspects. No aspect of the suit can be neglected in real life because life itself is multi-aspectual in nature like a system having multiple concerns. The day today life of human beings show that all aspects function because of the harmonious integration of the aspects. An aspect oriented system takes the disharmony that is created when aspectual properties are replicated as objects and uses the concept of aspects to harmonize them. In analogous to Dooyeweerd theory where areas of interest where splitted to fifteen aspects, in aspect oriented programming this can be seen as system requirements splitted into: logging, persistence, caching

and security et al. where each one is represented as aspect. In an aspect oriented program, each of these aspects coexist but one cannot be derived from other.

III. RELATED WORK

The primary ontology for AOP is by van den Berg et al [2]. This consists of fifteen ontology views, of which two are of particular interest in identifying ontology-enabled development from an AOSD perspective. These are the Software System View and the Weaving View, which between them encompass the high level view of the system and the core engineering perspective of managing aspects. In addition, Black and Harman [1] propose some extensions to this model, in particular the integration of spatial, lingual and social aspects. These three aspects can be defined as follows. Spatial- If only the system is viewed from spatial aspect, the user will be conscious that the system may be located in geographically dissimilar locations. Lingual- A system may be viewed as language independent if the concern that it is written in a particular language can be separated out.
Social-This is related to the computer programmers. Separating out the social aspects of the programmers helps to understand the cognitive thinking of the programmers. These views and extensions have been integrated together to provide a single ontology of aspect oriented software development.

IV. ONTOLOGY FOR AO METRICS

Since AOSD is very young and almost all terminology are adapted from AspectJ point of view, it is high time that aspect orientation getting a foundation that is not constrained by a programming language. An ontology enables the sharing of common terminology and associated conceptual models to communicate effectively within stakeholders. An ontology is essential to integrate the results from various activities that may occur in parallel. An ontology is expected to define the meaning of set of concepts for a particular domain. The development of ontology is the process of developing textual definitions of concepts with clear-cut formal specifications of their interdependencies. As the software development life cycle is divided into different phases the construction of ontology also involves the same phases. The activities in the each phase of ontological development is discussed below

4.1 Requirements

When building ontology for the software measurement in Aspect Oriented Paradigm, it should be able to satisfy certain requirements. The first being the ability to signify the terminology and concepts of AOSD [6]. In other words it should be able to give definition of the facts. The developed ontology must be generally accepted by AO metrics research community. This means that knowledge derived are applicable everywhere and the value and usefulness of the ontology must be acknowledged. The third requirement while building the ontology is that it should be accurate, complete, conflict free and non-redundant [4]. The third requirement specifies the properties the model should possess when it represents the semantic of AO metrics. The fourth requirement [14] while building the ontology for AO metrics requires that it should be verifiable (ability to check for correctness), traceable (origin of the definition could be determined) and unambiguous (single interpretation of the definition). The final requirement is that the model should be maintainable and usable [12]. Maintainability is the capability of the model to accept modification whereas Usability is the extend to which the product is understood, used and liked by a user under specified conditions

4.2 Design

The design or ontology engineering can be done using Common Warehouse Metamodel (CWM) [5]. The metamodel is described in the Unified Modelling Language (UML).In the CWM Business Nomenclature two

levels are distinguished viz a *taxonomy* with *concepts* at semantic level (conceptual model or domain model) and a *glossary* with *terms* at representation level (terminology). The design should be able to capture correct properties, avoid ambiguous language and be focusing only on relevant properties.

4.3 Implementation

In this phase the model can be implemented using modelling languages and tools. Various tools are available for supporting modification requests and modification tracking. So the disciplined process of ontology engineering falls on the line of production of software development with requirements, design and Implementation.

V. CONCLUSION

Ontology is about specification of a concept and provides a common vocabulary to communicate concerning a subject area. The paper describes Dooyeweerd theory of aspects and its relativity to aspect oriented programming. The paper also provides guidance to a theoretical basis upon which an ontology that gives a better and simple understanding of the aspect oriented programs can be constructed. Also the ontology can be used to give a strong philosophical basis for aspect oriented metrics as it is the case with object oriented metrics contributed by Chidamber and Kemerer.

REFERENCES

[1] S. Black, and M. Harman, “Aspect Oriented Software Development: Towards A Philosophical Basis,” Technical Report TR-06-01, Department of Computer Science, King’s College London, 2006

[2] K. van den Berg, J. M. Conejero, and R. Chitchyan, “AOSD Ontology 1.0 - Public Ontology of Aspect-Orientation,” AOSD Europe, 2005.

[3] Filman, R., et al., Aspect-Oriented Software Development. 2004: Addison-Wesley.

[4] Shanks, G., Tansley, E. & Weber, R. (2003). Using Ontology to Validate Conceptual Models. Communication of the ACM, October 2003, Vol 46, No 10, p. 85 - 98.

[5] CWM (2003). Common Warehouse Metamodel (CWM) Specification, March 2003,Version 1.1, Volume 1, formal/03-03-02

[6] Skulmoski, G. (2002). Shifting Gears: the De Facto Global Standard for Project Management.

[7] Kiczales, Gregor, et al. "An overview of AspectJ." ECOOP 2001—Object-Oriented Programming. Springer Berlin Heidelberg, 2001. 327-354.

[8] Basden, A. "The Dooyeweerd pages." (2000).

[9] Tarr, Peri, et al. "N degrees of separation: multi-dimensional separation of concerns." Proceedings of the 21st international conference on Software engineering. ACM, 1999

[10] Kiczales, Gregor, et al. Aspect-oriented programming. 11th European Conference on Object Oriented Programming in:LNCS,vol.1241,Springer Verlag,1997,pp 220-242 1997

[11] S.R.Chidamber and C.F. Kemerer. A metrics suite for object oriented design. IEEE transactions on Software Engineering,20(6):476-493,June 1994

[12] ISO/IEC9126 (1991). International Standard ISO/IEC 9126. Information technology Software product evaluation,Quality characteristics and guidelines for their use,International Organization for Standardization, International ElectrotechnicalCommission, Geneva

[13] Wand, Yair, and Ron Weber. "An ontological model of an information system."Software Engineering, IEEE Transactions on 16.11 (1990): 1282-1292.

[14] ANSI/IEEE 830 (1984). Guide to Software Requirements Specification

[15] Bunge, Mario. Treatise on basic philosophy: Ontology I: the furniture of the world. Vol. 1. Springer, 1977.

AN INTELLIGENT VEHICLE LOCATION SENSING SYSTEM USING KALMAN FILTER APPROACH

Mandeep Singh Walia

Assistant Professor, Department of Electronics and Communication Engineering,UIET, Panjab University SSG Regional Centre (India)

ABSTRACT

An intelligent vehicle may be defined as a vehicle that senses the environmental conditions which in turn produces some automatic action. The ability to accurately detect a vehicle's location and its status is the main goal of automobile trajectory monitoring systems. These systems are implemented using several hybrid techniques that include: wireless communication, geographical positioning and embedded applications. A Kalman filter is an optimal estimator - i.e. infers parameters of interest from indirect, inaccurate and uncertain observations. It is recursive so that new measurements can be processed as they arrive.

Keywords*: *Adaptive Cruise Control, Global Positioning System, Kalman Filter, Position Estimator, State Space Method.

I. INTRODUCTION

The intelligent systems concept seems to be very popular among transport management systems. Continuously increasing amount of vehicles in road, air and marine transport areas has put research in this area. Efficient, economical and more intelligent methods have to be deal with these challenging problems. The available intelligent system is vehicle platoons. In this framework research has been carried out in control and sensory requirements for platoons of vehicles. In this platform, vehicles are having shorter spacing between them. However, spacing with constant value is stable only if certain types of vehicle to vehicle communications are possible (Swaroop et al., 1994). This requires radio communication devices. Vehicle recognition plays an important role in field of traffic monitoring. It includes location identification, behavior identification of vehicles. Conventional loop detectors and video based systems are inefficient. The adaptive cruise control uses radar and stereovision sensing methods to detect the distance in defined environment (Kato et al., 2002). The smooth response filters out traffic disturbances and reduces air pollution and fuel consumption. This paper investigates the methods of location sensing systems. The paper is organized as follows. Section II gives an overview of location identification. Section III and IV describes the proposed Kalman filter approach and design of Kalman filter for location sensing respectively. In section IV, experimental results are presented, and conclusions are given in section V.

II. LOCATION SENSING SYSTEMS

Positioning systems determine the location of a person or an object either relative to a known position or within a coordinate system (G. M. Djuknic and R. E. Richton, 2001). In the last few decades, various positioning systems have been motivated by demand and have been developed. The comparison of different position estimators are shown in Table 1.

TABLE 1: Comparison of Different Position Estimators

Estimator	Advantages	Disadvantages
ML	High Accuracy	Global solution is not guaranteed Noise statistics are needed
LLS	Global solution is guaranteed Noise statistics are not needed	Low Accuracy
NLS	High Accuracy Noise statistics are not needed	Global solution is not guaranteed
WLLS	Global solution is guaranteed High Accuracy can be achieved	Noise statistics are needed

Some of the applications of positioning systems include (but are not limited to) law enforcement, security, road safety, tracking personnel, vehicles, and other assets, situation awareness, and mobile ad hoc networks. As shown in Fig. 1 positioning systems can be classified into two categories as global positioning and local positioning. Global positioning systems (GPS) allow each mobile to find its own position on the globe. A local positioning system (LPS) is a relative positioning system and can be classified into self - and remote positioning. Self - positioning systems allow each person or object to find its own position with respect to a static point at any given time and location. An example of these systems is the inertial navigation system (INS). Remote positioning systems allow each node to find the relative position of other nodes located in its coverage area. Here, nodes can be static or dynamic. Remote positioning systems themselves are divided into active target remote positioning and passive target remote positioning.

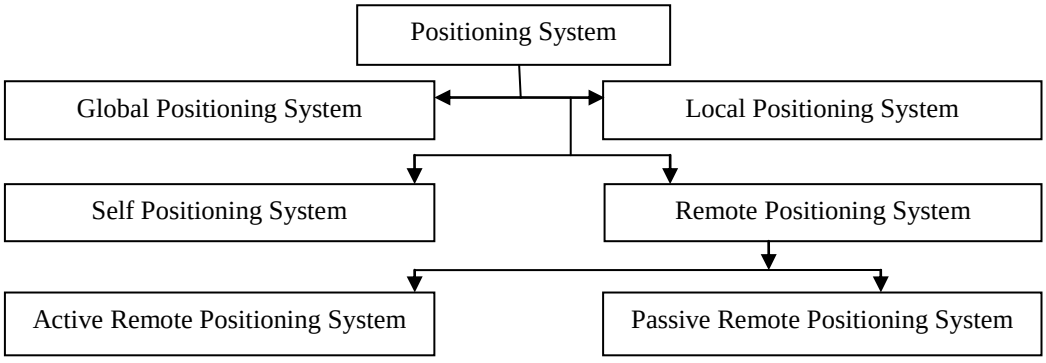

Fig.1: Positioning Sensing Systems

Location based technologies have been used for a number of years. However, advances in wireless technologies in location based technologies. It is possible to open a range of applications. The global positioning system finds the position of objects which are stationary or moving. Tracking systems have central processor that monitors the location of objects (B.T. Fang, 1986). The performance of location sensing system is dominated by its accuracy as a measure of systems expected error in terms of distance, Precision as a measure of expectation of location within the accuracy and Latency as a measure of how long it takes for a system to produce an estimate for a single location An analytical solution is the straightforward method to determine the position. It involves using a series of functions. The new expression used to calculate estimates the position. Measurement error is

results from noise effects of the system due to analytical solutions. Suppose there is a mathematical model and to understand its behavior and to find a solution to the set of equations. The best is the use calculus, trigonometry, and other math techniques to write down the solution. Now the model will behave under any circumstances can be found. This is called the analytic solution, because analysis is used to figure it out. It is also referred to as a closed form solution. Numerical solutions are iterative algorithms provided solutions where analytical solutions not exist. For more complex models, the math becomes much too complicated. Then numerical methods are used of solving the equations, such as the Runge-Kutta method. For a differential equation that describes behaviour over time, the numerical method starts with the initial values of the variables, and then uses the equations to figure out the changes in these variables over a very brief time period. It's only an approximation, but it can be a very good approximation under certain circumstances. It start with some initial information about variable x of $f(x) - g(x) = 0$. The problem of solving x is called as root finding as the solutions for roots, or zeros. It includes the bisection method and Newton Raphson Method. But, these solutions are not applicable for measurement error. Error minimization algorithm works by minimizing the difference between real world observations and predicted values of model equations which are called as errors or residuals. Errors are due to interference and instrumental noises. It finds the solution with lowest minimization error and it gives the optimal solution for the given data. Thus error minimization is also called as optimization algorithms. Simulated annealing and Particle Swarm Optimization called as stochastic algorithms can be used where the derivative of the error function is difficult for error minimization. This technique is used in real time position sensing. But, error minimization techniques are resource hungry for location sensing systems (S. Kirkpatrick, C. D. Gelatt, M. P. Vecchi, 1983). State space methods can be used to estimate the state of deterministic systems including physical processes like swing of pendulum or level of liquid. In location sensing, the position and movement of moving vehicle or object are considered (R. E. Kalman, 1960). States are a set of parameters that describe the instantaneous condition of a process at a set point of time. These methods predict the current state using model and the previous states and then corrects the predicted current measurements. These are also called as recursive time domain filters as they use temporal models. The feedback is based upon Markov assumptions. It is possible to provide estimates in real time environment as state space methods do not required storing long histories of states.

III. KALMAN FILTER APPROACH FOR VEHICLE LOCATION SENSING

A Kalman filter is an optimal estimator which infers parameters of interest from indirect, inaccurate and uncertain observations. It is recursive so that new measurements can be processed as they arrive as batch processing where all data must be present. Kalman filter is one of the most popular state space algorithms (C.K. Chui and G. Chen, 1987). It is an efficient algorithm used in real time navigation and positioning systems. Since the time of its introduction, the Kalman filter has been the subject of extensive research and application, particularly in the area of target tracking. This is likely due in large part to advances in digital computing that made the use of the filter practical, but also to the relative simplicity and robust nature of the filter itself. As a fruitful application for state estimation, the problem of tracking a moving object from radar measurements has received a great deal of attention in the literature. However a number of problems are still open, and reducing computational requirements, while achieving some desired tracking performance is another important issue in many practical applications. The kalman filter is an implementation of Bayes' rule that is a way of updating the stochastic

properties of the system for given input. Usually a Cartesian coordinate system is well suited to describe the target dynamics since the dynamic equations are often linear and uncoupled. Within the significant toolbox of mathematical tools that can be used for linear state estimation from noisy sensor observations, one of the most often-used tools in the target tracking field is what is known as the Kalman Filter (Hushino et al., 1996). But, because measurements of the target location are expressed as nonlinear equations in coordinates, the tracking problem is connected with nonlinear estimation. The natural way to generalize the methods applied to linear estimation was to extend the Kalman Filter to nonlinear recursive equations: this classical extended algorithm is called the Extended Kalman Filter. These two algorithms are the foundation of most moving vehicle tracking algorithms, but they have a lot of important flaws that need to be addressed.

The Kalman filter is essentially a set of mathematical equations that implement a predictor-corrector type estimator that is optimal in the sense that it minimizes the estimated error covariance-when some presumed conditions are met. Rarely do the conditions necessary for optimality actually exist, and yet the filter apparently works well for many applications in spite of this situation. The Kalman Filter has made a dramatic impact on linear estimation because of its adaptivity for implementation on a digital computer for on-line estimation and usefulness of the state-space approach. Today, the Kalman Filter is an established technique widely applied in the fields of navigation (Feng, Huifang, et al., 2014), guidance (Gao, Lian Zhou, 2014), aircraft (V. Gavrilets, A. Shterenberg, M.A. Dahleh, E. Feron, 2000), and missile tracking (D. Williams, B. Friedland, J. Richmans, 1983), reentry of space vehicles, etc.

The Kalman Filter is the foundation of our moving vehicle tracking method, because of it's adaptively for implementation on a digital computer for on-line estimation and usefulness of the state-space approach. The state-space equations are decomposed into two parts: the state equation and the measurement equation. The state equations describe the target dynamics and are chosen in order to be linear.

IV. DESIGN OF KALMAN FILTER

Designing a kalman filter to solve the problem of location sensing are known as the state transition and the measurement equations. The state transition equation known as the difference equation, describes the evolution of the process over time. It predicts the state changes between measurements. This equation models the dynamics of the object being positioned and will be different for different systems. The state transition equation is in the form:

$$\hat{X}_k = A_K X_{K-1} + w \tag{1}$$

where A_K is state transition matrix to calculate prediction for the current state vector $\hat{X}_k$ and X_{K-1} is the previous state vector. A_K is an NXN matrix. w_{k-1} is the normally distributed noise. The measurement equation allows the filter to predict measurements. The general form of measurement equation for position sensing is as:

$$\hat{Z}_k = H_k \hat{X}_k + v_{k-1} \tag{2}$$

where $\hat{Z}_k$ is the state prediction by the measurement sensitivity matrix H_k. H_k is an MXN matrix with M as measurements in number. v_{k-1} is the normally distributed measurement noise. The difference of $Z_k - \hat{Z}_k$ is the measurement residual. Firstly, integrate the measurements. Then, the Kalman filter predicts the confidence in the given state. It is measure of how accurately the filter estimates the state vector as:

$$\hat{P}_k = A_k P_{k-1} A_k^T + Q_k \tag{3}$$

where P_k is known as the apriori estimate of the covariance. Q_k is the covariance matrix for the noise w. It is added with the effect of decreasing the confidence in the state. The Kalman filter then calculates the Kalman gain matrix K which is a weighting factor to optimally integrate the measurements:

$$Y_k = \left(H_k \hat{P}_k H_k^T + R_k\right)^{-1} \quad (4)$$

where Y_k is the information matrix to incorporate the weight of the measurement noise by the addition of the measurement covarianceR_k. R_k is the covariance of the zero mean noise v.

$$K_k = \hat{P}_k H_k^T Y_k \quad (5)$$

where K_k represents the Kalman gain with multiplication of information matrix, measurement sensitivity matrix and a priori system covariance. The factor determines how the measurements will influence the state to detect or reject outlying measurements by:

$$\hat{z}_k = H_k \hat{x}_k \quad (6)$$

Finally, the Kalman filter integrates the measurement with the state:

$$x_k = \hat{x}_k + K_k(z_k - \hat{z}_k) \quad (7)$$

The filter uses the Kalman gain to update the current system covariance:

$$P_k = (I - K_k H_k)\hat{P}_k \quad (8)$$

where I is the identity matrix. The system covariance first expands with the passage of time and the contracts as the observation is integrated. For non-linear systems, more general representation is used. For example, the process equation relates the previous state to the current state:

$$\hat{x}_k = f \quad (9)$$

The measurement equation relating the state of measurements as:

$$\hat{z}_k = h(\hat{x}_k, v_{k-1}) \quad (10)$$

One such non linear Kalman filter is the extended Kalman filter (S.J. Julier, J.K. Unlmann, H.F. Durrant, 1995). It used first order Taylor series approximation to the process and measurement equations. Another, nonlinear Kalman filter is unscented Kalman filter (J.J. Laviala, 2003). It performs the sampled representations of mean and covariance through f ( ) and h ( ). It is easy to implement and more accurately models non-linear transformations.

V. EXPERIMENTAL RESULTS

The vehicle is initially located at the point x = 0 and moves along the X axis with velocity varying around a constant speed 10m/sec. The motion of the vehicle can be described by a set of differential equations:-

$$\dot{x}_1 = x_2,\ x_1(0) = 0 \quad (11)$$

$$\dot{x}_2 = w, x_2(0) = 10, w \sim N(0, (0.3^2)) \quad (12)$$

where $x_1$is the position and x_2 is the velocity, w the process noise due to road conditions, wind etc. Problem:

Using the position measurement to estimate actual velocity. The position of the vehicle is measured at every dt = 0.1 seconds. But, because of imperfect aperture, weather etc., the measurements are noisy, so the instantaneous velocity, derived from 2 consecutive position measurements (remember, we measure only position) is inaccurate. The Kalman filter is an accurate and smooth estimate for the velocity in order to predict train's

position in the future. The state space equation after discretisation with sampling time dt and the measurement model as:-

$$x_{k=1} = \phi_{x_k} + w_k, \qquad \phi = e^{A\Delta t},$$

$$A = [0\ 1\ ;0\ 0], w_k \ \ N(0,Q) \qquad ,Q = [0\ 0; 0\ 1] \tag{13}$$

$$y_{k=1} = [1\ 0]x_{k+1} + v_k, v_k \ \sim N(0,1) \tag{14}$$

Fig. 2 shows the position and velocity estimation results with Kalman estimated displacement and Kalman estimated velocity respectively. The key idea is to consider the accelerations not as inputs to the system, but as states, in the model. Besides, in that model, the accelerations are modeled as a weighted sum of the previous accelerations. A linear fitting is recursively performed using an LMS algorithm. The computed model (state transition matrix, state error covariance matrix) is then used in a classic Kalman filter that has the vehicle position and several accelerations as its outputs.

VI. CONCLUSION AND FUTURE SCOPE

In order for the Kalman Filters to be applicable, the assumption that the random variables have Gaussian probability distributions is used. We then consider that, after they propagate through the nonlinear functions, they are still Gaussian. Even if the approximation is accurate to at least the second order with the Unscented Transformation, the assumption is still wrong. To avoid those assumptions in the target tracking problem, the particle filter can be used. The Particle Filter is a sequential Monte Carlo based method that allows for a complete representation of the state distribution, using sequential importance sampling and resampling. It makes no assumption on the form of the probability densities in question, i.e. full nonlinear, non-Gaussian estimation. Nevertheless, the implementation of the Particle Filter is not yet very efficient. Research needs to be done in order for this algorithm to be implemented in hardware, and eventually be used in target tracking purposes.

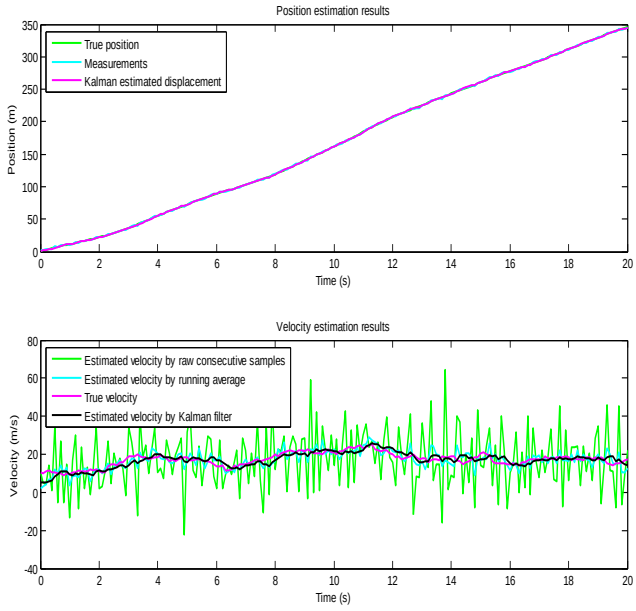

Fig. 2: Position and Velocity Estimation with Kalman Estimated Displacement and Velocity

REFERENCES

[1] Swaroop, D., Hedrick, K., Chien, C., and Loannou, P., Comparison of spacing and headway control laws for automatically controlled vehicles, Vehicle Syst. Dyn., 23, 1994, 597-625.

[2] Kato, T., Ninomiya, Y., and Masaki, I., An obstacle detection method by fusion of radar and motion stereo, IEEE Transaction on Intelligent Transaction Systems, 3, 2002, 182-188.

[3] Djuknic, G.M., and Richton, R.E., Geolocation and assisted GPS, IEEE Comput, 34 (2), 2001, 123 – 125.

[4] Fang, B.T., Trilateration and extension to global positioning system navigation, Journal of Guidance, Control, and Dynamics, 9, 1986, 715-717.

[5] Kirkpatrick, S., Gelatt, C.D., and Vecchi, M.P., Optimization by simulated annealing, Science, 220, 1983, 671-680.

[6] Kalman, R.E., A new approach to linear filtering and prediction problems, Journal of basic Engineering (ASME), 82, 1960, 35-45.

[7] Chui, C.K., and Chen, G., Kalman filtering with real-time applications, Springer- Verlag, Inc., NY, USA, 1987.

[8] Hushino, M., Gunji, Y., Oho, S., and Takano, K., A Kalman filter to estimate direction for automotive navigation, Proc. International Conference on Multisensor Fusion and Integration for Intelligent Systems, 1996, 145-150.

[9] Feng, Huifang, et al., Location prediction of vehicles in VANETs using a Kalman filter, Wireless Personal Communications, 2014, 1-17.

[10] Gao, Lian Zhou., Study on WSN localization algorithm and simulation model based on Kalman filtering algorithm, Advanced Materials Research, 945, 2014.

[11] Gavrilets, V., Shterenberg, A., Dahleh, M.A., and Feron, E., Avionics system for a small unmanned helicopter performing aggressive maneuvers, Proc. 19th Digital Avionics Systems Conferences,1, 2000, 1E2/1-1E2/7.

[12] Williams, D., Friedland, B., and Richman, J., Design of an integrated navigation, Guidance, and Control System for a Tactile Missile, Proc. Guidance and Control Conference, 1983, 57-66.

[13] Julier, S.J., Unlmann, J.K., and Durrant, H.F., A new approach for filtering nonlinear systems, Proc. American Control Conference, 1995, 1628-1632.

[14] Laviala, J.J., A comparison of unscented and extended Kalman filtering of estimating quaternion motion, Proc. American Control Conference, 2003, 2435-2440.

DESIGN AND ANALYSIS OF REDUCED SIZE H-CUT SHAPE MICROSTRIP PATCH ANTENNA

Akshay Patidar, Ms. Shivangi Saxena
[1]*Student*, [2]*Asst. Professor*
Elex. & Comm. Engg. , TCET, Indore (India)

ABSTRACT
Size reduction of microstrip antenna is very important design consideration. In this paper, I can design H-Cut shape microstrip patch antenna and hence the size of the antenna is reduced compared to an ordinary microstrip antenna with the same resonating frequency here, I can use 2.4GHz frequency for design of antennas. The antenna is simulated using High Frequency Structure Simulator (HFSS). The parameters like VSWR, Return loss, radiation pattern of ordinary microstrip antenna and H-Cut Microstrip Patch antenna are compared.

Keywords: Microstrip Patch Antenna, H-Cut Shape Patch Antenna, Hfss, Vswr, Return Loss, Radiation Pattern.

I INTRODUCTION
Microstrip antenna has many advantages like low cost, less size, light weight, dual and triple frequency operation. Because of less size of microstrip antenna it is used in many wireless applications like satellite communication system, Personal communication system and other wireless applications. In this paper, the main task is to implement more reduced sized microstrip patch antenna without degrading its radiation characteristics, VSWR, Return losses. During period of work first the ordinary microstrip antenna is designed for 2.4GHz then this antenna is simulated by using HFSS software. Then in next step the ordinary patch antenna is modified without changing its length and width and then again this antenna is simulated. Here, I can saw that the resonant frequency of modified antenna is reduced to 1.7GHz. But here I want to design the antenna for wireless band so in next step the Length and width of patch is reduced in such a way that antenna is operated in 2.4GHz band of frequency.

II DESIGNS AND ANALYSIS

The dimensions of the patch along its length have now been extended on each end by a distance ΔL, which is given empirically as: The effective length of the patch Leff now becomes:

$$L_{eff} = L + 2\Delta L$$

For a given resonance frequency f_0, the effective length is given by as:

$$L_{eff} = \frac{c}{2 f_o \sqrt{\varepsilon_{reff}}}$$

For a rectangular Microstrip patch antenna, the resonance frequency for any TMmn mode is given by as:

$$f_o = \frac{c}{2\sqrt{\varepsilon_{reff}}}\left[\left(\frac{m}{L}\right)^2 + \left(\frac{n}{W}\right)^2\right]^{\frac{1}{2}}$$

Where m and n are modes along L and W respectively. For efficient radiation, the width W is given as;

$$W = \frac{c}{2 f_o \sqrt{\frac{(\varepsilon_r + 1)}{2}}}$$

2.1 Ordinary Antenna

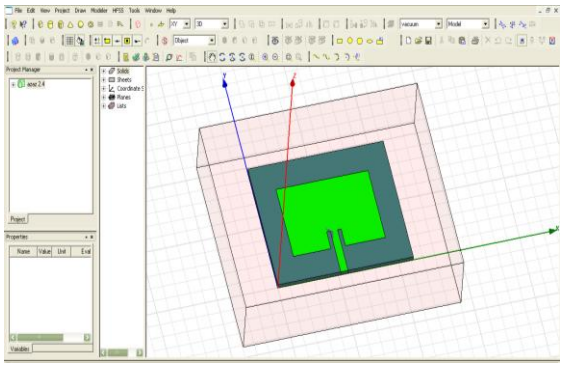

Figure 1.1 Simulation of Microstrip patch antenna at 2.4GHz frequency

Table 1: Antenna Dimension at 2.4GHz

PARAMETER	LENGTH	WIDTH	HEIGHT
SUBSTRATE	40MM	46MM	1.6MM
PATCH	28.9MM	38MM	0.05MM
FEED-LINE	10MM	5MM	0.05MM

The return loss for micro strip patch antenna is found to be -10dB as shown in Figure 1.2

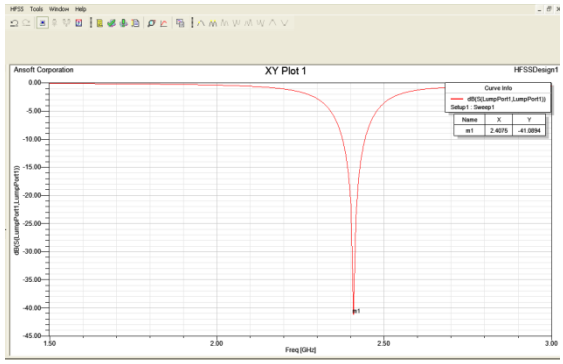

Figure. 1.2 Return Loss

Figure 1.3 Shows the 2 D Radiation Pattern of the Antenna.

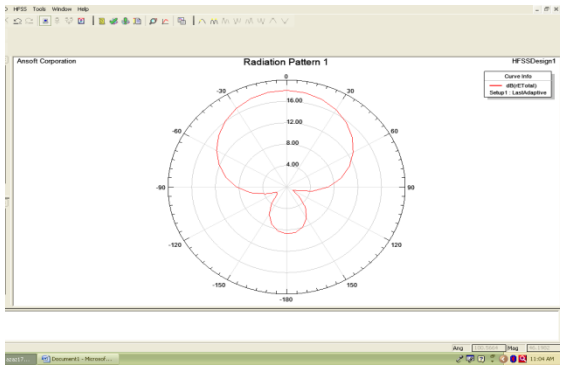

Figure 1.3 2D Radiation Patterns

Here ordinary antenna is design in HFSS software for AWS band fig. shows the radiation pattern, Return loss and VSWR of antenna and table shows the dimensions of the width length of patch here FR4 material is use as a dielectric because it has less cost. The height of FR4 is 1.5mm.Here substrate width=46mm and substrate length=40mm.

2.2 Ordinary Antenna is modified without Changing its Dimension (Cut)

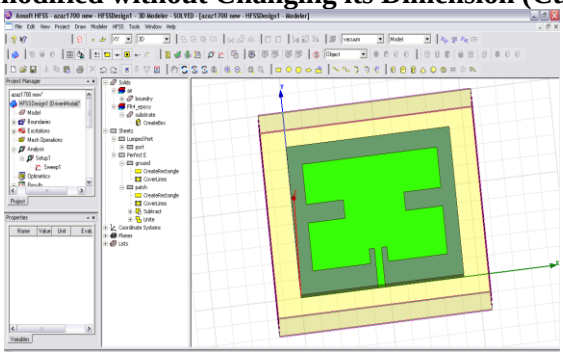

Figure 2.1 Simulation of Microstrip patch antenna at 1.7GHz frequency

Table 2: Modified Antenna Dimensions

ANTENNA WIDTH	38mm
ANTENNA LENGTH	28.9mm
SUBSTRATE HEIGHT	1.6mm

Here I can convert the ordinary antenna in to H Cut shape antenna without changing the dimensions of the antenna but because of this the resonant frequency of antenna is shifted to the 1.7 GHz approximately the figure shows the VSWR and return loss of the antenna.

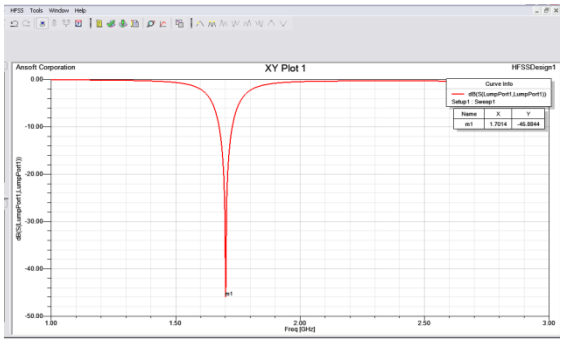

Figure 2.2 Return Loss

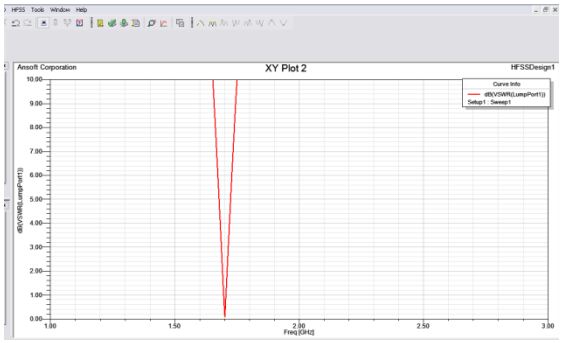

Figure 2.3 VSWR

2.3 Reduced size H-Cut Antenna

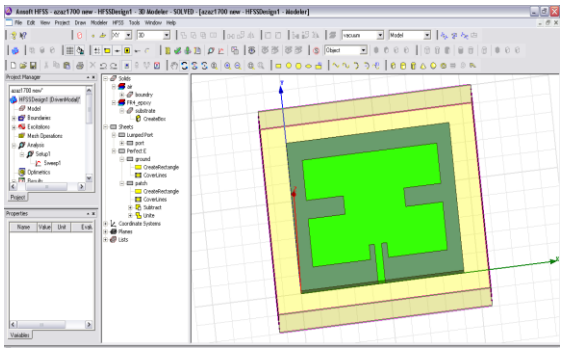

Figure 3.1 Simulation of Microstrip Patch Antenna With Reuced Size

Table 3: Modified Antenna Dimensions

ANTENNA WIDTH	27.25mm
ANTENNA LENGTH	23.9mm
SUBSTRATE HEIGHT	1.6mm

Here the width and length of patch is reduced this change in length is shown in table. And this antenna has resonating frequency 2.4GHz this is shown in VSWR and Return loss graph. Here substrate width is reduced to the 43mm and substrate length is reduced to the 38mm so total size and material cost of the antenna is reduced here.

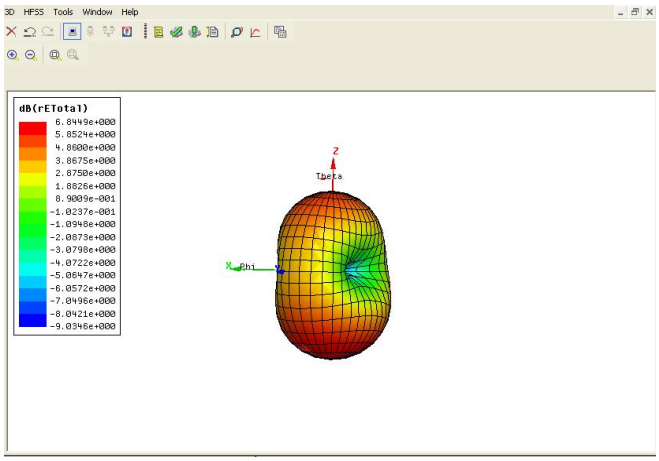

Figure 3.2 Radiation Pattern

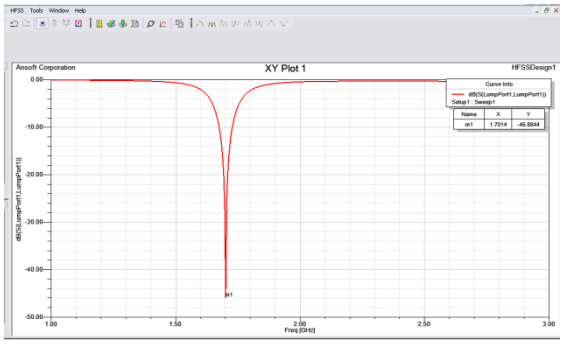

Figure 3.3 Return Loss

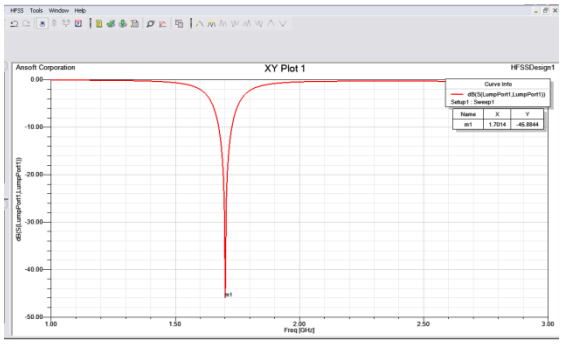

Figure 3.4 VSWR

III. CONCLUSION

This paper represents optimum design of rectangular microstrip patch antenna and here we say that if the rectangular microstrip patch antenna is converted into H- Cut shape antenna then size and cost of the antenna is reduced. The formulae for designing antenna are mentioned in paper. The results are simulated in HFSS.

REFERENCES

[1] Balanis,"Antenna theory analysis and design".

[2] Sihati, R. A,"CAD of Microstrip antenna for wireless applications", Artech House, Norwood, MA, 1996.

[3] Waterhouse, R, “Printed antenna for wires communications”, John wily and sons Inc, 2007.

[4] Shakaelfors,A.,Lee,K.M.,“Design of small size wide band width Microstrip patch antenna” Antenna and propagation magazine, IEEE, Vol. 45, Issue1, pp. 75-83 Feb-2003

[5] RaviKant, D.C.Dhubkarya, “Design and analysis of H-shape Microstrip patch antenna Publication”, In the Global Journal of Research in Engineering, Vol. 10, Issue 6 (Ver. 1.0), pp.26-29, Nov. 2010.

[6] R. Waterhouse, “Small Microstrip patch Antenna”, Electron. Lett. Vol. 31, No. 8, pp. 604-605, 1995.

A COMPARATIVE STUDY OF ECONOMIC LOAD DISPATCH BY USING GA AND PSO

Pooja Singh

Head, Department of Electrical Engineering, J.I.T. Nashik (India)

ABSTRACT

The economic load dispatch plays an important role in the operation of power system. The main objective of this paper is to determine the optimal combination of power outputs of all generating units so as to meet the required demand at minimum cost while satisfying all types of constraints. In this paper the lambda iteration method and the two main types evolutionary optimization technique genetic algorithm and particle swarm optimization which are generic population based probabilistic search optimization algorithms and can be applied to real world problem are respectively applied to solve an ELD problem and at last the comparison between all three method has been presented. The PSO provides the generation level such that the generation level is coming out to be lower than the cost resulted with genetic algorithm method.

Keywords: - Economic Load Dispatch, Genetic Algorithm, Particle Swarm Optimization Algorithm, Swarm Intelligence.

I. INTRODUCTION

The Economic load dispatch problem is one of the fundamental issues in power system operation. The economic load dispatch can be defined as the process of allocating generation levels to the generating units, so that the system load is supplied entirely and most economically. For an interconnected system it is necessary to minimize the expenses. Conventionally the cost function for each unit in ELD problem has been approximately represented by a quadratic function and is solved using mathematical programming techniques. Generally for obtaining the global optimum solution these mathematical methods are required some marginal cost information. Unfortunately, the real world input output characteristics of generating units are highly non-linear and non-smooth because of the different types of constraints like valve point effect, prohibited operating zones and multi fuel effects etc. Thus practical ELD problem is considered as a non-smooth optimization problem with equality and inequality constraints, which directly cannot be solved by the mathematical methods. Because these methods are highly sensitive to starting points and often converge to local optima. The ELD problem involves the solution of two different problems. The first of these is the unit commitment or pre dispatch problem wherein if is required to select optimally out of the available generating sources to operate meet the expected load and provide a specified margin of operating reserve over a specified period of time. The second aspect of Economic Dispatch is the online economic dispatch wherein it is required to distribute the load among the generating unit actually paralleled with the system in such manner as to minimize the total cost of supplying to minute requirements of the system. The main objective is to reduce the cost of energy production taking into

account the transmission losses. While the problem can be solved easily if the incremental cost curves of the generators are assumed to be monotonically increasing piece-wise linear functions, such an approach will not be workable for non-linear functions in practical systems. In past decade, conventional optimization techniques such as lambda iteration method, linear & quadratic programming, have been successfully used to solve power system optimization problem such as unit-commitment and economic load dispatch. for highly non-linear and combinatorial optimization problems, the conventional methods are facing difficulties to locate the global optimal solution. Recently there is an upsurge in the use of modern evolutionary computing techniques in the field of power system optimization. PSO first introduced by Kennedy and Eberhart, is one of the modern heuristic algorithm. It was developed through simulation of a simplified social system and has been found to be robust in solving continuous non linear optimization problems. The PSO technique can generate high quality solutions with in shorter calculation time and stable convergence characteristics.

II. ECONOMIC LOAD DISPATCH

The objective function & subjected constraints can be defined as:

2.1 The Problem Formulation: Objective Function-

The objective of economic load dispatch for power system consisting of thermal generating units is to find the optimal combination of power generations that minimises the total generation cost while satisfying the specified equality & inequality constraints. The fuel cost function of generator is represented as a quadratic function of generator active powers.

Objective function=

$$min \sum_{i=1}^{n} Fi(pgi)$$

$$F(P_{gi}) = a_i P_{gi}^{\ 2} + b_i P_{gi} + c_i$$

Where the $F_i(Pg_i)$ is the operation fuel cost of generator i and a_i, b_i, c_i are the cost coefficients for i^{th} unit.

2.2 Constraints

The problem is subjected to power balance constraints and generating capacity constraints as follows

2.2.1 Power Balance Constraints-Equality Constraints

$$\sum_{i=1}^{NG} P_{gi} = P_D + \mathrm{P_L}$$

2.2.2 Inequality Constraints

$$P_{gi}^{\ \min} \le P_{gi} \le P_{gi}^{\ \max}$$

Where P_D is the load demand. P_{gi} is output power of i[th] generator , P_L is the transmission loss. P_{gi}^{min} And P_{gi}^{max} are the maximum & minimum output powers of the i[th] generator respectively.

III. APPLIED METHODS

3.1 Lambda Iteration Method

In this method λ is a variable, introduced in solving constraint optimization problem and is already known as Lagrange Multiplier. It is significant to that Lambda can be solved at hand by solving systems of equations. Since all the inequality constraints to be satisfied in each trial the equations are solved by the iterative method.

- Assume a suitable value of $\lambda^{(0)}$.
- The value of lambda should be more than the largest intercept of the incremental cost characteristic of the various generators.
- Compute the individual generations.
- Check the equality constraint, $h = \sum_{i=1}^{ng} P_{gi} - P_d - P_L$ is satisfied.
- If not satisfied, make the second guess λ repeat above steps.

3.2 Genetic Algorithm

A global optimization technique known as Genetic algorithm has emerged as a candidate due to its flexibility and efficiency for many optimization applications. It is a stochastic searching algorithm. The method was developed by John Holland in 1975. GA is inspired by the evolutionary theory which is explaining by the origin of species. Normally in our nature weak and unfit species within their environment are faced with extinction with natural selections. The strong one has greater opportunity to pass their genes to the future generation via reproduction process. In the long run the species those are carrying the correct combination in their genes become dominant in their population. Some times during the slow process of evolution, random changes may occur in genes. If these additional advantages in the challenge for survival, new species evolve from the old ones, unsuccessful changes are eliminated by natural selection. The GA is a search heuristic technique that mimics the process of natural evolution. The heuristics technique is routinely used to generate useful solutions to optimization and search problems. GA belong to the larger class of evolutionary algorithm, which generate solutions to the optimization problems using natural evolution such as mutation, selection, crossover and inheritance. GA offer a new and powerful approach to the optimization problems make possible by the increasing availability of high performance of computers at relatively low cost. These algorithms have recently found extensive applications in solving global optimization searching problems when the closed form optimization techniques cannot be applied. GA are parallel and global search toward the global solution because, it simultaneously, evaluates many points in the parameter space. It does not need to assume that the search pace is differentiable or continuous.

3.2.1 Algorithm of Economic Load Dispatch using GA-

1. Read data, such as cost coefficients a_i, b_i, c_i number of iterations, length of strings population size, probability of mutation and crossover, power demand P^{min} and P^{max}.
2. Create the initial population randomly in the binary form.
3. Now decode the string, or obtain the decimal integer from the binary string.
4. Calculate the power which generated from the decoded population by using equation.

$$P_i^j = P_i^{min} + \frac{(P_i^{max} - P_i^{min}) y_i^j}{2^l - 1}$$

i = 1,2...NG

j = 1,2.....NG

L = Number of string or population size.

5. Check P_i^j ,

   If $Pi^j > P^{max,}$ then set $Pi^j = Pi^{max}$

   If $Pi^j < P^{max}$ then set $Pi^j = Pi^{min}$

6. Find the fitness or cost function from second equation.
7. Find the population with maximum fitness and average fitness of the population.
8. Perform the reproduction process, which includes these steps

- Set selection rate and number of mating in a pool.
- Define total fitness as the sum of values obtained by using above steps for all chromosomes which are selected.
- Select percentage of each chromosome which is equal to the ratio of its fitness value to the total fitness value i.e. find probability, which can be written as

  Probability=fitness/∑Fitness's.

- Calculate cumulative sum (CS) to normalize the values between 0.0 to 1.0.

9. Perform crossover operation:

- Choose a pair of random numbers between 0 and 1to select one mother and one father chromosome, so as to produce new offspring.
- Pairing the chromosome from different location, for different location the crossover point has to be selected which can be selected randomly. Generate offspring by applying crossover.

10. Perform mutation by randomly selecting the mutation point from the total no. Of bits in the population matrix.
11. Update the population.

12. If the no. Of iteration reaches the maximum then go to step (13) otherwise will go to step (6).
13. The fitness that generates the minimum total generation cost is the solution of the problem.

3.3 Particle Swarm Optimization

Kennedy and Eberhart developed a particle swarm optimization behavior (PSO) algorithm based on the behavior of individual (i.e. particles or agents) of the swarm. Its roots are in zoologist modeling of the movement of individuals (i.e. fishes, birds, and insects) with in a group. It has been noticed that members of the group seem to share information among them, a fact that leads to increase the efficiency of the group. PSO as an optimization tool provides a population based search procedure in which individuals called particles change their position (states) with time. In a PSO system particles flying around the multi dimensional space. In particle swarm optimization, each individual makes its decision based on its own experience together with other individual's experience. Particle swarm optimization (PSO) is a population based stochastic optimization technique which is inspired by a social psychological metaphor instead of the survival of fittest individual. During the flight period each particle adjusts its position according to its own experience and the experience of neighboring particles and making use of best position taken by it and neighbors. The swarm direction of a particle can be defined by the set of particles neighboring the particles and its history experience. In PSO we are not using evolutionary operation to manipulate the individuals, in the PSO each individual flies in the search space with a velocity which is dynamically adjusted according to its own flying experience and its companions flying experience also.

3.3.1 Algorithm Of Economic Load Dispatch By Using PSO

The algorithm for economic load dispatch by using particle swarm optimization is given as follows.

1. Initialize the individuals of the population according to the limit of each unit including the individual dimension, searching point, and velocities. This initial solution must be feasible candidate solution that satisfies the practical operation constraints.
2. To Each chromosome of the population the dependent unit output P_D will be calculated from the power balance equation and B_{mn} coefficient matrix.
3. Calculate the evaluation value of each individual P_{gi}, in the population using the evaluation function f given by

$$Minimize FC(i) = \sum_{i=1}^{ng} f_i(P_i)$$

4. Compare each individual's evaluation value with its P_{best}. The best evaluation value among P_{best} is denoted as G_{best}.
5. Modify the member velocity v of each individual P_g.

$$v_{id}(t+1) = wv_i(t) + C1Rand()(Pbest(Pg_{id}(t)) = C2Rand()$$
$$(gbest_{id} - Pg_{id}(t))$$

Where i=1,2….n and d=1,2….m

6. Check the velocity component constraint occurring in the limits from the following conditions.

$$\text{If } v_{ij}^{(r+1)} > v_j^{\max} \text{ then } v_{ij}^{(r+1)} = v_j^{\max}$$

$$\text{If } v_{ij}^{(r+1)} < v_j^{\min} \text{ then } v_{ij}^{(r+1)} = v_j^{\max}$$

Where, $v_j^{max} = -0.5P_j^{min}$

Where, $V_j^{max} = +0.5P_j^{max}$

7. Modify the member position of each individual P_g .

$$P_{gid}(t+1) = P_{gid}(t) + v_{id}(t+1)$$

$P_{gid}(t+1)$ Must be modified toward the near margin of the feasible solution.

8. If the evaluation value of each individual is better than previous P_{best} , the current value is set to be P_{best} . If the best P_{best} is better than the G_{best} , the value is set to be G_{best} .

9. If the number of iterations reaches the maximum, then go to step 2.

10. The individual that generates the latest G_{best} is the optimal generation power of each unit with the minimum total generator cost.

VI. COMPLETE WORK AND CALCULATIONS.

In this paper the result of economic load dispatch after the implementation of proposed method lambda-iteration method, genetic algorithm (GA) and particle swarm optimization (PSO) are discussed. The programs are implemented in MATLAB 7.6.0. The performance is evaluated with considering the total transmission losses using two generating test system i.e. three generator system, and six generator system whose input and output data are given below.

Case Study1: Solving Three Generator System By Using Lambda Iteration Method

The coefficients of fuel cost and maximum and minimum power limits are given below. the power demand is considered to be 850(MW). The results corresponding to Lambda iteration GA and PSO are detailed in section. The cost characteristic of the three units are given as

$$F_1 = .006P_1^2 + 8.4P_1 + 400 \text{ Rs/hr}$$

$$F_2 = .0042P_2^2 + 8.93P_2 + 600 \text{ Rs/hr}$$

$$F_3 = .0045P_3^2 + 6.78P_3 + 650 \text{ Rs/hr}$$

The unit operating constraints are

$$100MW \leq P1 \leq 600MW$$

$$60MW \leq P2 \leq 300MW$$

$$300MW \leq P3 \leq 650MW$$

For the above system considering the load of 550mw, 850mw, 900mw conventional lambda iteration method is applied to obtain the economic load dispatch. The table 1 shows that the economic load dispatch of above mentioned loads neglecting the transmission line losses.

Table-1: Lambda Iteration Method for Three Generating Unit System.

S. no.	Demand (mw)	P_1 (mw)	P_2 (mw)	P_3 (mw)	Lambda	Cost (Rs/hr)
1.	550	115.12	101.371	333.562	9.7815	6379.82
2.	850	194.87	215.291	439.831	10.77	9120.5
3.	900	208.16	234.282	457.552	10.89	9801.00

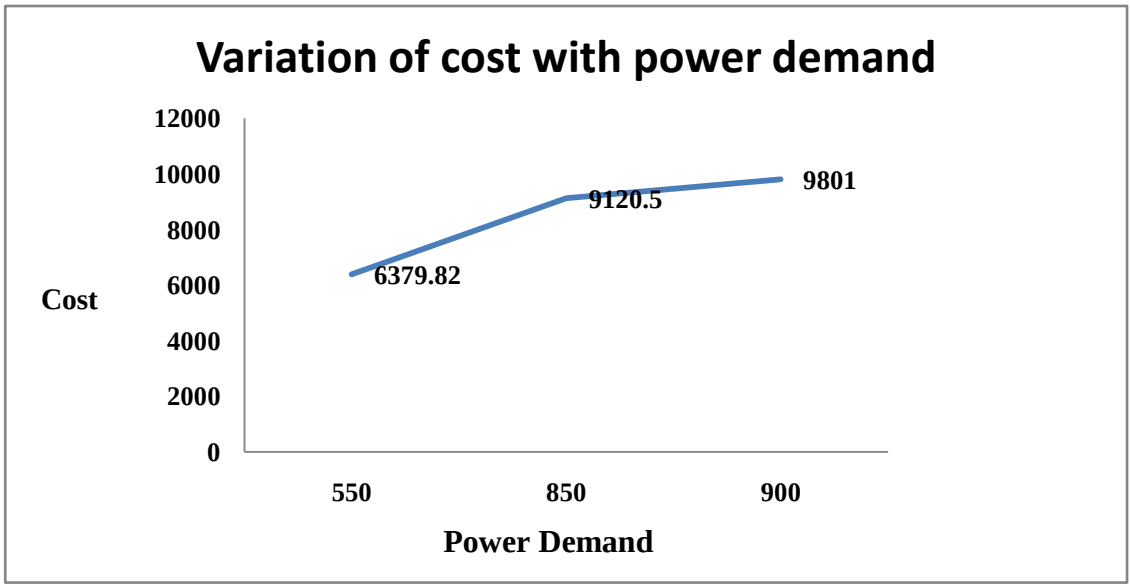

Fig .1: Variation of Cost with Power Demand for Three Unit System

Case Study2- Solving Three Generator Systems By Using Genetic Algorithm Method

The coefficients of fuel cost and minimum and maximum limits are given in table 2.

Table:2- Specification For GA Of Three Generating System

Unit no.	a_i	b_i	c_i	P_{min}	P_{max}
1.	.0001562	7.92	561	150	600
2.	.000194	7.85	310	100	400
3.	.00482	7.97	78	50	200

Optimal solution using genetic algorithm for case study (2) –

Table: 3- Optimal Result of GA

S.no.	Demand (MW)	P_1 (MW)	P_2 (MW)	P_3 (MW)	Total cost (Rs/hr)
1.	550	190.57	60.62	300.77	6299.00
2.	820	211.30	88.82	519.88	9000.60
3.	850	395.5	325.7	128.8	8719.55
4.	1500	560	290	650	17178.00

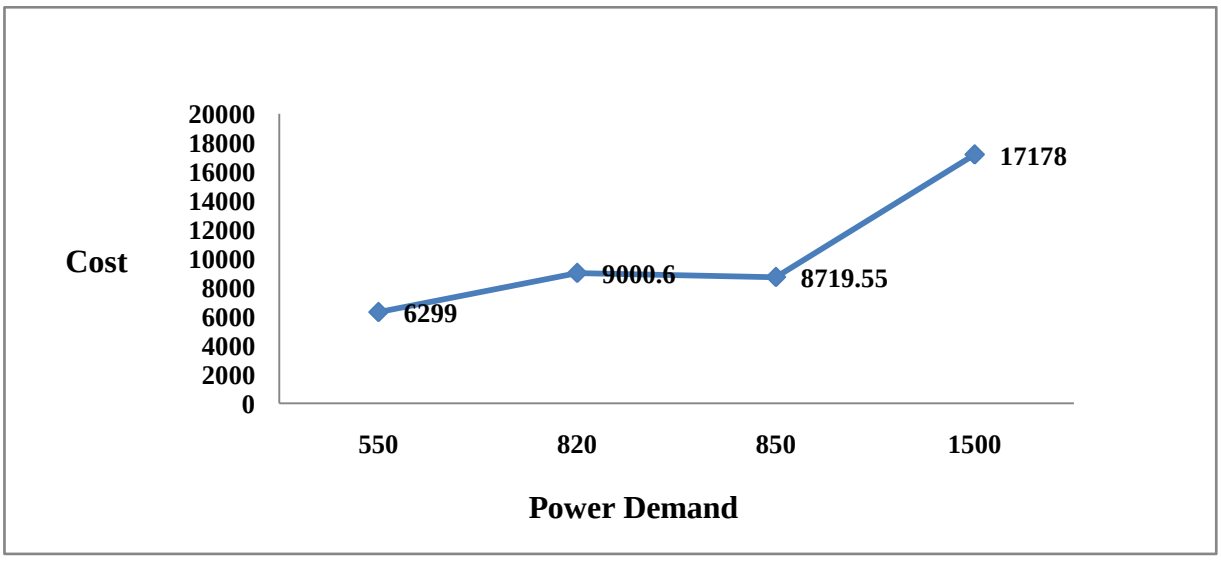

Fig.2: Cost Variation of Three Unit System By GA.

Case Study (3): Solving Three Generator Systems By Using PSO Method

Table:4- Specification For PSO Of Three Generating System

Unit no.	a_i	b_i	c_i	P_{min}	P_{max}
1.	.0001562	7.92	561	150	600
2.	.000194	7.85	310	100	400
3.	.00482	7.97	78	50	200

Optimal solution using PSO for case study (3)-

Table: 5- Results Of PSO For Three Generating Unit System.

P_1 (MW)	390.732
P_1 (MW)	388.976
P_1 (MW)	178.405
Total power(MW)	850
Total cost(Rs/hr)	8716.77

Comparison of Lambda-iteration, GA, and PSO-

Table No: 6- Comparison Of All Three Proposed Method

Demand (MW)	Cost by Lambda iteration method (Rs/hr)	Cost by GA (Rs/hr)	Cost by PSO (Rs/hr)
850	9120.5	8719.55	8716.77

Case study (4) - Solving six generator system by genetic algorithm method-

Table: 7- Specifications Of ELD Problem For GA.

S.no.	a_i	b_i	c_i	P_{min}	P_{max}
1.	.0070	7.0	240	100	500
2.	.0095	10.0	200	50	200
3.	.0090	8.5	220	80	300
4.	.0090	11.0	200	50	150
5.	.0080	10.5	220	50	220
6.	.0075	12	190	50	120

The loss coefficient matrix is given as,

B=1e-4*[0.13 0.12 0.12 0.19 0.22 0.17

0.16 0.7 0.12 0.15 0.14 0.4

0.16 0.12 0.66 0.18 0.25 0.18

0.18 0.15 0.16 0.70 0.2 0.23

0.25 0.16 0.25 0.2 0.67 0.30

0.23 0.1 0.18 0.24 0.34 0.82];

Optimal Solution By Using Genetic Algorithm For Case Study (4)-

Table: 8- The Result Of GA For Case Study-4.

S.no	Demand (MW)	P_1 (MW)	P_2 (MW)	P_3 (MW)	P_4 (MW)	P_5 (MW)	P_6 (MW)	P_L (MW)	Cost (Rs/hr)
1.	500	242.85	54.66	94.59	54.49	58.82	51.35	6.78	6153.03
2.	700	328.13	67.33	156.33	50.53	52.36	56.06	10.75	8357.44
3.	820	359.50	105.43	188.76	50.16	80.13	51.15	15.15	9807.092
4.	900	382.74	112.77	201.03	65.95	106.13	50.25	18.62	10813.59
5.	1100	429.50	191.22	266.89	144.94	167.90	90.44	41.22	13454.052

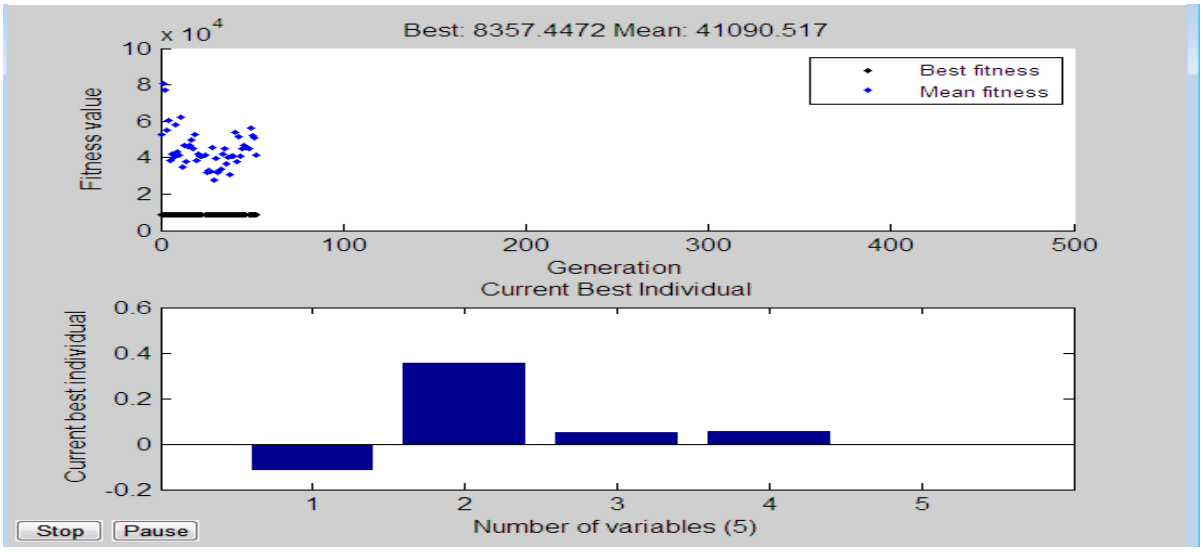

Fig.3: Convergence Characteristic Of PSO For Six Unit System (700mw Demand).

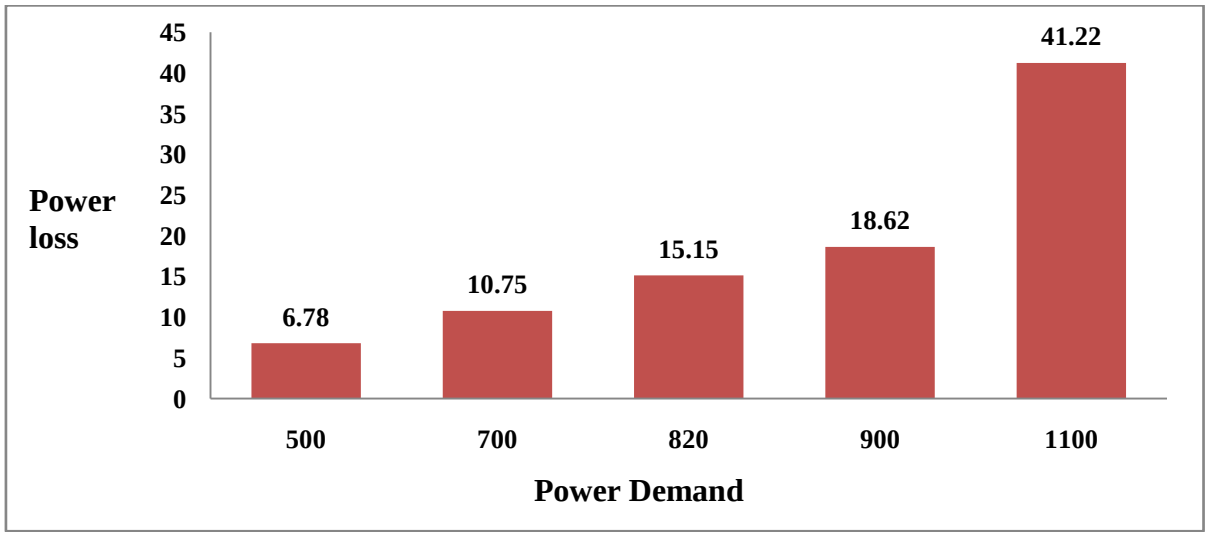

Fig .4: Variation Of Power Loss With The Load Demand For Six Unit System In GA.

Solving Six Generator System By Particle Swarm Optimization Method

The coefficient of fuel cost and minimum / maximum power limits are given in table 7, a number of power demands are considered here.

Optimal Solution By Using Particle Swarm Optimization For Case Study (4)

The initial particles are randomly generated within the feasible range. The parameters c1 and c2 and inertia weight are selected for best convergence characteristic. Here c1=1.99 and c2=1.99 are used, and the maximum value of w is chosen to be 0.9 and minimum value is 0.4. The velocity limits are selected as $V_{max}=0.5*P_{max}$ and minimum value is selected as $V_{min} = -0.5*P_{max}$. There are 10 number of particle are selected in the population. For different values of c1 and c2 the cost curves convergences in different region. So the best value is taken for the minimum cost of the problem. If we increase the number of particles then cost curve converges faster. From this solution analysis, it can be observed the loss has no effect on the cost characteristic, it has been observed even if number of units is increased the convergence is less affected.

Table: 9- Output Result Of PSO For Case Study-4

S.No	Demand (MW)	P_1 (MW)	P_2 (MW)	P_3 (MW)	P_4 (MW)	P_5 (MW)	P_6 (MW)	P_L(Losses) (MW)	Cost (Rs/hr)
1.	500	221.16	50	84.4	50	50	50	5.5842	6132.2
2.	700	322.81	77.01	158.56	50	52.34	50	10.74	8352.61
3.	820	361.42	103.35	185.74	52.31	82.29	50	15.13	9805.86
4.	900	383.04	118.76	201.21	67.42	98.04	50	18.50	10812.2
5.	1100	436.52	115.43	239.16	103.72	137.63	56.09	28.58	13452.42
6.	1300	482.67	187.68	271.81	135.90	171.39	91.76	41.26	16256.68

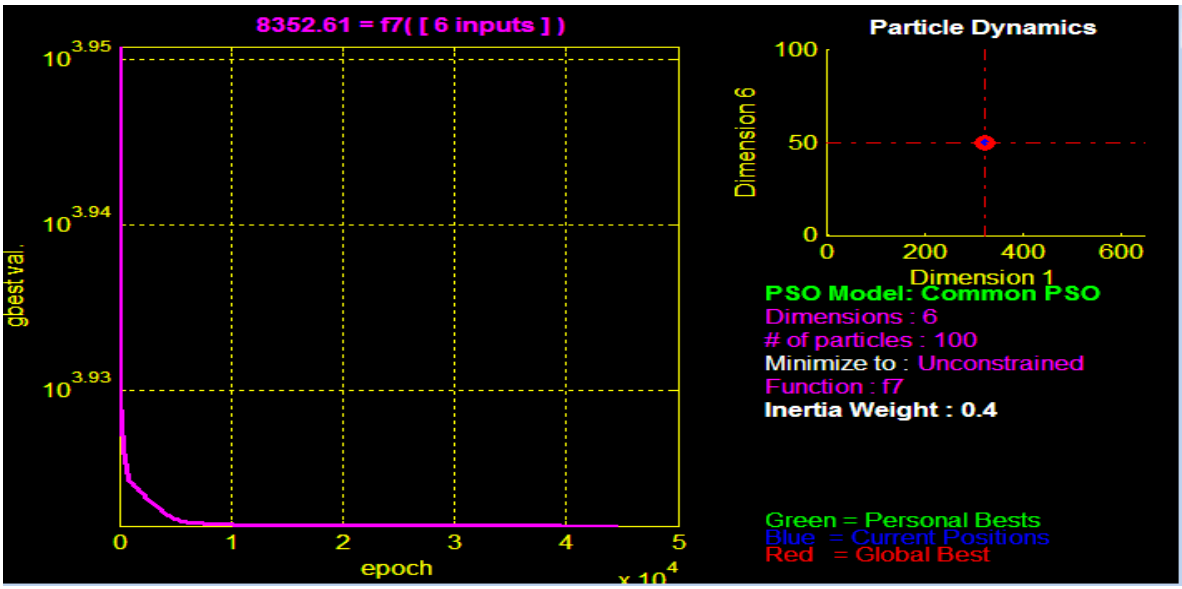

Fig.5: Convergence Characteristic Of PSO For Six Unit System (700mw Demand).

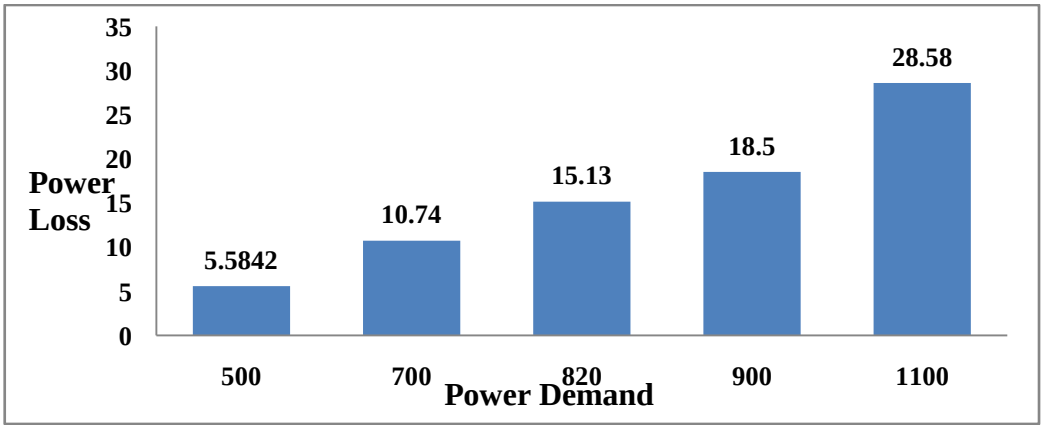

Fig .6: Variation Of Power Loss With The Load Demand For Six Unit System In GA.

Comparison Between GA And PSO-

Table No:10- Comparison Of Cost Between GA And PSO.

Demand (MW)	Cost by GA (Rs/hr)	Cost by PSO (Rs/hr)
500	6153.03	6132.2
700	8362.66	8352.61
820	9807.092	9805.86
900	10813.59	10812.2
1100	13454.052	13452.42

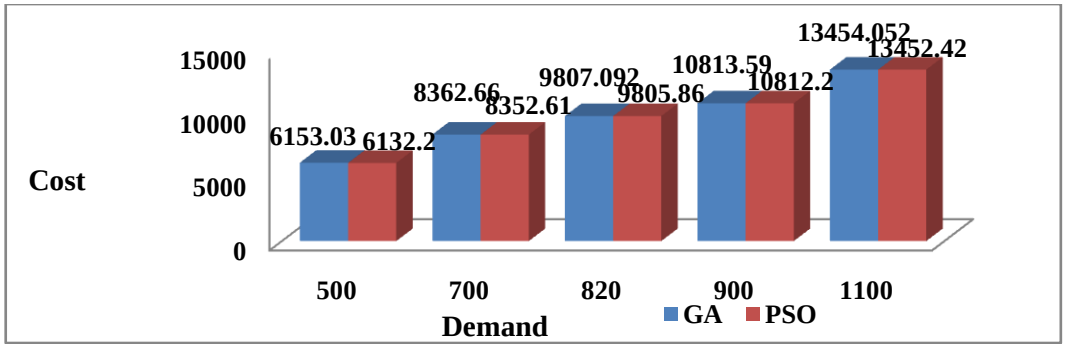

Fig: 7 Variation Of Cost In Six Generating Unit System By GA And PSO.

Comparison Of Losses From GA And PSO-

Table No: 11 Comparisons Of Losses Between GA And PSO.

Demand (MW)	Losses from GA (MW)	Losses from PSO (MW)
500	6.78	5.5842
700	10.75	10.74
820	15.15	15.13
900	18.62	18.50
1100	41.22	28.58

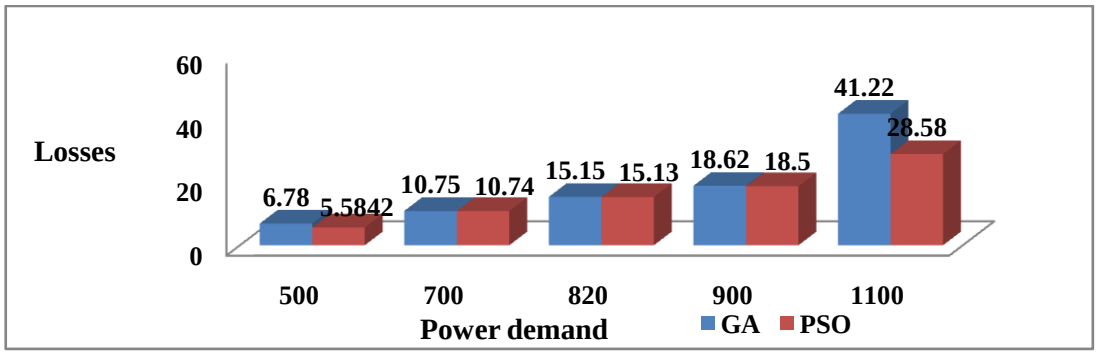

Fig: 8 Variations Of Losses In Six Generating Unit System By GA And PSO.

V. CONCLUSION

In this work the formulation and implementation of solution methods such as Lambda iteration method, Genetic Algorithm and Particle Swarm Optimization, to obtain the optimum solution of economic load dispatch. PSO can be used to solve many of the same kinds of problems as GA. This optimization technique does not suffer, from some of GA's difficulties: interaction in the group enhances rather than takes away from progress toward the solution. Further a particle swarm system has memory, which the genetic algorithm does not have. The change in genetic populations results in destruction of previous knowledge of the problem, except when elitism is employed, in which case usually one or a small number of individuals retain their "identities". The effectiveness of the developed program is tested for three generators and six generator test system. The

results obtained from these methods are also compared with each other. It is found that PSO is giving better results than GA and Lambda iteration method.

REFERENCES

[1] A.Y. Saber, T. Senjyu, T. Miyagi, N. Urasaki And T. Funabashi, Fuzzy Unit Commitment Scheduling Using Absolutely Stochastic Simulated Annealing, Ieee Trans. Power Syst, 21 (May2006), Pp. 955–964)

[2] A.J. Wood And B.F. Wollenberg, Power Generation, Operation, And Control, John Wiley And Sons., New York (1984).

[3] Ieee Committee Report, Present Practices In The Economic Operation Of Power Systems, Ieee Trans. Power Appa. Syst., Pas-90 (1971) 1768–1775.

[4] N. Sinha, R. Chakrabarti And P.K. Chattopadhyay, Evolutionary Programming Techniques For Economic Load Dispatch, Ieee Evol. Comput., 7 (February (1)) (2003), Pp. 83–94.

[5] H.T. Yang, P.C. Yang And C.L. Huang, Evolutionary Programming Based Economic Dispatch For Units With Nonsmooth Fuel Cost Functions, Ieee Trans. Power Syst., 11 (February 1996), Pp. 112–118.

[6] P. Attaviriyanupap, H. Kita, E. Tanaka And J. Hasegawa, A Hybrid Ep And Sqp For Dynamic Economic Dispatch With Nonsmooth Fuel Cost Function, Ieee Trans. Power Syst., 17 (May (2)) (2002), Pp. 411–416

[7] Zwe-Lee. Gaing, Particle Swarm Optimization To Solving The Economic Dispatch Considering The Generator Constraints, IEEE Trans. Power Syst. 18 (3) (2003), Pp. 1187–1195 Closure To Discussion Of 'Particle Swarm Optimization To Solving The Economic Dispatch Considering The Generator Constraints', IEEE Trans. Power Syst., 19 (November (4)) (2004) 2122–2123.

[8] D.N. Jeyakumar, T. Jayabarathi And T. Raghunathan, Particle Swarm Optimization For Various Types Of Economic Dispatch Problems, Elect. Power Energy Syst,. 28 (2006), Pp. 36–42.

[9] T.O. Ting, M.V.C. Rao And C.K. Loo, A Novel Approach For Unit Commitment Problem Via An Effective Hybrid Particle Swarm Optimization, IEEE Trans. Power Syst,. 21 (February (1)) (2006), Pp. 411–418.

[10] A.I. Selvakumar And K. Thanushkodi, A New Particle Swarm Optimization Solution To Nonconvex Economic Dispatch Problems, IEEE Trans. Power Syst,. 22 (February (1)) (2007), Pp. 42–51

[11] J.-B. Park, K.-S. Lee, J.-R. Shin And K.Y. Lee, A Particle Swarm Optimization For Economic Dispatch With Nonsmooth Cost Functions, IEEE Trans. Power Syst,. 20 (February (1)) (2005), Pp. 34–42.

[12] J. Kennedy And R.C. Eberhart, Particle Swarm Optimization, Proceedings Of The IEEE, International Conference On Neural Networks Perth, Australia (1995), Pp. 1942–1948.

[13] Y. Shi And R.C. Eberhart, Parameter Selection In Particle Swarm Optimization, Proceedings Of The Seventh Annual Conference On Evolutionary Programming, IEEE Press (1998).

[14] J. Kennedy And R.C. Eberhart, A Discrete Binary Version Of The Particle Swarm Algorithm, Proc. IEEE Conf. Syst. Man Cyberne, (1997), Pp. 4104–4109. .

[15] Y. Shi And R.C. Eberhart, Fuzzy Adaptive Particle Swarm Optimization, IEEE Int. Conf. Evol. Comput. (2001), Pp. 101–106.

APPLICATION OF FUZZY INFORMATION MEASURE TO CODING THEORY

H.D. Arora[1], Anjali Dhiman[2]

[1] *Department of Mathematics, Amity Institute Of Applied Sciences, Amity University, Noida, (India)*

[2]*Department of Mathematics, Ideal Institute Of Mgmt And Tech, G.G.S.I.P.University, Delhi, (India)*

ABSTRACT

The objective of the present communication is to develop new measure $\underline{L_{\alpha}^{\beta}}$ *, called average code word length of order* $\underline{\alpha}$ *and type* $\underline{\beta}$ *and establish its relationship with a result of generalized fuzzy information measures. Using* $\underline{L_{\alpha}^{\beta}}$*, Noiseless coding theorems connected with fuzzy information measure have been proved.*

Keywords: Fuzzy Information Measure, Codeword Length, Uniquely Decipherable Codes, Kraft's Inequality, Noiseless Channel.

I. INTRODUCTION

Information theory is a relatively new branch of Mathematics that was made mathematically rigorous only in the 1940s. Information theory deals with the study of problems concerning any system. This includes information processing, information storage, information retrieval and decision making. , information theory studies all theoretical problems connected with the transmission of information over communication channels. This includes the study of uncertainty (information) measures and various practical and economical methods of coding information for transmission. The first studies in this direction were undertaken by Nyquist [9] in 1924 and 1928 [10] and by Hartley in 1928 [27], who recognized the logarithmic nature of the measure of information. In 1948, Shannon [5] published a remarkable paper on the properties of information sources and of the communication channels used to transmit the outputs of these sources. Around the same time Wiener [22] also considered the communication situation and came up, independently, with results similar to those of Shannon. In the past fifty years the literature on information theory has grown quite voluminous and apart from communication theory it has found deep applications in many social, physical and biological sciences, for example, economics, statistics, accounting, language, psychology, ecology, pattern recognition, computer sciences, fuzzy sets, etc. A key feature of Shannon information theory is the term *"information"* that can often be given a mathematical meaning as a numerically measurable quantity, on the basis of a probabilistic model, in such a way that the solutions of many important problems of information storage and the transmission can be formulated in terms of this measure of the amount of information. As pointed out by Renyi [3] in his fundamental paper on generalized information measures, in other sort of problems other quantities may serve just as well, or even better, as measures of information. This should be supported either by their operational

significance or by a set of natural postulates characterizing them, or, preferably, by both. Thus the idea of generalized entropies arises in the literature. It started with Renyi [3] who characterized scalar parametric entropy as entropy of order r, which includes Shannon entropy as a limiting case. Fuzzy set theory has been studied extensively over the past 30 years. Most of the early interest in fuzzy set theory pertained to representing uncertainty in human cognitive processes. Fuzzy set theory is now applied to problems in engineering, business, medical and related health sciences, and the natural sciences. In 1978, Zadeh [16] first created the theory of fuzzy, which is related to fuzzy set theory. His study showed that the importance of the theory of fuzzy is based on the fact that much of the information on which human decisions is possibilistic rather than probabilistic in nature. Fuzzy set theory is being recognized as an important problem modeling and solution technique. The use of fuzzy set theory as a methodology for modeling and analyzing decision systems is of particular interest to researchers. In 1976, Zimmermann [11] first introduced fuzzy set theory into an ordinary linear programming problem with fuzzy objective and constraints. Zadeh [16] introduced the concept of fuzzy sets in which imprecise knowledge can be used to define an event.To explain the concept of fuzzy entropy in general, Kapur [12] considered the following vector:

$$(\mu_A(x_1), \mu_A(x_2), \ldots\ldots\ldots\ldots \mu_A(x_n))$$

Where $\mu_A(x_i)$ gives the perception of the grade of membership of the ith element of set A. Thus if $\mu_A(x_i)$ = 0 then the ith element certainty does not belong to set A and if $\mu_A(x_i)$ = 1, it definitely belongs to set A. If $\mu_A(x_i)$ =0.5, there is maximum certainty whether x_i belongs to set A or not. The above vector in which every element lies between 0 and 1 and has the interpretation given above, is called fuzzy vector and the set A is called a fuzzy set. If every element of the set is 0 or 1, there is no uncertainty about it and the set is said to be a crisp set.Thus there are 2^n crisp sets with n elements and infinity many sets with n elements.If Some elements are 0 or 1 and the others lie between 0 or 1 the set will still said to be a fuzzy set. With the ith element, we associate a fuzzy uncertainty f ($\mu_A(x_i)$), where f(x) has following properties:

I. f(x) = 0 when x = 0 or 1

II. f(x) increases as x goes from 0 to 0.5

III. f(x) decreases as x goes from 0.5 to1.0

IV. f(x)=f(1-x)

If the n elements are independent, the total fuzzy uncertainty is given by,

$$H(A) = \sum_{i=1}^{n} f(\mu_A(x_i))$$

The fuzzy uncertainty is called fuzzy entropy.

Klir and Folger [8] stated that the term fuzzy entropy was apparently due to clarity of product terms in the following two expressions:

$$H(A) = \sum_{i=1}^{n} \mu_A(x_i) \ln \mu_A(x_i) - \sum_{i=1}^{n} (1-\mu_A(x_i)) \ln(1-\mu_A(x_i))$$

After this development, a large number of measures of fuzzy entropy were discussed, characterized and generalized by various authors.

In coding theory, Error-correcting codes play an important role in many areas of science and engineering. Error-correcting codes constitute one of the key ingredients in achieving the high degree of reliability required in modern data transmission and storage systems. We come across the problem of efficient coding of messages to be sent over a noiseless channel and attempt to maximize the number of messages that can be sent through a channel in a given time. Therefore, we find the minimum value of a mean codeword length subject to a given constraint on code- word lengths. Let us assume that the messages to be transmitted are generated by a random variable X and each value x_i, i = 1, 2, ..., n of X must be represented by a finite sequence of symbols chosen from the set { a_1, a_2, ..., a_D }. This set is called code alphabet or set of code characters and sequence assigned to each i x , i = 1, 2,....., n is called code word. Let n_i be the length of code word associated with x_i satisfying Kraft's [13] inequality given by the following mathematical expression:

$$D^{-l_1} + D^{-l_2} + \cdots + D^{-l_n} \leq 1$$

Where, D is the size of alphabet. In calculating the long run efficiency of communications, we choose codes to minimize average code word length, given by

$$L = \sum_{i=!}^{n} n_i p_i$$

Where p_i is the probability of occurrence of x_i .For uniquely decipherable codes, Shannon's[4] noiseless coding theorem states that

$$\frac{H(P)}{\log D} \leq L < \frac{H(P)}{\log D} + 1$$

Determines the lower bounds on L in terms of Shannon's entropy H(P).

Campbell [17] for the first time introduced the idea of exponentiated mean codeword length for uniquely decipherable codes and proved a noiseless coding theorem.

He considered a special exponentiated mean of order α given by

$$L_\alpha = \frac{\alpha}{1-\alpha} log_D [\sum_{i=1}^{n} p_i D^{(1-\alpha)n_i/\alpha}]$$

And showed that its lower bound lies between $R_\alpha(P)$ and $R_\alpha(P) + 1$

Where $R_\alpha(P) = (1-\alpha)^{-1} log_D [\sum_{i=1}^{n} p_i^\alpha] ; \alpha > 0, \alpha \neq 1.$

The above is Renyi's [3] measure of entropy of order α.As $\alpha \to 1$, it is easily shown that $L_\alpha \to L$ and $R_\alpha(P)$ approaches H(P).

It may be seen that the mean codeword length had been generalized parametrically and their bounds had been studied in terms of generalized measures of entropies. Here we give another generalization and study its bounds in terms of generalized fuzzy information measures of order α and type β.

Generalized coding theorems by considering different information measure under the condition of unique decipherability were investigated by several authors.

Arun Choudhary and Satish Kumar[1] proved some noiseless coding theorem on generalized R- Norm entropy.

Also , Arun Choudhary and Satish Kumar [2] proposed some coding theorems on generalized havrda-charvat and tsalli's entropy.

M.A.K. Baig and Mohd Javid Dar [19] & [20] introduced some Coding theorems on Fuzzy entropy Function Depending Upon Parameter R and V . Further, Fuzzy coding theorem on generalized fuzzy cost measure.

Parkash and P. K. Sharma [23] & [24] proved some noiseless coding theorems corresponding to fuzzy entropies and introduced a new class of fuzzy coding theorems.

Guiasu and Picard [6] defined the weighted average length for a uniquely decipherable code as:

$$\bar{L} = \sum_{i=1}^{n} \frac{u_i n_i p_i}{\sum_{i=1}^{n} u_i p_i}$$

Longo [18] interpreted this as the average cost of transmitting letters x_i with probability p_i and utility u_i and gave some practical interpretation of this length. Lower and upper bounds for the cost function in terms of weighted entropy have also been derived.

Longo [18] gave lower bound for useful mean codeword length in terms of quantitative-qualitative measure of entropy introduced by Belis and Guiasu [4]. Guiasu and Picard [6] proved a noiseless coding theorem by obtaining lower bounds for similar useful mean codeword length. Gurdial and Pessoa [7] tried to extend the theorem by finding lower bounds for useful mean codeword lengths of order α in terms of useful measures of information of order α .

Some other pioneer who extended their results towards the development of coding theory are Korada and Urbanke [15], Szpankowski [28], Merhav [21] etc. Recently, Kapur [14] has established relationships between probabilistic entropy and coding. But there are many situations where probabilistic measures of entropy do not work and to tackle such situations, instead of taking the idea of probability, the idea of fuzziness can be explored.

In the next section, we have considered the fuzzy distributions and developed a new mean codeword lengths by proving noiseless coding theorems.

In this paper we study noiseless coding theorem by considering a fuzzy information measure depending on two parameters.

II. FUZZY NOISELESS CODING THEOREM

In this section, we consider the following generalized parametric measure of fuzzy entropy:

$$H_{\alpha}^{\beta}(A) = \frac{1}{(1-\alpha)\beta} \sum_{i=1}^{n} \left(\{ \mu_A^{\alpha\mu_A(x_i)}(x_i) + (1-\mu_A(x_i))^{\alpha(1-\mu_A(x_i))} \}^{\beta} - 2^{\beta} \right)$$

,where $\alpha > 0, \alpha \neq 1, \beta \neq 0.$ (2.1)

Under the assumption, $0^{0.\alpha} = 1$ we study the following properties:

1. $H_{\alpha}^{\beta}(A) \geq 0$
2. When $\mu_A(x_i) = 0$, $H_{\alpha}^{\beta}(A) = 0$
3. When $\mu_A(x_i) = \frac{1}{2}$,

$$H_\alpha^\beta(A) = \frac{n.2^\beta}{(1-\alpha).\beta}\left(\frac{1-2^{\frac{\alpha\beta}{2}}}{2^{\frac{\alpha\beta}{2}}}\right)$$

Hence, $H_\alpha^\beta(A)$ is an increasing function of $\mu_A(x_i)$ for $0 \leq \mu_A(x_i) \leq \frac{1}{2}$

4. When $\mu_A(x_i) = 1$, $H_\alpha^\beta(A) = 0.$ Hence $H_\alpha^\beta(A)$ is an decreasing function of $\mu_A(x_i)$ for $\frac{1}{2} \leq \mu_A(x_i) \leq 1$
5. $H_\alpha^\beta(A)$ does not change when $\mu_A(x_i)$ is changed to (1 - $\mu_A(x_i)$)

Under the above conditions, the generalized measure proposed in (2.1) is a valid measure of fuzzy entropy.

For this fuzzy measure of information of order α and type β we obtained the following mean codeword length L_α^β :

$$L_\alpha^\beta = \frac{1}{(1-\alpha)\beta}\sum_{i=1}^{n}\left[\frac{\beta^2}{1-\beta}\left\{1+\frac{(1-\beta)}{\beta}\left[\mu_A^{\alpha\mu_A(x_i)}(x_i)+(1-\mu_A(x_i))^{\alpha(1-\mu_A(x_i))}\right]D^{n_i\frac{\beta}{1-\beta}}\right\}-2^\beta\right]$$

,

where $\alpha > 0 >, \alpha \neq 1, \beta \neq 0$.

Now, corresponding to the proposed fuzzy information measure a noiseless coding theorem has been proved.

Theorem 2.1 : For all uniquely decipherable codes ,

$$H_\alpha^\beta(A) \leq L_\alpha^\beta \qquad (2.2)$$

Where,

$$L_\alpha^\beta = \frac{1}{(1-\alpha)\beta}\sum_{i=1}^{n}\left[\frac{\beta^2}{1-\beta}\left\{1+\frac{(1-\beta)}{\beta}\left[\mu_A^{\alpha\mu_A(x_i)}(x_i)+(1-\mu_A(x_i))^{\alpha(1-\mu_A(x_i))}\right]D^{n_i\frac{\beta}{1-\beta}}\right\}-2^\beta\right]$$

,

where $\alpha > 0 >, \alpha \neq 1, \beta \neq 0$. (2.3)

Proof : By Holder ‘s inequality, we have

$$x_i y_i \geq \frac{x_i^p}{p}+\frac{y_i^q}{q} \quad , 0 < p < 1, q < 0 \; or \; 0 < q < 1, p < 0. \qquad (2.4)$$

Set $x_i = [f(\mu_A(x_i),(\mu_B(x_i)]^{\frac{-1}{t}}D^{-n_i}$

$y_i = [f(\mu_A(x_i),(\mu_B(x_i)]^{\frac{1}{t}}$, $-1 < t < 0.$

Take $p = -t$, $q = \frac{t}{1+\frac{1}{t}}$.

Then equation (2.4) becomes

$$[f(\mu_A(x_i),(\mu_B(x_i)]^{\frac{-1}{t}}D^{-n_i}\;[f(\mu_A(x_i),(\mu_B(x_i)]^{\frac{1}{t}}$$

$$\geq \frac{\left\{[f(\mu_A(x_i),(\mu_B(x_i)]^{\frac{-1}{t}}\right\}^{-t}D^{n_i t}}{-t}+\frac{\left\{[f(\mu_A(x_i),(\mu_B(x_i)]^{\frac{1}{t}}\right\}^{\frac{t}{1+\frac{1}{t}}}}{\frac{t}{1+\frac{1}{t}}}$$

Or

$$D^{-n_i} \geq \frac{-[f(\mu_A(x_i),(\mu_B(x_i)]D^{n_i t}}{t} + \frac{\left(1+\frac{1}{t}\right)\{f(\mu_A(x_i),(\mu_B(x_i)\}^{\frac{1}{1+\frac{1}{t}}}}{t}$$

By Kraft's inequality,

$$\sum_{j=1}^{n} D^{-n_j} \leq 1$$

Or

$$\frac{\left(1+\frac{1}{t}\right)\{f(\mu_A(x_i),(\mu_B(x_i)\}^{\frac{1}{1+\frac{1}{t}}}}{t} \leq 1 + \frac{[f(\mu_A(x_i),(\mu_B(x_i)]D^{n_i t}}{t}$$

Take $t = \frac{\beta}{1-\beta}$,we have

$$\frac{(1-\beta)\{f(\mu_A(x_i),(\mu_B(x_i)\}^{\beta}}{\beta^2} \leq 1 + \frac{[f(\mu_A(x_i),(\mu_B(x_i)]D^{n_i\frac{\beta}{1-\beta}}}{\frac{\beta}{1-\beta}}$$

Or

$$[f(\mu_A(x_i),(\mu_B(x_i)]^{\beta} \leq \frac{\beta^2}{1-\beta}\{1\{+\frac{[f(\mu_A(x_i),(\mu_B(x_i)]D^{n_i\frac{\beta}{1-\beta}}}{\frac{\beta}{1-\beta}}\}$$

Subtracting 2^{β} from both sides, we get

$$[f(\mu_A(x_i),(\mu_B(x_i)]^{\beta} - 2^{\beta} \leq \left[\frac{\beta^2}{1-\beta}\left\{+\frac{[f(\mu_A(x_i),(\mu_B(x_i)]D^{n_i\frac{\beta}{1-\beta}}}{\frac{\beta}{1-\beta}}\right\} - 2^{\beta}\right]$$

Taking summation on both sides,

$$\sum_{i=1}^{n}\{[f(\mu_A(x_i),(\mu_B(x_i)]^{\beta} - 2^{\beta}\} \leq \sum_{i=1}^{n}\left[\frac{\beta^2}{1-\beta}\left\{+\frac{[f(\mu_A(x_i),(\mu_B(x_i)]D^{n_i\frac{\beta}{1-\beta}}}{\frac{\beta}{1-\beta}}\right\} - 2^{\beta}\right]$$

Let $f(\mu_A(x_i),(\mu_B(x_i) = \mu_A^{\alpha\mu_A(x_i)}(x_i) + (1-\mu_A(x_i))^{\alpha(1-\mu_A(x_i))}$ and multiplying both sides by $\frac{1}{(1-\alpha)\beta}$, we get,

$$\frac{1}{(1-\alpha)\beta}\sum_{i=1}^{n}\{[\mu_A^{\alpha\mu_A(x_i)}(x_i) + (1-\mu_A(x_i))^{\alpha(1-\mu_A(x_i))}]^{\beta} - 2^{\beta}\}$$

$$\leq \frac{1}{(1-\alpha)\beta}\sum_{i=1}^{n}\left[\frac{\beta^2}{1-\beta}\left\{+\frac{[\mu_A^{\alpha\mu_A(x_i)}(x_i) + (1-\mu_A(x_i))^{\alpha(1-\mu_A(x_i))}]D^{n_i\frac{\beta}{1-\beta}}}{\frac{\beta}{1-\beta}}\right\} - 2^{\beta}\right]$$

That is,

$H_{\alpha}^{\beta}(A) \leq L_{\alpha}^{\beta}$ which proves the result.

Theorem 2.2: For all uniquely decipherable codes, we have the following inequality:

$$H_\alpha^\beta(A,U) \leq L_\alpha^\beta(U) \qquad (2.5)$$

where

$$L_\alpha^\beta(U) = \frac{1}{(1-\alpha)\beta}\sum_{i=1}^{n}\left[\frac{\beta^2}{1-\beta}\left\{1+\frac{(1-\beta)}{\beta}\left[u_i\{\mu_A^{\alpha\mu_A(x_i)}(x_i)+\left(1-\mu_A(x_i)\right)^{\alpha(1-\mu_A(x_i))}\}\right]D^{n_i\frac{\beta}{1-\beta}}\right\}-2^\beta\right]$$

, is a new mean codeword length

where $\alpha > 0 >, \alpha \neq 1, \beta \neq 0$. (2.6)

Proof: Consider a quantitative –qualitative measure of information of order α and type:

$$H_\alpha^\beta(A,U) = \frac{1}{(1-\alpha)\beta}\sum_{i=1}^{n}\{u_i^\beta[\mu_A^{\alpha\mu_A(x_i)}(x_i)+\left(1-\mu_A(x_i)\right)^{\alpha(1-\mu_A(x_i))}]^\beta-2^\beta\}$$

For this quantitative–qualitative measure of information of order α and type β we obtain the following new mean codeword length of order α and type β:

$$L_\alpha^\beta(U) = \frac{1}{(1-\alpha)\beta}\sum_{i=1}^{n}\left[\frac{\beta^2}{1-\beta}\left\{1+\frac{(1-\beta)}{\beta}\left[u_i\{\mu_A^{\alpha\mu_A(x_i)}(x_i)+\left(1-\mu_A(x_i)\right)^{\alpha(1-\mu_A(x_i))}\}\right]D^{n_i\frac{\beta}{1-\beta}}\right\}-2^\beta\right]$$

Now, By Holder's inequality, we have

$$x_i y_i \geq \frac{x_i^p}{p}+\frac{y_i^q}{q} \quad , 0<p<1, q<0 \text{ or } 0<q< \quad 1, p<0. \qquad (2.7)$$

Set $x_i = [f(\mu_A(x_i),(\mu_B(x_i)]^{\frac{-1}{t}}D^{-n_i}$

$y_i = [f(\mu_A(x_i),(\mu_B(x_i)]^{\frac{1}{t}} \quad , -1<t<0.$

Take $p = -t, \; q = \frac{t}{1+\frac{1}{t}}$.

Then equation (2.6) becomes

$$[f(\mu_A(x_i),(\mu_B(x_i)]^{\frac{-1}{t}}D^{-n_i}\;[f(\mu_A(x_i),(\mu_B(x_i)]^{\frac{1}{t}}$$

$$\geq \frac{\left\{[f(\mu_A(x_i),(\mu_B(x_i)]^{\frac{-1}{t}}\right\}^{-t}D^{n_i t}}{-t}+\frac{\left\{[f(\mu_A(x_i),(\mu_B(x_i)]^{\frac{1}{t}}\right\}^{\frac{t}{1+\frac{1}{t}}}}{\frac{t}{1+\frac{1}{t}}}$$

Or

$$D^{-n_i} \geq \frac{-[f(\mu_A(x_i),(\mu_B(x_i)]D^{n_i t}}{t}+\frac{\left(1+\frac{1}{t}\right)[f(\mu_A(x_i),(\mu_B(x_i)]^{\frac{1}{1+\frac{1}{t}}}}{t}$$

By Kraft's inequality,

$$\sum_{j=1}^{n}D^{-n_j} \leq 1$$

Or

$$\frac{\left(1+\frac{1}{t}\right)\{f(\mu_A(x_i),(\mu_B(x_i)\}^{\frac{1}{1+\frac{1}{t}}}}{t} \leq 1+\frac{[f(\mu_A(x_i),(\mu_B(x_i)]D^{n_i t}}{t}$$

Take $t = \frac{\beta}{1-\beta}$,we have

$$\frac{(1-\beta)\{f(\mu_A(x_i),(\mu_B(x_i)\}^{\beta}}{\beta^2} \leq 1 + \frac{[f(\mu_A(x_i),(\mu_B(x_i)]D^{n_i\frac{\beta}{1-\beta}}}{\frac{\beta}{1-\beta}}$$

Or

$$[f(\mu_A(x_i),(\mu_B(x_i)]^{\beta} \leq \frac{\beta^2}{1-\beta}\{1 + \frac{[f(\mu_A(x_i),(\mu_B(x_i)]D^{n_i\frac{\beta}{1-\beta}}}{\frac{\beta}{1-\beta}}]$$

Subtracting 2^{β} from both sides, we get

$$[f(\mu_A(x_i),(\mu_B(x_i)]^{\beta} - 2^{\beta} \leq \left[\frac{\beta^2}{1-\beta}\left\{1 + \frac{[f(\mu_A(x_i),(\mu_B(x_i)]D^{n_i\frac{\beta}{1-\beta}}}{\frac{\beta}{1-\beta}}\right\} - 2^{\beta}\right]$$

Taking summation on both sides,

$$\sum_{i=1}^{n}\{[f(\mu_A(x_i),(\mu_B(x_i)]^{\beta} - 2^{\beta}\} \leq \sum_{i=1}^{n}\left[\frac{\beta^2}{1-\beta}\left\{1 + \frac{[f(\mu_A(x_i),(\mu_B(x_i)]D^{n_i\frac{\beta}{1-\beta}}}{\frac{\beta}{1-\beta}}\right\} - 2^{\beta}\right]$$

Let $f(\mu_A(x_i),(\mu_B(x_i) = u_i\{\mu_A^{\alpha\mu_A(x_i)}(x_i) + (1-\mu_A(x_i))^{\alpha(1-\mu_A(x_i))}\}$ and multiplying both Sides by $\frac{1}{(1-\alpha)\beta}$, we get,

$$\frac{1}{(1-\alpha)\beta}\sum_{i=1}^{n}\{u_i^{\beta}[\mu_A^{\alpha\mu_A(x_i)}(x_i) + (1-\mu_A(x_i))^{\alpha(1-\mu_A(x_i))}]^{\beta} - 2^{\beta}\}$$
$$\leq \frac{1}{(1-\alpha)\beta}\sum_{i=1}^{n}\left[\frac{\beta^2}{1-\beta}\left\{1 + \frac{u_i[\mu_A^{\alpha\mu_A(x_i)}(x_i) + (1-\mu_A(x_i))^{\alpha(1-\mu_A(x_i))}]D^{n_i\frac{\beta}{1-\beta}}}{\frac{\beta}{1-\beta}}\right\} - 2^{\beta}\right]$$

That is,

$H_{\alpha}^{\beta}(A,U) \leq L_{\alpha}^{\beta}(U)$ which proves the result.

III.MONOTONICITY OF THE MEAN CODEWORD LENGTH

Next, with the help of the data, we have presented the mean codeword length L_{α}^{β} graphically. For this purpose, we have computed different values of L_{α}^{β} for different values of the parameter α and β, corresponding to different fuzzy values $\mu_A(x_i)$. Next, we have presented L_{α}^{β} graphically and obtained the fig-3.1 which clearly shows that the codeword length L_{α}^{β} is monotonically decreasing function.

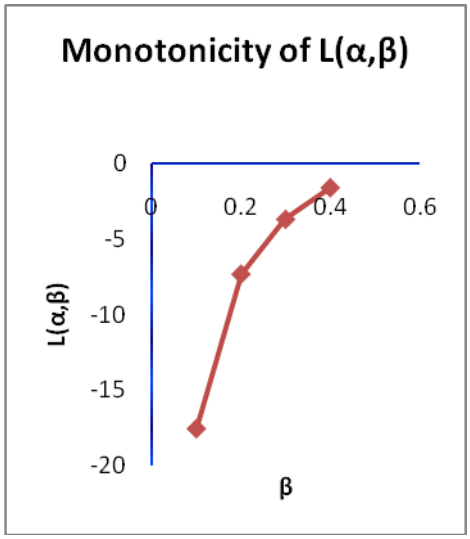

Fig-3.1

REFERENCES

[1] Arun Choudhary and Satish Kumar, "Some more noiseless coding theorem on generalized R- Norm entropy", *Journal of Mathematics Research*, vol.3, pp. 125-130, 2011.

[2] Arun Choudhary and Satish Kumar, "Some coding theorems on generalized havrda-charvat and tsalli's entropy", *Tamkang Journal of Mathematics*, vol.43, pp. 437-444, 2012.

[3] A.Renyi, *On Measures of Entropy and Information*, Proc. 4th Berk. Symp. Math. Statist. and Probl, University of California Press, pp.547-561, 1961.

[4] Belis, M. and Guiasu,, "*A quantitative-qualitative measure of information in cybernetic systems"*, IEEE Transactions on Information Theory 14, pp. 593-594,1968.

[5] C.E.Shannon, *A Mathematical Theory of Communication*, Bell Syst. Tech. J, pp.379-423, 623-659, 1948.

[6] Guiasu, S. and Picard, C. F., "Borne *in fericturde la longuerur utile de certains codes*", Comptes Rendus Mathematique Academic des Sciences Paris, pp.273, 248-251, 1971.

[7] Gurdial and Pessoa, F., "*On useful information of order* α" Journal of Combanatrics Information and System Sciences 2, pp.158-162, 1977.

[8] G.J. Klir, and T.A. Folger, *Fuzzy Sets, Uncertainty and Indetermination*, Prentice Hall, 1988.

[9] H.Nyquist, *Certain Factors Affecting Telegraph Speed*, Bell Syst. Tech.,pp. 324-325,1924.

[10] H.Nyquist, *Certain Topics in Telegraph Transmission Theory*, AIEEE Transactions, pp.617-619, 1928.

[11] H.J. Zimmermann, *Description and optimization of fuzzy systems*, International Journal of General Systems, pp. 209-215, 1976.

[12] J.N.Kapur, *Measures of Fuzzy Information*, Mathematical Sciences Trust Society, New Delhi, 1997.

[13] Kraft, "*A device for quantizing grouping and coding amplitude modulated pulses",* M.S. Thesis, Electrical Engineering Department, MIT.

[14] Kapur, J.N., "*Entropy and Coding*", Mathematical Sciences Trust Society, New Delhi, 1998.

[15] Korada, S. B. and Urbanke, R. L., "*Polar codes are optimal for lossy source coding*", IEEE Trans. Inform. Theory 56(4), pp.1751–1768, 2010.

[16] L.A. Zadeh, *Fuzzy sets as a basis for a theory of possibility*, *Fuzzy Sets and Systems*, pp. 3-28, 1978.

[17] L.L.Campbell, "*A coding theorem and renyi's entropy*", Information and control,8, pp.423-429,1965.

[18] Longo, G., "*Quantitative-Qualitative Measures of Information*", Springer-Verlag, New York, 1972.

[19] M.A.K. Baig and Mohd Javid Dar, "Some Coding theorems on Fuzzy entropy Function Depending upon Parameter R and V", *IOSR Journal of Mathematics*, vol.9, pp.119-123.

[20] M.A.K. Baig and Mohd Javid Dar, "Fuzzy coding theorem on generalized fuzzy cost measure", *Asian Journal of Fuzzy and Applied Mathematics*, vol.2, pp.28-34, 2014.

[21] Merhav, N., "*Shannon's secrecy system with informed receivers and its application to systematic coding for wiretapped channels",* IEEE Transactions on Information Theory 54,pp. 2723-2734,2008.

[22] N.Wiener, Cybernetics, MIT Press and Wiley, New York, 1948.

[23] Om Parkash and P. K. Sharma, "Noiseless coding theorems corresponding to fuzzy entropies", *Southeast Asian Bulletin of Mathematics*, vol.27, pp.1073–1080, 2004.

[24] Om Parkash and P. K. Sharma, "A new class of fuzzy coding theorems", *Caribb. J.Math. Comput.Sci.*, vol.12, pp. 1-10, 2002.

[25] R.K.Tuli, "Mean codeword lengths and their correspondence with entropy measures" , *International Journal of Engineering and Natural Sciences* , vol.4 , pp.175-180, 2010.

[26] R.P.Singh, R.Kumar and R.K.Tuteja, *Application of Holder's inequality in information theory*, Information Sciences, pp.145-154, 2003.

[27] R.T.V.Hartley, Transmission *of information*, Bell Syst. Tech. J, vol. 7, pp.535-563, 1928.

[28] Szpankowski, W., "*A one-to-one code and its anti-redundancy"*, IEEE Trans. Inform. Theory 54(10), pp. 4762–4766, 2008.

FACILITY LAYOUT DESIGN IMPROVEMENT IN ABC INDUSTRY

M.R. Jadhav[1] P.V. Mulik[2] G.S. Kamble[3] K.D. Joshi[4]

[1, 2, 3, 4] *Assistant Professor, Department of Mechanical Engineering, T.K.I.E.T. Warananagar, Maharashtra, India*

ABSTRACT

The aim of the paper was to investigate, analyze and implement improvements of the facility layout design for plant layout. Facility planning is a major undertaking that requires substantial resources and careful planning. Literature review was done to point out current knowledge on facility layout design and investigate tools, methods and approaches that could be followed in this paper to improve the processes.

In layout optimization study of existing plant layout and design implementation new proposed plant layout. The optimized machine layout in magnetic particle inspection (MPI) station and offset grinding station has resulted in to straight line material flow, reduced operator fatigue and reduced operator motion loss. Also it reduces material flow in plant for coil spring 210 meters to 140 meters and stabilizer bar 290 meters to 160 meters respectively.

Keywords: Critical analysis, offset grinding workstation, Magnetic particle test machine, Plant layout

I. INTRODUCTION

1.1 Facility Planning and design

Facility layout dates back to ancient times where it became important for rulers and planners to locate the locations for market centres, sport arenas and most living quarters. In those days, time and cost considerations were not of great importance because of the abundance of labour and other resources. Facility planning has a long history in finding the optimal or suboptimal facility design. S. Kulturel-konak et.al [1] The unequal area facility layout problem is studied considering both production uncertainty and routing flexibility. Stochastic production quantities are introduced under the assumption of dependent demands and incorporated into the usual objective of material handling cost minimization. Concurrently, alternative routings are considered based on production quantity. An efficient simulation approach is used to estimate the resulting department pair wise flows, both their expected values and variances. Using these estimates, a tabu search heuristic procedure performs the layout design optimization. Chawalit Jeenanunta [2] The facility layout design determines the best location of the production areas, support areas and personnel areas within the building. The typical plant layout objectives are to minimize investment in equipment and material handling cost, to minimize overall production time, to minimize variation in types of material handling equipment, to meet the requirement of quality of work

life and to meet the requirement of building and site constraints. The optimum plant layout was solved by using analytical approaches such as exact mathematical procedures, probabilistic model, graph theory, and heuristics methods. These procedures can be classified as construction method and improvement method. Construction methods develop a new layout from scratch whereas the improvement methods generate alternatives based on an initial layout.

N. R. Rajhans and Dr B. B. Ahuja [3] Plant layout decisions require strategic evaluations of the various important parameters specific to the manufacturing system of the industry concerned. As a consequence to this it is necessary to evaluate a number of alternative strategies each having characteristic criterion. Layout design is based on many factors such as flexibility in manufacturing, batch size, cost and accessibility to maintenance. These are the basic factors considered for the layout. Each factor can be further divided into sub factors and then a hierarchy of these can be found. It is not always necessary that all these factors be of equal importance while considering the redesigning. Analytical Hierarchy Process (AHP) calculates different weight ages to be given to each factor. Based on the selection criteria, different factors can be used with their weightages and a layout can be designed. Apple J.M. [4] Many heuristic methods for facility layout problems are developed by researchers over the last 20 years. A facility layout is an arrangement of everything needed for production of goods or delivery of service according to Moore[5] Facility planning has a significant impact upon manufacturing cost and an important effect on the performances and efficiency of a manufacturing system. A good placement of facilities contributes to the overall efficiency of operations and can reduce up to 50% of the total operating expenses. Muthur [6] considered facility layout as an industrial problem and the object is to minimize the cost of the materials that flow between workstations. Simulation studies are sometimes used to measure the benefits and performance of given layouts. Not all facility layouts are that simple, therefore research has been conducted through a number of decades to optimize and design complex layouts. In the early stage of a system design, it is important to strive for an optimal design and facility layout. It is expected that in the future, facility layout design will play a significant role for that extra space needed, for the growing demand of high quality products and a good performance system. A well known and popular layout planning method is the Systematic Layout Planning (SLP). This is a systematic approach that was developed by Muther. According to Muthur the following are common reasons for the redesigning of facilities:

- Material handling problems, bottlenecks and high costs that normally occur because of inefficient layouts.
- Safety hazards and possible occurring of accidents.
- Frequent changes in the design of the product or service.
- Introducing a new service.
- Changes in the volume or the mix of the output of products.
- Changes in methods, processes or equipment.
- Changes in legal requirements or environmental requirements.
- Morale problems (lack of face-to-face and teamwork).

There are ever increasing pressures on most manufacturing companies to be effective and efficient to stay competitive. The environment in which they operate are becoming more competitive with the increasing threat from international competition and customer demands for on-time delivery, consistent quality, low cost and customer specified product design and functionality. Today, algorithms and software tools are also used for these complex manufacturing environments to automate and optimize their facility layout designs. Facility

layout problems or inefficient layouts can occur in many ways and can have significant effects on the overall effectiveness of the production system. According to Apple J. M. at least 10% to 30% of material handling costs can be reduced by an effective facility planning.

II. BRIEF INTRODUCTION OF ABC INDUSTRY

ABC industry, was established in 1999 to design and manufacture of parts like Hot coil springs, Stabilizer bars, Torsion Bars and Strut bars for the automotive industry in line with customer expectations. The plant area is 35,600 m2 with a built up area of 5754 m2 . It is also supplying in OE spares market. The Major Strength of ABC industry is usage of special grade material locally developed for coil springs. The major advantage of this material is higher design stress leading to lesser weight & better fatigue life. ABC industry, has a concern about their plant because of excessive in process inventory, high material handling cost and excessive lead time. They suspect that an inefficient facility layout, process structure and material handling might be factors that contribute to the situation. According to their performance results they need to investigate these factors. An inefficient facility layout, process structure and material handling are possible reasons for the excessive inventory, high material handling cost and excessive lead time at the plant. The plant is lacking in performance and effectiveness.

III. METHODOLOGY

The aim of this paper is to improvement in plant layout and work stations by implementing lean principles; therefore the output of this paper should be applicable in improving the current situation. To be able to accomplish this, first theories are studied, and then those theories are implemented at ABC. Critical analysis of processes that are of concern with the design or improvement at the Finishing Station should be done. This will allow for inspections of standards, the manner of how material is handled, tool equipment and working conditions and methods. This is an important step in the designing of a new facility or material handling for improving an existing operation or system. According to Niebel and Freivalds [7] method analysts use operation analysis to increase productivity per unit of time by means of studying all productive and non-productive fundamentals of an operation. The means of using the questioning approach on all facets of the facility, process and material handling should help to develop an efficient facility layout design. Table 1 shows a template of the critical analysis technique that uses the questioning approach to analyse operations to study these operations, and focusing on the items likely to provide improvements. This can also help to identify problem areas and evaluate alternative facility layouts.

Table 1 Critical Analysis Template

CRITICAL ANALYSIS TECHNIQUE			
METHOD:			
PRESENT METHOD		ALTERNATIVES	SELECTED ALTERNATIVE
Purpose: What is achieved?	Is it necessary? (Y/N) If Yes - Why?	What else could be done?	What is the purpose?
Means: How is it done?	Why that way?	How else could it be done?	How should it be done?

Place: Where is it done?	Why there?	Where else can it be done?	Where should it be done?
Sequence: When is it done?	Why then?	When else could it be done?	When should it be done?
Person: Who does it?	Why that person?	Who else could do it?	Who should do it?

VI. STUDY OF EXISTING PLANT LAYOUT

Present plant layout is process type layout. Present layout divided in three areas i.e. initial area, bending area, final area. In initial area raw material storage, cutting machines, end heating furnace, forging press, walking beam furnace, new continuous tempering furnace, muffle furnace, tool crib area, maintenance area are covered. In bending area CNC bending machine, correction presses, tempering furnace, pit furnace, offset grinding are covered. In final area shot peening, pretreatment tank, powder coating, final inspection and packing are covered. In present plant layout it was observed that work in process (WIP) between each station was excessive and improper material flow. The following table 2 shows list of machines and area covered by machines in plant and table 3 shows new machine which will be part of new product layout. After studying the present plant layout it is found that work in process (WIP) between station is excessive and lead time also excessive due to which plant utilization is not done properly for detail material flow of stabilizer bar and coil springs.

Table 2: List Of Machines In Present Plant

Sr. No.	Name of Machine	Qty.	Size in M.	Area in Sq.M.	Total Area in Sq.m
1	Band Saw Cutting Machine	1	9.5 X 1.2	11.4	11.4
2	Abrasive Cutting Machine	1	10 X 1.5	15	15
3	Forging Press	2	2.2 X 1.8	3.96	7.92
4	End Heating Furnace	2	2.3 X 1.2	2.76	5.52
5	End Rolling Machine	1	2.3 X 1.9	4.37	4.37
6	Induction Heater	1	6 x 1.2	7.2	7.2
7	Walking Beam Furnace	1	6 X 1.3	7.8	7.8
8	Coiling Machine	1	3.2 x 0.9	2.88	2.88
9	Pig Tailing Machine	1	3 X 0.8	2.4	2.4
10	C.S. Quenching Tank	1	7.8 X 1.5	11.7	11.7
11	T.B. Quenching Tank	1	2.6 x 2.6	6.76	6.76
12	Upsetting machine	2	2 X 0.65	1.3	2.6
13	Continous Tempering Furnace	2	15.5 x 4.5	69.75	139.5
14	C.S. Hot Setting machine	1	1.2 x 0.8	0.96	0.96
15	Muffle Furnace	2	3 x 2.5	7.5	15
16	Bending Machine	8	5 x 1.4	7	56

17	Pit Tempering Furnace	1	Dia. 2.16	3.66	3.66
18	30 Ton Press with Power Pack	11	1.7 x 1	1.7	18.7
19	T.B.Hot Setting machine	1	2.6 x 1	2.6	2.6
20	Hardness Tester	2	0.6 X 0.6	0.36	0.72
21	C.S. Hot Setting machine	1	1 x 0.8	0.8	0.8
22	Drilling machine	2	1.2 x 0.7	0.84	1.68
23	C.S. Grinder	1	2 X 1.8	3.6	3.6
24	Stress Peening Fixture	4	2 x 1.2	2.4	9.6
25	Shot Peening Machine	1	10 x 8	66.5	66.5
26	M.P.I. machine	2	4 x 4	16	32
27	Pretreatement Tank Set up	1	13.5 x 5.5	74.25	74.25
28	Powder Coating Plant	1	19 x 11	209	209
29	Scragging machine	1	4.25 x 0.7	2.98	2.975
30	Crimping Machine	2	3.2 x 0.5	1.6	3.2

Table 3: List Of New Machines For Proposed Plant

Sr. No.	Name Of Machine	Qty.	Size in meters	Area in sq. meters
1	Shot peening machine	1	10x8	80
2	Resistance heating machine	1	8X2.5	20
3	Scragging machine	1	4.25X0.7	2.98
4	CNC Bending machines	2	5X1.4	14

V. ANALYSIS OF FACILITY LAYOUT DESIGN

In facility layout design new product type layout designed and phase wise implementation are to be carried out. machine layout improvement are carried out to reduce operator motion loss, fatigue and productivity improvements. Facility layout design involves the determination of the placement of the departments, work groups within the departments and workstations within production facility layouts. The objective is to arrange these elements in a way that it will ensure a smooth work flow of material, machines and people. General inputs to a layout design are the space requirements for the elements in the layout and the flow of elements between operations. Effective flow planning in the various workstations is an important aspect of facility layout design. Investigation revealed that there were numerous pattern and flow problems such as magnetic particle inspection station, offset grinding station etc. In proposed plant layout consists of two separate production lines for two products i.e. coil spring and stabilizer bar for this design some new machines required for achieving production demand that also consider. New plant layout material flow from raw material storage to packing for coil springs and stabilizer bar is 140 meters and 160 meters. In present layout material flow from raw material storage to packing for coil springs and stabilizer bar is 210 meters and 290 meters.

5.1 Magnetic Particle Inspection (MPI) Layout Improvement

5.1.1 Present Magnetic Particle Inspection Layout

In present magnetic particle inspection layout charging station and inspection station is covered by 4 m X 4 m dark room. The present method is one operator is required to pick up coil spring from incoming trolley and give

to the charging station operator then operator charge the coil spring and send to inspection table. In inspection table one operator is inspected coil spring in ultra violet light and send to outside of dark room. (shown in the fig. 2)

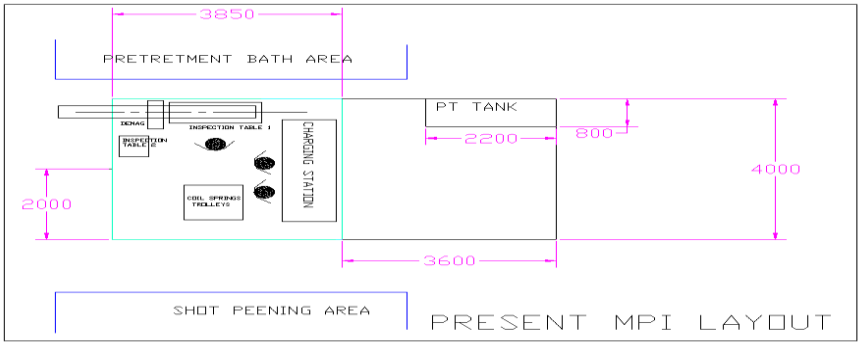

Fig. 2: Present magnetic particle inspection layout.

By first viewing the actual station, it does not look too bad but there is no chance to increase output with a second operator if the demand is increased. The improved process flow pattern as shown in the fig. 3 is a straight line shape, where two operators can work on single inspection table in both sides. It creates the potential to increase output with a second operator if needed. One of the several advantages of the straight line is better operator access. The straight line is also easier to balance and an extra operator can help to increase the output. Presently all process of MPI is under the close dark room. In new layout only inspection activity are carried out in dark room and magnetization is done outside the dark room. Following are advantages

- Work in process reduced between inspections and charging station.
- Two operators can work on single inspection table in both sides. It creates the potential to increase output with a second operator if needed.
- Straight line is better operator access. The straight line is also easier to balance and an extra operator can help to increase the output.

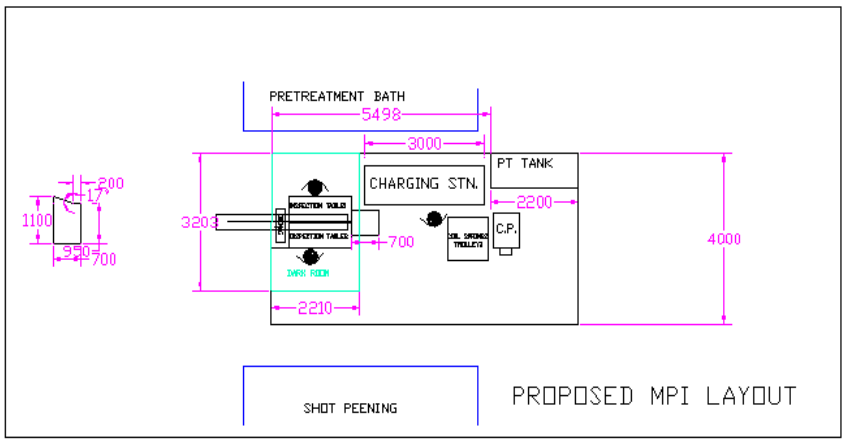

Fig. 3: New magnetic particle inspection layout.

5.2 Offset grinding layout improvement

5.2.1 Present offset grinding layout

Presently coil spring grinding coil spring trolleys are placed behind the surface grinder and one common outward trolley was placed in front of surface grinder. Due to this arrangement material flow are not in stream line,

operator motion loss is more due to movement of operator and no proper handling of coil springs. Present layout is shown in fig. 4. In modified offset grinding layout shown in fig. 5 input material trolley and outward material trolley are placed both sides of surface grinder. Due to modified layout material flow is streamline with zero operator loss and operator fatigue reduced.

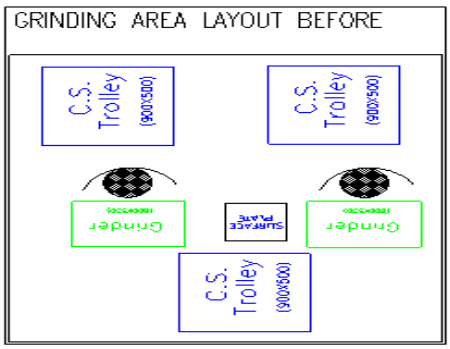

Fig. 4 Present offset grinding layout

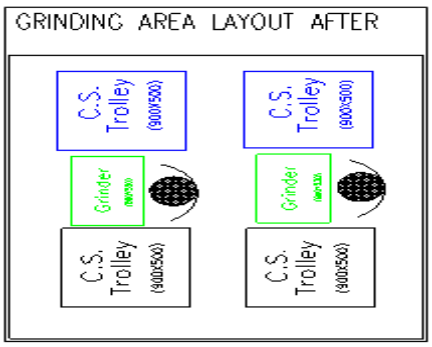

Fig. 5 Modified offset grinding layout

VI. CONCLUSION

- Optimized machine layout in magnetic particle inspection (MPI) station and offset grinding station has resulted in to straight line material flow, reduced operator fatigue and reduced operator motion loss.
- By implementing the above changes it is observed that new product oriented plant layout reduced material flow from raw material to packing area of coil spring is 33% and stabilizer bar is 45%

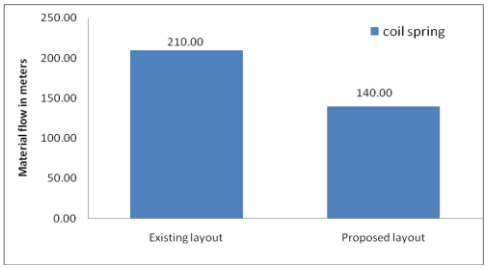

Fig. 6 Material flow of coil springs

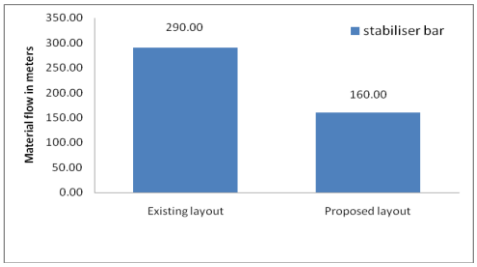

Fig. 7 Material flow of stabilizer bars

REFERENCES

[1] **S. Kulturel-konak, A. E. Smith and B. A. Norman: "**Layout optimization considering production uncertainty and routing flexibility**",** *int. j. prod. res.*, 1 November 2004, vol. 42, no. 21, 4475–4493

[2] **Chawalit Jeenanunta:**"Graphical layout design tool for facility layout", *Proceeding of IE(I) Journal-PR*, March 31,2005, PP 46-51.

[3] **N. R. Rajhans, Dr B. B. Ahuja:** "Analyzing decision factors for redesigning a plant layout using analytical hierarchical processing.**"** Retrived on June 15, 2008 from http://www.ieindia.org/pdf/86/faxdi85t2.pdf

[4] **Apple J.M.**: "Plant Layout and Material Handling", New York: Wiley.(1977)

[5] **Moore J. M.:** " Plant Layout and Design", New york: Macmillan(1962)

[6] **Muthur R.:** "Practical plant layout", McGraw Hill.(1955)

[7] **Niebel, B. & Freivalds, A.:** "Methods, Standards, and work design". New York: McGraw-Hill. (2003)

BER IMPROVEMENT IN OFDM USING CODING TECHNIQUES

[1]Mrs. Shubhangi S. Joshi, [2]Mrs. A. P. Laturkar

[1,2]Department of E&TC/University of Pune, (India)

ABSTRACT

In the last decade, Orthogonal Frequency Division Multiplexing (OFDM) based communication systems have been identified as one of the key transmission techniques for next generation wireless communication systems. The main objective is to transmit the OFDM signal with low bit error rate in the noisy environment. A cyclic prefix acts as a buffer region where delayed information from the previous symbols can get stored. Different modulation technique with respect to bit-error rate and SNR ratio is analyzed using MATLAB software. Here the performance of OFDM signal is analyzed by comparing the BER results of coding technique such as convolution [1]. As well various modulation methods are also used. Two decoding methods are used to analyze the signal. One is soft decoding and other is hard decoding with convolution code. Three types of modulation methods are used with normal OFDM to analyze the system performances which are Binary Phase Shift Keying (BPSK), Quadrature Phase Shift Keying (QPSK), and Quadrature Amplitude Modulation (QAM)[2]. The goal of this paper is to improve system performance by the mean of low bit error rate. Finally bit error rate of these three methods are analyzed by comparing SNR versus BER plots. Soft decoding method in convolution with high code rate gives better BER performance.

Keywords: OFDM, Convolution Code, Error detection, Error correction code, cyclic prefix, SNR, QPSK, BPSK, QAM, and BER

I INTRODUCTION

OFDM belongs to a family of transmission schemes called multicarrier modulation, which is based on the idea of dividing a given high-bit-rate data stream into several parallel lower bit-rate streams and modulating each stream on separate carriers often called subcarriers. Orthogonal frequency division multiplexing (OFDM) system has been proposed as a technique for broadcasting digital signals and for wireless communication. The bit-error-rate (BER) performance of the OFDM system is severely affected by the nonlinearity of the high power amplifier and by the impairments like noise. To reduce these effects caused by impairments, error rate of signal should be low and that can be obtained by FEC technique. Moreover, simulation results are presented to validate the analysis. It is shown that the resulting inter-carrier interference (ICI) due to noise generated by these impairments becomes very significant in a multi-hop relaying communication system, and severely degrades the BER performance of the system. Practical results show perfect agreement with those obtained by simulation. Three types of modulation methods with and without FEC techniques are used to analyze the system performances which are Binary Phase Shift Keying (BPSK), Quadrature Phase Shift Keying (QPSK) and Quadrature Amplitude Modulation (QAM). Out of two scenarios i.e. with FEC and without FEC, both the methods are analyzed by using three modulation techniques. In this paper bit error rate of three modulation methods without FEC is compared to achieve the goal. This paper is organized as follows. In section II a whole

system is described. Out of that implemented results are described in section IV. OFDM system using the BPSK, QPSK, QAM modulation method is described. Then, its exact BER performance is investigated based on the channel noise for OFDM system without FEC. Numerical results are plotted to analyze an OFDM with Convolution Code and finally, conclusions are provided in Section V.

II OFDM WITH AND WITHOUT FEC

Coding techniques is used for providing reliable information through the transmission channel to the user. In coding techniques the number of symbols in the source encoded message is increased in a controlled manner in order to facilitate two basic objectives at the receiver one is Error detection and other is Error correction.[2] It is used to reduce the level of noise and interferences in electronic medium. The amount of error detection and correction required and its effectiveness depends on the signal to noise ratio (SNR). In digital communication, coding techniques is a broadly used term mostly referring to the forward error correction code. The advantage of forward error correction is that a feedback-channel is not required, or that retransmission of data can often be avoided, at the cost of higher bandwidth requirements on average. This project is useful to get less number of errors in OFDM by using convolution coding scheme for different modulation technique with respect to bit-error rate and SNR ratio. In order to improve the error performance of the OFDM system forward error correction scheme can be utilized. In telecommunication, information theory, and coding theory, forward error correction (FEC) or channel coding is a technique used for controlling errors in data transmission over unreliable or noisy communication channels. The central idea is the sender encodes their message in a redundant way by using an error-correcting code (ECC). The American mathematician Richard Hamming pioneered this field in the 1940s and invented the first error-correcting code in 1950: the Hamming code. Many FEC schemes for multicarrier systems have been proposed in orthogonal FDM. Convolution is popular coding schemes for FEC. Convolution codes are binary code and it can operate on desired constraint length. One of the reasons that why CC-OFDM popular is that the same higher performance as Turbo code.[4] Turbo code is implemented using the structure of parallel concatenation of different FEC code and which may leads to high complexity. Convolutional codes are easy to implement and low complexity compared to Turbo code. Convolution codes are implemented with different code rates for improving the error performance of OFDM system. The BER performance of convolution coded OFDM is evaluated for various code rates in an AWGN channel.

2.1 OFDM

Simulation analysis gives the comparison of OFDM with and without FEC. OFDM system performance can be improved by using various kinds of modulation methods also. Three types of modulation methods without FEC techniques are used to analyze the system performances which are binary phase shift keying (BPSK), quadrature phase shift keying (QPSK), and quadrature amplitude modulation (QAM). Finally bit error rate of these three methods are analyzed by comparing SNR versus BER plots. QPSK gives better BER performance for low SNR value whereas QAM results are better for high SNR value.

2.2 CC-OFDM

The redundancy allows the receiver to detect a limited number of errors that may occur anywhere in the message, and often to correct these errors without retransmission. FEC gives the receiver the ability to correct

errors without needing a reverse channel to request retransmission of data, but at the cost of a fixed, higher forward channel bandwidth. FEC is therefore applied in situations where retransmissions are costly or impossible, such as one-way communication links and when transmitting to multiple receivers in multicast. FEC information is usually added to mass storage devices to enable recovery of corrupted data, and is widely used in modems.FEC processing in a receiver may be applied to a digital bit stream or in the demodulation of a digitally modulated carrier. For the latter, FEC is an integral part of the initial analog-to-digital conversion in the receiver. The Viterbi decoder implements a soft-decision algorithm to demodulate digital data from an analog signal corrupted by noise. Many FEC coders can also generate a bit-error rate (BER) signal which can be used as feedback to fine-tune the analog receiving electronics. The maximum fractions of errors or of missing bits that can be corrected are determined by the design of the FEC code, so different forward error correcting codes are suitable for different conditions. Evaluation of BER for OFDM without FEC reached to 10^{-1} and evaluation with CC-OFDM reached to 10^{-6}. Obviously CC-OFDM is the prominent solution to improve system performance. In CC-OFDM various decoding schemes are also. Hard decoding and soft decoding are two popular decoding methods. Then Performance analysis of CC-OFDM with hard decoding and soft decoding at different code rates have been analyzed. Hence, the BER performance of the CC-OFDM with higher code rate and soft decoding method with BPSK modulation has found to be best than the normal OFDM system. Hence the burst of errors has been reduced when CC-OFDM is used. Orthogonal Frequency Division Multiplexing has been employed in numerous wireless standards. However, the performance of OFDM systems is degraded by both the Inter Carrier Interference (ICI), Inter symbols Interference (ISI) and the channel noise. Hence new exact closed-form system model is designed for calculating the average BER of OFDM systems in the presence of both Interferences and channel noise in selective AWGN fading channels. By simulation results system model can be verified and the accuracy of our exact BER analysis is done. Consider an OFDM system having N subcarriers using the BPSK, QPSK, QAM modulation for communicating over frequency selective Additive white Gaussian noise channel.

1. FEC = Forward Error Correction
2. IFFT = Inverse Fast Fourier Transform
3. RF = Radio Frequency
4. FFT = Fast Fourier Transform

The transmitted sequence {bn} is obtained from the input information sequence {*an*} through an *N*-point inverse digital Fourier transform (IDFT). The {*an*} is created from the source data passed through a forward error correction (FEC) encoder, then interleaved and mapped into a constellation that can be Quaternary Phase Shift Keying (QPSK), 16-Quadrature Amplitude Modulation (QAM).

III OFDM MODEL WITH CC

In digital communication, coding techniques is a broadly used term mostly referring to the forward error correction code. The advantage of forward error correction is that a feedback-channel is not required, or that retransmission of data can often be avoided. Coding techniques is used for providing reliable information through the transmission channel to the user. In coding techniques the number of symbols in the source encoded message is increased in a controlled manner in order to facilitate two basic objectives at the receiver one is Error detection and other is Error correction. It is used to reduce the level of noise and interferences in electronic

medium. The amount of error detection and correction required and its effectiveness depends on the signal to noise ratio (SNR).

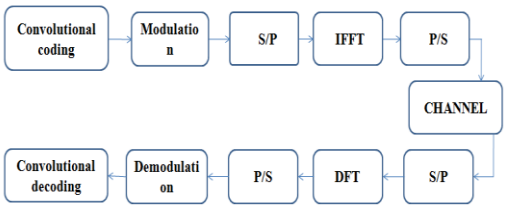

Fig.1. OFDM with Convolution Code

3.1 Code rates in CC-OFDM

Convolutional code can be generated at different code rates. Code rate is the ratio of number of input to the number of outputs. Following examples show the different code rate in convolutional code.1.The figure below is a rate 1/3 (k/n) encoder with constraint length (L) of 3. Generator polynomials $G_1 = (1,1,1)$ $G_2 = (0,1,1)$ $G_3 = (1,0,1)$. Output bits are calculated as follows $n_1 = m_1 + m_0 + m_{-1}$;

$n_2 = m_0 + m_{-1}$;

$n_3 = m_1 + m_{-1}$.

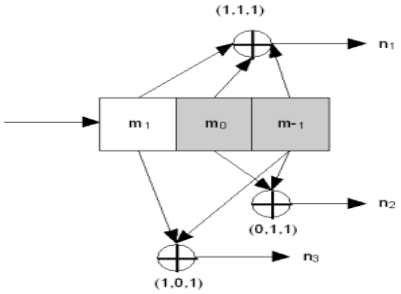

Fig 2. Rate 1/3 non-recursive CC-Encoder

The example of the encoder is systematic because the input data is also used in the output symbols. Codes with output symbols that do not include the input data are called non-systematic.

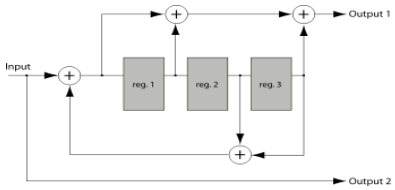

Fig.3. Rate 1/2 Recursive Systematic CC-Encoder

IV SIMULATION AND RESULTS

We have developed the simulator in Matlab™ using modular approach. Each block of the transmitter, receiver and channel is written in separate ´m´ file. The main procedure call each of the block in the manner a communication system works. The main procedure also contains initialization parameters, input data and delivers results. The parameters that can be set at the time of initialization are the number of simulated OFDM symbols, CP length, modulation and coding rate, range of SNR values. The input data stream is randomly

generated. Output variables are available in Matlab™ workspace while BER values for different SNR are stored in text files which facilitate to draw plots. Each single block of the transmitter is tested with its counterpart of the receiver side to confirm that each block works perfectly.

4.1 BER Plots of an OFDM

In this section various BER vs. SNR plots have been described for all the mandatory modulation and coding profiles as specified in the standard on same channel models. The value of signal to noise ratio (Eb/No) can be changed by following parameter in function block set. As we increase the value of SNR, getting result of decrease in error rate. Equally-spaced orthogonal sub-carriers are used to carry data. Each sub-carrier is modulated with a conventional modulation scheme. Here by using BPSK (Binary Phase Shift Keying) and QPSK (Quadrature Phase Shift Keying) phase shift keying modulation and demodulation for all the simulations, OFDM system without FEC is analyzed. The constellation points are displayed on discrete time scatter plot. As SNR increases by 6 dB, there is decrease in error rate. BPSK is good one in OFDM system performance. Reversal Keying or 2PSK is the simplest form of phase shift keying (PSK). It uses two phases which are separated by 180° and so can also be termed 2-PSK. It is, however, only able to modulate at 1 bit/symbol and so is unsuitable for high data-rate applications. As a result, the data is often differentially encoded prior to modulation. Binary PSK is functionally equivalent to 2-QAM modulation. QPSK gives better BER performance for low SNR value. QPSK uses four points on the constellation diagram, equispaced around a circle. With four phases, QPSK can encode two bits per symbol, shown in the diagram with gray coding to minimize the bit error rate (BER). QAM results are better for high SNR value.

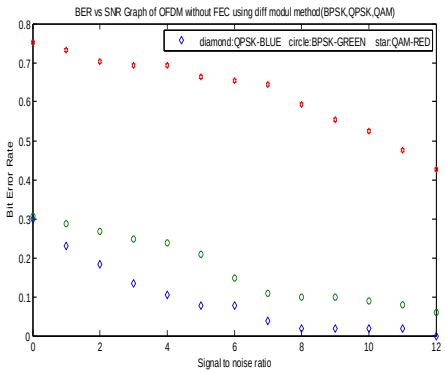

Fig 4. OFDM with Different Modulation Methods

Above graph as shown in fig.9 is obtained when all methods are combined. Arbitrarily high spectral efficiencies can be achieved with QAM by setting a suitable constellation size, limited only by the noise level and linearity of the communications channel. This paper is useful for analysis of physical layer of WIMAX[3] with different modulation techniques like BPSK, QPSK, QAM and comparison of these modulations with and without Forward Error Correction methods. Broadband Wireless Access (BWA) has emerged as a promising solution for last mile access technology to provide high speed internet access in the residential as well as small and medium sized enterprise sectors. IEEE 802.16 standard for BWA and its associated industry consortium, Worldwide Interoperability for Microwave Access (WIMAX) forum promise to offer high data rate over large areas to a large number of users where broadband is unavailable.

4.2 BER Plots Of CC-OFDM

The figure shows the convolution coding FEC scheme in OFDM. First figure is the result of simulated plot of Convolutional code with using four modulation methods QAM, QPSK, DBPSK, and BPSK. Black diamond gives rate of QAM whereas black stars give information about QPSK modulation. Green is for DBPSK and blue stars are of BPSK. Convolution code with BPSK modulation is found to be best which gives less number of errors as SNR increases.

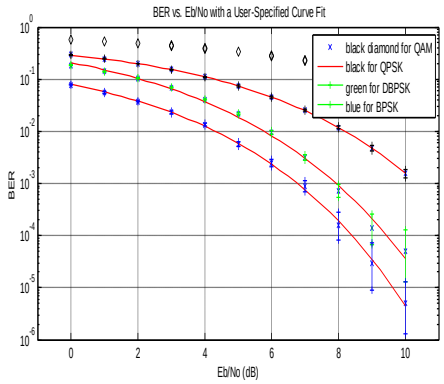

Fig.5. CC-OFDM at different modulation

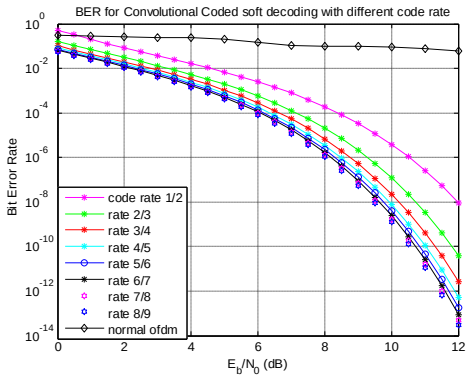

Fig.6. CC-OFDM at different code rates

The figure indicates comparison of eight code rates in CC-OFDM and BER of OFDM without FEC using BPSK modulation method. Higher code rate in convolution code i.e.8/9 code rate gives the best performance as SNR increases.

V CONCLUSION

Error detection and correction techniques are essential for reliable communication over a noisy channel. In this paper, a comparison of BER performance analysis of CC-OFDM and normal OFDM over AWGN channel has been presented. It has been found that the error performance of the OFDM system over AWGN and fading channel can be significantly improved by using Convolution codes for FEC. The improvement in the BER performance of the coded OFDM system increases by increasing the code rate (r). The BER performance of convolutionally coded OFDM system is found to be better than OFDM system.

Convolution codes are one of the most powerful and essential binary error correcting codes for detecting and correcting burst errors. The effect of errors occur during transmission is reduced by adding redundancy to the data prior to transmission. The redundancy is used to enable decoder in the receiver to detect and correct errors.

CC-OFDM is an efficient code to correct the errors by using code rates. It can reduce the bit-error in noisy environment and provide the efficient data through subscriber.CC-OFDM gives the all requirements required in wireless communication. It achieves the required channel capacity which leads to high data rate. Quality of an OFDM system is improved because it minimizes the probability of Error. It solves real life issues e.g. system complexity, cost of implementation, low transmission power required (SNR), minimum bandwidth etc. Performance analysis of BER evaluation of normal OFDM is poor than that of CC-OFDM. Obviously CC-OFDM is the prominent solution to improve system performance. BER performance of the CC-OFDM with higher code rate and soft decoding method with BPSK modulation has been found to be best than the normal OFDM system. Hence the burst of errors has been reduced when convolutional code with soft decoding method is used.

REFERENCES

[1] Ashish Goel, Manoj Kumar Garg, Dept.of ECE Jaypee Institute of Technology.,"Comparative Performance Evaluation of Convolutionally Coded and LDPC Coded OFDM System Over AWGN and SUI-5 Fading Channel",International Conference on Computer and Communication Technology 2012

[2] Prabhakar Telagarapu, G.B.S.R.Naidu, K.Chiranjeevi, Dept.of.ECE GMR Institute of Technology.,"Analysis of Coding Techniques in WiMAX", International Journal of Computer Applications (0975 – 8887) Volume 22– No.3, May 2011

[3] Arunabha Ghosh and David R. Wolter, SBC Laboratories Inc. Jeffrey G. Andrews and Runhua Chen, The University of Texas at Austin"Broadband Wireless Access With Wimax/8o2.16: Current Performance Benchmarks And Future Potential" by., IEEE Communications Magazine. February 2005.

[4] Alok Joshi, Davinder S. Saini.ECE Department JIIT, Noida.," Performance Analysis Of Coded-OFDM with RS-CC and Turbo codes in Various Fading Environment", Proceedings of the 5th International Conference on IT & Multimedia at UNITEN (ICIMU 2011) Malaysia .November 2011

Journal Papers:

1] IEEE 802.162004," IEEE Standard for Local and Metropolitan Area Networks Part 16: Air Interface forFixed Broadband Wireless Access Systems", 1 October,2004

2] J. G. Andrews, "Interference Cancellation in Cellular Systems: A Contemporary Overview," to appear, IEEE Wireless Commun.., Apr. 2005.

3] Israel Koffman, Runcom Technologies Vincentzio Roman, Paradise Consulting,"Broadband Wireless Access Solutions Based on OFDM Access in IEEE 802.16",IEEE Communications Magazine April 2002.

4] Dr.Kurt R.Matis (Director of Systems Research.,Visual System Simulator2002.,"Simulation of Convolutional Codes in VSS

5]"Signal Coding and Estimation Theory"by RanjanBose;"Digital Communication" by Simon Haykin.

6] Yun Hee Kim, Student Member, IEEE, Iickho Song, Senior Member, IEEE, Hong Gil Kim, Student Member, IEEE, Taejoo Chang, and HyungMyung Kim, Member, IEEE.,"Performance Analysis of a Coded OFDM System in Time-Varying Multipath Rayleigh Fading Channels", IEEE Transactions on vehicular technology, vol. 48, no. 5, September 1999

7] Shraddha Bansal, Raksha Upadhyay, Department of ECE,, IET-DAVV, Indore.," Performance Improvement of Wi-Max IEEE 802.16e in Presence of Different FEC Codes", First International Conference on Computational Intelligence, Communication Systems and Networks.2009.

8] Mario Huemer,Christian Hofbauer,Johannes B. Huber, .,"Non-Systematic Complex Number RS Coded OFDM by Unique Word Prefix ",IEEE transactions on Signal Processing, Vol. 60, No. 1, January 2012.

9] Tanaporn Payommai, Wichupong Wiboonjaroen ,SomsinWangkhuntod department of Electronic Engineering Rajamangala University of Technology Isan Nakhonrat chasima, Thailand .," Study on Sub-block Encoder of LDPC Code with OFDM for Image Transmission, 2012 IEEE.

10] HakanDo˘gan, HakanYıldız, Graduate Member, IEEE, TodorCooklev, Senior Member, IEEE,YusufAcar.," Coded OFDM Wireless Systems with Generalized Prefix, 2012 IEEE

11] Ding-Bing Lin, Member, IEEE, Ping-Hung Chiang, Student Member, IEEE, and Hsueh-Jyh Li, Senior Member, IEEE.," Performance Analysis of Two-Branch Transmit Diversity Block-Coded OFDM Systems in Time-Varying Multipath Rayleigh-Fading Channels, IEEE transactions on vehicular technology, vol. 54, no. 1, January 2005.

INVESTIGATIONS ON EFFECT OF INCORPORATION OF PHOTOVOLTAIC SYSTEM WITH COMBINED CYCLE GAS TURBINEPLANT

Naimul Hasan[1] , B.B .Arora[2], J.N. Rai[3]

[1]Department of Electrical Engineering, Jamia Millia Islamia .New Delhi

[2]Department of Mechanical Engineering, Delhi Technological University,Delhi, India

[3] Research Scholar, Dept. Of Elec. Engg, Jamia Miliia Islamia, N.Delhi

ABSTRACT

India is witnessing a huge demand in power requirement. Economic development has led to development in Industries and demand for housing has increased. To meet this ever-rising power demand, efforts have been made to increase the efficiency at the generating end. One of such efforts is the CCGT plant in which the exhaust of Gas Turbine is used to run the Steam Turbine; hence giving an overall efficiency upto 60%. But, the recent trends in electrical engineering has been shifted to renewable forms of energy via solar, wind et,.keeping in mind the emphasis is on importance ofsustainable development. This paper is a preliminary study of how solar energy can be used through photovoltaic panels for the excitation of GT and auxiliary purposes in CCGT plant. The results of the same have been plotted and the future developments of this research have been discussed in detail.

Keywords: Solar, PV, CCGT, Power, Photovoltaic

I INTRODUCTION

In power systems, various methods are employed to overcome the ever-rising electricity demand. In India, most Power Plants are driven by fossil fuels. A Combined Cycle Gas Turbine Plant(Fig. 1)is one themeans so as to make the efficiency of a plant to reach the 60% mark.[1][4].

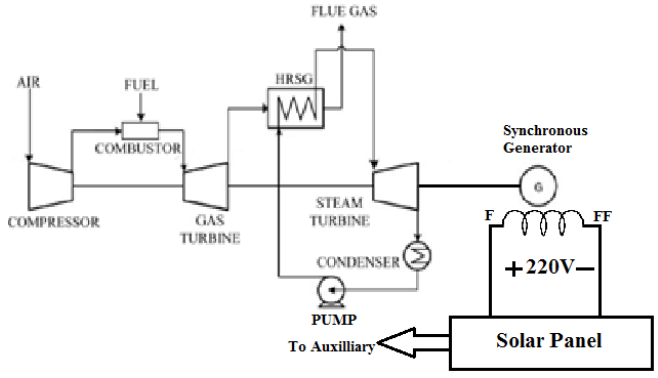

Fig 1. Combined Cycle Gas Turbine with Solar Panel

In a CCGT plant, the input temperature to a steam turbine is about 540°C and the exhaust can be maintained at the atmospheric pressure, due to design consideration the input temperature is limited and the efficiency of the about 45%. Theinput temperature of the gas turbine can be as high as 1100°C but the exhaust temperature can be lowered to about 550-650°C, the efficiency of a gas turbine is about 35%. It can be seen that to obtain higher efficiencies the exhaust of the gas turbine can used to drive the steam turbine giving efficiency up to 62%.The plant consists of a compressor, combustor, gas turbine, waste heat recovery boiler, steam turbine, and generator(s) associated with solar voltaic. [7][8]

Similarly, the emerging form of energy (Renewable Energy) is a socially and politically defined category of energy sources. Solar energy being one of them.Hence, we can employ solar panelswith the CCGT plant to make it less dependent on fossil fuels. The tariff for the consumers would also go down, since solar energy is at its peak in summer season, the time the electricity utilization is maximum in a year.

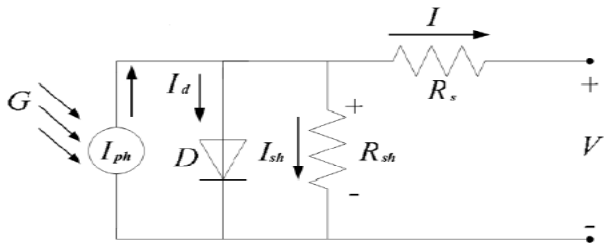

Fig 2. Equivalent Circuit of a PV cell

A simplest equivalent circuit(Fig. 2) of a solar cell is a current source in parallel with a diode. The output of the current source is directly proportional to the solar energy (photons) that hits on the solar cell (photocurrent I_{ph}). During darkness, the solar cell is not an active device; it works as a diode, i.e. a p-n junction. It produces neither a current nor a voltage. However, if it is allowed to connect to an external source (large voltage) it generates a current *Id*, called diode (D) current or dark current. [15]

Hence the combination of solar energy with CCGT plant could make a possible difference.

II THEORETICAL BACKGROUND

Equations which define the model of a CCGT Plant:The airflow (W) in the gas turbine is given as

$$W = W_a \frac{P_a}{P_{ao}} \frac{T_{io}}{T_i} \qquad (1)$$

Where Ti is ambient temperature and P_a denotes the atmospheric pressure.

$$\eta_{cc} = \eta_{gt} + \eta_{st}(1-\eta_{gt}) \qquad (2)$$

The Where η_{cc} is the efficiency of the combined cycle, η_{gt} is the efficiency of Gas Turbine and η_{st} is the efficiency of Steam Turbine.thermal efficiency of the simple gas turbine cycle is given as [6]

$$\eta = \frac{(1-\frac{1}{p_p})(a-p_p)}{\eta_c(k_1-1)-p_p+1} \qquad (3)$$

Where, $a = \eta_c \eta_t k_1$ [10][11][12]Equations which define the model of a PV cell:

$$V_t = \frac{kT_{op}}{q} \quad (4)$$

$$V_{oc} = V_t \ln\left(\frac{I_{ph}}{I_S}\right) \quad (5)$$

$$I_d = \left[e^{\frac{(V+IR_s)}{(nV_tCN_s)}} - 1\right] I_s N_p \quad (6)$$

$$I_S = I_{rs}\left(\frac{T_{op}}{T_{ref}}\right)^3 e^{\left[\frac{qE_g}{nk}\left(\frac{1}{T_{op}} - \frac{1}{T_{ref}}\right)\right]} \quad (7)$$

$$I_{rs} = \frac{I_{sc}}{\left[e^{\left(\frac{V_{oc}q}{kCT_{op}n}\right)} - 1\right]} \quad (8)$$

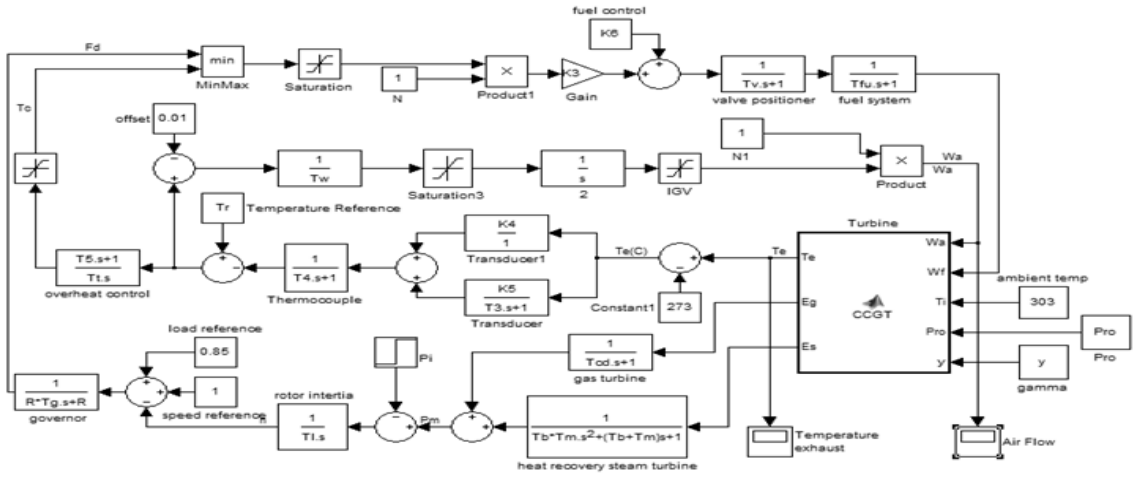

Fig 3. CCGT Simulink Model

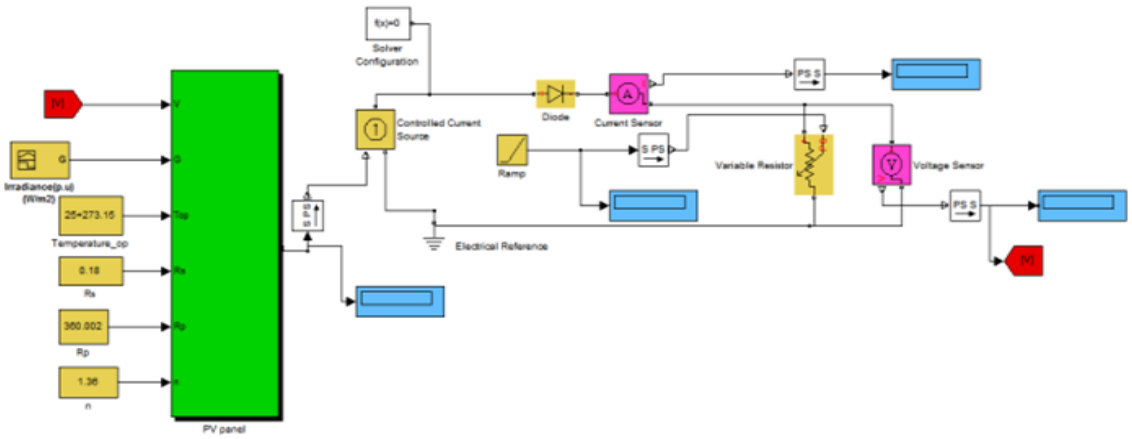

Fig 4. Simulink Model of Photovoltaic Panel

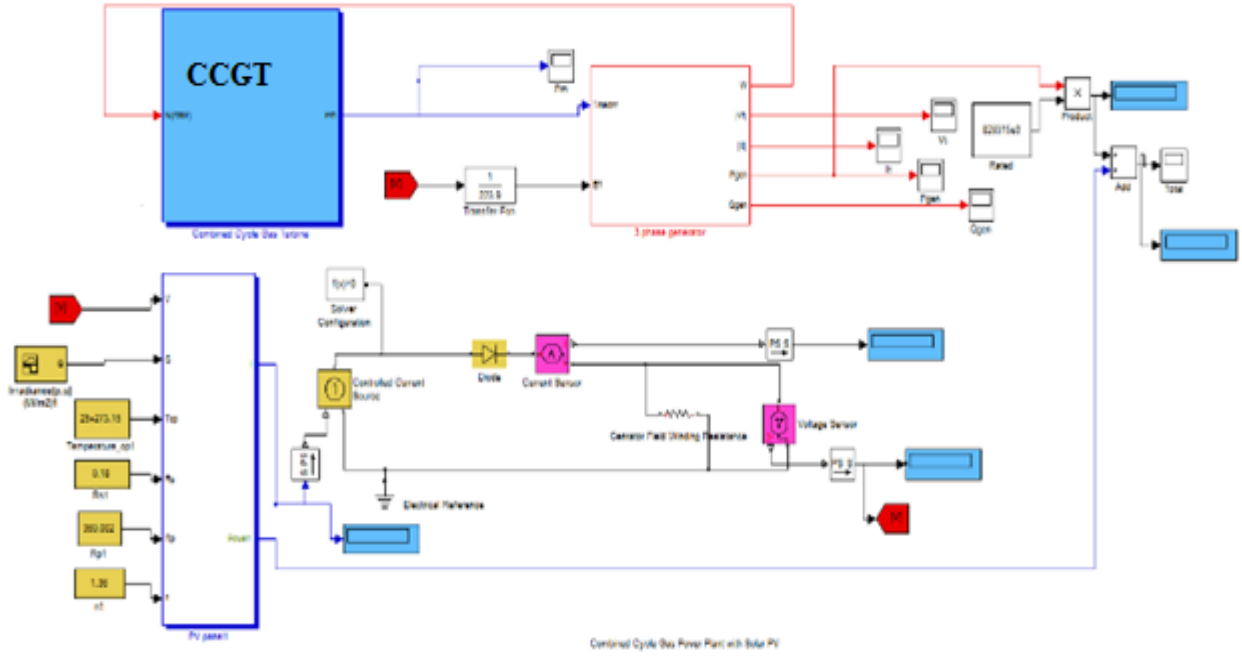

Fig 5. Simulink Model of Integrated Photovoltaic in CCGT

$$I_{sh} = \frac{V + IR_s}{R_p} \qquad (9)$$

$$I_{ph} = G_k \left[I_{sc} + K_I (T_{op} - T_{ref}) \right] \qquad (10)$$

$$I = I_{ph} N_p - I_d - I_{sh} \qquad (11)$$

where, $G_k$is solar insolation in W/m^2,

$T_{ref}$is reference temperature(298 K),

$T_{op}$is operating temperature of cell,

$R_s$is series resistance,

$R_{sh}$is shunt resistance,

k is Boltzmann constant,K is temperature coefficient,

N is data points used,

n is diode emission factor,

$I_{ph}$is photon current & I_d is dark current,

I_{sh} is short circuit current at reference state.

III DESCRIPTION OF SIMULINK MODEL AND RESULTS

The CCGT model (J. N. Rai. et.al. 2013)consists of various blocksdescribing various parameters whose variations have already been studied in order to optimize the performance of combined cycle. There are blocks related with speed/load, temperature control, fuel control, air control and other blocks for gas turbine, waste heat

recovery boiler/steam turbine, rotor shaft, and temperature transducer. All the parameters used in the model are given in Table I& II. [2] [3][5]

A circuit based simulation model for a PV cell for estimating the IV characteristic (temperature and irradiance) and cell parameters (parasitic resistance and idealty factor)has been discussed. The simulation model is used for analysing the behaviour of PV Panel by varying various parameters of the cell in accordance with the given equations. Using a Shockley diode equationan accurate *simulink* PV panel model was developed.The model is based on the equivalent diagram of the solar panel described in the theoretical background. [12] [13] [14]

Further with above Simulink model the response of CCGT. has been investigated which shows the variation of current with respect to the timeFigure 6.

Figure. 7 shows the Variation of Generated Electrical Power. It depicts the variation is almost constant. The output is stable. It can also be seen that the generator output falls which is also controllable with reactive power control as shown in Figure.8.

Further the effect of varying input condition of CCGT as Variation of CCGT parameter i.e Exhaust Temperature of Gas Turbine (^{o}C), Air Flow (p.u.) and Fuel Flow (p.u) (Figure. 9) has been investigated.

Turbine Output (input of generator) is constant for a while (Figure 10). As the system is uncontrollable, the output falls which can be brought to the near to its rated value by controlling the CCGT parameters. The Field Excitation for synchronous generator is accompanied with solar voltaic which shows the positive impact on the performance. It can also be seen that now the start-up time is higher than the normal plant model (J. N. Rai et.al. 2013) with increased power output.

IV CONCLUSION

The parameters considered above cannot be varied simultaneously due to complexity of system. Some parameters are located and the other parameters will be the function of critical parameters in one way or the other. Interrelations amongst the various parameters are balanced by superimposing some constraints on the parameters.The level of benefits achieved as a result of system optimization has included the following:

- Increased output-3 to 5%
- Reduced fuel consumption-3 to 5%
- Reduced power consumption-3 to 5%

Both, the CCGT and PV panel models are combined. PV panel is used to give the excitation to the CCGT Plant Generator and also the remaining energy developed can be used for driving the auxiliaries in the Plant. Since the solar output is DC itself, the conversion losses from AC to DC as was the earlier case in CCGT plant have been taken care of. Start-up Time would be high as compared to Normal Combined Cycle Gas Power Plant.

This paper provides a path for further research work in future by integrating solar plant to increase the clean energy generation and to enhance the existing plant capacity in India.

Table 1 : System Parameters

Symbol	Description	Value
T_i	Compressor inlet temperature	$30\,^{\circ}C$
T_{do}	Compressor discharge temperature	$390\,^{\circ}C$
T_{fo}	Gas turbine inlet temperature	$1085\,^{\circ}C$
T_{eo}	Gas turbine exhaust temperature	$535\,^{\circ}C$
P_{ro}	Compressor pressure ratio	11.5
γ	Ratio of specific heat	1.4
η_c	Compressor efficiency	0.85
η_t	Turbine efficiency	0.85
R	Speed Regulation	0.04
T_t	Temperature control integration rate	0.469
$T_{c\max}$	Temperature control upper limit	1.1
$T_{c\min}$	Temperature control lower limit	0
$F_{d\max}$	Fuel control upper limit	1.5
$F_{d\min}$	Fuel control lower limit	0
T_v	Valve positioner time constant	0.05
T_{fu}	Fuel system time constant	0.4
T_w	Air control time constant	0.4669
T_{cd}	Compressor volume time constant	0.2
K_0	Gas turbine output coefficient	0.0033
K_1	Steam turbine output coefficient	0.00043
T_g	Governor time constant	0.05
K_4	Gain of radiation shield	0.8
K_5	Gain of radiation shield	0.2
T_3	Radiation shield time constant	15
T_4	Thermocouple time constant	2.5
T_5	Temperature control time constant	3.3
K_3	Ratio of fuel adjustment	0.77
K_6	Fuel valve lower limit	0.23
T_m	Tube metal heat capacitance time constant of waste heat recovery boiler	5
T_b	Boiler storage time constant of waste heat recovery boiler	20
T_i	Turbine rotor time constant	18.5

Table II. Parameters of Three-Phase Synchronous Machine

Symbol	Description	Value
Fr	Rated Frequency	50
Poles	Number of poles of the generator	4
Pf	Rated Power Factor	0.9
V_R	Rated Voltage	11Kv
Pr	Rated output Power in Watt	82.831Mw
Rs	Synchronous Resistance	0.0048
X_d	Direct-Axis Reactance	1.790
Xq	Quadrature-Axis Reactance	1.660
X_{ls}	Leakage Reactance	0.215
H	Interia Constant	3.77
K_A	Gain Constant	50
T_A	Amplifier Time Constant	.06
V_{Rmax}	Maximum Voltage	1
V_{Rmin}	Minimum Voltage	-1
T_E	Exciter Time Constant	0.052
K_E	Exciter Gain	-0.0465
T_F	Field Time Constant	1.0
K_F	Field Gain	0.0832

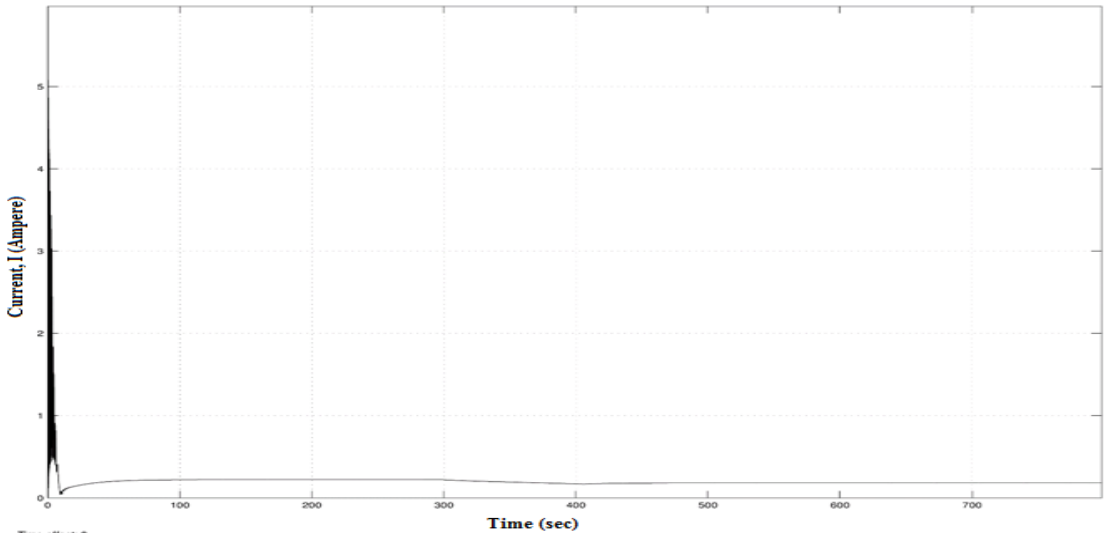

Fig 6. Variation of Current with Time

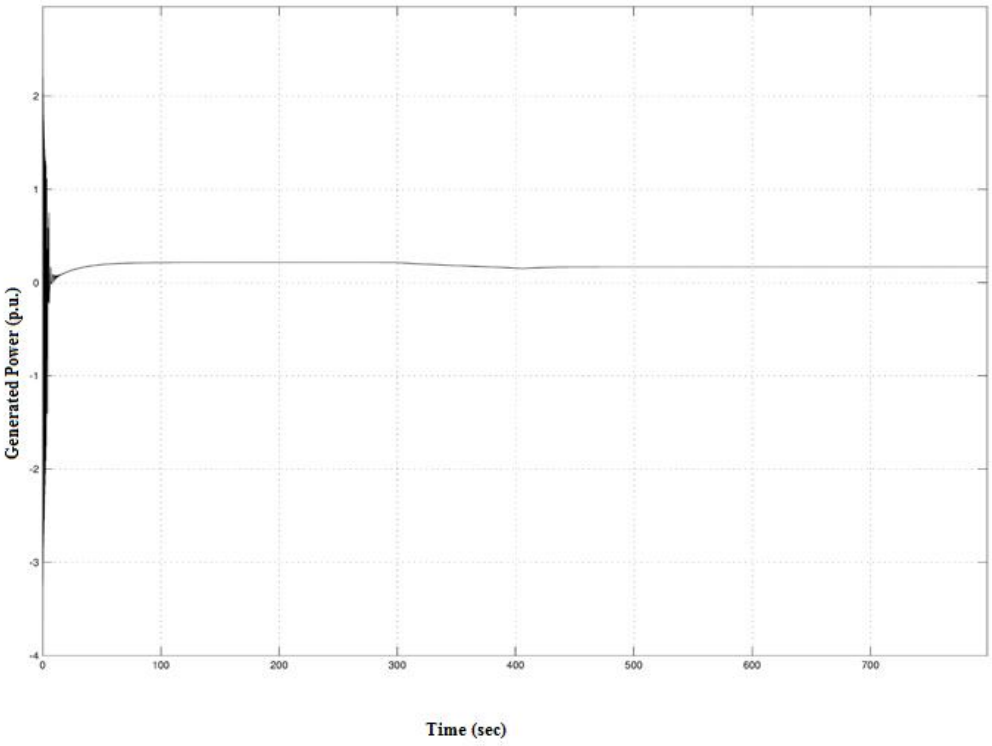

Fig 7. Variation of Generated Power with Time

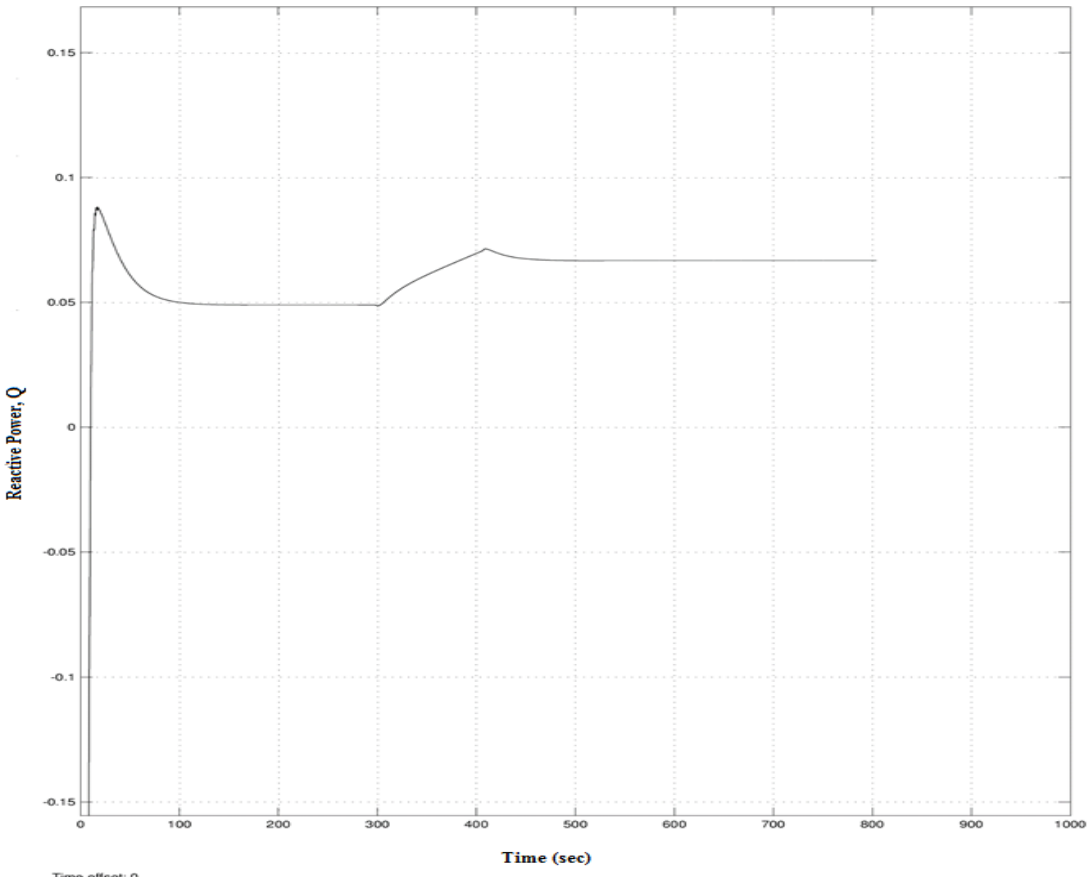

Fig 8. Variation of Reactive Power with Time

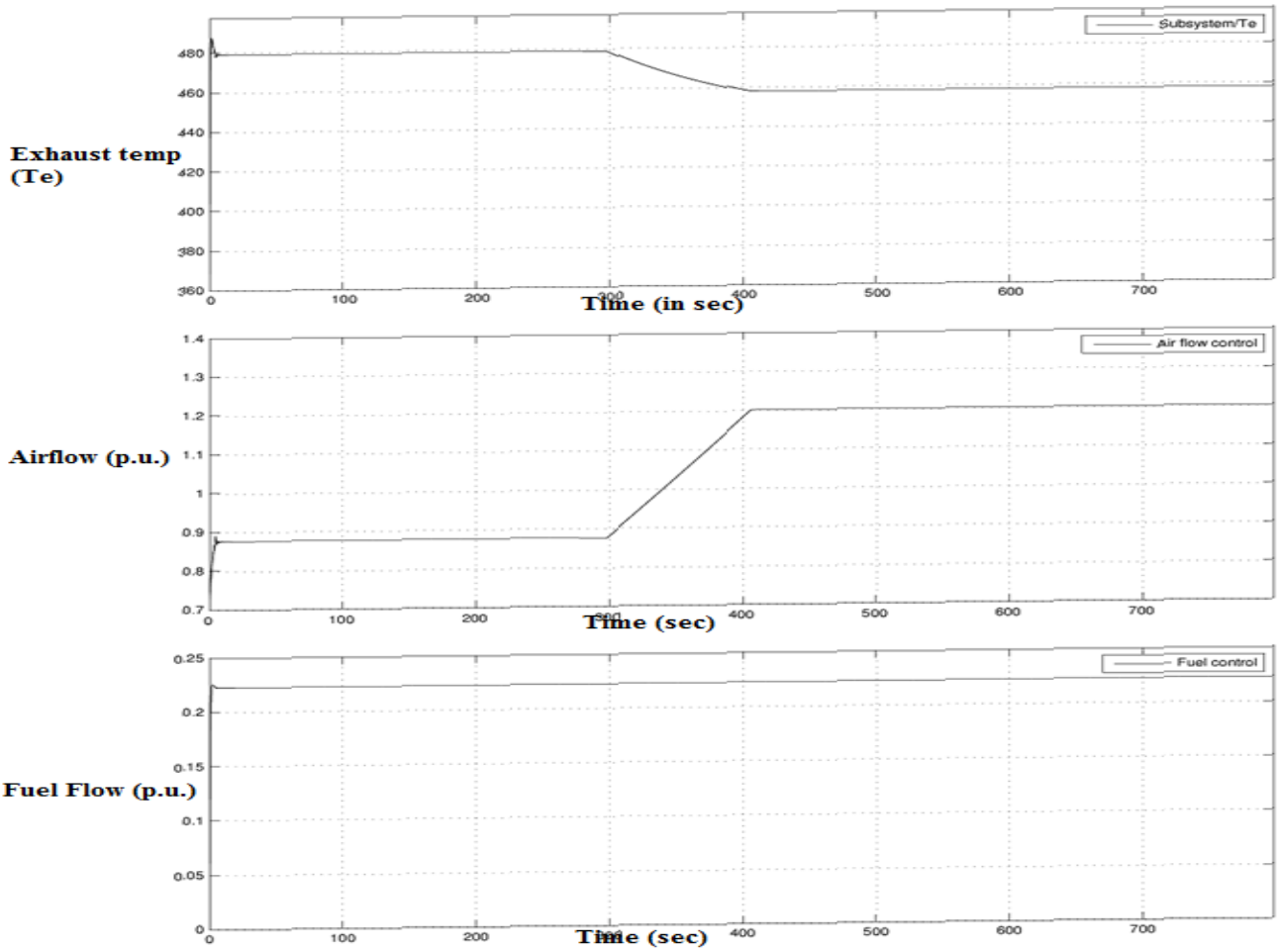

Fig 9. Variation of various System parameters with time

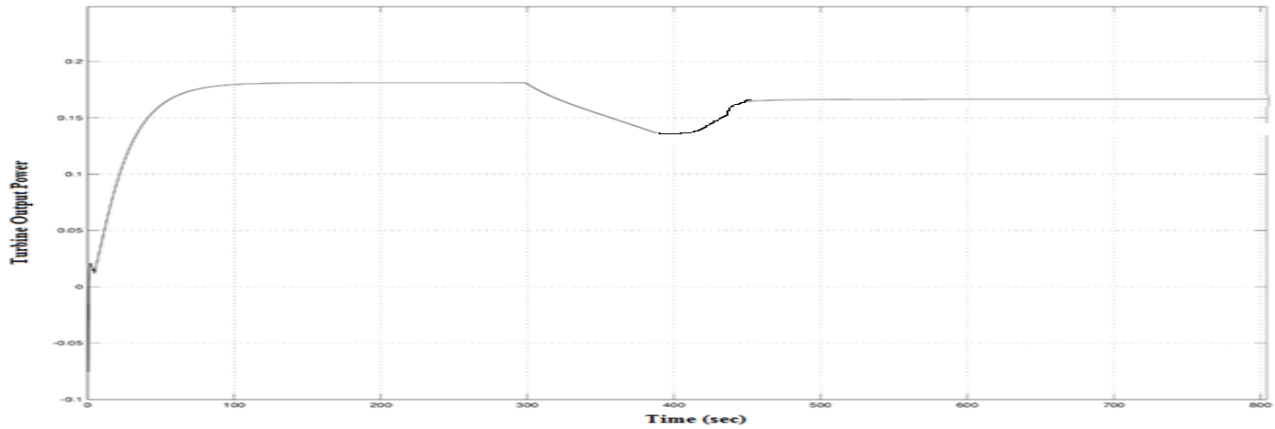

Fig 10. Variation of Turbine Output Power with Time

REFERENCES

[1]N. Kakimoto, K. Baba, , "Performance of gas turbine-based plants during frequency drops," IEEE Transactions on Power Systems,vol.18, pp. 1110- 1115, Aug. 2003.

[2]S. Al-Zubaidy, F.S. Bhinder, "Towards optimizing the efficiency of electrical power generation," Energy Conversion Engineering Conference, vol.3, pp. 1857-1862, Aug. 1996.

[3]K. Kunitomi, A. Kurita, H. Okamoto, Y. Tada, S. Ihara, P. Pourbeik, W. W. Price, A. B. Leirbukt, and J. J. Sanchez-Gasca, "Modeling frequency dependency of gas turbine output," Proc. IEEE/Power Eng. Soc. Winter Meeting, Jan. 2001.

[4]W. I. Rowen, "Simplified mathematical representations of heavy-duty gas turbines," Trans. Amer. Soc. Mech. Eng., vol. 105, pp. 865–869, Oct. 1983.

[5]F. P. de Mello and D. J. Ahner, "Dynamic models for combined cycle plants in power system studies," IEEE Trans. Power Syst., vol. 9, pp. 1698–1708, Aug. 1994.

[6]John H Horlock, "Advanced gas turbine cycles," Pergamon Press, 2003.

[7]Rolf Kehlhofer, Rukes Bert, Hannemann Frank, and Stirnimann Franz. "Combined-cycle gas & steam turbine power plants," PennWell, 2009.

[8]F. Drbal Lawrence, G. Boston Patricia, L. Westra Kayla, Black& Veatch. Power Plant Engineering. p. 241 Springer. 1996.

[9]Rai, J. N., Hasan, N., Arora, B. B., Garai, R., Gupta, R. K., & Kapoor, R. (2013). "Study the Effect of Temperature Control on the Performance of the Output of Combined Cycle Gas Turbine". International Journal of Theoretical and Applied Mechanics, 8(1), 15-23.

[10]J. N. Rai, NaimulHasan, B. B. Arora, Rajesh Garai, Rahul Kapoor, Ibraheem(2013) "Performance Analysis of CCGT Power Plant using MATLAB/Simulink Based Simulation" International Journal of Advancements in Research & Technology, Vol. 2(5), pp. 285-290

[11]Mantzaris, J., &Vournas, C. (2007). Modelling and Stability of a Single-Shaft Combined Cycle Power Plant. International Journal of Thermodynamics, 10(2).

[12]Patel, H., & Agarwal, V. (2008). MATLAB-based modeling to study the effects of partial shading on PV array characteristics. Energy Conversion, IEEE Transactions on, 23(1), 302-310.

[13]González-Longatt, F. M. (2005). Model of photovoltaic module in Matlab. II CIBELEC, 2005, 1-5.

[14]Tsai, H. L., Tu, C. S., & Su, Y. J. (2008, October). Development of generalized photovoltaic model using MATLAB/SIMULINK. In Proceedings of the world congress on Engineering and computer science (Vol. 2008, pp. 1-6).

[15]Rahim, N. A., Saidur, R., Solangi, K. H., Othman, M., & Amin, N. (2012). Survey of grid-connected photovoltaic inverters and related systems. Clean Technologies and Environmental Policy, 14(4), 521-533.

EMPLOYEE SURVEY ANALYSIS (ESA) SCRIPTS YET ANOTHER NATURAL LANGUAGE PROCESSING APPLICATION

[1]Aman Sharma, [2]Anuj Yadav

[1,2] Electronics and Computer Engineering
Dronacharya College of Engineering Gurgaon
Gurgaon, (India)

ABSTRACT

With this paper of our, we have particularly worked on one of the application of Data Analysis. We have proposed a novel method for finding out valuable information out of the bunch of raw data using Python and NLTK libraries. We have processed the Comments of the various Employees of a Company in the form of Raw Data. Each Comment follows different steps such as Cleansing which removes all the mistakes in the comments made by the user, Tagging which tags word according to the different types of verbs or adjectives used in the comments, Chunking which includes selecting a perticualr phrase out of the cleansed comment by use of a appropriate grammar rule, Category Generation which includes different types of category generated for the words which can be used for producing different categories user comments. This includes the use of Python as a tool where NLTk is added as a Natural Language Processor which is used for different kinds of languages. You may find the detailed explanation about our methodologies in the later parts of this paper.

Keywords: Python, NLTK, Tokenizer[8], Lemmatizer[9], Stemmer[9], Chunker, Tagger.

I INTRODUCTION

With the growth of IT sector over the past few years, data handling and its analysis had become very difficult. Many companies deals with a large amount of data and they have purchased different tools from different companies like IBM, Microsoft, etc for data storage and its analysis. Data Analysis basically provides us the method to extract some valuable information out of some raw facts. It contains several fields which are required to be undertaken such as removing all the mistakes, converting it into that form which our tool can understand, stating rules for it usage, finding the outcomes and take supportive actions on the basis of these outcomes. The field of Data Analytics is pity vast and have many approaches related to data extraction and modeling and in this paper we will be discussing on the one of the important application of Data Analytics.Let us better understand what Data Analysis is with example of a person named Lee who had a habit of writing dairy. He started noting each and every incident of his life starting from his birth till now. With the course of time, he have written a lot of information about himself which reflects different stages of his life. Suppose if another person goes through each and every incident of Lee's life and analysis what he used to like when he was below 10 years of age or which part of his life was unforgettable. This analysis of the raw information and find out the valuable information out of it is categorized with the term Data Analytics. I think now we are in a position to understand

the relevant terminologies used in this paper. So I would like to describe the real methodology of our research paper.

II A BRIEF METHODOLOGY

This paper demonstrates a novel method which help user to extract useful information from the bunch of a raw data. It includes a method/ codes which include the use of set of classes and functions which help in extracting a useful data out of input data. There are many useful functions which help in extracting information that are included here. Some of them may be named as, Tokenizer, Taggers, Chunkers, Stemmers, Transformation of Chunkers and Taggers and many more. These methods or classes work on the tool Named as Python 2.7.6 which is required to be downloaded and well configured in the system. Every Code that is executed required to be imported through various packages present in the library. In this project, we have processed the data and produced the different categories out of it and through that we have extracted what user actually meant to say in his/her comments. You may find the detailed explanation as what this paper is all about in later part.

2.1 Python

Python[1] is considered as a high level language, a level ahead of C and C++. It is basically developed for developing applications or scripts for transforming different forms of languages like English, French, German and many more. Python have a unique feature which differentiate it from other languages like C, C++ or java is that it uses white space indentation rather than curly brackets. Currently, the latest version of python in the market is Python 3.4.1 was released on May 18th, 2014. But we have used Python 2.7.6 .

2.2 NLTK

NLTK[3] is described as Natural Language Tool Kit. It comprises of library files in different languages that Python may use for data analysis. One is required to import the NLTK package in the Python Shell so that its library files can be used by the programmer. NLTK includes several features like graphical demonstration of data. Several books have been published on the exotic properties and facilities of NLTK which clearly explains things off to any programmer who is either beginner with python or NLTK or just an expert. NLTK finds several applications in research work when it comes to Natural Language Processing. It helps in processing text in several languages which itself is a big positive for modern researchers.

III IMPLEMENTATION OF EMPLOYEE SURVEY ANALYSIS (ESA) SCRIPTS

3.1 What's the Requirement of ESA Scripts.

In Today's world of Globalization and competitions, It is the trend which is followed by every company to organize a Engagement and Exit Survey for its employee within the organization to find out the reasons why people wants to join or leave their company. When any person leaves any company, he/she is required to fill an online survey that comprises of various fields which might be the reasons for his leaving the Organization. In that survey, the questions might be in various forms like Check Boxes, Scroll List, Text plain, etc. It is pity easy to record and analysis those questions which involve answering through Checkboxes or Scroll List but situation becomes very hectic for the person who is analyzing that data if the answer is recorded through Text plains or Text Paragraph. When talking about manually reading, the person, who is reading that data, will be required to go through each and every employees comments to find what were the reasons why they have left the job. Each

company comprises of thousands of employees and it is very common in industries that people moves from one organization to another organization. So, keeping the track of all those employees by just manual reading is a tough task.

Figure 1 – A Screen Shot of Employee Exit Survey[1]

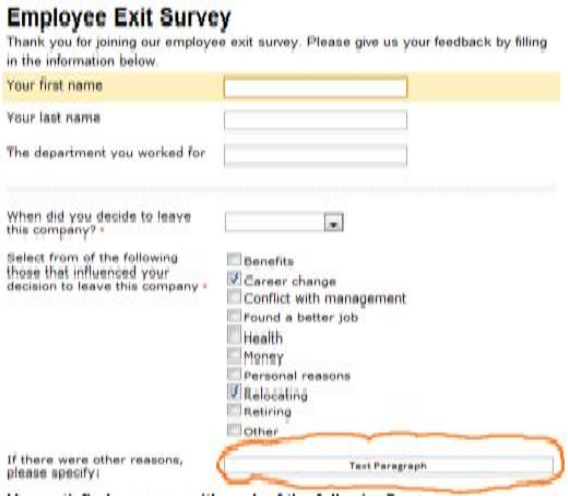

Each company spends a lot of money and resources on their employees on their training and growth and therefore, wants to find the reasons why their best employees are leaving them. Thus, we are in an urgent need of something which can help us finding the reasons why any person is leaving his/her organization. Although, there are several tools in the market by some remarkable companies like IBM. But the major point is they all are paid and hence, require a lot of money to invested to purchase them. In comparison with these paid tools, these Python Script are open source and are free of cost. Any organization can also make changes in the scripts according to its requirement. Hence, it is providing us the best reason why to opt for ESA Scripts.

3.2 Functionality of ESA Scripts

ESA Scripts performs following actions as specified below:-

- It corrects all the Spelling Mistakes.
- It corrects all the Repeated Words.
- It performs Lemmatization, Stemming and Tokenization of Data.
- It performs Antonyms and Synonym Operations on words.
- It find out what kind of Verb, Noun or Adjective is used by the Employee.
- It generates Phrases depending upon the type of Grammar Rule one select.
- Removal of Stop Words.
- Encryption and Decryption of Special Stop Words.
- Removal of ASCII Codes.

There are many more important operations which comes under these above specified operations which are discussed later as their roles comes.

3.3 Next Big Step

First of all, Comments of different employees are taken in a single Column of a CSV file and read line wise. Each Comment comprises of different paragraph having different Spelling mistakes, repeated characters in a word and many more mistakes which are required to be removed before we can find out what person meant in his/her reasons for leaving his/her job.

All the files are required to be stored by .py extension and all the important methods or classes are required to be defined in a single library file so that when using those functions and classes we can import them in a go and use them to do whatever we like to do. These methods/classes are defined in library file named as CustomClassLibrary.py and this file is required to be executed at the top before using any of the function or class so that these classes work accordingly whenever they are called in the main script.

There is yet another important thing that we are required to take care of. You must either place all you scripts in the current working directory or you must provide the path where you have placed your scripts. It is highly required and if we do not provide the path of our scripts properly then it will be going to show errors which will return an error that current file do not exist in our directory.

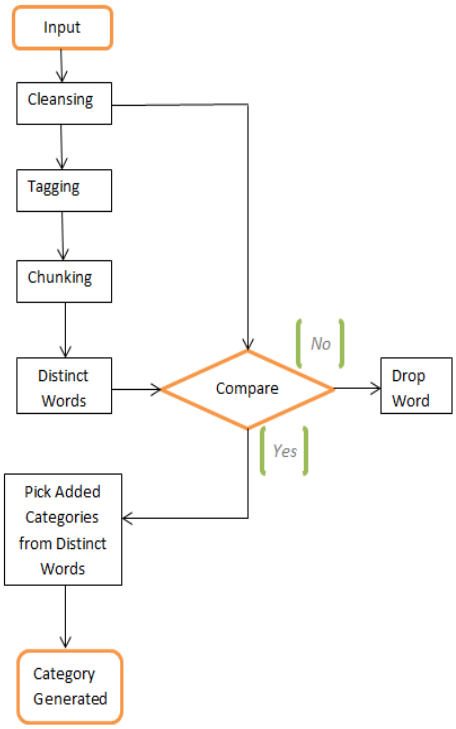

Figure-2 Block Diagram Representing Various Processes to be followed

This Purpose has been divided into 3 Categories which are as follows:

a. Cleansing.

b. Tagging and Chunking[12].

c. Category Generation.

The above described description can be better explained by the figure given below.

3.4 Cleansing

Cleansing, as its name suggests includes the methods which help in cleaning the data which the user has provided. It includes those methods or functions by which one can tokenize data, correct the spellings, remove all the repeated words like if any user wrote 'love' as 'llooovvvee' in a very passionate mode. So they are required to be corrected. There are several Abbreviations that people wrote which are required to be changed to their normal word form. Then there are several stop words in the sentences which do not contribute much to the meaning of that sentence are therefore required to be removed from that sentence. The procedure of this is explained as below. First of all, we break Paragraph into Sentences and in that procedure some of the words are changed into ASCII Codes which created problem when we further run the process on them and are required to be removed through strip_unicode command. After removing ASCII Codes we tokenize Sentences into words.
Now, explaining each category in detail below.

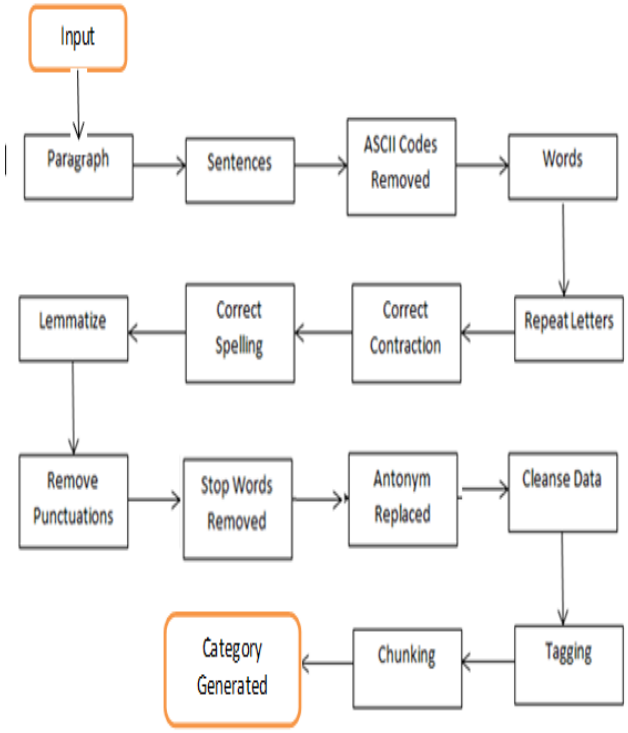

Figure-3 Step wise Explanation for Above Process

These words are processed and all the repeated words like "looovvee" are changed to "love" by using repeat replacer function. After that all the short forms or the Abbreviations are changed to their full forms. All the spelling mistakes are required to be corrected before proceeding further. This function is imported using import command and all the methods are required to be defined in our library file named as CustomClassLibrary.py After correcting all of our spelling mistakes, we lemmatize our word if they are found to be of Noun, Adjective or Verb. For any other category of words, it going to pass the word as it is. After that all the punctuations are removed such as Commas, Exclamation mark, Full Stops, etc.

Here, now we are required to encrypt some of the special words so that they can be used in upcoming process. We will be encrypting some of the words and them removing stop words from that list of words. All those word which do not help in analyzing the sentences like can, could, might, etc are removed from the list of words. Once, Stop words removed, we again decrypt those special words again so that they can be processed now. At

this step, we have got the list of words which are going to be passed to do Antonym of words which appears after "not" word.

For Example, "let's", "not", "uglify", "our", "code" is changed to "let's", "beautify", "our", "code". Thus, we are there with our Cleansed Data.

3.5 Tagging and Chunking

Tagging is a process of allotting different tags to the word in accordance with the part of speech tagging. For this, we have used Classifier based POS tagger[5][10] which is quite a good tagger. When calculated, its efficiency comes out to be over 90% which is quite good. For tagging, we passed the data word wise and find out to which part of speech category it belongs. Either it is a noun or it is a verb or adjective like vise.

We are doing tagging in order to generate tagged word from where we can create a grammar rule so that from them, all the words which comes, forms a meaningful phrase and thus can be wrote in different file.

IV GRAMMAR RULE[11] AND CHUNKING

4.1 Chunk Rule NP

{<RB|DT|NN.|VB.*>?<VB.*>?<.*>?<JJ.*>?<JJ.*|NN.?>+}*

This Chunk Rule can be described as the phrase formed will begin with optional Adverb or Determiner or any kind of Noun or any kind of Verb followed by any kind of optional Verb followed by optional any word followed by any kind of optional Adjective and ending with as many number of any kind of Adjective or any kind of Noun.

4.2 Category Generation

	A	B
1	**Word**	**Category**
2	abuse	harassment
3	attack	harassment
4	attitude	harassment
5	baby	personal/family reasons
6	child	personal/family reasons
7	career	lack of growth opportunities/promotion
8	branch	Location issues
9	building	Location issues
10	coffee	stress at work
11	department	work environment
12	dollar	dissatisfaction with salary/benefits
13	economy	dissatisfaction with salary/benefits
14	position	lack of growth opportunities/promotion
15	post	lack of growth opportunities/promotion
16	compassion	stress at work
17	debate	work environment
18	department	work environment

Figure-3 Distinct Categories defined for Chunked words

For Category Generation, we have selected those set of tokenized words which are generated from chunked output. These words are written separately in different file and we manually create category for that. Like if "salary" appears in the file then we have created its category as "salary problem" likewise if "family" appears in the word then we generated its category as "Personal Issues". Once this file is created then we compare each and every word of the file and if we find that word in our distinct words file then we are going to generate that category for that word.

Once the category is generated, this category is used to produce the results for the different comments made by user. It is here shown in the figure below.

	A	B	C
1	Input Text	Category	Mapping Word
2	"I have been with this company for the very long time. This job could never fullfil my desires for the better career position thats why i am resigning",	lack of growth opportunities/promotion	career
3	"I have been with this company for the very long time. This job could never fullfil my desires for the better career position thats why i am resigning",	lack of growth opportunities/promotion	position
4	I did't feel very good about what Income i was earning here. My income was low. When i shared this with higher management, It didn't bother them. I also wanted to get my shift timings changed as I was not able to spend time with my girlfriend, but my manager did not change my timings.	work environment	girlfriend
5	I did't feel very good about what Income i was earning here. My income was low. When i shared this with higher management, It didn't bother them. I also wanted to get my shift timings changed as I was not able to spend time with my girlfriend, but my manager did not change my timings.	dissatisfaction with salary/benefits	income
6	I did't feel very good about what Income i was earning here. My income was low. When i shared this with higher management, It didn't bother them. I also wanted to get my shift timings changed as I was not able to spend time with my girlfriend, but my manager did not change my timings.	my manager/supervisor	management
7	I did't feel very good about what Income i was earning here. My income was low. When i shared this with higher management, It didn't bother them. I also wanted to get my shift timings changed as I was not able to spend time with my girlfriend, but my manager did not change my timings.	work schedule/shift timing	shift
8	My spouce is not well and is hospitalised, so I need to take care of her.	personal/family reasons	spouse
9	I did not see a good work here in this organisation. I was expecting some other good work here as per my experience. I am not seeinf any learning here. I would like to seek some other oppertunity in other company rather than wasting my time here.	Quality of work	experience
10	I did not see a good work here in this organisation. I was expecting some other good work here as per my experience. I am not seeinf any learning here. I would like to seek some other oppertunity in other company rather than wasting my time here.	Lack of coaching/learning	learning
11	I did not see a good work here in this organisation. I was expecting some other good work here as per my experience. I am not seeinf any learning here. I would like to seek some other oppertunity in other company rather than wasting my time here.	lack of growth opportunities/promotion	opportunity

Figure-4 Categories Generated for different Employees comments

V APPLICATION OF EMPLOYEE SURVEY ANALYSIS (ESA) SCRIPTS

We can do sentimental analysis using this application.

Sentimental Analysis[7]- This is a process of analyzing the sentiments of a person, be it positive, negative or mixed emotions. We can use the same application for other domains as well like engagement of an employee with the organization.

VI CONCLUSION

This Paper provides a innovative idea which helps in reducing the human efforts as person who is analyzing the data of various employees who had left as now, is not required to go through each and every employee's comments. Thus, by running these scripts we will be able to generate what an employee is talking about, what are the various causes which he found in the company which forced him to resign. Hence, the value of this product goes up when you think analyzing the data of different users of different countries following different languages.

REFRENCES

[1] http://123facebooksurveys.com/wp-content/uploads/2011/10/employee-exit- interview-1.png.

[2] http://en.wikipedia.org/wiki/Python_(programming_language).

[3] https://www.python.org/download/releases/3.4.1/.

[4] http://www.nyu.edu/projects/politicsdatalab/workshops/NLTK_Presentation.pdf.

[5] https://www.packtpub.com/sites/default/files/3609-chapter-3-creating-custom-corpora.pdf.

[6] http://caio.ueberalles.net/ebooksclub.org__Python_Text_Processing_with_NLTK_2_0_Cookbook.pdf.

[7] http://fjavieralba.com/basic-sentiment-analysis-with-python.html.

[8] https://www.ics.uci.edu/~pattis/ICS-31/lectures/tokens.pdf

[9] http://nlp.stanford.edu/IR-book/html/htmledition/stemming-and-lemmatization-1.html.

[10] http://www.monlp.com/2011/11/08/part-of-speech-tags/

[11] http://danielnaber.de/languagetool/download/style_and_grammar_checker.pdf.

[12] http://www.eecis.udel.edu/~trnka/CISC889-11S/lectures/dongqing-chunking.pdf.

DUAL MODE BIQUADRATIC FILTER USING SINGLE VDTA

Navin Singhal[1] Rajeshwari Pandey[2] Neeta Pandey[3]

[1, 2, 3] *Department of Electronics and Communication, Delhi Technological University, Bawana Road, Delhi, (India)*

ABSTRACT

This paper presents a dual-mode biquad filter configuration using single voltage differencing transconductance amplifier (VDTA), three capacitors and two resistors. The proposed filter can be configured as voltage mode (VM) or current mode (CM) structure with appropriate input excitation choice and can be used to synthesize low pass (LP), high pass (HP) and band pass (BP) filter functions. The natural frequency (ω_0) and the quality factor (Q_0) of the proposed topology can be ortogonally tuned. The theoretical propositions are validated through SPICE simulations using 0.18 μm TSMC CMOS process parameters.

Keywords: VDTA, Voltage Mode, Current Mode, Filter, Signal Processing.

I. INTRODUCTION

The voltage differencing transconductance amplifier (VDTA) has emerged as an alternate analog building block (ABB) in recent past [1, 2] since it inherits all the advantages offered by current mode techniques [3]. It has been successfully used as an ABB for realizing a number of analog signal processing and generation circuits [1,2,4-10]. Several VDTA based filter circuits have been reported in the literature [1,2,6-10]. These structures can be classified as multiamplifier [2,8,10] or single amplifier based structures [1,6,7,9]. For the applications having power consumption as an important design constraint, single active element based filters are the useful choice. A detailed study of the existing literature on single VDTA based filters shows that

- Independent adjustment of ω_0 and Q_0 is not possible [1,7.9] in single VDTA based filters without using external resistor.

- Either VM [1, 10] or CM [2,6-9] outputs is provided by the existing structures

Therefore in this paper a single VDTA based dual-mode filter is proposed which can be used for either of the voltage or current mode operation with independently controllable ω_0 and Q_0.

II. THE PROPOSED CIRCUIT

The circuit symbol of the VDTA is shown in Fig. 1, where VP and VN are input terminals and Z, X+ and X- are output terminals. All terminals exhibit high impedance values. Using standard notation, the terminals relationship of an ideal VDTA can be written as:

$$\begin{bmatrix} I_{Z+} \\ I_{Z-} \\ I_{X^+} \\ I_{X^-} \end{bmatrix} = \begin{bmatrix} g_{m1} & -g_{m1} & 0 & 0 \\ -g_{m1} & g_{m1} & 0 & 0 \\ 0 & 0 & g_{m2} & 0 \\ 0 & 0 & -g_{m2} & 0 \end{bmatrix} \begin{bmatrix} V_{VP} \\ V_{VN} \\ V_{Z^+} \\ V_{Z^-} \end{bmatrix} \quad (1)$$

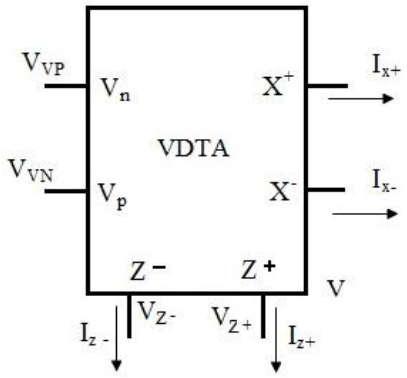

Fig. 1 Circuit symbol of VDTA

The CMOS realization of the VDTA [2] is shown in Fig. 2 and is based on two Arbel-Goldminz transconductances [11]. Input and output transconductance parameters of VDTA element, represented as g_{m1} and $g_{m2,}$ can be expressed as :

$$g_{m1} = \frac{g_1 g_2}{g_1 + g_2} + \frac{g_3 g_4}{g_3 + g_4} \quad (2)$$

$$g_{m2} = \frac{g_5 g_6}{g_5 + g_6} + \frac{g_7 g_8}{g_7 + g_8} \quad (3)$$

where, g_i is the transconductance value of the i-th transistor and is given by

$$g_i = \sqrt{\mu C_{ox} \left(\frac{W}{L}\right)_i I_{Bi}} \quad (4)$$

In (4) μ is effective carrier mobility; C_{ox} is the gate oxide capacitance per unit area, I_{Bi} represents the dc bias current and $(W / L)_i$ is the aspect ratio of the i-th MOS transistor.

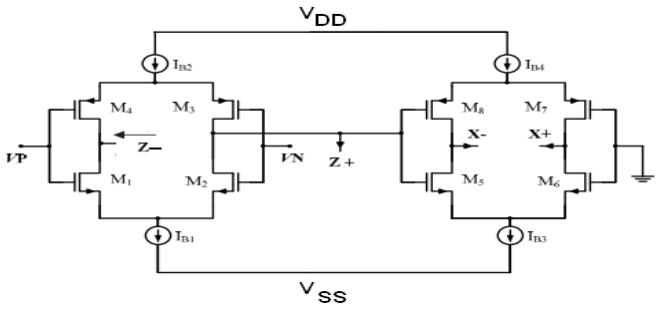

Fig. 2 The CMOS realization of the VDTA [2]

The proposed dual mode biquad filter is shown in Fig. 3 which uses single VDTA, two resistors and three capacitors. The proposed filter can be configured as VM or CM structure with appropriate input excitation choice and can be used to synthesize LP, HP and BP filter functions. Circuit analysis yields voltage-mode and current mode biquad transfer functions respectively as given by (5) – (10).

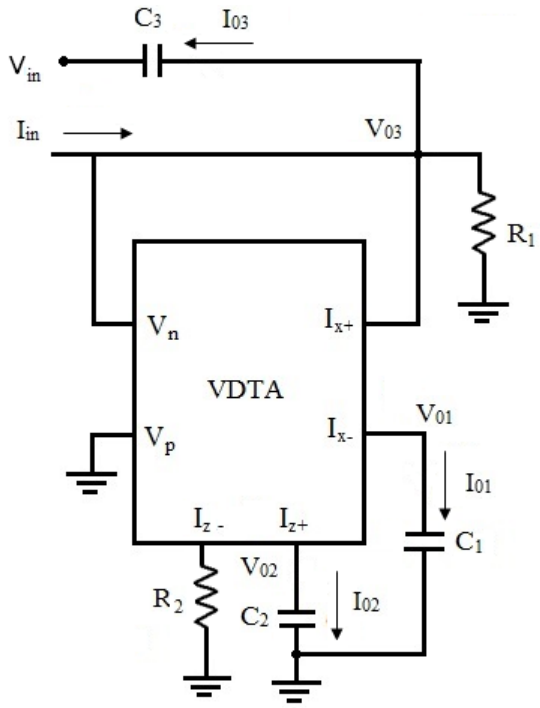

Fig. 3 The Proposed Dual Mode Biquad

2.1 Voltage Mode

The proposed configuration will work in voltage mode if I_{in} is removed and the transfer functions at various nodes can be derived as:

$$\left.\frac{V_{01}}{V_{in}}\right|_{LP} = \frac{-\frac{g_{m1}g_{m2}}{C_1C_3}}{s^2 + \frac{s}{R_1C_2} + \frac{g_{m1}g_{m2}}{C_2C_3}} \tag{5}$$

$$\left.\frac{V_{02}}{V_{in}}\right|_{BP} = \frac{\frac{g_{m1}}{C_1}s}{s^2 + \frac{s}{R_1C_2} + \frac{g_{m1}g_{m2}}{C_2C_3}} \tag{6}$$

$$\left.\frac{V_{03}}{V_{in}}\right|_{HP} = \frac{-g_{m1}R_3s^2}{s^2 + \frac{s}{R_1C_2} + \frac{g_{m1}g_{m2}}{C_2C_3}} \tag{7}$$

2.2 The CM Configuration

Removing voltage source V_{in} in Fig. 3 leads to CM operation of the filter.Using routine analysis the following transfer functions are obtained:

$$\left.\frac{I_{01}}{I_{in}}\right|_{LP} = \frac{\frac{g_{m1}g_{m2}}{C_2C_3}}{s^2 + \frac{s}{R_1C_2} + \frac{g_{m1}g_{m2}}{C_2C_3}} \tag{8}$$

$$\left.\frac{I_{02}}{I_{in}}\right|_{BP} = \frac{\frac{g_{m1}}{C_1}s}{s^2 + \frac{s}{R_1C_2} + \frac{g_{m1}g_{m2}}{C_2C_3}} \tag{9}$$

$$\left.\frac{I_{03}}{I_{in}}\right|_{HP} = \frac{s^2}{s^2 + \frac{s}{R_1C_2} + \frac{g_{m1}g_{m2}}{C_2C_3}} \tag{10}$$

The natural frequency ω_0 and quality factor Q_0 for both voltage and current mode is same and are given as follows

$$\omega_0 = \sqrt{\frac{g_{m1}g_{m2}}{C_2C_3}} \tag{11}$$

$$Q_0 = R_1\sqrt{\frac{g_{m1}g_{m2}C_2}{C_3}} \tag{12}$$

III. TRACKING ERROR

Considering the non-ideal characteristics of the VDTA, the port relations of current and voltage in equation (1) get modified as:

$$\begin{bmatrix} I_{Z+} \\ I_{Z-} \\ I_{X^+} \\ I_{X^-} \end{bmatrix} = \begin{bmatrix} \beta_1 g_{m1} & -\beta_1 g_{m1} & 0 & 0 \\ -\beta_1 g_{m1} & \beta_1 g_{m1} & 0 & 0 \\ 0 & 0 & \beta_2 g_{m2} & 0 \\ 0 & 0 & -\beta_2 g_{m2} & 0 \end{bmatrix} \begin{bmatrix} V_{VP} \\ V_{VN} \\ V_{Z^+} \\ V_{Z^-} \end{bmatrix} \tag{13}$$

where β_1 and β_2 respectively are the tracking errors for the first and second stages of the VDTA. Re-analysis the proposed circuit of Fig.3 using above equation yields the following non-ideal filter parameters.

$$\omega_0 = \sqrt{\frac{\beta_1\beta_2 g_{m1}g_{m2}}{C_2C_3}} \tag{15}$$

$$Q_0 = R_1\sqrt{\frac{\beta_1\beta_2 g_{m1}g_{m2}C_2}{C_3}} \quad (16)$$

It is evident that the values of ω_0, and Q_0 may be slightly changed by the effect of the VDTA's tracking errors. However, the small deviation can be minimized by properly adjusting the VDTA's transconductance values.

IV. SIMULATION RESULTS

The proposed dual mode structure is verified through SPICE simulations using TSMC CMOS 0.18 µm process parameters. The aspect ratios of the transistors as used are given in Table 1[2]. Supply voltages are taken as V_{DD} = −V_{SS} = 0.9 V and the bias currents are taken as I_{B1} = I_{B2} = I_{B3} = I_{B4} = 150 µA. The DC transfer characteristic of the VDTA is shown in Fig. 4 and the simulated transconductance values of VDTA are observed to be g_{m1} = g_{m2} = 636.3 µA/V.

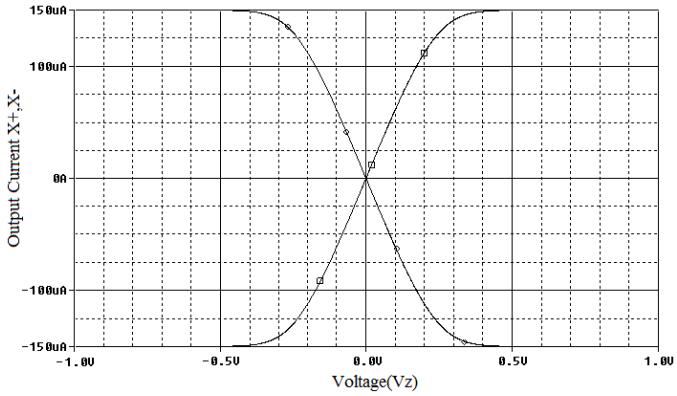

Fig. 4 The DC Transfer Characteristic Of The VDTA

The proposed circuit of Fig. 3 is simulated with the following passive element values C_1=C_2=C_3 = 1nF, R_1 R_2=1KΩ which results in f_0 = 101.27 KHz and Q_0 = 0.636. The frequency responses of voltage-mode and current mode filters, plotted by selecting voltage and current excitation respectively, are shown in Fig. 6(a) and (b) respectively.The simulated results are found in close agreement to the theoretical values.

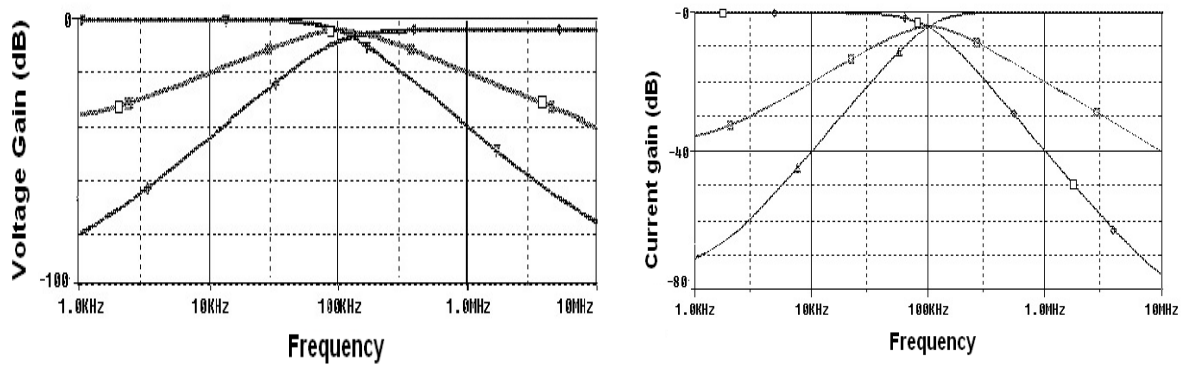

(a) (b)

Fig. 6. Frequency Response (a) Voltage Mode (b) Current Mode

V. CONCLUSION

A single VDTA based dual mode filter is presented in this paper which provides either of the voltage or current mode output with due selection of input excitation. The proposed filter provides LP, HP and BP responses simultaneously.The filter parameters namely ω_0 and Q_0 of the proposed topology can be ortogonally tuned. The theoretical propositions are validated through SPICE simulations using 0.18 μm TSMC CMOS process parameters.

REFERENCES

[1] D. Biolek and M. Shaktour, V. Biolkova and Z. Kolka, Current-Input Current-Output Universal Biquad Employing Two Bulk-Driven VDTAs, in proceeding of IV International Congress on Ultra Modern Telecommunications and Control Systems

[2] 2012A. Yesil, F. Kacar and H. Kuntman, New simple CMOS realization of voltage differencing transconductance amplifier and its RF filter application. Radioengineering, vol. 20, no. 3, p. 632-637, September, 2011.

[3] C. Toumazau, F. J. Lidgey and D. G. Haigh, Analogue IC Design: The Current-Mode Approach, Peter Peregrinus Limited, London, 1990.

[4] D. Prasad and D.R. Bhaskar, Electronically controllable explicit current output sinusoidal oscillator employing single VDTA, ISRN Electron. 2012 (2012) 5, http://dx.doi.org/10.5402/2012/382560.

[5] N. Herencsar, R. Sotner, J. Koton, J. Misurec and K. Vrba, New compact VM four phase oscillator employing only single Z-copy VDTA and all grounded passive elements, Electron. Electric. Eng. 19 (10) (2013) 87–90.

[6] D. Prasad, D. R. Bhaskar and M.Srivastava, Universal Current-Mode Biquad Filter Using a VDTA, Circuits and Systems, 2013, 4, 29-33

[7] J. Satansup and W. Tangsrirat, Single VDTA-based current-mode electronically tunable multifunction filter in Proceedings of the I-SEEC 2012, Petchburi,Thailand, 2012, pp. 266–272.

[8] J. Satansup, T. Pukkalanun and W. Tangsrirat, Electronically Tunable Current-Mode Universal Filter Using VDTAs and Grounded Capacitors, in Proceedings of the International MultiConference of Engineers and Computer Scientists 2013 Vol II, IMECS 2013, 2013, Hong Kong.

[9] J. Satansup and W.Tangsrirat, Compact VDTA-based current-mode electronically tunable universal filters using grounded capacitors, Microelectronics Vol. 45, Issue 6, June 2014, Pages 613–618

[10] J. Satansup, T. Pukkalanun and W, Tangsrirat, Electronically Tunable Single-Input Five-Output Voltage-Mode Universal Filter Using VDTAs and Grounded Passive Elements Circuits, Systems, and Signal Processing June 2013, Vol. 32, Issue 3, pp 945-957

NOVEL OSCILLATORS IN SUBTHRESHOLD REGIME

Neeta Pandey[1], Kirti Gupta[2], Rajeshwari Pandey[3], Rishi Pandey[4], Tanvi Mittal [5]

[1, 2,3,4,5] *Department of Electronics and Communication Engineering,*
Delhi Technological University, Delhi, (India)

ABSTRACT

In this paper, the implementation of oscillators in the subthreshold region is proposed. The ring and coupled ring oscillators are implemented. The techniques of swapped body biasing (SBB) and Dynamic threshold Voltage MOSFET (DTMOS) biasing are introduced for performance improvement of coupled ring oscillators. The functionality of the oscillators in subthreshold region is verified through simulations using 180 nm CMOS technology parameters. A comparison in performance of the oscillators is carried out. It is found that coupled ring oscillator based on the two biasing techniques shows improved performance.

Keywords: Coupled Ring Oscillator, Dynamic Threshold Voltage MOS Biasing, Ring Oscillator, Subthreshold Region, Swapped Body Biasing.

I. INTRODUCTION

The development of the applications demanding low energy application has generated significant scope for subthreshold circuits [1-5]. These circuits are suitable for two type of portable devices. There are energy constraint systems at one hand where the aim is energy conservation and speed of operation is largely irrelevant. The other application need high performance for fraction of time they are operational and spend significant time in non-critical tasks. The mobile phone is apparent example of the later class as it often remains in near idle computation mode while waiting for input from wireless link or user. Oscillator is a key component in a phase-locked loop (PLL) for providing the timing basis in clock control, data recovery, and synchronization [6]. It is also an integral part of voltage controlled oscillator which is employed in a wide variety of applications such as disk-drive read channels, on-chip clock distribution, integrated frequency synthesizers and microprocessor clock generation [7]. This paper proposes the implementation of two ring oscillators in subthreshold region. The first implementation uses a chain of odd numbers of CMOS inverters operating in subthreshold region. In the second implementation, a coupled ring oscillator [6] capable of producing quadrature outputs is proposed. The paper first briefly presents the operation of a MOSFET in subthreshold region in section II. The implementations of the ring and coupled ring oscillators in subthreshold region are presented in the section III. The different biasing techniques used for implementation are described briefly in section IV. The simulation results are presented in section V using CMOS 180nm technology parameters. The conclusion drawn from the results appear in section VI.

II. SUBTHRESHOLD DIGITAL DESIGN

The surface of the Metal-Oxide Semiconductor (MOS) structure is weakly inverted when the gate voltage is sufficient to cause band bending at the surface ranges between φF and 2φF. This region is also called subthreshold and current flows when drain to source potential is applied. The current flow mechanism is similar to that in bipolar transistors i.e. drain current shows exponential dependence on gate to source voltage. This current is called subthreshold current and is primarily a leakage current which flows even when gate to source voltage is below threshold voltage.

In the subthreshold, the power supply voltage VDD is made less than its threshold voltage V_{th}. In this case, the drain current I_{ds} region is exponentially related to the gate voltage V_{gs} as shown in Equation (1) [3]:

$$I_{sub} = I_0 \exp\left(\frac{V_{gs} - V_T}{nV_{th}}\right)\left(1 - \exp\left(\frac{-V_{ds}}{V_{th}}\right)\right) \qquad (1)$$

where V_{gs} is the gate-to-source voltage, V_{ds} is the drain-to-source voltage, n is the subthreshold slope factor and V_{th} is temperature equivalent of voltage (V_{th} = kT/q, where k is the Boltzmann constant, T the absolute temperature, and q the electron charge. The factor n of a long-channel uniformly doped device is calculated as:

$$n = 1 + \frac{C_b}{C_g} \qquad (2)$$

where C_g and C_b are the gate and bulk capacitances respectively.

A MOSFET operating in subthreshold region offers several advantages. The MOSFETs operating in this region generate low levels of the drain current, thereby creates a high-value resistor. These MOSFETs show low dynamic power consumption due to the lowering of power supply and the drain current [5]. Based on these advantages, we propose the implementation of ring oscillators in the subthreshold region.

III. RING OSCILLATOR

A ring oscillator (RO) is one of the most commonly used components in many integrated systems. The unique features of RO include ease of design with the state-of-art integrated circuit technology (CMOS, BiCMOS), ability to oscillate at lower values of voltage, high frequency oscillations can be achieved, electrically tunable with wide tuning range; attainment of multiphase outputs. Two popular implementations of a ring oscillator have been used in this paper. An RO is a cascade of odd number of delay stages connected in a close loop chain. Fig. 1 shows the traditional CMOS inverter and a ring oscillator using seven inverters. The frequency of oscillation of an RO varies with propagation delay τd of the individual inverter stage and the number of inverter stages used in the ring structure. There must be a phase shift of 2π and unity voltage gain at the oscillation frequency to achieve self-sustained oscillation. In a RO with m inverter stages, a phase shift of π/m is provided by each stage while the remaining phase shift of π is provided by the dc inversion. The signal undergoes m delay

stages in a time of $m\tau d$ to provide a phase shift of π and for another time in a time period of $2m\tau d$ to obtain the remaining phase of π [8]. Therefore, the frequency of oscillation *fo* can be found out using (3):

$$f_o = \frac{1}{2m\tau d} \quad (3)$$

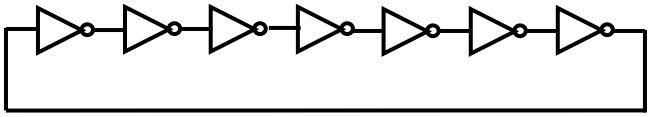

Fig. 1. Ring Oscillator with 7 inverter stages

A coupled ring oscillator (CRO) is designed by coupling two ring oscillators in such a way that only four distinguished nodes are formed. These four nodes generate quadrature outputs having a phase difference of 900 for a completely symmetrical coupling [6]. The implementation of a coupled ring oscillator employing 8 inverter stages is shown in Fig. 2.

IV. BODY BIASING TECHNIQUES

A CMOS inverter operating in the subthreshold region suffers from a drawback of reduced switching speed. This can be addressed by adopting body biasing techniques such as the swapped body biasing (SBB) [9] and the dynamic threshold MOS (DTMOS) biasing technique [10]. In SBB technique, the substrate of the NMOS devices are tied to the power supply voltage V_{DD} whereas those of the PMOS devices are tied to ground. Swapping the bulk terminals of the two MOSFETs increases the drive currents in the subthreshold operation from an exponential current increase, but degrades output node voltages when V_{DD} is greater than the zero bias threshold voltage [5]. Thus, SBB technique provides improved performance under subthreshold supply voltages. A CMOS inverter implemented using SBB technique is shown in Fig. 3. In DTMOS biasing technique, the substrate of the transistor is tied to its gate to allow the threshold voltage to change dynamically with the gate input voltage. With the increase in the gate voltage, the threshold voltage drops resulting in a much higher current drive than standard MOSFET for low-power supply voltages. A CMOS inverter implemented using DTMOS biasing technique is shown in Fig. 4. In this paper, the coupled ring oscillator (Fig. 2) is implemented using inverters with traditional biasing (Fig. 1), SBB (Fig. 3) and DTMOS biasing (Fig. 4).

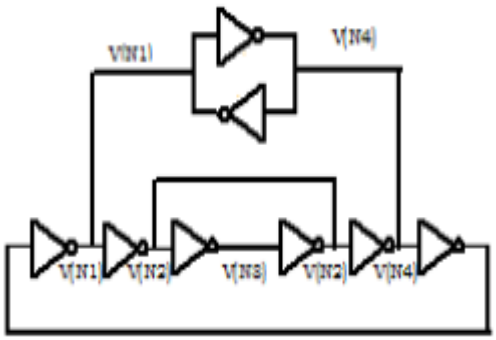

Fig. 2. Coupled Ring Oscillator Two Coupled 3-Stage Ring Oscillator

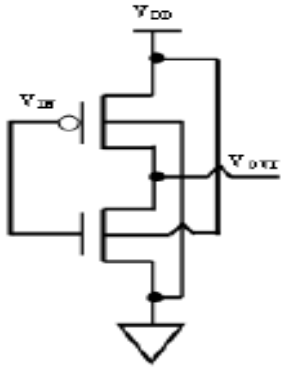

Fig.3. A CMOS Inverter Based On Swapped Body Biasing Technique

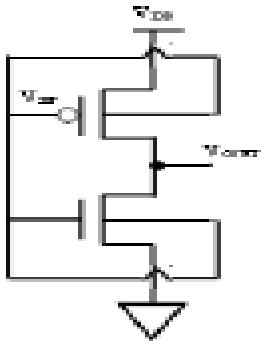

Fig. 4. A CMOS Inverter Based On DTMOS Biasing Technique

V. SIMULATION RESULTS

In the first sub-section, the functionality of ring oscillators in subthreshold region (Fig. 1) is verified. Further, the CRO is implemented using the inverters based on traditional, SBB and DTMOS biasing techniques. Then in the second section, the results of the comparison in performance of the ring oscillator and coupled ring oscillator are presented. All the simulations are carried with SPICE using 180 nm CMOS technology parameters. A power supply and load capacitor of 0.37 V and 1 fF have been taken in simulations respectively.

a. Functional Verification

The ring oscillator (Fig. 1) and the coupled ring oscillator (Fig. 2) are simulated. The waveform obtained for the ring oscillator output is shown in Fig. 5. It can be observed that the ring oscillator conforms to the functionality. The waveforms obtained at the four output nodes of the coupled ring oscillator using DTMOS biasing technique is shown Fig. 6. The waveforms for the coupled ring oscillator using traditional and SBB biasing are not shown for the sake of brevity

b. Performance Comparison

The simulation results for the ring oscillator and the coupled ring oscillator are listed in Table I. The results show that the coupled ring oscillators using SBB and DTMOS biasing techniques are better than the ring oscillators. It can be observed that the frequency of oscillation of the coupled ring oscillators increases by 16.62 MHz, 18.09 MHz in SBB and DTMOS biasing techniques respectively, with respect to traditional biasing. Though the power consumption increases by 859 nW and 757 nW respectively for both the techniques. Also, the SBB and DTMOS biasing based coupled ring oscillator outperforms the ring oscillator by reducing the propagation delay by 76.82 ns and 78.17 ns respectively.

TABLE I. PERFORMANCE COMPARISION OF OSCILLATORS

Performance Parameters	Ring Oscillator	Coupled Ring Oscillator		
		Traditional Biasing	Swapped Body Biasing	DTMOS Biasing
Frequency of oscillation (MHz)	2.19	2.954	19.571	21.040
Propagation Delay (ns)	50.53	89.822	13.008	11.654
Power Dissipation (W)	5.6×10^{-8}	1.14×10^{-7}	9.73×10^{-7}	8.71×10^{-7}

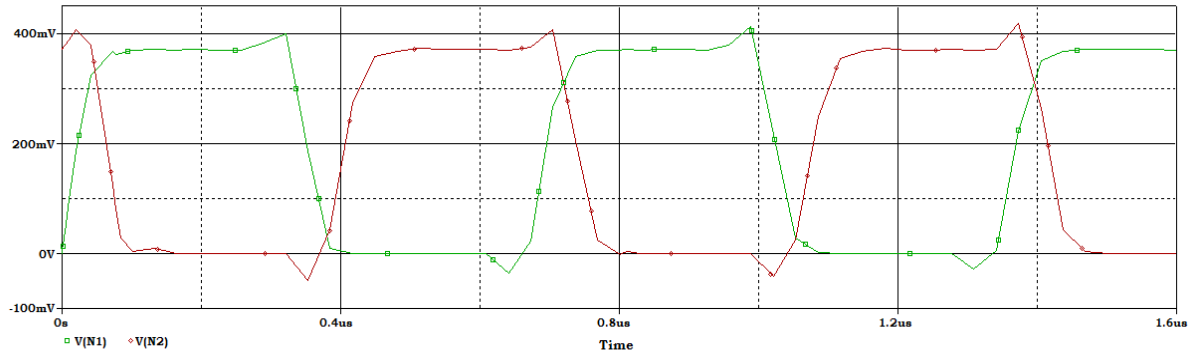

Fig. 5. Output Waveform Of Ring Oscillator Using Traditional Biasing

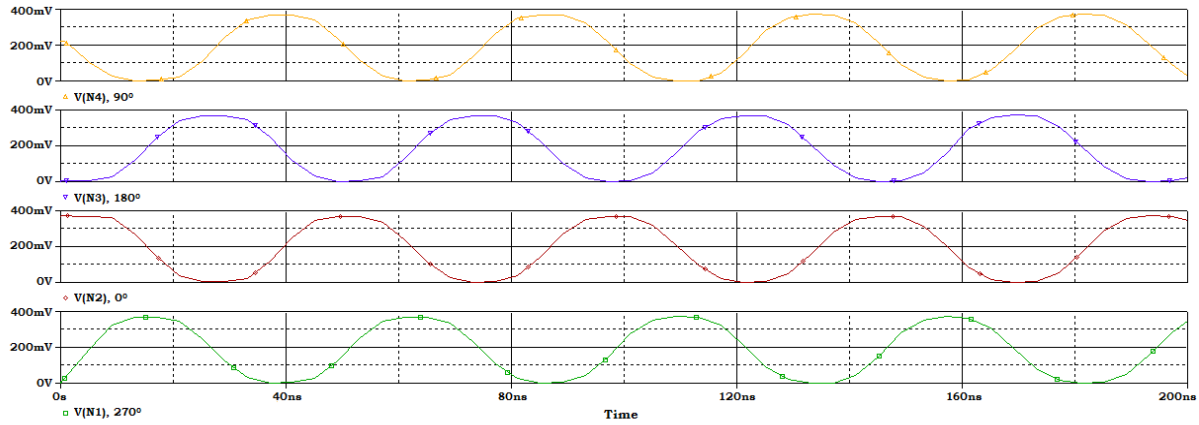

Fig. 6. Output Waveform Of Coupled Ring Oscillator Using DTMOS Biasing Technique

VI. CONCLUSION

This paper proposes the implementation of oscillators in the subthreshold regime. The ring and coupled ring oscillators are implemented. Improved CRO implementations based on swapped body biasing technique and dynamic threshold MOS biasing technique are proposed. The feasibility of the oscillators in subthreshold region is studied through simulations using 180 nm CMOS technology parameters. A comparison in performance of the oscillators show that the coupled ring oscillators based biasing techniques improves the performance significantly.

REFERENCES

[1] M. Alioto, "Understanding DC Behavior of Subthreshold CMOS Logic Through Closed-Form Analysis", IEEE Transactions on Circuits and Systems-I, Vol. 57, No. 7, July 2010, 1597-1607.

[2] H. Soeleman and K. Roy, "Digital CMOS Logic Operation in the Sub Threshold Region" CM Great Lakes Symposium on VLSI 2000: 107-112.

[3] A. Wang, B. H. Calhoun, A. P. Chandrakasan, "Sub-threshold Design for Ultra Low-Power Systems", Springer, 2006.

[4] A. Wang and A. Chandrakasan, "A 180-mV subthreshold FFT processor using a minimum energy design methodology," IEEE J. Solid-State Circuits, vol. 40, no. 1, Jan. 2005, 310-319.

[5] J. Rabaey, J. Ammer, B. Otis, F. Burghardt, Y. H. Chee, N. Pletcher, M. Sheets, and H. Qin, "Ultra-low-power design—The Roadmap to disappearing electronics and ambient intelligence," IEEE Circuits Devices Mag., pp. 23–29, Jul./Aug. 2006.

[6] J. Baker, H. W. Li, D. E. Boyce, "CMOS, Circuit Design, Layout, and Simulation", Wiley, 1997.

[7] I. A. Young, J. K. Gearson and K. L. Wong, "A PLL clock generator with 5 to 110 MHz of lock range for microprocessor," IEEE Journal of Solid State Circuits, Vol, 27, No. 11 1992. 51-52

[8] M.K. Mandal and B.C. Sarkar, "Ring Oscillators: Characteristics and applications", Indian Journal of Pure & Applied Physics Vol. 48, February 2010, 136-145.

[9] J. Nyathi, B. Bero and R. McKinlay, "A Tunable Body Biasing Scheme for Ultra-Low Power and High Speed CMOS Designs," International Symposium on Low Power Electronics and Design - 2006. October 4-6, 2006.

[10] F. Assaderaghi, D. Sinitsky, S. A. Parke, J. Bokor, P. K. Ko, and C. Hu, "Dynamic Threshold-Voltage MOSFET (DTMOS) for Ultra-Low Voltage VLSI," IEEE Transactions on Electron Devices, vol. 44, No. 3, March 1997. 414-422.

CDTA BASED CURRENT MODE ADC

Neeta Pandey[1], Rajeshwari Pandey[2], Ranjana Sridhar[3], Veepsa Bhatia[4], Alok Kumar Singh[5], Pradeep Kumar[6]

[1,2,3,4,5,6] *Department of Electronics and Communication Engineering*
Delhi Technological University, Delhi, (India)

ABSTRACT

This paper presents a CDTA based current mode analog to digital converter which shows the usefulness of CDTA as a building block in ADC design. The circuit is simple and is suitable for IC implementation as no external resistors or capacitors are required. The functionality of the circuit is verified with SPICE simulation using 0.35 μm CMOS technology parameters.

Keywords:Active Block; CDTA; Current Mode; Comparator; Flash ADC

I INTRODUCTION

Signal processing is an important part of myriad systems around us. The input signals be they speech, temperature, voltage, current etc. are in analog form and can be processed directly. But with the advent of digital signal processing two main advantages could be had: higher accuracy and faster processing of complex manipulations. Digital signal processing is a critical part diverse system like telecommunication, audio processing, medical diagnostic imaging, function generation etc.

In digital signal processing or other digital instruments, sensors measure process variables which are in the form of analog signals. Then an electronic circuit, termed the analog-to-digital converter (ADC), converts the analog signals into equivalent digital representation of required accuracy that can be stored and processed. The overall speed and accuracy of the digital signal processing system is influenced by the speed and accuracy of analog to digital conversion as processing is carried generally on high speed special purpose microprocessor or microcontroller. Thus, the design of an ADC is very crucial as it determines the speed, accuracy, power dissipation of the digital signal processing system.

These days, current mode circuits are gaining popularity because of the advantages offered such as wider bandwidth and the capability for working under low voltage [1]. Most modern designs employ voltage mode elements like op-amps for implementation of various electronic circuits. These elements are used widely due to their small sizes and good performance. With the demand for portable battery powered equipment increasing, designers have begun to look into different architectures to fit these demanding designs. This issue is not easily solved with voltage mode elements since the voltage supply if reduced will cause problems with realizing good, fully-functional circuits. Instead, current mode (CM) elements are now being considered for the same circuits and these issues can then be addressed.

In this paper we present the design of a current mode ADC using the recently introduced active building block (ABB) current differencing transconductance amplifier (CDTA). The CDTA is characterized by large

bandwidth and close-to-ideal terminal impedances. CDTA is a versatile sub circuit like the op-amp whose use in variety of applications in current mode signal processing, sinusoidal oscillators [2-13] has been explored. But, CDTA has not been used in applications like current mode ADCs and hence to check its viability, the paper focuses on this aspect. Section II discusses the basics of CDTA followed by Section III which enumerates the concept of CDTA based ADC. In Section IV, simulation results are presented followed by conclusion.

II CDTA BASICS

The circuit symbol of the CDTA is shown in Fig. 1 and the corresponding CMOS implementation in Fig. 2 [14] respectively. For Fig. 1, the terminal relationships can be described as $V_p=V_n=0$, $I_z = I_p - I_n$, $I_{x+} = g_m V_z$, $I_{x-} = -g_m V_z$, where V_p, V_n, V_x and V_z are the voltages at p , n, x and z terminals respectively, I_x is the output current at x terminal, I_0 is the input bias current and g_m represents transconductance. Here, from output terminal x, currents are equal in magnitude, but they flow in opposite directions, and the product of transconductance (g_m) and the voltage at the z terminal gives their magnitudes.

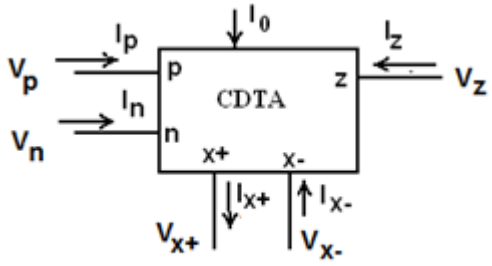

Fig. 1 Circuit symbol for CDTA

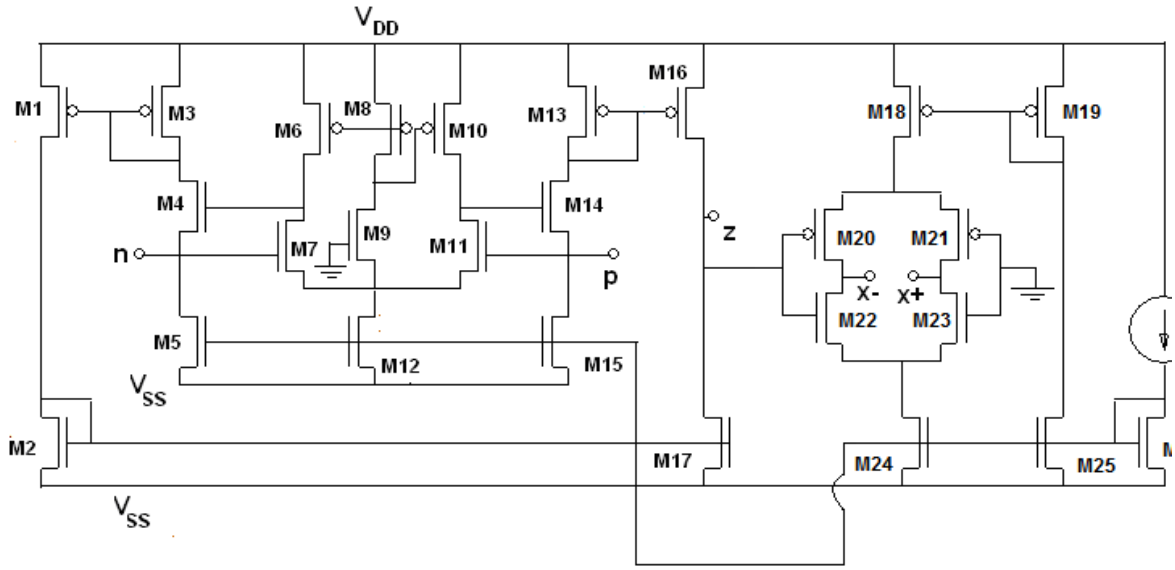

Fig. 2 CMOS CDTA implementation [14]

The p and n terminals are a pair of low-impedance current inputs and auxiliary terminal z has outgoing current which is the difference of input currents. Therefore, CDTA can be thought of as a combination of a current differencing unit followed by a dual-output operational transconductance amplifier, DO-OTA.

III CDTA BASED ADC

Current mode ADC plays an important role in front end signal processing and the design of a current mode ADC using CDTA is presented in this section. A current mode comparator performs comparison between two input currents and gives binary output voltage depending on which input current is greater. Generally, one of the two input currents is a constant, known as the reference current. The output equation of current comparator can be represented as in (1) where Ip(t) and In(t) are input currents and v_{out} is the output voltage.

$$v_{out}(t)=1, \text{ for } Ip(t)>In(t) \quad (1)$$

$$0, \text{ for } In(t)>Ip(t)$$

The input current and the reference current is supplied to p and n terminals of CDTA. The z terminal is left open therefore the voltage at X+ and X- terminals i.e. V_{X+} and V_X saturate at V_{DD} or V_{SS} [7]. The output of the CDTA is taken from X+ terminal and two cascaded CMOS inverters are used to bring the output voltage to 0-V_{DD} range.

The general schematic of a 2-bit current mode flash ADC is shown in Fig. 3. A flash ADC has the highest speed of any type of ADC [15]. It uses one comparator per quantization level and the 2^N -1 reference currents are generated and fed to each comparator. The input signal is compared to the reference level and the output of each comparator is a binary 1 or 0. The output of all the comparators together forms a thermometer code which is converted into binary code using a code converter circuit. The thermometer to binary encoder was designed using transmission gates and the implementation is shown in Fig. 4 with thermometer code (C1, C2 and C3) and the binary output (B0 and B1). The Boolean expression for the thermometer to binary code conversion is represented by (2) and (3).

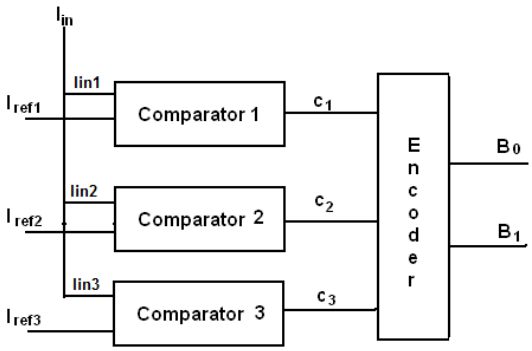

Fig. 3 2 bit Flash ADC

$$B_0 = C_1 * C_2 + C_3 * \overline{C_2} \quad (2)$$

$$B_1 = C_2 \quad (3)$$

The ADC was designed to work in the current range 0-40µA with a step size of 10µA. The reference currents I_{ref1}, I_{ref2}, I_{ref3} were accordingly set at 5µA, 15µA and 25µA respectively. The input current was mirrored into I_{in1}, I_{in2} and I_{in3} using a regulated cascode current mirror. The performance of the ADC is generally characterized by the parameters resolution, sampling rate, INL, DNL, offset and gain error. These parameters were measured through simulations and are presented in the simulation section.

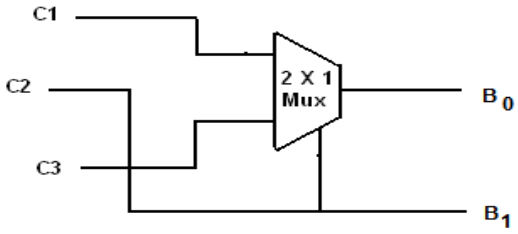

(a)

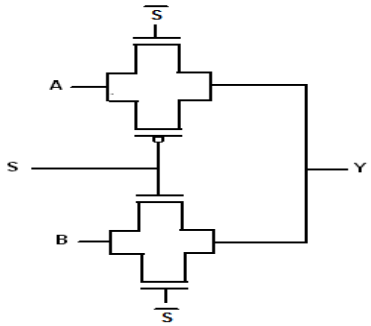

(b)

Fig. 4 (a) Encoder using multiplexer (b) TG based multiplexer implementation

IV SIMULATION RESULTS

The 2-bit flash current mode ADC using CDTA was implemented in 0.35µm CMOS technology in ORCAD PSIPCE and the corresponding transistor widths are reported in Table I. All the transistor lengths were set at 0.7 µm . The simulation conditions are reported in Table II.

TABLE I. TRANSISTOR DIMENSIONS FOR CMOS CDTA-ADC

Transistor No.	W(µm)
M1	9.8
M2-3,M13, M16-17	10.5
M4, M14	42
M5,M12,M15	35
M6,M8,M10, M21	28
M7,M9,M11	70
M18, M24-25	56
M19	58.8
M20	28.7
M22-23	16.1
M26	7

TABLE II. SIMULATION CONDITION FOR CDTA BASED CURRENT MODE ADC

Temperature	27^{o}C
Technology	0.35µm CMOS
Power Supply	1.8 V
$Iref_{i=1,2,3}$	5µA,15µA, 25µA

The CDTA based ADC was fed with input current in the range of 0-40µA and DC analysis was carried out. The corresponding output for is shown in Fig. 5. The input currents at which the ADC output transitions occurred

were noted and these were used to construct the actual ADC transfer characteristic. This is shown in Fig. 6 along with the ideal ADC transfer characteristic and it is seen that the ADC doesn't suffer from missing codes. The DNL and the INL were calculated from Fig. 6 and are plotted in Fig. 7 and Fig. 8 respectively. The DNL is -0.45LSB and the INL is -0.000225LSB and both are much lower than the maximum value of half of least significant bit (LSB), with LSB/2= 5 µA. The offset and the gain error were calculated as 0.5µA and 0.98 respectively. To characterize the speed of the CDTA based ADC, transient analysis was performed by feeding input pulse of 0-40 µA amplitude and frequency 500 KHz. The maximum delay under the above input conditions was found to be 81.332ns. The ADC was also subjected to sine input of frequency 6 MHz and it showed correct output as demonstrated by Fig. 9.

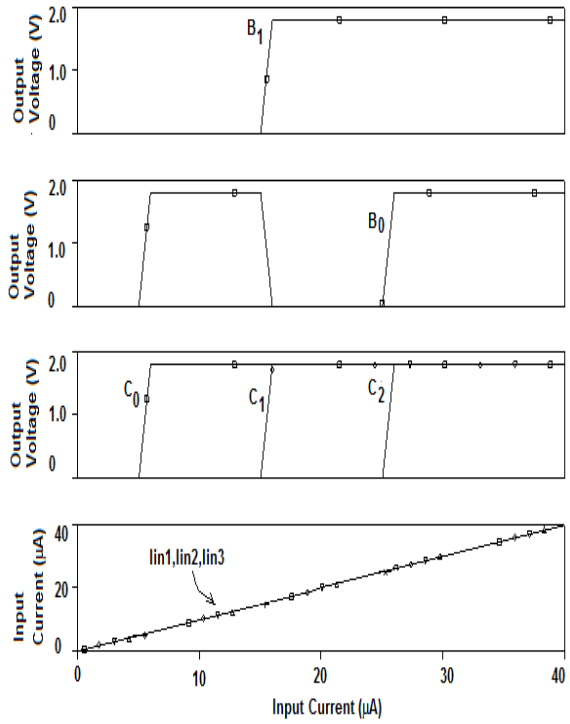

Fig. 5 ADC output for ramp input

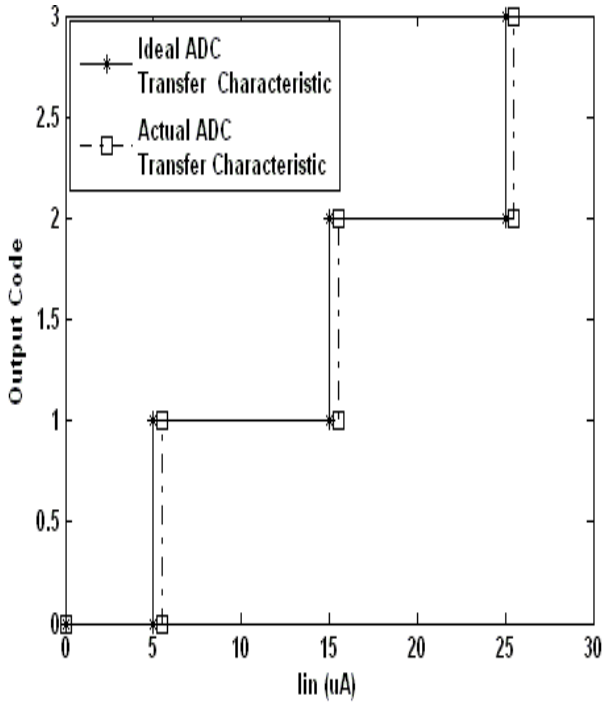

Fig. 6. Ideal and simulated ADC characteristics

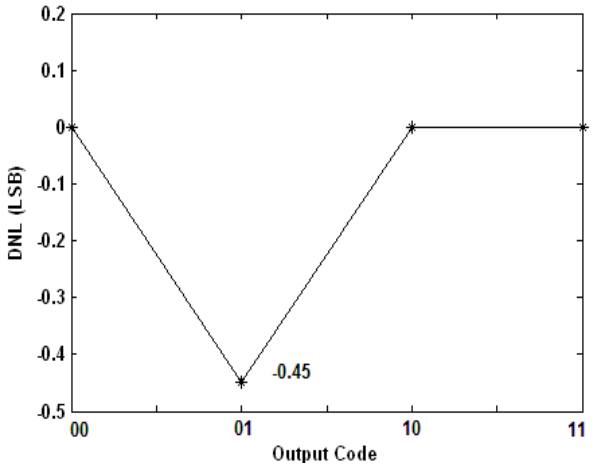

Fig. 7DNL versus Otput Code

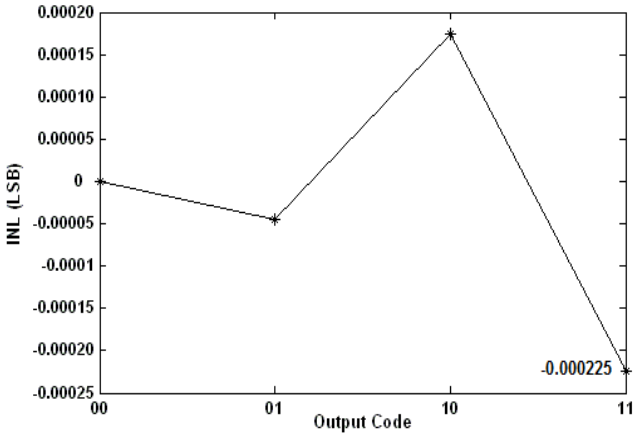

Fig. 8 INL versus Output Code

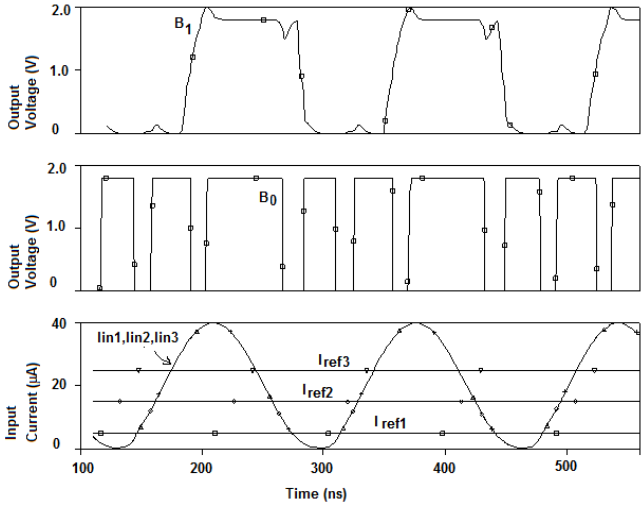

Fig. 9 ADC Output For Input Sine of Frequency 6 Mhz

V CONCLUSION

In this paper, a newly introduced active building block the current differencing transconductance amplifier (CDTA) is used for implementation of a current mode ADC. This application of CDTA has not yet been enumerated elsewhere and the results from the simulation section are promising. The INL and DNL of the CDTA based ADC is much lower than the maximum value of half of least significant bit (LSB). It also shows a delay of around 80ns at an input pulse of 500 KHz.

REFERENCES

[1] F. Yuan, “CMOS Current-Mode Circuits for Data Communications”, Springer, 2007.

[2] D. Biolek, "CDTA- Building block for current-mode analog signal processing”, Proceedings of ECCTD 03, Poland, Vol. III, pp. 397-400, 2003.

[3] A.U. Keskin, D. Biolek, E. Hancioglu and V. Biolkova, “Current-mode KHN filter employing current differencing transconductance amplifier”, AEU- International Journal of Electronics and Communications, 60 (6), 2006, 443-446.

[4] A. Uygur, H. Kuntman and A. Zeki, “Multi-input multi-output CDTA-based KHN filter”, Proc. of ELECO: The 4th International Conference on Electrical and Electronics, pp. 46-50, 2005.

[5] W. Tangsrirat, T. Dumawipata and W. Surakampontorn, "Multiple input single-output current-mode multifunction filter using current of Electronics and Communications, 61, 2006, 209-214.

[6] A. Uygur and H. Kuntman, "Seventh order elliptic video filter with 0.1dB pass band ripple employed CMOS CDTAs", AEU- International Journal of Electronics and Communications, 61, 2007, 320-328.

[7] N. Pandey and R. Pandey, "Current Mode Full-Wave Rectifier Based on a Single MZC-CDTA", Active and Passive Electronic Components, Volume 2013 (2013), Article ID 967057, 5 pages.

[8] A.U. Keskin and D. Biolek, "Current mode quadrature oscillator using current differencing transconductance amplifiers (CDTA)", IEE Proc.-Circuits Devices and Systems, 153(3), 2006, 214-218.

[9] D. Prasad, D.R. Bhaskar and A.K. Singh, "Realisation of Single-Resistance-Controlled Sinusoidal Oscillator: A new application of the CDTA", WSEAS Transactions on Electronics, 5(6), 2008, 257-259.

[10] W. Jaikla, M. Siripruchyanun, J. Bajer and D. Biolek, "A Simple Current-Mode Quadrature Oscillator Using Single CDTA", Radio engineering, 17(4), 2008, 33-40.

[11] A. Lahiri, "New current-mode quadrature oscillators using CDTA", IEICE Electronics Express, 6(3), 2009, 135-140.

[12] A. Lahiri, "Novel voltage/current-mode quadrature oscillator using current differencing transconductance amplifier", Analog Integrated Circuits and Signal Processing, 61(2), 2009, 199-203.

[13] W. Tangsrirat, "Current differencing transconductance amplifier-based current-mode four-phase quadrature oscillator", Indian Journal of Engineering and Materials Sciences, 14(7), 2007, 289-294.

[14] D. Biolek, E. Hancioglu, A. Ü. Keskin, High-performance current differencing transconductance amplifier and its application in precision current-mode rectification, International Journal of Electronics Communication (AEÜ), 62, 2008, 92 – 96.

[15] R.J.Baker, CMOS Circuit Design,Layout and Simulation, IEEE Press Series on Microelectronics, Second Edition.

RESIDUE ADDER BASED HIGH SPEED 8-BIT VEDIC MULTIPLIER

Ayush Tayal[1], Neeta Pandey[2], Rajeshwari Pandey[3]
[1, 2, 3] *Department of Electronics & Communication Engineering, DTU, Delhi (India)*

ABSTRACT

This paper aims at incorporating residue adder in the design of multiplier based on Nikhilam Sutra of Vedic mathematics. The residue adder employs residue number system (RNS). The performance is the proposition is compared with a Vedic multiplier employing carry save adder. The multiplier is coded in Very High Speed Integrated Circuits (VHSIC) Hardware Description Language (VHDL) while the simulation and synthesis is done using the Xilinx ISE Design Suite 14.2 software.

Keywords: Nikhilam Sutra, Residue Adder, Residue Number System (RNS), Vedic Mathematics, VHDL

I. INTRODUCTION

The use of multipliers is inevitable in any of the embedded system applications and they find great use in digital signal processing and high speed general purpose processor design. So, an important task is to design a multiplier which is efficient enough to help a designer design the final product with good performance parameters. VLSI deals with these methodologies and basically, there are three important parameters – power dissipation, chip area and delay. Due to the evolution and rapidly increasing use of the battery-based mobile embedded technology, design emphasis is now laid on optimizing the conventional delays and power dissipation while still maintaining high performance. To achieve this, different architectures and designs are explored. Some of the architectures of multipliers include array multiplier and Booth multiplier [1]. Booth multiplier is a way to perform multiplication of binary numbers in signed 2's complement notation. A modified Booth architecture has been proposed in [2] with improved performance. But the quest to find an optimized solution brought in the use of the ancient Vedic sutras. There are 16 different sutras in Vedic mathematics out of which two of them are used to design efficient multipliers. The performance of Urdhva Tiryagbhyam sutra of Vedic and the Booth multiplier architectures are compared in [3] in terms of the area, delay and power. In [4], a simple and basic Vedic multiplier is simulated while in others [5-8], the two sutras, Urdhva Tiryagbhyam Sutra and Nikhilam Sutra, are employed to design various 4-bit and 8-bit multipliers. Gunakasamuchyah Sutra is investigated in [9] for 4-bit Vedic multiplier implementation. The effectiveness of Vedic multipliers is demonstrated for convolution [10] and AES algorithm [11] which are used for digital signal processing and cryptography applications respectively. The adder is an integral part of all multipliers and influences the delay. The efficiency of the Vedic multiplier has also pronounced dependence on adder. Ripple Carry adders are used in [5-7] while [8] use Carry save adder in its architecture. Carry save adders have an obvious advantage of delaying the addition of the carry of different stages to next stages, thereby optimizing the delay. In [12-13], Pradhan and Panda have also worked on multipliers based on the Nikhilam Sutra and Urdhva Tiryagbhyam

Sutra using the carry save adder. It was found that the speed of 16-bit multiplier based on Nikhilam Sutra is better than Urdhva Tiryagbhyam Sutra when magnitude of both operands are more than half of their maximum values. Using this result, they have designed a Vedic multiplier based on Nikhilam Sutra [13] using the Carry Save adder. The speed of the multiplier can be further improved by residue adder which is based on Residue number system (RNS) [14]. This system removes the carry propagation and provides an efficient way to perform calculations faster. Vedic multipliers have been designed based on CSA but to the best of author's knowledge, residue adders have not been investigated in Vedic multipliers. In this paper, residue adder based 8-bit Vedic multiplier design is put forward . The performance is compared with Vedic multiplier having a carry save adder. The paper has been formulated in six sections: Section II and III present the concepts of Vedic mathematics and Residue Number System (RNS). The proposed multiplier has been presented inSection IV. Section V shows the results while the final conclusions are drawn in the last section.

II. VEDIC MATHEMATICS

Vedic Mathematics is the ancient system of mathematics which was rediscovered from the Vedas between 1911 and 1918 by Sri Bharati Krishna Tirthaji Maharaja (1884-1960). His research presented 16 Sutras & 16 Up-sutras from Atharva Veda. These sutras are word formulae which present an easy way to perform mathematical calculations [5]. Nikhilam Navatashcaramam Dashatah Sutra has been used to design the multiplier in this paper. A single line meaning of this sutra is "All from 9 and the last from 10". The basic description of Nikhilam sutra is as follows. The two numbers to be multiplied are complemented by subtracting them from a base. The numbers and their complements are written down vertically side by side. The right hand side of the result is obtained by multiplying the two complements while the left part is calculated by subtracting any of the diagonal numbers i.e. subtracting one's complement from the other number. The example below clearly depicts the above described sutra.

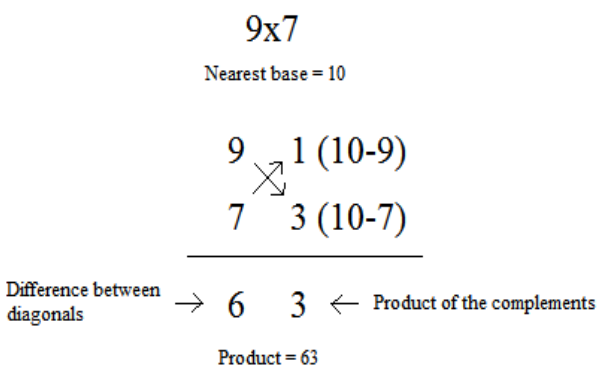

Fig. 1. Example Showing Multiplication Using The Nikhilam Sutra

Here the numbers to be multiplied are 9 and 7 written vertically. The complements of the two numbers 1 and 3 are also written vertically alongside the two numbers. The right part of the result is obtained by multiplying the two complements 1 and 3 which gives 3 while the left portion is obtained by subtracting the diagonal elements to obtain the difference as 6 (9-3 or 7-1). Thus the product is obtained as 63. This method can be extended to large numbers as well.

III. RESIDUE NUMBER SYSTEM

The speed of the arithmetic systems is of primary concern in any application. The conventional representations of numbers include decimal, binary and other weighted systems. The Residue Number System (RNS) represents numbers in a way which removes the carry propagation in an arithmetic unit. This in turn makes it high speed and low power arithmetic. RNS is very good for applications like digital signal processing, computer security, image & speech processing and also in embedded processors, especially those found in portable devices, for which power consumption is the most critical aspect of the design [14]. RNS involves the use of a set of relatively prime integers called moduli. This set can be of the form $\{m_1, m_2,\ldots,m_n\}$. Every number is then represented by n integers which correspond to the remainders with respect to each modulus. These n integers are called residues and are of the form $\{r_1, r_2,\ldots,r_n\}$. So, for any number X, we have,

$$X \bmod m_i = r_i \quad (1)$$

$$\& \quad X = \{r_1, r_2,\ldots,r_n\} \quad (2)$$

The dynamic range of this system is given by,

$$M = \pi m_i \quad (3)$$

All numbers lying in this dynamic range are uniquely represented in this system. Thus, we have a system which ensures parallel independent operations on small number of digits. This significantly speeds up the arithmetic operations especially the addition and the multiplication. Since each modulus is only of a small number of bits, the carries are strictly minimal. This makes it implementable through the use of Look-up Tables (LUTs).

The number in its binary form is first converted into the residual form by choosing a particular set of moduli. This set is chosen on the basis of some rules which uniquely represent the numbers. The largest modulus determines the speed of the operation, so the smallest possible moduli are taken. According to the dynamic range required for the application, the choice of the moduli is made. Here, for 8-bit operations, the range is 256. According to this range, moduli are chosen by taking prime numbers in sequence and including powers of smaller primes before moving to larger primes. The moduli are relatively prime and are represented by the smallest possible number of bits as this decides the speed of the arithmetic. After the set is decided, it is used for the conversion of binary numbers to RNS form. The moduli of powers of 2 ranging from 0 to 7 for 8-bit numbers with respect to the set of moduli chosen are stored in a LUT. The following equality is used for the conversion,

$$<(X_{k-1}X_{k-2}\ldots X_1X_0)>m_i = <<2^{k-1}X_{k-1}>m_i + <2^{k-2}X_{k-2}>m_i + \ldots\ldots + <2^1X_1>m_i + <2^0X_0>m_i>m_i \quad (4)$$

Corresponding to each modulus, the residues are obtained on the basis of the above equality. The arithmetic operations are performed on these residues which provide a carry free operation. The residue to binary conversion is performed using the Chinese Remainder Theorem (CRT). Digits of the residue number system (RNS) have position weightings s_i which are given by

$$s_i = M/m_i \quad (5)$$

According to the CRT, the binary form of the number is given by,

$$X = \{\Sigma\, s_i\, [(X_i s_i^{-1}) \bmod m_i]\} \bmod M$$

$$\text{where}(s_i s_i^{-1}) \bmod p_i = 1. \quad (6)$$

This is also most efficiently done through a LUT as a very small number of entries are required in the table which is equal to the sum of the moduli.

IV. PROPOSED MULTIPLIER

The proposed multiplier uses Nikhilam Sutra of Vedic mathematics along with a residue adder to get a high performance 8-bit Vedic multiplier. The block diagram of the proposed multiplier is shown in Fig. 2.

The two 8-bit numbers, the multiplicand and the multiplier, are both complemented when passed through the complementer block which corresponds to the subtraction of the numbers from the nearest base in the Nikhilam Sutra. The complements which are also of 8 bits each are then multiplied to obtain the right part of the product. The multiplication of the complements yields a 16-bit result. The lower 8 bits form the right part of the product while the higher 8 bits are carried over to the residue adder via a binary to residue converter. The multiplicand and the multiplier are also passed through binary to residue converters. The converters output three numbers in their residual form. These residues are added using a residue adder. The left part is then obtained by passing the output of the residue adder through a residue to binary converter which converts the residues back into their binary form. The complete product is obtained by concatenating the left and the right parts.

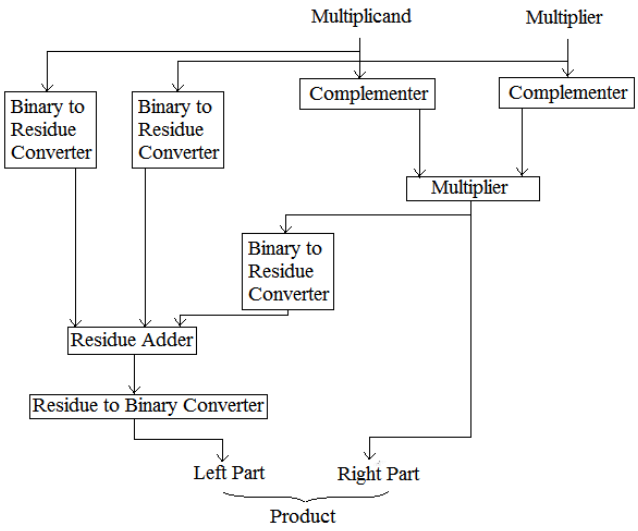

Fig. 2: Block Diagram of the proposed multiplier

The use of residue adder optimizes the performance parameters to obtain a highly efficient multiplier. The three inputs to the residue adder are of 8 bits and so the maximum value can be 255. Based on this and the concept of RNS, three moduli are chosen to represent the numbers. The three moduli taken here are 5, 11 and 14. The binary to residue converters convert binary numbers into residue numbers using these three moduli. Look-up tables are simulated using VHDL to carry out the conversion. The modulus operation is implemented using Finite State Machine (FSM) concept having three states. For any residue, the modulus is subtracted from the binary number until the remainders are obtained. Three residues then represent one binary number. This gives us in total nine residues, three for each binary number. These are added correspondingly by the residue adder to

give the output three residues of the sum. These are then converted back into binary form using the residue to binary converter which is based on CRT. This residue arithmetic enables us to improve the delays by removing the carry propagation due to smaller residues involved in addition rather than large 8-bit numbers.

V. RESULTS

The proposed multiplier using Nikhilam Sutra of Vedic mathematics incorporating a residue adder has been designed and simulated in Very High Speed Integrated Circuits (VHSIC) Hardware Description Language (VHDL) coding using the Xilinx Design Suite 14.2 and synthesis results are drawn for the XC3S50 device and PQ208 package of the Spartan 3 family. Table 1 compares the results with the multiplier using carry save adder proposed by Pradhan and Panda in [13]. The RTL schematic of the design is shown in Fig. 3. The external schematic with I/O's and one of the sub modules inside the complete design. The complete schematic is made up of many such sub modules and other sub modules combined together.

TABLE 1. Comparison of timings of the two multipliers

Device: Spartan 3 XC3S50: PQ208	Vedic multiplier based on CSA proposed by Pradhan & Panda	Proposed multiplier based on Residue Adder
Delay	19.851 ns	15.912 ns

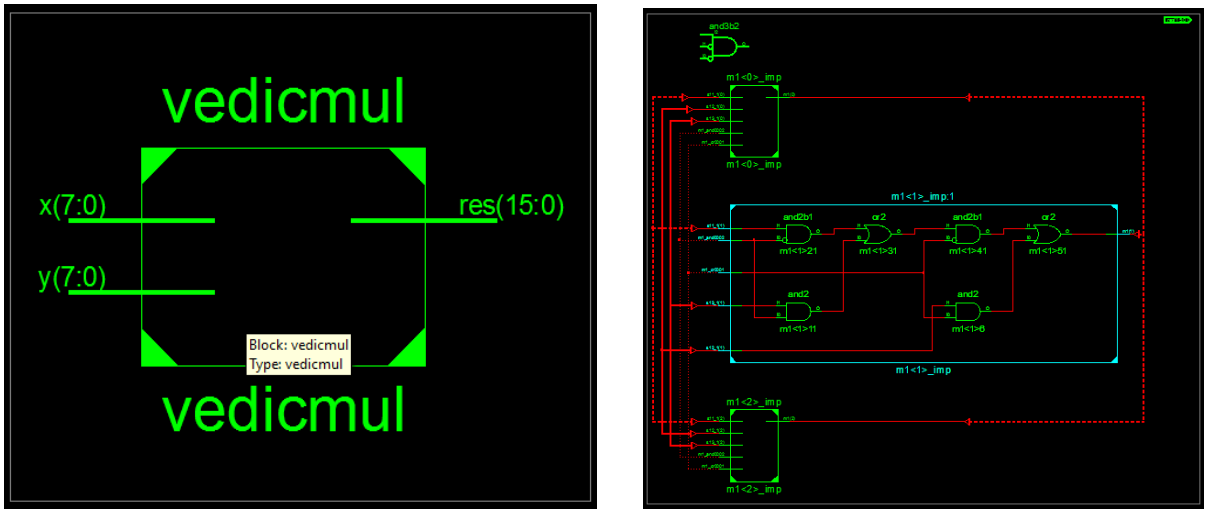

Fig. 3 (A) RTL Schematic Of The Proposed Multiplier (B) Schematic Of One Of The Sub Modules In The Design.

VI. CONCLUSION

In this paper, an efficient Vedic multiplier based on Nikhilam sutra of Vedic mathematics and residue number system based residue adder is proposed. The functionality is verified through VHDL simulations and synthesis on Xilinx Spartan platform. The simulation results show that the proposed RNS based vedic multiplier has

significant speed improvement over CSA based realization. The 8-bit multiplier presented here can easily be extended to 16 bits.

REFERENCES

[1] S Laxman, R Prabhu Darshan, M. Shetty, Manjula, C. Sharma, FPGA Implementation of different multiplier architectures, *IJETAE*, ISSN 2250-2459, Vol. 2, Issue 6, June 2012.

[2] M. Chaudhary, M. S. Narula, High Speed Modified Booth's Multiplier for Signed and Unsigned Numbers, *International Journal of Science and Engineering Investigations*, 2, 2013, 106 - 113.

[3] Anju, Performance Comparison of Vedic Multiplier and Booth Multiplier, *International Journal of Engineering and Advanced Technology*, 2, 2013, 336 - 339.

[4] G.Vaithiyanathan, K. Venkatesan, S. Sivaramakrishnan, S. Siva, S. Jayakumar, Simulation and Implementation of Vedic Multiplier using VHDL Code, *International Journal of Scientific & Engineering Research*, 4(1), 2013, 1-5.

[5] M. Poornima, S. K. Patil, Shivukumar , K. P. Shridhar , H. Sanjay, Implementation of Multiplier using Vedic Algorithm, *International Journal of Innovative Technology and Exploring Engineering*, 2 (6), 2013, 219 – 223.

[6] P. Sharma, Design of 4x4 bit Vedic Multiplier using EDA Tool, *International Journal of Computer Applications*, 48, 2012, 32-35.

[7] P. Verma, K. K. Mehta, Implementation of an Efficient Multiplier based on Vedic Mathematics Using EDA Tool, *International Journal of Engineering and Advanced Technology*, 1, 2012, 75-79.

[8] S. Karthik, P. Udayabhanu, FPGA Implementation of High Speed Vedic Multipliers, *International Journal of Engineering Research & Technology (IJERT)*, 1, 2012.

[9] Kavita, U. Goyal, FPGA Implementation of Vedic multiplier, *IJARET*, 4, 2013, 150-158.

[10] A. Haveliya, FPGA implementation of a Vedic convolution algorithm, *IJERA*, 2, 2012, 678-684.

[11] Ambika R , C S Mala , S K Pushpa, FPGA implementation of AES using Vedic Mathematics, *International Journal of Innovative Research in Science & Engineering*, 1(2), 2013, 1-8.

[12] M. Pradhan, R. Panda, S. K. Sahu, Speed Comparison of 16x16 Vedic Multipliers, *International Journal of Computer Applications* (0975 – 8887), 21(6), 2011, 16-19.

[13] M. Pradhan, R. Panda, High speed multiplier using Nikhilam Sutra algorithm of Vedic mathematics, *International Journal of Electronics*, vol. 101, pp. 300 – 307, 2014.

[14] *Residue Numbers and the Limits of Fast Arithmetic*, www.stanford.edu_class_ee486_doc_chap2.

AN IMPROVED WATERSHED AND MRI IMAGE SEGMENTATION

SNIGDHA RAI

Department of Electronics and communication, K.E.C, Mohan Nagar (INDIA)

ABSTRACT

Watershed Transformation in mathematical morphology is a powerful tool for image segmentation. Watershed transformation based segmentation is generally marker controlled segmentation. In the last decade medical image processing is immerged as one of the major area of research .In medical science, Magnetic Resonance Imaging(MRI) is a very popular technique used in details.MRI provides good contrast between the different soft tissues of the body, which makes it especially useful in imaging the different internal organs like brain ,heart, kidney etc. this paper presents a robust procedure for segmentation and edge detection of MRI images based on marker controlled watershed algorithm.

KEYWORDS: Image Segmentation, MR Image, Watershed Transform, Image Enhancement, Marker Controlled Watershed Segmentation, Prewitt's Operator.

I. INTRODUCTION

Image segmentation is an important and, perhaps, the most difficult task in image processing . Segmentation refers to the grouping of image elements that exhibit "similar" characteristics ,i.e. subdividing an image into its constituent regions or objects. For image unperceiving, analysis and pattern identification, image segmentation plays a very significant role. The most important role of the segmentation process is to segregate an image into regions with one or more characteristics like color and object and the segmentation results are mainly for better analyzing and meaningful understanding images. Several methods and approaches are introduced into area of segmentation among them a well known method is watershed algorithm or technique. The Watershed transform is a broadly used technique for image segmentation. The watershed transform can be classified as a region-based segmentation approach. The intuitive idea underlying this method comes from geography: it is that of a landscape or topographic relief which is flooded by water, watersheds being the divide lines of the domains of attraction of rain falling over the region. An alternative approach is to imagine the landscape being immersed in a lake, with holes pierced in local minima. Basins also called catchment basins will fill up with water starting at these local minima ,and, at points where water coming from different basins would meet, dams are built. Medical image segmentation is a very important field for the medical science. Medical images edge detection is an important work for object recognition of the human organs such as brain, heart, kidney etc. Medical images such as CT, MRI or X-RAY visualizes the various information's of internal organs which is very important for doctors diagnoses as well as medical teaching, learning and research. It is a tough job to locate the internal organ as these pictures contains noise or rough structure of human body organs. Image processing and segmentation technique plays a vital role for detecting edges of internal body organs for medical sciences and now a days

MRI (magnetic resonance imaging) images are very effective for the doctor's diagnoses. For a better understanding the following sections will give a better explanation with results, discussions and conclusion.

II. BACKGROUND AND PRELIMINARY

The idea that has been introduced in 1979 by S. Beucher and C.Lantuejoul.It consists in placing a water source in each regional minimum, to flood the relief from sources, and build barriers when different sources are meeting. The resulting set of barriers constitutes a watershed by flooding .By taking this concept several works has been done in various research fields .The main idea behind this in technique is to segmentation of images. We have tried to use this concept in a new dimension by detecting the human with MRI images. As an example we have chosen MRI images of human brains. Edge detection of human organs with MRI images is a major concerning problem in respect of the vision of the computer.

III. THE WATERSHED TRANSFORM

The watershed transform is a morphological based tool for image segmentation. The watershed transform can be classified as a region-based segmentation approach.Fig.1 Illustration of immersion process of watershed transforms. (CB: Catchment basins).The idea of watershed can be view as a landscape immersed in a lake; catchment basins will be filled up with water starting at each local minimum. Dams must be built where the water coming from different catchment basins may be meeting in order to avoid the merging of catchment basins. The water shed lines are defined by the catchment basins divided by the dam at the highest level where the water can reach in the landscape. As a result, watershed lines can separate individual catchment basins in the landscape. The idea is described in Fig.1 which describes the flooding or rain falling process of watershed algorithm. The process of rain falling is described in Fig.2.

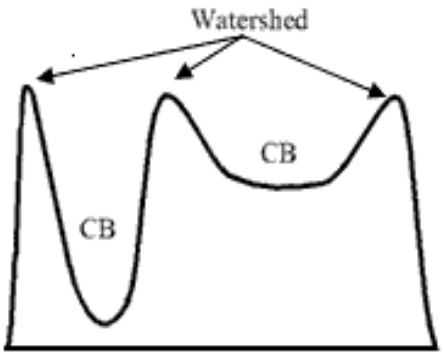

Fig.1: Illustration Of Flooding Transforms

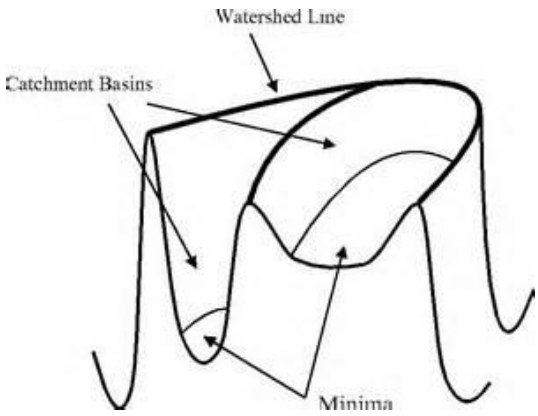

Fig.2: Illustration Of Immersion Process Of Watershed

IV. MARKER CONTROLLED WATERSHED SEGMENTATION

Watershed algorithm is a very good method for image segmentation, but this technique suffers from over segmentation problem. An approach used to control over segmentation is based on the concept of controlled marker. The concept of markers is a good approach to control over segmentation. The markers are connected component of an image. There are internal markers and external markers where internal markers are associated

with object of interest and external markers are associated with the background .This is a very useful technique for improvisation of watershed transform to overcome the over segmentation problem.

Marker -controlled watershed segmentation follows this basic procedure:

IV.1 : Compute a segmentation function. This is an image whose dark regions are the objects you are trying to object.

IV.2 : Compute foreground markers. These are connected blobs of pixels within each of the objects.

IV.3 : Compute background markers. These are pixels that are not part of any object.

IV.4 : Modify the segmentation function so that it only has minima at the foreground and background marker locations.

IV.5 : Compute the watershed transform of the modified segmentation function.

V. PROPOSED TECHNIQUE

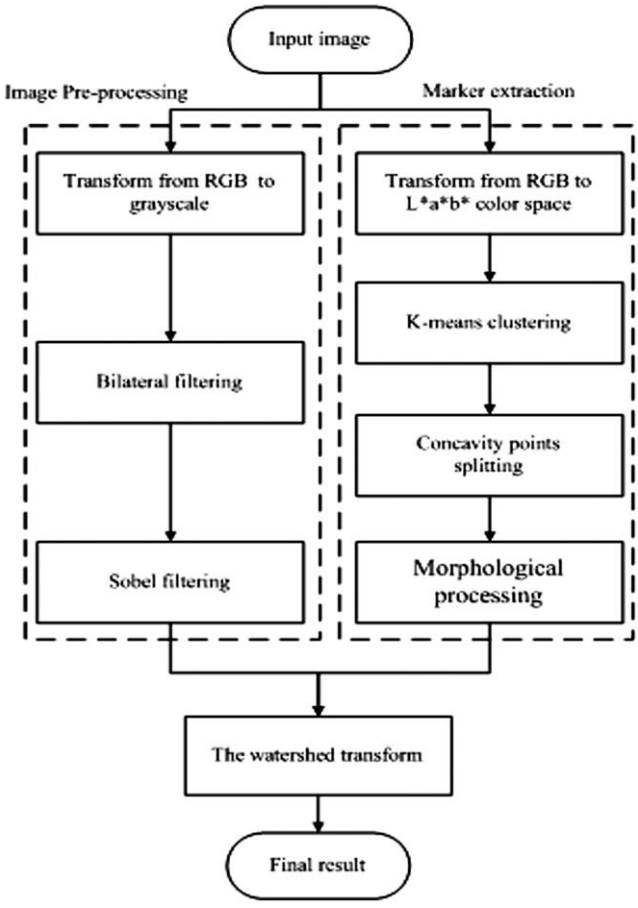

The marker controlled watershed transform is mainly for the problems where adjacent objects are there in an image and we have to separate them using image processing operations. This approach deals with catchment basins and watershed ridge lines in an image by assuming it as a surface where light pixels are low. In the initial step we have to convert a 3D color image into gray scale and compute the gradient magnitude as the segmentation function where gradient is highest at the borders of the object and generally low inside the object.

We will then use the internal marker to distinguish the foreground of adjacent objects. The background of image will then be segregated from the foreground objects using the external markers. Finally we will aggregate the computed result of the watershed transform and examine the final image .The detailed algorithm is the following:

STEP 1: Insert the original image as input.

STEP 2: Convert the image into gray scale.

STEP 3: Find out the gradient magnitude.

STEP 4: Mark the foreground objects.

STEP 5: Mark the background objects.

STEP 6: Estimate the watershed transform.

VI. RESULTS AND DISCUSSIONS

The designed algorithm has been tested on MRI brain images. Results indicate that the segmentation is very clear for the images where the region of interest where the region of interest is enhanced. An image segmentation approach based on Marker Controlled Watershed Transform has been discussed .This approach for segmentation of medical images can help in the proper detection of the region of interest and also can be very helpful for doctor's diagnoses, medical teaching, learning and research .We have tried to proposed a robust approach for 3D medical image segmentation with human brain images by using marker-based watershed segmentation. With this approach we can reduce user interaction and speeds up the entire segmentation process. In this paper this approach has been applied successfully on medical images where we have chosen MRI brain images. Furthermore the algorithm should be improved for more demanding tasks as brain, heart, liver or kidney segmentation with the CT image data in 3D nature.

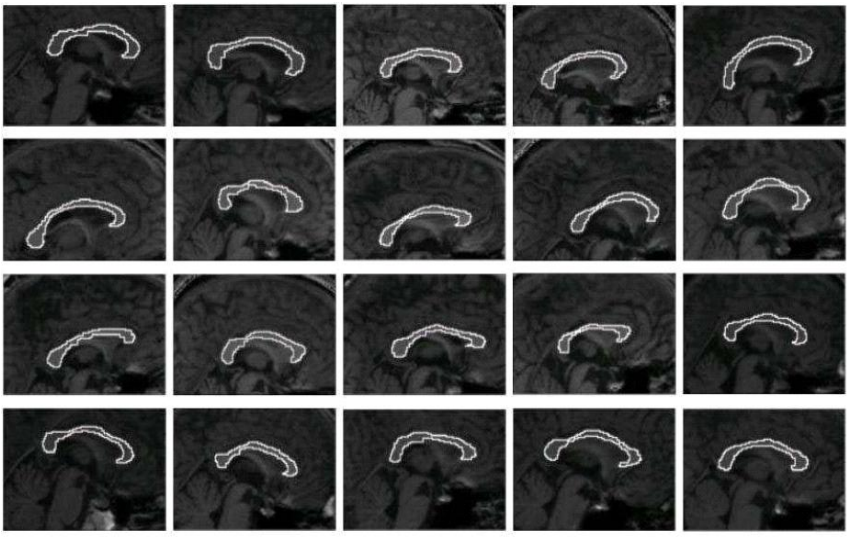

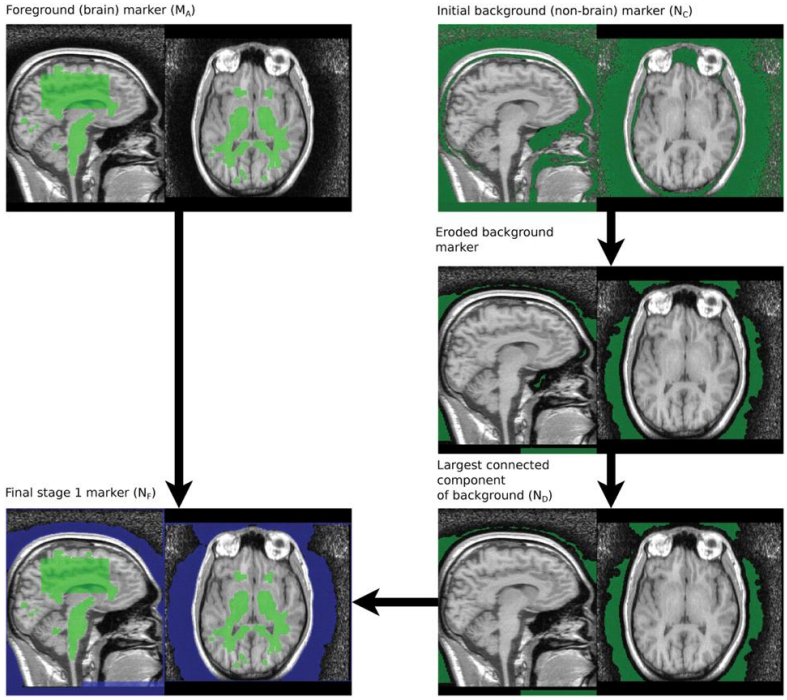

Fig. Illustrations Using Marker Foreground and Background Methods

REFERENCES

[1] Serra, J., Image analysis and mathematical morphology, Academic Press, New York, 1982.

[2] S.Beucher, F.Meyer,"The Morphological Approach to segmentation: The Watershed transform", in Mathematical Morphology Image Processing, E.R. Dougherty, Ed. New York Marcel Dekker, vol.12, pp.433-481, 1993.

[3] Beucher, S. "The Watershed Transform Applied to Image Segmentation", Proceedings of the pfefferkorn Conference on Signal and Image Processing in Microscopy and Microanalysis, pp. 299-314, September 1991.

[4] Rafael C. Gonzalez, Richard E. Woods, "Digital Image processing:, 2nd edition, Pearson Education, pp. 589-656, 2007.

[5] Malik Khan, "Modified Watershed Algorithm for Segmentation of 2D Images", Journal of Information Science & Information Technology, 6, No.3, pp.546-552,2009.

[6] S. Beucher,Watershed, hierarchial segmentation and water fall algorithm"' in Mathematical Morphology and its Application to Image Processing, Dordecht, The Netherlands: Kluwer, pp.69-76,1994.

[7] R.M. Haralick and L.G. Shapiro,"Survey: Image Segmentation Technique", Comput. vis. Graph. Im. Proc,29 (1985) 100-132.

[8] Rivest, J., Beucher, S., delhomme. J, "Marker-controlled segmentation: an application to electrical borehole imaging", Journal of Electronic Imaging, April pp.136-142,1992.

[9] MRI image segmentation by Dibyendu Goshal and Pinaki Pratim Acharjya, journal of Emerging Technology and advanced engineering.

[10] An improved watershed image segmentation by Anju Bala , Journal of Scientific and Engineering Research

LOAD BALANCING AND EFFICIENT CLUSTERING FOR IMPROVING NETWORK PERFORMANCE IN AD-HOC NETWORKS

Saranya.S[1], Menakambal.S[2]

[1]*M.E., Embedded System Technologies, Nandha Engineering College (Autonomous), (India)*

[2]*Asst. Professor, Dept. of Electrical and Electronics Engg., Nandha Engineering College,(India)*

ABSTRACT

Information gathering is a fast emergent and challenging field in today's world of computing. Sensors are tiny devices that are capable of gathering physical information like heat, light or motion of an object or environment. Sensors are deployed in an ad-hoc manner in an area of interest to monitor events and gather data about the environment. Sensors in such systems are typically disposable and expected to last until their energy drains. Therefore, energy is a very scarce resource and has to be managed wisely in order to extend the life of the sensors in order to provide dependable operation for the duration of a particular task. Mobile ad-hoc networks consist of freely moving nodes which are responsible of not only forwarding packets for other nodes but can also perform extensive computations. One of the most critical issues in these networks is the significant differences in term of processing and energy capacity between the nodes, inducing a load imbalance. Thus, sharing the load between the overloaded and idle nodes is a necessity in ad hoc networks. In this paper, we present a new load balancing algorithm based on clustering where a subset of nodes 'cluster heads' is elected to maintain some balance within their respective clusters while minimizing the overall communication cost. Our primary goal is to minimize the total execution time of the tasks by distributing the work load among nodes. Another goal is to extend the overloaded nodes lifetime inducing a stability of the network. The simulation results have shown that network performance can be reached by distributing load to idle nodes within the network.

Keywords: Ad-hoc network, Cluster head selection, Clustering, Load balancing, MANET

I. INTRODUCTION

Ad hoc is Latin meaning "for this purpose." Ad hoc networks therefore refer to networks created for a particular purpose. They are often created on-the-fly and for one-time or temporary use. Often, ad hoc networks are comprised of a group of workstations or other wireless devices which communicate directly with each other to exchange information. An ad-hoc network is one where there are no access points passing information between participants. In Fig.1, Infrastructure networks pass information through a central information hub which can be a hardware device or software on a computer. Office networks, for example, generally use a server to which company workstations connect to receive their information. Ad hoc networks, on the other hand, do not go through a central information hub.

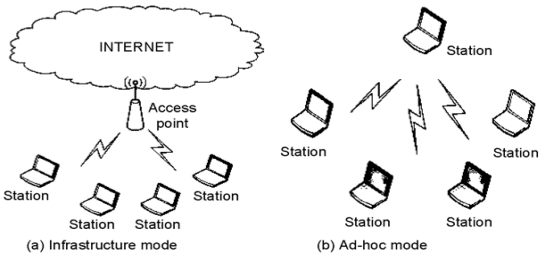

Fig.1: Infrastructure node and Ad-hoc network

An ad hoc network is defined as "an autonomous system of routers connected by wireless links the union of which forms an arbitrary graph. The routers are free to move randomly and organize themselves arbitrarily; thus, the network's wireless topology may change rapidly and unpredictably. Such a network may operate in a standalone fashion, or may be connected to the larger Internet operating as a hybrid fixed/ad hoc network." The areas of application range from school classes over well-known services like chat rooms to online shopping, but they are also used in places that do not come to mind immediately, like in the military. Furthermore, it is not even necessary to have a human interaction factor: ad-hoc networks can also be used to link together research computers or moving vehicles that exchange information "on the road".

II. AD-HOC NETWORK

Mobile Ad-Hoc Networks are wireless networks which do not require any infrastructure support for transferring data packet between two nodes. In these networks, nodes also work as a router that is they also route packet for other nodes. Nodes are free to move, independent of each other, topology of such networks keep on changing dynamically which makes routing much difficult. Therefore routing is one of the most concern areas in these networks. Normal routing protocol which works well in fixed networks does not show same performance in Mobile Ad Hoc Networks. In these networks routing protocols should be more dynamic so that they quickly respond to topological changes.

Fig.2: MANET

Mobile Ad hoc Network (MANET) is a collection of independent mobile nodes that can communicate to each other via radio waves is shown in Fig.2.The mobile nodes that are in radio range of each other can directly communicate, whereas others need the aid of intermediate nodes to route their packets. These networks are fully distributed, and can work at any place without the help of any infrastructure. This property makes these networks highly exile and robust.

The characteristics of these networks are summarized as follows:

- Communication via wireless
- Nodes can perform the roles of both hosts and routers.
- No centralized controller and infrastructure.
- Frequent routing updates.
- Autonomous, no infrastructure needed.
- Can be set up anywhere.
- Energy constraints

Despite the innumerable applications of Ad-Hoc Networks, these networks have several restrictions, e.g., limited energy supply, limited computing power, and limited bandwidth of the wireless links connecting sensor nodes. One of the main design goals of Ad-Hoc Networks is to carry out data communication while trying to prolong the lifetime of the network and prevent connectivity degradation by employing aggressive energy management techniques. The design of routing protocols in Ad-Hoc Networks is influenced by many challenging factors. These factors must be overcome before efficient communication can be achieved in Ad-Hoc Networks.

III. RELATED WORK

This section briefly outlines the related works taken in the area of Ad-Hoc networks challenges and issues. MANET's enable one or more mobile units to communicate with each other which can be done without using any physical connection. In such cases, load imbalance occurs in MANET nodes. This will cause packet dropping, end-to-end delay, energy consumption, etc. Load balancing improves the execution of tasks and better energy management. Many load balancing algorithms are used to improve the efficiency of the network. Two parameters such as Node ID and Node degree are used to balance the nodes in cluster with the help of cluster heads [1]. Many conventional routing algorithms are not supported with load balancing. So some kinds of load balancing algorithms are used [2].

The execution time improvement, energy, impact of mobility on energy, balance factor, communication cost threshold value are other important factors which are to be considered in case of Mobile Ad-hoc networks [3]. By this, the load is distributed among the idle nodes and overloaded nodes lifetime is extended by inducing the stability of the network. If the size of the network is large, then scalability issues can be increased which can increase the single-point bottleneck failures. So weight-based cluster head election strategy can be used [4]. Routing and scheduling of packets should be efficient to reduce the congestion [5]. Clustering should also be efficient to improve the network lifetime. Based on the residual energy, cluster head is elected. The cluster members are selected without considering the length of the base station [6]. Energy-efficient multi-hop hierarchical routing algorithm is used to improve the lifetime of the network [7].

IV. PROPOSED SYSTEM

In an ad-hoc network, with a decentralized and heterogeneous structure, some nodes may have different capabilities of processing and batteries, imbalances of load can occur. Indeed, a more powerful node in term of processing capacity can become idle, because it has finished its work quickly while the others, less powerful, are occupied most of the time, consuming more energy. Powerful nodes capacity can be exploited by overloaded nodes if a fraction of their load is shared with them. If the difference between the heaviest loaded and the

lightest loaded nodes is minimized, the average work execution time can be reduced, the energy of the nodes will be better exploited and the nodes lifetime can be extended. It is what contributes to the stability of the network topology that plays a principal role in different problems like: routing, scheduling, resource reservation etc. Load balancing is certainly one of the solutions for increasing the efficiency of applications and the network life time.

Load Balancing algorithms are designed essentially to distribute equally the load on nodes and maximize their utilization while minimizing the total task execution time. This issue has been of considerable interest in the network research community when it comes to wired and wireless networks. It aims to guarantee that no node is under loaded or overloaded. It looks at setting up a uniform load on all nodes. Then, it is expanded in order to take into account new environments and new applications (large scale applications, multimedia applications, etc.). Compared to the wired networks, the mobile environments introduce new highly variable parameters such as limited resources, wireless link communication and mobility.

V. MODULE DESCRIPTION

CLUSTER FORMATION

In our work, a cluster head is elected for its relatively high energy capacity and its low mobility. Energy is a critical resource in ad-hoc networks. A cluster head consumes more energy than an ordinary node since it has other functionalities: coordination between its members, cluster maintenance and load balancing. Mobility is also an important factor for a cluster head election. Indeed, to avoid frequent cluster head changes, it is important to choose the one that has a low mobility. If the cluster head moves quickly, the nodes can be detached from it, inducing re-affiliations which cause significant updated information exchanges.

CLUSTER FORMATION PROCEDURE

1. Find the neighbors of each node i (nodes within its transmission range). They are defined as follows: $V(i) = \{i_ \; ! = i / dist(i, i_) \leq txrange\}$ where *txrange* is the transmission range of node i.
2. Compute the speed average for every node. This gives a measure of its mobility.
3. Compute the battery power for each node
4. Choose the node which has the smallest value of mobility and the highest value of battery power as clustered. All its neighbors are designated as its members and they can no longer participate in the election procedure.
5. Repeat steps 2-4 for the remaining nodes not yet assigned to any cluster.

The following characteristics are considered in the cluster head election procedure:

- The nodes mobility causes changes in the network topology. If at a given time a node is detached from its current cluster and is attached to another, the corresponding cluster heads will update their members' tables.
- If a node leaves its cluster and doesn't find any other cluster to attach itself, the cluster heads election procedure is invoked.
- A cluster head keeps the information concerning its members (identifier ID, status, load, energy). It can detect if another cluster head is entered in its cluster. In these cases, one of them is constrained to give up its cluster head's role. In our case, it is the one which has less energy.

- Because of the additional functionalities for which the cluster head is intended, its energy is likely to be exhausted. A minimum threshold of energy is defined for each cluster head. If it is reached, the cluster heads election procedure is invoked.

When the network is set up, each node diffuses its identifier (ID) through a HELLO message which is recorded by all the other nodes in its transmission range. Once the neighbors list of each node is ready, the clustering procedure is executed. Each node maintains a record of its status: (cluster head or member). If it is not a cluster head, it must know the cluster head to which it is affiliated (CID: Cluster head Id).

Considering the dynamic nature of the system, the nodes and the cluster heads tend to move in various directions, causing a disorganization of the network configuration. The system must be updated from time to time. The updates are made in two cases:

- When renewing cluster formation.
- When a node changes its affiliation from one cluster head to a new one, in the existing cluster heads set; in this case, we speak about re-affiliation.

If a cluster head doesn't receive any message from a node, it updates its members list. When a node is attached to another cluster head, it updates its CID and the corresponding cluster head updates its members list. When the cluster head doesn't receive any more messages of a node, it updates its members list. It is important to note that, in this work, we make some assumptions. The number of nodes per cluster is limited to avoid the cluster head congestion and for better resources utilization .In all the analyses carried out on the proposed algorithm, we assumed that all nodes are cooperative and trusted. Considering these conditions allowed us to study only the characteristics specific to the proposed algorithm.

LOAD BALANCING ALGORITHM AT THE LEVEL OF EACH CLUSTER

As mentioned previously, a principal role of a cluster head is the maintenance of load balancing in each cluster. It is the principal coordinator of its cluster; it collects periodically information about each member node of its cluster, such as energy and load values. These data are collected in the members table. When a node reaches an overloaded or low energy state, a discharge message will be transmitted to its cluster head. The latter consults its members table and chooses the one which has the smallest load and the highest energy capacity. Then it sends a response to the concerned node.

Whenever a new node joins a cluster, or an existing node exits it, the members table is updated. The bases of our load balancing algorithm are as follows:

- Cluster head nodes maintain their member's tables in order to control their member's loads. Periodically, each node, member of a cluster, sends a HELLO message and communicates its energy and load values to the cluster head which updates its table.
- Two thresholds are defined for each node: the maximum load that a node is able to carry out and the minimum energy. When this is reached, the node knows that it is going to die soon, so it decides to transfer its load to another node.
- Periodically, each node checks its load and its energy and compares them with the two thresholds. Two cases are considered:

First case: the two thresholds are not reached, in this case nothing happens and the load balancing algorithm is not invoked.

Second case: if one of the two thresholds is reached (possibly both of them), the node sends a message (DR. Discharge Request) to its cluster head. This one consults its members table; it chooses the one which has the smallest load and the highest energy capacity.

- If one node is found, the cluster head sends a positive response (message RESPONSE) to that node indicating the address of the new node that will receive the extra load.
- If several nodes are found, it chooses one arbitrarily.
- If no node is found, the cluster head diffuses a solicitation message to its different neighbors cluster heads. If it is positive, a receiving node is designated and a quantity of work is transferred to it. If the response is negative, the node is constrained to execute the work locally.

VI. RESULT ANALYSIS

In this paper, we have implemented load balancing algorithm with efficient cluster head formation for ad-hoc networks. The implementations are carried out in NS-2.

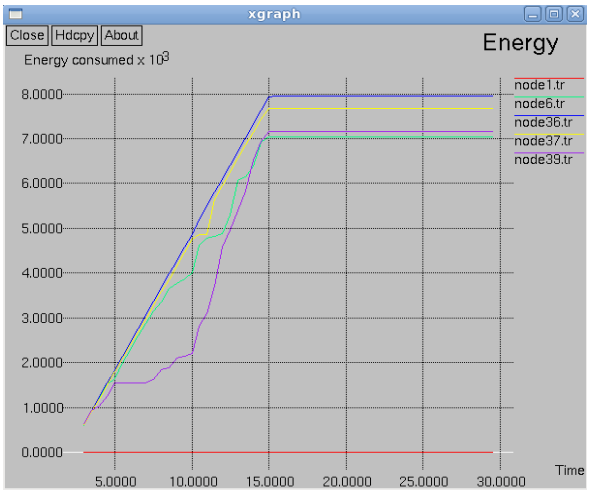

Fig. 3: Energy level graph

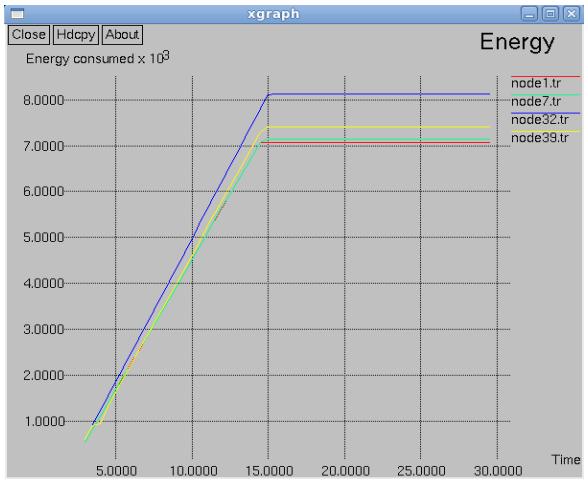

Fig. 4: Energy level graph

The energy level graph for the existing system is shown in the fig.3. The energy level graph for the proposed system is shown in the fig.4. Here we are taking node 1 and node 39 as common and this explains the improvement in energy efficiency which increases the life-time of the ad-hoc network.

VII. CONCLUSION

Load balancing is an important solution to improve the execution time of tasks and better management of the energy by reducing load imbalances in ad hoc networks. In order to take into account the limitations of these networks in terms of bandwidth and energy, clustering techniques have been suggested. In this paper, we have presented a new load balancing algorithm based on clustering where a subset of nodes 'clusterheads' is elected to coordinate their respective clusters.

The simulation results show a significant improvement of execution time (30%) and a good energy management for a great number of nodes and big sizes of work. This work is principally based on the clustering. We plan to use various clustering algorithms presented in the literature. The presented algorithm has implicitly assumed that all nodes are cooperative. In future, Cluster head selection can be more effective by choosing inner nodes of the cluster as cluster head to improve the network efficiency. If the border node of the cluster is chosen as cluster head then the data gathering in the border areas will be affected.

REFERENCES

[1] Aastha Singla, Saurabh Mittal, "Load Balancing in MANETS: A Review", International Journal of Advanced Research in Computer Science and Software Engineering, Volume 4, Issue 6, June 2014

[2] D Maheshwari and R Nedunchezhian, "Load Balancing in Mobile Ad Hoc Networks: A Survey", International Journal of Computer Applications 59(16):44-49, December 2012.

[3] Rachida Aoudjit, Mustapha Lalam, Abdelaziz M' zoughi, "Load Balancing: An Approach Based on Clustering in Ad Hoc Networks", Journal of Computing and Information Technology - CIT FEB 2009, 177–184 doi:10.2498/cit.1001194

[4] Gayathri V, Sabu E, Srikanthan T, "Size restricted cluster formation and cluster maintenance technique for mobile Ad Hoc Networks". International Journal of Network Management, Vol. 17, Issue 2, March 2007

[5] Zarifzadeh, S., Yazdani, N., Khanmirza, H., "A routing framework for load balancing of bandwidth sensitive traffic in differentiated service networks", Computer Networks: The International Journal of Computer and Telecommunications Networking, Vol. 51, Issue 4 (March 2007)

[6] H. Khamfroush, R. Saadat, A. Khademzadeh and K. Khamfroush, " Lifetime Increase for Wireless Sensor Networks Using Cluster-Based Routing", International Association of Computer Science and Information Technology - Spring Conference (IACSITSC), pp. 14–18, April 2009.

[7] W. W. Huang, Y. L. Peng, J. Wen and M. Yu, "Energy- Efficient Multi-hop Hierarchical Routing Protocol for Wireless Sensor Networks", Networks Security, Wireless Communications and Trusted Computing (NSWCTC), vol. 2, pp. 469-472, April 2009.

NEGATIVE IMPACT OF DIESEL AND USED ENGINE OIL SOAKING ON THE COMPRESSIVE STRENGTH OF CONCRETE

Girish S.Kulkarni[1], K.B.Prakash[2] , Nandini M.Naik[3]

[1]Professor Environmental science Department, Department of Technology, Shivaji University Kolhapur, Maharashtra.(India)

[2]Principal of Govt. Engineering College Haveri. Karnataka. (India)

[3]Associate Prof. Chemical Engineering Department, K.L.E Dr. MSSheshagiri College of Engineering & Technology, Udyambag, Belgaum. Karnataka. (India)

ABSTRACT

Concrete is one of the most important material used in construction. The concrete used for the construction should resist all types of loads imposed on it. Concrete tanks are used to store petroleum products. This paper attempts aims at the study of effect on compressive strength of concrete prepared with 30% Fly ash by weight of cement when soaked in water, soaked in diesel and soaked in used engine oil for 90 days and comparison of variation with water soaking. The change in compressive strength is indicative of the petroleum products on concrete. The non-randomness and ambiguity in results was analysed statistically.

Keywords:-Fly Ash, Concrete, Petroleum Products, Compressive Strength.

I INTRODUCTION

The exploitation of fly ash as cement replacement material in concrete or as an additive in cement introduces many benefits from economical, technical and the environmental points of view. Depending on the burning temperature, coal type and some other factors, fly ash shows different properties in different size fractions. In this study, different composition of fly ash varying from 0% to 40% by weight was taken. One of the previous studies showed that granulometry of fly ash has important effects on mortar strength [1]. In another study, concrete strengths were correlated to fly ash addition, amount and fineness [3]. Utilization of industrial solid wastes in concrete would help environmental abatement, in solving solid waste disposal problems.

Fly ash is the waste from the coal industries and poses serious problems of disposing. This present study focuses on the utilization of fly ash in concrete soaked in diesel and used engine oil. There has been a very comprehensive relation between concrete and petroleum products. Concrete tanks are used to store petroleum products. The cracking and deterioration of concrete due to spillage of petroleum products has been an area of interest in research. Spillage of petroleum products adversely affects marine life and environment [2]. Also petroleum comes in contact with concrete in areas like garages, automobile servicing stations, storage tanks, etc. The bore hole used in oil extraction may be lined up with concrete. Petroleum products poses a high degree of adverse effects on properties of concrete and thus degrades it. Petroleum products gets penetrated into concrete and thereby flows into underground water. The spillage of petroleum on roads leads to cracking. The study aims at avoiding these effects by mixing concrete with Fly-ash to an optimum extent. This technique is applied in the construction of roads, garage floorings and petroleum product's storage tanks. In all of the above mentioned

instances, petroleum products come in contact with concrete in one way or the other and have a specific impact on its characteristic behaviour.

The rest of the paper is organised as follows. Section 2 deals with the related work. Section 3 elaborates the materials used in the implementation. Section 4 deals with the results and discussion. The paper concludes in Section 5.

II RELATED WORK

Concrete is one of the most important materials used in construction. The concrete used for the construction should resist all the type of loads imposing on it. The service life and durability of concrete structure strongly depend on its transport material properties like permeability, sorptivity, diffusivity and water absorption [4]. The effect of oil soaking on the dynamic modulus of elasticity of concrete was investigated to study the deterioration rate due to concrete contact with crude oil [5](M.A.Matti ,1983). He has also studied the shrinkage of oil soaked concrete. He has found that the volume of concrete decreases when it comes in contact with crude oil [6](M.A Matti, 1982). [7](F. I. Faiyadh, 1985), investigated the bond characteristics of oil saturated concrete. The average bond strength of oil soaked specimens decreased with the soaking period. [8](Ramzi B.Abdul et al, 2000) analysed the compressive and tensile strength of concrete loaded and soaked in crude oil. Based on short and long term loading, the effect of crude oil on compressive, splitting tensile and flexural tensile strength of concrete was investigated. He found that the rate of crude oil absorption is high at the early stage of soaking, but later on, the rate decreases. This shows the reduction in the absorption by 30 to 40 % strength in specimens under loading versus unloaded specimens. Usage of fly ash in concrete considerably increases the compressive strength of concrete [9].

III MATERIALS AND METHODOLOGY

This section gives the details of the composition of the materials used for the experimentation. The details of Ordinary Portland cement, 43 grades conforming IS: 8112-1989 are provided in Table 1. Fly ash was obtained from Raichur Thermal Power Station, Shaktinagar, composition of Fly ash is given in Table 2. Locally available sand of specific gravity 2.64 and coarse aggregates of (10 mm and 20 mm) 2.90 were used. Water from city source is used for both concreting and for curing. Petroleum products like diesel and used engine oil are obtained from automobile service stations, composition of diesel and used engine oil given in Table 3 and 4.

Table 1. Physical Properties of Ordinary Portland Cement

Particulars	Experimental result	As per standard
Fineness	308 m^2/kg	Not less than 225 m^2/kg
Normal consistency	28.26	---
Soundness		
By Le-ChatelierExpn. (mm)	1.5 mm	Not more than 10 mm
By Autoclave Expn. (%)	0.070	Not more than 0.8
Setting time (minutes)		
Initial	180	Not less than 30
Final	250	Not more than 600
Compressive strength (MPa)		
3 days	23.98	Not less than 23
7 days	34.85	Not less than 33
28 days	45.36	Not less than 43

Table 2. Chemical Composition of fly ash

Chemical composition	Percentages
Silica (SiO_2)	56.88
Alumina (Al_2O_3)	27.65
Iron oxide (Fe_2O_3)	6.28
Alkalies (Na_2O+K_2O)	0.46
Calcium oxide (CaO)	3.62
Magnesium oxide (MgO)	0.34
Titanium oxide (TiO_2)	0.31

Table 3. Properties of diesel fuel of SAE 40

Properties	Results
Sp. Gravity @ 15.6 °c	0.897
Viscosity :cSt @ 40°C,cSt @ 100°C	142, 14.5
Viscosity Index	100
Flash Point, °c	230
Pour Point, °c	-12
Color (ASTM)	4.0
TBN	9.5
Sulfated ash, wt %	1.2

Table 4. Properties of used engine oil

Properties	Results
Kinematics viscosity at $40^{o}C$	111.32
Kinematics viscosity at $100^{o}C$	17.83
Viscosity index	99
Flash Point, °c	230
Pour Point, °c	-10
TBN	-
Sulfated ash, wt %	4.5
Specific gravity	0.928

3.1 Preparation of specimens

M 30 grade concrete designed as per IS: 10262-2009 which yielded a proportion of 1:1.76: 3.15 with a w/c ratio of 0.49 and Fly ash was added from 0 to 40 percent by weight of cement. Then the mix was placed layer by layer in the moulds to cast the specimens. The specimens were compacted by hand as well through vibrating table. The specimens were finished smooth and kept for 24 hours and then they were subjected to water curing for 28 days. After water curing, the specimens were soaked in diesel and used engine oil for 90 days. They were

tested for their respective compressive strengths as per IS specifications Standards, 150 mm x 150 mm x 150 mm.

It is convenient to use fly ash pozzolanic mineral admixture to replace a large quantity of cement in concrete. It not only enhances the quality of concrete, but it also helps in the preservation of many resources as well as it is eco-friendly. Cement shows high compressive strength without fly ash in the early stages. But though initially the fly ash mixed concrete shows lower compressive strength values, but it increases with time later [10]. Fly ash significantly increases concrete's strength and workability. It can also nurture the durability and chemical resistance of concrete [11].

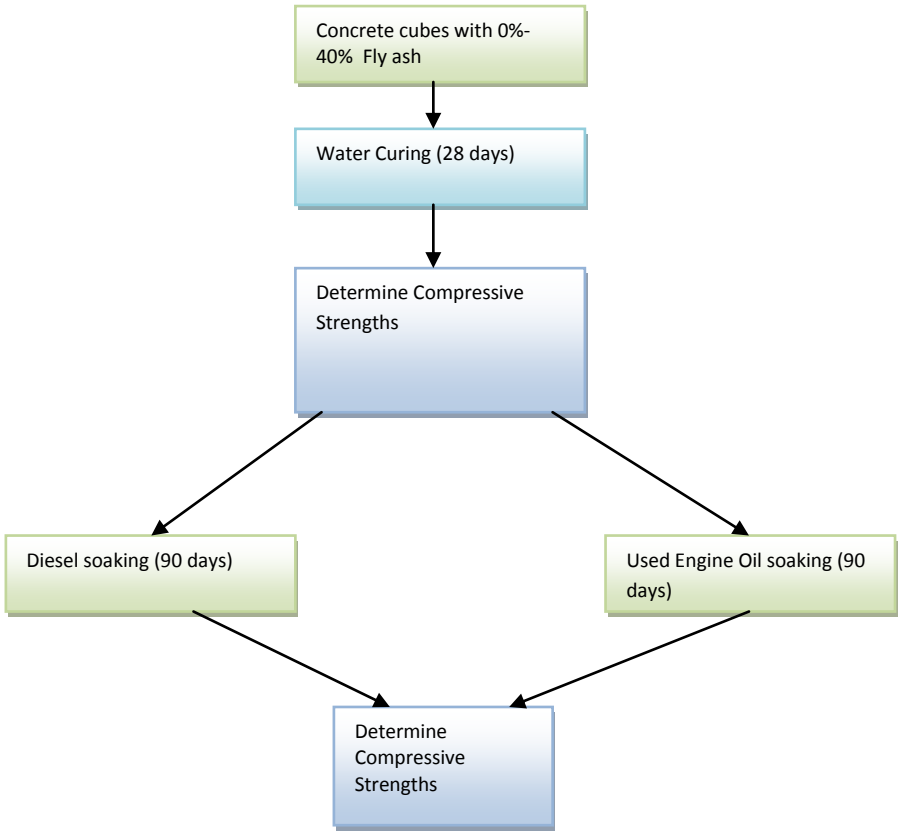

Fig. 1 Overall System Implementation Schema

Fig. 1 shows the system implementation. As is evident from the figure, concrete cubes were subjected to water curing for 28 days and the compressive strengths of few samples were noted (since all the other samples were identical in composition and size, their strengths)

IV RESULTS AND DISCUSSIONS

Studies reveal the fact that compressive strength of concrete increases when cured in water. It has been observed experimentally that the addition of fly ash exhibit considerable increase in compressive strength and durability characteristics. Fig. 2 indicates the variation in compressive strength of concrete specimens prepared with 30% of fly ash by weight of cement cured 28 days in water and soaked in diesel oil for total period of 90 days.

Similarly, Fig. 3 shows the variation in compressive strength of concrete specimens prepared with 30% of fly ash cured in water for the first 28 days and soaked in used engine oil for a total period of 90 days.

Variations of compressive strength results of concrete indicate the effect of petroleum products, Results exhibit considerable reduction in strength of concrete. The sharp decrease in compressive strength due to petroleum products curing is an indicative of the degradation that concrete undergoes after being used in contact with petroleum products. Since there is not enough work available on petroleum products curing of concrete, we use statistical analysis to judge the relation and non-randomness of the data sets.

In case of diesel curing, the regression analysis was as follows:-

Co-relation factor R^2=0.5373.

Slope= -0.1164.

The relation can be obtained as:-

Y=-0.1164x+43.375.

Similarly in case of used engine oil curing, the regression analysis bore:-

Co-relation factor R^2=0.406.

Slope= -0.0981

The relation can be obtained as:-

Y=-0.0981x+42.35

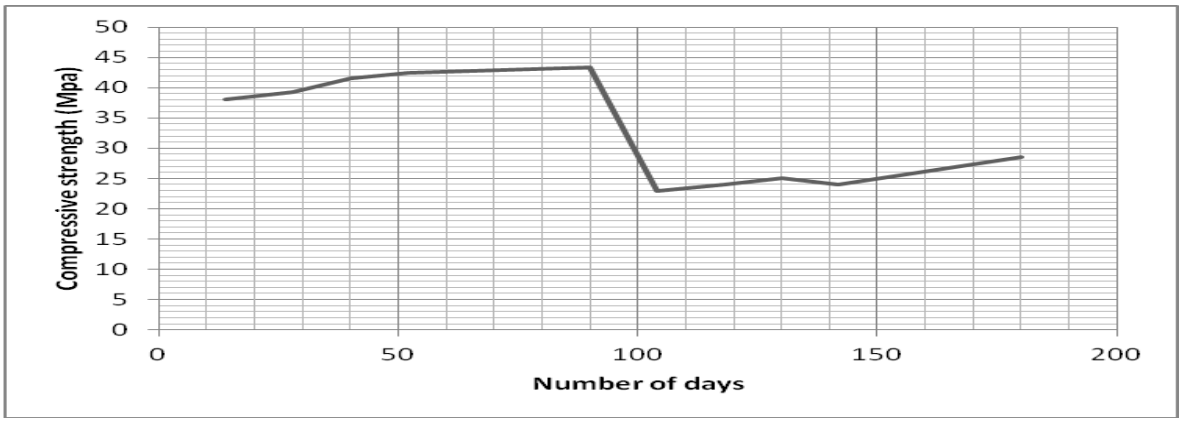

Fig 2. Variation in compressive of Diesel cured concrete.

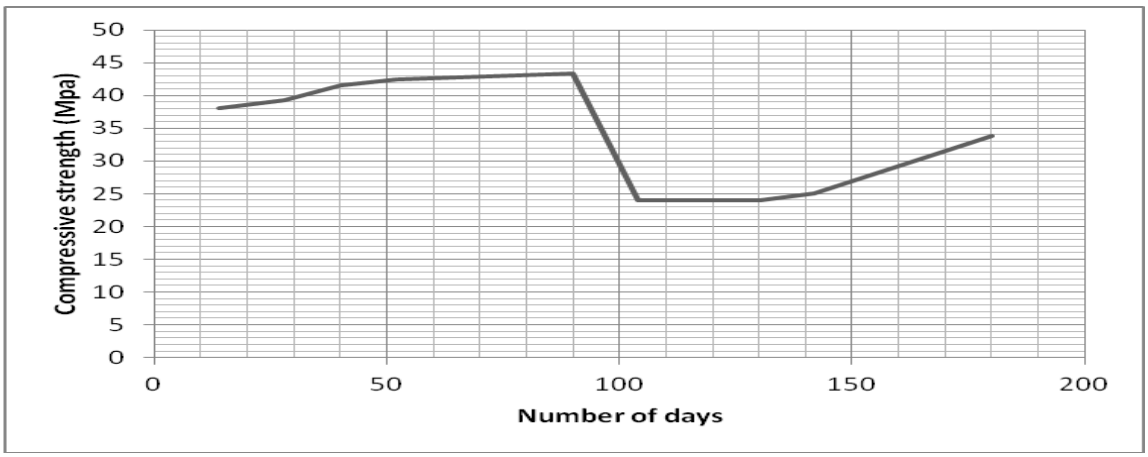

Fig 3. Variation in compressive strength of Used engine oil cured concrete.

Randomness checking in this case is of paramount importance as it yields us the conclusion whether or not obtained data is random. Proving randomness of this data is indicative of wrong experimentation. But the data were not random here. Runs test was used in this context. It is basically a statistical procedure which examines whether the data in a given distribution occurs randomly.

Randomness is doubted when there are too many or too few runs.

Hypothesis:

H_0: The observations in the sample are random.

H_1: The observations in the sample are not random.

The procedure requires calculating the values for the following variables:

n=Total sample size.

n_0=Number of sample members of one type (number of samples below mean).

n_1=Number of sample members of another type (number of samples above mean).

Calculate $n=n_0+n_1$.

Reject H_0,

If R<=lower critical values (few runs)

If R>=upper critical values (many runs).

If both n_0 and n_1 are <=20, the small sample runs test is appropriate.

The algorithm for carrying out the runs test is as follows:

Small Sample Runs test:

α=0.05

Calculate R.

If $n_0-1 < R < n_1-1$, do not reject the null hypothesis, H_0.

Else reject H_0.

Large Sample Runs test:

If n_0 or n_1 is greater than 20, then calculate

$$\text{Mean}=\frac{2\times n0\times n1}{n+1}$$

$$\text{Variance}=\frac{2\times n0\times n1\times(2\times n0\times n1-n)}{(n-1)\times n^2}$$

Standard Deviation=√Variance

$$Z=\frac{R-Mean}{Standard\ deviation}$$

If -1.96<=Z<=1.96, do not reject H_0,

Otherwise, reject H_0.

The runs test a result on the above cases is as follows:

1). Diesel curing

Number of runs=2

Z-value= 2.01

2). Used engine oil curing

Number of runs=3

Z-value=1.99

It can be observed that the fewest number of runs and the value of Z are indicative of the non-randomness of the datasets. Also the larger value of R^2, holds this argument.

V CONCLUSION

The negative impact of diesel and used engine oil on fly ash concrete was assessed. The non-randomness in the datasets was assessed using the correlation test and the runs test.

VI ACKNOWLEDGEMENTS

The authors are immensely grateful to the Principal, KLE Dr. M. S. S. College of Engineering and Technology, Belgaum, and to the Department of Technology, Shivaji University, Kolhapur; for all the crucial amenities provided for the experimentation.

REFERENCES

1 J. Monzo, J. Paza, and E.P. Mora, Cem. Concr. Res. 24, 791–796 (1994).

2 S.P.Ejeh, at al, (2009) Effect of Crude Oil Spill on Compressive Strength of Concrete Materials.,*Journal of applied sciences Research*,5(10): 1756-1761.

3 S. Slanicka, Cem. Concr. Res. 21, 285–296 (1991).

4 Martys NS. Survey of concrete transport properties and their measurement. NISTIR 5592, US Department of Commerce, 1996, pp. 1–40.

5 M.A.Matti (1983), The Effect of oil soaking on the dynamic modulus of concrete, *International journal of cement composites and lightweight concrete*, Vol.5, No. 4.

6 Matti A. M (1976) Shrinkage of oil soaked concrete *University of Sheffield*, U.K.

7 F. I. Faiyadh (1985). The Bond characteristics of oil saturated concrete *International journal of cement composites and lightweight concrete*, Vol.7, No. 2.

8 Ramzi B. Abdul, et al(2000). Compressive and tensile strength of concrete loaded and soaked in crude oil. *Engineering journal of the University of Qatar*, vol.13, 2000, pp.

9 Prediction model of compressive strength development of fly-ash concrete

10 Kwangryul Hwanga, et al(2004)., Building Research Institute, Department of Architecture, College of Science and Technology, Nihon University, Tokyo, Japan Received 18 March 2003, accepted 7 April 2004.

11Neville A.M. (2000),Properties of concrete, 4th and final edition, *Pearson Education Asia Pte. Ltd*., England, First Indian reprint.

SYNTHESISCHARACTERIZATION AND STUDY OF COBALTDOPED LYSINE CARBONNANOTUBESINAQUEOUSMEDIUM

Sarvesh Kumar Shailesh[1] ,K Yadav[2]

[1]*Department of Chemistry, Mewar University, Chittorgarh, Raj, (India)*
[2]*Department of Chemistry ,Samastipur College Samastipur, Bihar, (India)*

ABSTRACT

Carbon Nano tubes have been considered as one of the most promising material for a wide range of applications, in virtue of their outstanding properties. During the last two decades, both single walled and muti-walled CNT's probably represented the hottest research topic covering materials science. Due to various application of CNT's, it is a very interesting research area for new research to develop feasible, efficient and economical methods for the synthesis of CNT's. The work in this paper deals with the synthesis of multi-walled CNT's from step of number of unit processes and operations. CNT's have been synthesizing from the complexes of transition metal Co (II) with amino acid present in egg albumin in aqueous medium. The complex so formed, is analyzed on the basis of spectroscopic method using IR and NMR Spectra confirmed the cobalt-lysine complexes. The cobalt-lysine complex is decomposed at higher temperature using muffle furnace to get metal carbon nanotubes. These metal carbon nanotubes are characterized using scanning probe instruments like AFM, TEM, X-RD . The properties examined from the analysis shows a very high thermal stability as well as electrical conductivities. This result shows that CNT's made by this process can be further used in various applications of Electrical & Electronics devices.

Keywords:-Co (II), Albumin-Metal-Complex, IR, NMR , AFM, TEM, XRD.

I. INRTODUCTION

Carbon Nanotubes (CNT's) are allotropes of Carbon with a Nano structure. Due to the unique properties of carbon nanotubes, such as high specific surface area, thermal conductivity, chemical stability, optical, mechanical and electrical properties, carbon nanotubes are considered as one of the best area for replacing traditional conventional processes with this new emerging science aimed at miniaturizing of processes with almost efficient uses compared to others. It consists of Graphite like Carbon, having a length of 1-100 nm and a diameter up to several micrometers or even up to millimeters.The transition from micro particles to nanoparticles leads to a number of changes in physical properties. One of the major factors is the increase in the ratio of surface to volume area. As the surface area of a particle increases, the portion of its constituent atoms at or near the surface increases exponentially, creating more sites for bonding, catalysis or reaction with surrounding materials, resulting in improved properties such as increased strength or chemical or heat resistance. Additionally, the fact that nanoparticles have dimensions below the critical wavelength of light can render them transparent, which has implications for part aesthetics. They are among the stiffest and strongest

fiber known and have remarkable electronic properties with many other unique characteristics. Carbon nanotubes have a broad range of potential applications in Nano electronics, gas sensors, cancer therapy and diagnoses. Nano medicine provides a great potential in fighting many dangerous diseases like cancer and also it has great efficiency in drug delivery. [1,2,6] Due to huge application of CNT's, it is required to develop new economical methods and techniques to prepare Carbon Nanotubes and characterized them. For the economical production of carbon nanotubes protein source can be taken as the key material. It is also required to discover some desired properties in them, so that they can be used in various applications.

II. SYNTHESIS OF CARBON NANOTUBES BY CHEMICAL METHOD

2.1 Material and Method

2.1.1 Preparation of CNTs in Aqueous Medium

It takes place in two steps. First is formation of Cobalt egg albumin complex and second is decomposition of complex material to form multi-walled CNT's.

2.1.2 Preparation Of Cobalt Doped Lysine Complex

To prepare the carbon nanotubes the solution of cobalt metal salt with concentration of 1N was prepared in distilled water solution by AR grade techniques. The concentration of Cobalt metal ion was then allowed to react with egg albumin to give Cobalt metal doped lysine complex. The Cobalt doped lysine complex is taken out and kept in desiccator for drying. The complex has to be dried for forty days. Protein comprising of amino acid present in egg albumin as a monomer, when reacted with alcoholic solution of cobalt salt forms complex with Co^{2+} ions. In this complex lone pair present on the nitrogen of NH_2 and oxygen of COO^- of COOH group formed cross link between two amino acid chains as shown below. The complex formed was characterized by **NMR**described in characterization of complex and CNT's later in this paper.

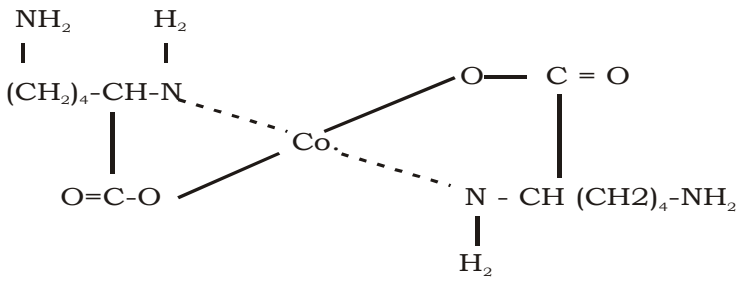

Fig-1: Lysine – Cobalt (II) Complex

2.1.3 Synthesis Of CNT'S.

In order to obtain CNT's the complex was decomposed in muffle furnace. The decomposition takes place at either of temperatures at 800 °, 900° or 1000°c. [3,4,5].After the preparation of cobalt doped lysine complex, the extra metal ion are removed from the surface by washing it from 1N HCl solution. Multi-walled CNT's are prepared mostly at temperature as high as 800-900^{0}C as at high temperature than this range the formation tends to single walled structure. The characterization of multi-walled CNT's are done from AFM, DLS, TEM,andXRD, explained in the next section of this paper.

III. CHARACTERIZATION

3.1 Spectral Studies Of Formation Of Cobalt Doped Lysine Complex

Though it is very difficult to analyze the complexes of albumin and metal but certain important feature can be identified which give valuable information about the structure.

3.1.1NMR (Nuclear Magnetic Rasonance) Spectra

NMR Spectra of Cobalt Amino acid complex is shown in fig-3. The information from the NMR Spectra is summed up in the table -2 shows the chemical shift of the protons.

Table-2: Characteristics Proton Chemical Shift:

Types of proton	Chemical shift S(PPM)
$R.CH_3$	0.839
$R_2. CH_2$	1.220
H-C-COOH	2.486
NH_2	3.310

Fig-2: NMR Spectra Of The Synthesized Cobalt Doped Lysine Complex In Aqueous Medium

In the "H NMR spectra of the synthesized cobalt Amino acid Complex with chemical shifts within the range 3.310 PPM the NH_2 Protons was observed. In the spectra, signal with chemical shift at 2.486 PPM C-H Protons attached to the COOH in the amino acids was observed in the spectra signal with chemical shifts at 1.220 PPM is related to the R_2 -CH_2 (secondary type) Protons and the signal with chemical shift with the 0.839 PPM corresponds to the $R.CH_3$ (Primary type) protons also observed.

The above examination of the material by IR and NMR spectroscopy shows the presence of Cobalt doped lysine complex.

3.2 Characterization Of Cnt's By Scanning Probe Instrument

3.2.1 AFM (Atomic Forces Microscopy)

Surface imaging studies were performed using Atomic force microscopy (AFM) to estimates surface morphology and particle size distribution. By this investigation we came to know that the linear dendritic shape of metal ions presents at the surface of Carbon nanotubes. The white spots in figure 5 show the presence of Co metal ions in rare linear dendritic form with mutli-walled structures .The particle size predicted is 90 nm in . The maximum peak height obtained is of 179.25 nm with no peaks in between[8,9,10]. The distance between peak to peak in y-direction is 179 nm and in z-direction is 89.78 nm shown in figure 8-. Average sizes of peaks are 101.38 nm or Defined line distanced from the mean line (z_i) with roughness approximately 20.93 nm can be calculated by $R_a = \frac{1}{L}\int_0^L [z(x)]\,dx$ [11,12,13,14,15]

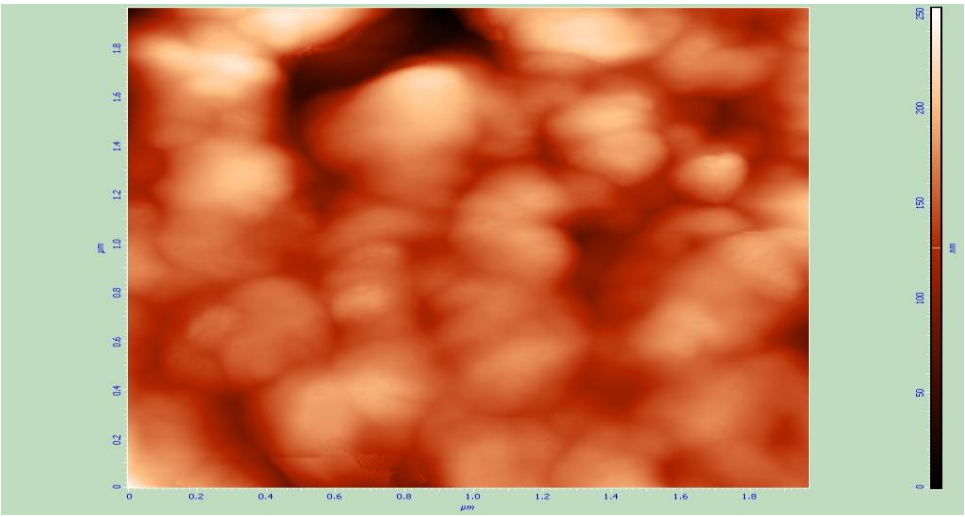

Fig 3 (a): The white spots in fig show the presence of Co metal ions in rare linear dendritic form with mutli-walled structures.

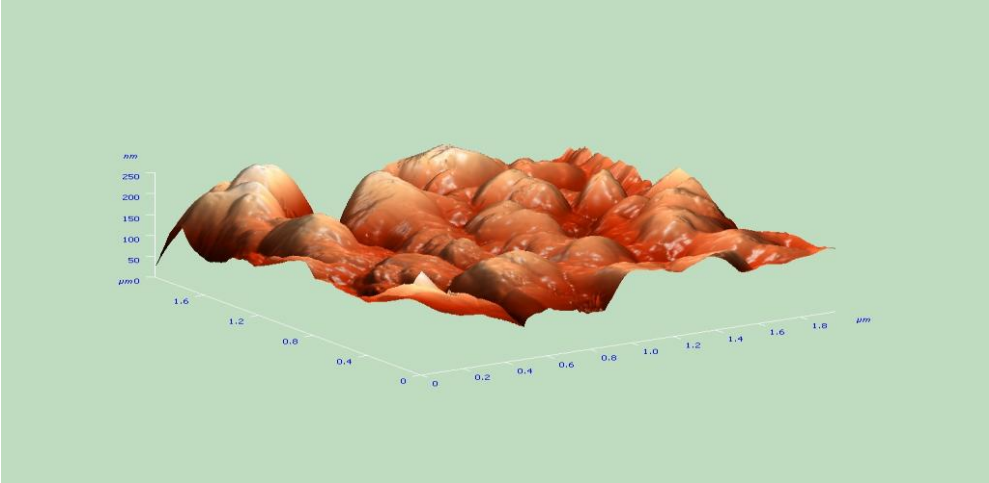

3 (b) : shows 3D morphology of Co metallic ion made CNT'sFig

3.2.2 TEM (Transmission Electron Microscopy)

As a result, a specimen having non-uniform density, shape and thickness can be examined by this technique.Figure 4 shows a TEM micrograph of cobalt nanoclusters, where almost all of the particles stick together as one can see better in the picture taken with 500 K magnification. In such cases, reliable particle counting is impossible with or without touching particles being ignored. This is not due to any inherent inability of Image; instead, it is due to the inherent tendency of thenanoparticales to aggregate[16]. This analysis confirmed that the diameter of the particle is in between 10- 20 nm.It also predicted the zig-zagdendrimer shape of carbon nano tubes [17,18,19].

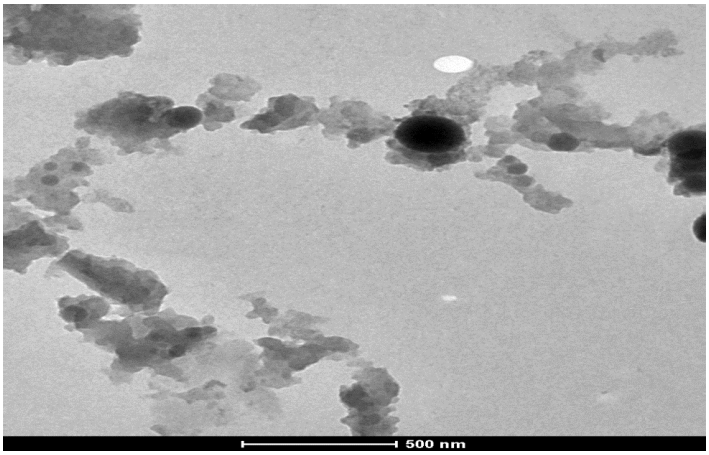

Fig 4:- TEM Images Of Carbon Nanotubes Synthesized On Decomposition Of Cobalt Egg Albumin Complex At 900

3.2.3 X-Ray Diffraction

The X-Ray power diffraction pattern of product were recorded with Cu K*a*radiation (1.54056 λ = A°) in 2 θ range from 15° to 80°.The analysis of the X-RD report we find different peaks at different value of 2ɵ and degree. e.g ((2Theta, d) = (24.662^0,3.60692; 48.877^0,1.86191;50.208^0,1.81560;69.804^0,1.34626)), this shows that the analysed sample is multi-walled carbon nanotubes. The report of sample given in figure 5

Dynamic light scattering (DLS) method has been employed for obtaining the microstructure zetapotential value, average cumulate diameter and the characteristics of the microstructure. The Malvern instrument has been used with Parameter Value **of** Sizing range 0.6 nm to 6 µmDiam, Concentration range 0.1 mg/mL ,Lys to 30w% ,Min sizing sample volume 12 µL ,Min zeta sample volume 0.75 mL, Temperature control 2 to 90 oC, Conductivity range 0 to 200 mS/cm , Laser 3 mW 633 nm He-Ne. the dispersant used is ethylene glycol with RI 1.452 the CNT has RI value of 1.59.

Dynamic light scattering techniques will give an intensity weighted distribution, where the contribution of each particle in the distribution relates to the intensity of light scattered by the particle. It also measures the time dependent fluctuation in the scattering intensity to determine the translational diffusion coefficient(D_T) and subsequently hydrodynamic radius(R_H).

Z-analysis or comulant mean from the dynamic light scattering comes out to be 94.03 nm. The Bimodal curves for each colored lines shows presence of impurities of Co ion complex and the polydespersity index value is 1 which shows broad size distribution of Co ion composites. The y-intercept can be used to evaluate the signal-to-noise ratio from a measured sample and thus is often used to judge data quality , the intercept value is 0.939

which shows a very good sytem as an ideal system gives value of 1.0 .the three curves in the fig shows number, volume and intensity distribution respectively.

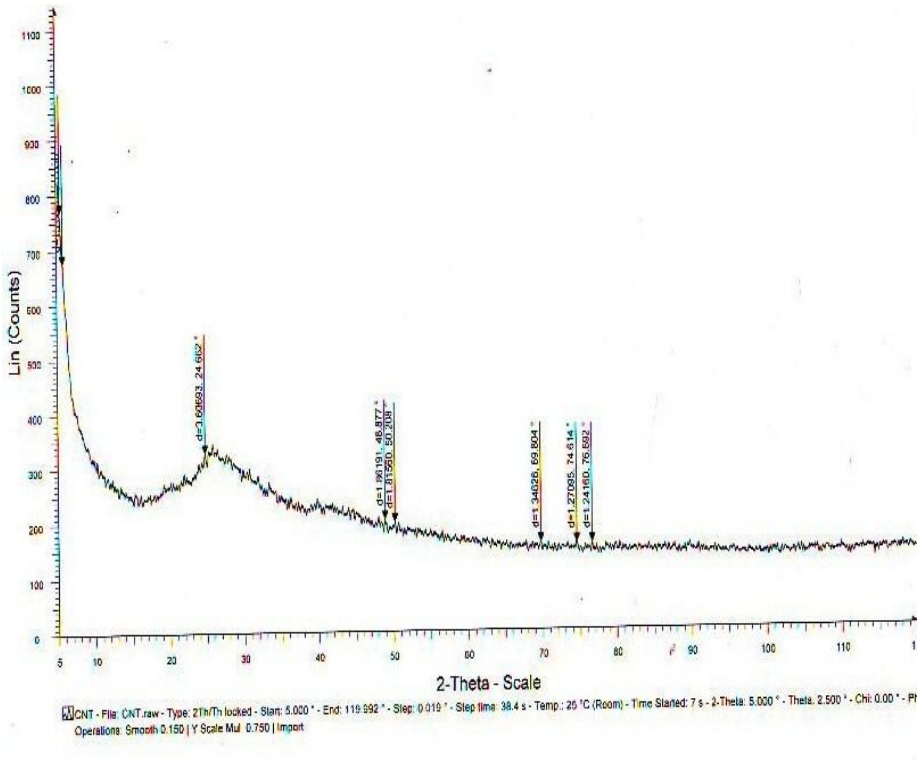

Fig-5: The X-RD Image Of Carbon Nanotubes Synthesized At Decomposition Of Cobalt Egg Albumin Complex At 800^{0}C

3.2.4 Dynamic Light Scattering

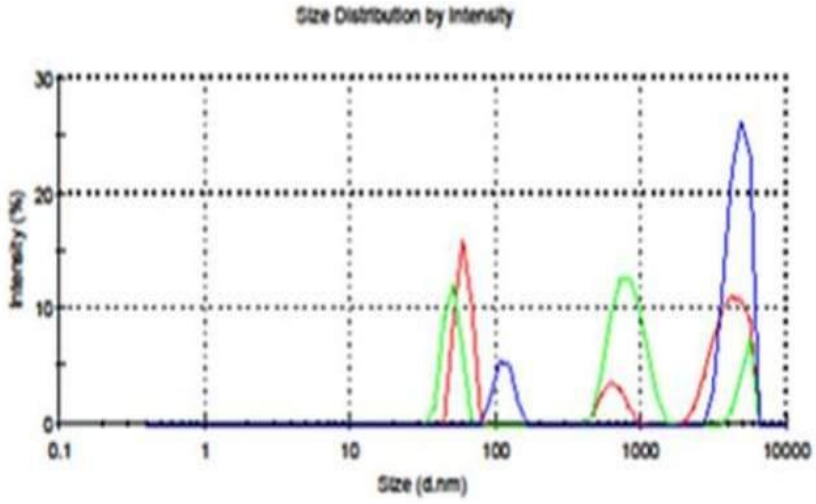

Fig.-6.Dynamic Light Scattering Of Carbon Nano Tubes Synthesized At The Decomposition Of Cobalt Doped Lysine Complex

IV. RESULT & DISCUSSION

Carbon nanotubes are prepared by the decomposition of Cobalt doped lysine complex. These Carbon metal nanotubes are formed to exhibit electrical conductivity proves by dynamic light scattering. This shows the presence of unpaired electron and exhibit Para magnetic behavior. It is also predicted to exhibit thermal conductivity.The TEM analysis confirmed that the diameter of the particle is in between 10- 20 nm.It also predicted the zig-zagdendrimer shape.

V. CONCLUSION

Multi-walled Carbon nanotubes have been prepared by AR grade technique using egg albumin and CO metal ion in aqueous medium. The NMR spectra of sample proves the preparation of Cobalt doped lysine complex. The AFM, TEM image confirms that metal ion present has a linear dendritic copolymers on to the surface of CNT's which can show a great advantages for drug delivering or chemical catalytic reactions in controlled and efficient manner. The large surface to volume ratio can be used in replacing silicon with CNT's for maximizing energy production in solar cells and electrical conductivity. The X-RD studies of the CNT confirm the multi-walled structure of carbon nanotubes. The DLS analysis proves the nano range of the carbon nanotubes and its electrical conductivity.

REFERENCES

[1] Banerjee, K.; What are Carbon Nanotubes?; ACM/SIGDA E- Newsletter, Vol. No.**22, 2006.**

[2] Iijima, S.; Helical Microtubules of Graphitic Carbon," Nature, Vol**. 354, pp. 56-58, 1991**

[3] Dresselhaus M.S., Dresselhaus G. et al.; Carbon Nanotubes: Synthesis, Structure, Properties and Applications, Springer -Verlag; **2000**.

[4] Meo, S.B.; Andrews R..; " Carbon Nanotubes: Synthesis, Properties, and Application". Crit. Rev. Solid State Mater. Sci. **26(3): 145-249,(2001**).

[5] Cao ,G.; Nanostructures and Nanomaterials: Synthesis, Properties and Application, Imperial college Press, **pp. 245-450,(2001**).

[6] Ratnar, M. ,Ratnar, D.; Nanotechnology "A gentle introduction to next big idea", **pp. 120-130 (1999).**

[7] Whatmough, R.; Automatic threshold selection from a histogram using the "exponential hull", CVGIP: Graphical Models and Image Processing, vol. **53, no. 6, pp. 592-600, 1991.**

[8] Russ, J.; Computer-Controlled Microscopy: The Measurement and Analysis of Images, Plenum Press, New York, **1999**

[9] Lindley, C.; Practical Image Processing in C, John Wiley & Sons, Inc., New York, **1991.**

[10] Parker,J.; Gray level thresholding in badly illuminated images, IEEE Transactions on

[11] Pattern Analysis and Machine Intelligence, **vol. 13, no. 8, pp. 813-819, 1999.**

[12] Oliveira, R. et. al.; Measurement of the Nanoscale Roughness byAtomic Force Microscopy:Basic Principles and Applications; Federal University of São Carlos**;2012**

[13] Wilson, R. A., &Bullen, H. A.; (2007). Introduction to Scanning Probe Microscopy. Department of Chemistry, Northern Kentucky University, Highland Heights, KY 41099. Accessed 10;03;2011.

[14] Czifra, A., & Horvath, S. Complex microtopography analysis in sliding friction of

[15] steel-ferodo material pair. Meccanica.Vol. 46, No. 3, (jun 2011), pp**. 609-616, 1572- 9648(2011).**

[16] Freitas, A. C. P.; Influencia do tipo de polimentopós-clareamentonaalteração de

[17] rugosidade, cor e brilho da superfície de esmalte dental humano. 110 p. Thesis (Phd in Dentistry) – University of São Paulo, USP, Brazil, São Paulo, 2010.

[18] Rohit K. et. al.; Preparation, Texture, and Magnetic Properties of Carbon Nanotubes/Nanoparticles Doped with Cobalt; J. Phys. Chem. B **2002, 106, 4079-4084.**

[19] Khassin, A. A.; Yurieva, T. M.; Zaikovskii, V. I.; Parmon, V. N. React. Kinet. Catal. Lett. **1998, 64, 63.**

[20] Nikolaev, P.; Bronikowski, M. J.; Bradley, R. K.; Rohmund, F.; Colbert, D. T.; Smith, K. A.; Smalley, R. E. Chem. Phys. Lett. **1999, 313,91** TEM

[21] Gerd H.; WOEHRLE ; Analysis of Nanoparticle Transmission Electron Microscopy Data Using a Public-Domain Image-Processing Program, Image; Turk J Chem**30 (2006) , 113.**

[22] Kiskinova, M. P. Surf. Sci. **1981, 111, 584.**

NEXT GENERATION GSM TECHNOLOGIES: 3GPP VS. LTE

Susmit Paul[1], Sakshi Arya[2]

[1]*Department of Electronics & Communication Engineering, Tula`s Institute, Dehradun (India)*

[2]*Department of Electronics & Communication Engineering, Tula`s Institute, Dehradun (India)*

ABSTRACT

Mobile communication is continuously one of the hottest areas that are developing at a booming speed, with advanced techniques emerging in all the fields of mobile and wireless communications. Wireless services have the highest demand in wireless and internet world. Mobile phones are rapidly becoming the preferred means of personal communication. Communication system has evolved from wired button telephone system to wireless mobile phone in the few years. With wider use of mobile communication which provides an easement to fast and easy communication mode. Nowadays the use of 3G mobile communication systems seem to be the standard, while 4G stands for the next generation of wireless and mobile communications. Due to the increase in demand for speed, multimedia support and other resources, the wireless world is looking forward for a new generation technology to replace the third generation. The 4G system provides mobile ultra-broadband, internet access with very high speed data rate. Currently marketed technologies such as LTE (Long Term Evolution) and Wi-MAX have been around for a few years and are being marketed as 4G whilst not meeting the requirements set by the ITU. In this paper firstly we will introduce a brief study of the generations of the wireless GSM system. Currently we are using the 3G connection almost all over world. But somewhere when we count the no of users in developing countries, we get the reality. Till the date, maximum users use 2G wireless system. But instead of 3G, 4G technology is used in developed countries. Here we will compare the 4G technology with 3G. After comparing this, we will introduce the future GSM technology 5G which will revolute the whole world.

***Keywords*: Mobility, wireless system, 3G, 4G, 3GPP, LTE, Wi-Max, ITU, CDM, WCDMA, GPRS.**

I. INTRODUCTION

Over the past decade, wireless communications has seen an exponential growth and will certainly continue to amazing developments due to the emergence of new interactive multimedia applications and its highly integrated systems driven by the rapid growth in information services and microelectronic devices. So far, most of mobile systems are mainly targeted to voice communications with low transmission rates. In the near future, however, broadband data access at high transmission rates will be needed to provide users packet-based connectivity to a plethora of services. It is also almost certain that the next Generation (XG) wireless systems will consist of complementary systems having a set of different standards and technologies along with different requirements and complementary capabilities that will offer users ubiquitous wireless connectivity between mobile and

desktop computers, machines, game systems, cellular phones, consumer electronic products, and other hand-held devices. A key requirement of wireless system in future is their ability to provide broadband connectivity with end-to-end Quality of Service (QoS), a high network capacity, and throughput at a low cost. To support the above services, a host of new issues and problems have to be addressed. This talk will discuss the challenges facing the 3G communication networks and at some of the important issues pertaining to the evolution of mobile communication networks from GSM (Global System for Mobile Communications) to GPRS (General Packet Radio Service) to 3G (Third Generation) and to CDMA and WCDMA. And also describe some of the leading enabling technologies and comparison of CDMA2000 and WCDMA.

II. CONCEPT OF 3G TECHNOLOGIES

In present investigation, the experiment test rig was built in the vibration lab. The vibration characteristics of UMTS (Universal Mobile Telecommunications System) is a so-called "third-generation (3G)," broadband, packet-based transmission of text, digitized voice, video, and multimedia at data rates up to and possibly higher than 2 megabits per second (Mbps), it offers a compatible set of services to mobile computer and phone users no matter where they are located in the world. Based on the GSM communication standard, UMTS, endorsed by major standards bodies and manufacturers, is the planned standard for mobile users around the world by 2002. Once the implementation in UMTS completed computer and phone users can be constantly attached to the Internet whether they travel or as they roaming service, it has the same set of capabilities no matter where they travel to. Users will have access through a combination of terrestrial wireless and satellite transmissions. Until UMTS is fully implemented, users can have multi-mode devices that switch to the currently available technology where UMTS is not yet available.

2.1 Spread Spectrum of 3G System

It is a kind of modulation system in which the modulated (spread spectrum) signal bandwidth is much greater than the message signal bandwidth. The spectral spreading is independent to the massage signal and is only performed by a code. The same code is used at receiver to dispread the received signal and to recover the message signal. It is very secure, is nearly impossible to intercept without knowing the chip code. A large number of codes can support a large number of users. The system is less liable to distortion as a large bandwidth is used . Since the power is distributed in a large bandwidth so the power spectral density goes below to noise level so it resist to jamming and remain invisible to unintended users. It provides asynchronous multiple access.

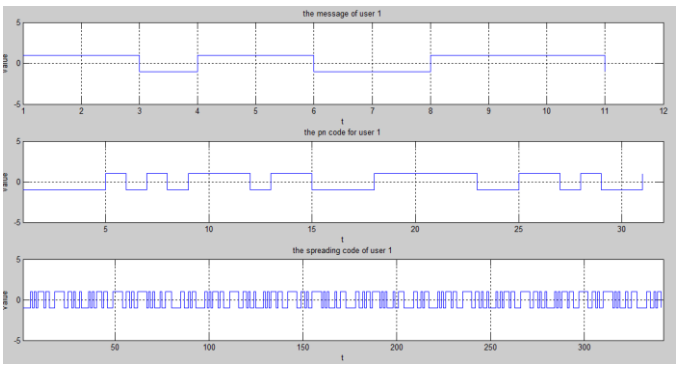

Fig: 1 Spread Spectrum of 3G

In direct sequence spread spectrum, the stream of information to be transmitted is divided into small pieces, each of which is allocated across to a frequency channel across the spectrum. At the point of transmission data signal is combined with a higher data-rate bit sequence (also known as a chipping code) that divides the data according to a spreading ratio. If the data bits are damaged then the redundant chipping code helps the signal resist interference and also enables the original data to be recovered. In an FH-CDMA system, a transmitter "hops" between available frequencies according to a specified algorithm, which can be either random or replanted. The transmitter and receiver are synchronized and remains tuned to the same centre frequency. A short burst of data is transmitted on a narrowband. Then, the transmitter tunes to another frequency and transmits again. The receiver thus is capable of hopping its frequency over a given bandwidth several times a second, transmitting on one frequency for a certain period of time, then hopping to another frequency and transmitting again. Frequency hopping requires a much wider bandwidth than is needed to transmit the same information using only one carrier frequency. The Near-Far problem of DS/SS is avoided here. FH-CDMA devices use less power and are generally cheaper, but the performance of DS-CDMA systems is usually better and more reliable. The biggest advantage of frequency hopping lays in the coexistence of several access points in the same area, something not possible with direct sequence.

2.2 WCDMA Protocol Architecture for 3G

CDMA is a form of multiplexing, which allows numerous signals to occupy a single transmission channel, optimizing th e use of available bandwidth. The technology is used in ultra-high-frequency (UHF) cellular telephone systems in the 800-MHz and 1.9-GHz bands. CDMA employs analog-to-digital conversion (ADC) in combination with spread spectrum technology. Audio input is first digitized into binary elements. According to the defined pattern (code), the frequency of the transmitted signal is then made to vary, so it can be intercept only by a receiv er whose frequency response is programmed with the same code, so it follows exactly along with the transmitter frequency. There are trillions of possible frequency-sequencing codes; this enhances privacy and makes cloning difficult. The original CDMA standard, also known as CDMA One and still common in cellular telephones in the U.S.,In single channel form , it offers a transmission speed of only up to 14.4 Kbps and up to 115 Kbps in an eight-channel form. The next version of CDMA, CDMA2000, also known as IMT-CDMA Multi-Carrier or 1xRTT, can support mobile data communications at speeds ranging from 144 Kbps to 2 Mbps. In CDMAOne and CDMA2000, a 1.25 MHz wide radio signal is multiplied by a spreading signal (which is a pseudo-noise code sequence) with a higher rate than the data rate of the message. The resultant signal appears as seemingly random, this process is reversed and the original signal is extracted, if the intended recipient has the right code. Uses of unique codes mean that in all cells, the same frequency is repeated, which is commonly referred to as a frequency re-use of 1. WCDMA is a step further in the CDMA technology. It uses a 5 MHz wide radio signal and a chip rate of 3.84 Mcps, which is about three times higher than the chip rate of CDMA2000 (1.22 Mcps).

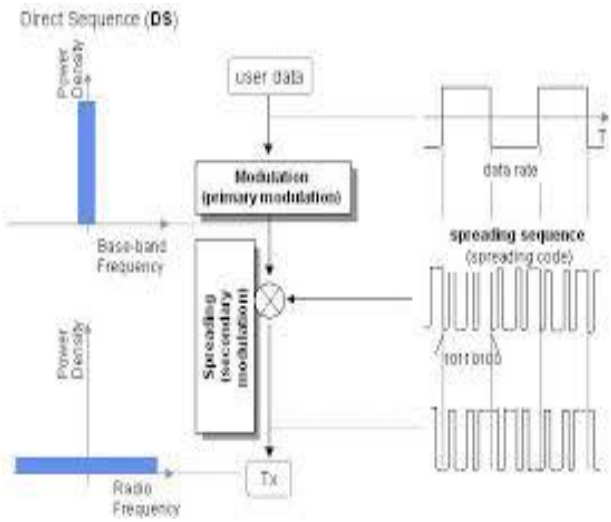

Fig: 3 CDM structure

2.21 The main benefits of a wideband carrier with a higher chiprate are:

- Higher bit rates is supported by it• Higher spectrum efficiency thanks to improved trunking efficiency (i.e. a better statistical averaging)
- Higher QoS :Further, experience from second-generation systems like GSM and cdmaOne has enabled improvements to be incorporated in WCDMA. Focus has also been put on ensuring that as much as possible of WCDMA operators' investments in GSM equipment can be re- used. Examples are the re-use and evolution of the core network, the focus on co-sitting and the support of GSM handover. The subscribers need dual mode handsets in order to use GSM handover

The Physical Layer (Layer 1) offers Transport Channels to the MAC layer. With different characteristics of the transmission there are different type of transport channels Common transport channels can be shared by multiple handsets (e.g. FACH, RACH, DSCH, BCH, PCH). Dedicated transport channels (DCH) are assigned to only one handset at a time. The transmission functions of the physical layer include channel coding and interleaving, multiplexing of transport channels, mapping to physical channels, spreading, modulation and power amplification, with corresponding functions for reception. The following is the physical layer frame structure of WCDMA A frequency and a code characterize a physical channel. The specifications include two modes: the FDD mode (Frequency Division Duplex) and the TDD mode (Time Division Duplex). The mainstream mode is the FDD mode that operators are now deploying in WCDMA. The TDD mode may eventually be deployed as well, as a complement to the FDD mode.

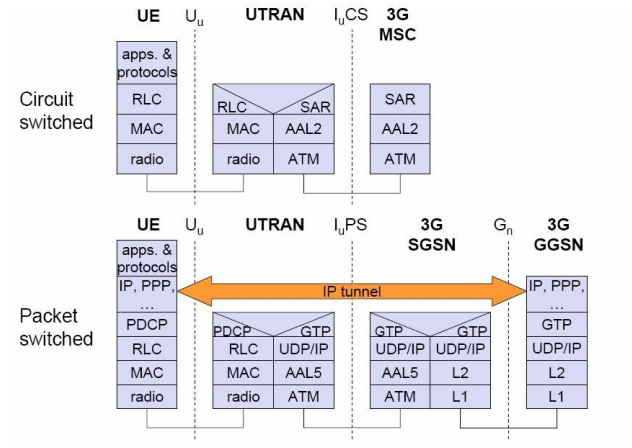

Fig: 2 UMTS Architecture

2.3 Goals for 3G Technology

- Global standards to allow for low cost and worldwide roaming.
- High Quality of Service (QoS) especially for voice.□ Support for advanced services: Multimedia, Bandwidth on Demand, High speed data.

2.4 Disadvantages of 3G

There are some issues in deploying 3G:

- The cost of upgrading base stations and cellular infrastructure to 3G is very high.
- Requires different handsets and there is the issue of handset availability. 3G handsets will be a complex product. Roaming and making both data/voice works has not yet been demonstrated. Also the higher power requirements (more bits with the same energy/bit) demand a larger handset, shorter talk time, and larger batteries).
- Base stations need to be closer to each other (more cost).
- Tremendous spectrum-license costs, network deployment costs, handset subsidies to subscribers, etc.
- Wireless service providers in Germany and Britain who won spectrum licenses in auctions, paid astronomical prices for them. As a result, they have little money left for building the infrastructure. Consequently, deployment of 3G in Germany and Britain will be delayed.

III CONCEPT OF 4G TECHNOLOGIES

4G is the term used to refer to the next wave of high-speed mobile technologies and 3G networks will be replace by this technology. LTE and Wi-MAX are the two top contenders, both of which are IP based networks that are built from similar, yet incompatible, technologies. 4G WI-MAX service is currently offering sprint and clear wire in the USA, while Verizon and AT&T have committed to the use of LTE and are trialing their own 4G networks. Carriers that use orthogonal frequency-division multiplexing (OFDM) instead of time division multiple access (TDMA) or code division multiple access (CDMA) even when their data speed are not as fast as the international telecommunication union specifies care increasingly marketing their services as to be 4G. According to the ITU, a 4G network requires a mobile device to be able to exchange data at 100 Mbit/sec. A 3G network, on the other hand, can offer data speeds as slow as 3.84 Mbit/sec.

From the consumer's point of view, 4G is more a marketing term than a technical specification, but carriers feel justified in using the 4G label because it lets the consumer know that he can expect significantly faster data speeds.

Although carriers still differ about whether to build 4G data networks using Long Term Evolution (LTE) or Worldwide Interoperability for Microwave Access Wi-MAX, all carriers seem to agree that OFDM is one of the chief indicators that a service can be legitimately marketed as being 4G. A signal is split into several narrowband channels at different frequencies in OFDM, which is a digital modulation This is more efficient than TDMA, which divides channels into time slots and has multiple users take turns transmitting bursts or CDMA, which simultaneously transmits multiple signals on the same channel.

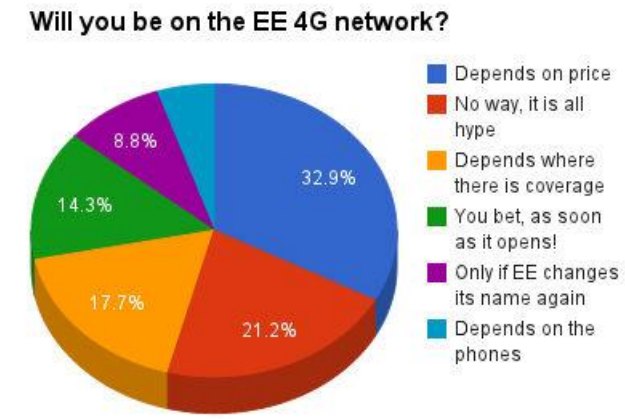

Fig: 4 Evolutions of 4G

When fully implemented, 4G is expected to enable pervasive computing, in which simultaneous connections to multiple high-speed networks will provide seamless handoffs throughout a geographical area. Coverage enhancement technologies such as femtocell and picocell are being developed to address the needs of mobile users in homes, public buildings and offices, which will free up network resources for mobile users who are roaming or who are in more remote service areas.

3.1 LTE Protocols

LTE is a standard for wireless data communications technology and an evolution of the GSM/UMTS to increase the capacity and data rates of wireless data networks, improve spectrum efficiency, improve coverage, reduced latency and packet-optimized system that support multiple Radio Access, are the main goals of LTE .Thus, in order to achieve the goals, the architecture of the network if different from the previous wireless data transfer network, GPRS. So, in post, a comprehensive overview of the network architecture and basic working principle of LTE network is going to be discussed.

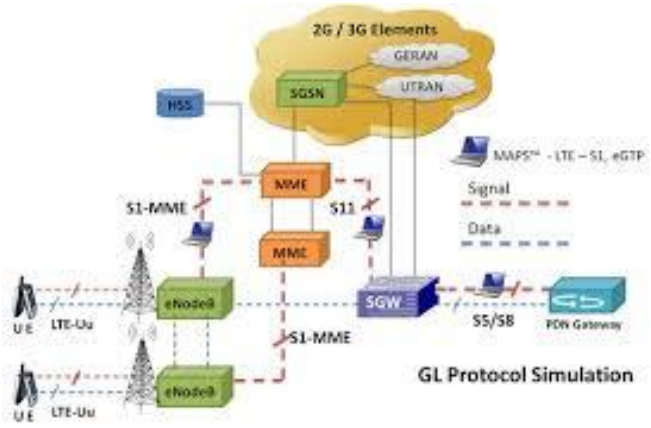

Fig: 5 LTE Protocol Simulations

Basically, the LTE standard only supports packet switching with its all-IP network. The reason why LTE is designed only for packet switching is because without any disruption to the end user application during mobility it aims to provide seamless Internet Protocol (IP) connectivity between user equipment (UE) and the packet data network (PDN). Due to this characteristic, voice calls and text message natively (which are typically handled by circuit-switched networks like GSM and CDMA). In LTE architecture, Evolved UTRAN (E-UTRAN) is an important role which is the air interface of LTE upgrade path for mobile networks meanwhile it is accompanied by an evolution of the non-radio aspects under the term "System Architecture Evolution" (SAE), which includes the Evolved Packet Core (EPC) network. Together LTE and SAE comprise the Evolved Packet System (EPS). Besides that, LTE network uses an eNodeB (evolved node B, essentially an LTE base station), a MME (Mobile management entity), a HSS (home subscriber server), a SGW (serving gateway), and a PGW (a packet data network gateway). These are considered as part of the EPC except eNodeB.

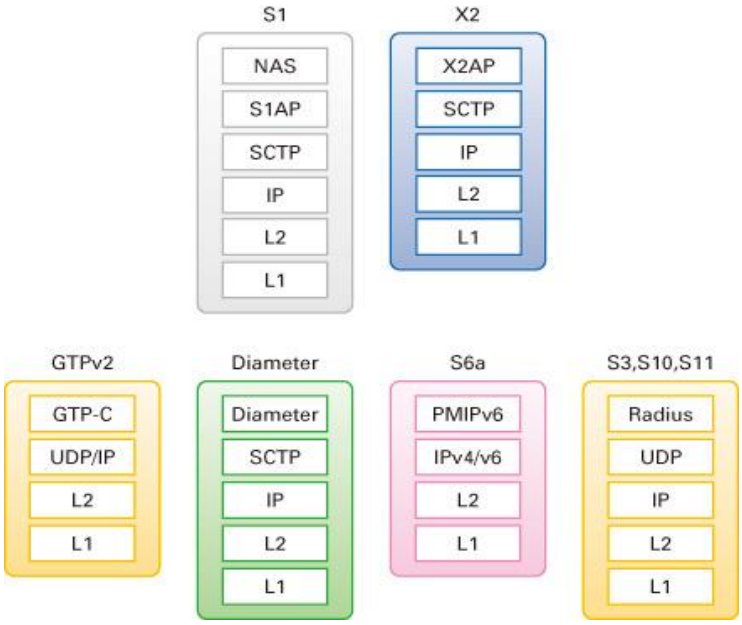

Fig: 6 LTE Protocol

3.2 Goals for 4G Network

- Support for Multiple and Efficient Applications and Services: 4G provides support for unicast, multicast and broadcast services and the applications that depend on them. Prompt enforcement of Service level Agreements (SLA) along with privacy and other security features.
- Quality of Service: Regardless of underlying infrastructure and operator diversity, dependable applications of admission control and scheduling algorithms leads to an increased quality of service (QoS) to the users.
- Network detection selection: A mobile terminal that features multiple radio technologies or possibly uses software defined radios if economical, allows participation in multiple networks simultaneously, thereby connecting to the best network with the most appropriate service parameters (cost, QoS and capacity among others) for the application. For defining eligibility of a terminal to attach to a network and to determine the validity of link layer configuration ,this requires .establishing a uniform process
- Seamless Handover and Service Continuity With zero or minimal interruption, without a noticeable loss in service quality, a base station that features intra and inter technology handover, assuring service continuity. Support for this function requires continuous transparent maintenance of active service instances and inclusion of various access technologies, from Wi-Fi to OFDMA.

3.3 Disadvantages of 4G

- Very high start-up costs of service providers and consumers for equipment upgrades a; new equipments will be needed to be installed.
- For data transmission LTE technology need to use additional antennas at network base stations as a result to the network upgrades users need to buy new cell phones to make use of new network infrastructure.

IV BASICS OF 3GPP

Calculated values of crack growth rate were plotted at frequency 60 Hz, 80 Hz, 100 Hz and 120 Hz. From fig. 3, 3GPP specifications are published - free of charge - up to four times a year following the quarterly Technical Specification Group (TSG) plenary meetings. At each TSG round, specs can be

- Newly brought under change control (i.e. at least 80% complete)
- Unaltered from their previous versions
- Revised as a result of incorporating approved Change Requests (either in existing Releases or in the latest Release)
- Upgraded to that Release with no technical change at the release freeze time

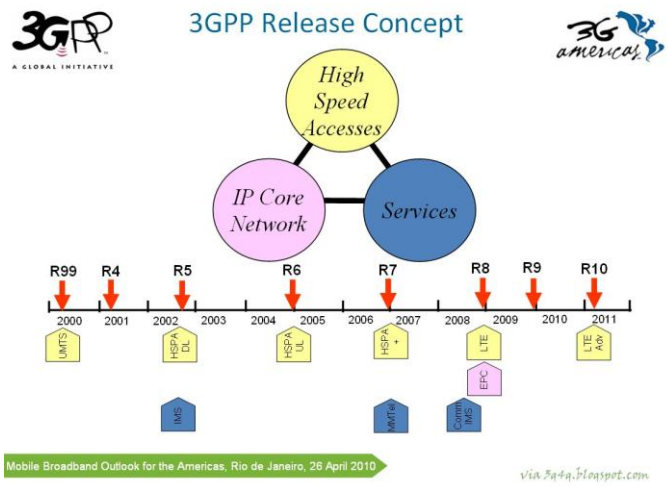

Fig: 7 3GPP Network Overview

The 3GPP Mobile Competence Centre (MCC) aims to make all Specs available following a TSG round as soon as possible. The target dates are shown in the table below. Where very many CRs have to be implemented, or very many specifications are to be produced, a further week beyond the above deadlines may be required. These dates are agreed by the TSG Chairmen. Over the Christmas and New Year period, when the winter TSG round finishes shortly before the holiday period, an extra week or so is normally added to the final deadlines.

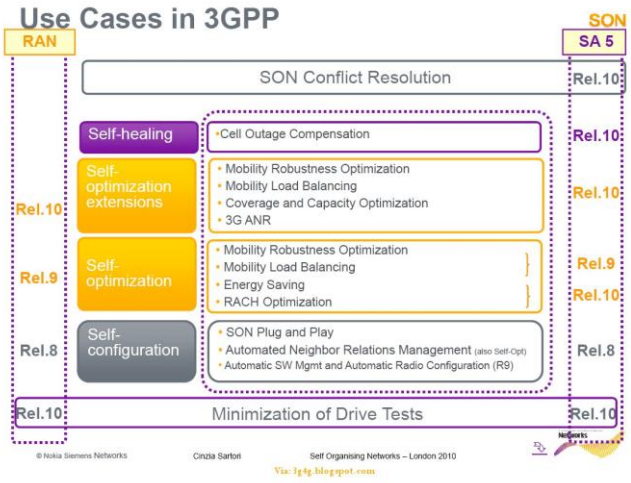

Fig: 8 3GPP Architecture

Across much of the established GSM market.3GPP system are deployed they are primarily *Release 6* systems, but as of 2010, growing interest in HSPA+ and LTE is driving adoption of *Release 7* and its successors. Since 2005, as 3GPP2 system 3GPP systems were also seeing deployment in the same markets (for example, North America). With LTE the official successor to 3GPP2's CDMA systems, 3GPP-based systems will eventually become the single global mobile standard.

V INTRODUCTION TO LTE

LTE (Long Term Evolution) is a wireless broadband technology designed to support roaming Internet access via cell phones and handheld devices. Because over older cellular communication standards, LTE offers significant improvements, some refer to it as a *4G* (fourth generation) technology along with Wi-Max. With its architecture based on Internet Protocol (IP) unlike many other cellular Internet protocols, Browsing Web sites, VoIP and other IP-based services are well supported by Long Term Evolution. LTE can theoretically support downloads at 300 Megabits per second (Mbps) or more based on experimental trials. However, the actual network bandwidth available is significantly less to an individual LTE subscriber sharing the service provider's network with other customers.

5.1 The high-level network architecture of LTE is comprised of following three main components:

- The User Equipment (UE).
- The Evolved UMTS Terrestrial Radio Access Network (E-UTRAN).
- The Evolved Packet Core (EPC).

5.2 The User Equipment (UE): The internal architecture of the user equipment for LTE is actually a Mobile Equipment (ME) which is identical to the one used by UMTS and GSM. The mobile equipment comprised of the following important modules:

- **Mobile Termination (MT):** This handles all the communication functions.
- **Terminal Equipment (TE):** This terminates the data streams.
- **Universal Integrated Circuit Card (UICC):** This is also known as the SIM card for LTE equipments. It runs an application known as the Universal Subscriber Identity Module (USIM).

A USIM stores user-specific data very similar to 3G SIM card. Information about the user's phone number, home network identity and security keys etc .are also secure by this.

5.3 The Evolved UMTS Terrestrial Radio Access Network (E-UTRAN)

The radio communications between the mobile and the evolved packet core are handle by E-UTRAN and just has one component, the evolved base stations, called **eNodeB** or **eNB**. Each eNB is a base station that controls the mobiles in one or more cells. The base station that is communicating with a mobile is known as its serving eNB. A home eNB (HeNB) has been purchased by a user to provide femtocell coverage within the home which is a base station. A home eNB belongs to a closed subscriber group (CSG) and can only be accessed by mobiles with a USIM that also belongs to the closed subscriber group.

5.4 The Evolved Packet Core (EPC)

The architecture of Evolved Packet Core (EPC) has been illustrated below To keep the diagram simple .few more components have not shown in it these components are like the Earthquake and Tsunami Warning System (ETWS), the Equipment Identity Register (EIR) and Policy Control and Charging Rules Function (PCRF).

VI RELATION WITH 3GPP OF LTE

GSM was developed to carry real time services, in a circuit switched manner (blue in figure 1), with data services only possible over a circuit switched modem connection, with very low data rates. The first step towards an IP based packet switched (green in figure 1) solution was taken with the evolution of GSM to GPRS, using the same air interface and access method, TDMA (Time Division Multiple Access).

A technology WCDMA (Wideband Code Division Multiple Access) was developed to reach higher data rates in UMTS (Universal Mobile Terrestrial System). UMTS emulates a circuit switched connection for real time services and a packet switched connection for data com services to access network in it. In UMTS when a data com service is established IP address is allocated to the UE and it released when the service is released. Incoming data com services are therefore still depending upon the circuit.

The Evolved Packet System (EPS) is purely based on IP by using IP protocol both real time services and data com services will be carried When the mobile is switched on the IP address is allocated and it released when the mobile is switched off.

The new access solution, LTE, is based on OFDMA (Orthogonal Frequency Division Multiple Access) and in combination with higher order modulation (up to 64QAM), large bandwidths (up to 20 MHz) and spatial multiplexing in the downlink (up to 4x4) high data rates can be achieved. On the transport channel the highest theoretical peak data is 75 Mbps in the uplink, and in the downlink, using spatial multiplexing, the rate can be as high as 300 Mbps. The LTE access network is simply a network of base stations, evolved NodeB (eNB), generating a flat architecture (figure 2).there is no concentrated intelligent controller, and the eNBs are normally inter-connected via the X2-interface and towards the core network by the S1-interface. In LTE the reason for distributing the intelligence amongst the base-stations is to speed up the connection set-up and reduce the time required for a handover. The connection set-up time for a real time data session is in many cases crucial for an end user, especially in on-line gaming. When end-users tend to end calls if the handover takes too long , the time for a handover is essential for real time services.

VII COMPARE 3G VS. 4G

How much faster is 4G compared to 3G? Unfortunately for consumers, the answer to this question is more nuanced than one would like. The speed of a 3G network depends upon its implementation. In the US, by 2010 Sprint and Verizon (both CDMA networks) had reached the limits of how fast they could make their 3G networks. Upgrading to 4G networks allowed them to offer data transmission speeds up to four times faster than their 3G networks. However, the 3G networks of GSM carriers AT&T and T-Mobile were designed such that there was room to upgrade 3G speeds. As of mid-2010, it is anticipated that when AT&T and T-Mobile upgrade their 3G networks, their speeds will become comparable to 4G from Sprint and Verizon.

Comparison Topics	3G	4G
Data Throughput	Up to 3.1Mbps with an average speed range between 0.5 to 1.5 Mbps	Practically speaking, 2 to 12 Mbps (Telstra in Australia claims up to 40 Mbps) but potential estimated at a

		range of 100 to 300 Mbps.
Peak Upload Rate	5 Mbps	500 Mbps
Switching Technique	packet switching	packet switching, message switching
Network Architecture	Wide Area Cell Based	Integration of wireless LAN and Wide area.
Service & Applications	Concatenated codes are used for error corrections in 4G.	Wimax2 and LTE-Advance
Forward Error Correction	3G uses Turbo codes for error correction	Concatenated codes are used for error corrections in 4G.
Peak Download Rate	100 Mbps	1Gbps
Frequency Band	1.8-2.5 GHz	2-8 GHz

VIII INTRODUCTION TO 5G

5G mobile telecommunication standards stand for fifth-generation advancements made in the mobile communications field. These comprise packet switched wireless systems using orthogonal frequency division multiplexing (OFDM) with wide area coverage, high throughput at millimetre waves (10 mm to 1 mm) covering a frequency range of 30 GHz to 300 GHz, and enabling a 20 Mbps data rate to distances up to 2 km. The millimetre-wave band is the most effective solution to the recent surge in wireless Internet usage. These specifications are capable of providing 'wireless world wide web' (WWWW) applications.

The WWWW allows a highly flexible network (flexible channel bandwidth between 5 and 20 MHz, optimally up to 40 MHz), and dynamic ad-hoc wireless network (DAWN). This technique employs intelligent antennae (e.g., switched beam antennae and adaptive array antennae) and the flexible modulation method, which helps in obtaining bidirectional high bandwidth, i.e., transfer of a large volume of broadcasting data in giga bytes, sustaining more than 60,000 connections and providing 25 Mbps connectivity. Users of 5G technology can download an entire film to their tablets or laptops, including 3D movies; they can download games and avail of remote medical services. With the advent of 5G, Piconet and Bluetooth technologies will become outdated. The 5G mobile phones would be akin to tablet PCs, where you could watch TV channels at HD clarity without any interruption.

8.1 Key Features of 5G

- Wearable devices with artificial intelligence (AI)
- Internet Protocol version 6 where the IP address is assigned according to location and the connected network.

- The ability to connect the user to different wireless access technologies, like 2.5G, 3G, 4G or 5G mobile networks, as well as Wi-Fi and WPAN (wireless personal area network)—or even any other technology to be developed in the future. This is basically a concurrent data transfer path technique.

- Smart radio. In order to share the same spectrum efficiently during a wireless transmission scheme, the system will adaptively find (search) unused spectrum. This dynamic radio resource management will be achieved in a distributed fashion and rely on software defined transmission.

- High altitude stratospheric platform station (HAPS) system. This is based on beam division multiple access (BDMA) and group relay techniques.

8.2 5G Hardware

Ultra wideband networks (UWB). It is already known that Wi-Fi, Wi-Max and cellular wide area communications are long-range radio technologies. But systems like WPAN need short-range radio technology, which helps in achieving higher bandwidths (around 4000 Mbps) but at low energy levels (UWB network) for relaying data from host devices to devices in the immediate vicinity, i.e., distances of around 10 metres or so. This higher bandwidth (4000 Mbps) level is almost 400 times faster than today's wireless networks. Each network will be responsible for handling user-mobility while the user terminal will make the final choice among different wireless/mobile access network providers for a given service. However, there should be different radio interfaces for each radio access technology (RAT) in the mobile terminal.

Smart antennas:

These include the following:

- *Switched beam antennae. :*This type of antenna supports radio positioning via angle of arrival (AOA). Information is collected from nearby devices.

- *Adaptive array antennae (Samsung has used 64 antennae elements):* Such antennae promise to improve the capacity of wireless systems by providing improved safety through position-location capabilities. This technique rejects interference through spatial-altering-position location through direction-ending measurements and developing improved channel models through angle-of-arrival channel sounding measurement.

- *CDMA (code division multiple access) technique:* This technique converts audio analogue input signals into digital signals (ADC) in combination with spread spectrum technology. The signal is transmitted using modulation according to some predefined code (pattern), and is demodulated using the same pattern since there can be billions of code patterns which can provide privacy and sufficient security.

8.3 5G Software

1. 5G will be a single unified IP standard of different wireless networks and a seamless combination of broadband, including wireless technologies, such as IEEE802.11, LAN, WAN, PAN and WWWW.

2. 5G will enable software-defined radio, packet layers, implementation of packets, encryption flexibility, etc.

8.4 Chronological Evolution Of Mobile Technologies

- Although the 1G system (NMT) was introduced in 1981, 2G (GSM) started to come out in 1982, and 3G (W-CDMA)/FOMA first appeared in 2001, the complete development of these standards (e.g., IMT-2000 and UMTS) took almost 10 years. It is still unclear how much time it will take to launch the standards for 5G.

- 5G technologies will ensure the convergence of networks, technologies, applications and services, and can serve as a flexible platform. Wireless carriers will have an opportunity to shorten their return-on-investment periods, improve operating efficiency and increase revenues. In short, this will change people's lives in numerous ways.

IX LITERATURE REVIEW

Wi-MAX is exactly not a technology; it is rather than a certification mark, or 'stamp of approval', it is given to equipment that meets certain conformity and interoperability tests for the IEEE 802.16 families of standards. A similar confusion surrounds the term Wi-Fi, which like Wi-MAX, is a certification mark for equipment based on a different set of IEEE standards from the 802.11 working group for wireless local area networks (WLAN). Neither Wi-MAX, nor Wi-Fi is a technology but their names have been adopted in popular usage to denote the technologies behind them. This is likely due to the difficulty of using terms like 'IEEE 802.16' in common speech and writing.

In case of wireless networks, the behavior of cellular networks, examining 3G, 4G, and Wi-Fi networks for both single-path and multi-path data transport. Our contribution is two-fold: First, we perform measurements of single path transport using TCP over major US cellular wireless networks (both 4G and 3G), and characterize them in terms of throughput, packet loss, and round-trip time. Second, we measure and evaluate transport using multi-path TCP in cellular environments and show that leveraging path diversity under changing environments is a promising solution for more reliable and efficient TCP transfer. We also identify potential issues in using multi-path TCP which can limit performance.

The high bandwidth of 3G networks will lead to the creation of new services, some of which we have no idea about at this time. The big question is what services will be big revenue makers for the wireless service providers. In 2G networks, the big winners have been short text messaging in GSM networks (Europe and countries other than USA) and image downloads and forwarding on iMode networks in Japan. Two candidate services for big winners in 3G networks are video streaming and video conferencing.

The Parallel to Wi-MAX, LTE (Long Term Evolution) is introduced by the Verizon. LTE is considered to be promising high data transfer speed. LTE is supposed to provide the internet facility using both systems. It has

the ability of a transition from one mode to another. LTE is developed on the radio waves technology. This is not only increases the speed but also the amount of data allowed through the same bandwidth and results into lower cost. As LTE is compatible with 3G technology so it not only increases the speed but also prevents the need of new network and it can work through the same infrastructure. In LTE will not only support the functions of 3G but also incorporate some newer ones. LTE using MIMO (Multiple input multiple output) able to send and receive huge data negative in the sense that it will overload the base stations networks. While we seeing the working methodologies of both technologies considered being the standards of 4G, the future is of mobile business.

Wi-MAX could not be commercially available until the second half of 2005, and even then at a very controlled level. This is primarily due to standardization issues. In fact, it could not be until 2006 that a robust production and implementation would happen due to the ramp-up period for manufacturers. This is certainly one challenge to the widespread adoption of WiMax. Additionally, WiMax will have issues of pricing, and will remain far more expensive than Wi-Fi. WiMax will be primarily adopted by businesses to replace or displace DSL, and offices that want to cover a lot of territory without entering the world of endless repeaters that are necessary with the 802.11 technologies. It will take some time (2 years) for WiMax to significantly reduce its price-point for residential uptake. WiMax will not displace Wi-Fi in the home because Wi-Fi is advancing in terms of speed and technology. Each year brings a new variant to the 802.11 area with various improvements.

X POSSIBLE FUTURE TECHNOLOGIES

It's a term used to describe the forthcoming fifth generation of mobile network technology. It's not a reference to any specific standard of that technology, in the way that 4G and LTE have become closely entwined. That's because no such 5G standard has yet been fully agreed upon, though a couple of likely technologies are emerging. We'll discuss those in a moment.

Most of us in the UK today still connect to the internet on our phones using crusty old 3G technology, while those who live in the right areas can connect via 4G extremely fast. As in, you'll be able to download a film to your iPhone 12 or Google Contact Lens in less than a second. Chinese mobile giant Huawei reckons that 5G will be 100 times faster than fastest 4G LTE standard currently available.

One of the chief complaints with 4G is that it offers a new level of speed, but sticks its users with the same old data restrictions. At their worst, current 4G contracts are a little like someone giving you the keys to a new Ferrari, but only allowing you to drive to the end of your street and back.

It's estimated 5G technology will offer upwards of 1,000 times the capacity of 4G. This means that there'll be more space for everyone to access this advanced network, which should negate the need for mobile operators to throttle or limit your access to their networks.

Another benefit of 5G that everyone seems to agree on is reduced latency. It should take significantly less time for data transfers to take place, which means that those streaming videos should start pretty much immediately after you press play.

As we've mentioned elsewhere, the plan is to get London up and running with 5G by 2020. This should make it among the first areas in the world to receive this next gen network.

We're a little far out to speculate on when the rest of the country might get the benefits of 5G, but if the recent switch to 4G is anything to go by, it should start spreading out pretty soon after its capital debut. Of course, the likely need for new antenna installations could see a longer delay on the rest of the UK getting 5G, but its all speculation at this point.

XI FUTURE WORK

5G mobile technology changed the use of cell phones within a very high bandwidth. The user never experienced ever before such as high value technology. Nowadays the mobile users have much awareness of cell phone (mobile) technology. 5G technologies include all of advanced features that make 5G mobile technology most powerful and huge demand in near future. The gigantic array of an innovative technology being built into new cell phones is stunning and 5G technologies which are on hand held phone offering an more power and features than at least a 1000 lunar modules. A user can also hook their 5G technology cell phone with their Laptop to get a broadband internet access. 5G technology including the camera, MP3 recording, video player, large phone memory, dialing speed, audio player and much more you never imagine. For children rocking the fun Bluetooth technology and Pico nets has become in market.

But the main problem is the LTE and 4G networks are used only some finger counting developed countries. 3G networks are not satisfying the users. Here a question arise that, when we are till the date unable to use 4G networks, then when 5G technology will satisfy us. In the era of this civilization, within 10 years the 6^{th} generations would be invented. But we are not getting those facilities in the regular basics. So we need to invent new technologies, but we should follow the availability on the market.

XII CONCLUSION

We have already discussed the all technologies here. From the last 3 decades the wireless communication systems are going to be vast uses in all over world. But in the superfast updated industry a new technology can`t be new for more than 1 year. That`s why the GSM generations are flowing from 1G to 5G within 20 years. Here a question arise that, in the next 10 years which technology will be used. 4G is a very promising generation of wireless communication that already changed the people's life in the wireless world. There are many striking attractive features proposed for 4G which ensures a very high data rate, global roaming etc. New ideas are being introduced by researchers throughout the world, but new ideas introduce new challenges. There are several issues yet to be solved like incorporating the mobile world to the IP based core network, efficient billing system, smooth hand off mechanisms etc. 5G is expected to be launched by 2020 and the world is looking forward for the most intelligent technology that would connect the entire globe.

5G technology has changed the means to use cell phones within very high Bandwidth. Nowadays mobile users have much awareness of the cell phones technology. The 5G technology may include all type of advanced features which makes it most powerful technology upcoming years. New mobile generations are typically assigned new frequency bands and wider spectral bandwidth per frequency channel (1G up to 30 KHz, 2G up to

200 KHz, 3G up to 5MHz, 4G up to 40 MHz), but the main issue that there is little room for new frequency bands or larger channel bandwidths.

REFERENCES

[1] Yung-Chih, Don Towsley, Erich M. Nahum, Richard J. Gibbens, Yeon-sup Lim, "Characterizing 4G and 3G Networks: Supporting Mobility with Multi-Path TCP", UMass Amherst Technical Report: UM-CS-2012-022.

[2] P. Sarolahti and A. Kuznetsov. Congestion control in Linux TCP. In Proceedings of the FREENIX Track: 2002 USENIX Annual Technical Conference, pages 49–62, Berkeley, CA, USA, 2002. USENIX association.

[3] 3GPP LTE. http://www.3gpp.org/lte.

[4] AT&T 4G LTE coverage. http://www.att.com/network/.

[5] Cradlepoint. http://www.cradlepoint.com.

[6] IEEE Standard 802.16. Broadband wireless metropolitan area networks (MANs) http://standards.ieee.org/about/get/802/802.16.html

[7] Sprint 4G WiMax coverage. http://www.clear.com/coverage

[8] W. Wei, C. Zhang, H. Zang, J. Kurose, and D. Towsley. Inference and evaluation of split-connection approaches in cellular data networks. In Proc. PAM (Passive and Active Measurement), 2006.

[9] Verizon Wireless 4G LTE coverage. http://news.verizonwireless.com/lte/markets.html

[10] WIRELESS NETWORK (3G & 4G), Arti Rana[1], Kamaljeet Kaur [2], Anuj Aggarwal[3]

[11] S. Y. Hui, K. H. Yeung, " Challenges in the migration to 4G mobile systems," Communications Magazine, IEEE , Volume: 41 , Issue: 12 , Dec. 2003, pp:54 – 59

[12] K. R. Santhi, V. K. Srivastava, G. SenthilKumaran, A. Butare, "Goals of true broad band's wireless next wave (4G-5G)," Vehicular Technology Conference, 2003. VTC 2003-Fall. 2003 IEEE 58th, Volume: 4, 6-9 Oct. 2003, Pages:2317 - 2321 Vol.4

[13] J. Z. Sun, J. Sauvola, D. Howie, "Features in future: 4G visions from a technical perspective," Global Telecommunications Conference, 2001. GLOBECOM'01,IEEE, Volume:6, 25-29,Nov.2001, pp:3533 - 3537 vol.6

[14] W. Zhou, X. Lu, J. Zhu, "M-ary MC-CDMA system for 4G," Vehicular Technology Conference, 2001. VTC 2001 fall. IEEE VTS 54th , Volume: 4, , 7-11.Oct.2001, pp:2234 - 2238 vol.4

[15] IJCSI International Journal of Computer Science Issues, Vol. 8, Issue 5, No 3, September 2011 ISSN (Online): 1694-0814 www.IJCSI.org, "Comparative Study of 3G and 4G in Mobile Technology", K. Kumaravel.

[16] C. R. Casal, F. Schoute, and R. Prasald, "A novel concept for fourth generation mobile multimedia communication," in 50th Proc. IEEE Vehicular Technology Conference, Amsterdam, Netherlands, Sep. 1999, Vol. 1, pp. 381–385.

[17] J. B. Chia, "Video services over 4G wireless networks: not necessarily Streaming," Wireless Communications and Networking Conference, 2002. WCNC2002. 2002 IEEE , Volume: 1 , 17-21 March 2002 , pp:18 - 22 vol.1

[18] K. R. Santhi, V. K. Srivastava, G. SenthilKumaran, A. Butare, "Goals of true broad band's wireless next wave (4G- 5G)," Vehicular Technology Conference, 2003. VTC 2003-Fall. 2003 IEEE 58th, Volume: 4 , 6-9 Oct. 2003, Pages:2317 - 2321 Vol.4

[19] S. Chatterjee, W. A. C Fernando, M. K. vasantha, "Adaptive modulation based MC- CDMA systems for 4G wireless consumer applications," Consumer Electronics, IEEE Transactions on , Volume: 49 , Issue:4, Nov.2003, pp:995 – 1003

[20] C. R. Casal, F. Schoute, and R. Prasald, "A novel concept for fourth generation mobile multimedia communication," in 50th Proc. IEEE Vehicular Technology Conference, Amsterdam, Netherlands, Sep. 1999, Vol. 1, pp. 381–385.

[21] "Comparative study between the generations of mobile communication 2G, 3G & 4G", Rajasweta Datta[1], Niharika[2], International Journal on Recent and Innovation Trends in Computing and Communication ISSN 2321 – 8169, Volume: 1 Issue: 4, 327 – 331

[22] Vijay K. Garg ph.d., P.E, camuel halpern M.S, and Kenneth F.Smolik,ph.D., P.E. ―Third Generation (3G) mobile communication system‖.

[23] Neerav Dalal Award Solutions, Inc. IEEE METROCON- 2001 ‖ A Comparative Study of UMTS (WCDMA) and cdma2000 Networks‖.

[24] 3G and 4G Cellular Standards, Prof. Jeffrey G. Andrews the University of Texas at Austin, November 5, 2008.

[25] "The 4G Technology V/S other G Technologies", Volume 3, Issue 3, March 2013, ISSN: 2277 128X International Journal of Advanced Research in Computer Science and Software Engineering.

[26] http://www.diffen.com/difference/3G_vs_4G

[27] http://www.blogsolve.com/difference-between-1g-2g-2-5g-3g-pre-4g-and-4g

Biographical Notes

Mr. Susmit Paul is presently pursuing B. Tech. 3rd year in Electronics & Communication Engineering Department from Tula`s Institute, Dehradun, India.

Ms. Sakshi Arya is presently pursuing B. Tech. 2nd year in Electronics & Communication Engineering Department from Tula`s Institute, Dehradun, India.

A STUDY ON EFFECTIVE APPROACH FOR INTRUSION DETECTION IN MANETS

Ayesha Unnisa [1], G. Narayana[2], T. Shesagiri[3]

[1] *M.Tech, Department of Computer Science Engineering, J.B.R.E.C, Hyderabad (India)*

[2] *Professors, Department of Computer Science Engineering, J.B.R.E.C, Hyderabad (India)*

[3] *Associate Professor, Department of Computer Science Engineering, J.B.R.E.C, Hyderabad (India)*

ABSTRACT

Now a day's most of the people are moving form wired to wireless networks. Among the wireless networks MANETS are being mostly being used. Some of the features of MANETS are that it does not require any fixed infrastructure, self-configuring ability, dynamic topology and decentralized network. Due to its features MANETS can be used in a military and emergency recovery situations .In MANETS the nodes can work both as transmitter and receiver, can communicate with each other directly and indirectly or depend on neighboring nodes to relay their messages. One of the primary concerns related to ad hoc network is to provide a secure communication among mobile nodes in a hostile environment. The ad hoc networks can be easily reached by malicious attackers so it is vital to address its security issue. In this paper we propose a new intrusion detection mechanism EAACK specially designed for MANETS which uses ACK, S-ACK and MRA methods .The acknowledgment packets are being protected using digital signature and detects malicious nodes based on their malicious behavior.

Keyword: Mobile Ad Hoc Network (MANET), Intrusion Detection, Digital Signature, Digital Signature Algorithm, Enhanced Adaptive Acknowledgment (EAACK).

I. INTRODUCTION

Mobile Ad hoc networks or MANETs are the category of wireless networks which do not require any fixed infrastructure or base stations. They can be easily deployed in places where it is difficult to setup any wired infrastructure. There are no base stations and every node must co operate with each other in forwarding packets in the network. Thus, each node acts as a router which makes routing complex when compared to Wireless LANs, where the central access point acts as the router between the nodes.A sensor network is a special category of ad hoc wireless networks which consists of several sensors deployed without any fixed infrastructure. The difference between sensor networks and ordinary ad hoc wireless is that the sensor nodes may not be necessarily mobile. Further, the number of nodes is much higher than in ordinary ad hoc networks. The nodes have more stringent power requirements since they operate in harsh environmental conditions.

Fig-1 MANETs

1.1 Advantages Of Mobile Ad Hoc Networks

1.1.1 Low cost of deployment*:* As the name suggests, ad hoc networks can be deployed on the fly, thus requiring no expensive infrastructure such as copper wires, data cables, etc.

1.1.2 Fast deployment: When compared to WLANs, ad hoc networks are very convenient and easy to deploy requiring less manual intervention since there are no cables involved.

1.1.3 Dynamic Configuration*:* Ad hoc network configuration can change dynamically with time. For the many scenarios such as data sharing in classrooms, etc., this is a useful feature. When compared to configurability of LANs, it is very easy to change the network topology.

1.2 Intrusion Detection System

Intrusion detection can be defined as a process of monitoring activities in a system which can be a computer or a network. The mechanism that performs this task is called an Intrusion Detection System

II. PROBLEM DEFINITION

We mainly describe the existing approach, namely, the Watchdog to detect the misbehaving nodes. Watchdog aims to improve throughput of network with the presence of malicious nodes. The watchdog scheme is consisted of two parts, namely Watchdog and Path rater. Watchdog serves as an intrusion detection system for MANETs. It is responsible for detecting malicious nodes misbehaviors in the network. Watchdog detects malicious misbehaviors by promiscuously listening to its next hop's transmission. The Watchdog-IDS fails to discover malicious nodes in the following situations: 1) ambiguous collisions 2) receiver collisions 3) limited transmission power 4) false behavior report 5) collusion and 6) partial dropping

2.1 Existing System

Security has become a most important service in Mobile Adhoc Network (MANETs)[5], Zhou and Haas have proposed using threshold cryptography for providing security to the network. To secure an ad hoc network, the following attributes are to be considered: availability, authentication and key management, confidentiality, integrity, non-repudiation, and scalability. In order to achieve this goal, the security solutions for each layer which are providing complete protection for MANETs are to be described.

There are five main layers on the network, as follows:

Application layer is used for detecting and preventing viruses, worms, malicious codes. Transport layer: is used for authenticating and securing end-to-end communication through data encryption, Network layer does the job of protecting the ad hoc routing and forwarding protocols. Link layer is used for protecting the wireless MAC

protocol and providing link-layer security support and last the physical layer is used to prevent signal jamming, denial-of-service attacks. Intrusion Detection System (IDS) should be added to enhance the security level of MANETs. If MANET can detect the attackers as soon as they enter the network, we will be able to completely eliminate the potential damages caused by compromised nodes at first time. IDSs usually act as the second layer in MANETs, and it is a great complement to existing proactive approaches and presented a very thorough survey on contemporary IDSs in MANETs. The existing approach, namely, the Watchdog to detect the misbehaving nodes. Watchdog aims to improve throughput of network with the presence of malicious nodes. The watchdog scheme is consisted of two parts, namely Watchdog and Pathrater. Watchdog works as an intrusion detection system for MANETs. It is responsible for detecting malicious nodes misbehaviors in the network.

2.2 Watchdog Scheme

Watchdog detects malicious misbehaviors by promiscuously listening to its next hop's transmission. If Watchdog node overhears that its next node fails to forward the packet within a certain period of time, it increases its failure counter. Whenever a node's failure counter exceeds a predefined threshold, the Watchdog node reports it as misbehaving. In this case, the Pathrater cooperates with the routing protocols to avoid the reported nodes in future transmission. Many following researches and implementations have proved that the Watchdog scheme to be efficient. Compared to some other schemes, Watchdog is capable of detecting malicious nodes rather than links. These advantages have made Watchdog scheme a popular choice in the field. Many MANET IDSs either based on or developed as an improvement to the Watchdog scheme.

The Watchdog-IDS fails to discover malicious nodes in the following situations: 1) ambiguous

Collisions; 2) receiver collisions; 3) limited transmission power; 4) false misbehavior report; 5) collusion and 6) partial dropping.

Intrusion Detection System must be added to enhance the security level of MANETS.

2.3 TWOACK

TWOACK is neither an enhancement nor a Watchdog based scheme. Aiming to resolve the receiver collision and limited transmission power problems of Watchdog, TWOACK detects misbehaving links by acknowledging every data packets transmitted over each three consecutive nodes along the path from the source to the destination. Upon retrieval of a packet, each node along the route is required to send back an acknowledgement packet to the node that is two hops away from it down the route .TWOACK is required to work on routing protocols such as Dynamic Source Routing (DSR).

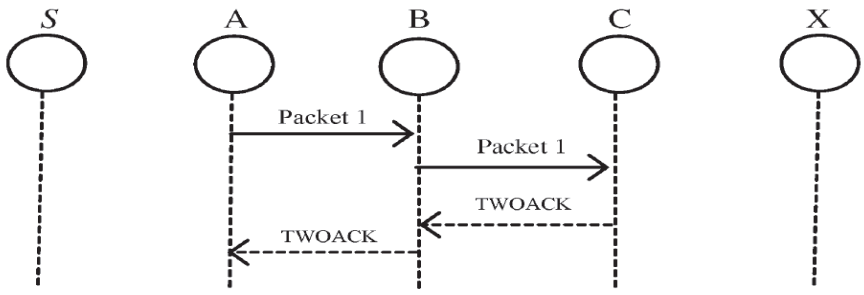

Fig-2: TWO ACK

The working of the TWO ACK scheme is as follows in Fig. 2, node A first forwards packet 1 to node B, and then node B forwards Packet 1 to node C. When node C receives Packet 1, as it is two hops away from node A, node C is obliged to generate a TWOACK packet, which contains reverse route from node A to node C, and sends it back to node A. The retrieval of this TWOACK packet at node A indicates the transmission of Packet 1 from node A to node C is successful. Otherwise, if this TWOACK packet is not received in a predefined time period, both nodes B and C are reported malicious. TWOACK scheme successfully solves the receiver collision and limited transmission power problems posed by Watchdog. However, the acknowledgement process required in every packet transmission process added a significant amount of unwanted network overhead. Due to the limited battery power nature of MANETs, Such redundant transmission process can easily degrade the life span of the entire network.

2.4 AACK

It is based on TWOACK Acknowledgement (AACK) similar to TWOACK,AACK is an acknowledgement based network layer scheme which can be considered as a combination of a scheme call ACK (identical to TWOACK) and an end-to-end acknowledgement scheme called ACK. Compared to TWOACK, AACK significantly reduced network overhead while still capable of maintaining or even surpassing the same network throughput. Source node S will switch to TACK scheme by sending out a TACK packet. The concept of adopting a hybrid scheme in AACK greatly reduces the network overhead, but both TWOACK and AACK still suffer from the problem that they fail to detect malicious nodes with the presence of false misbehavior report and forged acknowledgement packets. In fact, many of the existing IDSs in MANETs adopt acknowledgement based scheme, including TWOACK and AACK. The function of such detection schemes all largely depend on the acknowledgement packets. Hence, it is crucial to guarantee the acknowledgement packets are valid authentic. To address this concern, we adopt digital signature in proposed scheme EAACK.

III. PROPOSED METHOD

Our proposed approach EAACK is designed to tackle three of the six weaknesses of Watchdog scheme, namely false misbehavior, limited transmission power and receiver collision. In this section, we discuss these three weaknesses in details. In a typical example of receiver collisions, demonstrated in Fig. 3 after node A sends Packet 1 to node B, it tries to overhear if node B forwarded this packet to node C; meanwhile, node X is forwarding packet 2 to node C. In such case, node A overhears that node B has successfully, forwarded Packet 1 to node C, but failed to detect that node C did not receive this packet due to a collision between Packet 1 and Packet 2 at node C.

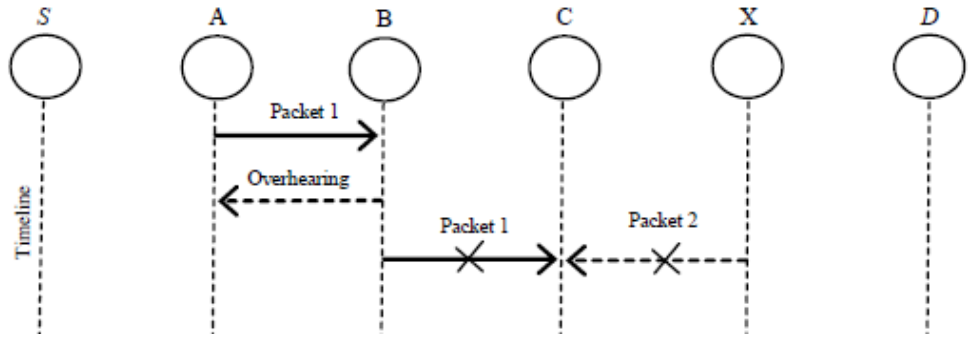

Fig-3 Receiver Collision

In limited transmission power, in order to preserve its own battery resources, node B intentionally limits its transmission power so that it is strong enough to be overheard by node A but not strong enough to be received by node C, as shown in Fig. 4

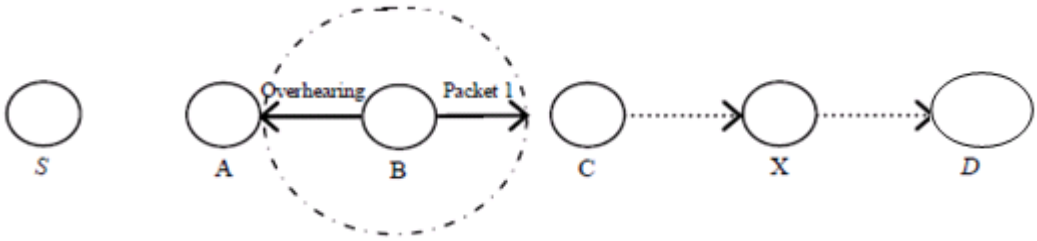

Fig-4 Limited transmission power

In the false misbehavior report, although node A successfully overheard that node B forwarded Packet 1 to node C, node A still reported node B as misbehaving as shown in Fig. 5. Due to the open medium and remote distribution of typical MANETs, attackers can easily capture and compromise one or two nodes to achieve this false misbehavior report attack. As discussed in previous sections, TWOACK and AACK solve two of these three weaknesses, namely receiver collision and limited transmission power. However, both of them are vulnerable to the false misbehavior attack. In this research work, our goal is to propose a new intrusion detection system specially designed for MANETs, which solves receiver collision, limited transmission power, and also the false misbehavior.

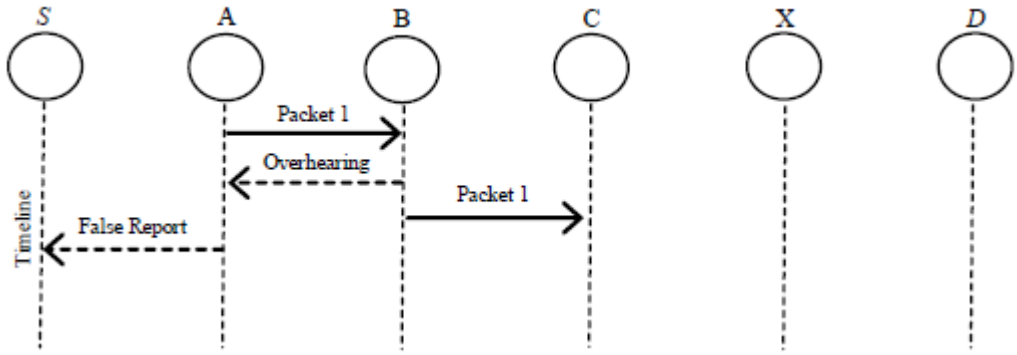

Fig-5 False Misbehavior Report: Node A Send Back Misbehavior Report Even Node B Forwarded The Packet To Node C

IV. METHODOLOGY

EAACK is consisted of three major parts, namely, ACK, secure ACK (S-ACK), and misbehavior report authentication (MRA). It uses the ACK and TWO ACK scheme and integrate digital signature for the acknowledgement packets. In order to distinguish different packet types in different schemes to include a 2-b packet header in EAACK. According to the Internet draft of DSR [7], there is 6 b reserved in the DSR header. In EAACK, use 2 b of the 6 b to flag different types of packets. In this secure ID, It is assumed that the link between each node in the network is bidirectional. Furthermore, for each communication process, both the source node and the destination node are not malicious. All acknowledgment packets are required to be digitally signed by its sender and verified by its receiver.

4.1 ACK

ACK is basically an end-to-end ACK IDS. It acts as a part of the hybrid IDS in EAACK, aiming to reduce network overhead when no network misbehavior is detected. Consider the scenario source node first sends out an ACK data packet to the destination node D. If all the intermediate nodes along the route between nodes S and D are cooperative and node D successfully receives packet, node D is required to send back an ACK acknowledgment packet along the same route but in a reverse order. Within a predefined time period, if node S receives packet, then the packet transmission from node S to node D is successful. Otherwise, node S will switch to S-ACK mode by sending out an S-ACK data packet to detect the misbehaving nodes in the route.

4.2 S-ACK

It is an improved extension of the TWOACK IDS [6] incorporating digital signature. The principle is to let every three consecutive nodes work in a group to detect misbehaving nodes. For every three consecutive nodes in the route, the third node is required to send an S-ACK acknowledgment packet to the first node.

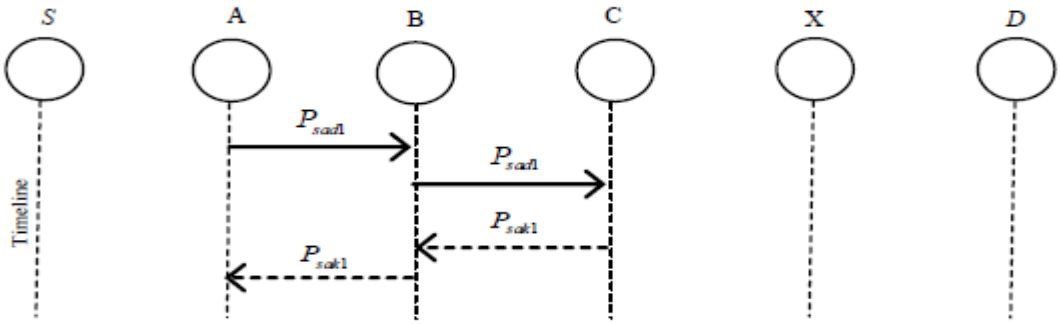

Fig-6 S-ACK scheme: Node C is required to send back an acknowledgment packet to node A.

The intention of introducing S-ACK mode is to detect misbehaving nodes in the presence of receiver collision or limited transmission power.

4.3 MRA

Unlike the TWOACK IDS, where the source node immediately trusts the misbehavior report, EAACK requires the source node to switch to MRA mode and confirm this misbehavior report. This is a vital step to detect false misbehavior. The MRA field is designed to tackle the weakness of Watchdog when it fails to detect misbehaving nodes. The false misbehavior report can be generated by malicious attackers to falsely report innocent nodes as malicious. The core of MRA field is to authenticate whether the destination node has received the reported missing packet through a different route. To initiate the MRA mode, the source node first searches its local knowledge base and seeks for an alternative route to the destination node. If there is no other that exists, the source node starts a DSR routing request to find another route. Due to the nature of MANETs, it is common to find out multiple routes between two nodes. When the destination node receives an MRA packet, it searches its local knowledge base and compares if the reported packet was received. If it is already received, then it is safe to conclude that this is a false misbehavior report and whoever generated this report is marked as malicious. Otherwise, the misbehavior report is trusted and accepted. By the adoption of MRA scheme, EAACK is capable of detecting malicious nodes despite the existence of false misbehavior report.

4.4 Digital Signature

EAACK is an acknowledgment-based IDS. All three methods of EAACK, namely, ACK, S-ACK, and MRA, are acknowledgment-based detection schemes. They all rely on ACK packets to detect misbehaviors in the network. Thus, it is extremely important to ensure that all acknowledgment packets in EAACK are authentic and untainted. Otherwise, if the attackers are smart enough to forge acknowledgment packets, all of the three schemes will be vulnerable. To overcome this problem, need to integrate digital signature in secure IDS. In order to ensure the integrity of the IDS, EAACK requires all ACK packets to be digitally signed before they are sent out and verified until they are accepted [1].

The signature size of DSA is much smaller than the signature size of RSA. So the DSA scheme always produces slightly less network overhead than RSA does. However, it is interesting to observe that the Routing Overhead differences between RSA and DSA schemes vary with different numbers of malicious nodes. The more malicious nodes there are, the more ROs the RSA scheme produces. Assume that this is due to the fact that more malicious nodes require more acknowledgment packets, thus increasing the ratio of digital signature in the whole network overhead. With respect to this result, find DSA as a more desirable digital signature scheme in MANETs [1]. The reason is that data transmission in MANETs consumes the most battery power. Although the DSA scheme requires more computational power to verify than RSA, considering the tradeoff between battery power and performance, DSA is still preferable [1].

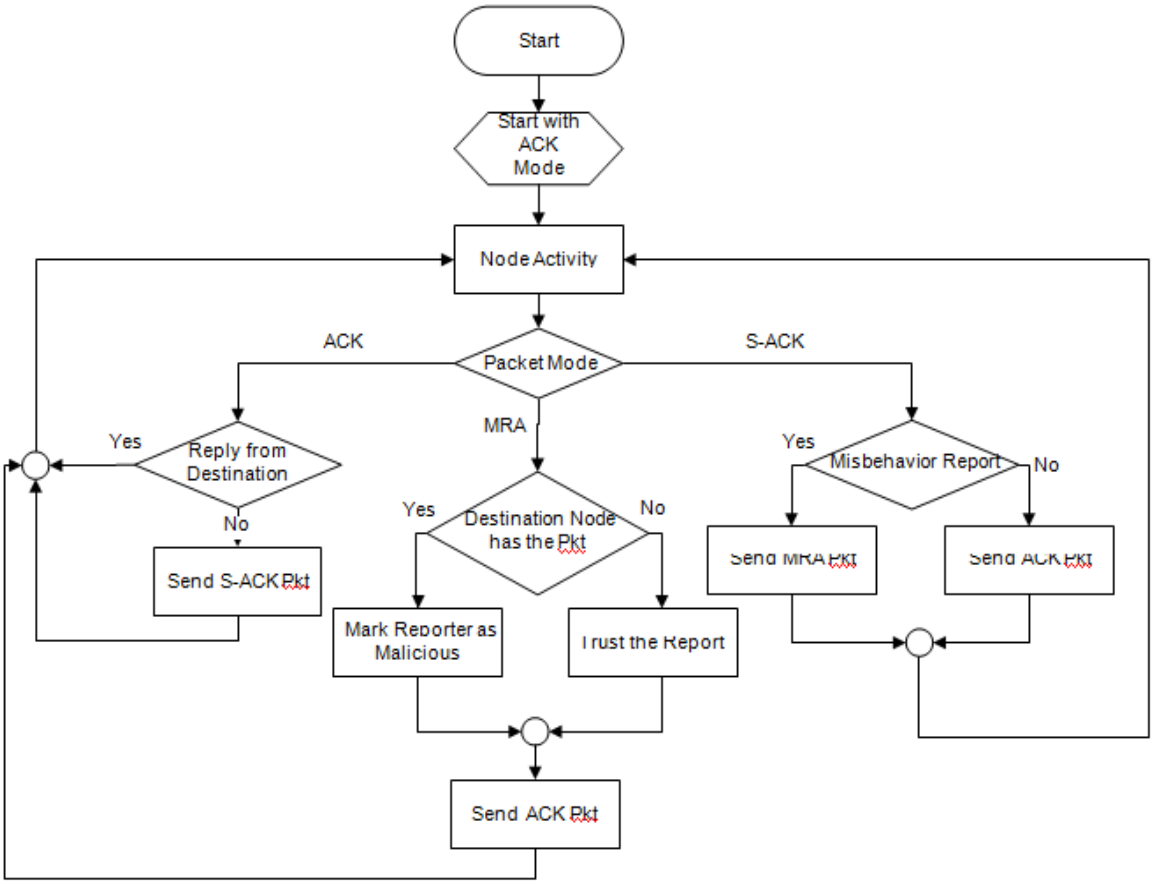

Fig-7 A. System Flow of EAACK

V. CONCLUSION

In this paper, a comparative study of Secure Intrusion- Detection Systems (SIDS) for discovering malicious nodes and attacks on MANETs is presented. Due to some of the characteristics of MANETs, prevention mechanisms alone are not adequate to manage the secure networks Therefore, security was always the major threat for MANETS so intrusion detection must be designed to address its security issues for MANET's .So in our proposed system a novel IDS (EAACK) was designed using digital signature. All three parts of EAACK, namely: ACK, SACK and MRA acknowledgement based detection schemes. They all rely on acknowledgement packets to detect misbehaving nodes in the network. Thus, it is extremely important to ensure all acknowledgement packets in EAACK are authentic and untainted .EAACK requires all acknowledgement packets to be digitally signed before they are sent out, and verified until they are accepted. However, we fully understand the extra resources that are required with the introduction of digital signature in MANETs. To address this concern, we implemented both DSA and RSA digital signature scheme in our proposed approach. The goal was to find the most optimal solution for using digital signature in MANETs. Although the DSA scheme requires more computational power to verify than RSA, considering the tradeoff between battery power and performance, DSA is still preferable [1].

REFERENCES

[1] EAACK – A Secure Intrusion Detection System for MANETs Elhadi M. Shakshuki, Senior Member, IEEE, Nan Kang and TarekR.Sheltami, Member, IEEE.

[2] R. Akbani, T. Korkmaz and G.V.S Raju. "Mobile Ad hoc Network Security", Lecture Notes in Electrical Engineering, vol. 127, pp. 659-666, Springer, 2012 – here1

[3] R.H. Akbani, S. Patel, D.C. Jinwala. "DoS Attacks in Mobile Ad Hoc Networks: A Survey", the proceedings of the Second International

Meeting of Advanced Computing & Communication Technologies (ACCT) , pp. 535-541, Rohtak, Haryana, India. 2012.

[4] T. Anantvalee and J. Wu. *A Survey on Intrusion Detection in Mobile Ad hoc Networks. In Wireless/Mobile Security,* Springer, 2008.

[5] L. Buttyan and J.P. Hubaux. Security and Cooperation in Wireless Networks. Cambridge University Press, Aug. 2007.

[6] D. Dondi, A. Bertacchini, D. Brunelli, L. Larcher, L. Benini, "Modeling and Optimization of a Solar Energy Harvester System for Self-Powered Wireless Sensor Networks," IEEE Trans. on Industrial Electronics, vol. 55, no. 7, pp. 2759-2766, July 2008.

[7] V. C. Gungor, G. P. Hancke, "Industrial Wireless Sensor Networks: Challenges, Design Principles, and Technical Approach," IEEE Trans. on Industrial Electronics, vol. 56, no. 10, pp. 4258-4265, Oct 2009.

Electrical Prototype Model of Pantograph-Catenary System

Rachana Garg[1], Senior Member, IEEE, Priya Mahajan[2], Member, IEEE, Parmod Kumar[3], Member, IEEE and Vidushi Gupta[4]
Deptt. of Electrical Engg. Delhi Technological University, Delhi, India[1,2,4]
Deptt. of Electrical Engg. MAIT, Delhi, India[3]
rachana16100@yahoo.co.in, priyamahajan.eed@gmail.com, pramodk2003@yahoo.co.in, vdushigupta@gmail.com

***Abstract*- The pantograph-catenary (PAC) system is one of the important interfaces between supply system and loco drive. The aim of this paper is to develop an electrical analogous of the mechanical model of PAC system. The response of the developed analogous electrical model and mechanical model are compared using simulink. Further, the hardware prototype of this electrical analogous of the PAC system is fabricated on a PCB using electric circuit elements and the response of hardware prototype and the developed electrical simulink model are compared. This model shall be useful in the designing and testing of PAC system.**

I. INTRODUCTION

Pantograph acts as an active link between the catenary and electric drive used for driving the electric loco. Till date many dynamic mechanical models of PAC system have been developed for studying its static and dynamic performance. However, no researcher has tried to develop the prototype electrical model of this system. S.D. Eppinger[1] et al have designed high performance pantograph employing two degrees of freedom, one for the head mass and one for the frame. It was shown that two degree of freedom models have been appropriate to represent a number of symmetric pantograph designs and an additional degree of freedom representing frame dynamic has been added to represent the asymmetric designs. The model has been evaluated with experimental data obtained from laboratory dynamic testing of an asymmetric pantograph. Most of the pantograph models used in initial studies are low order models with few translational degrees of freedom[2]-[10]. A first prototype of servo-actuated pantograph is developed by B.Allotta et al [11] and some simulation and experimental results were obtained. A. Balestrino [12] have proposed a modified pantograph model by adding wire simulation, in order to exert a constant force on the moving pantograph and overhead wire. Liu et al[13] presented an extended Mayr's equation-based model for the pantograph detachment arc of the high-speed railway traction system. Multibody models of pantographs have also been discussed by many researchers. These models give more realistic simulation results and new design concepts based on the simulation can be introduced[14]-[17].

Most of the models discussed above are mechanical models. These models are analyzed through simulation. Electrical analogous of these models are not available in the literature. The authors in this paper have developed an electrical analogous model of PAC system and compared the response of developed electrical analogous model and mechanical model of a symmetric pantograph. Further, the fabrication of electrical hardware prototype is done on PCB with the help of electric circuit elements.

II. RAILWAY ELECTRIC TRACTION SYSTEM

Electric rail traction system is a high speed and green technology based transportation system for metro urban as well as semi urban cities. In many countries, 25kV, 50Hz single phase ac supply is fed to the electric loco which is stepped down to different voltage levels by the loco transformer for various functions[18]. One of the winding of loco transformer is used to feed the traction drive through converter-inverter system. The single phase, 25kV supply from traction substation transformer is first fed to catenary at suitable point using the three core cable. The catenary conductor is made of cadmium-copper material to increase its tensile strength. The catenary conductor is supported at towers of approximately 63-72 m span and has sag between the span. Hence the pantograph cannot be fed directly through catenary. A contact wire of pure copper material is used below the catenary. This power conductor is supplied through the catenary and held in horizontal straight position using droppers of suitable lengths spaced at around 9m apart. The pantograph draws up the current through carbon brushes/metalized carbon strip and feed it to the loco transformer for supplying the power to the traction drives. The metalized carbon strip provides lubrication and has high current collecting capacity. Fig.1 shows the simplified diagram of power supply from power conductor to pantograph to electric rail loco system[19].

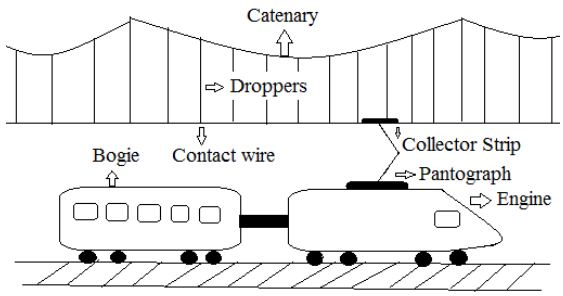

Fig.1. Electric loco supply system

III. Mechanical Model of PAC System

Pantograph is a crucial link between the power conductor and electric drive. It transfers the electric energy from the power conductor to loco transformer which feeds to the loco drive. It is a mechanical system composed of an articulated frame, carrying a collector head on which the collector strips for current collection are mounted. Constant pressure is applied at the head of the pantograph through pneumatic control mechanism to ensure that it always remain in contact with the contact wire. The supply from catenary to the power conductor to loco transformer through pantograph form a dash pot mass spring system. Fig. 2 shows the physical representation of pantograph[20].

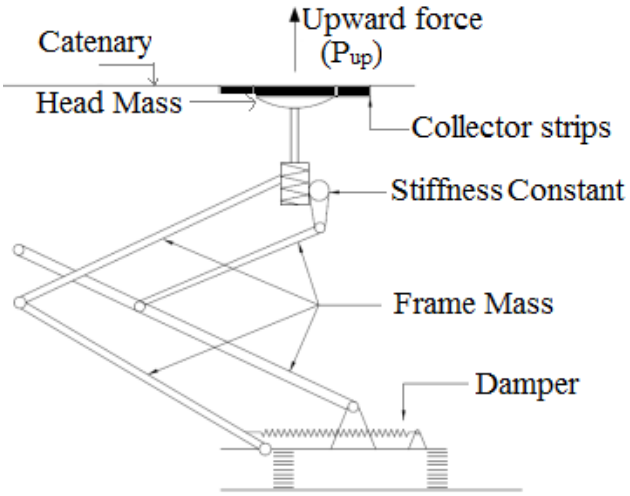

Fig.2. Physical Representation of Pantograph

The pantograph is modeled as a set of masses, springs and shock absorbers. For a symmetric pantograph, it is assumed that complete pantograph frame moves as a rigid body[1] and the pantograph can be represented by the two degrees of freedom of mechanical system as shown in Fig. 3.

In this dual mass system, the upper mass represents the head mass, M_h and lower mass represents the inertia of frame linkages M_f[1]. The stiffness of the contact strips and pantograph shoe is represented by shoe spring constant, K_s. The head spring constant, K_h, represents the stiffness of the torsional spring between the head link and the frame. Damper is included at each of the joints which is represented with a viscous damper, B_{vh}, in parallel with the spring constant. The suspension between the frasme and ground is modeled by viscous damper, B_{vf}. The input force P_{up} is applied to the frame mass which not only provides an uplift force against the catenary but must also overcome the weight of the mechanism due to gravity.

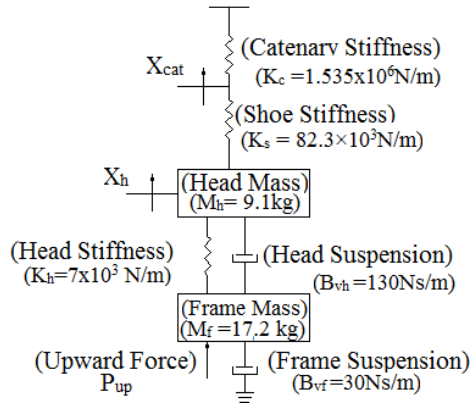

Fig. 3. Mechanical model of PAC system.

Modeling the PAC system as dash-pot spring system, the relation between displacement in catenary and force applied is given by (1)[2],

$$\frac{X_h - X_{cat}}{P_{up}} = \frac{(K_1-1)(sB_{vh}+K_h)}{K_1(c_4 s^4 + c_3 s^3 + c_2 s^2 + c_1 + c_0)} \quad (1)$$

where $c_4 = M_f M_h$,$c_3 = (M_f B_{vh} + M_h B_{vf} + M_h B_{vh})$,

$c_2 = (M_f K_2 + B_{vh} B_{vf} + M_h K_h)$,

$c_1 = (B_{vf} K_2 + B_{vh} K_2 + 3B_{vh} K_h)$, $c_0 = (K_2 K_h - K_h^2)$,

$K_1 = \frac{K_c + K_s}{K_s}$, $K_2 = K_h + K_s - \frac{K_s}{K_1}$

IV. Electrical Analogous of Mechanical Model

Mechanical systems are analogous to electrical systems. They have three passive, linear components. Two of them, spring and mass, are energy storage elements and the third, viscous damper, dissipates energy. The two energy storage elements viz. spring and mass are analogous to two electrical energy storage elements viz. inductor and capacitor. Energy dissipating element viscous damper is analogous to electrical resistance.

Using force-voltage analogy, where the mechanical force is considered analogous to the electrical voltage, mechanical velocity is analogous to the electrical current or mechanical displacement is represented by the charge, spring is analogous to the capacitor, the viscous damper is analogous to the resistor and the mass is analogous to the inductor. Thus, summing forces, written in terms of the velocity, is analogous to the summing voltages, written in terms of the current, and the resulting mechanical differential equations are analogous to mesh equations.

Using above analogy, the above mechanical model can be represented by electrical parameters as shown in Fig. 4.

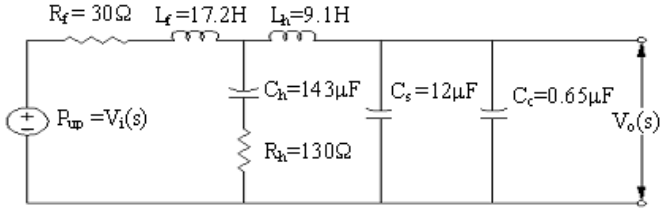

$V_i(s)=P_{up}$, $R_f=B_{vf}$, $L_f=M_f$, $C_h=1/K_h$, $R_h=B_{vh}$, $C_s=1/K_s$, $C_c=1/K_c$.

Fig. 4. Electrical model of PAC system

The transfer function of above circuit is given by (2).

$$\frac{V_o(s)}{V_i(s)} = \frac{1+n_1 s}{d_4 s^4+d_3 s^3+d_2 s^2+d_1+d_0} \quad (2)$$

The corresponding displacement of the catenary, $X_h - X_{cat}$, is represented by charge, Q_o, given by (3),

$$\frac{Q_o(s)}{V_i(s)} = \frac{(C_s-C_c)(1+n_1 s)}{d_4 s^4+d_3 s^3+d_2 s^2+d_1+d_0} \quad (3)$$

where, $n_1 = R_h C_h$, $d_4 = L_f L_h C_h (C_s + C_c)$
$d_3 = \left[(C_s + C_c)(R_f L_h C_h + R_h L_h C_h + R_h L_f C_h\right]$,
$d_2 = \left[L_f C_h + L_h (C_s + C_c) + L_f (C_s + C_c) + R_h R_f C_h (C_s + C_c)\right]$,
$d_1 = [R_f C_h + R_h C_h + (C_s + C_c) R_f]$, $d_0 = 1$

V. NUMERICAL RESULTS AND SIMULATION STUDIES

The transfer functions of mechanical model (model 1) and the corresponding electrical analog model (model 2), represented by Fig. 3 and Fig. 4, are given by (4) and (5). It is observed that both the transfer functions are approximately same.

$$\frac{X_h - X_{cat}}{P_{up}} = \frac{s+53.8}{1.27s^4+29.92s^3+1.24\times10^4 s^2+1.32\times10^5 s+4.43\times10^6} \quad (4)$$

$$\frac{Q_o(s)}{V_i(s)} = \frac{s+53.7}{1.29s^4+31.00s^3+1.3\times10^4 s^2+1.2\times10^5 s+4.5\times10^6} \quad (5)$$

The simulink response of displacement of catenary for mechanical model and the corresponding charge for analogous electrical model is studied under two input conditions i)when pantograph is fed with 1 p.u. step input representing constant contact force and ii) when pantograph is fed with 1 p.u. step input, with sinusoidal offset of 0.2 p.u. of frequency 5Hz added to it representing the oscillations in the contact force due to the translational movement of electric train. The responses with both inputs are as shown in Fig.5 and Fig. 6 respectively.

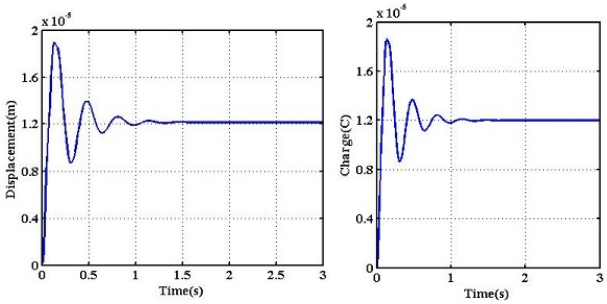

(a) (b)

Fig. 5. Response for step input of 1 p.u.
(a) Displacement for mechanical model (b) Charge for electrical model

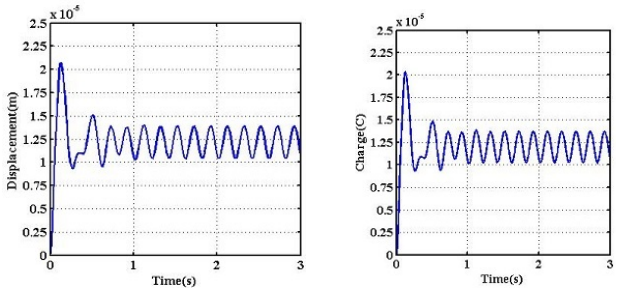

(a) (b)

Fig. 6. Response for 1 p.u. step input with sinusoidal offset of 0.2 p.u. added to it (a) Displacement for mechanical model (b) Charge for electrical model

VI. HARDWARE SET-UP

The hardware set up comprises of hardware electrical analogous model consisting of electrical circuit elements, a Tektronix TDS 2014B four channel digital storage oscilloscope, 100 Hz ,1GS/s, a dual output DC regulated power supply of $\pm$ 15V, a Tektronix AFG3021B Signal Generator.

For the electrical hardware model, two inductors of values 17.2 H and 9.1H are required. Both of these inductors are of floating type as none of their end is connected to ground and the value of these inductances is very high. Wire wound inductors of large value are bulky, costly and also produce noise. As a result, RC-active devices are used to simulate inductors on silicon chips. In this paper, Antoniou's simulated inductor [21]-[25] known as Generalized Impedance Converter (GIC) is used as shown in Fig. 7.

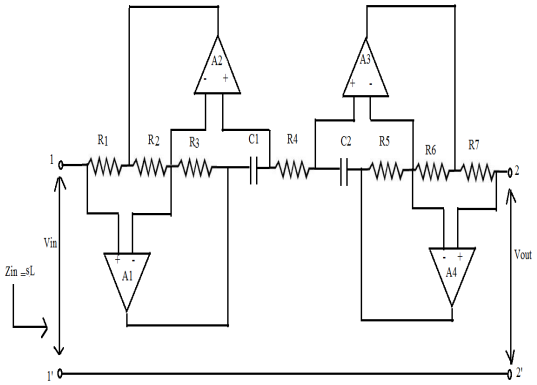

Fig. 7. Floating Inductor realization using two GIC circuits

In the above circuit, four op amps, seven resistors of identical rating and two capacitors of same ratings are used. A Generalized Impedance Converter (GIC) consists of active and passive elements. The input impedance of the converter is given by (6),

$$Z_{in} = \pm \frac{Z1}{Z2}\frac{Z3}{Z4} \ldots\ldots \frac{Z_{N-2}}{Z_{N-1}} Z_N \quad (6)$$

where N is total no. of active and passive elements (mostly an odd number with only a few exceptions).

The positive/negative sign signifies the positive/negative impedance converter respectively. The input terminals, between which the impedance is measured, can be either floating or one of them is grounded. The equivalent impedance as seen at the input node 1-1' of the simulated floating inductance is given by (7)

$$Z_{in} = sL = sR^2C \quad (7)$$

with all the resistances and capacitances are matched appropriately as follows:

R1 = R2 = R3 = R4 = R5 = R6 = R7 = R; C1 = C2 = C

The corresponding hardware set up is as shown in Fig. 8. The values of different components used for developing the hardware model are
Resistors=100Ω, 30Ω, Capacitors=144μF, 12μF, 1μF

For inductor of 17.2H, resistors for 4.7kΩ and capacitors of 1μF are used. For inductor of 9.1H, resistors for 3.3k Ω and capacitors of 1μF are used.

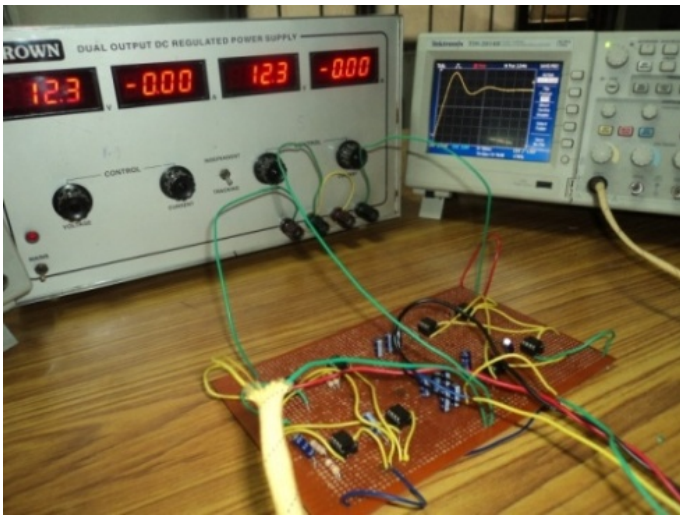

Fig. 8. Hardware Set-up

VII. VALIDATION OF RESULTS

Fig. 9 shows the response of the hardware prototype of developed electrical analog model of the PAC system under two input conditions.

Although the displacement of the catenary is proportional to charge $Q_o(s)$, since it is difficult to take the waveform of charge on CRO, therefore, voltage across capacitor is taken which will represent charge when multiplied by $(C_s - C_c)$. The simulink response of voltage, $V_o(s)$, of electrical model of PAC system are shown in Fig. 10. The simulink response for corresponding force for the mechanical model is shown in Fig. 11.

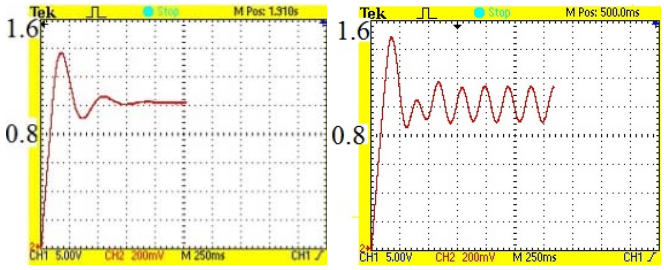

(a) (b)

Fig. 9. Voltage Response of electrical hardware prototype for both inputs

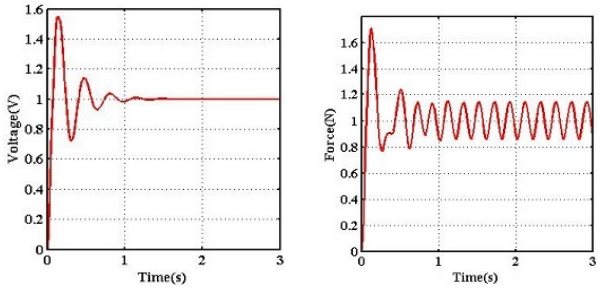

(a) (b)

Fig. 10. Voltage response of electrical simulink model for both inputs.

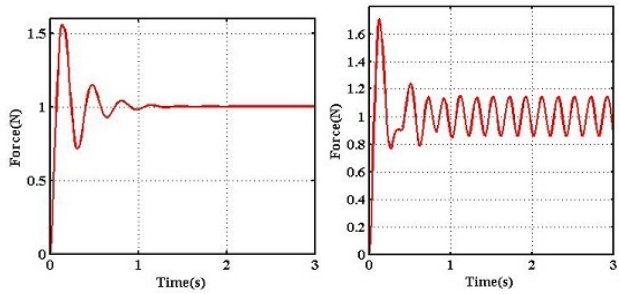

(a) (b)

Fig. 11. Force for mechanical model for both inputs

The results for three models are compared in table I. It is observed that for both the inputs, the settling time and the steady state values are same for all the models. However, for the peak overshoot, results for model 1 and model 2 are similar while the small deviation in the corresponding value of model 3 may be due to slight variation of values for capacitor and inductor used in actual hardware circuit from their synthesized values and due to the tolerance of the components and experimental errors.

TABLE I
COMPARISON OF RESULTS

Para-meters	Step Input (1 p.u.)			Step input (1p.u.) with sinusoidal offset of 0.2 p.u. added to it		
	Model 1	Model 2	Model 3	Model 1	Model 2	Model 3
t_s(s)	1.12	1.12	1	1	1	1
M_p(%)	55.9	55.9	40	55.7	55.7	50

VIII. CONCLUSIONS

An electrical analogous of mechanical model of PAC system is developed and its hardware prototype is fabricated in the laboratory of Electrical Engineering Department, Delhi Technological University. The prototype of mechanical model of PAC system is difficult to develop in the laboratory conditions due to its heavy weight and large force involved. But its electric analogous prototype is simple in design and can be easily realized under test conditions. Further, the hardware electrical prototype model shall be quite closer to the actual mechanical system as compared to simulated mechanical model. This model once developed can be very useful for the system designer for the real time studies of the PAC system and can be used to design robust active controllers for the high speed trains.

REFERENCES

[1] S.D. Eppinger, D.N.O. Conoor, W.P. Seering and D.N. Wormley, "Modeling and experimental evaluation of asymmetric pantograph dynamics", *ASME Transactions,* vol. 110, pp.168-174 , 1988.

[2] T.X. Wu and M.J Brenman, " Dynamic Stiffness of a Railway Overhead Wire System and Its Effect on Pantograph- Catenary System Dynamics," *Journal of Sound and Vibration*, vol. 219(3), pp. 483-502, 1999.

[3] Tong-Hin Park, Chang-Soo Han and Jin-Hee Jang, "Dynamic sensitivity analysis for the pantograph of a high speed rail vehicle," *Journal of Sound and Vibration*, vol.266, pp. 235-260, 2003.

[4] Jin-Woo Kim, Ho-chol Che, Bum-Scok Park, Seung-Yeol Lee, Chang-Soo Han and Jin-Hee Jang, "State sensitivity analysis of the pantograph system for a high-speed rail vehicle considering span length and static uplift force," *Journal of Sound and Vibration*, vol. 303, pp. 405-427, 2007.

[5] Jin-hee Ledd, Young-Guk Kim, Jin-Sung Park and Tae-Won Park, "Performance evaluation and design optimization using differential evolutionary algorithms of the pantograph for the high-speed train," *Journal of Mechanical Science and Technology*, vol 26(10), pp. 3253-3260, 2012.

[6] Yong Hyeon Cho , Young Park , Bubyoung Kang and Ki – nam Kim, " Influence of contact wire pre – sag on the dynamic of pantograph – railway catenary," *International Journal of Mechanical Sciences*, vol.52 pp 1471 -1490, 2010 .

[7] Lin, Y.C., Lin, C.L., Yang C.C.: 'Robust active vibration control for rail vehicle pantograph', *IEEE Trans. Vehicular Technology*, vol.56 (4), pp. 1994-2004, 2007.

[8] S. Walter, "Simulation of fuzzy control applied to a railway pantograph-catenary system," *International Conference on Knowledge based Intelligent Information and Engineering Systems*, 2010.

[9] E. Karakose, T. Gencoglu, "Adaptive fuzzy control approach for dynamic pantograph-catenary interaction," *MECHATRONIKA*, 2012.

[10] R.Garg, P. Mahajan, P. Kumar, "Effect of controller parameters on pantograph-catenary system," *American International Journal of Science, Technology, Engineering and Mathematics*, vol. 2(2), pp. 233-239, 2013.

[11] B. Allotta, M. Papi, L. Pugi, P. Toni and A.G Violi, "Experimental Campaign on a Servo-Actuated Pantograph," *IEEE/ASME International Conference on Advanced intelligent Mechatronics Proceeding*, pp. 237-242, 8-12 July 2001.

[12] Aldo Balestrino, Ottorinio Bruno, Alberto Landi and Luca Sani, " Innovative solutions for overload catenary-pantograph system: wire actuated control and observed contact force," *Vehicle System Dynamics*, vol. 33, pp 69-89, 2000.

[13] Yu-Jen Liu, G.W Chang and H.M. Huang, "Mayr's Equation-Based Model for Pantograph Arc of High-Speed Railway Traction System," *IEEE Transactions on Power Delivery*, vol.25, Issue 3, pp 2025-2027, July 2010.

[14] S.H. Kia, F. Bartolini, A. M. Mabwe and R. Ceschi, "Pantograph-catenary interaction model comparison," *Proceedings of IEEE, IECON*, pp. 1584-1589, 7-10 Nov., 2010.

[15] B. Simeoni and A. Arnold, " Coupling DAE and PDEs for simulating the interaction of pantograph and catenary," *Journal of Mathematical and Computer Modeling of Dynamical Systems*, vol. 6, no. 2, pp. 129-144, Jun.2000.

[16] J.H.Seo, SW. Kim, IH. Jung, TW. Park, JY. Mok, YG. Kim, and JB. Chai, "Dynamic analysis of a pantograph-catenary system using absolute nodal coordinates," *Journal of Vehicle System Dynamics*, vol. 44, no. 8, pp.615-630, 2006.

[17] C. Vera, B. Suarez, J. Paulin and P. Rodríguez , "Simulation model for the study of overhead rail current collector system dynamics, focused on the design of a new conductor rail," *Vehicle System Dynamics: International Journal of Vehicle Mechanics and Mobility*, vol. 44, no. 8, pp.595- 614, 2006.

[18] R.Garg, P.Mahajan and P.Kumar, "Sensitivity analysis of characteristic parameters of railway electric traction system," *International Journal of Electronics and Electrical Engineering*, vol.2(1), pp. 8-14, 2014.

[19] P. Mahajan, R. Garg and P. Kumar, "Sensitivity Analysis of Railway Electric Traction System", *IICPE 2010, India International Conference on Power Electronics*, [Online]. Available: IEEE Xplore, DOI 10.1109/IICPE.2011.5728107.

[20] P. Mahajan, R. Garg and P. Kumar, "Senstivity Analysis of Pantograph Catenary System Model", *Presented at IICPE 2012*, [Online]. Available: IEEE Xplore, DOI: 10.1109/IICPE.2012.6450475.

[21] K.C. Smith and A.S. Sedra, "*Microelectronic Circuit*," vol. V, New York: Oxford University, 2004.

[22] D. Susan and S. Jayalalitha "Frequency Dependent Negative Resistance -A Review" *Research Journal of Applied Sciences, Engineering and Technology*, vol. 4(17), pp. 2988-2994, 2012.

[23] Vimal Singh "On Floating Impedance Simulation*" IEEE transaction on circuits and systems*, vol. 36, pp. 161-162,1989.

[24] Umesh Kumar and Sushil kr. Shukla," Analytical Study of inductor Simulation Circuits," *Gordon and Breach Science Publishers*, vol. 13, pp. 211-227, 1989.

[25] R. Senani, "Realisation Of Single Resistance Controlled Lossless Floating Inductance", *Electronics Letters*, vol. 14(25), pp. 828-829, 1978. doi:10.1049/el:19780560.

Empirical Validation of Website Quality Using Statistical and Machine Learning Methods

Poonam Dhiman[#1] Anjali[*2]

Department of Software Engineering, Delhi Technological University, Delhi, India

[1]poonamdhiman19@gmail.com
[2]anjaliakg17@gmail.com

Abstract- **The analysis of quantitative measure of large set of websites plays a significant role in evaluating the quality of websites. The paper, computes 22 metrics using a tool developed in MATLAB. Website quality prediction is developed using statistical and some machine learning methods. The work has been validated using dataset collected from webby awards web site. The results are analyzed using Area Under the Curve (AUC) obtained from Receiver Operating Characteristics (ROC) analysis. The results show that the model predicted using the random forest and Bayes Net methods outperformed over all the other models. Hence, based on these results it is reasonable to claim that quality models have a significant relevance with design metrics and the machine learning methods have a comparable performance with statistical methods. Univariate analysis results provide an empirical view for website design guidance and suggest which metrics are more important for website development.**

Keywords: Empirical Validation, Receiver Operating Characteristics, Statistical Methods, Machine Learning, Web page.

I. INTRODUCTION

Web applications are different from traditional software system in terms of the involvement of diverse technologies in software as well as in hardware. Basic building blocks of web application are web pages which are static or dynamic in nature. Static web pages are written in HTML and dynamic web pages are written using various scripting languages such as PHP etc. Dynamic pages are generated at run time and the backend is typically written by database management system. Web metrics are used for better understanding of web page attributes and elements that we develop. Web metrics are used to determine the quality of web application. Since metrics are important source of information for decision making, a large number of web metrics have been proposed in the last few years to compare the structural quality of a web page [1][2]. As quality is an important factor in web engineering and an influential facet of website. Every organisation wants to determine the quality of web product at early stage so that overall cost and time can be saved. This would lead to early detection of poor website design that will be responsible for the poor product quality.

Hence, the main contributions of the paper are: (1) establishing relationship between web metrics and status of website (good or bad) - There are a number of website design metrics such as total number of links, web page size, total number of embedded text and complexity of a web page etc.; but all the metrics cannot predict the quality of a web site. Thus, it is very important to understand the relationship of web metrics and its status. In other words, we must find out which of the metrics are significant in predicting the status (good and bad) of a website. Identifying metrics will help web developers to predict goodness of a website. (2) Analyzing machine learning methods: Nowadays, machine learning is widely used in various domains. Seven machine learning methods have been used in this study to predict the accuracy of the model predicted. Amongst the various models predicted, our objective is to determine the one of the most optimised model, which can be used by researchers in further studies to predict the goodness of a website.

In this paper, to meet the above objective following procedure has been followed: a large set of metrics have been used and their values computed for different web sites (2012 - 2013 webby awards data). The inferences are drawn to find the subset of attributes which are related to the goodness of website design. Further, these attributes can be used to assess the data into good sites and bad sites. One statistical method (logistic regression) and six machine learning methods (Random Forest, Adaboost, Bagging,

978-1-4799-4236-7/14/$31.00 ©2014 IEEE

Multilayer Perceptron, Bayes Net) have been used in this study. The performance of the models is analyzed by calculating area under the Receiver Operating Characteristic (ROC) curve [3].

The paper comprises of five sections. Section 2 contains the literature review. Section 3 describes our research methodology with description of various metrics selected for the study and descriptive statistics of dataset that have been collected. Univariate results and ROC curve is used for model prediction in section 4. Finally section 5 includes conclusion remarks.

II. LITERATURE REVIEW

In the field of evaluating quality of web page there has been many research carried out, that is depend upon the statistical analysis of user behaviour [5]. Another method proposed in [20] for evaluating web page quality, investigates many factor related to browsing behaviour of user e.g. form input, number of scroll etc. In [9] comparative analysis of web page has been perform by using Gentler tool but there is no clear guidelines is given for large class of web page measure. Ivory et. al. [4] provides an analysis of web pages but does not predict the model that provides high accuracy. In [11] quality of website is analysed using fuzzy technique but the result is not validated and there is no classification of websites has been done. The recent work related to our study is that of Malhotra et. al[21] in which quality of web pages is analysed using Neuro-fuzzy model and result is validated using ROC curves. The study has been used nine web page metrics. In our research work we have been used 22 web page metrics and six machine learning methods to predict the best suited model that provide the high accuracy.

III. RESEARCH METHODOLOGY

This section describes list of metrics used in this study that are listed in table I and their descriptive statistics is given. Data collection process explained in this section. The section also explains the evaluation measure of performance that is being taken for the result analysis. We did quantitative analysis of web metrics like total number of links, complexity of web page, embedded Text, total graphics etc. These metrics have been calculated for websites downloaded from webby awards site. The webby awards site contains 70 different categories of websites like news, entertainment, sports, kids, education, fashion etc. To honour excellence on the Internet, there is a leading International award named, The Webby Award, which was established in 1996 during the Web's infancy. It is given by the International Academy of Digital Arts and Sciences (IADAS), which has more than thousand members for judging including executive members of leading Web experts, creative celebrities, business figures, visionaries, luminaries and Associative members who previously have been Webby Award Winners and Nominees and other Internet professionals [7].

I. TABLE

LIST OF METRICS

Total words length	Total words on a page
Body text length	Total words in body that are displayed.
Title text length	Words in title of the page
Total links	Total links including external, internal, embedded links etc.
Internal links	Total internal links of a web page
Size of page in KB	Total size of a page in kilo byes
Emphasize text	Total emphasized text
Total no. of !'s	Exclamation sign on a page
Average Number of Lines	Number of lines for all functions or methods.
HTML Lines	Number of all html lines.
JavaScript Lines	Number of all java Script lines.
Blank Lines of Code	Number of blank lines
Source Lines of Code	Number of lines containing source code
Lines with Comments	Number of lines containing comment
Paths	Number of possible paths, not counting abnormal exits or gotos.
Statements	Number of statements
Cyclomatic Complexity	Cyclomatic complexity
Nesting	Maximum nesting level of control constructs.
Frames	Total number of frames used on a page
Total list	Total list on a page
Number of tables	Number of tables present on a web
Graphic	Total number of images

A) Data Collection Process

Data consists of nearly 200 websites having different categories selected from webby award site. This organisation consists of six judges who examined many websites that have submitted for the awards based upon many criteria. All the award winning sites have been considered as good data points and other nominated sites as bad data points for our research. The home page of each website has been downloaded which is processed using our tool implemented in MATLAB. For evaluation 94 good data points and 101 bad data points have been selected. After processing the web pages of the selected websites the various web metrics like body text length, page size and total number of tables, frames etc were determined. After determining all the metrics for both good and bad data points the relationship between each metrics with the status of the website, that is, good or bad site is analysed. This is accomplished by using univariate analysis with the help of SPSS tool and the model is predicted using seven machine learning algorithm using weka tool [6]. Result of this tool is fed into the SPSS tool to predict the ROC curve which helps in predicting the best method for model prediction. The process of data collection is explained in block diagram as shown in fig 1.

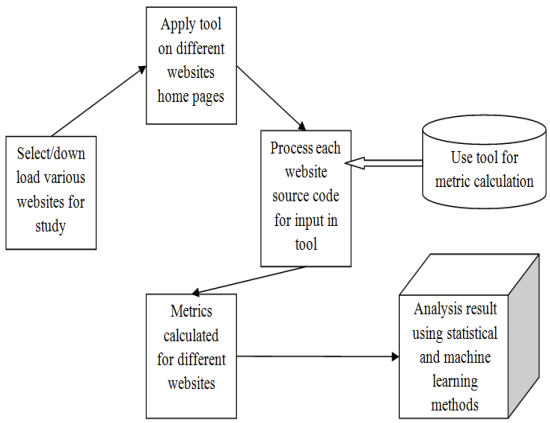

Fig1Block Diagram of Research Methodology

B) Descriptive Statistics

The table II presents the mean, median, standard deviation, standard error of mean for all the metrics that we have considered.

II. TABLE

STATISTICAL DESCRIPTION OF WEB METRICS

Metrics	Mean	Minimum	Maximum	Std. Deviation
Total words length	8005.272	1470	665260	10031.1
Body text length	6318.467	0	665200	9770.740
Title text length	3.491	0	310	4.8170
Table count	1.166	0	460	5.1855
Frame count	000	0	0	0000
Graphics	28.769	0	6310	64.8988
List count	006	0	10	0769
Links	150.639	0	9050	178.1218
Internal links	1042	0	270	3.3624
Size of Page In KB	12008	3	1497	160.723
Emphasize Text	19.179	0	18990	173.9611
Total No. of !'S	70.892	1	19070	158.3657
Average Number Of Lines	3.627	0	240	4.4505
HTML Lines	721.225	10	188780	1763.3180
Javascript Lines	91.544	0	9910	159.1810
Blank Lines Of Code	264089	0	181090	1522.6956
Source Lines Of Code	74.976	0	8010	130.77
Lines With Comments	35024	0	8500	79.5308
Path	69656450	0	999999999	78038086.3
Statements	79.751	0	12900	150.6374
Cyclomatic Complexity	3.343	0	510	6.7762
Nesting	.988	0	80	1.1902

C) Evaluation Measures of Performance

We have used following evaluation measures:

Sensitivity: It measures the correctness of predicted model and defined as the percentage of data points correctly measured. *Specificity:* measures the correctness of the predicted model.

Receiver Operating Characteristic (ROC):

It is an efficient method for model prediction and ROC analysis is used to evaluate the performance of the output of the predicted models. The ROC curve is a graph between sensitivity and 1-sensitivity. Where sensitivity corresponds to y coordinate and 1-sensitivity corresponds to x coordinate [3]. We have selected many cut-off points while plotting the ROC curves between 0 and 1 and then at each cut-off point sensitivity and specificity are determined. ROC curve is used to obtain the optimal cut-off point that maximizes both sensitivity and specificity [3].

The 10-cross validation method has been used for our study. In this method data points are divided into 10 equal partitions, among them one partition is used for testing and remaining partitions are used for training the model at a time [8].

IV. RESULT ANALYSIS

The final result after validation of web page quality is being provided in this section. Initially the subsets of the web metrics related to quality has been analysed using a statistical method, called univariate logistic regression. To predict the model that would provide highest accuracy, seven machine learning methods have been used. The performance of each model is analysed based on following parameter: sensitivity, specificity, ROC and cut-off points.

A) Result Univariate LR Analysis

Univariate logistic regression results have been analysed to find how each independent metric is associated significantly with the status (good or bad) of website, which is taken as dependent variable and is listed in Table III. It shows the coefficient (B), standard error (S.E.), statistical significance (sig.), and odds ratio (exp (B)) for each metric [10]. The "sig" parameter describes whether each metric significantly predicts the dependent variable or not. The metric is said to be significant if value of "sig" parameter of metric is nearly in the range of 0.001 to 0.005, that is, a significance threshold and range between 0.01 and 0.05 is considered to be moderate.

III. TABLE.

UNIVARIATE ANALYSIS

Metric name	B	S.E.	Sig.	Exp(B)
Total words in a page	0.000	.000	0.167	1.000
Words between body tag	0.00	.000	**0.016**	1.000
Words between title tag	-0.017	0.32	0.603	.983
Total links	-0.002	0.01	**0.030**	1.002
No. of Internal links	0.127	0.075	0.090	1.135
Size of page in KB	0.004	0.002	0.025	1004
Embbed text	0.000	0.01	0.0904	1.000
Total no. of!'s	-0.002	0.002	0.294	0.994
Average Number of Lines	-0.145	.042	**0.001**	0.865
HTML Lines	0.000	0.000	0.883	1.000
JavaScript Lines	-0.003	0.001	**0.030**	0.997
Blank Lines of Code	0.000	0.000	0.883	1.000
Source Lines of Code	-0.003	0.001	**0.030**	0.997
Lines with Comments	-0.010	0.004	**0.008**	.990
Paths	0.000	.000	.523	1.000
Statements	-0.002	0.001	0.125	.998
Cyclomatic Complexity	-0.125	0.46	**0.007**	0.883
Nesting	-0.759	0.172	**0.000**	0.468
Graphic	-0.001	0.002	0.728	0.999
List count	-21.49	40192.970	1.000	0.000
Frame count	0.274	0.155	**0.078**	1.315
Table count	0.32	0.38	0.392	1.033

Table III represents the significant values in bold. The coefficient (B) tells the strength of independent variable, higher the value of coefficient (B), higher is the impact of the independent variable. The sign of coefficient represents whether the impact is positive or negative. We can observe that total words in a page, HTML Lines, Paths and Statements are not significant therefore they are not taken for further analysis. Thus, in this way we can reduce the independent variable and take only significant metrics for analysis of website quality.

B) Model Evaluation Using the ROC Curve

The machine learning algorithms have been used for model prediction e.g. Bagging [12], Adaboost[13], multinomial naive bayes[14], Random Forest[15], Bayes Net[16], decision table[17] and MLP[18].Table IV presents the result of 10 fold cross validation of model predicted by applying machine learning algorithms. It also shows sensitivity, specificity, AUC and the cut-off point for the model prediction. Sensitivity corresponds to y-axis and 1-specificity corresponds the x-axis of the ROC curve. The cut-off point can be called as the point at which 1-specificity is equal to sensitivity. The ROC curve for Random Forest and Bayes Net is represented in fig 2 and fig 3 respectively.

From the above, we observed that Random forest provides the best result as compared to other methods. Random forest has highest value of area under curve i.e. 0.82 and for Bayes Net AUC value is 0.813. The Adaboost and bagging gives almost similar result i.e., values of AUC are 0.804 and 0.805 respectively. Naive Bayes Multinomial and decision table shows average results, AUC values for these methods are 70.8 and 71.1 respectively. MLP shows poor results having AUC value 66.8. Thus, this method is not considered as a better method for prediction in our case. We can also observe that the logistic regression [19] is poor as compared to machine learning methods. Thus, from the above discussion that the machine learning methods give better results as compared to the statistical methods.

Amongst the machine learning methods under consideration, random forest and Bayes Net have shown the best results.

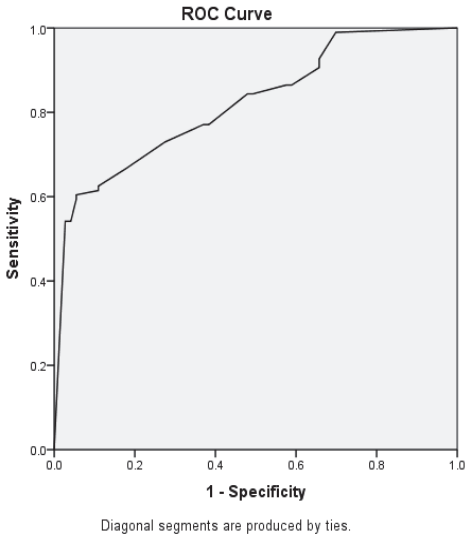

Fig2. ROC curve for random forest

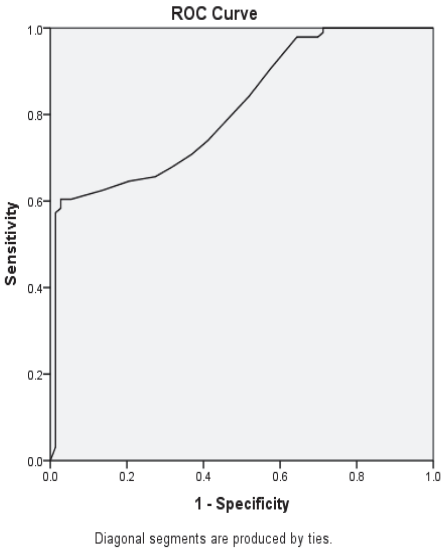

Fig3. ROC curve for Bayes Net

IV. TABLE

RESULTS OF 10-CROSS VALIDATION

S.NO.	Method used	Sensitivity	specificity	AUC	Cut-off point
1.	Adaboost	70.8%	70%	80.4	0.48
2.	Bagging	69.8%	70%	80.5	0.49
3.	Bayes Net	67.7%	69.5%	81.3	0.27
4.	MLP	64.4%	65%	66.8	0.64
5.	Random Forest	72.9%	72.6%	82	0.55
6.	Decision Table	66.7%	63%	71.1	0.39
7.	Naive Bayes Multinomial	69.8%	69.9%	70.8	0.99
8.	Logistic Regression	67.7	67.9	69.8	0.55

V. CONCLUSION

The objective of this paper is to evaluate the quality of web sites. The E-commerce is an emerging platform and we frequently deal with different web- based interactive applications like shopping and management applications etc. We can expect an increased interest in developing such applications with the wide acceptance of the same. Hence maintenance, quality and security inclusion for websites become very crucial. We empirically validated the relationship between quality and web metrics using statistical and machine learning methods. In this study we considered all web metrics as independent variable and status (good or bad) of a website as a dependent variable. For predicting quality of a website, we used univariate logistic regression. It was found that the metrics average number of lines, complexity, nesting, lines with comments, total links is more significant predictor of quality of website. For model prediction we have used seven machine learning methods which determine the accuracy in terms of specificity, sensitivity, AUC (area under curve) and cut-off points. Cut-off points maintain the balance between quality data points. We observed that the random forest and Bayes Net gave the best result as compared to other models. MLP method is poor predictor as compared to others for our study. Decision table and Naive Bayes Multinomial have shown average results.

References

[1] George W. Furans, "Effective view navigation", *in proceedings of ACM CHI 97 conference on human factors in computing systems*, volume 1 of PAPERS: information structures, pp. 367-374, 1997.

[2]Izzat Alsmadi, Ahmad T. Al-Taani, and Nahed Abu Zaid Web Structural Metrics Evaluation 978-0-7695-4160-0/10 $26.00 © 2010 IEEE DOI 10.1109/DeSE.2010.43

[3] K. El Emam, S. Benlarbi, N. Goel, and S. Rai, "A *validation of object-oriented metrics*," *NRC Technical report ERB-1063,*1999.

[4] Melody Y. Ivory, Rashmi R. Sinha and Marti A. Hearst "Empirically Validated Web Page Design Metrics" *SIGCHI'01*, March 31-April 4, 2001, Seattle, WA, USA.Copyright 2001 ACM 1-58113-327-8/01/0003.

[5] Li,P., yamada, S.: Automated web site Evaluation- an approach based on ranking SVM, international joint conference on web intelligent and intelligent agent technologies, IEEE/WIC/ACM ,pp.34-37(2009).

[6]weka Available: http://www.cs.waikato.ac.nz/ml/weka/

[7] http://WWW.webby awards.com/

[8] M.Stone, "*Cross-validatory choice and assessment of statistical predictions*," *Journal Royal Stat. Soc*., Vol.36, 1974, pp.111-147.

[9] Thimbleby, h.: Gentler: A tool for systematic web authoring, international journal of human- computer studies, 47, pp. 139-168 (1997).

[10] Y. Singh, A. Kaur, and R. Malhotra, "Empirical vlidation of object-oriented metrics for predicting fault proneness models," Software Quality Journal, Vol.18,No.1, 2010,pp.3-35.

[11] Mittal, H., Sharma, M., Mittal, J.P.2012: Analysis and modelling of websites quality using fuzzy technique. Proceeding of the second international conference on advanced computing & communication technologies (ACCT), pp. 10-15, IEEE 2012.

[12] L.Breiman, "*Bagging predictors*," *Machine Learning*, Vol.24, 1996, pp.123-140.

[13] Yoav Freund and Robert E. Schapire" *A Short Introduction to Boosting", Journal of Japanese Society for Artificial Intelligence,14(5):771-780, September, 1999.*

[14] Kibriya, A.M., Frank, E., Pfahringer, B., Holmes, G.: Multinomial naive bayes for text categorization revisited. In: Proceedings of the 17th Australian joint conference on Advances in Artificial Intelligence. AI'04, Berlin, Heidelberg, Springer- Verlag (2004) 488-499.

[15] Y. Freund and R.E. Schapire, "*A Short Introduction to Boosting*," *Journal of Japanese Society for Artificial Intelligence,* Vol.14, No.5, 1999, pp.771-780.

[16] Jiang Su jiang.su@unb.ca,Harry Zhang" Full Bayesian Network Classifier" Faculty of Computer Science, University of New Brunswick, Canada, Appearing in Proceedings of the 23 rd International Con- ference on Machine Learning, Pittsburgh, PA, 2006.

[17] Barry G. Becker, INFOVIS '98 Proceedings of the 1998 IEEE Symposium on Information Visualization Pages 102-105 IEEE Computer Society Washington, DC, USA ©1998.

[18] Mashor M.Y, "Hybrid Multilayer Perceptron Networks", *International Journal of Systems Sciences*, 2000, Vol 31, No 16, pp. 771-785.

[19] Goran Mauša, Tihana Galinac Grbac and Bojana Dalbelo Bašić "Multivariate Logistic Regression Prediction of Fault-Proneness in Software Modules" MIPRO 2012, May 21-25,2012, Opatija, Croatia.

[20] Velayathan, G.,Yamada, s.: Behaviour based web page evaluation proceedings of the IEEE/WIC/ACM international conference on web intelligence and intelligent agent technology (WI-IAT workshops), pp. 409-412 (2006).

[21] Malhotra, r., Sharma, A,a neuro-fuzzy classifier for website quality prediction, proceeding of international conference of advances in computing, communication and informatics (ICACCI), 978-1-4673-6217-7/13,IEEE 2013.

Hindawi Publishing Corporation
International Scholarly Research Notices
Volume 2014, Article ID 175464, 9 pages
http://dx.doi.org/10.1155/2014/175464

Review Article

Forward Osmosis in India: Status and Comparison with Other Desalination Technologies

Dhruv Mehta, Lovleen Gupta, and Rijul Dhingra

Department of Environmental Engineering, Delhi Technological University, Shahbad Daulatpur, Main Bawana Road, Delhi 110042, India

Correspondence should be addressed to Dhruv Mehta; dhruv.meh19@gmail.com

Received 23 June 2014; Revised 19 September 2014; Accepted 22 September 2014; Published 29 October 2014

Academic Editor: Shaobin Wang

Copyright © 2014 Dhruv Mehta et al. This is an open access article distributed under the Creative Commons Attribution License, which permits unrestricted use, distribution, and reproduction in any medium, provided the original work is properly cited.

With an increase in demand of freshwater and depleting water sources, it is imperative to switch to seawater as a regular source of water supply. However, due to the high total dissolved solid content, it has to be desalinated to make it drinkable. While desalination technologies have been used for many years, mass deployment of such technologies poses a number of challenges like high energy requirements as well as high negative environmental impact through side products and CO_2 emissions. The purpose of this paper is to present a sustainable technology for desalination. Forward osmosis, an emerging technology, is compared with the other commonly used technologies worldwide, namely, multieffect distillation, multistage flash distillation, and reverse osmosis as well as other emerging technologies like vapour compression, solar humidification dehumidification, nanofiltration, and freezing desalination. As energy consumption and associated greenhouse gas emissions are one of the major concerns of desalination, this paper concludes that forward osmosis is an emerging sustainable technology for seawater desalination. This paper then presents the challenges involved in the application of forward osmosis in India and presents a plant setup. In the end, the cost comparison of a forward osmosis and reverse osmosis plant has been done and it was concluded that forward osmosis is economically better as well.

1. Introduction

Three-fourths of the earth's surface is covered with water. Out of this three-fourths, only 0.6 percent is found in the form of lakes and rivers [1]. The rest is found in the form of salt water in oceans, which cannot be directly used for human consumption. The world's population is expected to reach 8.1 billion by the end of 2025 [2]. With depleting fresh water sources, additional water supplies will be important in determining the future of humans on this planet. Like fossil fuel resources, the need for water is likely to be a major factor for world stability in the coming few years [3, 4]. There are technological innovations being made, as well as new water sources being explored, to cater to the growing water demand around the world. If used efficiently, the concept of desalination is a very viable option for addressing the problem of water scarcity.

Desalination is slowly becoming a popular concept among the public. The worldwide desalination industry is expected to grow 140 percent over the next decade, with 25 billion United States Dollar (USD) in capital investment by 2010 and 56 billion USD by 2015 [5]. Thermal methods of desalination such as multistage flash (MSF) and multiple-effect distillation (MED) have been found successful in converting seawater into pure water, but the energy required for this process makes it unviable to be used on a large scale. Membrane technology, such as reverse osmosis (RO), suffers from membrane fouling and a high rate of brine production [6]. Current methods of brine disposal cause major environmental problems. Therefore, research is continually being carried out in order to find out the sustainable way of desalting seawater. One such method is forward osmosis (FO). It is found to be highly efficient with a low rate of brine production; FO is an area of active research. If adopted, this technique might be the answer to all of our water problems.

India has a coastline of 7516 km [7]. Since, 9 Indian states and 4 union territories are surrounded by seawater along one or more sides, desalination can play a major

role in augmenting the fresh water requirements of the country if technically and economically efficient desalination technology is implemented for obtaining pure water from sea water in these regions. Additionally, areas such as Tamil Nadu, Gujarat, and Andhra Pradesh have a huge problem of water scarcity due to poor river water availability, low ground water levels, and high water demand [8]. Since the launch of the first five-year plan in 1951, 1105 billion Indian Rupees [9] have been spent to provide safe drinking water, yet it continues to be a major issue. Thus, it is imperative that India focuses its attention on seawater in order to meet the water demands of the growing population.

Of all the desalination techniques available, in this paper, we focus our attention on FO. The review begins by discussing the current situation of the desalination sector in India. The key part of this paper is the comparison of FO with all of the other prevalent, as well as emerging, techniques in India. We also cite all the benefits of adopting FO. Then we discuss the application of FO in seawater desalination along with its advantages and disadvantages. In the final part of the review, we look at the challenges of bringing FO into the Indian market. Due to limitations on literature on the topic, a complete comparison of the techniques on all 14 parameters could not be made.

2. Desalination in India

India represents 16 percent of the world's population and at its present growth rate is expected to hit the 1.5 billion mark within the next four decades [10]. The Government of India's Planning Commission estimates the water demand to increase to 1180 BCM (billion cubic meters) by the year 2050. This represents a nearly 66 percent increase from the known 710 BCM of water demand in 2010 [11]. With the depleting water sources and increase in the demand, it becomes imperative to switch to seawater to meet the water requirements in India. Suryanarayanan says that desalination technologies are still evolving in India [12] and Indo-Asian News Service report suggests that the Indian desalination water market is expected to grow at a compounded annual growth rate (CAGR) of 30 percent over a period of five years from 2013 to 2018 [13]. There has been a sudden increase in the capacity of plants desalinating saline water from year 2006 as shown in Figure 1. In addition, the desalination capacity in India is seen at 5.35 million m^3/d by 2018 [13], which is 342.1% increase from its capacity in 2013. Thus, it can be concluded that desalination water market in India is expected to grow at a rapid rate.

The two main desalination technologies are those based on thermal and membrane processes. Thermal processes include multistage flash (MSF), multiple-effect distillation (MED), and vapour compression (VC), whereas membrane processes include reverse osmosis (RO), electrodialysis (ED), and forward osmosis (FO). Figure 2 shows the distribution of the desalination technologies adopted in India in the financial year 2012-13. Since membrane based technologies are considered to be 23 percent cheaper than thermal based technologies for generating desalinated water, plants in India

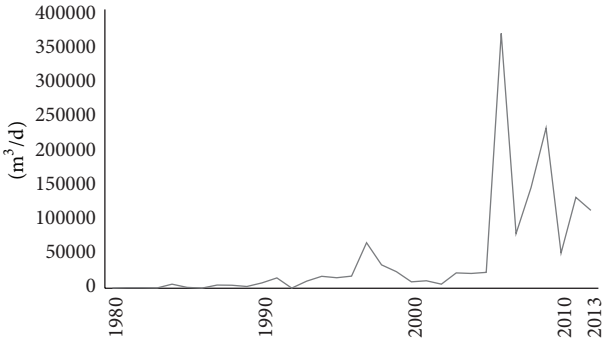

Figure 1: Increase in capacity of plants desalinating saline water in India (DesalData).

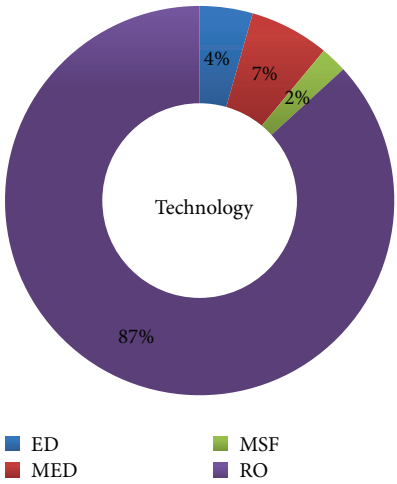

Figure 2: Desalination technologies adopted in India in 2012-13 (DesalData).

are mostly membrane based [14]. It can be seen that RO dominated.

Figure 3 illustrates the breakup of the desalination plants currently operating in India by capacity. It can be seen that currently desalination plants in India are mostly of sizes up to 10,000 cubic meters per day (m^3/d). These plants are mostly used for industrial and irrigational purposes. Gujarat and Tamil Nadu have emerged as desalination hubs due to poor water availability, low ground water levels, and high demand [8]. Desalination is also used in the coastal regions of Maharashtra, Andhra Pradesh, Karnataka, and West Bengal.

3. Desalination Techniques

3.1. Current Techniques Employed in India

3.1.1. Reverse Osmosis. Reverse osmosis (RO) is a membrane separation process in which the seawater permeates through a membrane by applying a pressure larger than the osmotic pressure of the seawater. The membrane is permeable for water but not for the dissolved salts. In this way, a separation between a pure water fraction (the product) and

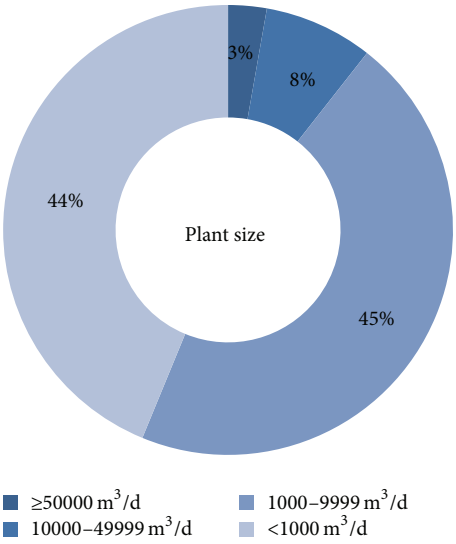

Figure 3: Plant size breakup in India in 2012-13 (DesalData).

a concentrated fraction (the retentate or concentrate) is obtained [15]. A typical RO desalting plant consists of three sections, namely, pretreatment section, membrane section, and posttreatment section. Energy consumption depends on the salt content of the feed water. Development of RO membranes of very high rejection, while maintaining high permeability, has the potential to reduce energy consumption [16].

Bhabha Atomic Research Centre erected desalination plants in Andhra Pradesh, Gujarat, Rajasthan, Tamil Nadu, Port Blair, and Lakshadweep. Bharat Heavy Electricals Limited (BHEL) operated 12 desalination plants using RO technology in Tamil Nadu [17].

3.1.2. Multistage Flash. Multistage flash (MSF) starts with saline feed water being passed through a series of tubes which preheat the water. Water then enters the brine heater where it is heated using thermal energy. The heated water is then passed through a vessel, called the stage, with pressure lower than that of the brine heater, which results in flashing of the saline water. Vapours formed during boiling condense on the tubes carrying the input saline water. Distillate is collected in the distillate trays. Only a small percentage of the heated water is converted into steam, depending upon the pressure maintained at the next stage. The remaining water is then introduced to a subsequent stage, which has a lower pressure. This process continues until the saline water is cooled down and discharged [18].

BARC built a 425 KLD MSF pilot plant in Bombay and a 4.5 MLD MSF unit as a part of 6.3 MLD Hybrid MSF-RO plants [16].

3.1.3. Multieffect Distillation. Multieffect distillation (MED) takes place in a series of vessels or effects and uses the principle of evaporation and condensation at reduced ambient pressures. The feed water, after being preheated in the final condenser, is fed in equal proportions to the various vessels. The water is sprayed on the evaporator surface (tubes) after being heated to its boiling point. The evaporator tubes in the first effect are heated with steam. The steam comes from the steam turbines of a power plant, or boiler, where the steam inside condenses as the water sprayed on the evaporators vaporizes. The vapours from the first effect are used to heat the surfaces of the succeeding effects. The vapours produced in the last effect are condensed in the final condenser—cooled by incoming saline feed water—to yield pure water [18].

At reliance industries ltd. (RIL) in India, four MED plants have been in operation since 1998, each with a nominal production of 12,000 m^3/d. A fifth MED unit of 14,400 m^3/d capacity was operational in February 2005 [19].

3.2. Other Techniques Being Researched

3.2.1. Vapour Compression. Vapour compression (VC) is a highly reliable and efficient process which uses mechanical energy to desalinate water. Heat is pumped from a reservoir which is at a low temperature to a reservoir which is at higher temperature. The basic system consists of an evaporator-condenser and a compressor where water vapours act as a working fluid. Water vapour at the evaporation side of a heat transfer surface is compressed. This results in a rise of the saturation temperature and pressure, which is then condensed to form condensate releasing latent heat of condensation in the process. The latent heat is transferred across the heat transfer surface into the water layer side causing further evaporation.

3.2.2. Solar Humidification-Dehumidification. In solar humidification-dehumidification (SHDH), solar energy is used to heat sea water, which results in the humidification of air. This air acts as a carrier gas. The humidified air rises up to form clouds, which upon dehumidification pours down as rain. The man-made version of this cycle is called the humidification-dehumidification desalination cycle.

3.2.3. Electrodialysis Reversal. The electrodialysis reversal (EDR) process is based on the principle that most dissolved salts are positively and negatively charged and are attracted towards an electrode of the opposite charge. Selective membranes allow either passage of anions or cations, leading to the separation of ions. Anion selective membranes allow the passage of anions but block cations, whereas cation selective membranes allow the passage of cations but block anions. Polarity of the electrode is frequently reversed to free up accumulated charge on the membrane surface, thus minimizing membrane fouling.

3.2.4. Freezing Desalination. The process of freezing desalination (FD) is based on the principle that the formation of ice crystals leads to the exclusion of dissolved solids. During freezing, the nonfrozen saline component is removed at the appropriate time. The frozen water is rinsed to remove the

remaining salts adhering to the ice crystals. The ice is then melted to get fresh water [20].

3.2.5. Nanofiltration. In nanofiltration (NF), a pressure driven membrane separation process, the separation takes place across a semipermeable membrane. Membranes have pores that measure in the nanometers. The pressure difference between the feed and filtrate side of membrane leads to the separation of salt from water. Lower operation pressure, higher flux, and higher retention of multivalent anion salts provide it an advantage over RO.

3.2.6. Forward Osmosis. Forward osmosis (FO) is a natural phenomenon where a difference in osmotic pressure drives the solvent from a region of lower concentration to a region of higher concentration across a selectively permeable membrane [21]. The low-concentration solution is called the feed solution and the high-concentration solution is called the draw solution [22]. Feed solution is generally seawater or brackish water that needs to be desalinated, while the draw solution is prepared in a laboratory using a solute of high osmotic pressure. Osmotic pressure difference between the feed and draw solution causes the water to flow into the draw solution from the feed solution [23]. Energy efficient techniques are used to draw pure water from the draw solution [24]. Regeneration of the draw solution is the most expensive stage in the FO desalination process. Nanofiltration, reverse osmosis, or other thermal processes are proposed for the regeneration of draw solution [25].

4. Comparison between the Desalination Technologies

Table 1 provides a detailed comparison of the traditional techniques as well as techniques being researched for desalination. It can be seen that FO requires less energy per m^3 of water than the other thermal and membrane techniques. Solar energy is in abundance, but the technical knowledge to harness it efficiently is still primitive. Nanofilters have also shown early promise but there is still time before its theoretical knowledge can be efficiently applied to desalination. Stand-alone nanofilters face many problems, such as fouling, and therefore need to be incorporated with another suitable technique as a hybrid system. The cost required to construct an FO plant is considerably less than most of the other thermal technologies, even reverse osmosis. Compared to RO, FO has less membrane fouling, scaling, and brine discharge. Even though the product water quality varies over a wider range than the thermal methods, this is not of much importance since the dissolved solid content is well under the specified world health organization (WHO) guidelines. Greenhouse gas (GHG) emissions are also considerably less in membrane techniques compared to the thermal techniques. However, the draw solutions and membranes in FO are still areas of active research in order to improve upon the process. Additionally, though FO membranes suffer from fouling which other techniques besides membrane techniques do not, the advantages of FO outweigh its disadvantages. Therefore, if efficiently used, FO can prove to be an efficient way of desalinating seawater.

5. Challenges in Settingup of FO Plant

(i) Membrane development: an appropriate membrane should be able to reduce the effect of concentration polarization, fouling, and reverse solute diffusion. Values of FO flux calculated using solution diffusion theory tend to have higher values than experimental values. This is attributed to the presence of internal and external concentration polarization which reduces the osmotic force.

(ii) Draw solution development: a suitable draw solution should have high osmotic pressure, be easily recoverable, and exhibit minimal internal concentration polarization. Factors such as low cost, zero toxicity, and low fouling are also important.

(iii) Membrane fouling: membranes having low fouling are still being researched. Low membrane fouling would lead to better quality product water. Membranes would have a longer working life leading to reduction in capital and operational costs.

(iv) Brine discharge: disposal of brine produced is a major issue since it causes environmental problems. However, not only is it a challenge for FO, but also it is a challenge for every other desalination technology.

(v) Fragmentation: creating an industrial standard would be a problem because most of the Indian market is fragmented with many regional players [26].

(vi) Bureaucratic hurdles: new technology adopted has to be approved by the government before it can be introduced into the market. Slow execution and bureaucratic hurdles may prove to be time consuming and cause problems before the technology can be adopted [26].

(vii) Improper training: as the technology is new, lack of adequate training of the staff handling the plant would be a major problem for the industry.

6. Proposed FO Setup in India

Figure 4 presents the FO setup as proposed for India. 50 leading scientists and professionals working in the field of desalination in India were surveyed on the potential FO setup that can be viably operated in the Indian market. According to the results of the survey, the FO membranes which can be easily synthesized using the existing setup in India are (a) cellulose triacetate membrane and (b) polybenzimidazole. The possible draw solutions which can be used in the Indian market are (a) sulphur dioxide solution, (b) glucose solution, (c) ammonium carbonate solution, (d) sodium chloride solution, and (e) potassium nitrate + sulphur dioxide solution. Also, for regeneration purposes, RO or any thermal process can be employed, as the technical knowhow of these processes is very good in India considering the data presented

Table 1: Comparison of different desalination techniques.

Desalination technique	MSF	MED	RO	VC	SHDH	EDR	FD	NF	FO
Energy consumption (kWh/m^3)	Electrical: 4–6 Thermal: 55–120 [30]	Electrical: 2–2.5 Thermal: 30–120 [31]	Electrical: 3.5–4.5 Thermal: None [30]	Electrical: 7–12 Thermal: None [32]	140–550 [33]	<0.6 [34]	90–120 [35]	0.3–1 [36]	Total: 0.84 [37]
Product water quality (mg/L TDS)	1–50 [30]	1–50 [38]	1–350 [30]	1–50 [39]	50–90 [40]	0–10 [41]	Not available	30–45 [42]	120–200 [43]
Total capital costs	Very high	High	Low-medium	Medium	Very high	Low-high	Very high	Low	Low
Tolerance to changes in seawater composition	Medium-high	High	Very low	High	Very high	Very high	high	Very low	Very low
Maintenance requirements	Medium	Low	High	High	Higher than RO	High	Very high	low	High but with less frequent cleaning than RO
Scaling potential	Low-medium	Low	High	Medium	Low	Very low	Very low	Less than RO	High but lower than RO
Chemical consumption	High	Medium	High	Medium	—	Low	Low	Low	Medium
Ratio between product to total seawater flow	0.1-0.2 [30]	0.1–0.25 [30]	0.3–0.5 [30]	0.7 [44]	0.85 [45]	0.8-0.9 [41]	0-1 [46]	0.7 [47]	0.3–0.85 [48]
Technical know how	High	High-medium	Medium	Medium	Low	Medium	Medium	Low	Low
Membrane fouling	NA	NA	High	NA	NA	Low	NA	High	Low
GHG emission	Yes	Yes	Negligible	Yes	No emission	Can't say	Can't say	Negligible	Negligible
Fully automatic operation	Possible	Possible	Possible	Possible	No information available	Possible	No information available	Possible	Possible
Limiting factors	Pumps, valves, and vacuum unit [30]	Erection and construction aspects; plant reliability [30]	Pumps [30]	Volumes of vapour to be handled are large, thus demanding high volumetric capacity centrifugal compressors. [44]	Low productivity and thermal efficiency, and large land area required [49]	Microbial contamination [34]	High capital cost and operating cost, and retention of aroma from original water [50]	Membrane fouling, limited lifetime of membranes, and low chemical resistance [51]	Lack of an optimized membrane to produce high water flux, and lack of ideal draw solution [52]

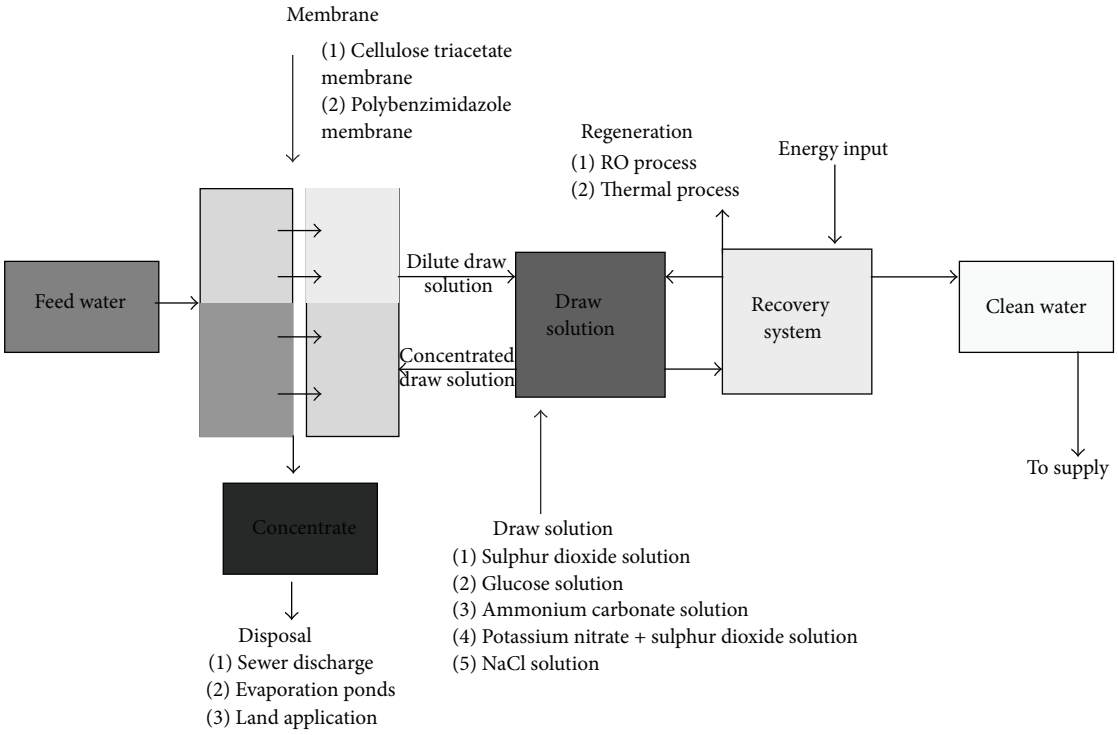

Figure 4: Proposed FO setup viable for use in the Indian market.

in Figures 2 and 3. It is proposed that the concentrate from the process is disposed of using any of the following three techniques independently or in combination of each other: (a) sewer discharge, (b) evaporation ponds, and (c) land application.

7. Cost Analysis

The costs of desalination vary significantly depending on the size and type of the desalination plant, the source and quality of incoming feed water, the plant location, site conditions, qualified labour, energy costs, and plant lifetime. Lower feed water salinity requires less power consumption and dosing of antiscale chemicals. Larger plant capacity reduces the unit cost of water due to economies of scale. Lower energy costs and longer plant period reduce unit product water cost [27].

The primary elements of desalination costs are capital cost and annual running cost. The capital cost includes the purchase cost of major equipment, auxiliary equipment, land, construction, management overheads, and contingency costs. Annual running costs consist of costs for energy, labour, chemicals, consumables, and spare parts [28].

As is evident from Figure 2, approximately 88% of the desalination plants operating in India are based on RO, and the cost analysis of RO and FO has been done. We have used the model developed by CH2M Hill (a global environmental consulting company), which estimates the cost involved in setting up an FO plant and RO plant [29]. The model has been found useful in estimating costs involved up to 15 mgd capacity of recovered water from impaired solution.

The important assumptions on which cost model of both SWRO and FO depends are [29]

(i) number of hours per day the plant operates—24 hours,

(ii) number of days per year the plant operates—329 days,

(iii) membrane replacement frequency—6 years,

(iv) number of membrane replacements in 20 years—3.

Membrane replacement costs, cartridge filter replacement costs, labour, and chemical costs are included in the Annual Operation and Maintenance cost in both SWRO and FO models.

Table 2 shows the estimated costs involved in setting up both FO and RO plants of design capacity 1 mgd.

A plant operating on FO technology can be constructed at 90% of the construction cost and operated at 80% of the operation cost of an SWRO plant, with the current options of FO membranes and draw solution available. Extensive research is being carried out to develop FO membranes offering better flux performance and draw solutions which can be much more easily regenerated. As and when better membranes and draw solutions are available, the construction and operating cost of FO plants is expected to reduce further.

8. Conclusion

Most of the present desalination techniques are currently areas of active research, which is being performed to constantly find ways of improving the technologies and reducing

Table 2: Cost comparison between RO and FO seawater desalination plant.

Seawater reverse osmosis	Forward osmosis
Design capacity = 1 mgd	Design capacity = 1 mgd
Construction cost (in USD) = $-39877 * C^2 + 3E + 06 * C + 7E + 06$, where C is the design capacity in mgd [29]	Construction cost (in USD) = 86.82 (A) + $3E$ + 06, where A is membrane area in sq ft. [29]
$= -38977 * (1) + 3E + 06 + 7E + 06$ = **USD 9.96 million**	FO membrane area required = design capacity/water flux performance Water flux performance = 15 gfd [53]. This value is for a pilot plant developed by Yale University which used ammonia-carbon dioxide as draw solution and cellulose acetate membrane. Thus, FO membrane area required (A) = $10^6/15$ A = 66666.6 sq ft. Thus, construction cost = 86.82 (66666.6) + $3E$ + 06 = **USD 8.78 million**
Annual operation and maintenance cost (in USD) = $697283 * C + 368927$, where C is the design capacity in mgd [29]	Annual operation and maintenance cost (in USD) = $3E - 06 * A^2 + 10.631 * A + 116981$, where A is membrane area in sq ft. [29]
$= 697283 + 368927$ = **USD 1.06 million**	$= 3E - 06 * (66666.6)^2 + 10.631 * 66666.6 + 116981$ = **USD 0.83 million**

the capital cost as well as increasing the efficiency. Early signs show FO to be the most promising technique that can be used efficiently to meet India's water demand. FO requires low capital input and results in lesser membrane fouling, and the product water is of high quality. Low capital cost is going to act as an incentive, resulting in increased expenditure for the adoption of this technique. However, lack of trained personnel will prove to be a hindrance and so there is still time before this technique proves to be a major player in the Indian market.

Conflict of Interests

The authors declare that there is no conflict of interests regarding the publication of this paper.

References

[1] A. S. Moon and M. Lee, "Energy consumption in forward osmosis-desalination compared to other desalination techniques," *World Academy of Science, Engineering and Technology*, vol. 65, pp. 537–539, 2012.

[2] United Nations Department of Economic and Social Affairs, *World Population Prospects : The 2012 Revision, Key findings and Advanced Tables*, United Nations, Department of Economic and Social Affairs, New York, NY, USA, 2013.

[3] M. McKeon-Slattery, "Two approaches to desalination," AIChe, March 2010.

[4] H. Perlman, "Saline water: desalination," 2013, from The USGS Water Science School, http://ga.water.usgs.gov/edu/drinkseawater.html.

[5] S. Shah, "Desalination in India overview—process, methods (reverse osmosis), list of companies and plants," 2013, from Green World Investor, http://www.greenworldinvestor.com/2011/07/05/desalination-in-india-overview-processmethod-sreverse-osmosislist-of-companies-and-plants/.

[6] B. L. Pangarkar, M. G. Sane, and M. Guddad, "Reverse osmosis and membrane distillation for desalination of groundwater: a review," *ISRN Materials Science*, vol. 2011, Article ID 523124, 9 pages, 2011.

[7] K. Venkataraman, "Coastal and marine wetlands in India," in *Proceedings of the Taal2007: the 12th World Lake Conference*, pp. 392–400, 2008.

[8] H. Subramaniam, *Fresh from the Sea*, The Hindu, Chennai, India, 2013.

[9] I. Khurana and R. Sen, "Drinking water quality in rural India: Issues and approaches," WaterAid.

[10] K. Sampathkumar, T. V. Arjunan, and P. Senthilkumar, "Water desalination by solar energy," in *Wastewater Reuse and Management*, S. K. Sharma and R. Sanghi, Eds., pp. 323–351, Springer, Amsterdam, The Netherlands, 2013.

[11] Central Pollution Control Board, *Status of Water Treatment Plants in India*, Central Pollution Control Board.

[12] S. Suryanarayanan, "Water Security: Old Problems, New Solutions," 2011, http://www.strategicforesight.com/inner-articles.php?id=121#.UksOQoZHJjs.

[13] Indo Asian News Service, "Water desalination has big potential in India, says a firm," 2013, http://in.news.yahoo.com/water-desalination-big-potential-india-says-firm-120314740–finance.html.

[14] India Water Review, "India desalination market to grow at 22% CAGR till 2017," 2012, http://www.indiawaterreview.in/Story/News/india-desalination-market-to-grow-at-22-cagr-till-2017/542/1#.UksqnYZHJjs.

[15] B. van der Bruggen and C. Vandecasteele, "Distillation vs. membrane filtration: overview of process evolutions in seawater desalination," *Desalination*, vol. 143, no. 3, pp. 207–218, 2002.

[16] B. A. Centre, *Desalination & Water Purification Technologies*, Bhabha Atomic Research Centre, 2010.

[17] T. S. Subramanian, "Desalination thrust," *Frontline*, vol. 18, no. 25, 2001.

[18] T. Mezher, H. Fath, Z. Abbas, and A. Khaled, "Techno-economic assessment and environmental impacts of desalination technologies," *Desalination*, vol. 266, no. 1–3, pp. 263–273, 2011.

[19] A. Ophir and A. Gendel, "Latest developments in MED and MVC thermal desalination processes," in *Proceedings of the IDA World Congress*, Gran Canaria, Spain, 2007.

[20] M. S. Rahman, M. Ahmed, and X. D. Chen, "Freezing-melting process and desalination: I. review of the state-of-the-art," *Separation and Purification Reviews*, vol. 35, no. 2, pp. 59–96, 2006.

[21] J. Su, S. Zhang, M. M. Ling, and T. S. Chung, "Forward osmosis: an emerging technology for sustainable supply of clean water," *Clean Technologies and Environmental Policy*, vol. 14, no. 4, pp. 507–511, 2012.

[22] T. S. Chung, X. Li, R. C. Ong, Q. Ge, H. Wang, and G. Han, "Emerging forward osmosis (FO) technologies and challenges ahead for clean water and clean energy applications," *Current Opinion in Chemical Engineering*, vol. 1, no. 3, pp. 246–257, 2012.

[23] T.-S. Chung, S. Zhang, K. Y. Wang, J. Su, and M. M. Ling, "Forward osmosis processes: yesterday, today and tomorrow," *Desalination*, vol. 287, pp. 78–81, 2012.

[24] Q. Ge, M. Ling, and T.-S. Chung, "Draw solutions for forward osmosis processes: developments, challenges, and prospects for the future," *Journal of Membrane Science*, vol. 442, pp. 225–237, 2013.

[25] A. Altaee, "Forward osmosis: potential use in desalination and water reuse," *Journal of Membrane and Separation Technology*, vol. 1, no. 2, pp. 79–93, 2012.

[26] Frost & Sullivan, *Assessment of Indian Desalination Market—"Water Without a Pinch of Salt"*, Frost & Sullivan, Chennai, India, 2009.

[27] Y. Zhou and R. S. Tol, "Evaluating the costs of desalination and water transport," *Water Resources Research*, vol. 41, no. 3, pp. 1–10, 2005.

[28] B. Djebedjian, M. S. Mohamed, S. El-Sarraf, and M. A. Rayan, "Evaluation of desalination and water transport costs (case study: Abu Soma bay, Egypt)," in *Proceedings of the 9th International Water Technology Conference (IWTC '05)*, pp. 199–207, Sharm El-Sheikh, Egypt, 2005.

[29] J. D. Gomez, R. P. Huehmer, and T. Cath, *Assessment of Osmotic Mechanisms Pairing Desalination Concentrate and Wastewater Treatment*, Texas Water Development Board, Austin, Tex, USA, 2011.

[30] I. S. Al-Mutaz, "The continued challenge of capacity building in desalination," *Desalination*, vol. 141, no. 2, pp. 145–156, 2001.

[31] J. Koschikowski, *Water Desalination: When and Where will It Make Sense?* Fraunhofer Institute for Solar Energy Systems ISE, Freiburg, Germany, 2011.

[32] Desware, "Energy requirements of desalination processes," May 2013, http://www.desware.net/desa4.aspx.

[33] G. P. Narayan, M. H. Sharqawy, E. K. Summers, J. H. Lienhard, S. M. Zubair, and M. A. Antar, "The potential of solar-driven humidification-dehumidification desalination for small-scale decentralized water production," *Renewable and Sustainable Energy Reviews*, vol. 14, no. 4, pp. 1187–1201, 2010.

[34] F. Valero, A. Barceló, and R. Arbós, "lectrodialysis technology—theory and applications," in *Desalination, Trends and Technologies*, D. M. Schorr, Ed., pp. 1–20, Intech, Vienna, Austria, 2011.

[35] J. B. Michel, O. Sari, P. Egolf, and N. Erbeau, "Desalination using ice slurry manufacturing," in *Sustainable Environmental Solutions for Emerging Countries*, Geneva, Switzerland, 2005.

[36] Nanofiltration, 2010, http://emis.vito.be/node/22626.

[37] G. Danasamy, *Sustainability of seawater desalination technology: assessing forward osmosis as a potential [M.S. thesis]*, Imperial College London, Centre for Environmental Policy, London, UK, 2008.

[38] S. Ariyanto and S. Alimah, *Economic Aspect for Nuclear Desalination Selection in Muria Peninsula*, International Atomic Energy Agency, Vienna, Austria, 2009.

[39] J. A. Cotruvo, *Desalination Guidelines Development for Drinking Water: Background*, World Health Organization, Geneva, Switzerland, 2004.

[40] M. Zamen, M. Amidpour, and S. M. Soufari, "Experimental investigation of a two-stage solar humidification dehumidification desalination process," in *Proceedings of the 25th International Conference on Efficiency, Cost, Optimization, Simulation and Environmental Impact of Energy Systems (ECOS '12)*, Perugia, Italy, 2012.

[41] URS Australia, *Introduction to Desalination Technologies in Australia*, AFFA, 2002.

[42] M. Metaiche and J. Palmeri, *Optimization of Reverse Osmosis (RO) and Nanofiltration (NF) Desalination Systems*, 2009.

[43] Surrey, "The Most Promising Desalination Technology Invented and Developed by Surrey Engineers," 2012, http://www.surrey.ac.uk/cpe/files/The%20Most%20Promising%20Desalination%20Technology%20Developed%20by%20Modern%20water%20and%20Surrey%20Scientists.pdf.

[44] F. Lokiec and A. Ophir, *The Mechanical Vapor Compression: 38 Years of Experience*, IDA World Congress-Maspalomas, Gran Canaria, Spain, 2007.

[45] G. P. Narayan, R. K. McGovern, G. P. Thiel, J. A. Miller, and V. J. H. Lienhard, *Status of Humidification Dehumidification Desalination Technology*, World Congress/Perth Convention and Exhibition Centre, Perth, Australia, 2011.

[46] Y. Cerci, Y. Cengel, B. Wood, N. Kahraman, and E. S. Karakas, "Improving the thermodynamic and economic efficiencies of desalination plants: minimum work required for desalination and case studies of four working plants," Desalination and Water Purification Research and Development Program Final Report 78, University of Nevada, Reno, Nev, USA, 2003.

[47] A. M. Hassan, M. A. K. Al-Sofi, A. S. Al-Amoudi et al., "A new approach to membrane and thermal seawater desalination processes using nanofiltration membranes (Part 1)," *Desalination*, vol. 118, no. 1–3, pp. 35–51, 1998.

[48] ModernWater, "Forward osmosis applied to desalination and evaporative cooling make-up water," in *Proceedings of the 3rd Osmosis Summit*, April 2012.

[49] J. Lindblom, *Solar Thermal Technologies for Seawater Desalination: State of the Art*, Luleå University of Technology, Luleå, Sweden, 2003.

[50] M. S. Rahman, M. Ahmed, and X. D. Chen, "Freezing-melting process and desalination: review of present status and future prospects," *International Journal of Nuclear Desalination*, vol. 2, no. 3, pp. 253–264, 2007.

[51] A. W. Mohammad, "Nanofiltration membranes in desalination—from fundamental to applications," in *Proceedings of the 3rd International Conference on Water Resources and Arid Environments and and the 1st Arab Water Forum*, 2008.

[52] S. Chaudhry, "An overview of industrial desalination technologies," in *Proceedings of the ASME Industrial Demineralization*

(Desalination): Best Practices & Future Directions Workshop, Washington, DC, USA, January 2013.

[53] J. L. McCutcheon, R. L. McGinnis, and M. Elimelech, *The Ammonia-Carbon Dioxide Forward Osmosis Desalination Process*, Water Conditioning & Purification, 2006.

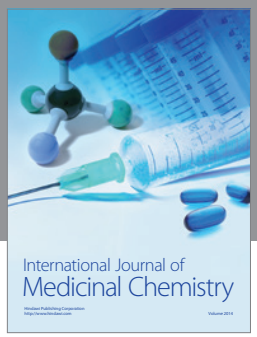

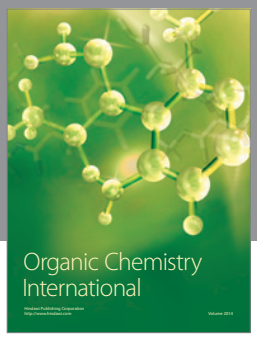

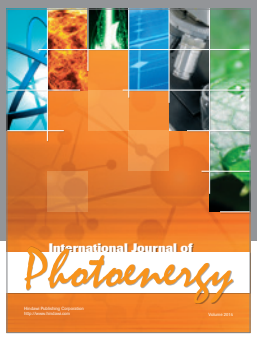

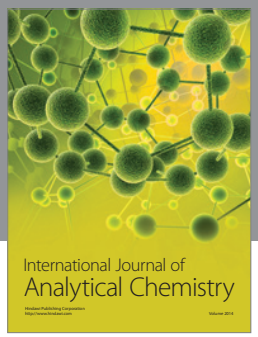

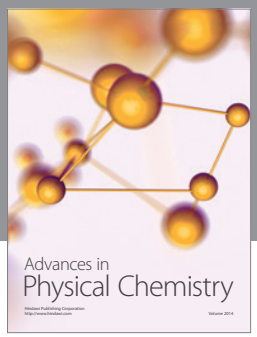

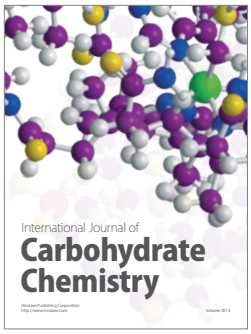

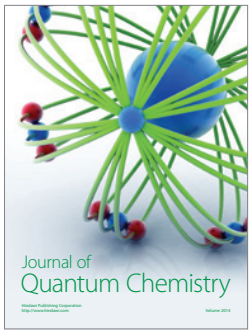

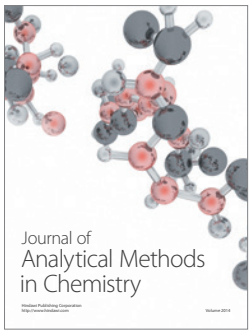

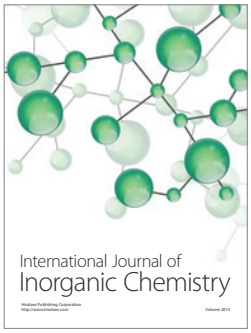

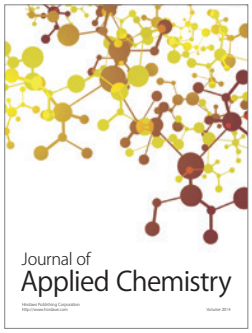

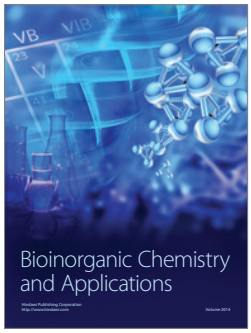

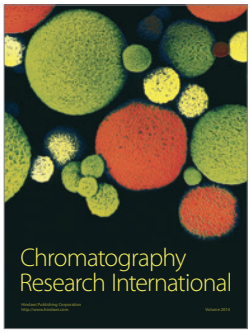

Hindawi

Submit your manuscripts at
http://www.hindawi.com

INVESTIGATIONS ON EFFECT OF INCORPORATION OF PHOTOVOLTAIC SYSTEM WITH COMBINED CYCLE GAS TURBINEPLANT

Naimul Hasan[1] , B.B .Arora[2], J.N. Rai[3]

[1]Department of Electrical Engineering, Jamia Millia Islamia .New Delhi

[2]Department of Mechanical Engineering, Delhi Technological University,Delhi, India

[3] Research Scholar, Dept. Of Elec. Engg, Jamia Miliia Islamia, N.Delhi

ABSTRACT

India is witnessing a huge demand in power requirement. Economic development has led to development in Industries and demand for housing has increased. To meet this ever-rising power demand, efforts have been made to increase the efficiency at the generating end. One of such efforts is the CCGT plant in which the exhaust of Gas Turbine is used to run the Steam Turbine; hence giving an overall efficiency upto 60%. But, the recent trends in electrical engineering has been shifted to renewable forms of energy via solar, wind et,.keeping in mind the emphasis is on importance ofsustainable development. This paper is a preliminary study of how solar energy can be used through photovoltaic panels for the excitation of GT and auxiliary purposes in CCGT plant. The results of the same have been plotted and the future developments of this research have been discussed in detail.

Keywords: Solar, PV, CCGT, Power, Photovoltaic

I INTRODUCTION

In power systems, various methods are employed to overcome the ever-rising electricity demand. In India, most Power Plants are driven by fossil fuels. A Combined Cycle Gas Turbine Plant(Fig. 1)is one themeans so as to make the efficiency of a plant to reach the 60% mark.[1][4].

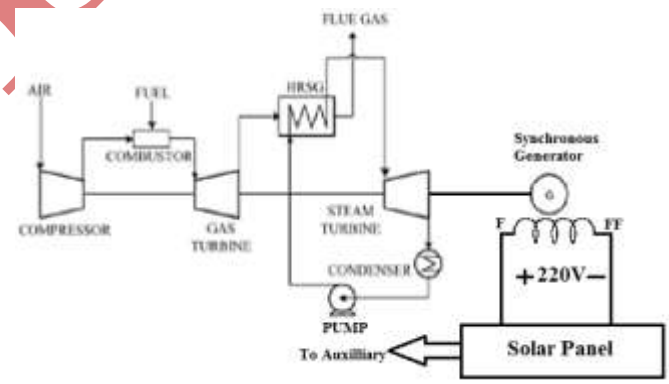

Fig 1. Combined Cycle Gas Turbine with Solar Panel

In a CCGT plant, the input temperature to a steam turbine is about 540°C and the exhaust can be maintained at the atmospheric pressure, due to design consideration the input temperature is limited and the efficiency of the about 45%. Theinput temperature of the gas turbine can be as high as 1100°C but the exhaust temperature can be lowered to about 550-650°C, the efficiency of a gas turbine is about 35%. It can be seen that to obtain higher efficiencies the exhaust of the gas turbine can used to drive the steam turbine giving efficiency up to 62%.The plant consists of a compressor, combustor, gas turbine, waste heat recovery boiler, steam turbine, and generator(s) associated with solar voltaic. [7][8]

Similarly, the emerging form of energy (Renewable Energy) is a socially and politically defined category of energy sources. Solar energy being one of them.Hence, we can employ solar panelswith the CCGT plant to make it less dependent on fossil fuels. The tariff for the consumers would also go down, since solar energy is at its peak in summer season, the time the electricity utilization is maximum in a year.

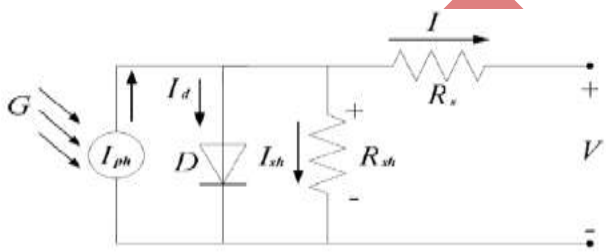

Fig 2. Equivalent Circuit of a PV cell

A simplest equivalent circuit(Fig. 2) of a solar cell is a current source in parallel with a diode. The output of the current source is directly proportional to the solar energy (photons) that hits on the solar cell (photocurrent I_{ph}). During darkness, the solar cell is not an active device; it works as a diode, i.e. a p-n junction. It produces neither a current nor a voltage. However, if it is allowed to connect to an external source (large voltage) it generates a current *Id*, called diode (D) current or dark current. [15]

Hence the combination of solar energy with CCGT plant could make a possible difference.

II THEORETICAL BACKGROUND

Equations which define the model of a CCGT Plant:The airflow (W) in the gas turbine is given as

$$W = W_a \frac{P_a}{P_{ao}} \frac{T_{io}}{T_i} \qquad (1)$$

Where Ti is ambient temperature and P_a denotes the atmospheric pressure.

$$\eta_{cc} = \eta_{gt} + \eta_{st}(1 - \eta_{gt}) \qquad (2)$$

The Where η_{cc} is the efficiency of the combined cycle, η_{gt} is the efficiency of Gas Turbine and η_{st} is the efficiency of Steam Turbine.thermal efficiency of the simple gas turbine cycle is given as [6]

$$\eta = \frac{(1 - \frac{1}{p_p})(a - p_p)}{\eta_c(k_1 - 1) - p_p + 1} \qquad (3)$$

Where, $a = \eta_c \eta_t k_1$ [10][11][12]Equations which define the model of a PV cell:

$$V_t = \frac{kT_{op}}{q} \quad (4)$$

$$V_{oc} = V_t \ln\left(\frac{I_{ph}}{I_S}\right) \quad (5)$$

$$I_d = \left[e^{\frac{(V+IR_s)}{(nV_tCN_s)}} - 1\right] I_s N_p \quad (6)$$

$$I_S = I_{rs}\left(\frac{T_{op}}{T_{ref}}\right)^3 e^{\left[\frac{qE_g}{nk}\left(\frac{1}{T_{op}} - \frac{1}{T_{ref}}\right)\right]} \quad (7)$$

$$I_{rs} = \frac{I_{sc}}{\left[e^{\left(\frac{V_{oc}q}{kCT_{op}n}\right)} - 1\right]} \quad (8)$$

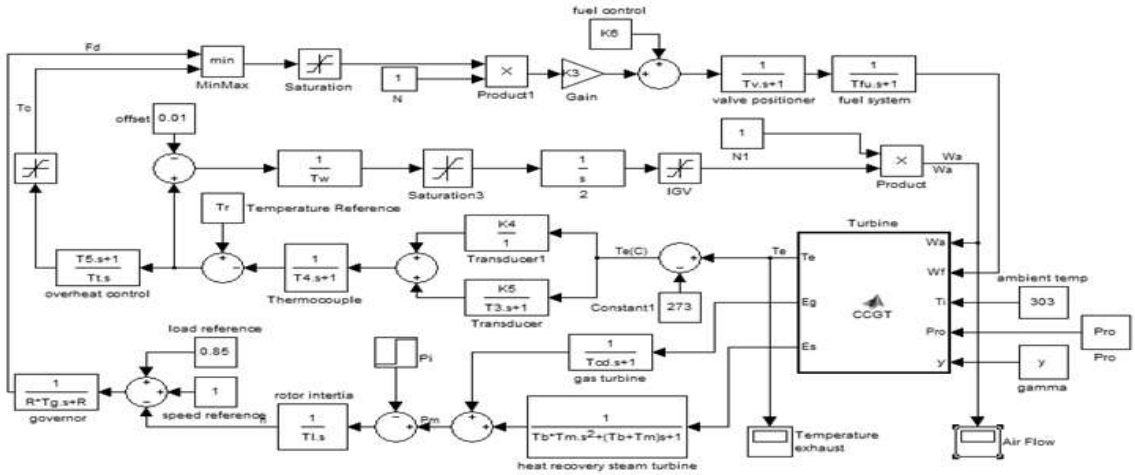

Fig 3. CCGT Simulink Model

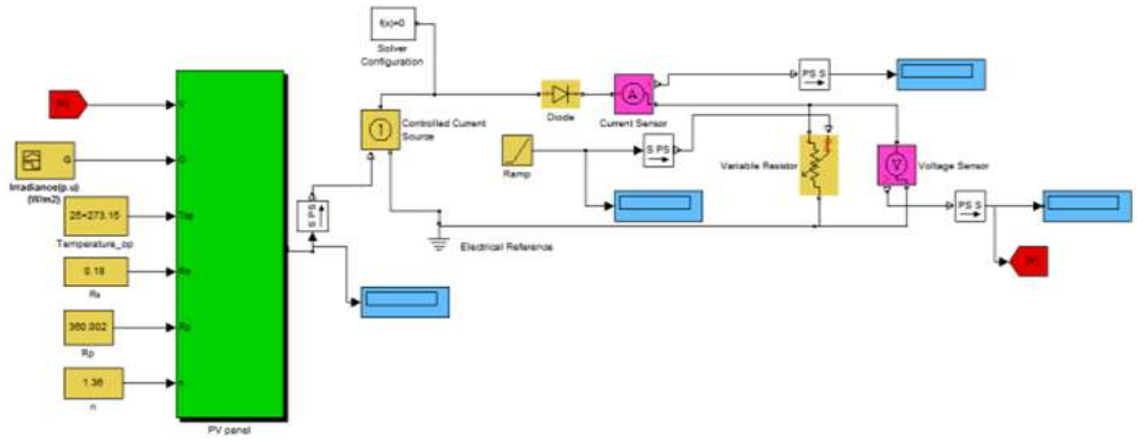

Fig 4. Simulink Model of Photovoltaic Panel

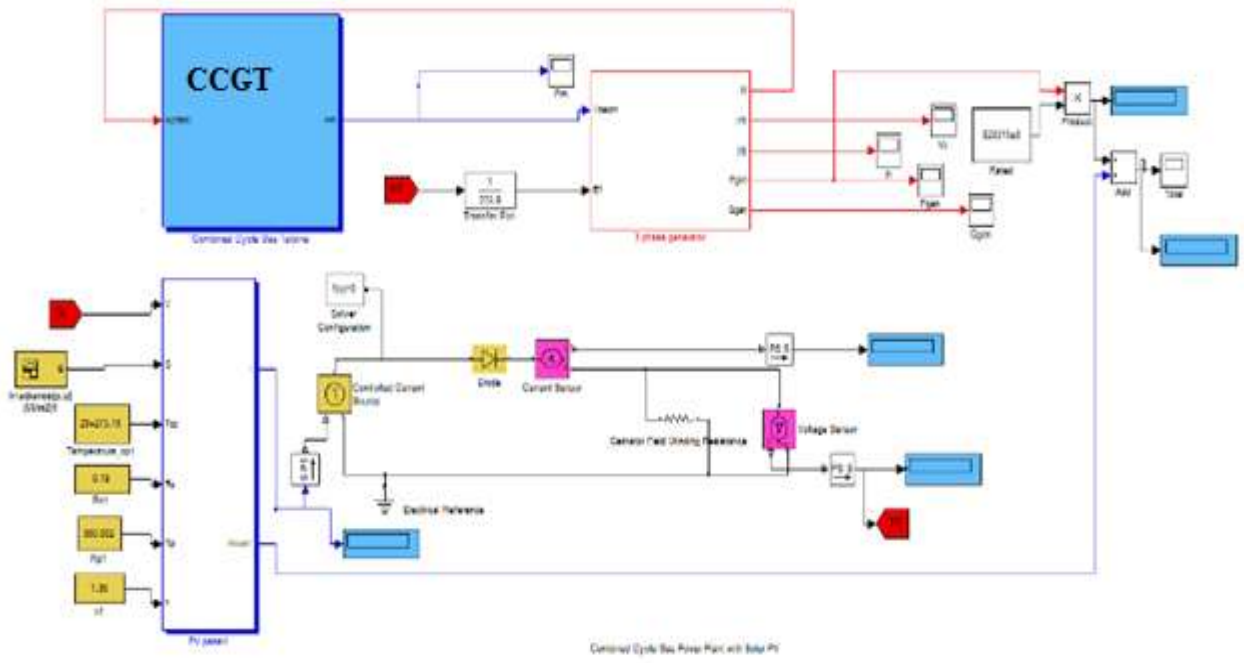

Fig 5. Simulink Model of Integrated Photovoltaic in CCGT

$$I_{sh} = \frac{V + IR_s}{R_p} \quad (9)$$

$$I_{ph} = G_k \left[I_{sc} + K_I (T_{op} - T_{ref}) \right] \quad (10)$$

$$I = I_{ph} N_p - I_d - I_{sh} \quad (11)$$

where, G_k is solar insolation in W/m^2,

T_{ref} is reference temperature(298 K),

T_{op} is operating temperature of cell,

R_s is series resistance,

R_{sh} is shunt resistance,

k is Boltzmann constant,K is temperature coefficient,

N is data points used,

n is diode emission factor,

I_{ph} is photon current & I_d is dark current,

I_{sh} is short circuit current at reference state.

III DESCRIPTION OF SIMULINK MODEL AND RESULTS

The CCGT model (J. N. Rai. et.al. 2013)consists of various blocksdescribing various parameters whose variations have already been studied in order to optimize the performance of combined cycle. There are blocks related with speed/load, temperature control, fuel control, air control and other blocks for gas turbine, waste heat

recovery boiler/steam turbine, rotor shaft, and temperature transducer. All the parameters used in the model are given in Table I& II. [2] [3][5]

A circuit based simulation model for a PV cell for estimating the IV characteristic (temperature and irradiance) and cell parameters (parasitic resistance and idealty factor)has been discussed. The simulation model is used for analysing the behaviour of PV Panel by varying various parameters of the cell in accordance with the given equations. Using a Shockley diode equationan accurate *simulink* PV panel model was developed.The model is based on the equivalent diagram of the solar panel described in the theoretical background. [12] [13] [14]

Further with above Simulink model the response of CCGT. has been investigated which shows the variation of current with respect to the timeFigure 6.

Figure. 7 shows the Variation of Generated Electrical Power. It depicts the variation is almost constant. The output is stable. It can also be seen that the generator output falls which is also controllable with reactive power control as shown in Figure.8.

Further the effect of varying input condition of CCGT as Variation of CCGT parameter i.e Exhaust Temperature of Gas Turbine (^{o}C), Air Flow (p.u.) and Fuel Flow (p.u) (Figure. 9) has been investigated.

Turbine Output (input of generator) is constant for a while (Figure 10). As the system is uncontrollable, the output falls which can be brought to the near to its rated value by controlling the CCGT parameters. The Field Excitation for synchronous generator is accompanied with solar voltaic which shows the positive impact on the performance. It can also be seen that now the start-up time is higher than the normal plant model (J. N. Rai et.al. 2013) with increased power output.

IV CONCLUSION

The parameters considered above cannot be varied simultaneously due to complexity of system. Some parameters are located and the other parameters will be the function of critical parameters in one way or the other. Interrelations amongst the various parameters are balanced by superimposing some constraints on the parameters.The level of benefits achieved as a result of system optimization has included the following:

- Increased output-3 to 5%
- Reduced fuel consumption-3 to 5%
- Reduced power consumption-3 to 5%

Both, the CCGT and PV panel models are combined. PV panel is used to give the excitation to the CCGT Plant Generator and also the remaining energy developed can be used for driving the auxiliaries in the Plant. Since the solar output is DC itself, the conversion losses from AC to DC as was the earlier case in CCGT plant have been taken care of. Start-up Time would be high as compared to Normal Combined Cycle Gas Power Plant.

This paper provides a path for further research work in future by integrating solar plant to increase the clean energy generation and to enhance the existing plant capacity in India.

IJEE

Table 1 : System Parameters

Symbol	Description	Value
T_i	Compressor inlet temperature	$30\,^{\circ}C$
T_{do}	Compressor discharge temperature	$390\,^{\circ}C$
T_{fo}	Gas turbine inlet temperature	$1085\,^{\circ}C$
T_{eo}	Gas turbine exhaust temperature	$535\,^{\circ}C$
P_{ro}	Compressor pressure ratio	11.5
γ	Ratio of specific heat	1.4
η_c	Compressor efficiency	0.85
η_t	Turbine efficiency	0.85
R	Speed Regulation	0.04
T_t	Temperature control integration rate	0.469
$T_{c\max}$	Temperature control upper limit	1.1
$T_{c\min}$	Temperature control lower limit	0
$F_{d\max}$	Fuel control upper limit	1.5
$F_{d\min}$	Fuel control lower limit	0
T_v	Valve positioner time constant	0.05
T_{fu}	Fuel system time constant	0.4
T_w	Air control time constant	0.4669
T_{cd}	Compressor volume time constant	0.2
K_0	Gas turbine output coefficient	0.0033
K_1	Steam turbine output coefficient	0.00043
T_g	Governor time constant	0.05
K_4	Gain of radiation shield	0.8
K_5	Gain of radiation shield	0.2
T_3	Radiation shield time constant	15
T_4	Thermocouple time constant	2.5
T_5	Temperature control time constant	3.3
K_3	Ratio of fuel adjustment	0.77
K_6	Fuel valve lower limit	0.23
T_m	Tube metal heat capacitance time constant of waste heat recovery boiler	5
T_b	Boiler storage time constant of waste heat recovery boiler	20
T_i	Turbine rotor time constant	18.5

IJEEE

Table II. Parameters of Three-Phase Synchronous Machine

Symbol	Description	Value
Fr	Rated Frequency	50
Poles	Number of poles of the generator	4
Pf	Rated Power Factor	0.9
V_R	Rated Voltage	11Kv
Pr	Rated output Power in Watt	82.831Mw
Rs	Synchronous Resistance	0.0048
X_d	Direct-Axis Reactance	1.790
Xq	Quadrature-Axis Reactance	1.660
X_{ls}	Leakage Reactance	0.215
H	Interia Constant	3.77
K_A	Gain Constant	50
T_A	Amplifier Time Constant	.06
V_{Rmax}	Maximum Voltage	1
V_{Rmin}	Minimum Voltage	-1
T_E	Exciter Time Constant	0.052
K_E	Exciter Gain	-0.0465
T_F	Field Time Constant	1.0
K_F	Field Gain	0.0832

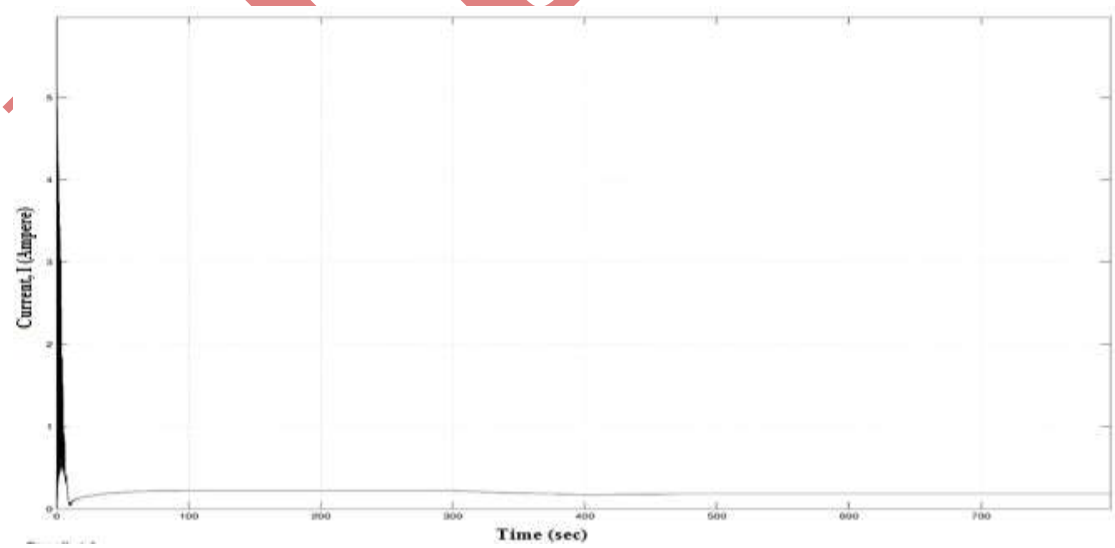

Fig 6. Variation of Current with Time

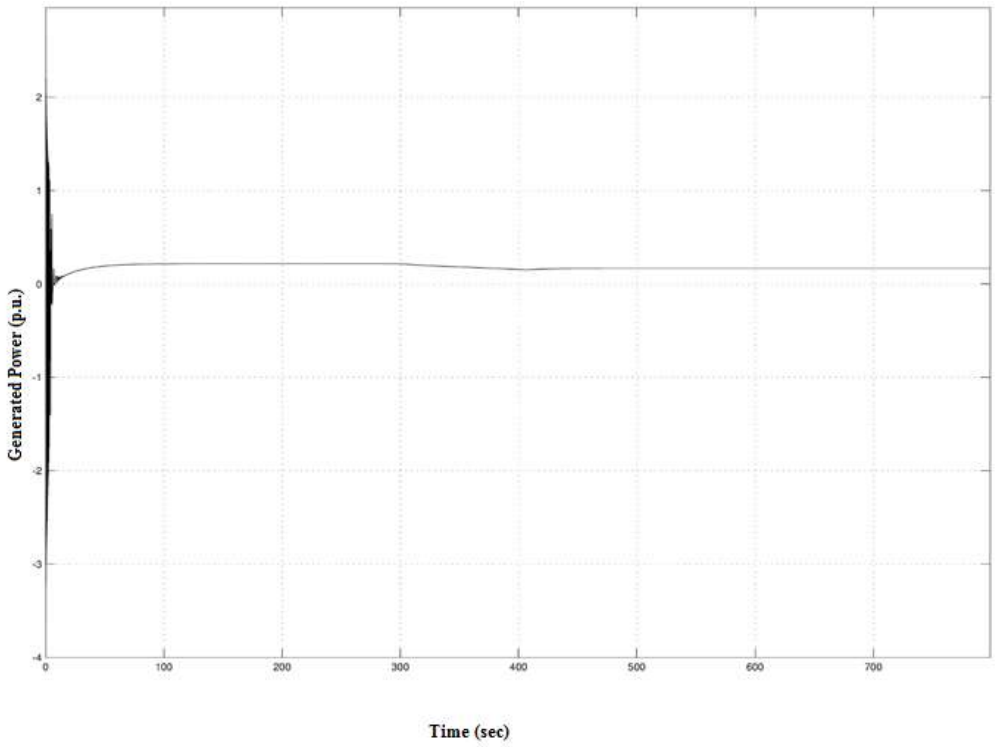

Fig 7. Variation of Generated Power with Time

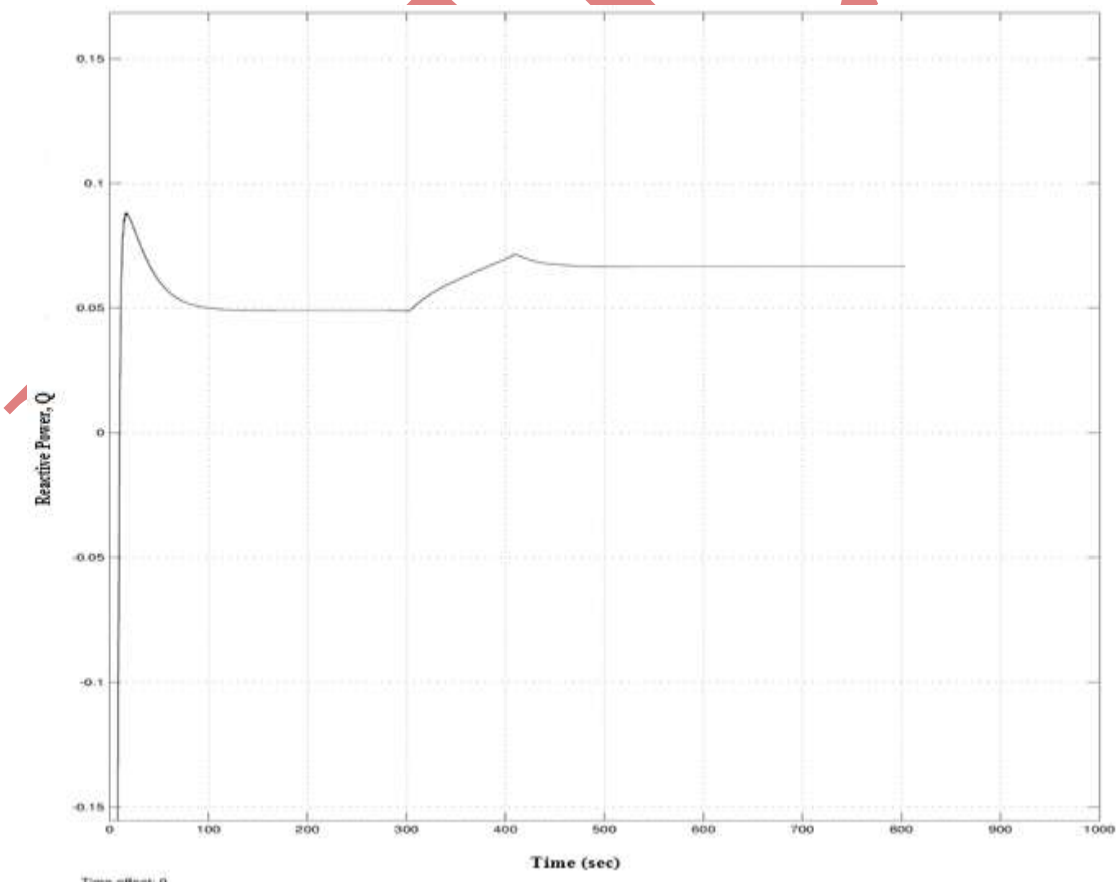

Fig 8. Variation of Reactive Power with Time

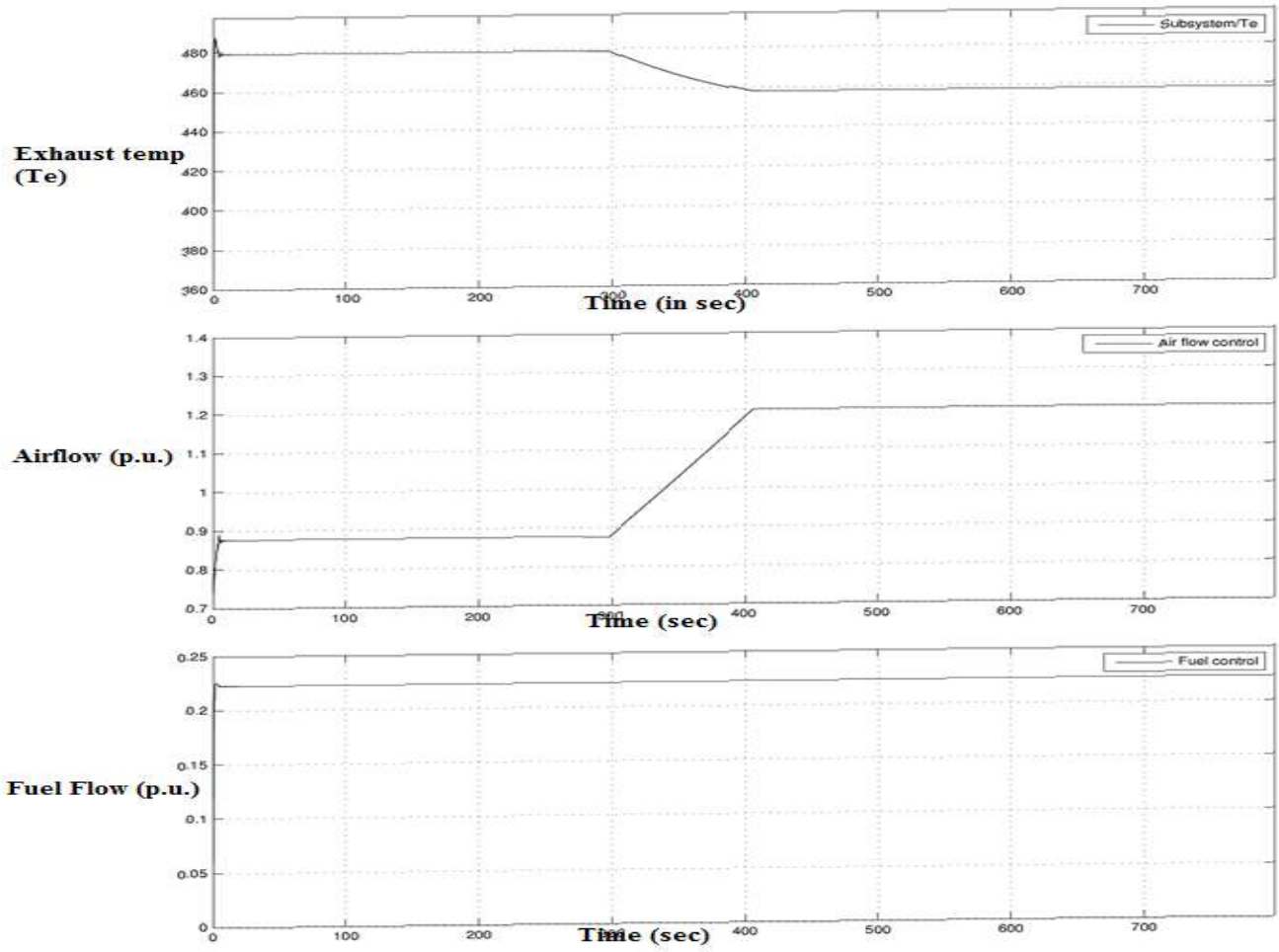

Fig 9. Variation of various System parameters with time

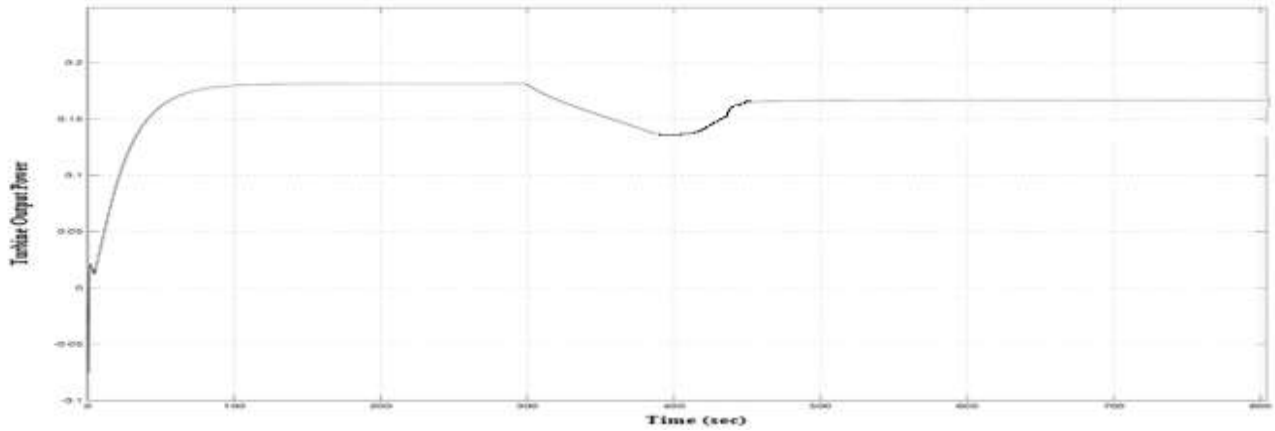

Fig 10. Variation of Turbine Output Power with Time

REFERENCES

[1]N. Kakimoto, K. Baba, , "Performance of gas turbine-based plants during frequency drops," IEEE Transactions on Power Systems,vol.18, pp. 1110- 1115, Aug. 2003.

[2]S. Al-Zubaidy, F.S. Bhinder, "Towards optimizing the efficiency of electrical power generation," Energy Conversion Engineering Conference, vol.3, pp. 1857-1862, Aug. 1996.

[3]K. Kunitomi, A. Kurita, H. Okamoto, Y. Tada, S. Ihara, P. Pourbeik, W. W. Price, A. B. Leirbukt, and J. J. Sanchez-Gasca, "Modeling frequency dependency of gas turbine output," Proc. IEEE/Power Eng. Soc. Winter Meeting, Jan. 2001.

[4]W. I. Rowen, "Simplified mathematical representations of heavy-duty gas turbines," Trans. Amer. Soc. Mech. Eng., vol. 105, pp. 865–869, Oct. 1983.

[5]F. P. de Mello and D. J. Ahner, "Dynamic models for combined cycle plants in power system studies," IEEE Trans. Power Syst., vol. 9, pp. 1698–1708, Aug. 1994.

[6]John H Horlock, "Advanced gas turbine cycles," Pergamon Press, 2003.

[7]Rolf Kehlhofer, Rukes Bert, Hannemann Frank, and Stirnimann Franz. "Combined-cycle gas & steam turbine power plants," PennWell, 2009.

[8]F. Drbal Lawrence, G. Boston Patricia, L. Westra Kayla, Black& Veatch. Power Plant Engineering. p. 241 Springer. 1996.

[9]Rai, J. N., Hasan, N., Arora, B. B., Garai, R., Gupta, R. K., & Kapoor, R. (2013). "Study the Effect of Temperature Control on the Performance of the Output of Combined Cycle Gas Turbine". International Journal of Theoretical and Applied Mechanics, 8(1), 15-23.

[10]J. N. Rai, NaimulHasan, B. B. Arora, Rajesh Garai, Rahul Kapoor, Ibraheem(2013) "Performance Analysis of CCGT Power Plant using MATLAB/Simulink Based Simulation" International Journal of Advancements in Research & Technology, Vol. 2(5), pp. 285-290

[11]Mantzaris, J., &Vournas, C. (2007). Modelling and Stability of a Single-Shaft Combined Cycle Power Plant. International Journal of Thermodynamics, 10(2).

[12]Patel, H., & Agarwal, V. (2008). MATLAB-based modeling to study the effects of partial shading on PV array characteristics. Energy Conversion, IEEE Transactions on, 23(1), 302-310.

[13]González-Longatt, F. M. (2005). Model of photovoltaic module in Matlab. II CIBELEC, 2005, 1-5.

[14]Tsai, H. L., Tu, C. S., & Su, Y. J. (2008, October). Development of generalized photovoltaic model using MATLAB/SIMULINK. In Proceedings of the world congress on Engineering and computer science (Vol. 2008, pp. 1-6).

[15]Rahim, N. A., Saidur, R., Solangi, K. H., Othman, M., & Amin, N. (2012). Survey of grid-connected photovoltaic inverters and related systems. Clean Technologies and Environmental Policy, 14(4), 521-533.

IJEEE

IJCAES
ISSN: 2231-4946
Volume IV, Special Issue, September 2014

International Journal of Computer Applications in Engineering Sciences
Special Issue on First International Conference on Microelectronics,Circuits and Systems-Micro'2014
www.caesjournals.org

Luminous TCAD Analysis of Transparent ITO Gate Recessed Channel MOSFET using Elliptical Lenslet

Anuj Kumar Sinha*[1], Rishu Chaujar*[2]

[*]*Microelectronics Research Lab, Department of Engineering Physics,*
Delhi Technological University, Bawana Road, Delhi-110042

[1]anujsinhadce@gmail.com, [2]rishu.phy@dce.edu

***Abstract*—In this paper, we report the effect of luminous behaviour of transparent gate Recessed Channel MOSFET (RC-MOSFET).Aggressive scaling is associated with a number of higher order effects such as short channel effects, hot carrier effects and heating effect which significantly affect the device performance. The Ray trace method in MOSFET has emerged to be the ultimate solution. The proposed device has an elliptical lenslet above the RC MOSFET to focus the raytrace in to the transparent indium tin oxide (ITO) gate. The effect of illumination with the improved photogeneration rate, optical intensity, switching ratio and light absorption is studied. The work proves the effectiveness of transparent gate RC-MOSFET for higher efficiency, speed, ON current, reduction in power dissipation and better temperature stability. Luminous-3D RC-MOSFET is fully integrated with ATLAS and Device 3D.**

***Keywords* — DEVEDIT -3D, Illumination, ITO, Photogeneration, Ray Trace, RC-MOSFET.**

I. INTRODUCTION

In order to achieve high speed, low power dissipation and low noise, the device feature size is reduced. Short channel effect (SCE) degrades the controllability of drain current, which leads to degradation of the subthreshold slope and increase in subthreshold current [1]. As the device length is reduced to increase the speed of operation and the number of components per chip, the so-called short channel effect arises [3]. Recessed channel MOSFET is a promising device for suppressing SCEs, punch through and hot carrier effects. This is due to shallow junctions or even negative junctions in RC MOSFET which can be fabricated without any increase in the series resistance [1-3]. Thinning gate oxide and using shallow source/drain junctions are known to be effective ways of preventing SCEs.
In this paper luminous analysis is performed for Recessed channel MOSFET and conventional MOSFET for DC and AC under small signal condition of the incident frequency range of 600nm to 900nm [6]. Use of transparent ITO as a gate material has the advantage of minimal reflection of the gate surface so that most of the raytrace by an elliptical lens incident at the gate reach the channel region. The transparent ITO RC MOSFET shows the possibility to operate at relatively low temperature of 100 ^{0}C, due to the characteristics of downsizing and cost reduction in fabrication of integrated circuits [4]. Tin-doped ITO semimetal gate electrodes of the RC MOSFET is a solid solution of indium oxide (In_2O_3) and Tin oxide (SnO_2) material of 91:9 weight percent with a purity of 99.99% [5]. The advantage of ITO is that it possesses very high electrical conductivity and optical transparency in the visible region. The purpose of using ITO in Recessed channel MOSFET is to obtain stable film for large-area coatings with exceptionally low resistivity, improve switching ratio, which causes the decrease in device power consumption and high transmittance within the visible spectrum range [7].

While nanoscale MOSFET can do many things, but one thing it cannot do very well is to generate power at high frequencies. This is because as transistors become smaller, they tend to breakdown very easily with even a small amount of voltage or current. Up to now, all the research work has been focused on improving the photoresponse by implementing methods of enhancing the photocurrent such as use of transparent gate electrode [8] and channel material engineering [4]. Luminous3D analysis calculates the optical intensity and the photogeneration rate within the semiconductor device. It consistently solves drift diffusion or energy balance equations with photogeneration from an optical source for steady state, time domain and small signal analysis [9]. The light absorption and photogeneration effects of the reflection coefficients and the integrated loss due to absorption over the ray path are saved for each ray [15].

In luminous analysis, lenslets are not meshed for drift diffusion type analysis and is only used for raytracing. In elliptical lens, we specify the semi major axis, center and index. The light rays when pass through the lens converge on a single point. The single point to which the light rays are converging is called the focal point. The lens is used to specify lenslet characteristics used for light propagation analysis [15].

A. Device Structure: Parameters And Simulation Approach

Analysis of Recessed channel MOSFET using Transparent ITO gate has been performed using the ATLAS and DEVEDIT 3D device simulator. Silvaco ATLAS advanced luminous 3D optical device simulator has been used to extract the device characteristics under illumination [16]. Fig 01(a) and Fig 01(b) shows the simulated device structure of the RC MOSFET and conventional MOSFET under illumination. The RC MOSFET uses a p-type substrate of concentration of 1×10^{16} cm^{-3}, source and drain regions have peak concentration of 1×10^{19} cm^{-3}. The channel threshold voltage of the fabricated structure extracted is 0.28V. All simulations were carried out at 300K and bias voltage V_{gs}=0.8V and V_{ds}=0.5V. We use a light source which ranges between 600nm to 900nm wavelength. The models used in the simulations of the RC MOSFET are Shockley–Read–Hall (SRH), Fermi Statistics (FERMI), AUGER, FLDMOB and Lombaerdi mobility model (CVT) for transverse field dependence. The CVT model sets general aim mobility ideal to include concentration, temperature, parallel field and transverse field effects [4]. The SRH model accounts for recombination/generation effects and uses fixed minority carrier lifetimes. Ray trace method has been used in simulator to solve photogeneration rate at each grid point. For the study of I-V characteristics, gate currents, transconductances (g_m) the impact ionization and hot-electron-injection models are used to provide an exact measure of hot-carrier-injection in short-channel devices [17].

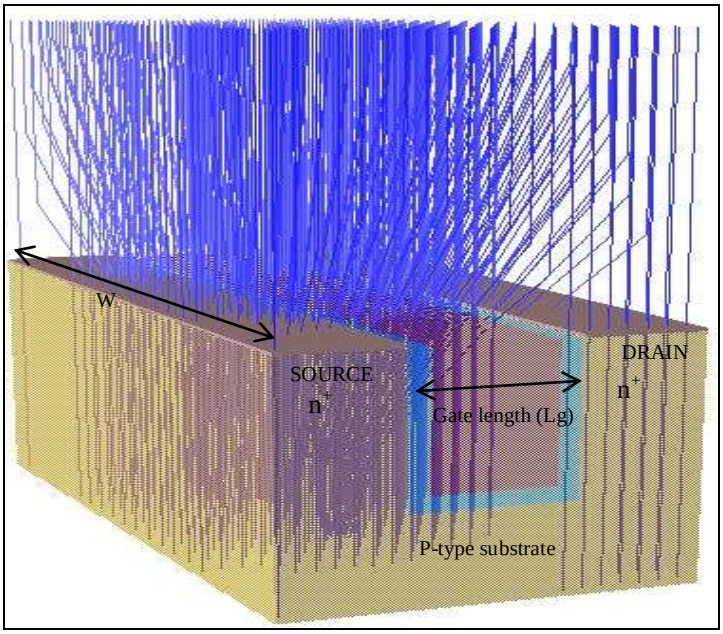

Fig. 01(a): Simulated Device structure of RC- MOSFET.

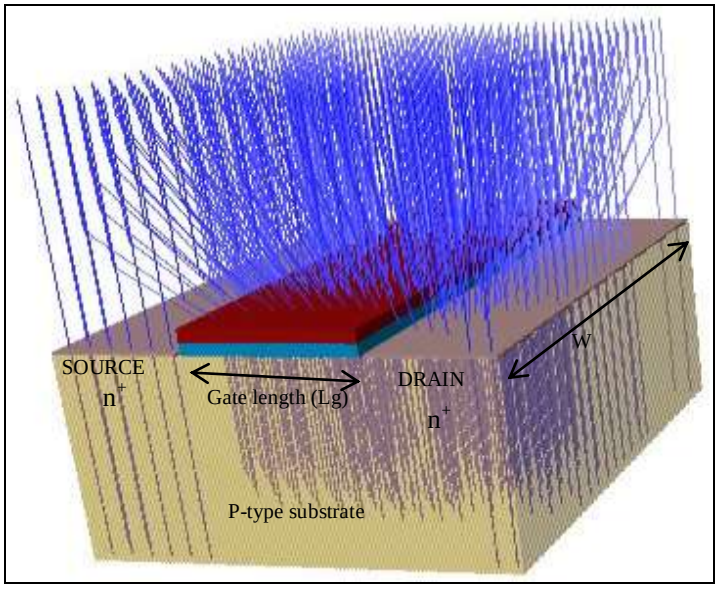

Fig. 01(b): Simulated Device structure Conventional MOSFET.

When light falls on elliptical lens, then the rays converge on a single point i.e. focal point on the surface of a transparent ITO gate and the photon whose energy is greater than that of the band-gap energy of the ITO material, are absorbed. This absorption excites an electron to leap into the valence band to the conduction band and as a result, a hole is left in the valence band. These electrons and holes behave as free particles and travel below intrinsic or extrinsic applied electric field [8]. There is continuous separation of electron–hole pairs due to the absorption of photons. The intensity of the incident light is directly proportional to the photocurrent. The aluminium electrodes in source and the drain side block the incident light. The real and imaginary values of refractive index for calculation of reflection coefficient at the transparent ITO Gate are taken from SOPRA database [19].

TABLE I: Design Parameters for Conventional MOSFET & RC-MOSFET device designs

Channel Length (L_G)	30nm
Device Width (W)	200nm
Groove Depth (d)	40nm
Source/Drain Junction Depth	30nm
Negative Junction Depth (NJD)	20nm
Substrate Doping (N_A)	1×10^{16} cm^{-3}
Source/Drain Doping (N_D^+)	1×10^{19} cm^{-3}
Physical Oxide Thickness (t_{ox})	5.0nm
Permittivity of SiO_2	Ɛox= 3.9
Wavelength	600nm to 900nm
Gate to Source voltage (V_{GS})	0.8V
Drain to Source voltage(V_{DS})	0.55V
Work function(Φ) Conventional MOSFET	4.7eV
Work function(Φ) RC MOSFET	4.7eV
Dimension	100×80nm

1) Results And Discussion

In this paper, we compare transparent gate RC MOSFET and conventional MOSFET and demonstrated that the proposed device design possesses superior switching ratio in comparison to other devices. The present analysis is carried out for a channel length, L_g=30nm, wavelength=600nm angle=90^0,Theta=90^0,and thickness of oxide, t_{ox}= 5.0nm, work function Φ_{ITO}=4.7eV.

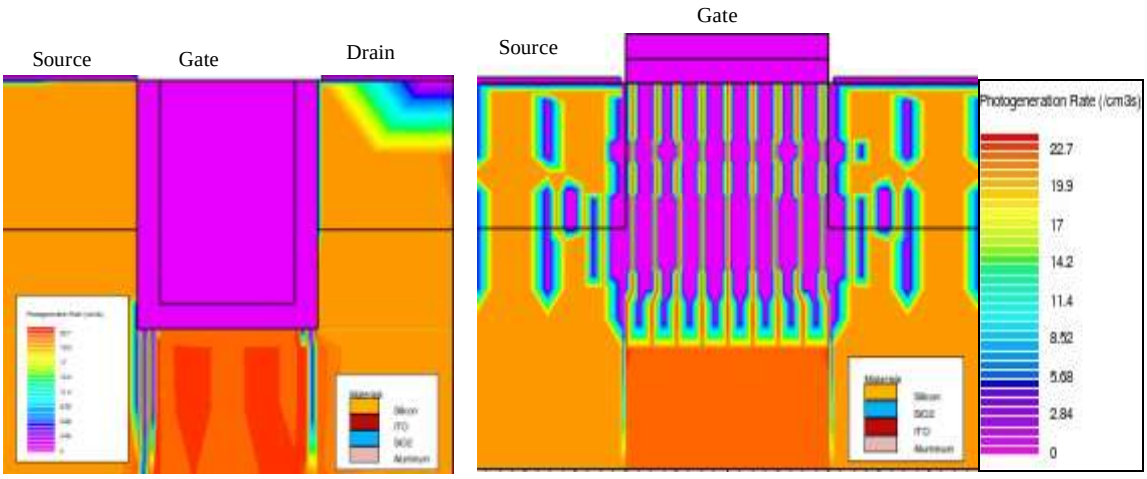

Fig. 02: Contour plot showing photogenerated carriers within the channel region of the incident radiation in RC and conventional MOSFET.

Fig.02: shows a contour plot of photogeneration rate along the channel length of RC and conventional MOSFET. Photogeneration or the photocurrent is the most important factor in luminous analysis. It is the process where mobile electron and holes are created due to absorption of electromagnetic radiation in the channel region. The photon has an enormous energy than the bandgap i.e hv > Eg [12]. Photogeneration rate is maximum in the channel region (Red colour) in RC-MOSFET as comparsion to conventional MOSFET. This is mainly due to ITO gate and moreover, the gate oxide is taken to be thin so that most of the incident radiation generates EHPs due to the absorption of incident photons in the channel region of RC-MOSFET [13].

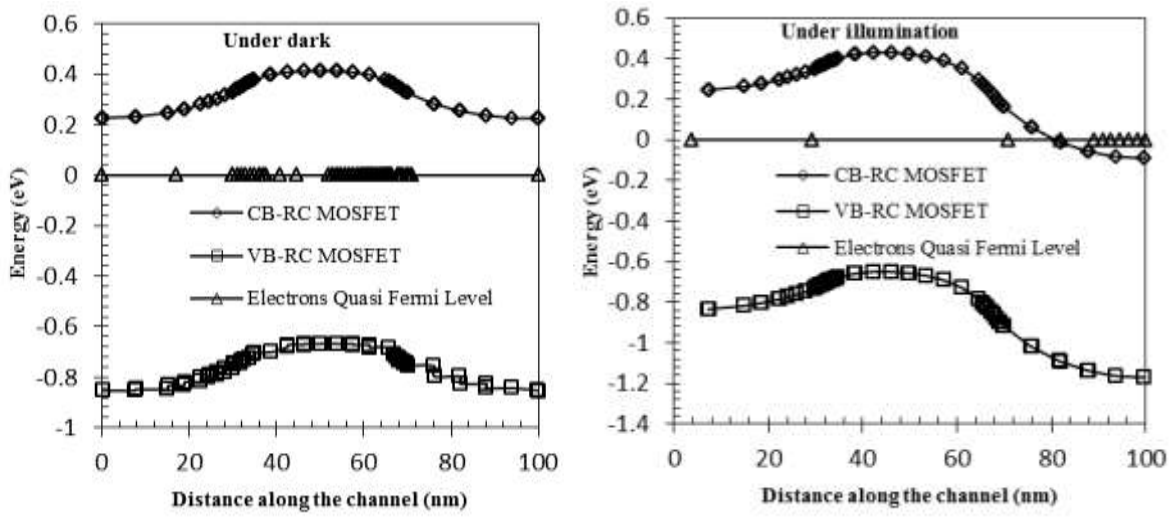

Fig. 03: Conduction band energy and Valence band energy variation along the channel at Electron Quasi Fermi Level at zero bias Under dark and under illumination for RC-MOSFET.

Fig. :03 shows the variation of conduction band and valence band with electron quasi Fermi level along the channel length of RC MOSFET examined under dark and illuminated conditions & it is mainly due to electron quasi Fermi level which lies within the valence band and conduction band at source and drain region. It helps to analyze the motion of the carriers i.e. carriers always flow from the source to drain. In normal operation of n-channel MOSFET, free electrons move from source to drain, but the current direction is from drain to source. Since the hole current is negligible everywhere, it is assumed that the electron quasi Fermi energy (level) is constant where hole concentration is significant. Under illumination, the free carriers are increased so that thermalisation happens so fast that the carriers relax to the conduction band edge long before they reach the contacts [11]. Hence, it is the thermalised carriers that determine the quasi-Fermi levels.

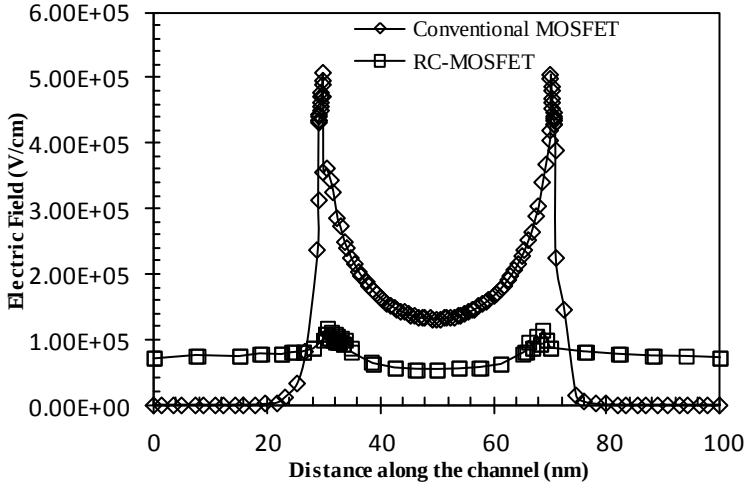

Fig. 04: Electric field variation along the channel for Conventional MOSFET and RC-MOSFET at L_G=30 nm, V_{ds}=0.5 V, V_{gs}=0.8 V, t_{ox}=5nm and wavelength=650nm.

Fig. 04: shows the variation of the electric field, along the channel from source to drain side for RC-MOSFET and conventional MOSFET. It can be seen that there is an appreciable increase in the electric field near the source side as compared to drain side in RC MOSFET. It clearly shows that electron velocity near the source is improved, thereby improving the carrier injected into the channel. This is mainly due to the photocurrent available at 650nm wavelength of the incident light because maximum light is reaching the channel region in RC MOSFET.

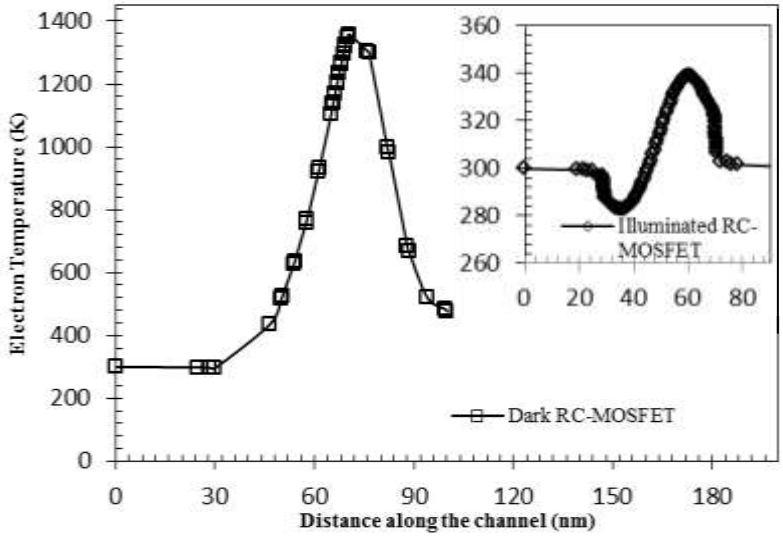

Fig. 05: Electron temperature variation along the channel for wavelength= 650nm in dark and illumination RC-MOSFET.

Fig. 05: shows the variation of electron temperature along the channel length from source to drain under dark and illumination RC MOSFET. As is clear from the results, an appreciable reduction in electron temperature for illuminated RC MOSFET at the drain side is observed. This is because incident radiation results in a large amount of photon-generated electron hole pair in the depletion layer. Indium tin oxide has a low electrical resistivity, high optical transparency of visible light and exhibits metallic character of high conductivity, so it is directly dependent upon temperature [18]. When the carrier concentration increases, mobility decreases and hence, the increase in electron temperature is less in an illuminated RC MOSFET as compared to under dark condition.

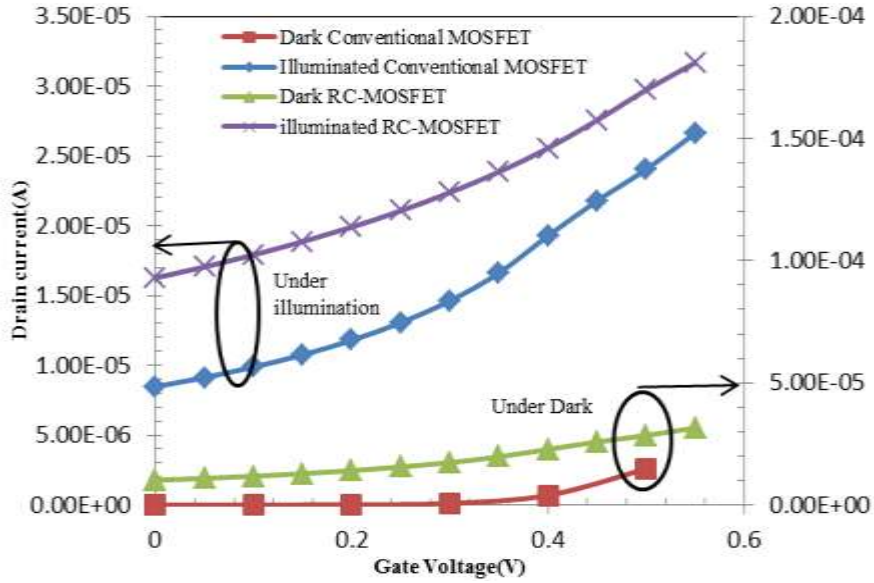

Fig. 06: Drain current Vs Gate Voltage for V_{DS}= 0.5 V in under illumination and dark RC-MOSFET & Conventional MOSFET.

Fig 06: shows the variation of drain current with respect to gate voltage V_G varying from 0 to 0.8V with V_D=0.5 V in dark and under illumination. It is evident from the figure that there is an increase in drain current under illumination as compared to the dark condition. It is due to more electron hole pair generation in the depletion region and the effective threshold voltage reduces under illumination [10]. It clearly shows that RC MOSFET is a better photo-sensing device because it has lower dark current and enhanced photo sensitivity due to its better gate controllability. This higher effective gate bias enhances the device conductivity and consequently the drain current increases.

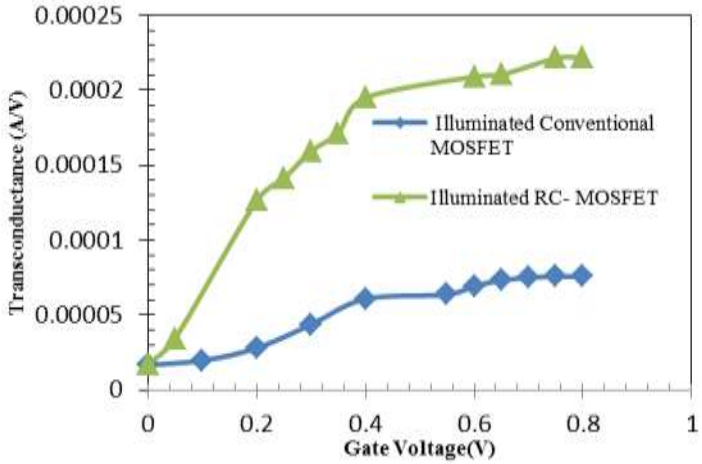

Fig. 07: Transconductance Vs Gate Voltage for V_{DS}= 0.5V in under illumination RC-MOSFET & Conventional MOSFET.

Fig. 07: shows the variation of transconductance with respect to drain voltage under varying gate voltage from 0V to 0.8V. The drain current is low until the device goes in the inversion layer. Due to this, the change in gate transconductance in RC MOSFET is seen at higher gate voltage as shown in figure. It is evident from the figure that the transconductance curve reaches a top and then remains constant in the saturation region. This is due to the effect of V_{GS} on enhanced electron mobility. The transconductance is use in integrated circuit design as it decides power dissipation and transition frequency. A substantial rise in transition frequency can contribute towards an increase in drain current and hence improvement in transconductance [14].

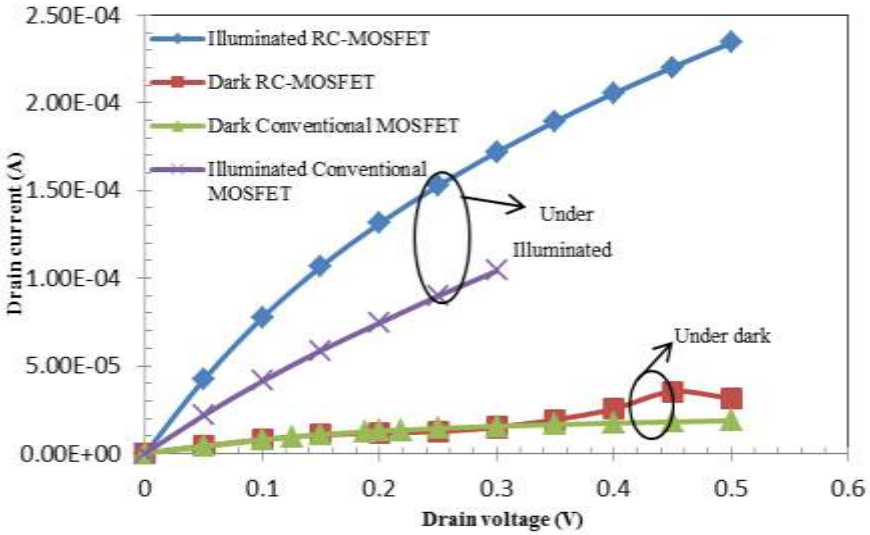

Fig. 08: Drain current Vs Drain Voltage for V_{GS}= 0.5V in under illumination RC-MOSFET & Conventional MOSFET.

Fig. 08: shows the variation of drain current with respect to drain voltage V_D varying from 0V to 0.8V with V_{GS}=0.5 V in dark and under illumination. It can be seen that the effective threshold voltage reduces because of optical radiation due to photo voltage created across the gate terminal. It is due to higher magnitude of photogenerated current than the dark current that effective gate control and subthreshold characteristics enhance [16].

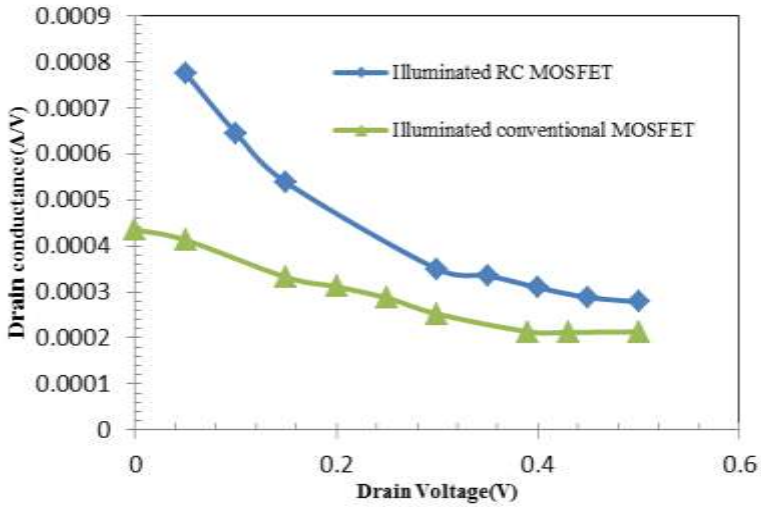

Fig. 09: Drain Conductance Vs Drain Voltage for V_{GS}= 0.8 in under illumination RC & conventional MOSFET.

Fig. 09: shows the variation of drain conductance with respect to drain voltage with V_D varying from 0V to 0.5V and V_G=0.8 in under illumination. This shows the drain conductance is constant with increasing drain voltage. As it is clear from the figure that output drain conductance is proportional to the drain current, and drain current is constant in saturation region of the RC and conventional MOSFET at higher drain voltage. So the drain conductance remains constant in saturation region under illumination RC and conventional MOSFET.

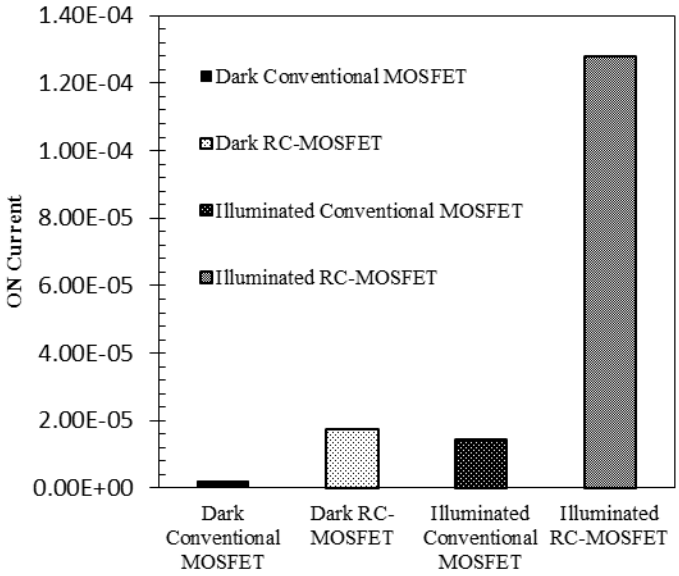

Fig. 10: ON Current for RC-MOSFET and conventional MOSFET under dark and illuminated at L_G=30 nm.

Fig. 10: shows high ON current in illuminated RC-MOSFET in comparison to dark RC and conventional MOSFET which favours pertinence in switching applications as compared to conventional MOSFET. In ITO, indium oxide (In_2O_3) and Tin oxide (SnO_2) contributes many free electrons which increases the electrical conductivity and decreases the resistivity [18]. As a result, the electron velocity near the source side is higher in an illuminated RC MOSFET which magnifies the source carrier injected into the channel Hence it improved the transconductance, low power dissipation and current driving capability in illuminated RC MOSFET.

CONCLUSION

Luminous analysis of the transparent RC MOSFET has been studied using silvaco TCAD software. In this paper, we emphasize our focus on transparent ITO gate RC MOSFET for improved switching ratio, transconductance and reduction in power dissipation. The high photogeneration rate is attributed to improved transmittance of the transparent ITO gate RC MOSFET compared to conventional MOSFET. The work thus presents a transparent RC MOSFET design as a promising solution for high-performance optical applications in the visible range of wavelength.

ACKNOWLEDGMENTS

The authors would like to thank the Microelectronics Research Lab, Department of Engineering Physics, Delhi Technological University (formerly Delhi College Engineering) to carry out this work.

REFERENCES

[1] R. Wemer, C. Zimmermann, and A. Kalz, "Light Dependence of Partially Depleted SOI-MOSFET's Using SIMOX Substrates", IEEE Trans. On Elec.Dev., Vol. 42, No. 9, pp. 1653- 1656, 1995.

[2] P. Jain and B.K Mishra, "Evaluation of Optically Illuminated MOSFET Characteristics by TCAD SIMULATION" International journal of VLSI design & Communication Systems (VLSICS) Vol.4, No.2, April 2013.

[3] R. Chaujar, R. Kaur, M. Saxena, M. Gupta and R.S. Gupta, "Solution to CMOS Technology for high Performance Analog Applications: GEWE-RCMOSFET", ACMD 2008.

[4] Y. Liu, K. Gopalafishan, P. B. Griffin, K. Ma, M.D. Deal, J. D. Plummer, "MOSFETs and Highspeed Photodetectors on Ge-on-Insulator Substrates Fabricated Using Rapid Melt Growth**",** *IEDM*, pp1001-1004, 2004

[5] N.arora, "MOSFET models for VLSI circuit simulation theory and practice", Springer Verlag Wien New York, pp. 87-89.

[6] R. Chaujar, R. Kaur, Manoj Saxena, M. Gupta, and R. S. Gupta, "TCAD Assessment of Gate Electrode Workfunction Engineered Recessed Channel (GEWE-RC) MOSFET and Its Multilayered Gate Architecture"—Part I: Hot-Carrier-Reliability Evaluation." IEEE Trans. Electron Devices, vol.55, no. 10, pp 2602-2612,2008.

[7] E. Lee, D. Moon, J. H. Yang, K. S. Lim, and Y. K.Choi, "Transparent Zinc Oxide Gate Metal–Oxide–Semiconductor Field-Effect Transistor for High- Responsivity Photodetector", IEEE Electron Device Letters, Vol. 30, No. 5, pp. 493-495, 2009.

[8] R. Gautam, M. Saxena, R. S.Gupta, and M. Gupta, "Analytical Model of Double Gate MOSFET for High Sensitivity Low Power Photosensor", Journal of semiconductor technology and science, VOL.13, NO.5, October, 2013.

[9] ATLAS User's Manual: 3-D Device Simulator, SILVACO International, Version 5.14.0.R, 2010.

[10] R. A. Ismail, W. K. Hamoudi, "Characteristics of Novel Silicon Pin Photodiode Made By Rapid Thermal Diffusion Technique", Journal of Electron Devices, Vol. 14, pp. 1104-1107, 2012.

[11] A. K. Okyay, D. Kuzum, S. Latif, D. A. B. Miller, and K. C. Saraswat, "Silicon Germanium CMOS Optoelectronic Switching Device: Bringing Light to Latch", IEEE Transactions On Electron Devices, Vol. 54, 3252-3259, 2007.

[12] N. S. Roy, B. B. Pal, and R. U. Khan, "Analysis of GaAs OPFET with Improved Optical Absorption under Back Illumination", IEEE Transactions On Electron Devices, Vol.46, pp.2351-2353, 1999.

[13] P. Jain and B.K. Mishra, "CV Investigation in Optically Illuminated MOSFET," International Journal of Engineering Research and Applications, vol. 47, pp. 1881-1885, Nov-Dec 2012.

[14] T. Yamagata and K. Shimomura, "Optically Controlled Metal –Oxide Semiconductor Field Effect Transistor Operated by Long – Wavelength Light", *Jpn. J. Appl. Phys.*, Vol.35, pp.L1589-1592, 1996.

[15] T. Minami, Present status of transparent conducting oxide thin-film development for Indium-Tin-Oxide (ITO) substitutes. Thin Solid Films 2008, 516, 5822–5828.

[16] Z.M. Jarzebski, Preparation and physical properties of transparent conducting oxide films. Phys. Stat. Sol. 1982, 71, 13–41.

[17] J-H Lim, C-K Kang, Kim K-K, Park I-K, Hwang D-K, Park SJ 2006 UV electroluminescence Emission from ZnO light emitting diodes grown by high-temperature radiofrequency sputtering. Adv. Mater. 18, 2720–4

[18] H. Ouyang, C. C. Striemer, and P. M. Fauchet, "Quantitative analysis of the sensitivity of porous silicon optical biosensors", Appl. Phys. Lett. Vol.88.

[19] N. S. Roy, B. B. Pal, and R. U. Khan, "Analysis of GaAs OPFET with Improved Optical Absorption under Back Illumination", IEEE Transactions On Electron Devices, Vol.46, pp.2351-2353, 1999.

MODELING OF 5-LEVEL CHB AS DSTATCOM FOR COMPENSATION OF POWER QUALITY ISSUES

T Rakesh[1], Dr M Sushama[2]
[1]Research Scholar JNTUH, Hyderabad, (India)
[2]Professor & Head EEE Department, JNTUCEH, Hyderabad, (India)

ABSTRACT

With the widespread use of harmonic generating devices, the control of harmonic currents to maintain a high level of power quality is becoming increasingly important. An effective way for harmonic suppression is the harmonic compensation by using active power filter. This paper presents a comprehensive survey of DSTATCOM and is aimed at providing a broad perspective on the status of DSTATCOM control methods to researchers and application engineers dealing with harmonic suppression issues. Many control techniques have been designed, developed, and realized for active filters in recent years. This paper presents different types of Synchronous reference frame methods for real time generation of compensating current for harmonic mitigation and reactive power compensation. All the techniques are analyzed mathematically and simulation results are obtained which are being compared in terms of its compensation performance with different parameters under steady state condition. Shunt compensation for medium voltage distribution systems requires higher rating for voltage source converters (VSCs). Ratings of the semiconductor devices in a VSC are always limited; therefore, for higher rated converters it is desirable to distribute the stress among the number of devices using multilevel topology. Cascaded multilevel configuration of the inverter has the advantage of its simplicity and modularity over the configurations of the diode-clamped and flying capacitor multilevel inverters. Application of cascaded multilevel converters for shunt compensation of distribution systems has been described in Literature. This paper presents an investigation of five-Level Cascaded H – bridge (CHB) Inverter as Distribution Static Compensator (DSTATCOM) in Power System (PS) for compensation of reactive power and harmonics. The advantages of CHB inverter are low harmonic distortion, reduced number of switches and suppression of switching losses. A CHB Inverter is considered for shunt compensation of a 11 kV distribution system. Finally a level shifted PWM (LSPWM) and phase shifted PWM (PSPWM) techniques are adopted to investigate the performance of CHB Inverter. The results are obtained through Matlab/Simulink software package. The proposed DSTATCOM is simulated for both linear and nonlinear loads.

Keywords- DSTATCOM, Power Quality Level Shifted Pulse Width Modulation (LSPWM), Phase Shifted Pulse Width Modulation (PSPWM), Proportional-Integral (PI) Control.

I. INTRODUCTION

One of the most common power quality problems today is voltage dips. A voltage dip is a short time (10 ms to 1 minute) event during which a reduction in r.m.s voltage magnitude occurs. It is often set only by two

parameters, depth/magnitude and duration. The voltage dip magnitude is ranged from 10% to 90% of nominal voltage (which corresponds to 90% to 10% remaining voltage) and with a duration from half a cycle to 1 min. In a three-phase system a voltage dip is by nature a three-phase phenomenon, which affects both the phase-to-ground and phase-to-phase voltages. A voltage dip is caused by a fault in the utility system, a fault within the customer's facility or a large increase of the load current, like starting a motor or transformer energizing. Typical faults are single-phase or multiple-phase short circuits, which leads to high currents. The high current results in a voltage drop over the network impedance. At the fault location the voltage in the faulted phases drops close to zero, whereas in the non-faulted phases it remains more or less unchanged [1, 2]. Voltage dips are one of the most occurring power quality problems. Off course, for an industry an outage is worse, than a voltage dip, but voltage dips occur more often and cause severe problems and economical losses. Utilities often focus on disturbances from end-user equipment as the main power quality problems. This is correct for many disturbances, flicker, harmonics, etc., but voltage dips mainly have their origin in the higher voltage levels. Faults due to lightning, is one of the most common causes to voltage dips on overhead lines. If the economical losses due to voltage dips are significant, mitigation actions can be profitable for the customer and even in some cases for the utility. Since there is no standard solution which will work for every site, each mitigation action must be carefully planned and evaluated. There are different ways to mitigate voltage dips, swell and interruptions in transmission and distribution systems. At present, a wide range of very flexible controllers, which capitalize on newly available power electronics components, are emerging for custom power applications [3, 4]. Among these, the distribution static compensator and the dynamic voltage restorer are most effective devices, both of them based on the VSC principle. The STATCOM used in distribution systems is called DSTACOM (Distribution-STACOM) and its configuration is the same, but with small modifications. It can exchange both active and reactive power with the distribution system by varying the amplitude and phase angle of the converter voltage with respect to the line terminal voltage. A multilevel inverter can reduce the device voltage and the output harmonics by increasing the number of output voltage levels. There are several types of multilevel inverters: cascaded H-bridge (CHB), neutral point clamped, flying capacitor [2-5]. In particular, among these topologies, CHB inverters are being widely used because of their modularity and simplicity. Various modulation methods can be applied to CHB inverters. CHB inverters can also increase the number of output voltage levels easily by increasing the number of H-bridges. This paper presents a DSTATCOM with a proportional integral controller based CHB multilevel inverter for the harmonics and reactive power mitigation of the nonlinear loads. This type of arrangements have been widely used for PQ applications due to increase in the number of voltage levels, low switching losses, low electromagnetic compatibility for hybrid filters and higher order harmonic elimination.

II. DESIGN OF MULTILEVEL BASED DSTATCOM

2.1 Principle Of DSTATCOM

A D-STATCOM (Distribution Static Compensator), which is schematically depicted in Figure-1, consists of a two-level Voltage Source Converter (VSC), a dc energy storage device, a coupling transformer connected in shunt to the distribution network through a coupling transformer. The VSC converts the dc voltage across the storage device into a set of three-phase ac output voltages. These voltages are in phase and coupled with the ac system through the reactance of the coupling transformer. Suitable adjustment of the phase and magnitude of the

D-STATCOM output voltages allows effective control of active and reactive power exchanges between the DSTATCOM and the ac system. Such configuration allows the device to absorb or generate controllable active and reactive power.

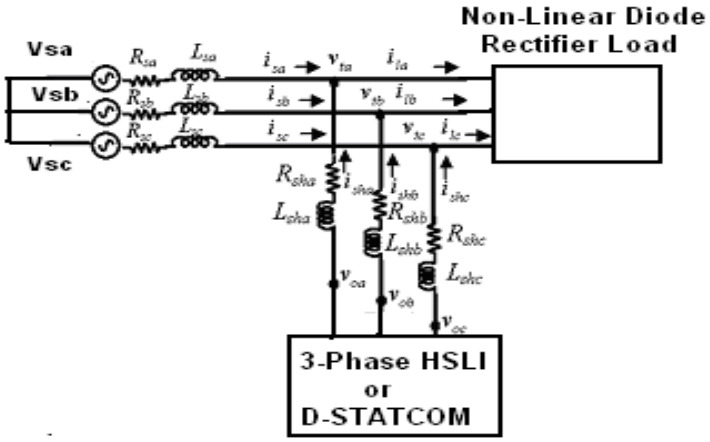

Figure – 1 Schematic Diagram of a DSTATCOM

The VSC connected in shunt with the ac system provides a multifunctional topology which can be used for up to three quite distinct purposes:

1. Voltage regulation and compensation of reactive power;
2. Correction of power factor
3. Elimination of current harmonics.

2.1 Control For Reactive Power Compensation

The aim of the control scheme is to maintain constant voltage magnitude at the point where a sensitive load under system disturbances is connected. The control system only measures the rms voltage at the load point, i.e., no reactive power measurements are required. The VSC switching strategy is based on a sinusoidal PWM technique which offers simplicity and good response. Since custom power is a relatively low-power application, PWM methods offer a more flexible option than the fundamental frequency switching methods favored in FACTS applications. Apart from this, high switching frequencies can be used to improve on the efficiency of the converter, without incurring significant switching losses.

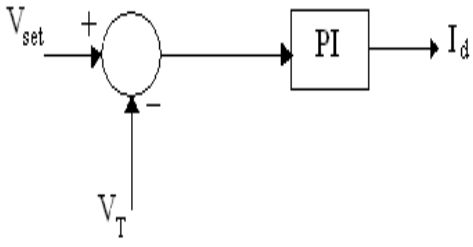

Figure-2 PI Control For Reactive Power Compensation

The controller input is an error signal obtained from the reference voltage and the rms terminal voltage measured. Such error is processed by a PI controller; the output is the angle δ, which is provided to the PWM signal generator. It is important to note that in this case, of indirectly controlled converter, there is active and reactive power exchange with the network simultaneously. The PI controller processes the error signal and

generates the required angle to drive the error to zero, i.e. the load rms voltage is brought back to the reference voltage.

2.3 Control For Harmonics Compensation

The Modified Synchronous Frame method is presented in [7]. It is called the instantaneous current component (id-iq) method. This is similar to the Synchrous Reference Frame theory (SRF) method. The transformation angle is now obtained with the voltages of the ac network. The major difference is that, due to voltage harmonics and imbalance, the speed of the reference frame is no longer constant. It varies instantaneously depending of the waveform of the 3-phase voltage system. In this method the compensating currents are obtained from the instantaneous active and reactive current components of the nonlinear load. In the same way, the mains voltages V (a,b,c) and the available currents i_l (a,b,c) in α-β components must be calculated as given by (4), where C is Clarke Transformation Matrix. However, the load current components are derived from a SRF based on the Park transformation, where 'θ' represents the instantaneous voltage vector angle (5).

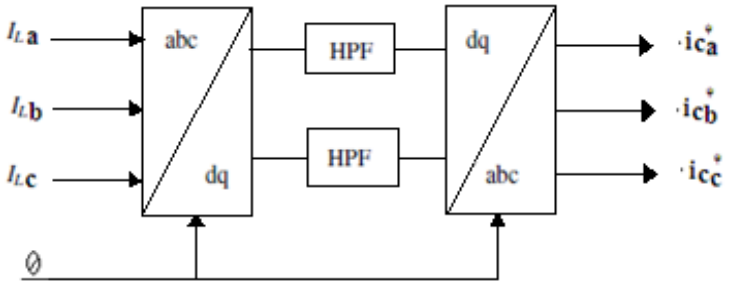

Figure-3 Block diagram of SRF method

Switches Turn ON	Voltage Level
S1,S2	Vdc
S3,S4	-Vdc
S4,D2	0

Table-1 Switching table of single CHB inverter

2.4 Cascaded H-Bridge Multilevel Inverter

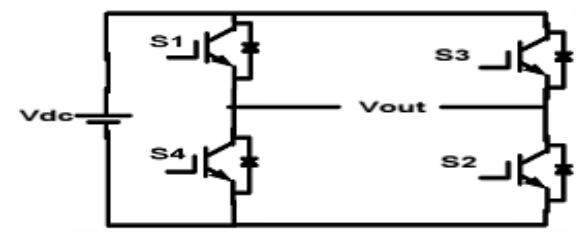

Figure-4 Circuit of the single cascaded H-Bridge Inverter

Fig.4 shows the circuit model of a single CHB inverter configuration. By using single H-Bridge we can get 3 voltage levels. The number of output voltage levels of CHB is given by 2n+1 and voltage step of each level is given by Vdc/2n, where n is number of H-bridges connected in cascaded. The switching table is given in Table 1.

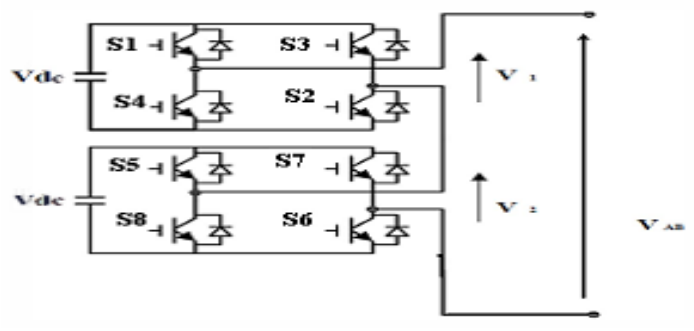

Figure-5 Block diagram of 5-level CHB inverter model

The switching mechanism for 5-level CHB inverter is shown in table-2.

Table 2.Switching table for 5-level CHB Inverter

Switches Turn On	Voltage Level
S1, S2	Vdc
S1,S2,S5,S6	2Vdc
S4,D2,S8,D6	0
S3,S4	-Vdc
S3,S4,S7,S8	-2Vdc

2.5 PWM Techniques For CHB Inverter

The most popular PWM techniques for CHB inverter are 1. Phase Shifted Carrier PWM (PSCPWM), 2. Level Shifted Carrier PWM (LSCPWM).

2.1.1 Phase Shifted Carrier PWM (PSCPWM)

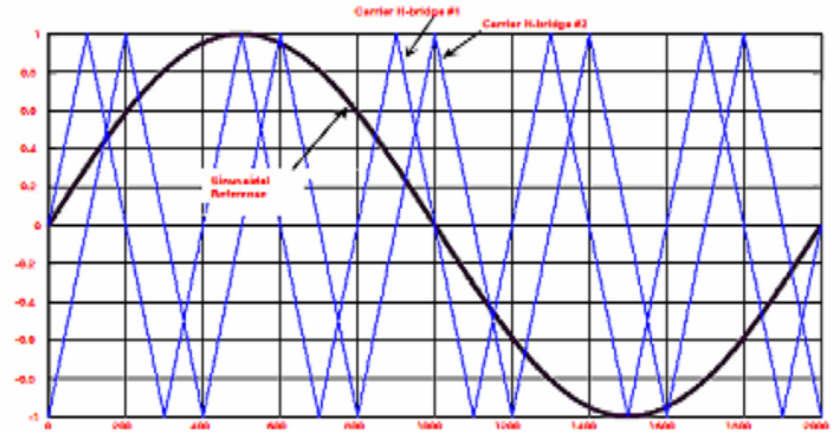

Fig. 6 phase shifted carrier PWM

Fig6 shows the Phase shifted carrier pulse width modulation. Each cell is modulated independently using sinusoidal unipolar pulse width modulation and bipolar pulse width modulation respectively, providing an even power distribution among the cells. A carrier phase shift of 180°/m (No. of levels) for cascaded inverter is introduced across the cells to generate the stepped multilevel output waveform with lower distortion.

2.1.2 Level Shifted Carrier PWM (LSCPWM)

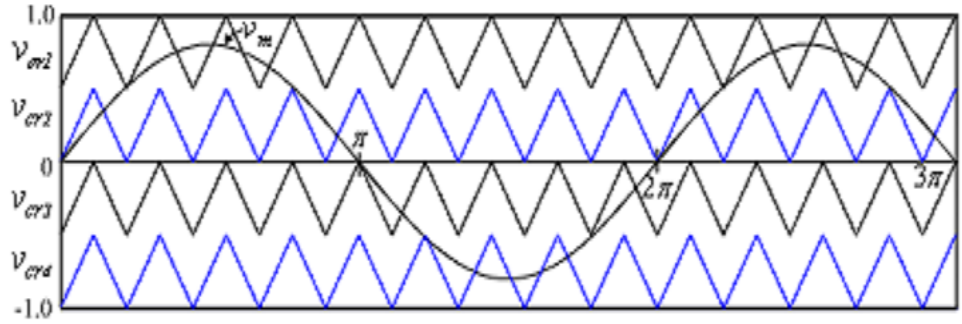

Fig.7 Level shifted carrier PWM

Fig.7 shows the Level shifted carrier pulse width modulation. Each cell is modulated independently using sinusoidal unipolar pulse width modulation and bipolar pulse width modulation respectively, providing an even power distribution among the cells. A carrier Level shift by 1/m (No. of levels) for cascaded inverter is introduced across the cells to generate the stepped multilevel output waveform with lower distortion.

III. MATLAB/SIMULINK MODELING AND SIMULATION RESULTS

Here Matlab/Simulink modle is developed for two cases. In case one DSATCOM with Linear load and in case two DSTATCOM with nonlinear load are simulated.

3.1 Case One

Fig8 shows the Matab/Simulink power circuit model of DSTATCOM. It consists of five blocks named as source block, non linear load block, control block, APF block and measurements block.

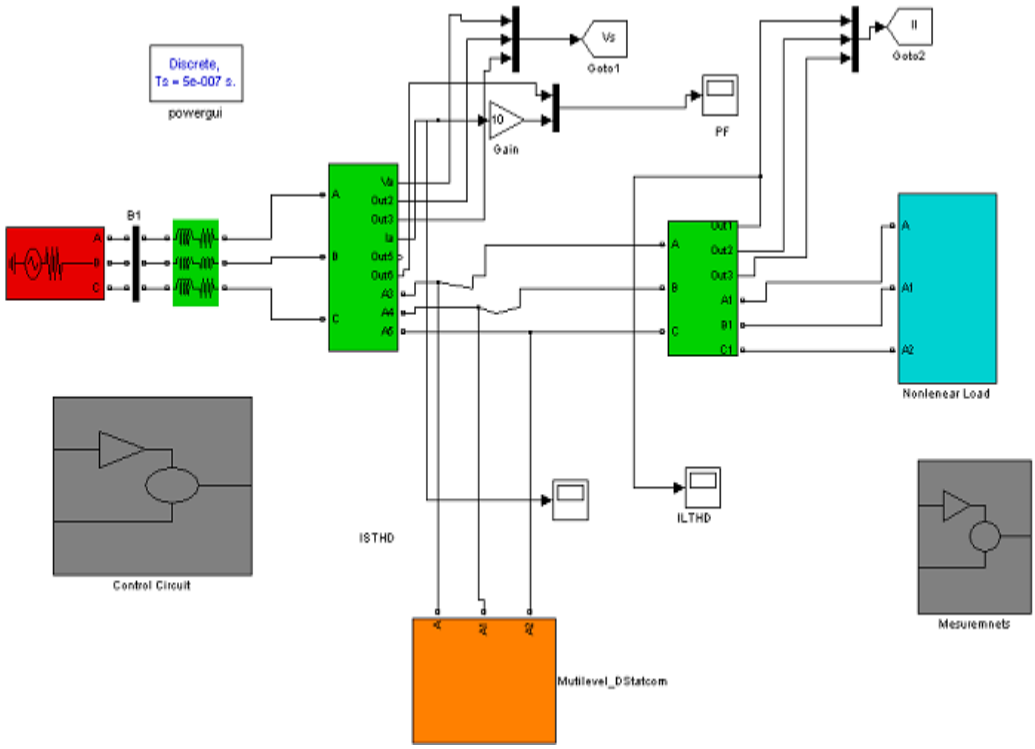

Fig. 8 Matlab/Simulink power circuit model of DSTATCOM

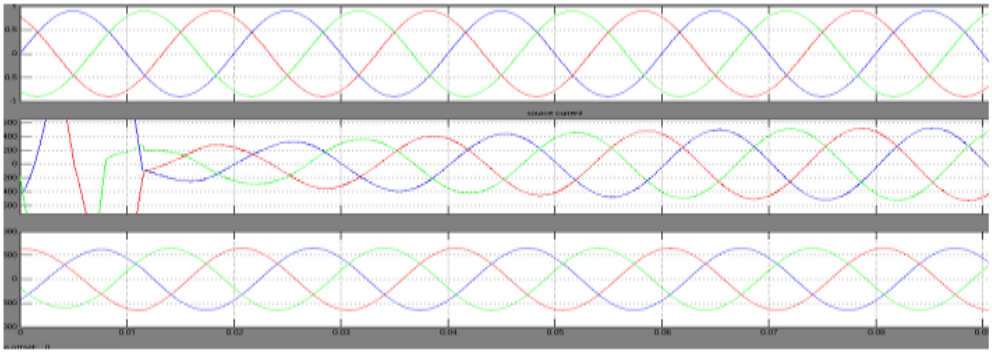

Fig. 9 Source Voltage, Current And Load Current With DSTATCOM

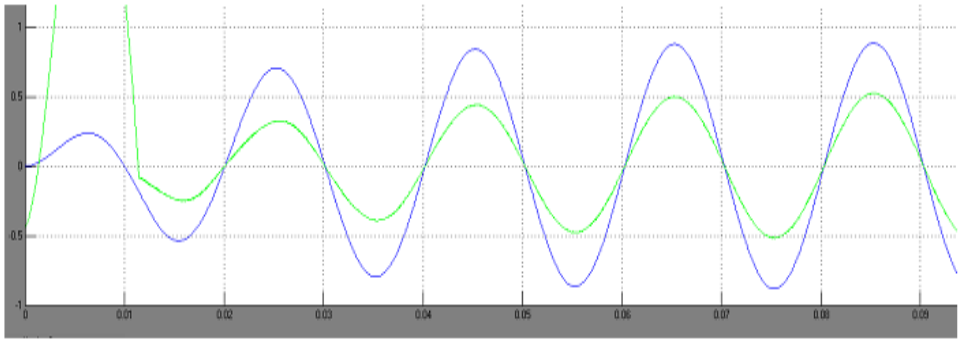

Fig.10 Phase-A Source Voltage And Current

Fig.10 shows the phase-A source voltage and current, even though the load is non linear RL load the source power factor is unity.

3.2 Case Two

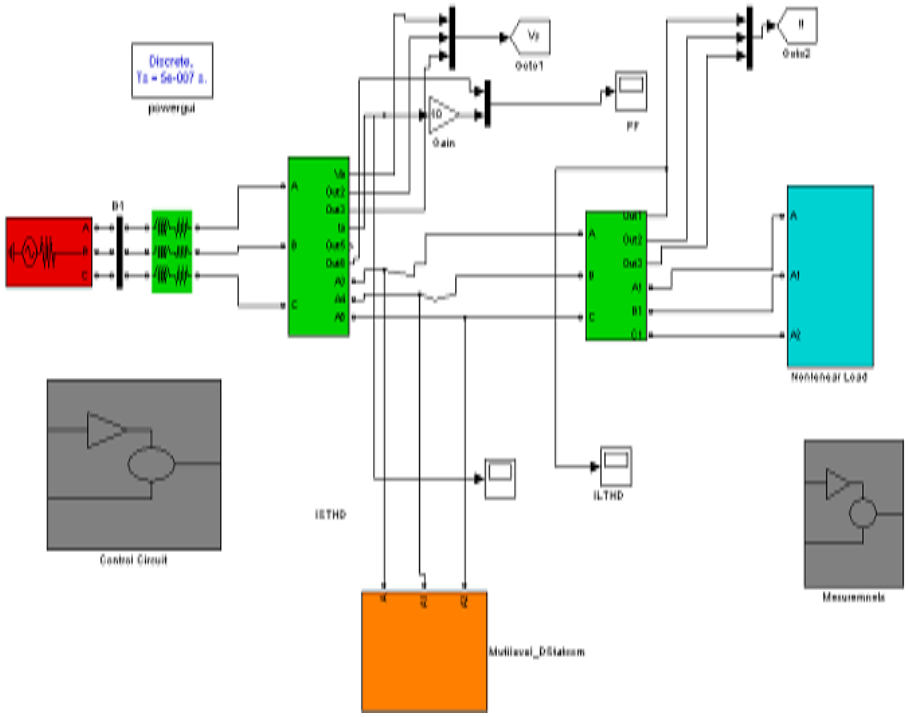

Fig.11 Matlab/Simulink Power Circuit Model Of DSTATCOM

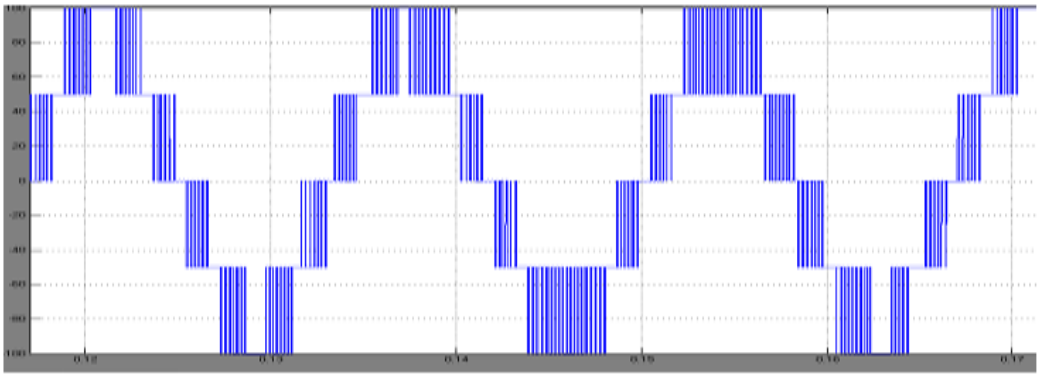

Fig. 12 five levels PSCPWM output

Fig. 13 shows the three phase source voltages, three phase source currents and load currents respectively without DSTATCOM. It is clear that without DSTATCOM load current and source currents are same.

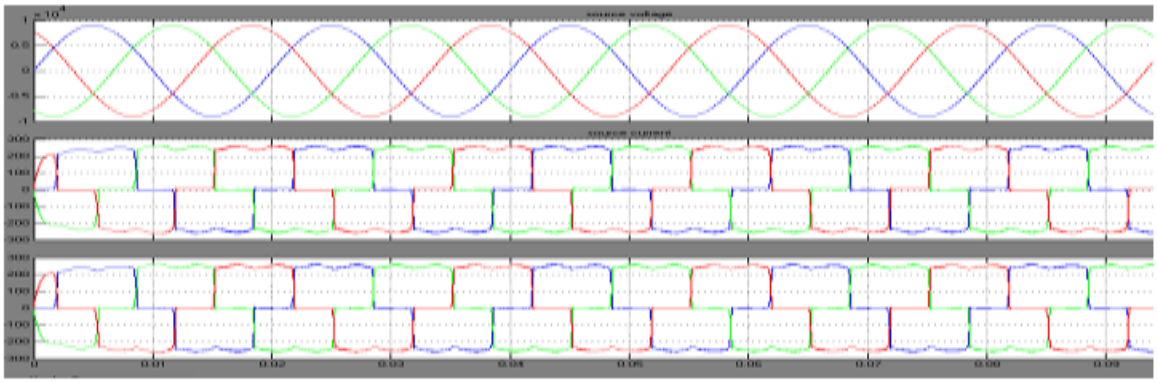

Fig. 13 Source voltage, current and load current without DSTATCOM

Fig. 14 shows the three phase source voltages, three phase source currents and load currents respectively with DSTATCOM. It is clear that with DSTATCOM even though load current is non sinusoidal source currents are sinusoidal.

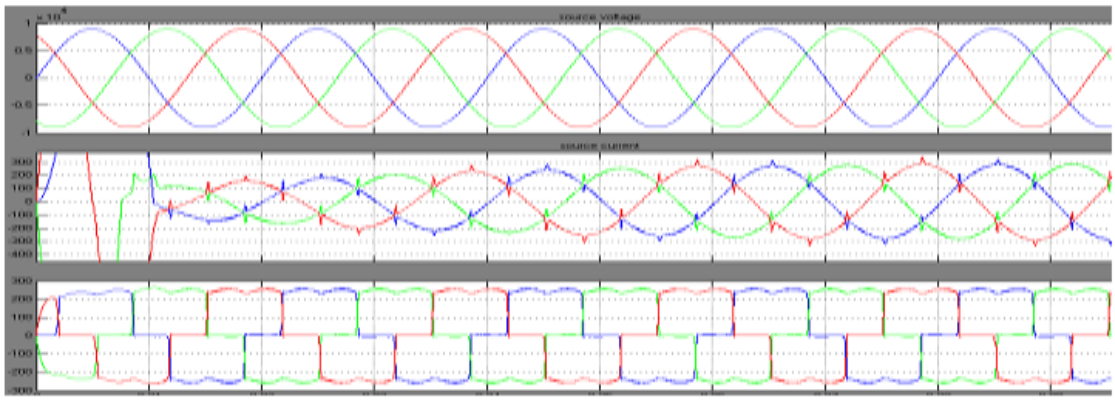

Fig. 14 Source voltage, current and load current with DSTATCOM

Fig. 15 shows the DC bus voltage. The DC bus voltage is regulated to 11kv by using PI regulator.

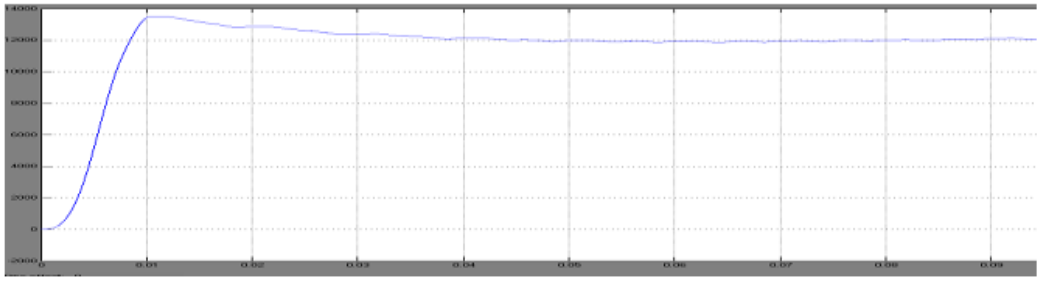

Fig. 15 DC Bus Voltage

Fig. 16 shows the phase-A source voltage and current, even though the load is non linear RL load the source power factor is unity.

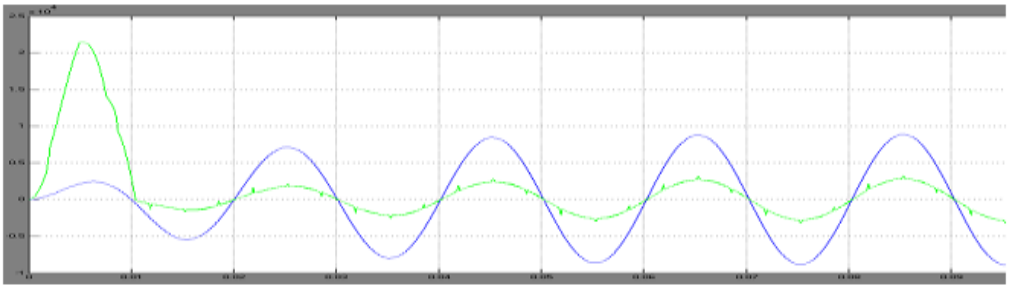

Fig. 16 Phase-A source voltage and current

Fig. 17 shows the harmonic spectrum of Phase –A Source current without DSTATCOM. The THD of source current without DSTACOM is 36.89%.

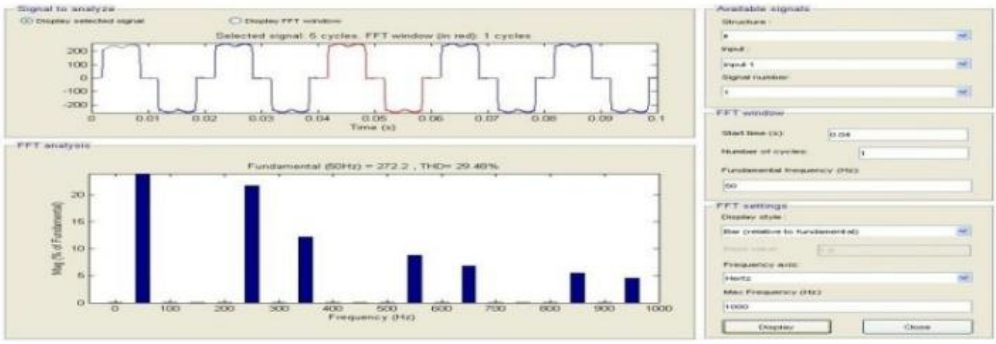

Fig. 17 Harmonic spectrum of Phase-A Source current without DSTATCOM

Fig. 18 shows the harmonic spectrum of Phase –A Source current with DSTATCOM. The THD of source current without DSTACOM is 5.05%

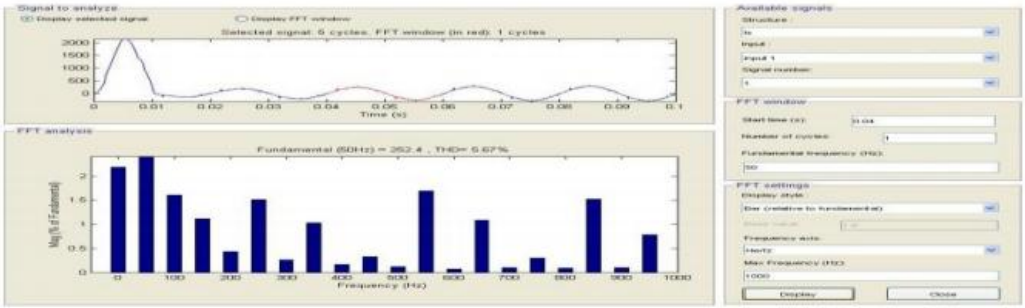

Fig. 18 Harmonic spectrum of Phase-A Source current with DSTATCOM

IV. CONCLUSION

This paper studied a five level inverter used in a DSTATCOM in PS and has been successfully demonstrated in MatLab/Simulink. The befits of five level inverter has low harmonics distortion, reduced number of switches to achieve the seven- level inverter output over the cascaded seven level inverter and reduced switching losses. A DSTATCOM with five levels CHB inverter is investigated. Mathematical model for single H-Bridge inverter is developed which can be extended to multi H-Bridge. The source voltage , load voltage , source current, load current, power factor simulation results under non-linear loads are presented. Finally Matlab/Simulink based model is developed and simulation results are presented for both linear and non linear loads.

REFERENCES

[1]. K.A Corzine, and Y.L Familiant, "A New Cascaded Multi-level H-Bridge Drive," IEEE Trans. Power.Electron., vol.17, no.1, pp.125-131. Jan 2002.

[2]. J.S.Lai, and F.Z.Peng "Multilevel converters – A new breed of converters, "IEEE Trans. Ind.Appli., vol.32, no.3, pp.509-517. May/ Jun. 1996.

[3]. T.A.Maynard, M.Fadel and N.Aouda, "Modelling of multilevel converter," IEEE Trans. Ind.Electron., vol.44, pp.356-364. Jun.1997.

[4]. P.Bhagwat, and V.R.Stefanovic, "Generalized structure of a multilevel PWM Inverter," IEEE Trans. Ind. Appln, Vol.1A-19, no.6, pp.1057-1069, Nov./Dec..1983.

[5]. J.Rodriguez, Jih-sheng Lai, and F Zheng peng, "Multilevel Inverters; A Survey of Topologies, Controls, and Applications," IEEE Trans. Ind. Electron., vol.49,no4., pp.724-738. Aug.2002.

[6]. RoozbehNaderi, and Abdolrezarahmati, "Phase-shifted carrier PWM technique for general cascaded inverters," IEEE Trans. Power.Electron., vol.23, no.3, pp.1257-1269. May.2008.

[7]. Bhim Singh, Kamal AlHaddad&Ambrish Chandra, 1999, A Review of Active Filter for Power Quality Improvements, IEEE Trans on Industrial Electronics, 46(5), pp.960970

[8]. Mauricio Angulo, Pablo Lezana, Samir Kouro, Jos´eRodr´ıguez and Bin Wu,"Level-shifted PWM for Cascaded Multilevel Inverters with Even Power Distribution" IEEE Power Electronics specialist conference, 17-21 june 2007, pp.2373-2378.

[9]. P. McGrath and D. G. Holmes, "Multicarrier PWM strategies formultilevel inverters," IEEE Trans. Ind. Electron., vol. 49, no. 4, pp. 858–867, August 2002.

[10]. M. Meinhardt and G. Cramer, "Past, present and future of grid-connected photovoltaic- and hybrid-power-systems," in Proc. IEEE-PES Summer Meeting, Jul. 2000, vol. 2, pp. 1283–1288.

[11]. S. Kouro, J. Rebolledo, and J. Rodriguez, "Reduced switching-frequency modulation algorithm for high-power multilevel inverters," IEEE Trans.Ind. Electron, vol. 54, no. 5, pp. 2894–2901, Oct. 2007.

[12]. S. J. Park, F. S. Kang, M. H. Lee, and C. U. Kim, "A new single-phase five level PWM inverter employing a deadbeat control scheme," IEEE Trans. Power Electron., vol. 18, no. 18, pp. 831–843, May 2003.

A COMPREHENSIVE REVIEW OF POWER SYSTEM STABILIZER MODELING, ANALYSIS AND CONTROL STRATEGY

V Sanjeeva Rao[1], Dr B V Sanker Ram[2]
[1]*Research Scholar JNTUH, Hyderabad, (India)*
[2]*Professor EEE Dept. JNTUCEH, Hyderabad, (India)*

ABSTRACT

A Power System Stabilizer (PSS) is the most cost effective approach of increase the system positive damping, improve the steady-state stability margin, and suppress the low-frequency oscillation of the power system. A PSS has to perform well under operating point variations. Some of the major issues in the application of PSS are the choice of the input signal, the location of the PSS, the control algorithms and coordination with flexible AC transmission system (FACTS) devices. This paper presents an exhaustive review of power system stabilizer in terms of operation, dynamics, and control technique. It also reviews various methods for optimal placement of PSS. Studies have shown that PSS are designed to provide additional damping torque without affecting the synchronizing torque at critical frequencies in order to improve power system dynamic stability.

Keywords: ***Power System Stabilizer (Pss), Flexible Ac Transmission System (Facts), Single-Machine Infinite-Bus (SMIB).***

I. INTRODUCTION

Power system dynamic performance is improved by the damping of system oscillations. Generally, there are two kinds of power oscillation damping controllers in power systems: PSS and FACTS controllers [1-5]. PSS is widely used in the electric power industry for improve the performance and functions of power systems during normal and abnormal operations. It can increase the system positive damping, improve the steady-state stability margin, and suppress the low-frequency oscillation of the power system [6-12]. Design and application of PSS has been the subject of continuing development for many years. All part of the PSS topic are numerous and various. These are classified as: (a) mathematical modeling and proper signal selection, (b) finding the optimal placement of PSS, (c) coordination between the PSS and the FACTS, (d) the optimal parameters of the controller, and effect of PSS on system stability [13-21]. A field test to adequately assess the oscillation damping effectiveness of the PSS in a multi-generator power plant is presented in [22], which the test allows estimating the location of the dominant open-loop poles from frequency response measurements of the closed-loop multivariable system. The conic programming is an effective tool to solve robust PSS design problems by simultaneously considering several operating scenarios is show in. Optimal multi-objective design of robust multi-machine power system using Genetic Algorithms is presented in, which a conventional speed-based lead-

lag PSS is used. A method based on a model predictive control for robust tuning of PSS and AVR in multi-machine power systems to improve the stability of the wide-area power system with distribution systems including dispersed generations is presented in. This paper will review some of the published work in application, operation and control technique of PSS. The principle of operation of PSS such as input signals and block diagram is described in section II. The Multi-Band PSS (MB-PSS) is described in section III. Section IV provides an overview of the conventional techniques of controllers to enhance performance of a PSS. Section V presents the review of various methods for selecting the PSS location in multi-machine power systems. A detailed overview of the modes oscillations is presented in section VI. The effects of PSS on the Sub-Synchronous Resonance (SSR) damping characteristics show in section VII. FACTS devices and PSS can help the damping of power system oscillations. The basic concepts of coordination between PSS and FACTS devices have been presented in section VIII. In power system stability, the damping torque and the synchronous torque are both important. Section IX covers the mathematical modeling of the single-machine infinite-bus (SMIB) installed with PSS. Section X presents the summary and the conclusions of the paper.

II. SUPPLEMENTARY EXCITATION

The idea of supplementary excitation is to apply a signal through the excitation system to increase the damping torque of the generator in a power system. Power System Stabilizer (PSS) is used to generate supplementary control signals to excitation systems in order to dampen the low frequency oscillations.

2.1 Excitation System

Figure 1 shows the functional block diagram of a typical of a large synchronous generator. Fast acting exciters with high gain AVR (Automatic Voltage Regulator) gives good voltage control and increases the possibilities of keeping the generator synchronized at large disturbances, but can contribute to oscillatory instability in power systems.

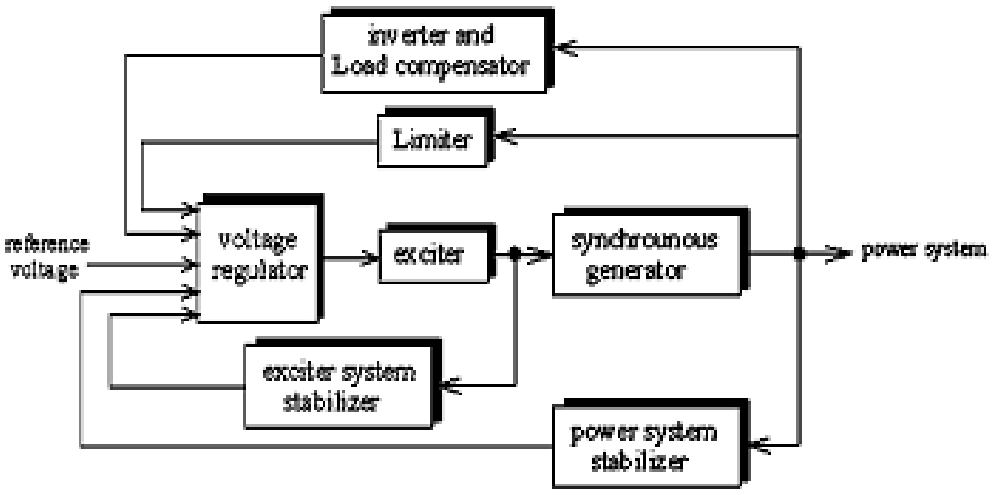

Figure 1. Block diagram of synchronous generator excitation system and structure diagram of power system stabilizer

The objective of PSS control is to directly target the control of the generator. Therefore, the PSS control is a direct control on the generator side.

2.2 Input Signals

A PSS can be viewed as an additional block of a generator excitation control or automatic voltage regulator, added to improve the overall power system dynamic performance, especially for the control electromechanical oscillations. The input signal for the PSS in the system is a point of debate. The input signals that have been identified as valuable include deviations in the shaft speed, the accelerating power, the terminal frequency and the active power output and linear combinations of these have been extensively investigated and recommendations regarding their use have been reported in the literature. Since the main action of the PSS is to control the rotor oscillations, the input signal of rotor speed has been the most frequently advocated in the literature. One of the limitations of the speed input PSS is that it may excite torsional oscillatory modes. It is important to select the PSS parameters carefully depending on its input signal and location in the power system. In, an indirect adaptive PSS is designed using two input signals, the speed deviation, and the power deviation to a neural network controller. A design method for PSS using the power flow of a remote transmission line and a remote bus voltage is proposed in, which it was possible to improve the damping of inter-area oscillations and the power transfer capability.

2.3 Block Diagram

A PSS model is viewed as an additional control block to enhance system stability. To provide damping, PSS must produce a component of electrical torque in phase with the rotor speed deviations. Controllers based on speed deviation would ideally use a differential type of regulation and a high gain, a typical PSS block diagram is shown in Figure 2. It consists of an amplifier block of gain constant *KP*, a block having a washout time constant $T_{\omega}$and one or two lead-lag compensators. The output signal of PSS is a voltage signals here it is *US*. In practice, two or more first-order blocks can be used to achieve desired phase compensation. It is accomplished by adjusting the PSS to compensate for phase lags through the generator, excitation system, and power system, such that PSS provides torque changes in phase with speed changes. The signal washout block serves as high pass filter, which remove any DC offsets in output of PSS in steady state. Without it, steady changes in speed would modify the terminal voltage. Controllers based on speed deviation would ideally use a differential type of regulation and a high gain. Since this is impractical in reality, the previously mentioned lead-lag structure is commonly used. The gain and the lead-lag compensator time constants are to be selected for optimal performance over a wide range of operating conditions. All of the variables of the PSS must be determined for each type of generator separately because of dependence on machine parameters.

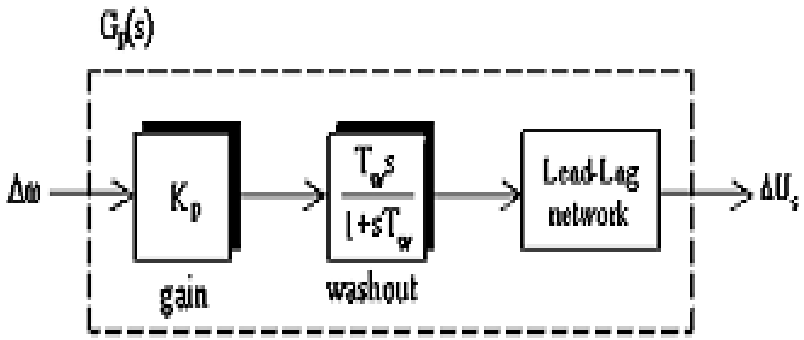

Figure 2. Block diagram of general power system stabilizer

III. MULTIBAND PSS

The need for improving the damping of a wide range of electromechanical oscillations motivated the concept of the multiband PSS. It structure is based on multiple working bands. As for conventional PSS, the MB-PSS with three kinds of frequency bands action function are used, dedicated to low, intermediate, and high frequency modes of oscillations.

IV. CONTROL TECHNIQUES

Two of the most important factors for selecting a control technique are valid in a wide range of operating conditions and unexpected equipment failures. The proper selection of PSS parameters to accommodate variations in the power system dynamics is important. The parameters of the excitation system and PSS are chosen to enhance the overall system stability. The PSS design methods can be divided into three categories: (a) linear control methods such as pole placement, linear quadratic regulation, eigenvalue sensitivity analysis and sliding mode control, (b) nonlinear control methods such as adaptive control, fuzzy logic, and (c) empirical control methods such as artificial intelligence techniques. PSS has to perform well under various loading conditions and stability of system is guaranteed. Robustness of a PSS is a major issue. Many robust control techniques have been used in the design of PSS. Some of major approaches to robust control are H-infinity optimal control, structured singular value, parameter space method, pole placement, Quantitative Feedback Theory (QFT), Variable Structure Control (VSC) and Linear Matrix Inequality (LMI). Generally, PSS control design methodologies can be categorized as (a) classical methods, (b) adaptive and variable structure methods, (c) robust control approaches, (d) artificial intelligent techniques and (e) digital control schemes.

4.1 State Feedback Control

The state feedback power system stabilizers possess superior control capabilities when compared to the conventional lead-lag power system stabilizers. They require feedback of all the state variables, which are generally not measurable. However, in this method robustness may not be always possible. The design of robust PSS base on full state feedback, which place the system poles in an acceptable region in the complex plane for a given set of operating, and system conditions is presented in. In, Hybrid Differential Evolution (HDE) has been used to investigate a decentralized pole placement design method of output feedback PSS, which HDE method is originally an optimal searching approach.

4.2 Particle Swarm Optimization

The Particle Swarm Optimization (PSO) technique belongs to class of evolutionary programming approaches for optimization. It is computationally simple since it neither requires gradient calculations nor necessitates the convexity of the function to be optimized. A modified PSO algorithm with a small population for the design of optimal PSS used to determine the optimal parameters of several PSS simultaneously in a multi-machine power system is presented in. A simultaneous coordinated design of the Thyristor Controlled Series Capacitor (TCSC) damping controller and PSS in multi-machine power system is presented in , which the optimization problem with the time domain-based objective function is solved by a PSO technique which has a strong ability to find the most optimistic results. A method based on the PSO algorithm, based on the optimization of a suitable

objective function, for tuning PSS parameters is presented in , which optimal values for PSS controlling parameters including lead-lag compensator time constants as well as the controller gain are calculated.

4.3 Adaptive And Variable Structure Method

The power systems are complex and highly nonlinear systems. The linearized system models are valid only at the operating point that is used to linearize the system. If the parameters of the stabilizer are kept fixed, PSS performance is degraded whenever the operating point changes. The basic function of adaptive control is to adjust the parameters, in real time and according to the behavior of the power system and provided good damping over a wide operating range. All adaptive control techniques can be divided into two different groups, Direct Adaptive Control (DAC) and Indirect Adaptive Control (IAC). In DAC such as Model Reference Adaptive Control (MRAC) the controller parameters are adjusted, so that the output of the controlled system to follow the output of a reference model. In IAC such as self-tuning control, the aim is to control the system so that its behavior has the given properties. In comparison with the self-tuning control, MRAC has some advantages, such as fast adaptation process and lower computing complexity of adaptation algorithm. The damping effects of an adaptive PSS by simulations and compared its damping effect with a conventional PSS in both time domain and frequency domain is studied in. An adaptive PSS estimates some uncertainty within the system, and then automatically designs a controller for the estimated plant uncertainty. An adaptive PSS consisting of an online-identified planet model and self-learning fuzzy logic controller, for PSS application is described in. Application of a neural adaptive PSS to a five-machine power system is described in, which the proposed technique comprises two sub networks: the ‘Adaptive Neuro-Identifier’ to dynamically identify the nonlinear plant, and the Adaptive Neuro-Controller to damp output oscillations. An adaptive PSS, which consists of a recurrent neural network controller to supply an adaptive control signal to the exciter or governor with the adaptive law and a compensator to damp the oscillations of power system, is presented in. An indirect adaptive fuzzy PSS used to damp inter-area modes of oscillation following disturbances in power systems is proposed in, which the gains of the controller are tuned via a PSO routine to ensure system stability and minimum sum of the squares of the speed deviations.

4.4 Artificial Intelligent Techniques

Artificial Intelligence Techniques are Artificial Neural Network (ANN), Fuzzy Logic, Intelligent Optimization, Hybrid Artificial Intelligent Techniques and Expert System. The application of fuzzy logic control has been motivated by following reasons: (a) improved robustness over conventional linear control algorithms, (b) simplified control design for difficult system models, (c) simplified implementation. A fuzzy logic based adaptive PSS is proposed in, which neural networks online tune the parameters of fuzzy logic based PSS. An approach based on Traditional Frequency Domain method for designing fuzzy logic based adaptive PSS for multi-machine power systems is presented in. The optimal design of settings of PSS parameters that shift the system eigenvalues associated with the electromechanical modes to the left in the S-Plane using Evolutionary Programming Optimization technique is presented in. The systematic optimal tuning of all parameters PSS based on the Hessian Matrix estimated by Feed-Forward Neural Network and the Eigen value analysis for the linear parameters is presented in, which can improve the system damping performance immediately following a large disturbance. In, the simultaneous stabilization of a power system over a wide range of operating conditions via a single-setting conventional power system stabilizer using GA is investigated.

4.5 H-Infinity Control

It cannot provide good transient behavior. In addition, design is complex because of dynamic output feedback. In robust control theory, $H2$ performance and $H\infty$ performance are two important specifications. In, the effectiveness of the power system stabilizer designed through weighted mixed sensitivity $H\infty$ robust control theory is demonstrated by simulation of a sample power system for various load conditions using MATALB. In an $H\alpha$ optimal control method is design for PSS using a nominal model with an uncertainty description which represents the possible perturbation of a synchronous generator around its normal operating point. A method of designing $H\alpha$ loop shaping based robust PSS for a dynamic equivalent large power system is presented in , which the simulation show that it very effectively.

4.6 Linear Matrix Inequality

Linear Matrix Inequality (LMI) is flexible in controller design since it provides an incredibly powerful way to solve convex or quasi-convex optimization problems. It is the way to specify system dynamic performance. In, the robust control using fuzzy controller is designed by satisfying certain LMI conditions, to improve the angular stability at multiple operating points. A $H2$ controller design approach for PSS based on LMI pole constraints analysis for damping low frequency oscillations is presented in, which the $H2$ robust control guarantees the damping performance for different operating conditions and its robustness is better than that of conventional PSS. In, a mixed $H2/H\alpha$ control that is solved using LMI technique is used as a PSS for a SMIB system, which proposed controller show robustness over a wide range of operating conditions and parameters change.

4.7 Sliding Mode Controls

The parameters of a power system are varied continuously according to the conditions of the generation system, networks, and the load. In Sliding Mode Control (SMC), the parameter insensitivity and the realization simplicity, it is very robust. The main disadvantage in SMC are: (a) stability is dependent on the sampling period when implemented using digital controllers, (b) full state-feedback structure may not be available at all times, and (c) limitation on amount of parameter variations. In, a Neural Networks based Adaptive Sliding Mode Controller has been applied to a PSS of a single machine power system, which Neural Networks are used for online prediction of the optimal SMC gains when the operating point changes. In a model reference discrete time Sliding Mode Controller for design of the PSS is presented, which a number of studies demonstrates the effectiveness of the proposed approach. A PSS for a small-signal stability study using three kinds of controllers to solve the problem of the immeasurable state variables in the conventional sliding mode control is presented in, which the effectiveness of the proposed controller is verified by linear time-domain simulation under normal load operation and under parameter variation of AVR gain.

V. PSS OPTIMAL LOCATION

A PSS on a machine in a power system represents a closed-loop controller. The first step in designing such a PSS to increase the damping of a certain oscillation mode in a multi-machine power system is to find its optimum location. The PSS is important to quickly damping the inter-area oscillations. The probabilistic approach for the optimum location of power system stabilizers is presented in , which the probabilistic

distribution of an eigenvalue is expressed by its expectation and variance under the assumption of normal distribution. Local controllers for machines that need to have stabilizers have been designed in , which by using sensitivity analysis, the relation between system states and oscillatory modes is considered.

VI. OSCILLATION MODES

Power system dynamic performance is improved by damping of system oscillations. The small-signal stability of the following types of electromechanical oscillations is of concern: Local Modes, Inter-Area Modes, Control Modes and Torsional Modes. The PSS are designed mainly to stabilize local and inter-area modes. By varying the terminal voltage, the PSS affects the power flow from the generator, which efficiently damps local modes. Damping of both local and Inter-Area modes requires suitable phase compensation over a wider frequency range, which may be difficult to achieve. Proper tuning and coordination of multiple PSS controller can adequately damp out oscillations with any local rotor angle oscillatory modes. Dynamic stability enhancement of electromechanical modes of multi-machine power systems by means of an adaptive PSS is proposed in , which it is a varietal configuration to self-adjusted tracking system operation condition. A method based on modal decomposition for tuning PSSs for damping of the concerned inter-area mode is proposed in, while minimizing its effect on other modes by weakening the interactions among different modes. An extended quasi-steady-state model of long-term dynamics that includes low-frequency inter-area oscillations can be used effectively for the design of PSS is show in, which all local and intra-area electromechanical oscillations are replaced in this model by algebraic equations.

VII. EFFECT OF PSS ON SSR

SSR is an electromechanical power system instability, which occurs due to interaction between series capacitors and nearby turbine-generators. It can break generator shafts and must be studied and prevented when series compensation is used. The PSS keep the power system in a secure state and protect it from dangerous phenomena. The effects of different types of excitation systems and PSS on the SSR damping characteristics in a SMIB system are studied in, which the effects of the parameters of PSS on the electrical damping are investigated. A LQR based-PSS to control the SSR presented in, which eigenvalue analysis and time domain simulations using a nonlinear system model show that proposed PSS can control the SSR efficiently. The behavioral aspects of two types of PSS in are studied in a fixed series capacitor comp-ensated system employing the IEEE first benchmark system for SSR study.

VIII. PSS AND FACTS DERIVES

Electromechanical oscillations of small magnitude and low frequency exist in the interconnected power system and often persist for long periods of time. PSS and FACTS devices are applied to increase the system stability and improve system performance. They can help the damping of power system oscillations. PSS increases damping torque of a generator by affecting the generator excitation control, while FACTS devices improve damping by modulating the equivalent power-angle characteristic of the system.

Figure 3. Overview of compensation devices

There are several methods proposed in literatures on coordination between PSS and FACTS devices, in multi-machine power systems from different operating conditions viewpoint. Several kinds of FACTS-devices have been developed. It can be divided into two categories as shown in Figure 3. In general, from control of view, FACTS controllers can be divided into four categories: Series Controllers, Shunt Controllers, Combined Series-Shunt Controllers, and Combined Series-Series Controllers.

8.1 Shunt Controller and PSS

An optimal designing method, which is based on adaptive genetic algorithm, is applied in the cooperation control of PSS and STATCOM proposed in, that simulation results show the stability of power angle and voltage can be effectively enhanced. A systematic approach for designing of SVC based damping controllers for damping of low frequency oscillations in a SMIB power system is presented in.

8.2 Series Controller and PSS

The tuning of Proportional Integral Derivative (PID) PSS and TCSC is studied in, which the Genetic Algorithm (GA) is used to search for optimal settings of controller parameters. An output feedback controller for PSS and TCSC based on genetic algorithm in order to damp the low frequency oscillations in a single machine infinite bus is design in, which TCSC located at the terminal of generator, is considered. Based on multivariable model, and by using the concept of the minimization of column dominance measure, a multi-input multi-output controller is designed in to minimize interaction among the control variables of PSS and Series Static Synchronous Compensators (SSSC).

8.3 Series-Shunt Controller and PSS

A control scheme to design an advanced PSS, comprehensive analysis, and result obtained for the dynamic control of power transmission, damping of oscillations with Unified Power Flow Controller (UPFC) presented in. The study and design a controller capable of doing the task of damping in less economical control effort for coordination between PSS and thyristor controlled phase shifter (TCPS) is presented in .

8.4 Series-Series Controller and PSS

In, fuzzy logic controller by selecting effective control signal based supplementary controller is installed with Interline Power Flow Controller (IPFC) to damp low frequency oscillations.

IX. SINGLE-MACHINE INFINITE-BUS

Numerous different control techniques, which are based on classical or optimum control techniques, have been applied to design PSS but many of them are use a linearized model of an electrical machine connected to a power system. The basic block diagram of power system linear model is show in Figure 4 [145], where *K*1 and *K*2 are the constant derived from electrical torque, *K*3 and *K*4 are the constant derived from field voltage equation, and *K*5 and *K*6 are the constant derived from terminal voltage magnitude . The electrical torque can represent as:

$$\Delta T_E = \Delta T_{E1} + \Delta T_{E2} = \underbrace{[K_1 + H_Q(s) + H_P(s)]}_{H_E(s)} \Delta\delta \qquad (1)$$

The action of the PSS is effective through the transfer function block between the electric torque output and the reference voltage input with variation in the machine speed assumed to be zero.

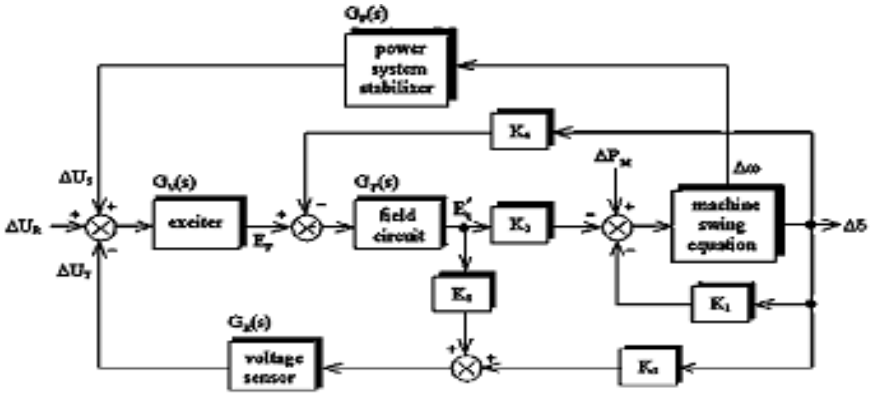

Figure 4. Block diagram of SMIB system

The main objective of designing PSS is to increase the damping torque without affecting the synchronizing torque at critical frequencies. To provide damping, PSS must produce a component of electrical torque in phase with the rotor speed deviations. The *KS* and *KD* are synchronizing torque and damping torque is defined:

$$K_S(\omega) = \mathrm{Re}[H_E(j\omega)] \qquad (2)$$

$$K_D(\omega) = \frac{\omega_b}{\omega}\mathrm{Im}[H_E(j\omega)] \qquad (3)$$

In small oscillations, the damping torque in phase with Δω, and the synchronous torque is in phase with Δδ. They are sensitive to generator operating conditions, parameters of power system network, excitation system and PSS parameters. The block diagram representing the small signal stability model can be simplified as shown in Figure 5, where the transfer functions *HQ*(*s*) and *HP*(*s*) are defined as:

$$H_Q(s) = -\frac{K_2 G_F(s)[K_4 + K_5 G_V(s) G_R(s)]}{1 + K_6 G_V(s) G_F(s) G_R(s)} \quad (4)$$

$$H_P(s) = \frac{K_2 G_V(s) G_F(s) G_P(s)}{1 + K_6 G_V(s) G_F(s) G_R(s)} \frac{s}{\omega_b} \quad (5)$$

$$H_P(s) = \frac{s}{\omega_b} G_E(s) G_P(s) \quad (6)$$

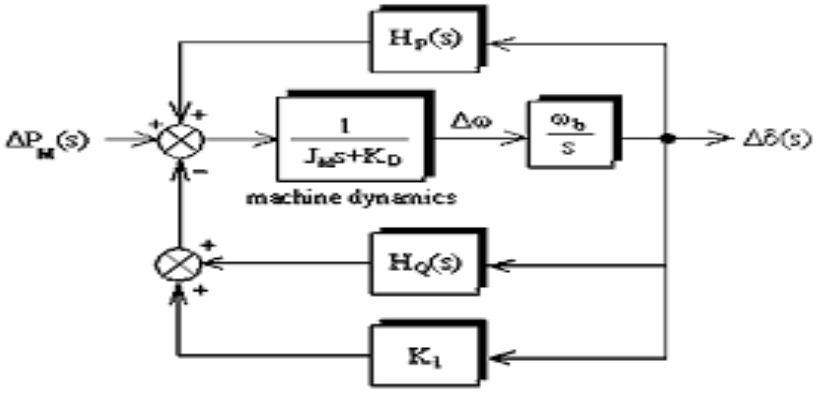

Figure 5. System transfer function model

The control transfer function of excitation system as shown in Figure 6.

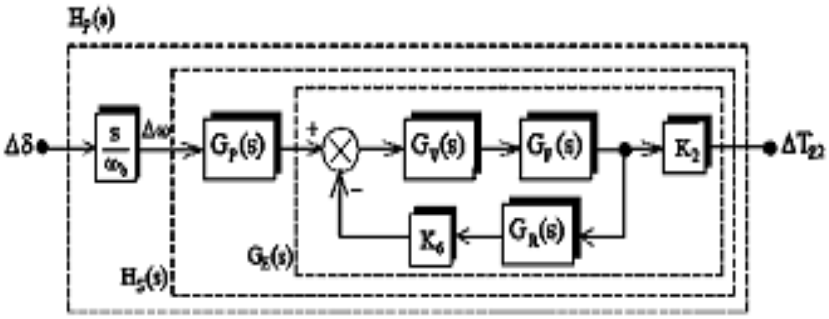

Figure 6. Control block diagram of excitation system

Where *GE*(*s*) is the transfer function of the electrical loop between the incremental terminal voltage (Δ*US*) and the internal voltage variation (Δ*E'q*). The effects of PSS on synchronizing and damping torque components are defined as:

$$K_{s(PSS)}(\omega) = \mathrm{Re}[H_P(j\omega)] \quad (7)$$

$$K_{d(PSS)}(\omega) = \frac{\omega_b}{\omega} \mathrm{Im}[H_P(j\omega)] \quad (8)$$

X. CONCLUSIONS

This paper presents a critical review of the recent philosophies in the area of PSS. A simple, economical and effective for improve the steady-state stability margin, increase system positive damping, suppress low-frequency oscillation of the power system and improve power system dynamic stability is with PSS. It has been widely used in the electric power industry in order to increase the damping ratios of electromechanical modes, extend power transfer limits of system and maintain the reliable operation of the grid.

REFERENCES

[1] Gh. Shahgholian, J. Faiz, "Static Synchronous Compensator for Improving Performance of Power System - A Review", Int. Rev. of Elec. Eng., Vol. 4, No. 2, pp. 2333-2342, Oct. 2010.

[2] M. Farahani, "Damping of Sub-Synchronous Oscillations in Power System Using Static Synchronous Series Compensator", IET Gen., Trans. and Dist., Vol. 6, No. 6, pp. 539-544, June 2012.

[3] M. Bouhamida, M.A. Denai, "Robust Stabilizer of Electric Power Generator Using $H\square$ with Placement Constraints", Jour. of Elec. Eng. (JEE), Vol. 56, No. 7-8, pp. 176-182, 2005.

[4] A.A. Ba-Muqabel, M.A. Abido, "Review of Conventional Power System Stabilizer Design Methods", IEEE/GCC, pp. 1-7, Manama, March 2006.

[5] B. Tang, M.L. McAnelly, G. Gu, "Experimental Parameter Tuning of Power System Stabilizer", IEEE/CCDC, pp. 2132-2137, Taiyuan, May 2012.

[6] J. Murgas, A. Dobrovic, E. Miklovicova, J. Dubravsky, "Two Level Turbogenerator Control System", Jour. of Elec. Eng., Vol. 55, No. 3-4, pp. 83-88, 2004.

[7] A. Safari, R. Jahani, M. Hajinasiri, A.H. Araskalaei, H.A. Shayanfar, "COA Based Coordinated Design of FACTS and PSS Output Feedback Controllers", Int. Rev.of Elec. Eng. (IREE), Vol. 5, No. 6, pp. 2803-2808, Aug. 2010.

[8] H. Taliyat, J. Sadeh, R. Ghazi, "Design of Augmented Fuzzy Logic Power System Stabilizer to Enhance Power System Stability", IEEE Trans. on Ene. Con., Vol. 11, pp. 97-103, March 1996.

[10] M.O. Hassan, S.J. Cheng, Z.A. Zakaria, "Design and Parameters Optimization of Power System Stabilizer to Improve Power System Oscillations", IEEE/ICCAE, Vol. 5, pp. 107-111, Singapore, Feb. 2010.

[11] S. Panda, N.P. Padhy, R.N. Patel, "Robust Coordinated Design of PSS and TCSC Using PSO Technique for Power System Stability Enhancement", Jour. of Elec. Sys., Vol. 3, No. 2, pp. 109-123, 2007.

[12] A. Soos, "An Optimal Adaptive Power System Stabilizer", Master Thesis, Calgary, Alberta, Oct. 1997.

[13] F.M. Hughes, O. Anaya-Lara, G. Ramtharan, N. Jenkins, G. Strbac, "Influence of Tower Shadow and Wind Turbulence on the Performance of Power System Stabilizers for DFIG-Based Wind Farms", IEEE Trans. on Eng. Con., Vol. 23, No. 2, pp. 519-528, June 2008.

[14] S. Jalilzadeh, R. Noroozian, M. Sabouri, S. Behzadpoor, "PSS and SVC Controller Design Using Chaos, PSO and SFL Algorithms to Enhancing the Power System Stability", Ener.and Pow. Eng., pp. 87-95, No. 3, 2011.

[15] A. Dysko, W.E. Leithead, J. Reilly, "Enhanced Power System Stability by Coordinated PSS Design", IEEE Trans. on Power System, Vol. 25, No. 1, pp. 413-422, Feb. 2010.

[16] N.M. Tabatabaei, M. Shokouhian Rad, "Desiging Power System Stabilizer with PID Controller", International Journal on Technical and Physical Problems of Engineering (IJTPE), Issue 3, Vol. 2, No. 2, pp. 1-7, June 2010.

[17] T.T. Nguyen, R. Gianto, "Optimization Based Control Coordination of PSSs and FACTS Devices for Optimal Oscillations Damping in Multi-Machine Power System", IET Gen., Tran. and Dist., Vol. 1, No. 4, pp. 564-573, July 2007.

[18] M. Ahmadzadeh, S. Mortazavi, S. Mohammadzadeh, S.V. Heydari, "Application of Multi Objective Optimization Approach in Designing of Power System Stabilizers and Power System Stability Enhancement", Int. Rev. of Elec. Eng., Vol. 5, No. 6, pp. 2846-2854, Aug. 2010.

[19] M. Solimana, A.L. Elshafei, F. Bendarya, W. Mansoura, "Robust Decentralized PID-Based Power System Stabilizer Design Using an ILMI Approach", Elec. Power System Res., No. 80, pp. 1488-1497, 2010.

[20] M.O. Hassan, S.J. Cheng, Z.A. Zakaria, "Optimization of Conventional Power System Stabilizer to Improve Dynamic Stability", IEEE/ICIEA, pp. 599-604, Taichung, June 2010.

[21] O. Abedinia, N. Amjady, H.R. Izadfar, H.A. Shayanfar, "Multi-Machine Power System Oscillation Damping - Placement and Tuning PSS via Multi-Objective HBMO", Int. Jour. on Technical and Physical Problems of Eng. (IJTPE), Vol. 4, No. 3, pp. 1-8, Sep. 2012.

[22] A. Alfi, M. Khosravi, "Optimal Power System Stabilizer Design to Reduce Low-Frequency Oscillations via an Improved Swarm Optimization Algorithm", International Jour. on Technical and Physical Problems of Engineering (IJTPE), Vol. 4, No. 2, pp. 24-33, June 2012.

[23] T. Henrique, S. Bossa, N. Martins, R. Jovita, G. Correa, D. Silva, P.C. Pellanda, "A Field Test to Determine PSS Effectiveness at Multi-Generator Power Plants", IEEE Trans. on Power System, Vol. 26, No. 3, pp. 1522-1533, Aug. 2011.

[24] R.A. Jabr, B.C. Pal, N. Martins, "A Sequential Conic Programming Approach for the Coordinated and Robust Design of Power System Stabilizers", IEEE Trans. on Power Sys., "Vol. 25, No. 3, pp. 1627-1637, Aug. 2010.

[25] Y.L. Abdel-Magid, M.A. Abido, "Optimal Multi-Objective Design of Robust Power System Stabilizers Using Genetic Algorithms", IEEE Trans. on Power Sys., Vol. 18, No. 3, pp. 1125-1132, Aug. 2003.

[26] Y.S. Qudaih, Y. Mitani, T.H. Mohamed, "Wide-Area Power System Oscillation Damping Using Robust Control Technique", IEEE/APPEEC, pp. 1-4, Shanghai, March 2012.

[27] D. Sabapathi, R. Dhanasekaran, R. Lakshmipathy, "Design of Fuzzy Based Power System Stabilizer for a Multi-Machine System", Int. Jour. of Elec. and Power Eng., Vol. 2, No. 4, pp. 248-253, 2008.

LOCOMOTIVE RAIL POWER DISTRIBUTION SYSTEM (A REVIEW)

Pragati Deb[1], Isha Rajput[2], Aarti Aggarwal[3]

[1(]*Electrical & Electronics Deptt., ABES, Ghaziabad, U.P. (India)*
[2] *(Electrical & Electronics Deptt., ABES, Ghaziabad, U.P. (India)*
[3] *(Electronics and communication Deptt., ABES, Ghaziabad, U.P. (India)*

ABSTRACT

Conventionally locomotives are connected in succession to add motive powers of the locomotives depending on the train length and power requirements. In this scheme the pulling force is not uniformly distributed throughout the length of the train which affects adversely hauling capacity , fuel efficiency, train safety , brake pipe pressure etc. It overall gives an inefficient and unsafe operation for longer trains. In a microprocessor based locomotive, a computer is located usually in the driver's cab which controls most of the locomotive operations. When the locomotives are joined together in succession, control signals are transferred from one locomotive to the adjacent locomotive via coupling between two connectors, those are located at the front and rear of the locomotives. Control signals are transferred to a connector from computer via a bus. It is a physical connection between locomotives. These two or more locomotives joined together are called multiple unit or multiple consist. First locomotive in the direction of motion of a train becomes the lead locomotive and other becomes simply consists. For example Indian Railways uses multiple unit operation of locomotives to add the motive powers of the locomotives but not Distributed Power. In this paper a concept of Distributed Power (DP) has been given to obtain an optimized performance of a train and an architecture to achieve DP has been proposed. This enables distribution of power along the train which enhances hauling capacity, fuel efficiency, more uniform and controlled coupling forces, and allows quicker brake pipe charging and efficient operation.

Keywords: Multiple Consists, Distributed Power (DP), Lead Locomotive, DP Computer, Locomotive Computer.

I. INTRODUCTION

Distributed power means the placing of additional locomotives at intermediate points in the middle of the train, remotely controlled from the lead locomotive. Distributed power thus describes the physical distribution throughout the length of a train of separate motive power groups. Such 'groups' may be single units or multiple consists. While locomotive consist refers to having one or more locomotives in succession, connected together so as to provide motoring and /or braking capability. The train can have more than one consist in its composition. Specifically, there can be a lead consist, and more than one remote consists. A system for establishing distributed power operations of the locomotive consist from a single location includes a communication network [3] providing communications to and from at least one distributed power system, and a distributed power setup unit in communication with the distributed power system [1]. Without wireless

communication network or a remotely controlled system , a train having locomotives that may operate in distributed power are set up manually, usually at a rail yard. Operators must physically enter each locomotive to enter data into the distributed power system aboard the locomotive to enable “linking” of the locomotives so that distributed power operations may commence. For example, suppose locomotives are included in a train where the locomotives may be facing different directions, meaning that some may be facing forward whereas others may be facing backward. The operator must physically enter each locomotive and select the direction the locomotive should motor. The operator must also initiate and attempt to complete the linking process prior to any unforeseen problems with equipment or systems in the train being detected. Train operators and owners may realize a financial savings and reduction in manpower from remotely setting up, linking and testing distributed power operations of a train. With a remotely controlled distributed power [3], railroads can optimize the distribution of power and braking control over the entire length of a train. A locomotive that has been fitted with Distributed Power (DP) equipment may be set up as either a Lead or Remote 'active' unit; the Lead unit being the controlling locomotive. Only one distributed power-equipped locomotive in any Lead or Remote consist (group) is active. Other locomotives coupled to this 'active' unit operate conventionally as multiple units [2]. There are two basic modes for over-the-road distributed power operation. Locomotive control can be *synchronous*, whereby control commands made by the engineer in the Lead unit are transmitted instantly via radio telemetry to - and are followed immediately by - all Remote units in the train, or *independent* whereby the engineer may set up and independently operate the Remote locomotives as a 'front' and a 'back' group [4]. The front group always includes the Lead locomotive, and all Remote locomotives in the front group follow the commands made by the engineer using the Lead locomotive controls. Which Remote locomotives are in the front or back groups are selectable by the engineer in real time. One DP train cannot affect another DP train and an individual DP - equipped locomotive not in a train cannot affect any DP train or other individual DP locomotive regardless of proximity. When operating in distributed power, an operator, usually located in the lead locomotive, can control operating functions of remote locomotives in the remote consists via a control system, such as a distributed power control element. Thus when operating in distributed power, the operator can command each locomotive consist to operate at a different notch power level (or one consist could be in motoring and other could be in braking), or each individual locomotive in the locomotive consist operates at the same notch power. Wireless System provides a RF link between the Lead and Remote Locomotive(s) [1].The Lead Locomotive gains Wireless Control over the consist.

II. PROPOSED SCHEME AND ARCHITECTURE

Embodiments of the scheme are directed towards a system, method, and a computer software code for remotely establishing distributed power operations of a train [3]. A system for establishing distributed power operations of a locomotive consist from a single location in a locomotive consist that has a lead locomotive and/or a remote locomotive with a distributed power system on each locomotive in the locomotive consist is considered. The system includes a communication network. The distributed power setup unit has minimum a processor, display, and/or an input device to allow a user to establish distributed power operations. The method is for autonomously establishing distributed power operations of a locomotive consist from a single location where the locomotive consists has a lead locomotive and/or a remote locomotive with a distributed power system on each locomotive [2]. It includes receiving data remotely from a distributed power system on a locomotive specific to the

locomotive, and involves sending data remotely to the distributed power system on the locomotive pertaining to distributed power settings to configure the locomotive for distributed power operations. A computer software code is to be used. The computer software code is for autonomously establishing distributed power operations of the locomotive consist from a single location that has a processor. The locomotive consist has a lead locomotive and/or a remote locomotive with a distributed power system on each locomotive and a processor connected to each distributed power system. The computer software code includes a computer software module for receiving data remotely from a distributed power system on a locomotive specific to the locomotive; A computer software module is to be used for sending data remotely to the processor connected to the distributed power system on the locomotive pertaining to distributed power settings to configure the locomotive for distributed power operations. It also includes a computer software module for confirming the locomotive is configured for distributed power operations. A data collection, data management and wireless transmission system, provides railroads with locomotive data. Fig.1 shows DP architecture and functional diagram.

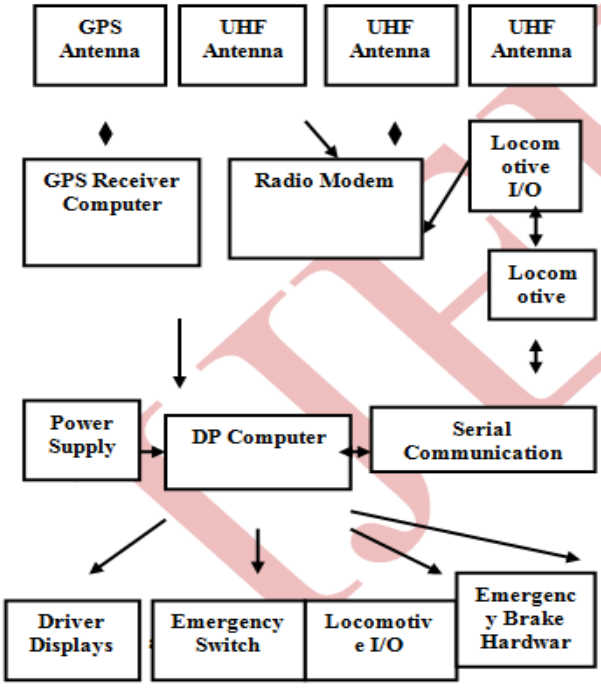

Fig1: DP Architecture and Functional Diagram

III. DISCUSSION

Conventionally locomotives have microprocessor based control on their operations; thereby locomotives are fitted with a computer which controls operations of different locomotive systems. It receives various inputs via sensors and sends signals to control locomotive operations. When two locomotives are coupled together in succession then one locomotive works as a lead locomotive and control signals are transferred via a physical connector between the locomotives. But this is a multiple unit operation [5] not a distributed power. In a distributed power operation same connector signals are to be transmitted to different multiple units via a wireless system and these multiple units work together in coordination. DP computer is connected to Lead Locomotive Computer as add on via a serial communication link. It accesses all important features from Locomotive Computer and transmits them via radio modem and UHF antenna to other multiple units where they

have similar system. A GPS antenna gives location of the locomotive. Four antennas are to be used one GPS and three UHFs. Three UHF antennas have one transmitter and two receivers to have strong reception. All these communicate with DP Computer which is energised by a power supply. And this DP Computer communicates bidirectional with Locomotive Computer via a serial communication physical link. Two driver displays are used to view input and output signals and facilitate locomotive operations. Locomotive I/O signals and emergency brake control signals to be transmitted to other multiple units via wireless communication system. Every locomotive in distributed power is to be fitted with such system. There is a serial communication between locomotive computer and DP computer under a protocol say CAN bus for better speed. Motoring, Braking and other locomotive operations should be in coordination with the lead locomotive otherwise coupling forces between may lead to train partitioning or an accident. A Software is needed to control operations between DP Computer and Locomotive Computer. Usually locomotives have microprocessors of different make they need to share their architecture and information to communicate with wireless system or a common platform is required for software and microprocessors.

IV. CONCLUSION

An architecture for distributed power application in locomotives using a wireless system for train optimization has been proposed and implementation of given architecture should establish an automatic distributed power system via a wireless communication network and railroads can optimize the distribution of power and braking control over the entire length of a train.Train operators and owners may realize a financial savings and reduction in manpower from remotely setting up, linking and testing distributed power operations of a train. A data collection, data management and wireless transmission system, provide railroads with locomotive data well beyond the capabilities of a traditional system.

REFERENCES

[1] A. T. Chronopoulos, J. Sarangapani, S. Ponipireddy, ”Distributed Power Control in Wireless Communication Systems”, at the IEEE International Conference on Computer Communications and Networks (ICCCN 2002), Oct. 2002, pp 493-496.

[2] Lustig, David. (September 2010). "Freight Train, Unbounded: Distributed power: It's a bigger deal than you think". Trains Magazine (Kalmbach) 70 (9).

[3] Method, system, and computer software code for automated establishment of a distributed power train, US 8280566 B2, Robert James Foy, James Glen Corry

[4] Railroad vehicles, IEEE Transactions on Vehicular technology, 2011, 60, 2,406–420.

[5] S.Lu, S. Hillmansen, and C.Roberts, “A power-management strategy for multiple-unit.

PERFORMANCE ANALYSIS OF CCGT POWER CYLCE USING MAT LAB CODING

Neelam Khandelwal[1], Nikita Agarwal [2], Binit Kumar Jha[3]

[1]*Assistant Professor, Department of Manufacturing Technology, JSSATE, Noida (India)*
[2]*Assistant Professor, Department of Manufacturing Technology, JSSATE, Noida (India)*
[3]*Professor & Head Department of Manufacturing Technology, JSSATE, Noida (India)*

ABSTRACT

A combined cycle is a synergistic combination of two or more power cycles operating at different temperatures running independently. Normally the cycles are classified as a 'topping' and a 'bottoming' cycle. Presently, the gas steam combined cycle is widely accepted, where Brayton Cycle has high source temperature and rejects heat at suitable temperature that is conveniently used as the energy source for the Rankine Cycle. The performance of combined cycle depends upon number of parameters like TIT, component efficiencies, turbine exhaust temperature, degree of supplementary firing and condition of steam generation. Our work is to find specific work output and optimize the thermal efficiency of combined cycle by reheating without supplementary firing and reheating with supplementary firing when steam is generated at 12 bar 325^{0}C for a given set of parameters like temperature, pressure ratio and A/f ratio. MAT lab coding has been used for validation of research work.

Keywords: Combined Cycle, Optimization, Steam turbine, Gas turbine, Efficiency, Supplementary heating, , A/F ratio, Pressure ratio.

I. INTRODUCTION

The introduction of combined cycle had opened new avenues in the field of power generation. The gas turbines that were initially used in peak load power generation and emergency conditions could be used in base load power generation. Combined Cycle is a synergistic combination of gas cycle and power cycle. Thus performance of combined cycle depends upon the performance of gas cycle and steam cycle. So in order to achieve this objective the parameters that affect the performance of gas turbine (maximum temperature, component efficiency, a/f ratio and pressure ratio) the limitations that restrict the performance of gas turbine (space, cost and metallurgical limitations) were determined .One of the major limitations of gas cycle is the unavailability of materials that could withstand high temperature. So, gas turbines are provided with high a/f ratio to maintain the temperature of turbine blades. Due to this turbine exhaust have high amount of unused oxygen in which additional fuel can be burnt. Thus concept of supplementary heating comes into picture.

S. De and P.K. Nag[1] has been done the exergy analysis of various components at different degree of supplementary heating . It is found that the most favorable benefit of supplementary heating is for a low temperature ratio only and for

higher temperature ratio gain in work output is at an expense of overall efficiency of the plant. .Louis JF Hirao Ka K and E.I. Masri M.A [2] have proposed the comparative study of the influence of different means of turbine cooling on gas turbine performance G.CARRY et. Al. [3] has discussed the effect of steam cycle regeneration on combined cycle. They find out that efficiency could rise for low turbine pressure ratio and for small regeneration degree and regeneration degree causes an increase in efficiency when it is small enough .Considerable work on comparative evaluation of advanced combined cycle alternatives is reported in literature [4].IG RICE [5] have discussed the effect of pressure ratio and firing temperature on power output, thermal efficiency, turbine exit temperature. According to this reheat cycle gas turbine efficiency is degrade slightly over the simple cycle for equal firing temperature and the reheat cycle gas turbine output is increased significantly. It has been also mentioned that as the pressure ratio is increased the compressor discharge temperature also increase. However gas generator exit temperature decreases with increase in pressure ratio. He emphasize on the role of pressure ratio on specific power output and thermal efficiency. And find that as the pressure ratio for compression increases the specific work output for gas turbine increases whereas work output in steam turbine is decrease .M.A. Da Cunha et. Al. [6] has discussed the concept of inter cooling and reheat for gas turbines and the effect of position of inter-cooling and reheating on gas turbine performance. In our analysis we discuss the optimized efficiency of the combined cycle with given sets of constraints and variables. The optimized result will give the maximum efficiency of the Combined Cycle which defines the running conditions of both the Gas Turbine and Steam Turbine Cycles. In 2012 Thamir K. Ibrahim 2(7) has discussed the effect of compression ratio on performance of Combined Cycle Gas Turbine. R-I Crane [8] has discussed the critical analysis of the thermodynamic advantages of reheat in Gas Turbines.

In the present analysis, the specific work output and thermal efficiency of combined cycle is determined at different a/f ratio in the range of 50-130 and pressure ratio in the range of 4-40. It is observed that specific work output and thermal efficiency improve at lower a/f ratio and higher-pressure ratio.

II. THERMODYNAMIC MODELING OF COMBINED CYCLE

In the present analysis of combined cycle, the effect of various parameters like a/f ratio), pressure ratio on specific work output and thermal efficiency. The effect of reheat, supplementary heating and condition of steam generation i.e. pressure and temperature on specific work output and thermal efficiency are also analyzed.

To analyze the present study the methodology adopted are

Firstly calculate worknetl, work net2 and efficiency 1, efficiency 2 at different a/f ratio and pressure ratio for

a) Reheat , inter-cooling without supplementary firing

b) Reheat , inter-cooling with supplementary firing

when the steam is generated at 12 bar and 325^{o}C

Once the exhaust gas has temperature higher than the temperature needed for steam generation, the steam cycle would contribute.

Thus we can calculate work3 and efficiency3. Here,

work 3 = work net 1 + work net 2

efficiency 3 = efficiency 1 + efficiency 2

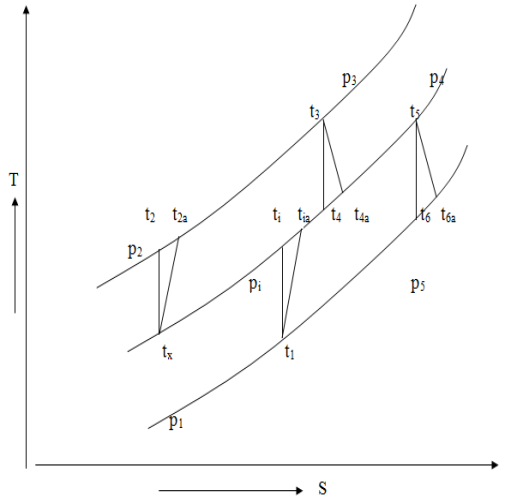

Fig. 1 Gas Turbine Cycle (Brayton Cycle) without Supplementary heating with Reheat and with Inter-cooling.

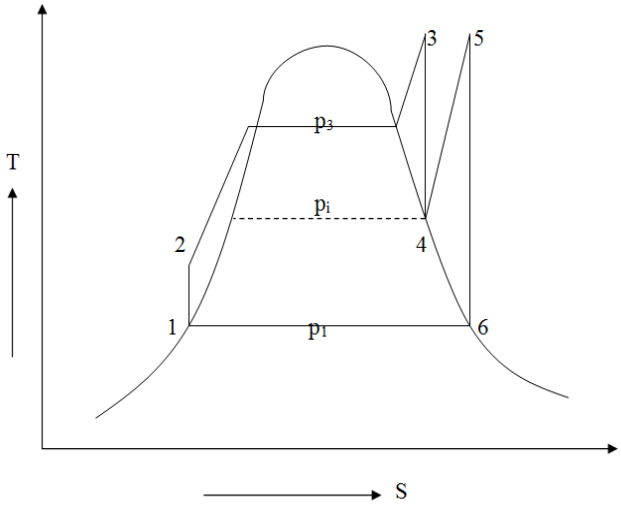

Fig. 2 Rankine Cycle without Supplementary heating with Reheat and with Inter-cooling.

III. ANALYSIS OF GAS TURBINE CYCLE

3.1 With Reheat Without Supplementary Heating

$$\frac{t_i}{t_1} = \frac{p_i}{p_1}^{\gamma-1/\gamma}$$

where $\frac{\gamma-1}{\gamma} = 0.2857$

Also, $p_i = \text{sqrt}(p_1 \times p_2)$, where Sqrt = Square Root

Now,

$$\frac{t_i - t_1}{t_{ia} - t_1} = \eta_c$$

$$t_{ia} = \frac{t_i - t_1}{} + t_1$$

η_c

Now, similarly

$$t_{2a} = \frac{t_2 - t_x}{\eta_c} + t_x$$

Here, for perfect inter-cooling, $t_x = t_1$

So $$t_{2a} = \frac{t_2 - t_1}{\eta_c} + t_1$$

Now, to calculate t_3

$m_f \times L.C.V = (m_f + m_a) \times C_{pg} \times (t_3 - t_{2a})$

$m_a = 1 \times a/f$

$$t_3 = \frac{m_f \times L.C.V}{(m_f + m_a) \times C_{pg}} + t_{2a}$$

$$\frac{t_3}{t_4} = \left(\frac{p_3}{p_4}\right)^{0.2857}$$

and $p_4 = \text{sqrt}(p_3 \times p_5)$

$$t_4 = \frac{t_3}{(p_3 / p_5)^{0.2857}}$$

and $t_5 = t_3$

$$t_6 = \frac{t_5}{(p_4 / p_5)^{0.2857}}$$

$$\eta_t = \frac{t_5 - t_{6a}}{t_5 - t_6}, \quad t_{6a} = t_5 - \eta_t (t_5 - t_6)$$

Here,

$w_t = (m_f + m_a) \times C_{pg} \times (t_3 - t_{4a} + t_5 - t_{6a})$

and

$w_c = m_a \times C_{pa} \times (t_{2a} - tx + t_{ia} - t_1)$

Now,

$$\text{Thermal Efficiency} = \frac{\text{Work 1}}{m_f \times L.C.V + (m_f + m_a) \times C_{pg} \times (t_5 - t_{4a})}$$

3.2 Reheat With Supplementary Heating

We have,

$$w_t = Z \times (m_f + m_a) \times C_{pg} \times (t_3 - t_{4a} + t_5 - t_{6a})$$

IV ANALYSIS OF STEAM CYCLE

4.1 With Reheat Without Supplementary Heating

Mass of steam generated by utilization of waste energy.

$$\text{Work (steam)} = m_s \times (h_3 - h_2)$$

Now to calculate 'm_s'

$$m_s = \frac{(m_f + m_a) \times C_{pg} \times (t_8 - t_9)}{(h_3 - h_2)}$$

Also,

$$\text{work net 2} = \frac{\text{(work 2)}}{(m_f + m_a)}$$

$$\text{Efficiency 2} = \frac{\text{(work 2)}}{m_f \times L.C.V + (m_f + m_a) \times C_{pg} \times (t_5 - t_{4a})}$$

4.2 With Supplementary Heating With Reheat With Inter Cooling

To calculate mass of steam

$m_s(h_1 - h_{f3}) = Z \times (m_f + m_a) \times C_{pg} \times (t_8 - t_9) + Z_a \times m_f \times L.C.V$

Here $Z_a = 1 - Z$,

Where Z is supplementary fuel fired.

$$m_s = \frac{Z \times (m_f + m_a) \times C_{pg} \times (t_8 - t_9) + Z_a \times m_f \times L.C.V}{(h_3 - h_2)}$$

$$\text{work net2} = \frac{\text{work2}}{}$$

$(m_f + m_a)$

Here,

$$Efficiency\ 2 = \frac{work2}{m_f \times L.C.V + (m_f + m_a) \times C_{pg} \times (t_5 - t_{4a})}$$

V. ANALYSIS THROUGH MATLAB CODING

5.1 – Analysis Of Combined Cycle With Reheat Without Supplementary Heating

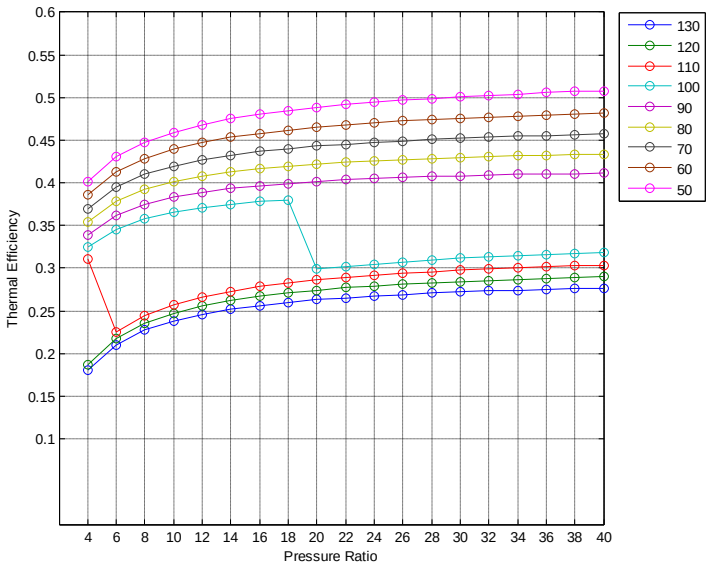

Fig. 3: Thermal Efficiency v/s Pressure Ratio at Different A/F Ratio with Reheat without Supplementary Heating When Steam is generated at 12 bar 325^{0}C

The Optimized Value of Efficiency at Air/Fuel Ratio 50.00 and Pressure Ratio 40.00 is 0.508.

1) Steam cycle become effective for A/F ratio 110 and lower.

2) At A/F ratio of 100 Efficiency 3 increases from pressure ratio 4 to pressure ratio 18. Efficiency 3 decreases sharply in the range of 18 to 20 bars. From 20 bar onward Efficiency 3 continuously increase with pressure.

3) At a particular pressure ratio the Efficiency 3 increases with lowering of A/F ratio.

4)It is also seen that Efficiency 3 continuously increases with pressure for all A/F ratio.

5)The optimized value of Efficiency 3 is at A/F ratio 50 and pressure ratio 40.

5.2 – Analysis Of Combined Cycle With Reheat With Supplementary Heating.

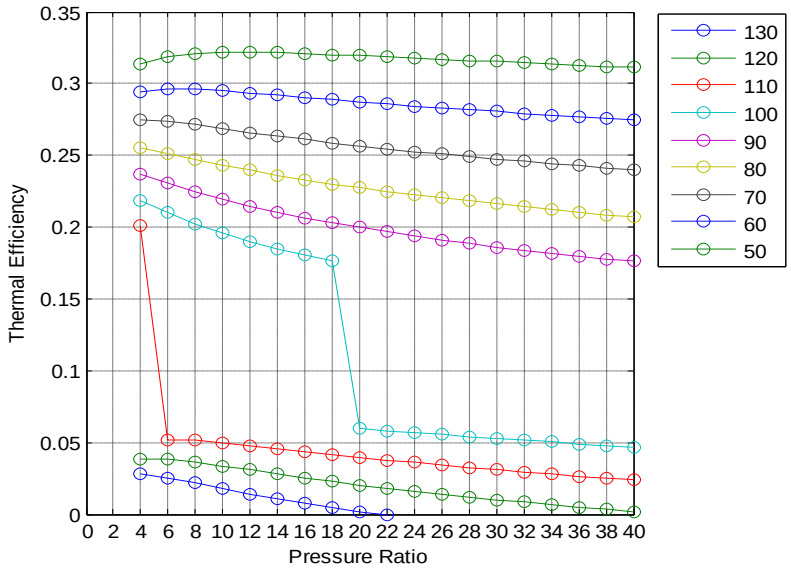

Fig.4 : Thermal Efficiency v/s Pressure Ratio at Different A/F Ratio with Reheat with Supplementary Heating When Steam is generated at 12 bar 325^{0}C

The Optimized Value of Efficiency at Air/Fuel Ratio 50.00 and Pressure Ratio 10.00 is 0.322.

1) The steam cycle becomes effective for A/F ratio 110 and lower.

2) It is seen that when steam is generated at high pressure and temperature, Efficiency 3 increases.

3) The optimization point-shift downward if we opt for lower A/F ratio and is located at A/F ratio 50 and pressure ratio 10.

VI. CONCLUSION

Turbine exit temperature is decreasing as pressure ratio is increased keeping A/F ratio constant because turbine maximum temperature does increase with pressure ratio but this effect is marginalized by the increase of expansion ratio owing to higher pressure ratio. At a particular pressure ratio if a higher A/F ratio is optimized then turbine maximum temperature goes on decreasing as the mass of fuel is constant and at higher A/F ratio the heat released due to combustion of same mass of fuel is used for raising the temperature of higher quantity of flue gas resulting in low temperature of turbine inlet temperature. In the gas turbine cycle the efficiency first increase and then decreases with increasing pressure ratio when steam is generated at, 12 bar 325^{0}C with reheat .A steam cycle does not effective at higher A/F ratio. Generally steam cycle is effective at A/F ratio 110 and less than it. Efficiency of steam cycle is decreases as pressure ratio increases when steam is generated at 12 bar 325^{0}C, with or without reheating and with or without supplementary heating. In combined cycle for A/F 130 to A/F 100 the turbine exit temperature is less than 325^0 C i.e. (the condition of Steam generated)so steam cycle does not contribute and, Efficiency = Efficiency 1.Steam cycle became effective at A/F ratio of 100 and lower. Here Efficiency = Efficiency 1 + Efficiency 2.At a particular pressure ratio the efficiency of combined cycle is increases at lower A/F fuel ratio.

NOMENCLATURE

m_f	Mass of fuel
m_a	Mass of Air
a/f	Air Fuel Ratio
η_c	Isentropic compressor efficiency
η_t	Isentropic turbine efficiency
h_1	Enthalpy of steam at turbine Inlet temperature
h_2	Enthalpy of steam after expansion in turbine.
h_{f3}	Enthalpy of feed water after considering pump work.
Work 1	Work output in gas turbine per kg of fuel burnt.
Work net 1	Work output in gas turbine cycle per kg of flue gas.
m_s	Mass of steam
Work 2	Work output (steam cycle.) per kg of fuel burnt.
Work net 2	Work output (steam cycle.) per kg of flue gas.
Efficiency 1	Thermal efficiency for gas turbine cycle.
Efficiency 2	Thermal efficiency for steam cycle.
Work 3	Specific work output for combined cycle.
Efficiency3	Thermal efficiency for combined cycle.
p_2	Compressor exit pressure.
t_2	Compressor exit temperature.
t_3	Turbine Inlet Temperature
t_4	Isentropic Turbine Exit Temperature (w/o Reheating)
t_5	Temperature after Reheated.
t_6	Isentropic Turbine exit temperature (with Reheating).
p_3	Pressure in combustion chamber for gas turbine cycle.
p_4	Reheat Pressure.
t_i	Isentropic Temperature of air after intercooler.
p_i	Intercooler Pressure.
T.I.T	Turbine Inlet Temperature
w/o	Without
H.R.S.G	Heat Recovery Steam Generator
H.P.C	High Pressure Compressor
L.P.C	Low Pressure Compressor
H.P.T	High Pressure Turbine
L.P.T	Low Pressure Turbine
t_i	Actual temperature of air after passing low pressure Compressor
t_{2a}	Actual temperature of air after passing high pressure Compressor

t_{4a}	Actual temperature of flue gas after passing high pressure Turbine
t_{6a}	Actual temperature of flue gas after passing low pressure Turbine
t_x	Temperature of air after passing through intercooler.
w_t	Work output of turbine.
w_c	Work required in the compressor.
t_{ia}	Actual temperature after compression
L.C.V	Lower Calorific Value.
.p_1	Ambient pressure.
t_1	Ambient temperature.
C_{pg}	Specific heat of flue gas.
C_{pa}	Specific heat of air.
Z	The percentage of fuel that is burnt in Combustion Chamber when supplementary heating is considered.
Z_a	The percentage of fuel that bypass the Combustion Chamber when supplementary heating is considered.

REFERENCES

[1] S-De and P.K. Nag, "Effect of Supplementary Firing on the Performance of an Integrated Gasification Combined Cycle Power Plant" I Mech E, Vol. 214 Part A, 2000

[2] Louis JF Hirao Ka K and E.I. Masri M.A. "Comparative study of the influence of different means of turbine cooling on gas turbine performance" ASME paper 83 - GT 180.

[3] G.CARRY and A.COLAGE July "Steam cycle regeneration influence on Combined Gas-Steam power plant performance" ASME paper, 1985

[4] Bolland April, "A Comparative Evaluation of Advanced Combined Cycle Alternatives". Journal of Engineering for Gas Turbine and Power, Vol.113 Pages 190-202, 1991

[5] I.G Rice January "The Combined Reheat Gas Turbine & Steam Turbine Cycle" Journal for Engineering for power vol. 102, PP 35-41, 1980

[6] M.A Da Cunha Alves H F De Franca Mendes Carneiro, J R Barbosa, l.E.Travieso, P pilidis and K W Ramsden, "An insight on inter-cooling and reheat Gas Turbine". Proc Institute of Mechanical Engineers Vol. 215 Part A, 2001

[7] Thamir .K.Ibrahim "Thermodynamic analysis of gas turbine power plant" internal journal of physical science vol 6 (14), 2011

[8] R-I Crane,1998 "A Critical Analysis of the Thermodynamic Advantages of Reheat in Gas Turbines." Proc Institute Mech. Engineers Vol 212 Part A.

[9] Cohen H. Rogers, Gas Turbine Theory (G.F.C. and Sarvanmutto HIH, 1972) 4th Edition.

[10] Cox H.R., Gas Turbine Principles and Practice (George Newton Ltd. London, 1955)

[11] R.Yadav, Steam and Gas Turbines(Central Publishing House, Allahabad).

ROBUST FORMANT TRACKING ALGORITHM IN REAL TIME NOISE ENVIRONMENT

Mandeep Singh Walia

Assistant Professor, Department of Electronics and Communication Engineering, UIET, Panjab University SSG Regional Centre (India)

ABSTRACT

The traditional approaches for formant frequency estimation are misled by spectral peaks in unvoiced speech and perform very poorly in transient background noise. Also, these traditional algorithms are not robust in real life noise environment and are unable to recover quickly after periods of silence. Robust formant tracking algorithm is discussed. Testing of the algorithm using various speech sentences has shown promising results over a wide range of signal to noise ratio's (SNR's) for various types of background included the babble (crowd of people), car, exhibition hall, restaurant, street, airport, train station and train recordings from different places. By observing the limitations of the traditional formant tracking algorithms it can be seen that the robust formant tracking algorithm is the most accurate algorithm. Results from algorithm showed that the robust formant tracking algorithm gives very good tracking performance in every environment.

Keywords*: AZF, *CEFS, DTF, LPC, Vocal Tract.

I. INTRODUCTION

The resonance frequencies of the vocal tract are called the formant frequencies or formants when vowels are pronounced. Formants can be found where there are large concentrations or peaks of energy in the spectrogram reading of a voiced sample. Accurate formant estimation for continuous speech (in real time noise environments) is a challenge because formant frequencies are not simple to track in such a dynamic environment. The formant estimation algorithm needs to be robust and be able to operate in a wide range of real-time noise scenarios. The vocal tract is generally considered as the speech production organ above the vocal folds. As the acoustic wave passes through the vocal tract, its frequency content (spectrum) is altered by the resonances of the vocal tract. Vocal tract resonances are called formants. Thus, the vocal tract shape can be estimated from the spectral shape (e.g., formant location and spectral tilt) of the voice signal. Voice verification systems typically use features derived only from the vocal tract. The human vocal mechanism is driven by an excitation source, which also contains speaker-dependent information. The excitation is generated by airflow from the lungs, carried by the trachea (also called the "wind pipe") through the vocal folds (or the arytenoids cartilages). The excitation can be characterized as phonation, whispering, frication, compression, vibration, or a combination of these. Then model is made as like human speech production model.
The robust formant tracking algorithm discussed in the present work is the most accurate formant tracking algorithm. This algorithm provides reliable formant frequency estimates for contrast enhanced frequency shaping (CEFS) amplification (R. L. Miller, B. M. Calhoun, E. D. Young, 1999) and other applications. The

Robust formant tracking algorithm (K. Mustafa and I. C. Bruce, 2006) is the most accurate algorithm for tracking formant frequencies of a speech signal. The paper is organized as follows. Section II gives an overview of traditional formant estimation techniques. Section III describes the proposed robust formant tracking algorithm. In section IV, experimental results are presented, and conclusions are given in section V.

II. TRADITIONAL FORMANT ESTIMATION TECHNIQUES

Development of accurate formant estimation algorithms began in the 1950s. Since then numerous techniques have been proposed for formant analysis. Most of the work can be classified as frequency domain techniques (such as picking peaks in the short-time frequency spectrum), parametric techniques (also called "analysis by synthesis") (R. W. Schafer and L. R. Rabiner, 1970) in which one generates a best match to the incoming signal based on a model of speech production.

III. TRADITIONAL FORMANT ESTIMATION TECHNIQUES

The traditional formant tracking algorithms do not track formants accurately. Robust formant tracking algorithm (K. Mustafa and I. C. Bruce, 2006), represent the best known formant analysis techniques and have been implemented in MATLAB. Fig. 1 shows a block diagram of the Robust Formant Tracker. A speech samples has been taken as an input signal for which formant estimation and tracking has to be done. After taking speech signal the first step in formant tracking with this algorithm is silence removal and pre-emphasis. Silence detection is usually based on the measuring some signal characteristics as relative energy level, zero crossing rate, first autocorrelation coefficient, first LPC linear predictor coefficient, first Mel – frequency cepstrum coefficient, and normalized prediction error. The easiest method proposed in this work to detect silent regions in speech is based on the computing of variations of the signal samples in speech frame, against the frame mean. If variations are big enough, the frame is considered as a speech frame, otherwise as a silence. Silent region is detected in the ways shown in Fig. 2 and Fig. 3. First, the mean of the frame samples is computed and then cumulative sum of absolute magnitude of differences between samples and mean is collected. Then if this sum exceeds predefined threshold the frame is considered as a speech frame, otherwise as a silent frame. Pre-emphasis is a system process designed to increase, within a band of frequencies, the magnitude of some (usually higher) frequencies with respect to the magnitude of other (usually lower) frequencies in order to improve the overall signal-to-noise ratio by minimizing the adverse effects of such phenomena as attenuation differences or saturation of recording media in subsequent parts of the system. Voiced speech signals have a natural spectral tilt, with the lower frequencies (below 1 kHz) having greater energy than the higher frequencies. The lower frequencies have more energy because they contain the glottal waveform and the radiation load from the lips. In some speech processing applications it is desirable that this spectral tilt be removed by pre-emphasis or spectral equalization of the signal. A common method of pre-emphasis is to filter the speech signal using a High-Pass Filter (HPF) that attenuates the lower frequencies. Pre-emphasis is a system process designed to increase, within a band of frequencies, the magnitude of some (usually higher) frequencies with respect to the magnitude of other (usually lower) frequencies in order to improve the overall signal-to-noise ratio by minimizing the adverse effects of such phenomena as attenuation differences or saturation of recording media in subsequent parts of the system. Voiced speech signals have a natural spectral tilt, with the lower frequencies (below 1 kHz) having

greater energy than the higher frequencies. The lower frequencies have more energy because they contain the glottal waveform and the radiation load from the lips. In some speech processing applications it is desirable that this spectral tilt be removed by pre-emphasis or spectral equalization of the signal. A common method of pre-emphasis is to filter the speech signal using a High-Pass Filter (HPF) that attenuates the lower frequencies. The result of the pre-emphasis is the approximate removal of the contribution of the glottal waveform and the radiation load effect from the lower frequencies of the signal, i.e. the energy in the speech signal is redistributed to be approximately equal in all frequency regions. Fig. 4 shows a spectrogram of a speech signal before and after it has been pre-emphasized using the filter from

Fig. 5.

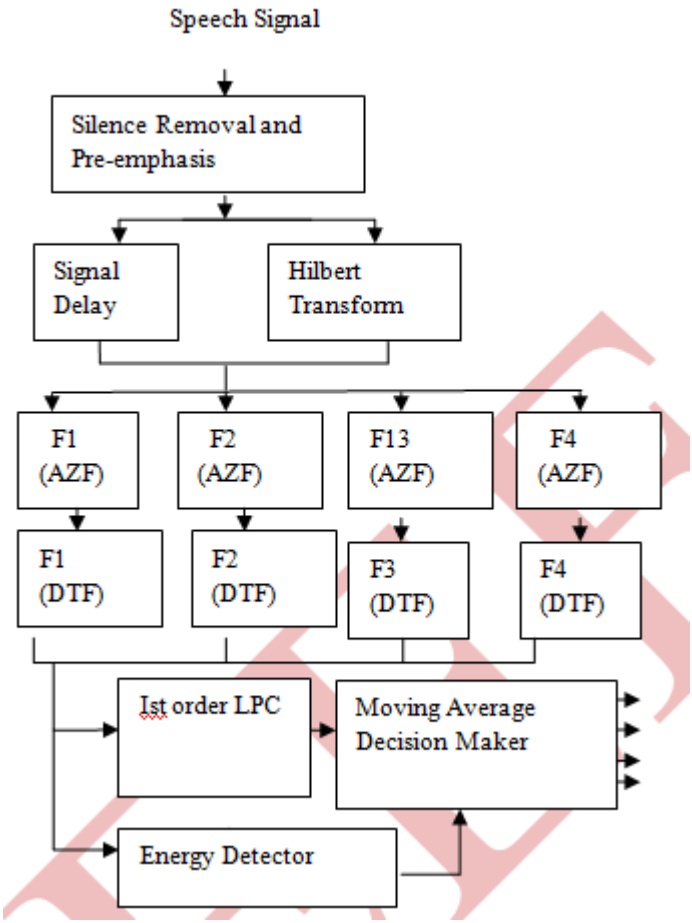

Fig. 1: Robust Formant Tracker

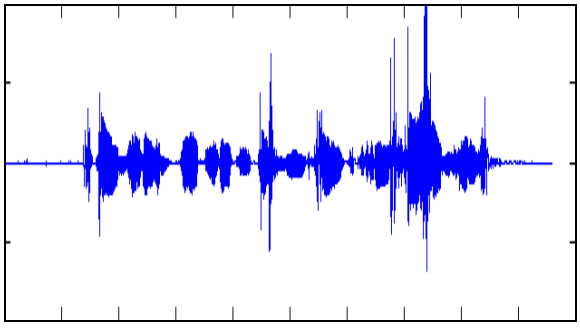

Fig. 2: Waveform Before Silence Removal

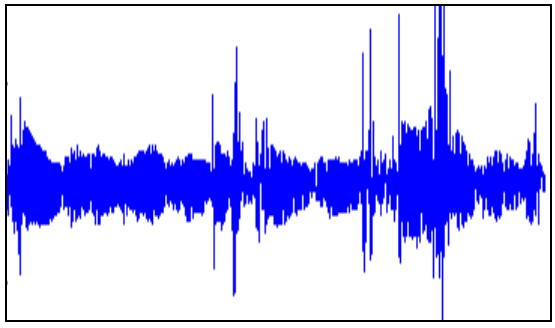

Fig. 3: Waveform After Silence Removal

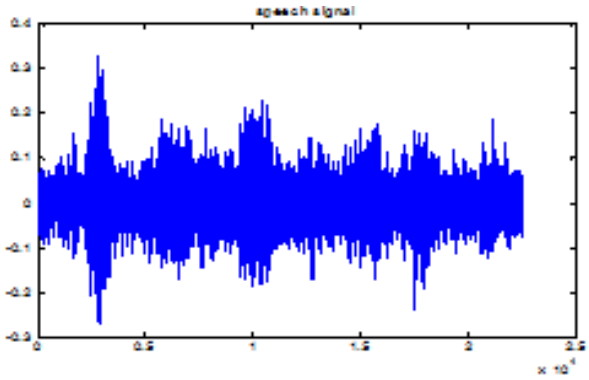

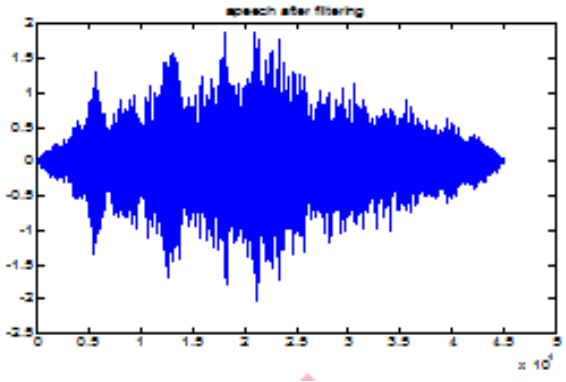

Fig. 4 Waveform before pre-emphasis **Fig. 5: Waveform after Pre-emphasis**

Pre-emphasis is used due to voiced section of the speech signal usually falls at high frequencies due to high frequency formants have small amplitude compared to low frequency formants, and to reduce the DC effect. The frequency response of pre-emphasis is shown in Fig. 6.

After the signal has been pre-emphasized it is equalized to have a global RMS energy value of 0 dB. This equalization ensures that the energy threshold levels are set properly and to appropriate energy levels. An approximate, analytic version of the signal is then calculated to increase spectral accuracy for the formant estimates through an approximate Hilbert transformer (K. Mustafa and I. C. Bruce, 2006). The Hilbert transform of a function is defined as:

$$H\{f\}(y) = \frac{1}{\pi} PV \int_{-\infty}^{+\infty} \frac{f(x)}{x-y} dx \quad (1)$$

Where PV stands for "principal value" and the primary reason behind converting the signal into its complex representation is to allow the use of complex filters in the formant filter bank (AZF's and DTF's). The real-time discrete signal, SR[n], can be represented by its complex form, SC[n], as:

$$SC[n] = SR[n] + jSH[n] \quad (2)$$

Where SH[n] is the Hilbert transform of SR[n]. The particular technique used to implement the Hilbert transformer in the formant tracking algorithm uses an optimum FIR filter.
The Hilbert transformer is implemented with a 20th-order linear-phase FIR filter designed using the Parks-McClellan algorithm (Remez exchange algorithm). The frequency and phase responses of the filter are shown in Figure 7. The filter is designed using the Remez exchange algorithm and Chebyshev approximation to have an optimal fit between the desired and actual frequency responses. The analytic signal is then filtered into four different bands using a bank of adaptive band-pass filters (called Formant filters). Each of the four formant filters (F1, F2, F3 and F4) in the filter bank is made up of an All- Zero Filter (AZF) and a Dynamic Tracking Filter (DTF) (A. Rao and R. Kumaresan, 2000).

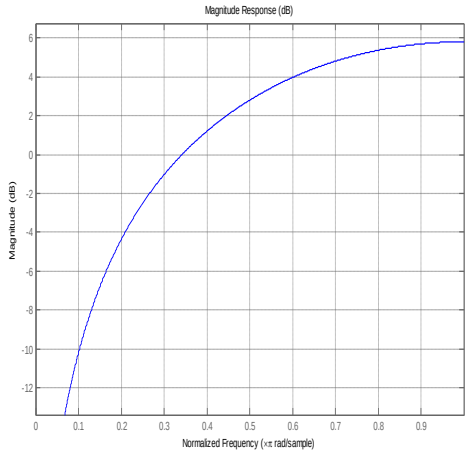

Fig. 6: Frequency Response of Pre-emphasis

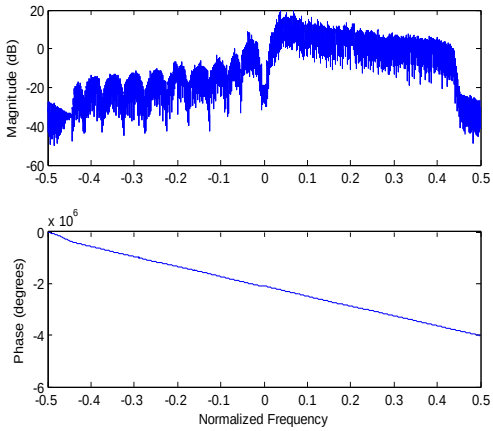

Fig. 7: Frequency Response and Phase Response of the Filter

The zeros of each of the AZF's are set to the latest estimate of the formant frequencies from the other three bands. The DTF provide the single pole located at the latest estimate of the formant frequency for that band. This cascade arrangement results in each of the filters having a pole around its own formant frequency and zeros at the other formant frequency locations. Each of the four band-pass filters allows only the signal around the frequency region of the desired formant to pass and suppresses the other frequency regions. The formant filter bank has a fundamental modification that the F1 filter of the filter bank has an added zero at the pitch frequency (F0) for further suppression of the region below the F1 frequency (the pitch region). This decreases the effects of the pitch on the F1 estimate.

The adaptive band-pass filter bank used in the formant tracking algorithm is similar to the one proposed (A. Rao and R. Kumaresan, 2000) but it has a modified first formant filter that removes the effects of the pitch from the first formant filter band. Each channel of the filter bank consists of an all-zero filter (AZF) cascaded with a single pole dynamic tracking filter (DTF). The combination of the AZF and the TF is called a formant filter (A. Rao and R. Kumaresan, 2000) and is responsible for tracking one individual formant frequency. The filters are designed in the complex domain because it is easier to design the unity gain and zero phase lag filters in the complex domain. Adaptively varying the zeros and pole of each formant filter, allows the suppression of interference from neighboring formant frequencies and from other spectral noise sources, while tracking an individual formant frequency as it varies with time.

The transfer function of the kth AZF at time sample index n is:

$$H_{AZFK}(n,z) = K_k[n]\ X \prod_{\substack{l=1 \\ l\neq k}}^{4} (1 - r_z e^{2\pi f_l[n-1]} z^{-1} \quad (3)$$

Where

$$K_k[n] = \frac{1}{\prod_{\substack{l=1 \\ l\neq k}}^{4} (1 - r_z e^{2\pi (f_l[n-1] - f_k[n-1]_)}} \quad (4)$$

and rz is the radius of the zeros on the Z-plane, fl[n-1] is the formant frequency of the l^{th} filter estimated at time index n–1 and, fk[n] is the formant frequency of this filter (k^{th} filter) estimated at index n–1. The gain of $K_k[n]$ ensures that the AZF has unity gain and zero phase lag at the estimated formant frequency of the k^{th} component. A wide range of values for rz were tested and the best results were obtained (for the range of values tested) for rz = 0.98.

The 'DTF' in each formant filter is a single-pole dynamic tracking filter. The pole location is always set to the previous estimate of the formant frequency of that formant filter. The transfer function of the kth DTF at index n is:

$$H_{DTFk}(n,z) = \frac{1-r_p}{(1-r_p e^{j2\pi fk[n-1]z^{-1}})} \quad (5)$$

Where r_p is the radius of the pole and $f_k[n-1]$ is the formant frequency of the k^{th} filter at time index n-1. A wide range of values for r_p were tested and the best results were obtained (for the range of values tested) using r_p = 0.90. The transfer function of the 1st formant AZF is slightly different than that of the other AZFs. The AZF of the first formant filter has an additional zero at the location of the pitch estimate to suppress pitch effects on the first formant estimate. The transfer function of the 1st AZF at index n is:

$$H_{AZF1(n,z)} = K_k[n] X \prod_{\substack{l=1 \\ l\neq k}}^{4} (1 - r_z e^{j2\pi(f_l[n-1]z^{-1})}) \quad (6)$$

Where

$$K_k[n] = \frac{1}{\prod_{\substack{l=1 \\ l\neq k}}^{4} (1-r_z e^{2\pi(f_l[n-1]-f_k[n-1])})} \quad (7)$$

and f0 [n-1] is the pitch estimate at time index n-1, that is provided to the 1st formant filter by the gender detector (K. Mustafa and I. C. Bruce, 2006). After the placement of the pole and zeros for each of the formant filters, the transfer function and the complex filter coefficients of the four formant filters are calculated. These complex filter coefficients are then used to filter the analytic speech signal into four band-limited spectral regions from which the four formant frequencies are estimated.

The frequency responses of the four formant filters are set as; pitch (F0) is set to 200 Hz, the first formant frequency (F1) is set to 700 Hz, the second formant frequency (F2) is set to 1500 Hz, the third formant frequency (F3) is set to 2200 Hz and the fourth formant frequency (F4) is set to 3500 Hz. After the speech signal has been filtered using the adaptive band-pass filterbank of the signal over the previous 20 ms in each band is calculated. In order for the algorithm to estimate a particular formant frequency from the spectrum (instead of using the moving average value), the energy calculated in that formant band has to be above a certain 'energy threshold level', in addition to that speech segment being voiced. Linear prediction provides a good model of the speech signal. This is especially true for the quasi steady state voiced region of speech in which the all pole model of LPC (Kaneko, Takuma, and Tetsuya Shimamura, 2014) provides a good approximation to the vocal tract spectral envelope. During unvoiced transient region of speech, the LPC model is less effective than for voiced regions, but it still provides acceptably useful models. The linear prediction method provides a robust, reliable, and accurate method for estimating the parameters that characterize the linear time varying system. Linear prediction models the human vocal tract as an infinite impulse response (IIR) system that produces the speech signal. For vowel sounds and other voiced regions of speech, which have a resonant structure and high degree of similarity overtime shifts that are multiples of their

pitch period, this modeling produces an efficient representation of the sound. The linear prediction problem can be stated as finding the coefficients a_k which results in the best prediction (which minimizes mean-squared prediction error) of the speech sample s [n] in terms of the past samples as s[n-k], k = {1… P}.The idea behind linear prediction is to approximate each sample of the speech signal as a linear combination of past samples. By minimizing sum of squared differences between the actual speech samples and the predicted ones, a unique set of predicted coefficients can be determined. A linear predictor of order p is defined as:

$$\tilde{s}[n] = \sum_{k=1}^{p} \alpha_k s[n-k] \quad (8)$$

Where $\tilde{s}[n]$ is the prediction of s[n] by the sum of p past weighted samples of s[n]. The system function of the p^{th} order predictor is a FIR filter of length p given by:

$$p(z) = \sum_{k=1}^{p} \alpha_k z^{-k} \quad (9)$$

The associated prediction error filter is:

$$A(z) = 1 - \sum_{k=1}^{p} \alpha_k z^{-k} = 1 - p(z) \quad (10)$$

And prediction error is defined by:

$$e[n] = s[n] - \tilde{s}[n]$$

$$= s[n] - \sum_{k=1}^{p} \alpha_k s[n-k] \quad (11)$$

The roots of the inverse of the prediction error filter corresponds to the poles placed to model the original signal as closely as possible while minimizing the mean squared error between the estimated and original signals. First order linear prediction (p = 1) obtains one linear predictive coefficient and the corresponding single pole is placed to model the original signal as well as possible. Second order LPC tries to model the original signal using two poles, and so on. The first four formant frequencies of the speech signal are estimated from the four filter bands of the adaptive band pass filter bank using first-order LPC. The analytic signal from each of the bands is first windowed using a 20-ms periodic Hamming window and then the linear predictive coefficient (one per band) of the previous 20 ms of the windowed signal from each band is calculated. LPC tries to fit a single pole model to each signal and the location of the pole corresponds roughly to the vocal tract pole (formant frequency) in that band, for voiced segments of speech. The LPCs are only calculated from the bands if the entire previous 20-ms window of the speech signal is voiced. A first-order Linear Prediction Coefficient (LPC) (Sahoo, D. K., et al., 2013) is then calculated for the analytic signal in each of the four bands. From each of these coefficients a formant frequency estimate is obtained. As the value of the four formant frequencies vary with time, the formant pre-filters are modified to track them by changing their pole and zero locations. Due to the band-pass pre-filtering of each formant frequency region prior to LPC, the frequency estimates provided by LPC are more accurate and the algorithm is less susceptible to errors due to background noise. The formant estimation is further refined by adding an adaptive voicing detector to detect a voiced and unvoiced speech segments. LPC estimates for the formant frequencies are only used during the voiced segments of speech. During the unvoiced

speech segments or when the signal energy of a particular formant frequency region (determined by the adaptive energy detector) is below a set threshold level, the formant frequency estimates are assigned their moving average value. This approach ensures that the formant tracker is able to recover quickly and with minimum error to the formant estimates, after unvoiced or low-energy speech segments. The energy detector threshold levels are also made adaptive for each of the formant filters so that they can adjust to long term changes in the energy levels of each formant frequency region. The voicing detector calculates the log ratio between the energy in the lower and higher frequencies of the speech to determine if a speech segment is voiced or unvoiced. If there is more energy in the lower frequencies than the higher ones, the speech segment is classified as being voiced. The voicing detector also has a threshold with hysteresis to ensure that switching from voiced to unvoiced speech (or vice versa) does not erroneously occur too quickly. Finally, an autocorrelation-based energy test is performed to ensure that voicing is not detected erroneously when there is no actual voicing in the speech but sufficient energy is present in the lower frequencies due to 'colored Gaussian noise' (or other background noises) . The voicing detector provides a sample by sample decision on whether a segment is voiced or unvoiced. In order for the voicing detector to work properly for both male and female speakers, various parameters of the voicing detector need to be modified. The main purpose of the gender detector is to determine the gender of the speaker and pass this information to the voicing detector so that it is able to modify its parameters. The gender detector uses a pitch based method to classify the gender of the speaker where the pitch is calculated using an autocorrelation based method. The gender detector also provides the pitch estimate to the first formant filter so that an additional zero can be added at the location of the pitch in the AZF of the first formant filter. Extensive testing of the robust formant tracking algorithm has been done which showed that the formant tracking algorithm is robust to a wide variety of real-time background noise conditions. The algorithm is able to provide reliable formant frequency estimates from continuous speech for both male and female speakers. It recovers quickly and with minimal error when problems do occur and when there is a switch in speakers. The moving average decision maker assigns the estimated value to the formant frequencies (from the LPCs) only when the segment is voiced and the energy of the formant frequency is above its respective threshold level. If the segment is unvoiced or if the energy of a particular formant is below its respective threshold level, then the current value of the formant frequency decays toward the moving average value for that formant frequency according to:

$$F_i[n] = F_i[n-1] - (0.002 * (F_i[n-1] - F_i^{MA}[n-1])) \quad (12)$$

Where F_i is the formant estimate of ith formant frequency at time index n and $F_i^{MA}[n-1]$ *i* is the previous value of the moving average for the ith formant frequency. The update rule for the moving average value of each formant frequency:

$$F_i^{MA}[n] = \frac{1}{n} F_i[k] \quad (13)$$

Where F_i^{MA} the moving average is value for the ith formant frequency at index n and $F_i[n]$ is the estimate of the ith formant frequency at index n.

IV. EXPERIMENTAL RESULTS

The primary goal of formant tracking algorithms is to develop a reliable formant tracking algorithm that is robust in real-time noise scenarios. Different test cases are described and the performance of the algorithms under these conditions has been discussed. The formant tracking algorithms has been tested using a noisy speech corpus (NOIZEUS) (ITU-T P.56, 1993). The noisy database contains IEEE sentences (produced by three male and three female speakers) corrupted by eight different real-world noises at different SNRs. The noise was taken from the AURORA database (H. Hirsch, and D. Pearce, 2000) and includes suburban train noise, babble, car, exhibition hall, restaurant, street, airport, and train-station noise. The noise signals were added to the speech signals at SNRs of 0dB, 5dB, 10dB, and 15dB. This corpus is available free of charge. Algorithm is tested for both male and female voices. The spectrogram of male speaker saying "Her purse was full of useless trash is shown in fig. 8. The spectrogram of female speaker saying "The clothes dried on a thin wooden rack" shown in fig. 9.

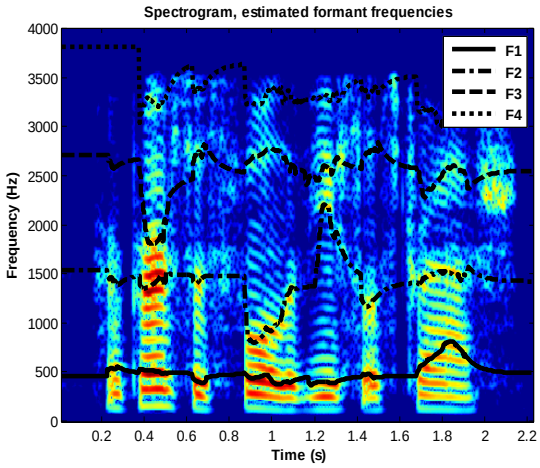

Fig. 8: Spectrogram and Formant Frequencies for a Male Speaker Saying "Her Purse was full of Useless Trash"

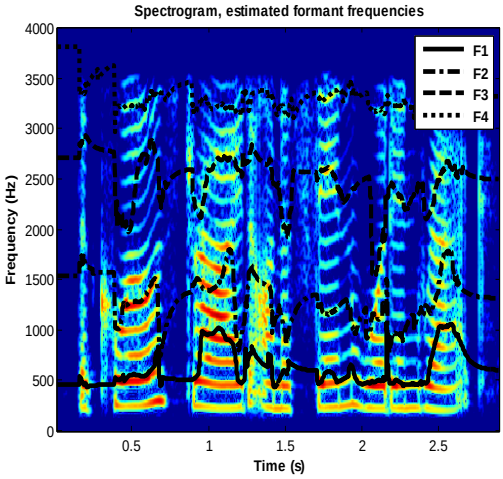

Fig. 9: Spectrogram and Formant Frequencies for a Female Speaker Saying "The Clothes Dried on a Thin Wooden Rack"

The IRS filter is independently applied to the clean and noise signals. The active speech level of the filtered clean speech signal is first determined using the method B of ITU-T P.56 (ITU-T P.56, 1993). Table 1 shows the range of first four formant frequencies. Generally the estimated formant frequencies vary in these ranges.

TABLE 1: Ranges for Formant Frequencies

Formants	Minimum Frequency (Hz)	Maximum Frequency (Hz)
F1	270	730
F2	840	2290
F3	1690	3010
F4	2500	4500

V. CONCLUSION

Robust formant tracking algorithm has been discussed in this work. The present work shows the testing of robust tracking algorithm for a speech signal in different environmental conditions. The operation of the algorithm is tested and analyzed in the presence of background noises. Quantitative analysis has shown that it provides accurate formant frequency estimates for both male and female speakers for a wide range of SNR's in real-time noise conditions. The robust formant tracking algorithm recovers quickly after erroneous estimates to go back to tracking the actual formant frequencies in the speech signal. The algorithm occasionally gives choppy and oscillating formant frequency estimates. This is an undesirable result because the actual formant frequencies of speech normally vary slowly with time and have smooth transitions. Furthermore, the estimated formant frequencies have to be smooth and the algorithm has to be able to identify formant transitions accurately. The oscillating formant frequency problem may be solved in future updates to the formant tracking algorithms by either smoothing the formant frequency estimates or by incorporating additional logical limitations to prevent abnormal jumps in the formant estimates. Another future improvement may be to modify the formant pre-filters to have variable bandwidths that are dependent on the magnitudes of the poles estimated by the linear prediction coefficients.

REFERENCES

[1] Miller, R. L., Calhoun, B. M., and Young, E. D., Contrast enhancement improves the representation of /E/-like vowels in the hearing-impaired auditory nerve, J. Acoust.Soc. Am., 106, 1999, 2693–2708.

[2] Mustafa, K., and Bruce I. C., Robust formant tracking for continuous speech with speaker variability, IEEE Transactions on Audio, Speech and Language Processing 14(2), 2006, 435–444.

[3] Schafer, R. W., and Rabiner, L. R., System for automatic formant analysis of voiced speech, J. Acoust. Soc. Am., 47, 1970, 634–648.

[4] Rao, A., and Kumaresan, R., on decomposing speech into modulated components, IEEE Trans. Speech Audio Processing, 8, 2000, 240–254.

[5] Kaneko, Takuma, and Tetsuya Shimamura, Noise-Reduced complex LPC analysis for formant estimation of noisy speech, 2014

[6] Sahoo, D. K., et al, Estimation of formant frequency of speech signal by linear prediction method and wavelet transform, International Journal of Engineering Research and Technology, 2(3), 2013.

[7] ITU-T P.56, Objective measurement of active speech level, 1993.

[8] Hirsch, H., and Pearce, D., The Aurora Experimental Framework for the Performance Evaluation of Speech Recognition Systems under Noisy Conditions, ISCA ITRW ASR, Paris, France, 2000, 18-20.

Biographical Notes

Mandeep Singh Walia is working as an Assistant Professor in Electronics and Communication Engineering Department, PUSSGRC, Hoshiarpur.

DESIGN AND STUDY OF A SOLAR THERMAL SYPHON PUMP

Md. Zishan Akhter[1], Md. Sarwar Khan[2], Md Sameer Farooque[3], Kaushalendra K. Dubey[4], Gopal P. Sinha[5]

[1,2,3]U.G.Student,Dept of M & AE, School of Engg & Tech, Sharda University,Gr Noida,U.P. India
[4] Research Scholar, Dept of Mechanical, Production, Industrial & Automobile Engg, Delhi Technological University, New Delhi, India
[5]Professor,Dept of M & AE, School of Engg & Tech, Sharda University,Gr Noida,U.P. India

ABSTRACT

This paper describes the idea and the development of a solar thermal energy driven pump for lifting of ground water for irrigation as well as for meeting urban supply system. This has the potential of saving over 93billion kWh of electrical energy and 3.3 billion litres of diesel (fossil fuel) per year, for India. The invention has been patented. The most attractive feature of the pump is the absence of any moving part, which makes it almost maintenance-free. Solar thermal energy is used to create a pressure higher than the atmospheric pressure, over the surface of liquid to be pumped to height H. The estimated thermal efficiency of solar thermal syphon pumping is four times of photovoltaic pumping system.

Keywords - Solar Thermal Energy, Syphon Pump, Overall Efficiency.

NOMENCLATURE

Aa = aperture area of PTC in m^2
Sc = solar constant in KW/m^2
Pc = pressure created by solar energy in Pascal,
P_A = Atmospheric pressure in Pascal
Ƥ = Mass density of liquid in kg /m^3.
g = acceleration due to gravity in m/s^2.
h = Enthalpy of steam.
H = Discharge height.
m_w = mass flow rate of water in m^3/s.
m_s = mass flow of steam in m^3/s.
V = flow velocity of water in m/s
Hs = friction loss in pipe.
ϕ = Latitude angle of location where system is installed in degree
β = Inclination angle of PTC system from horizontal in degree.
r_r = Rim Radius in meter.
ϕ_r = Rim Angle in degree
f = Focal Distance in meter.

h_p = Parabolic Height in meter.

D = Receiver or Boiler Diameter in meter.

C_R = Concentration Ratio

Θ = Incidence Angle in degree.

ω = Hour angle

γ = System Azimuth angle in degree

δ = Solar Incidence angle in degree.

n = Total no of day in month measured from 1st January.

$\eta_{opto\text{-}thermal}$ = Opto-Thermal efficiency of Syphon system

Ib = Solar Irradiation

q_u = Rate of use full energy in joule

U_L = heat loss co-efficient (W / m^2k)

Tc = Receiver Temperature in ^0C

Tr = Mean Receiver Temperature in ^0C

Ta = Ambient Temperature in ^0C

Rk = Thermal Resistance of Receiver or Boiler Tube

Acond = Effective area of conduction in m^2

ϵr = Non selective absorber parameter.

$\tau\alpha$ = Effective Transmission.

Qgen = Heat generated from PTC.

Qreq = Required Heat for steam generation.

$\eta_{thermo\text{-}syphon}$ = Thermal Efficiency of system.

ηo = Overall Efficiency.

η_{SPV} =Solar Photovoltaic panel Efficiency.

η_{pump} = Irrigation pump Efficiency.

η_{CC} = Charge-Controller Efficiency.

η_B = Battery Efficiency.

l = Length

b = Width

t = Thickness

PTC=Parabolic Through Collector.

STSP= Solar Thermal Syphon Pump.

SPVP= Solar Photovoltaic Pump System.

I. INTRODUCTION

Most of the developing countries have large needs of irrigation for meeting their agricultural requirements for food-security. The drinking water requirement also necessitates lifting of ground water to a height ranging from 50 to 200 feet. This requires huge amount of energy which is currently supplied through electricity and fossil fuel based engines. For a country like India the energy consumed for lift irrigation has been 93225.28MU, (in the year 2011),1MU= 1M kWhr [6].In most of the cases the developing countries are endowed with rich solar

energy. Some of it has been used for lift irrigation using photovoltaic panels electrically coupled to a conventional motor pump system, or Stirling cycle based engine coupled through a conventional pump. The potential number of SPV pumps is estimated at 70 million, with extending irrigation support to untapped markets [7]. This work reports the use of direct solar thermal energy for creating pumping action. The uniqueness of this development is that the pumping action requires no moving parts-reciprocating, rotating or expander action. Therefore there is no possibility of wear and tear or lubrication requirement or loss of energy due to friction between moving parts. Syphon action created by water vapour picked-up from the source, lifts the water from the reservoir through the delivery head. This is being demonstrated for the first time. The efficiency of the entire system is also high on account of no moving parts. An excellent review of the development of solar energy based pumps have been carried out by Y.Wong et al [11].The proposed thermo-syphon pump is a high pressure steam forced pump where there is no limitation of a suction head of less than 34 feet of water, the delivery head is unlimited based on the concentration of solar energy and the aperture area requirement of the solar collector has been worked out in subsequent paragraphs.

A model has been fabricated for proving the concept. This model demonstrates lifting of water through a head of nearly 5 to 10 feet Fig.2, shows a sketch of the parabolic trough collector (PTC) used for concentrating the solar thermal energy.

In most of the developing countries are endowed with rich solar energy. Some of it has been used for lift irrigation using photovoltaic panels electrically coupled to a conventional pump, or Stirling cycle based engine coupled through a conventional pump. The potential number of SPV pumps is estimated at 70 million, with extending irrigation support to untapped markets [7]. Total cost (before subsidy) for installation and commissioning of SPV water pump system varies from Rs. 190,000 to 290,000 or even Rs. 450,000/- [8][9].Capital cost of a 1.8 kWp solar PV pump is about Rs. 0.3 million. The payback period of solar PV pump (without subsidy) replacing a diesel pump is about 9 years (at a cost of diesel is Rs. 32/litre) [12].Purohit evaluated the financial attractiveness of different renewable energy technologies for irrigation water pumping in India. He calculated the following unit costs for water for SVP pumping systems [10]. The unique part of this development is that the pumping action requires no moving parts, reciprocating or rotating and therefore there is no possibility of wear and tear or lubrication requirement. A model has been fabricated for proving the concept as shown in Fig.1a and Fig.1b. This model demonstrates lifting of water through a head of nearly 5 to 10 feet.

II. WORKING OF SOLAR THERMAL SYPHON PUMP.

Solar Thermal Syphon pumping system (STSP) may be used to lift water from the ground or any liquid to a height without using any moving mechanical-part by pressurized steam through syphon action. The steam is generated by solar energy concentrator on a tube filled with the liquid. The concentration of solar energy can be achieved by parabolic trough collector (PTC) / concave / plane mirrors type solar concentrator or through Fresnel lenses based solar thermal system.

Water liquid enters into a boiler cell, through an inlet regulated by a float valve action, for maintaining a uniform level. Steam generated in the boiler flows through a perfectly insulated and sealed pipe into an enclosures connected to ground water to be pumped. The discharge pipe is dipped below the ground water. The

pressurized steam lifts the water to the delivery head H, through a syphon action. The conversion of water in to steam at boiling temperature of water depends upon the thermal energy obtained from the area of PTC (Aperture Area of concentrator).The heat raise the temperature of boiler and water gets converts into steam. The water feeding pipe use some amount of steam pressure feeding water to the boiler [8]. Fig.1a and Fig.1b, show the model and working set up of the thermo-syphon pump. This system has been developed in mechanical

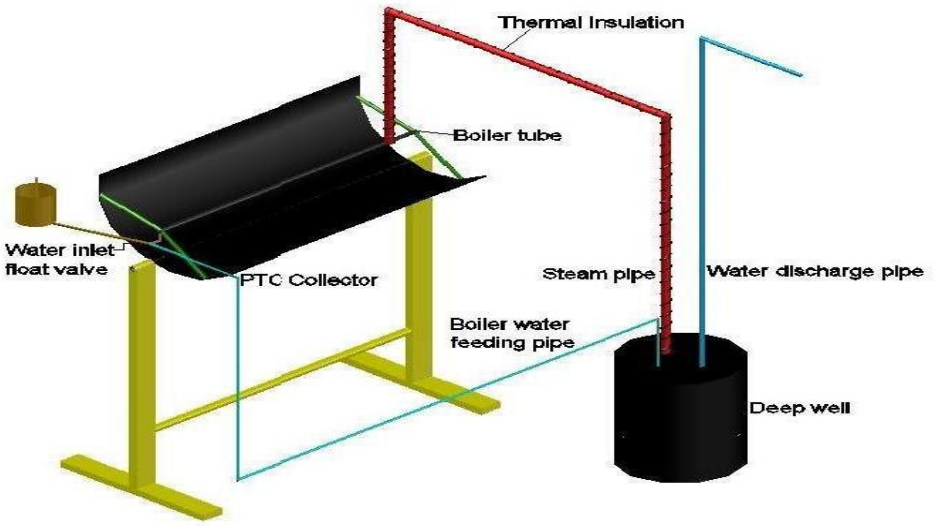

engineering department sharda university greater noida,u.p. state, India. Dimension of all parts of STSP listed in Table-1

Fig. 1a: Schematic of Solar thermal Syphon Pump.

Fig. 1b: Working set up of Solar thermal Syphon Pump at Sharda University Greater Noida campus.

III. PRINCIPLES OF THE SOLAR THERMAL SYPHON SYSTEM.

The solar thermal syphon pump derives its pumping action by putting additional pressure on the surface of the liquid, to be lifted. This additional pressure is obtained using solar thermal energy in concentrated form. The concentrated solar thermal energy obtained by a parabolic trough collector (PTC) is given by

[2]

$Q_{gen} = Aa\ Ib\ W$……..(1)

The useful solar gain by the collector $Qu = Aa\ (\tau\alpha)\ Ib\ W$

$\tau\alpha$ = Effective Transmission

The head of lifted water or liquid is given by

H = (Pc - P_A)/ βg meters .Where Pc is pressure created by solar energy in Pascal, P_A is Atmospheric pressure in Pascal ,β is Mass density of liquid in kg /m^3 and g is acceleration due to gravity in m/s^2.

3.1 Collection and concentration of solar thermal energy using PTC.

For generating steam, whose pressure is used for pumping of liquid to a height, we require concentrated solar thermal energy for super heated high pressure steam at a high pressure. This is achieved by a PTC or a Fresnel lens or a combination of the two. The concentrated thermal energy obtained through PTC is given by Heat required for steam generation [4],

$Q_{reqired} = m_{water} [Cp_{water} (T_{boiling} - T_{ambient}) + LH_{water}] +$

$m_{steam} [Cp_{steam} (T_{sup} - T_{boiling}) + LH_{vaporisation}]$ KJ…….....…….(2)

For system to work continuously

Qgen >. Qreq……..(3)

Boiling Temperature of water for the exerting the required steam pressure ($T_{boiling}$) is directly taken from steam table corresponding to the pressure Pc.This heat can generate steam at a pressure Pc is given by

Pressure required on water table for achieving the discharge head

Pc = $10^5 + 10^4$ H Pa…….……..(4)

This pressure on the surface of the liquid can lift it by 'H' meter through syphon action is given by

H = (Pc - Pa)/ βg meter…….……...(5)

3.2 Estimation of specified head H and flow rate Q.

Heat from PTC is mainly required to meet the heat loss occurring due to imperfect insulation and the temperature difference between the superheated steam and the ambient. It is given by,

Total energy in steam = Energy given to discharge

$m_s h = m_w g H + ½ m_w v^2 + hs$…….…….....(6)

Conduction loss in pipe = Effective surface area for conduction (Acond) / thermal resistance (R_k).

$$[\frac{(Tr-Ta)}{Rk} \times \frac{Acond}{Aa}]$$……..……..(7)

3.3 Design parameters of PTC.

Parabolic through collector (PTC) are preferred for solar steam generation because high temperature can be obtained without any degradation of collector efficiency. The specifications of PTC shown in fig.2 of PTC design for steam generation. All design calculations provide by equations below.

Projected area for heat require = Aperture area of PTC = Aa m^2

Solar Constant [2] = 1000W/m^2 (Standard for India)

Solar radiation (Ib) = 750W/m^2. (Taken average value for month of April-May)

Parabolic Aperture area of PTC = Aa m^2 = 550 W / Q_{gen}.

Dimensions of PTC on the basis of aperture area, Aa = b × h.

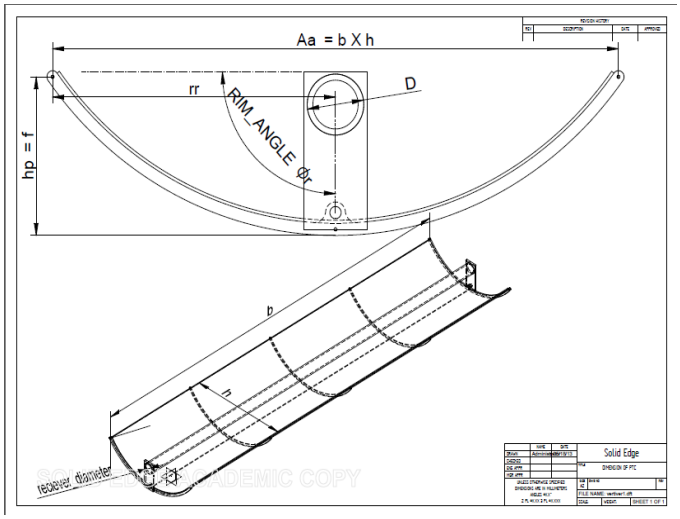

Fig. 2: Schematic of parabolic through collector.

Rim Angle [5] = $\phi_r = \text{Sin}^{-1}(Aa/2\ r_r)$……..…….(8)

Focal Distance [5] = $f = \frac{Aa}{4\tan\frac{\Phi r}{2}}$……..……..(9)

Parabolic Height [5] = $h_p = f$

Receiver or Boiler Diameter [5] = $D = \sqrt{\frac{4}{1000\ \pi\ b}}$ m……..…..……(10)

Concentration Ratio [5] = $C_R = \frac{Aa-D}{\pi D}$……..……(11)

Incidence Angle (Θ) [2] = Cos Θ = Sin ϕ (Sin δ * Cos β + Cos δ* Cos γ * Cos ω * Sin β) + Cos ϕ (Cos δ * Cos ω * Cosβ – Sin δ * Cos γ * Sin β) + Cos δ * Sin γ * Sin ω * Sin β…….……(12)

ω = Hour angle [2] = (Solar Time – 12:00)15^0.

(Afternoon solar time taken as +ve hour angle, whereas forenoon solar time taken as –ve solar time.)

δ = Solar Incidence angle [2] = 23.45 × Sin $[\frac{360}{365}(n + 284)]$……..……(13)

3.4 Dimensions of STSP parts.

Table-1 Dimensions of STSP

STSP Parts	**Dimensions**
Reflector	l = 2.44 m, b= 1.25 m, t= 0.4 m. Aperture Area = 2.44 m^2
G.I Sheet for reflector support.	l = 2.44 m, b= 1.25 m, t= 0.36 m.
Copper Water Tube	L = 2.44m,Diameter = 20mm, Volume = 7.6 ×10^{-5} m^3
PVC Steam Tube	Diameter =14mm, Thermally insulated with glass wool.
Supporting Iron Frame **Arc** **Rods** **Rivets** **Mounting Nut**	No. Of Arc = 5, No of Rods = 3 t = 3 mm, Arc length = 1.25 m t = 3mm, l = 2.44 m 10 (Aluminium with head), l = 10mm, diameter = 4mm. Diameter = 9mm (5mm from top and each side)
Iron Stand	l = 1.17 m, t = 5mm.

IV. EFFICIENCY INVOLVED.

4.1 Opto-Thermal Efficiency ($\eta_{opto\text{-}thermal}$)

$$\eta_{opto\text{-}thermal} = qu / Ib\ Aa = \eta_O - \frac{1}{Ib}\left[\frac{(Tr-Ta)}{Rk} \times \frac{Acond}{Aa}\right] + \epsilon r\left[\frac{Tr4-Tc4}{CR}\right] \quad \text{.....(14)}$$

Rate of use full energy = $q_u = \eta o\ I_b\ Aa - U_L(Tr - Ta)Aa$ .....(15)

Rk = Thermal Resistance of Receiver or Boiler Tube =

$$\frac{\text{Distence Travel by conductive heat in boiler tube or recevier } (x)}{\text{Thermal conductivity of recevier metal } (K) \times \text{Condution Area } (A)}$$

4.2 Thermal Efficiency ($\eta_{thermo\text{-}syphon}$)

$\eta_{thermo\text{-}siphon}$ or η_I = $Q_{required} / Q_{gen}$ .....(16)

4.3 Over All Efficiency (ηo)

$\eta o = \eta_{opto\text{-}thermal} \times \eta_{thermo\text{-}syphon}$ .....(17)

V. ESTIMATION OF STSP EFFICIENCY WITH PHOTOVOLTAIC PUMP EFFICIENCY.

Efficiency of Solar Photovoltaic Pump (η_{SPVP})

$$\eta_{SPVP} = \eta_{SPV} * \eta_B * \eta_{CC} * \eta_{pump}$$

η_{SPV} = 15%

η_{pump} = 50%

η_{CC} = 90%

η_B = 85%

Lead-acid batteries typically have columbic efficiency of 85% and energy efficiencies in order of 70 % [9]. Columbic efficiency is the ratio of number of charges that enter the battery during charging compared to the number that can be extracted from the battery during discharging [9].

η_{CC} depend on the input-output level of voltage-current. DC-AC conversion efficiency as 100% but practically it is not possible because some account of heat dissipated by the passive components. Therefore, there is no way to simulate 100% charge-controller efficiency. We can assume more than 90%.

Farm irrigation pumping is around 70 to 80% of total farm electricity usage [10].

η_{SPVP} = 15% * 85% * 90% * 70% = 8.08 %

VI. RESULTS AND DISCUSSION.

An experiment with the fabricated model was carried out in the month of April-May. In a mid day when the sun rays were focused on the copper boiler, the pump lifted the water from the down reservoir and sprayed a stream up to a height of 10 feet. This gave a feel that about 50% of energy was lost in reflector. A more reflective surface with better focussing power is recommended. The concept was clearly demonstrated.

The result of energy and exergy analysis of STSP shown in Table 2:

Table-2, STSP Efficiency results

System/Efficiency (%) → ↓	$\eta_{optical}$	$\eta_{thermal}$ or η_I	$\eta_{overall} = \eta_{optical} \times \eta_{thermal}$
STSP	75	46.6	34.9
SPV Pump			8.08

VII. CONCLUSION.

It is possible to use direct solar thermal energy for pumping action instead of going through the photovoltaic electrical route, where the SPV pumpinjg system overall efficiency comes to 8% against 35 % (η_{opt} and η_I comes 75% and 46% respectively) of solar thermal syphon pump system. Apart from this significant gain in utilisation of solar energy, there is further indirect savings in energy required for production of solar photovoltaic panel. The solar thermal syphon pump would be a significant environment friendly attempt for harnessing solar energy.

The unique part of this development is that the solar thermal syphon pump has no moving parts and it is thus maintenance free.

VIII. ACKNOWLEDGMENT

This project has been funded by Sharda University and we are very thankful for this.

REFERENCES.

[1] Principles of solar engineering by Frank Kreith, Jan F. Kreider, McGraw-Hill, 1981.

[2] Solar Energy: Principles of Thermal Collection and Storage By S.P. Sukhatme.Tata McGraw-Hill,2008.

[3] Introduction to Fluid Mechanics by Fox & McDonald,John Wiley & Sons,2008

[4] Basic and applied Thermodynamics by P.K.Nag,Tata McGraw-Hill, 2004

[5] Kalogirou, S.; and Lloyd, S.Use of solar parabolic trough collectors for hot water production in Cyprus. A feasibility study. Renewable Energy 2(2): 117-124.1992.

[6] State-wise Electricity Consumption & Conservation Potential in India. Bureau Of Energy Efficiency (BEE) Ministry of Power, Government of India, Report2009, www.emt india.net/eca2009/14Dec2009/CombinedSummaryReport.pdf.

[7] HWWI (2005): CDM potential of SPV pumps India. http://www.hwwi.org/uploads/tx_wilpubdb/HWWI_Research_Paper_4.pdf.

[8] "Solar Thermal Syphon pump System for Irrigation",Gopal P Sinha,Kaushalendra Kr Dubey, India Patent,Patent Docket No- 9684,Application No-1626/DEL/2013,Reference No- E-2/5773/2013-DEL, E-3/5571/2013-DEL, E-5/5240/2013-DEL,Date of Patent filied-30/05/2013.

[9] Cral John Rydh, BjornA. Sanden, Energy Analysis of batteries in photovoltaic syste,Part-ll, Energy return factors and overall efficiencies, Journal of energy conversion and management,Elsevier,46 (2005),1980-2000.

[10] Jamse Curaan, Agricultural Resource Management. Irrigation Pump Efficiency, www.farmpoint.tas.gov.au.

[11] Solar thermal water pumping systems-a review Y.W. Wong,K.Sumathy_ Department of Mechanical Engineering\ University of Hong Kong\ Hong Kong, August 1998.

PROCESS TRANSFORMATION AT DISTRICTS: A CASE STUDY OF E-GOVERNANCE IN INDIA

M. K. Singh[1], M. P. Gupta[2] and Jitendra Madaan[3]

[1,2,3]*Department of Management Studies, Indian Institute of Technology Delhi, Delhi 110016, (India)*

ABSTRACT

Under the E-governance Projects several services and procedures of government are being automated to enhance citizen services and experiences. It has been found that if a system is made IT enabled then it renders several activities redundant or one process becomes flexible and efficient at the cost of another, simultaneously it requires reengineering, prioritisation of process and optimisation of resources of the system to garner all benefits. A suitable IT based model is engineered backed up by computerised decision making. One such decision point is taken and decision support is developed through the use of logic available in Operations Research (Travelling Sales Man Problem).

Keywords: E-governance, Information Technology Reengineering, Decision Support. Process Mapping, Workflow, As-Is Process Map, To-Be Process Map, What if Analysis, IT enabled.

I. INTRODUCTION

Government across the world are focusing on various ways to provide efficient and transparent services with high flexibility. These services must reach the citizen at affordable cost. Also from 49 empirical studies it was concluded that there were positive e-government impacts on data access, efficiency and productivity of government performance [1] from earlier studies also found that e-government enhances communication between government and citizens [2] Country like India, with high population, the successful model of E-governance is at urge, simultaneously the policy makers must be enough flexible to integrate the various challenges at system level. The innovation is essential for economic development [3]. Standardisation of the processes, providing online services, Database management, open source of the data, by means of this the government expenditure in terms of expenditure can be reduced. Government of India has taken initiatives under National E-governance Plan (NeGP) for the growth of E-governance within the country. The E-governance plan can help to seek the right governance and institutional mechanisms. The Government plan at the Centre, State and local level with integrated service levels to create a citizen-centric as well as business-centric environment for good governance. Under this plan government has vision that all government services accessible to the common man in his locality through a one stop shop (integrated service delivery) ensuring flexibility, efficiency, transparency and reliability at affordable costs to meet the basic needs of the common man" with support of IT. E-district is a Project under the NeGP. The districts in India are the delivery channels for government administration which caters various services to the citizens such as ration card, certificate issuing, pension etc; therefore e-district can project can significantly improve government service deliveries.

The backbone of above implementation is IT in government processes the benefit of same can helpful to extract the flow of real time information of services which can further help firstly interlinking the functioning of the various departments by increasing the flexibility and efficiency in the system; secondly innovating web enabled applications; thirdly developing management information central data base and lastly utilisation of the computational power.

As the computer capability enhanced with time problems gets solved faster speed. The computers can collect the real time information and can be integrated with mathematical algorithm to solve complex models at very fast speed. In organisations computing power are being used by managers, decision makers, stake holders etc. The solving of large and unstructured problem which are very difficult and time consuming when solved manually for taking decision now can be solved utilising the computing power. This is what precisely known as Decision Support System (DSS). The paper focuses on IT based model for e-district. There are various citizens centric a service delivered at district level, one among is allocation of ration card.

II LITERATURE REVIEW

2.1 E-governance

E-governance has been defined as that which, "seeks to realize processes and structures for harnessing the potentialities of information and communication technologies (ICTs) at various levels of government and the public sector and beyond, for the purpose of enhancing good governance. E-governance puts the citizen at the centre giving citizens the choice of when and where government services. In other terms it gives the flexibility to citizen to accesses the government information and to completion of government transactions anywhere and anytime efficiently and effectively. “Creating an open and transparent government is an ideal index of the effectiveness of gross government activity and progress” [4]. E-government utilizes technology to accomplish reform by fostering flexibility, transparency, accountability, eliminating distance and other divides, and empowering people to participate in the political processes. These services are offered at district level to ensure citizen centric services. In the research paper e-governance is defined as the application of electronic means firstly in interaction between government and citizens and government and businesses and secondly in internal government operations.

E-government can be said to have function of four components namely governance, IT, reengineering and citizen (familiar with computer). The four independent variables require a little elaboration that is e-government without good governance, sound IT infrastructure support, a critical examination of existing administrative procedures followed by appropriate administrative reforms, here designated as reengineering and finally, meeting the needs of citizen, a citizen who seeks public service delivery and interacts with governance online.

The objectives of e-government is to transform government, the same is based on two basic premises: firstly, current government functioning, as exhibited by its public service delivery, is far from satisfactory level. And secondly, government can perform better, with emerging IT. “E-government managers need to be responsible for the quality of service they deliver through the portals and try to understand the need of the citizens” [5]. In this conceptualization, therefore, e-government is transformation of the government functioning. This

conceptualization of e-government gives rise to four important corollaries, namely, first e-government is an intermediary stage for transforming government. Thus e-government is not an end in itself but a means for reaching an end. Secondly, e-government must aim at government transformation without which its full potential will not be harnessed. Thirdly, any e-government attempt must be based on administrative reforms, failing which the e-government attempt may not give desired results. And lastly, e-government should strive to reach the ultimate stage, still eluding the developing countries, when e-government becomes synonymous with government.

E-District is a State Mission Mode Project under the National E-governance Plan. The project aims to target high volume services through Common Service Centres. Districts are the primary delivery channels of governance to deliver a large number of services to the citizens; therefore E-governance can significantly improve government service delivery. e-District project covers ten services at Nation and State level. These services are certificates, pension, utilities, dues and recovery, ration card (PDS), electoral services, grievance, revenue court, employment exchange and police department.

2.2 Objectives of e-district Model:

a. To establish fundamental relationship with citizen;
b. To integrate and seamlessly deliver citizen services by district administration through backend digitization and reengineering;
c. Fast processing of public cases/appeals/grievances by IT advantage;
d. Focus on backend computerization
e. Infusion of transparency and accountability in operations
f. Implementation of an efficient electronic workflow system in order to reduce the workload of the district personnel;
g. To create a smart interface between citizens, governments, public utilities and other information providers;

2.3 Holistic View of Reengineering for e-district model

"Reengineering is the fundamental rethinking and radical redesign of business processes to achieve dramatic improvements in critical, contemporary measure of performance, such as cost quality, services etc (Hammer & Champy, 1993.). Today most of the process used for delivering the services are old age, obstructive, complex and require major rethinking and re-orientation. The reengineering entails dramatic improvement rather than marginal. Reengineering advocates streamlining these processes for today requirements with a scope of continuous improvement [7]. The process of reengineering can deliver radical change in performance, firstly by reducing redundant and non-value added activities secondly by reducing the number of stages/transfer points of work and thirdly by speeding up the work flow often through the use of IT System.

2.4 Fundamental Attributes of reengineering:

a. Results in radical change;
b. Assumes clean slate change;

c. Focuses on end-to-end processes;
d. It is top-down directed;
e. It is information technology enabled.

2.5 Need of Reengineering in the Government Services

The changing environment necessitates government to switch from task orientation to a performance, result orientation and complete revamping so good governance has to be the driving force instead of government. Government has to restructure its structure, processes, rules, regulations and transformation of behavioural attitude of government officials. It has to eliminate redundant hierarchical levels, overheads, obsolete rules and practices and significant reduction in cost and response-time

2.6 Benefits of Applying Reengineering in Government Services

The benefits of reengineering may be simple and one-dimensional, but are more likely to be complex and multi-dimensional; some of the benefits are listed below:

a. Financial performance gets improved because things get streamlined.
b. Customer satisfaction improves because he gets services at faster rate.
c. Cost reduction.
d. Service quality gets improved.
e. Delivery performance gets improved.
f. Productivity increases ideal time reduces.
g. Flexibility/responsiveness increases.
h. Process times of services reduce.
i. Innovation of new ideas those can be applied to other application.
j. Employee development in terms capability, value, efficiency etc.
k. Competitiveness among other departments.
l. Organisational flexibility increases, for example decision can be taken at any level of stake holders, forwarding of application of request has eliminated the middle personal involved in services deliveries.

Government organizations are required to deliver or produce at a low cost, high quality, fast and flexible responsiveness to customer requirements. Therefore, there seems a pressure on organizations to redesign. Out of such pressures was born the idea of reengineering. While reengineering promised radical change the attainment of true reengineering remained elusive for most organizations, with 50-70 per cent of reengineering projects failing. From above it is felt that there is still a need for process change in holistic and more incremental manner.

2.7 Holistic Approach to Reengineering in e-district model

Traditional approach of reengineering and many literature reviews have emphasized changed based one aspect of an organization for example on with inadequate treatment of human aspect. Reengineering programme can be

powerful change approach if it is integrated with verities of change initiatives such as cultural and structural change within an organisation. Therefore, the need for holistic view of change management of government and district administration has to be highlighted as well as incorporated.

2.8 IT Enablement of e-district Services

Role of Information Technology (IT) have reached to long height in various sectors in India. Finance and Insurance sectors are playing a leading role in IT enabled processes. At the same time Government of India had initiated project at district level.

Presently the interacting bodies as shown in figure 1 are:

a. Users/Applicants;
b. Process Owner and;
c. Service Counters

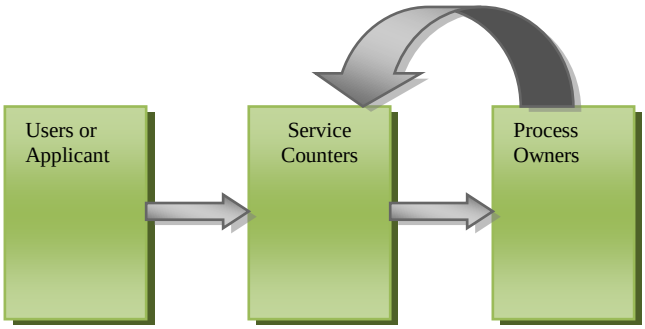

Figure: 1 Traditional Way of Interaction of Bodies

These interacting bodies are responsible for delivery of services and there no role of Information Technology, the service delivery takes lot of time, movement of papers is manual, status tracking is quite difficult, and service levels are not fixed for any work. These deficiencies can be overcome by proposed by Services Architecture shown in figure 2 below in which service counters are being replaced by computer service centres and users can also interact with Web Portal.

2.9 Use of IT and the framework

Incorporation of IT into tradition processes will try to make them more efficient, transparent, aid in compliance, increase visibility, aid in performance measurement, aid in planning etc.

Now the questions are who needs the services? Who will do it? How to avail the services? And how it is possible?

The above figure may be helpful in giving the answers. The interacting bodies are the User, CSCs and the various process owners. They are collectively responsibly for forming successful system and delivery to the citizen.

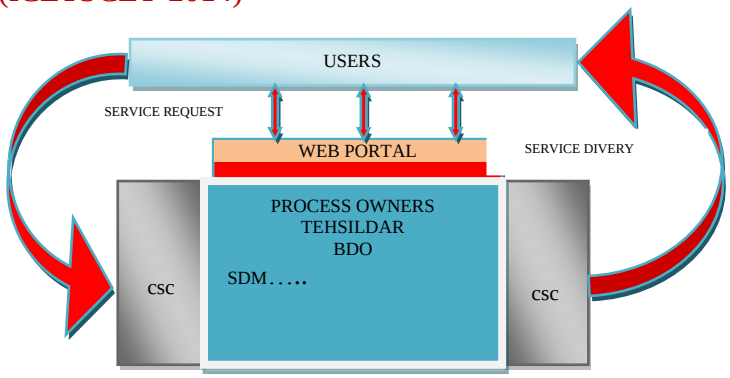

Figure: 2 IT Enabled for Interaction of Bodies

Now again the question arises how these bodies responsible for services are facilitated by the Information Technology for delivery of services?

They are interacting through the various components of IT and the new system is called as e-District system. These components of IT are namely Web Services, Application System, Data warehousing, Notification System and Decision Support System. Details of these components are explained systematically. The requirement of reengineering is necessitated by the integration of the information system. Without discussing the architecture of the information system the entire framework of E-governance will be futile. These components have always remained in the background while performing reengineering and as it is shown in the figure 3.

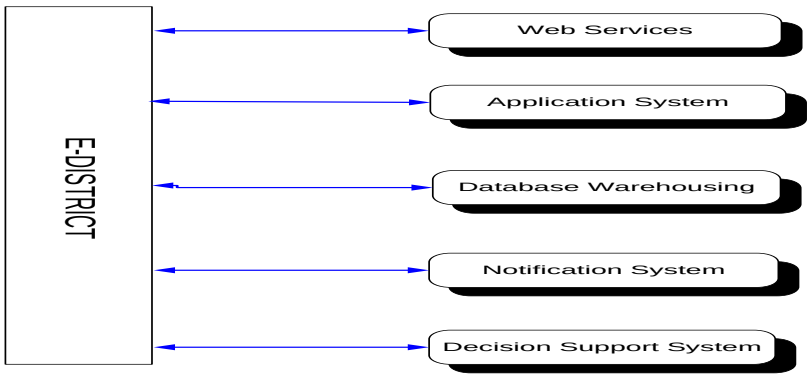

Figure: 3 It Components in e-district

Now the Question is how these IT components are connected with each other and interacting with the interacting bodies. For that we need to understand the IT Architecture. The System architecture shown in above figure 4 can be explained with example of domicile certificate. The applicant/user arrives at CSC for domicile certificate. CSCs are connected through satellite or leased line for accessing the web services. The applicant requests for domicile certificate to CSC operator, operator opens the web portal and enters the particulars, these particulars are stored in temporary database (part of central database) connected to system application. System application generates the receipt number/application number. CSC operator gives the stipulated time for collecting the domicile certificate. CSC operator on applicant request enters the receipt no./application no. and

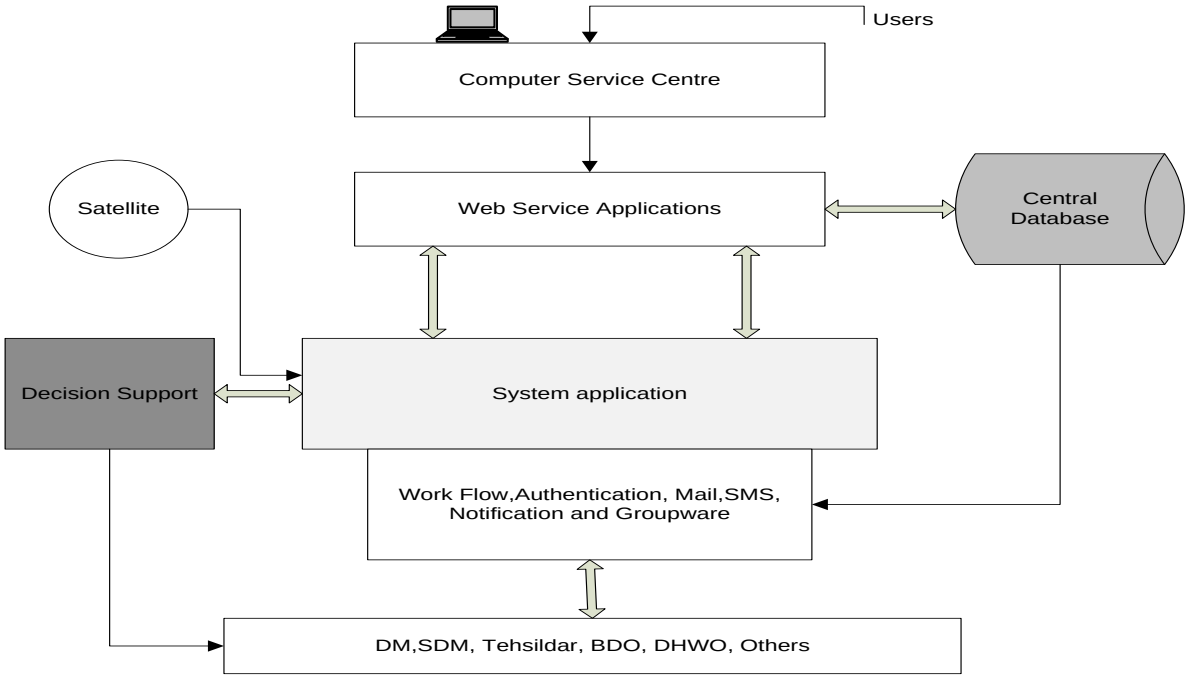

Figure: 4 Overall System Architecture

checks the WIP database if the request is approved takes the print out, stamp it and hand over to applicant, system upgrade the service database

Now the system application notifies to service owner (SDM) connected to LAN. SDM logs in to Personal Database (part of central database) and approves the application if details found and matched either marks for physical verification to Accountant. Accountant does the physical verification and update the Personal database, report sent to SDM. SDM approves the request and update WIP database (part of central database), applicant is send mail or SMS. .

Lastly the DSS connected to system application helps to decide the route for various locations in case if there are many applications for verification of different location for Accountant.

2.10 Decision Making for E-Governance

"Decision Support Systems is an integrated, interactive computer system, consisting of analytical tools and information management capabilities, design to aid decision makers in solving relatively large and unstructured problem" [8]. "A number of frameworks or typologies have been proposed for organizing knowledge about Decision Support. In the expanded framework, the two most widely implemented approaches for delivering decision support are called data-driven and model-driven DSS" (Adla, 2007a). "Data-driven DSS help managers organize, retrieve, and analyse large volumes of relevant data using database queries and OLAP techniques" [10]. "Model-driven DSS use formal representations of decision models and provide analytical support using the tools of decision analysis, optimization, stochastic modelling, simulation, statistics, and logic modelling" [9] The three other types of DSS have become more widespread and sophisticated because of Web

technologies. Communication- driven DSS rely on electronic communication technologies to link multiple decision makers who might be separated in space or time or to link decision makers with relevant information and tools.

The Web has expanded this technology. "Knowledge driven DSS can suggest or recommend actions to managers". The Web helps deliver this type of DSS to a much broader audience of decision makers. Finally, document-driven DSS integrate a variety of storage and processing technologies to provide managers document retrieval and analysis. Our primary focus in this paper and discussion is on the first two categories of Decision Support Systems: data driven and model-driven DSS for decision making.

III METHODOLOGY

3.1 Decision Making Opportunities in the e-district Model

There are several opportunities for decision making which has been identified. These are discussed below:

- Decision for Ration Card: Numbers of Ration Card are allocated to several villages after getting the quota for district. This allocation requires frequent changes and updates of number of possible allocations based on the changes done at the central level. This decision may be well facilitated by such decision support.

- Decision for Pension Services: Pension issued to citizen should be equally distributed in the given area. Concentration of pension in one area is should not be allowed. But again such decision is difficult to taken manually. This decision caters to this need.

- Decision for predicting the next year demand of ration card: It is prudent for the district services to inform the centre of next year expected demand rise in the ration card. It better equips the centre to meet the increasing year on year demand and release the quota. Such exercise requires the forecasting techniques and past data and must not be relied on simply hunch of process owners.

- Decision for Routing Accountant: Accountant has the duty of verifying personal details of citizen like name, addresses, age, family members, stay at particular location etc. For this Accountant has to visit the people living in the District physically. This itself is a time taking process and offers several opportunities such as reduction of time, etc.

From above discussed various decision making opportunities routing Accountant has been taken, Accountant does all the work related to field verifications and reports back to higher authorities required deliver the services, for his convenience decision making is described below.

3.2 Decision support for routing accountant

See figure 5, Accountant does physical verification for personal details. The Accountant had to travel various locations for various services. The decision where to go first and complete the verification process in minimum

time is the goal. But it becomes physically difficult to decide and this is almost routine work for him. Even the manager (process owner) must know about the status of the verification process in order to maintain the smooth work flow. Services where accountant does the verification are certificate services, pension services, electoral services and other services

The computerised decision support aid the Accountant for determining its shortest possible route. For example the process map of As-Is Certificate Services is as given below:

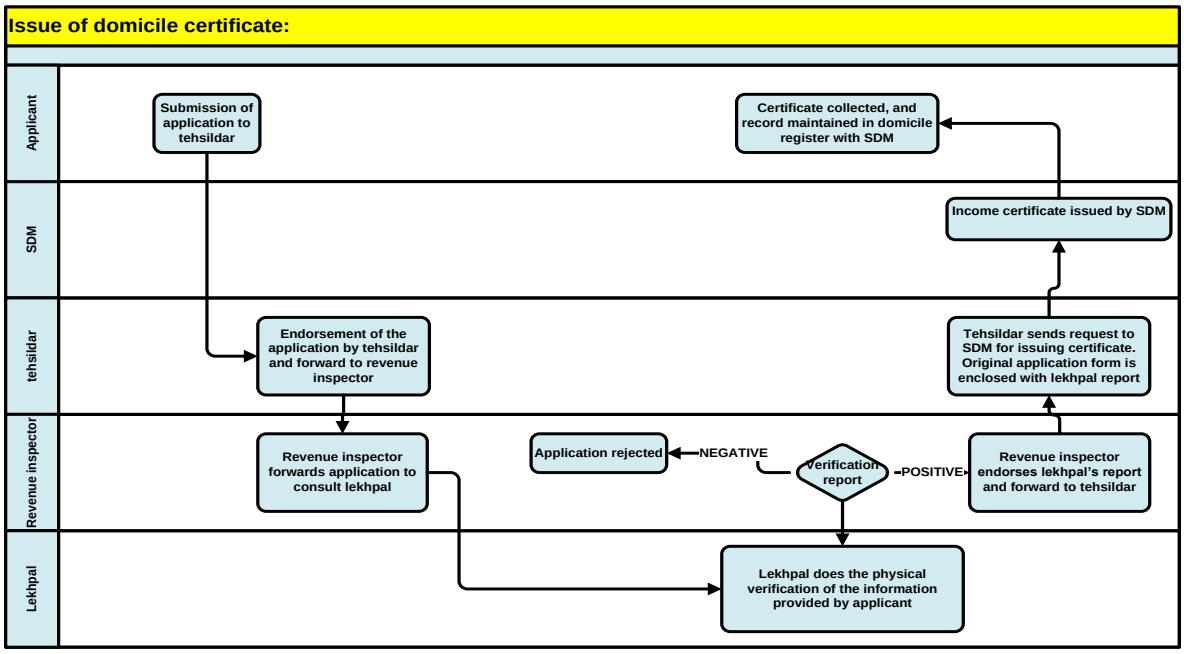

Process mapping of domicile certificate

.

Figure: 5 Process Making For Domicile Certificate (As-Is)

Applicant visits the Tehsil office and enquires about the procedure and documents required for enclosing with the request for domicile certificate. Once he completes the all the requirement for certificate and submits in the office of Tehsildar, Tehsildar forwards the application to Revenue Inspector (RI), who assists the work of Tehsildar. Revenue Inspector forwards the application for physical verification to Accountant. Similarly verification for other services would also require Accountant. Accountant does the physical verification and forward the application back to RI, RI endorses verification report sends to the Tehsildar. Tehsildar forwards the request to SDM for issuing the certificate. Applicant arrives at SDM office and collects the domicile certificate; manual copy of the same is maintained at SDM office. In this process the Accountant faces problem in taking the decision and he decides of his own and takes decision on hunch

3.3 To-Be Model:

Below model is combined model for all types of certificates services. In new model two more new components are involved namely CSC and System Application described in early section. The applicant arrives

at CSC and request for the same. The operator at CSC opens the web portal login the details of applicant in the system application which generates the receipt no. at the same time the operator gives the applicant stipulated time. The system application notifies Accountant for physical verification and at the same time to process owner for further processing. The Accountant logs into personal database and looks if physical verification required otherwise marks the application to Tehsildar (Income and Caste) or SDM (Domicile) if Personal Database available.

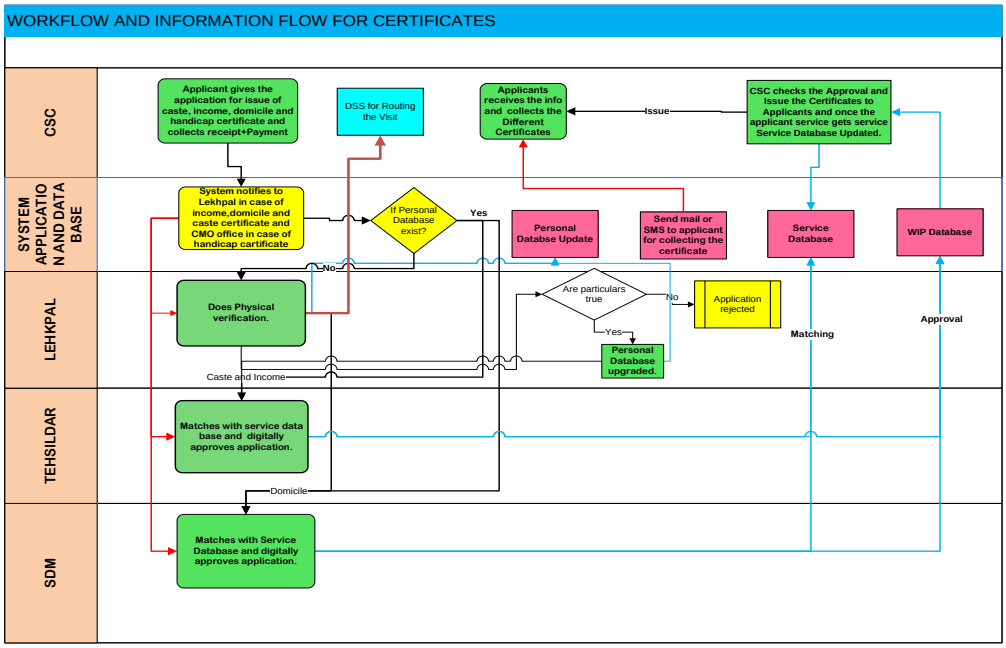

Figure: 6 Process Making for Domicile Certificate (To-Be)

The respective process owner verifies with personal database and digitally approves the application which is stored in WIP database. Once the application stored in WIP database the system notifies the applicant by email or SMS. Applicant visits the CSC with the receipt no. and asks for domicile certificate. The operator logs into WIP database and checks the status of the request if approved by the process owner print the digitally approved application, stamp and sigh it to hand over for the applicant, as enumerated in figure 6. In both the processes As-Is and To-Be the Accountant is assigned the work of Physical verification. But the To-Be process designed is IT enabled, has computing power and Computerised decision making component within the system. The problem faced by him in As-Is process is solved with the help of computerised decision making, such decision making may work on Travelling Sales Problem and the Assignment (Manoj, 2009).

IV CONCLUSIONS

The performance of decision making system can be further improved by considering more decision parameters like taking onto account verification of remaining family members, pending application, dividing the area into more small components, considering the real distance, counting the verification done per day etc. Likewise more decision support could be developed for an example in case of ration card distribution. The problem faced by the service owner is in allocating the ration cards with even distribution coordinating with the supply and demand of

quota allocated in district. The same decision support could work for pension allocation with a little modification.

REFERENCES

[1] J. N. Danziger and K. V. Andersen, "the Impacts of Information Technology on Public Administration: an Analysis of Empirical Research From the 'Golden Age' of Transformation[1]," Int. J. Public Adm., vol. 25, no. 5, pp. 591–627, Apr. 2002.

[2] Scavo and Shi, World Wide Website Design and Use in Public Management. Idea Group Publishing, 1999, pp. 246–66.

[3] M. Janssen and E. Estevez, "Lean government and platform-based governance—Doing more with less," Gov. Inf. Q., vol. 30, pp. S1–S8, Jan. 2013.

[4] M. . Gupta and D. Jana, "E-government evaluation: a framework and case study," Gov. Inf. Q., vol. 20, no. 4, pp. 365–387, Jan. 2003.

[5] D. Bhattacharya, U. Gulla, and M. P. Gupta, "Asia Pacific Business Review," 2011.

[6] M. Hammer and J. Champy, "Reengineering the Corporation A Manifesto For Business Revolution," 2000.

[7] M. Al-mashari, Z. Irani, and M. Zairi, "Holistic Business Process Reengineering : An International Empirical Survey," vol. 00, no. c, p. 7695, 2001.

[8] "Book reviews.," J. Psychother. Pract. Res., vol. 1, no. 4, pp. 387–90, Jan. 1992.

[9] A. Adla, "A Distributed Architecture for Cooperative Intelligent Decision Support Systems," vol. 2, no. 2, pp. 22–29, 2007.

[10] N. Taghezout, A. Adla, and P. Zaraté, "A Multi-agent Framework for Group Decision Support System : Application to a Boiler Combustion Management System (GLZ)," vol. 3, no. 2, pp. 9–20, 2009.

[11] Singh, M.K. (2009), "Development of Decision Support System for E- District Project of Gaziabhad Through Analysis of BPR", M.Tech Thesis, Indian Institute of Technology, Delhi

JAVA VIRTUAL MACHINE

Manjeet Saini[1], Abhishek Jain[2], Ashish Chauhan[3]

[1, 2, 3]*Department Of Computer Science And Engineering, Dronacharya College Of Engineering Khentawas, Farrukh Nagar, Gurgaon, Haryana*

ABSTRACT

*This machine or the '***Simulated computer within the computer***' is known as the "***Java Virtual Machine***" or* ***JVM****. It is an abstract machine. It is a specification that provides runtime environment in which java byte code can be executed. JVM loads, verifies and executes the code. It provides a runtime environment. It provides definitions for the Memory area, Class file format, Register set, Garbage-collected heap, fatal error reporting etc. The Java Virtual Machine forms part of a large system, the Java Runtime Environment (JRE). Each operating system and CPU architecture requires a different JRE.*

Keywords: Just-In-Time, Interpreter, Compiler, Ahead Of Time Compilation, Transpiler, Cross Compiler, De-Compiler, Low Level Language, Assembly Language, High Level Language, Object Code, Translator.

I. INTRODUCTION

Java virtual machine is a virtual machine which is used to execute the java byte code files. It is the code execution component of java development kit.

A Java virtual machine (JVM) works as an interpreter. It interprets compiled java byte code also known as java binary code for computer processor or hardware platform so that it can perform java program's instruction. James Gosling introduces JVM concept to make java platform independent language. Java allows programmers to write code that could run on any platform without the need for rewriting and recompilation for each separate platform. Java use just in time compilation, not interpreting to achieve faster speed.

Creating a Virtual Machine within our computer's memory requires building every major function of a real computer down to the very environment within which programs operate. These functions can be broken down into seven basic parts:

- A set of registers
- A stack
- An execution environment
- A garbage-collected heap
- A constant pool
- A method storage area
- An instruction set

II. COMPILER

A compiler is a computer program (or set of programs) that transforms source code written in a programming language (the source language) into another computer language (the target language, often having a binary form known as object code).The most common reason for transforming the source code is to create an executable program. The name "compiler" is primarily used for programs that translate source code from a high-level programming language to a lower level language (e.g., assembly language or machine code). If the compiled program can run on a computer whose CPU or operating system is different from the one on which the compiler runs, the compiler is known as a cross-compiler. A program that translates from a low level language to a higher level one is a de-compiler. A program that translates between high-level languages is usually called a source-to-source compiler or transpiler. A language rewriter is usually a program that translates the form of expressions without a change of language. More generally, compilers are sometimes called translators.

III. INTERPRETER

Interpreter is a computer program that directly executes or performs instructions written in programming or scripting language without previously compiling them into a machine language program while in java JVM uses JIT for purpose of compiling byte code into machine executable code.

An interpreter generally uses one of the following strategies for program execution:

1. Parse the source code and perform its behavior directly.
2. Translates source code into some efficient intermediate representation and immediately execute this.
3. Explicitly execute stored precompiled code made by a compiler which is part of the interpreter system.

Source programs are compiled ahead of time and stored as machine independent code, which is then linked at run-time and executed by an interpreter and/or compiler (for JIT systems).
While interpretation and compilation are the two main means by which programming languages are implemented, they are not mutually exclusive, as most interpreting systems also perform some translation work, just like compilers. The terms "interpreted language" or "compiled language" signify that the canonical implementation of that language is an interpreter or a compiler, respectively.

IV. C TO BYTE-CODE COMPILER

From the viewpoint of a compiler, the Java virtual machine is just another processor with an instruction set, Java byte-code, for which code can be generated. The JVM was originally designed to execute programs written in the Java language. However, the JVM provides an execution environment in the form of a byte-code instruction set and a runtime system that is general enough that it can be used as the target for compilers of other languages. Because of its close association with the Java language, the JVM performs the strict runtime checks mandated by the Java specification. That requires C to byte-code compilers to provide their own lax machine abstraction, for instance producing compiled code that uses a Java array to represent main memory (so pointers can be compiled to integers), and linking the C library to a centralized Java class that emulates system calls. Most or all of the compilers listed below use a similar approach.
Several C to byte-code compilers exist:

- Nested-VM translates C to MIPS machine language first before converting to Java byte code.
- Cybil works similarly to Nested-VM but targets J2ME devices.
- LLJVM compiles C to LLVM IR, which is then translated to JVM byte-code.
- C2J is also GCC-based, but it produces intermediary Java source code before generating byte-code supports the full ANSI C runtime. Available as a Win32 binary or as a Java executable.
- Java Backend for GCC, possibly the oldest project of its kind, was developed at The University of Queensland in 1999.
- Javum is an attempt to port the full GNU environment to the JVM, and includes one of the above compilers packaged with additional utilities.
- Compilers targeting Java byte-code have been written for other programming languages, including Ada and COBOL

V. JVM (JAVA VIRTUAL MACHINE)

5.1 Just-In-Time Compilation

Just in time compilation is used by java JVM which is also known as dynamic translation. Just in time compilation is done during execution of a program at run time rather than prior to execution. This consists of translation to machine code which is directly executed. JIT compilation is a combination of two traditional approaches to translation to machine code- ahead of time compilation (AOT) and interpretation and combines some advantages and drawbacks of both. JIT compilation is a form of dynamic compilation and allows adaptive optimization such as dynamic recompilation thus in principle JIT compilation can yield faster execution than static compilation. Interpretation and JIT compilation are particularly suited for dynamic programming languages, as the runtime system can handle late-bound data types and enforce security guarantees. JIT compilation fundamentally uses executable data, and thus poses security challenges and possible exploits. Implementation of JIT compilation consists of compiling source code or byte code to machine code and executing it. This is generally done directly in memory – the JIT compiler outputs the machine code directly into memory and immediately executes it, rather than outputting it to disk and then invoking the code as a separate program, as in usual ahead of time compilation. In modern architectures this runs into a problem due to executable space protection – arbitrary memory cannot be executed, as otherwise there is a potential security hole. Thus memory must be marked as executable; for security reasons this should be done after the code has been written to memory, and marked read-only, as writable/executable memory is a security hole

5.2 AOT (Ahead of Time Compilation)

Dynamic recompilation is a feature of some emulators and virtual machines, where the system may recompile some part of a program during execution. By compiling during execution, the system can tailor the generated code to reflect the program's run-time environment, and potentially produce more efficient code by exploiting information that is not available to a traditional static compiler. Adaptive optimization is a technique in computer science that performs dynamic recompilation of portions of a program based on the current execution profile. With a simple implementation, an adaptive optimizer may simply make a trade-off between Just-in-time compilation and interpreting instructions Ahead-of-time (AOT)

compilation is the act of compiling a high-level programming language such as C, or an intermediate language such as Java byte-code, .NET Common Intermediate Language (CIL), IBM System/38 or IBM System "Technology Independent Machine Interface" code, into a native (system-dependent) machine code. Most languages with a managed code runtime that can be compiled to an intermediate language take advantage of just-in-time (JIT). This, briefly, compiles intermediate code into machine code for a native run while the intermediate code is executing, which may decrease an application's performance. Ahead-of-time compilation eliminates the need for this step by performing the compilation before execution rather than during execution.

AOT compilation is mostly beneficial in cases where the interpreter (which is small) is too slow or JIT is too complex or introduces undesirable latencies. In most situations with fully AOT compiled programs and libraries it is possible to drop considerable fraction of runtime environment, thus saving disk space, memory and starting time. Because of this it can be useful in embedded or mobile devices. AOT in most cases produces machine optimized code, just like a 'standard' native compiler. The difference is that AOT transforms the byte-code of an existing virtual machine into machine code. AOT compilers can perform complex and advanced code optimizations which in most cases of JIT will be considered much too costly. On the other hand AOT can't usually perform some optimizations possible in JIT, like runtime profile-guided optimizations, pseudo-constant propagation or indirect/virtual function in lining.

V1. EXECUTION OF INSTRUCTION

The class loader subsystem is responsible for more than just locating and importing the binary data for classes. It must also verify the correctness of imported classes, allocate and initialize memory for class variables, and assist in the resolution of symbolic references. These activities are performed in a strict order:

a. Loading: finding and importing the binary data for a type
b. Linking: performing verification, preparation, and (optionally) resolution
c. Verification: ensuring the correctness of the imported type
d. Preparation: allocating memory for class variables and initializing the memory to default values
e. Resolution: transforming symbolic references from the type into direct references.
f. Initialization: invoking Java code that initializes class variables to their proper starting values.

6.1 Startup Delay And Optimizations

JIT typically causes a slight delay in initial execution of an application, due to the time taken to load and compile the byte-code. Sometimes this delay is called "startup time delay". In general, the more optimization JIT performs, the better the code it will generate, but the initial delay will also increase. A JIT compiler therefore has to make a trade-off between the compilation time and the quality of the code it hopes to generate. However, it seems that much of the startup time is sometimes due to IO-bound operations rather than JIT compilation (for example, the rt.jar class data file for the Java Virtual Machine (JVM) is 40 MB and the JVM must seek a lot of data in this contextually huge file). One possible optimization, used by Sun's Hot-Spot Java Virtual Machine, is to combine interpretation and JIT compilation. The application code is initially interpreted, but the JVM monitors which sequences of byte-code are frequently executed and translates them to machine code for direct execution on the hardware. For byte-code which is executed only a few times, this saves the compilation time and reduces the initial latency; for frequently executed byte-code, JIT compilation is used to

run at high speed, after an initial phase of slow interpretation. Additionally, since a program spends most time executing a minority of its code, the reduced compilation time is significant. Finally, during the initial code interpretation, execution statistics can be collected before compilation, which helps to perform better optimization. The correct tradeoff can vary due to circumstances. For example, Sun's Java Virtual Machine has two major modes—client and server. In client mode, minimal compilation and optimization is performed, to reduce startup time. In server mode, extensive compilation and optimization is performed, to maximize performance once the application is running by sacrificing startup time. Other Java just-in-time compilers have used a runtime measurement of the number of times a method has executed combined with the byte-code size of a method as a heuristic to decide when to compile. Still another uses the number of times executed combined with the detection of loops. In general, it is much harder to accurately predict which methods to optimize in short-running applications than in long-running ones. Native Image Generator by Microsoft is another approach at reducing the initial delay. Native Image Generator pre-compiles byte-code in a Common Intermediate Language image into machine native code. As a result, no runtime compilation is needed. .NET framework 2.0 shipped with Visual Studio 2005 runs Native Image Generator on all of the Microsoft library DLLs right after the installation. Pre-jitting provides a way to improve the startup time. However, the quality of code it generates might not be as good as the one that is jitted, for the same reasons why code compiled statically, without profile-guided optimization, cannot be as good as JIT compiled code in the extreme case: the lack of profiling data to drive, for instance, inline caching. There also exist Java implementations that combine an AOT (ahead-of-time) compiler with either a JIT compiler (Excelsior JET) or interpreter (GNU Compiler for Java.)

VII. SUMMARY

In a byte-code-compiled system, source code is translated to an intermediate representation known as byte-code. Byte-code is not the machine code for any particular computer, and may be portable among computer architectures. The byte-code may then be interpreted by, or run on, a virtual machine. The JIT compiler reads the byte-codes in many sections (or in full, rarely) and compiles them dynamically into machine language so the program can run faster. Java performs runtime checks on various sections of the code and this is the reason the entire code is not compiled at once. This can be done per-file, per-function or even on any arbitrary code fragment; the code can be compiled when it is about to be executed (hence the name "just-in-time"), and then cached and reused later without needing to be recompiled. In contrast, a traditional interpreted virtual machine will simply interpret the byte-code, generally with much lower performance. Some interpreters even interpret source code, without the step of first compiling to byte-code, with even worse performance. Statically compiled code or native code is compiled prior to deployment. A dynamic compilation environment is one in which the compiler can be used during execution. For instance, most Common Lisp systems have a compile function which can compile new functions created during the run. This provides many of the advantages of JIT, but the programmer, rather than the runtime, is in control of what parts of the code are compiled. This can also compile dynamically generated code, which can, in many scenarios, provide substantial performance advantages over statically compiled code, as well as over most JIT systems. A common goal of using JIT techniques is to reach or surpass the performance of static compilation, while maintaining the advantages of byte-code interpretation: Much of the "heavy lifting" of parsing the original source code and

performing basic optimization is often handled at compile time, prior to deployment: compilation from byte-code to machine code is much faster than compiling from source. The deployed byte-code is portable, unlike native code. Since the runtime has control over the compilation, like interpreted byte-code, it can run in a secure sandbox. Compilers from byte-code to machine code are easier to write, because the portable byte-code compiler has already done much of the work.

JIT code generally offers far better performance than interpreters. In addition, it can in some cases offer better performance than static compilation, as many optimizations are only feasible at run-time:

1. The compilation can be optimized to the targeted CPU and the operating system model where the application runs. For example JIT can choose SSE2 vector CPU instructions when it detects that the CPU supports them. However there is currently no mainstream JIT that implements this. To obtain this level of optimization specificity with a static compiler, one must either compile a binary for each intended platform/architecture, or else include multiple versions of portions of the code within a single binary.
2. The system is able to collect statistics about how the program is actually running in the environment it is in, and it can rearrange and recompile for optimum performance. However, some static compilers can also take profile information as input.
3. The system can do global code optimizations (e.g. in lining of library functions) without losing the advantages of dynamic linking and without the overheads inherent to static compilers and linkers. Specifically, when doing global inline substitutions, a static compilation process may need run-time checks and ensure that a virtual call would occur if the actual class of the object overrides the in lined method, and boundary condition checks on array accesses may need to be processed within loops. With just-in-time compilation in many cases this processing can be moved out of loops, often giving large increases of speed.
4. Although this is possible with statically compiled garbage collected languages, a byte-code system can more easily rearrange executed code for better cache utilization.

VIII. FUTURE SCOPE

Continuing porting more of Perl to the JVM via Kawa is the most open area for future work . Currently, only a small subset of Perl is supported, but the path is clear. The task of porting Perl to the JVM becomes much more feasible via the Kawa's architecture. The Kawa/JVM environment can be a real competitor to Microsoft's .NET system. Kawa/JVM system has the added advantage of being completely open and free software, while Microsoft's .NET will remain proprietary. This advantage can surely carry a Kawa/JVM-based language system, along with a Perl port to Kawa/JVM, to success for users and programmers alike.

IX. REFERENCES

[1] Compiler textbook references a collection of references to mainstream Compiler Construction Textbooks.
[2] How the Java Virtual Machine Works by Bikash Shaw.
[3] Compiler textbook references A collection of references to mainstream Compiler Construction Textbooks.
[4] Aho, Alfred V.; Sethi, Ravi; Ullman, Jeffrey D. (1986). Compilers: Principles, Techniques, and Tools (1st Ed.). Addison-Wesley. ISBN 9780201100884.

[5] Allen, Frances E. (September 1981). "A History of Language Processor Technology in IBM". IBM Journal of Research and Development (IBM) **25** (5). (Subscription required (help)).

[6] Allen, Randy; Kennedy, Ken (2001). Optimizing Compilers for Modern Architectures. Morgan Kaufmann Publishers. ISBN 1-55860-286-0.

[7] Appel, Andrew Wilson (2002). Modern Compiler Implementation in Java (2nd Ed.).Cambridge University Press. ISBN 0-521-82060-X.

[8] Apple, Andrew Wilson (1998). Modern Compiler Implementation in ML. Cambridge University Press. ISBN 0-521-58274-1.

[9] Bornat, Richard (1979). Guide. MacMillan. ISBN 0-333-21732-2.

[10] Cooper, Keith D.; Torczon, Linda (2004). Engineering a Compiler. Morgan Kaufmann. ISBN 1-55860-699-8.

[11] Leveret, Bruce W.; Catelli, R. G. G.; Newcomer, Joseph M.; Hobbs, S.O.; Reiner, A.H.; Schatz, B.R.; Wulf, W.A. (August 1980). "An Overview of the Production – Quality Compiler – Compiler Project". Computer (Carnegie-Mellon University) 13 (8): 38–49.Doi: 10.1109/MC.1980.1653748. ISSN 0018-9162. (Subscription required (help)).

[12] McKee-man, William Marshall; Horning, James J.; wort-man, David B. (1970). A Compiler Generator. Englewood Cliffs, NJ: Prentice-Hall. ISBN 0-13-155077-2.

[13] Much-nick, Steven (1997). Advanced Compiler Design and Implementation. Morgan Kaufmann Publishers. ISBN 1-55860-320-4.

[14] Scott, Michael Lee (2005). Programming Language Pragmatics (2nd ed.). Morgan Kaufmann. ISBN 0-12-633951-1.

[15] Srikant, Y. N.; Shankar, Priti (2003). The Compiler Design Handbook: Optimizations and Machine Code Generation. CRC Press. ISBN 0-8493-1240-X.

KERNEL OPERATING SYSTEM

Manjeet Saini[1], Abhishek Jain[2], Ashish Chauhan[3]

Department Of Computer Science And Engineering, Dronacharya College Of Engineering
Khentawas, Farrukh Nagar, Gurgaon, Haryana, (India)

ABSTRACT

The central module of an operating system (OS) is the Kernel. It is the part of the operating system that loads first, and it remains in main memory. It is necessary for the kernel to be very small while still providing all the essential services needed by other parts of the OS because it stays in the memory. To prevent kernel code from being overwritten by programs or other parts of the operating system it is loaded into a protected area of memory. The presence of an operating system kernel is not a necessity to run a computer. Directly loading and executing the programs on the "bare metal" machine is possible, provided that the program authors are willing to do without any OS support or hardware abstraction. Many video game consoles and embedded systems still constitute the "bare metal" approach. But in general, newer systems use kernels and operating systems.

Keywords: Scalability, Multicore Processors, Message Passing

I. INTRODUCTION

In computing, the kernel is a computer program that manages input/output requests from software, and translates them into data processing instructions for the central processing unit and other electronic components of a computer. When a computer program (in this context called a process) makes requests of the kernel, the request is called a system call. Various kernel designs differ in how they manage system calls and resources.

For example, a monolithic kernel executes all the operating system instructions in the same address space in order to improve the performance of the system. A microkernel runs most of the operating system's background processes in user space, to make the operating system more modular and, therefore, easier to maintain. Because of its critical nature, the kernel code is usually loaded into a protected area of memory, which prevents it from being overwritten by other, less frequently used parts of the operating system or by application programs. The kernel performs its tasks, such as executing processes and handling interrupts, in kernel space, whereas everything a user normally does, such as writing text in a text editor or running programs in a GUI (graphical user interface), is done in user space. This separation is made in order to prevent user data and kernel data from interfering with each other and thereby diminishing performance or causing the system to become unstable (and possibly crashing).

II. FUNCTIONS OF KERNEL

The kernel's primary function is to mediate access to the computer's resources, including:

This central component of a computer system is responsible for running or executing programs. The kernel takes responsibility for deciding at any time which of the many running programs should be allocated to the processor or processors.

Random-access memory is used to store both program instructions and data. Typically, both need to be present in memory in order for a program to execute. Often multiple programs will want access to memory, frequently demanding more memory than the computer has available. The kernel is responsible for deciding which memory each process can use, and determining what to do when not enough is available. I/O devices include such peripherals as keyboards, mice, disk drives, printers, network adapters, and display devices. The kernel allocates requests from applications to perform I/O to an appropriate device and provides convenient methods for using the device (typically abstracted to the point where the application does not need to know implementation details of the device). Kernels also usually provide methods for synchronization and communication between processes called inter-process communication (IPC). The kernel has full access to the system's memory and must allow processes to safely access this memory as they require it. Often the first step in doing this is virtual addressing, usually achieved by paging and/or segmentation. Virtual addressing allows the kernel to make a given physical address appear to be another address, the virtual address. Virtual address spaces may be different for different processes; the memory that one process accesses at a particular (virtual) address may be different memory from what another process accesses at the same address. This allows every program to behave as if it is the only one (apart from the kernel) running and thus prevents applications from crashing each other. On many systems, a program's virtual address may refer to data which is not currently in memory. The layer of indirection provided by virtual addressing allows the operating system to use other data stores, like a hard drive, to store what would otherwise have to remain in main memory (RAM). As a result, operating systems can allow programs to use more memory than the system has physically available. When a program needs data which is not currently in RAM, the CPU signals to the kernel that this has happened, and the kernel responds by writing the contents of an inactive memory block to disk (if necessary) and replacing it with the data requested by the program. The program can then be resumed from the point where it was stopped. This scheme is generally known as demand paging. Virtual addressing also allows creation of virtual partitions of memory in two disjointed areas, one being reserved for the kernel (kernel space) and the other for the applications (user space). The applications are not permitted by the processor to address kernel memory, thus preventing an application from damaging the running kernel. This fundamental partition of memory space has contributed much for current designs of actual general-purpose kernels and is almost universal in such systems, although some research kernels (e.g. Singularity) take other approaches. To perform useful functions, processes need access to the peripherals connected to the computer, which are controlled by the kernel through device drivers. A device driver is a computer program that enables the operating system to interact with a hardware device. It provides the operating system with information of how to control and communicate with a certain piece of hardware. The driver is an important and vital piece to a program application. The design goal of a driver is abstraction; the function of the driver is to translate the OS-mandated function calls (programming calls) into device-specific calls. In theory, the device should work correctly with the suitable driver. Device drivers are used for such things as video cards, sound cards, printers, scanners, modems, and LAN cards.

The common levels of abstraction of device drivers are:

1. **On The Hardware Side**:

- Interfacing directly.
- Using a lower-level device driver (file drivers using disk drivers).
- Using a high level interface (Video BIOS).

- Simulating work with hardware, while doing something entirely different.

2. On The Software Side:

- Allowing the operating system direct access to hardware resources.
- Implementing only primitives.
- Implementing an interface for non-driver software (Example: TWAIN).
- Implementing a language, sometimes high-level (Example PostScript).

For Example, to show the user something on the screen, an application would make a request to the kernel, which would forward the request to its display driver, which is then responsible for actually plotting the character/pixel. A kernel must maintain a list of available devices. This list may be known in advance (e.g. on an embedded system where the kernel will be rewritten if the available hardware changes), configured by the user (typical on older PCs and on systems that are not designed for personal use) or detected by the operating system at run time (normally called plug and play). In a plug and play system, a device manager first performs a scan on different hardware buses, such as Peripheral Component Interconnect (PCI) or Universal Serial Bus (USB), to detect installed devices, then searches for the appropriate drivers. As device management is a very OS-specific topic, these drivers are handled differently by each kind of kernel design, but in every case, the kernel has to provide the I/O to allow drivers to physically access their devices through some port or memory location. Very important decisions have to be made when designing the device management system, as in some designs accesses may involve context switches, making the operation very CPU-intensive and easily causing a significant performance overhead.

1. In computing, a system call is how a program requests a service from an operating system's kernel that it does not normally have permission to run. System calls provide the interface between a process and the operating system. Most operations interacting with the system require permissions not available to a user level process, e.g. I/O performed with a device present on the system, or any form of communication with other processes requires the use of system calls. A system call is a mechanism that is used by the application program to request a service from the operating system. They use a machine-code instruction that causes the processor to change mode. An example would be from supervisor mode to protected mode. This is where the operating system performs actions like accessing hardware devices or the memory management unit. Generally the operating system provides a library that sits between the operating system and normal programs. Usually it is a C library such as Glibc or Windows API. The library handles the low-level details of passing information to the kernel and switching to supervisor mode. System calls include close, open, read, wait and write. To actually perform useful work, a process must be able to access the services provided by the kernel. This is implemented differently by each kernel, but most provide a C library or an API, which in turn invokes the related kernel functions. The method of invoking the kernel function varies from kernel to kernel. If memory isolation is in use, it is impossible for a user process to call the kernel directly, because that would be a violation of the processor's access control rules.

   A few possibilities are:

- Using a software-simulated interrupt. This method is available on most hardware, and is therefore very common.
- Using a call gate. A call gate is a special address stored by the kernel in a list in kernel memory at a location known to the processor. When the processor detects a call to that address, it instead redirects to

the target location without causing an access violation. This requires hardware support, but the hardware for it is quite common.

- Using a special system call instruction. This technique requires special hardware support, which common architectures (notably, x86) may lack. System call instructions have been added to recent models of x86 processors, however, and some operating systems for PCs make use of them when available.
- Using a memory-based queue. An application that makes large numbers of requests but does not need to wait for the result of each may add details of requests to an area of memory that the kernel periodically scans to find requests.

III. TYPES OF KERNELS

Naturally, the above listed tasks and features can be provided in many ways that differ from each- other in design and implementation. The principle of separation of mechanism and policy is the substantial difference between the philosophy of micro and monolithic kernels. Here a mechanism is the support that allows the implementation of many different policies, while a policy is a particular "mode of operation". For instance, a mechanism may provide for user log-in attempts to call an authorization server to determine whether access should be granted; a policy may be for the authorization server to request a password and check it against an encrypted password stored in a database. Because the mechanism is generic, the policy could more easily be changed (e.g. by requiring the use of a security token) than if the mechanism and policy were integrated in the same module. In minimal microkernel just some very basic policies are included, and its mechanisms allows what is running on top of the kernel (the remaining part of the operating system and the other applications) to decide which policies to adopt (as memory management, high level process scheduling, file system management, etc.). A monolithic kernel instead tends to include many policies, therefore restricting the rest of the system to rely on them. Mr Per Brinch Hansen presented arguments in favor of separation of mechanism and policy. The failure to properly fulfill this separation is one of the major causes of the lack of substantial innovation in existing operating systems a problem common in computer architecture. The monolithic design is induced by the "kernel mode"/"user mode" architectural approach to protection (technically called hierarchical protection domains), which is common in conventional commercial systems; in fact, every module needing protection is therefore preferably included into the kernel. This link between monolithic design and "privileged mode" can be re-conducted to the key issue of mechanism-policy separation; in fact the "privileged mode" architectural approach melts together the protection mechanism with the security policies, while the major alternative architectural approach, capability-based addressing, clearly distinguishes between the two, leading naturally to a microkernel design (see Separation of protection and security). While monolithic kernels execute all of their code in the same address space (kernel space) microkernels try to run most of their services in user space, aiming to improve maintainability and modularity of the code base. Most kernels do not fit exactly into one of these categories, but are rather found in between these two designs. These are called hybrid kernels. More exotic designs such as Nano and Exo-kernels are available, but are seldom used for production systems. The Xen hypervisor, for example, is a Exo-kernel.

3.1 Monolithic Kernels

In a monolithic kernel, all OS services run along with the main kernel thread, thus also residing in the same memory area. This approach provides rich and powerful hardware access. The main disadvantages of monolithic kernels are the dependencies between system components — a bug in a device driver might crash the entire system — and the fact that large kernels can become very difficult to maintain.

Monolithic kernels, which have traditionally been used by Unix-like operating systems, contain all the operating system core functions and the device drivers (small programs that allow the operating system to interact with hardware devices, such as disk drives, video cards and printers). A monolithic kernel is one single program that contains all of the code necessary to perform every kernel related task. Every part which is to be accessed by most programs which cannot be put in a library is in the kernel space: Device drivers, Scheduler, Memory handling, File systems, Network stacks. Many system calls are provided to applications, to allow them to access all those services. A monolithic kernel, while initially loaded with subsystems that may not be needed can be tuned to a point where it is as fast as or faster than the one that was specifically designed for the hardware, although more in a general sense. Modern monolithic kernels, such as those of Linux and FreeBSD, both of which fall into the category of Unix-like operating systems, feature the ability to load modules at runtime, thereby allowing easy extension of the kernel's capabilities as required, while helping to minimize the amount of code running in kernel space. In the monolithic kernel, some advantages hinge on these points:

- Since there is less software involved it is faster.
- As it is one single piece of software it should be smaller both in source and compiled forms.
- Less code generally means fewer bugs which can translate to fewer security problems.

This design has several flaws and limitations:

Coding in kernel can be challenging, in part because one cannot use common libraries (like a full-featured libc), and because one needs to use a source-level debugger like gdb. Rebooting the computer is often required. This is not just a problem of convenience to the developers. When debugging is harder, and as difficulties become stronger, it becomes more likely that code will be "buggier". Bugs in one part of the kernel have strong side effects; since every function in the kernel has all the privileges, a bug in one function can corrupt data structure of another, totally unrelated part of the kernel, or of any running program. Kernels often become very large and difficult to maintain. Even if the modules servicing these operations are separate from the whole, the code integration is tight and difficult to do correctly. Since the modules run in the same address space, a bug can bring down the entire system. Monolithic kernels are not portable; therefore, they must be rewritten for an each new architecture that the operating system is to be used on. In the microkernel approach, the kernel itself only provides basic functionality that allows the execution of servers, separate programs that assume former kernel functions, such as device drivers, GUI servers, etc.

3.2 Microkernels

Microkernel) is the term describing an approach to Operating System design by which the functionality of the system is moved out of the traditional "kernel", into a set of "servers" that communicate through a "minimal" kernel, leaving as little as possible in "system space" and as much as possible in "user space". A microkernel that is designed for a specific platform or device is only ever going to have what it needs to operate. The microkernel approach consists of defining a simple abstraction over the hardware, with a set of primitives

or system calls to implement minimal OS services such as memory management, multitasking, and inter-process communication. Other services, including those normally provided by the kernel, such as networking, are implemented in user-space programs, referred to as servers. Microkernels are easier to maintain than monolithic kernels, but the large number of system calls and context switches might slow down the system because they typically generate more overhead than plain function calls. Only parts which really require being in a privileged mode are in kernel space: IPC (Inter-Process Communication), Basic scheduler, or scheduling primitives, Basic memory handling, Basic I/O primitives. Many critical parts are now running in user space: The complete scheduler, Memory handling, File systems, and Network stacks. Micro kernels were invented as a reaction to traditional "monolithic" kernel design, whereby all system functionality was put in a one static program running in a special "system" mode of the processor. In the microkernel, only the most fundamental of tasks are performed such as being able to access some (not necessarily all) of the hardware, manage memory and coordinate message passing between the processes. Some systems that use micro kernels are QNX and the HURD. In the case of QNX and Hurd user sessions can be entire snapshots of the system itself or views as it is referred to. The very essence of the microkernel architecture illustrates some of its advantages:

- Maintenance is generally easier.
- Patches can be tested in a separate instance, and then swapped in to take over a production instance.
- Rapid development time and new software can be tested without having to reboot the kernel.
- More persistence in general, if one instance goes hay-wire, it is often possible to substitute it with an operational mirror.

Most micro kernels use a message passing system of some sort to handle requests from one server to another. The message passing system generally operates on a port basis with the microkernel. As an example, if a request for more memory is sent, a port is opened with the microkernel and the request sent through. Once within the microkernel, the steps are similar to system calls. The rationale was that it would bring modularity in the system architecture, which would entail a cleaner system, easier to debug or dynamically modify, customizable to users' needs, and more performing. Other services provided by the kernel such as networking are implemented in user-space programs referred to as servers. Servers allow the operating system to be modified by simply starting and stopping programs. For a machine without networking support, for instance, the networking server is not started. The task of moving in and out of the kernel to move data between the various applications and servers creates overhead which is detrimental to the efficiency of micro kernels in comparison with monolithic kernels.

Disadvantages in the microkernel exist however. Some are:

- Larger running memory footprint
- More software for interfacing is required, there is a potential for performance loss.
- Messaging bugs can be harder to fix due to the longer trip that they have to take versus the one off copy in a monolithic kernel.
- Process management in general can be very complicated.
- The disadvantages for micro kernels are extremely context based. As an example, they work well for small single purpose (and critical) systems because if not many processes need to run, then the complications of process management are effectively mitigated.

So, what the bare minimum that MicroKernel architecture recommends in kernel space?

- Managing memory protection

- Process scheduling
- Inter Process communication (IPC)

A microkernel allows the implementation of the remaining part of the operating system as a normal application program written in a high-level language, and the use of different operating systems on top of the same unchanged kernel. It is also possible to dynamically switch among operating systems and to have more than one active simultaneously.

3.3 Hybrid (Or Modular) Kernel

These kernels represent a compromise that was implemented by some developers before it was demonstrated that pure micro kernels can provide high performance. These types of kernels are extensions of micro kernels with some properties of monolithic kernels. Unlike monolithic kernels, these types of kernels are unable to load modules at runtime on their own. Hybrid kernels are micro kernels that have some "non-essential" code in kernel-space in order for the code to run more quickly than it would were it to be in user-space. Hybrid kernels are a compromise between the monolithic and microkernel designs. This implies running some services (such as the network stack or the file system) in kernel space to reduce the performance overhead of a traditional microkernel, but still running kernel code (such as device drivers) as servers in user space. Hybrid kernels are used in most commercial operating systems such as Microsoft Windows NT 3.1, NT 3.5, NT 3.51, NT 4.0, 2000, XP, Vista, 7, 8, and 8.1 . Apple Inc's own Mac OS X uses a hybrid kernel called XNU which is based upon code from Carnegie Mellon's Mach kernel and FreeBSD's monolithic kernel. They are similar to micro kernels, except they include some additional code in kernel-space to increase performance. Many traditionally monolithic kernels are now at least adding (if not actively exploiting) the module capability. The most well-known from these kernels is the Linux kernel. The modular kernel essentially can have parts of it that are built into the core kernel binary or binaries that load into memory on demand. It is important to note that a code tainted module has the potential to destabilize a running kernel. Many people become confused on this point when discussing micro kernels. It is possible to write a driver for a microkernel in a completely separate memory space and test it before "going" live. When a kernel module is loaded, it accesses the monolithic portion's memory space by adding to it what it needs, therefore, opening the doorway to possible pollution. A few advantages to the modular (or) Hybrid kernel are:

- Faster development time for drivers that can operate from within modules. No reboot required for testing (provided the kernel is not destabilized).
- On demand capability versus spending time recompiling a whole kernel for things like new drivers or subsystems.

Modules, generally, communicate with the kernel using a module interface of some sort. The interface is generalized (although particular to a given operating system) so it is not always possible to use modules. Often the device drivers may need more flexibility than the module interface affords. Essentially, it is two system calls and often the safety checks that only have to be done once in the monolithic kernel now may be done twice. Some of the disadvantages of the modular approach are:

- With more interfaces to pass through, the possibility of increased bugs exists (which implies more security holes).
- Maintaining modules can be confusing for some administrators when dealing with problems like symbol differences.

1. **Nano-kernels:-**

Nano-kernel delegates virtually all services — including even the most basic ones like interrupt controllers or the timer — to device drivers to make the kernel memory requirement even smaller than a traditional microkernel.

2. **Exo-kernels:-**

Exo-kernels are a still experimental approach to operating system design. They differ from the other types of kernels in that their functionality is limited to the protection and multiplexing of the raw hardware, providing no hardware abstractions on top of which to develop applications. This separation of hardware protection from hardware management enables application developers to determine how to make the most efficient use of the available hardware for each specific program. Exo-kernels in themselves are extremely small. However, they are accompanied by library operating systems, providing application developers with the functionalities of a conventional operating system. A major advantage of Exo-kernel-based systems is that they can incorporate multiple library operating systems, each exporting a different API, for example one for high level UI development and one for real-time control.

IV. MONOLITHIC KERNELS VS. MICROKERNELS

As the computer kernel grows, a number of problems become evident. One of the most obvious is that the memory footprint increases. This is mitigated to some degree by perfecting the virtual memory system, but not all computer architectures have virtual memory support. To reduce the kernel's footprint, extensive editing has to be performed to carefully remove unneeded code, which can be very difficult with non-obvious interdependencies between parts of a kernel with millions of lines of code. Due to the various shortcomings of monolithic kernels versus microkernels, monolithic kernels were considered obsolete by virtually all operating system researchers. As a result, the design of Linux as a monolithic kernel rather than a microkernel was the topic of a famous debate between Linus Torvalds and Andrew Tanenbaum. There is merit on both sides of the argument presented in the Tanenbaum–Torvalds debate.

V. PERFORMANCE

Monolithic kernels are designed to have all of their code in the same address space (kernel space), which some developers argue is necessary to increase the performance of the system. Some developers also maintain that monolithic systems are extremely efficient if well-written. The monolithic model tends to be more efficient through the use of shared kernel memory, rather than the slower IPC system of microkernel designs, which is typically based on message passing. Studies that empirically measured the performance of these microkernels did not analyze the reasons of such inefficiency. The explanations of this data were left to "folklore", with the assumption that they were due to the increased frequency of switches from "kernel-mode" to "user-mode" to the increased frequency of inter-process communication and to the increased frequency of context switches.

The reasons for the poor performance of microkernels might as well have been:

(1) An actual inefficiency of the whole microkernel approach,

(2) The particular concepts implemented in those micro-kernels, and

(3) The particular implementation of those concepts. Therefore it remained to be studied if the solution to build an efficient microkernel was, unlike previous attempts, to apply the correct construction techniques. On the other end, the hierarchical protection domains architecture that leads to the design of a monolithic kernel has a significant performance drawback each time there's an interaction between different levels of protection (i.e. when a process has to manipulate a data structure both in 'user mode' and 'supervisor mode'), since this requires message copying by value. The hybrid kernel approach combines the speed and simpler design of a monolithic kernel with the modularity and execution safety of a microkernel.

VI. CONCLUSION

A monolithic OS kernel is faster due to small source and compiled code size. Less code means also less bugs and security issues. Bug fixing or adding new features requires the compilation of the whole source code which is a time and resource consuming process. The idea behind microkernel OS is to reduce the kernel to only basic process communication and IO control and let other system services run in user space just like any other normal processes. Easy and faster integration with 3d party modules is an advantage of Microkernel OS. The conclusion is no OS architecture is better than the other in the general sense because every monolithic operating system meets different needs.

VII. FUTURE SCOPE

The increased resemblance of multi core machines with complex networked systems can prove to be helpful in proposing the multi kernel architecture as a way forward. Current OS structure is tuned for a coherent shared memory with a limited number of homogeneous processors, and is not made for efficiently managing the diversity and scale of future hardware architectures. Viewing the OS as a distributed system rather than centralized system can help in scaling to a network like environment of a modern or future machine.

REFERENCES

[1] A. Baumann, S. Peter, A. Schüpbach, A. Singhania, T. Roscoe, P. Barham, and R.Isaacs. Your computer is already a distributed system. Why isn’t your OS? In Proceedings of the 12th Workshop on Hot Topics in Operating Systems, May 2009.

[2] S. Borkar. Thousand core chips: a technology perspective. In Proceedings of the 44th Annual Design Automation Conference, pages 746–749, 2007.

[3] P. Charles, C. Grotho_, V. Saraswat, C. Donawa, A. Kielstra, K. Ebcioglu, C. von Praun, and V. Sarkar. X10: an object-oriented approach to non-uniform cluster computing. In Proceedings of the ACM Symposium on Object-Oriented Programming Systems, Languages, and Applications, pages 519–538, 2005.

[4] M. Kistler, M. Perrone, and F. Petrini. Cell multiprocessor communication network: Built for speed. IEEE Micro, 26(3):10–23, 2006.

[5] SQLite database engine. http://www.sqlite.org/.

USING TECHNOLOGY IN AGRICULTURE TO SAVE THE FALLING WATER TABLE IN INDIA

Ravinder Singh[1], Tripatjot Singh Panag[2]

[1]*Department of Electronics and Communication Engineering, B.B.S.B.E.C (India)*
[2]*Assistant Professor, Department of Electronics and Communication Engineering, B.B.S.B.E.C (India)*

ABSTRACT

Today India faces several problems and one of the major problems is the shortage of water for irrigation purposes. Ground water is an important source of irrigation mainly in Punjab. Due to irrational irrigation of paddy the utilization of ground water has increased manifold. So to save this underground water table we thought of designing a Wireless Sensor Network (WSN) based irrigation regulator system. The system uses the soil moisture level along with the weather forecast information to regulate the irrigation process. The weather forecast information is acquired from the mobile service provider (IDEA) using Weather Forecast Unit (WFU). This enquiry is made in response to a dry signal generated by Moisture Sensor Unit (MSU).After checking through the weather condition the Main Control Unit (MCU) of the system makes a decision whether to switch ON the motor or not. The system was deployed to regulate the irrigation process for the onion crop during the period Feb-2014 to May-2014. The results indicate that the system can reliably be used to regulate the irrigation process.

Keywords: Wireless Sensors, Soil Moisture, Weather Forecast, Irrigation Regulator, GSM Modem.

I. INTRODUCTION

"Water is not a commercial product like any other, rather a heritage that must be protected, defended and *treated* as such". A recent study based on satellite data conducted by NASA has found that ground water levels in northern India have been declining at an alarming rate, by as much as one foot per year over the last decade [1]. According to the report, it is being pumped and consumed by human activities principally to irrigate the cropland. Ground water is an important source of irrigation in our country. In the coming years the ground water utilization is likely to increase manifolds for expansion of irrigated agriculture and to achieve National targets of food production. The fall in water table in Punjab has been a serious issue. One of the main reasons for it has been the early transplanting of rice (before mid-June), which means severe withdrawal of groundwater, as the monsoon is still far away, temperatures are very high and evapo-transpiration rate (ETR) is maximum. Several water management strategies have been suggested e.g. drip irrigation and on-farm management practices, change in cropping pattern, banning early plantation of paddy etc. New technologies and practices based on WSNs are being developed and implemented in agriculture around the whole world, but their deployment in Punjab is still at the beginning stage. So there is a great challenge before us to implement these technologies practically in the

fields. In this paper, we have taken a step towards the deployment of WSN and Weather Forecast based irrigation regulator system practically in the fields to save the falling water table.

II. SYSTEM DESCRIPTION

In this system we make use of wireless network and sensors to know whether to **ON/OFF** the irrigation system to water the field. Here in addition to the sensor network a GSM system is also used to send and receive the weather report as per requirement. A wireless sensor network is a system comprised of radio frequency (RF) transceivers, sensors, microcontrollers and power sources. Wireless sensor networks with self-organizing, self-configuring, self-diagnosing capabilities have been developed to solve problems or to enable applications that traditional technologies could not address.

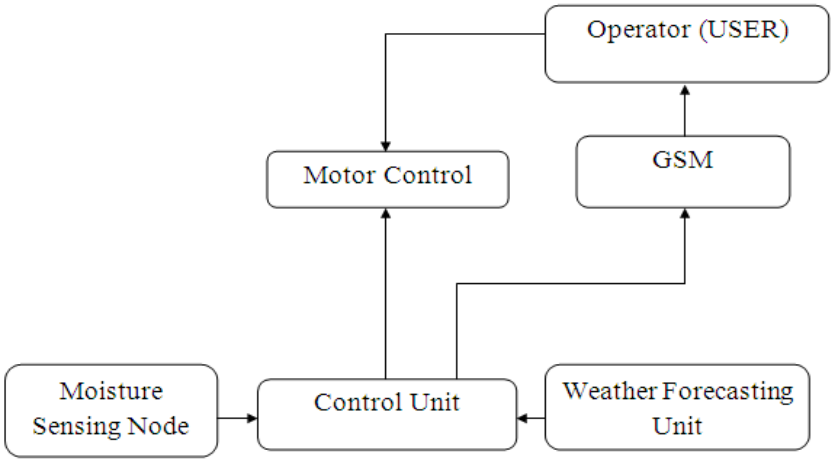

Fig. 1: Block Diagram of WSN and Weather Forecast Based Irrigation Regulator System

For The block diagram consists of the four basic parts i.e. MSN (Moisture Sensing Node), WFU (Weather forecasting Unit), Control unit and GSM, etc.

1. MSU (Moisture Sensing Unit)

This is the most important unit. In this two stainless steel rods are inserted into the soil acting as electrodes. Depending upon the moisture level in the soil, its conductivity will change. This variation shall be measured and used to make a decision.

2. WFU (Weather Forecast Unit)

This is a challenging block here it is intended to access the available weather forecast information. Using GSM, the weather information is obtained through an SMS from a telecommunication company or data can be received from some specific weather forecast station.

3. Control Unit

This unit will act as the brain of the complete hardware. The soil moisture sensed in the first unit plus the weather forecast information from the second unit is given to the control unit. Depending upon these two signals the control units makes a decision. The decision may be sent to the relay to switch the motor ON/OFF or it can be controlled manually by the user as it can cause chaos in the experimental setup.

4. GSM Module

This can be a mobile set or a special modem for sending an SMS to the user indicating the final decision of the control unit. This SMS would tell the user whether to switch the motor ON/OFF for irrigation process.

2.1 Working

The working of the whole system can be divided into three parts or steps. As soon as the system is turned ON, all the three parts starts working. These three parts work in the following manner:

2.1.1. Moisture Sensing Unit (MSU)

The continuous monitoring signals from all the sensors are received by the receiver at the Base Station. The signal received here indicates the soil condition i.e. wet or dry. If the wet signal is received from all the sensors then MSU further performs no action and it waits until the signal gets DRY. As soon as the DRY signal is received, the MSU sends a signal to the second unit i.e. control unit that the soil is DRY. The whole working is shown in Fig.2.

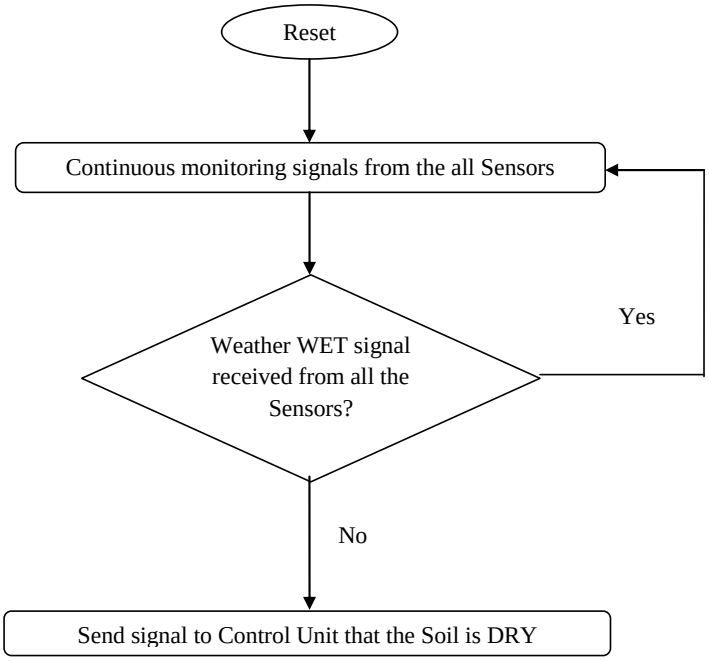

Fig.2: Working of Moisture Sensing Unit.

2.1.2. Control Unit

This unit acts as the brain of the complete hardware. It will check the signal from MSU. If the signal indicates the soil to be DRY, then it sends the signal to Weather Forecasting Unit (WFU) to update weather conditions. Along with this it will also send an alert message to the user regarding the weather enquiry made. In the mean time WFU will send weather information to the control unit. The control unit will interpret this message and carry out the decision making process. If the weather remains conducive for irrigation it will send a message to the user to turn ON the motor otherwise it will send a message “No Need”. The working of the control unit is shown in Fig.3.

2.1.3 Weather Forecasting Unit (WFU)

The WFU will wait for the command signal from the control unit to update the weather condition. On receiving the command from the control unit for updating the weather, the WFU will send a SMS “Weather” to the Idea service centre for weather information. On receiving information, it will forward this information to the control

unit otherwise it will wait for the SMS from the Idea service centre. The complete working of WFU is shown in Fig.4.

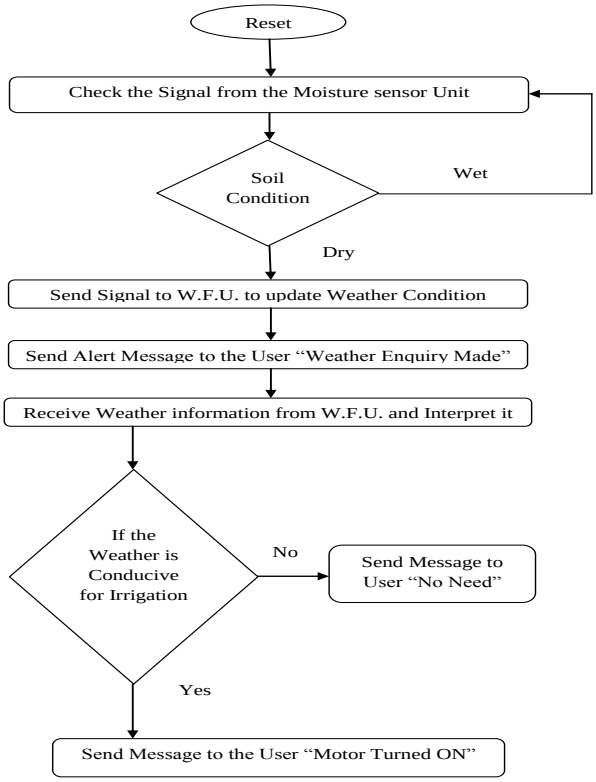

Fig.3: Working of Control Unit

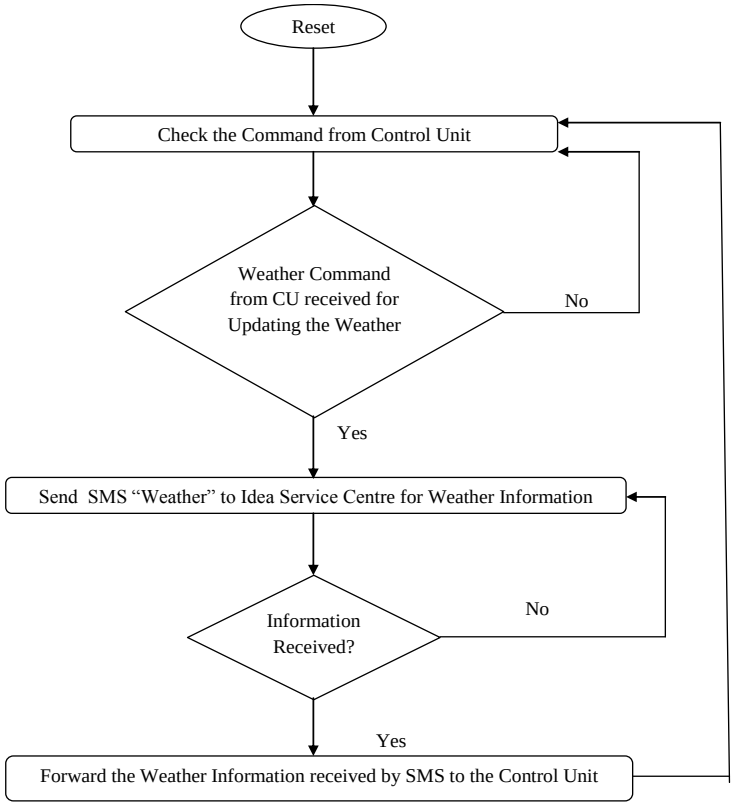

Fig.4: Working of Weather Forecasting Unit

2.2. Hardware

2.2.1. Moisture Sensing Unit (MSU)

It consists of light weight circuit comprising of two stainless steel rods inserted into the soil acting as electrodes. A comparator circuit is used for checking the moisture level in the soil as shown in Fig. 3.9. The TWS-434 and TWS-330 are used for transmitting the moisture level to the base station.

2.2.2. Base station (Control Unit and Weather Forecast Unit (WFU)

It is the unit where whole processing takes place. The signal from the sensors is received by the receivers (RWS-434 & RWS-330) working at different frequencies. The receiver forwards the signal to the controller. The controller AVR Mega series is interfaced with GSM module (SIM300AT) and LCD LMB162A. The GSM modem is used for sending and receiving the weather updates. Along with the weather information it also sends alert messages to the user. The LCD indicates the status of all the sensor units and final decision made by the control unit.

III. RESULT AND DISCUSSION

The project was installed to monitor the irrigation of onions in the current season. The crop was sowed in the month of February in 2014. The system was installed to regulate irrigation process of onions in the month of March in 2014. The system checked the moisture level of the soil. Whenever the soil was found to be dry, it went on to check the weather forecast. If the weather was found to be sunny for the day and also for the next couple of days, it recommended switching ON of the motor. Otherwise it suggested not switching ON the motor as rains were expected. Thus it helped us in saving underground water as well as the crop. The data thus obtained is presented in the table below. The decision made by the system was also verified by manual enquiring about the weather (using IDEA message services) whenever there was a need to water the crop. The manual verification was needed because the project was in the evaluation phase. The data thus obtained is presented in the last column.

S.No.	Date	Soil Condition	Alert Message Received	Decision made by the User	Manual Verification
1.	25-Feb-2014	Nil	Nil	No Need	Nil
2.	27-Feb-2014	Nil	Nil	Watering	Nil
3.	08-Mar-2014	Nil	Nil	Watering	Nil
4.	14-Mar-2014	Nil	Nil	Rain	Nil
Installation of Irrigation Regulator System					
S.No.	**Date**	**Soil Condition**	**Alert Message Received**	**Decision made by the System**	**Manual Verification**
1.	20-Mar-2014	Wet	No	Motor turned OFF	
2.	25-Mar-2014	Dry	Yes	No Need	Rain
3.	29-Mar-2014	Wet	No	Motor turned OFF	
4.	02-Apr-2014	Dry	Yes	No Need	Rain

5.	06-Apr-2014	Wet	No	Motor turned OFF	
6.	10-Apr-2014	Wet	No	Motor turned OFF	
7.	14-Apr-2014	Dry	Yes	Motor turned ON	Sunny
8.	19-Apr-2014	Wet	No	Motor turned OFF	
9.	24-Apr-2014	Dry	Yes	Motor turned ON	Clear
10.	27-Apr-2014	Wet	No	Motor turned OFF	
11.	02-May-2014	Dry	Yes	Motor turned ON	Sunny
12.	04-May-2014	Wet	No	Motor turned OFF	
13.	08-May-2014	Wet	No	Motor turned OFF	
14.	12-May-2014	Wet	No	Motor turned OFF	
15.	13-May-2014	Wet	No	Motor turned OFF	

As can be observed from the table after the installation of system, the fields were found to be dry on five occasions. We will discuss each of these situations one by one. Firstly on 25 March 2014 the Moisture Sensor Unit of the system checks the soil to be dry. On detecting the soil to be dry, the system sends a message "Weather" to the Idea service centre for weather enquiry. In the meantime the system also sends another alert message to the user that the weather enquiry message has been sent. On receiving this alert message a manual verification was carried out by the user in the same way by sending a message "Weather" to the Idea service number 51115. In response to this message user receives a reply message from Idea describing the weather condition for almost a week. The manual verification was needed because the project was in the evaluation phase. The same message was received and interpreted by the system also. The decision made as per the weather conditions of 25 March 2014, 26 March 2014 & 27 March 2014 was sent to the user. It means it was decided by the system to keep the motor OFF during this period as rain was expected. And the rain was experienced on 26 March 2014, evening. Secondly the soil was found to be dry on 2 Apr 2014. Hence the same steps were carried out by the system as in previous case. Decision was made by the system as per the weather conditions on 2 Apr 2014, 03 Apr 2014 & 04

Apr 2014. The weather condition was again not suitable for turning the motor ON. Showers were experienced on 03 Apr 2014, morning. Thirdly the soil was found to be dry on 14 Apr 2014. Decision making process was carried out by the system as per the weather conditions on 14 Apr 2014, 15 Apr 2014 & 16 Apr 2014. So here the decision was made to water the crop because the weather was felt conducive for irrigation process. Weather was sunny for these days. Then the soil was found to be dry on 24 Apr 2014. Decision making process was carried out by the system as per the weather conditions on 24 Apr 2014, 25 Apr 2014 & 26 Apr 2014. It was decided to water the crop because the weather was felt conducive for irrigation process. Last occasion when the soil was found to be dry was on 02 May 2014. On the basis of the weather forecast for 2 May 2014, 3 May 2014 & 4 May 2014, the system suggested to water the crop

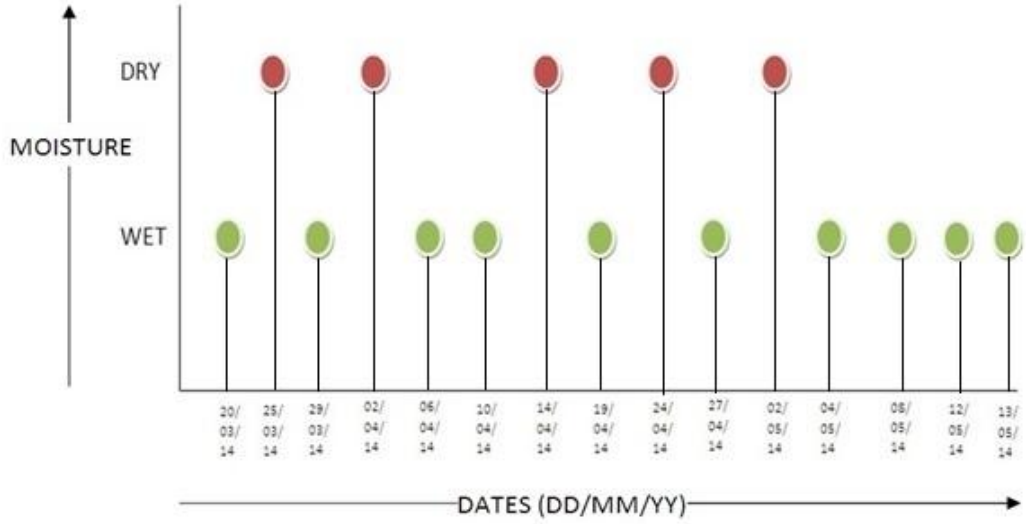

Graph 1 Indicates Moisture Level on different dates

Graph 1 Indicates Moisture Level on different dates. The soil was found to be wet on all occasions except on 25/03/2014, 2/04/2014, 14/04/2014, 24/04/2014, 02/05/2014.

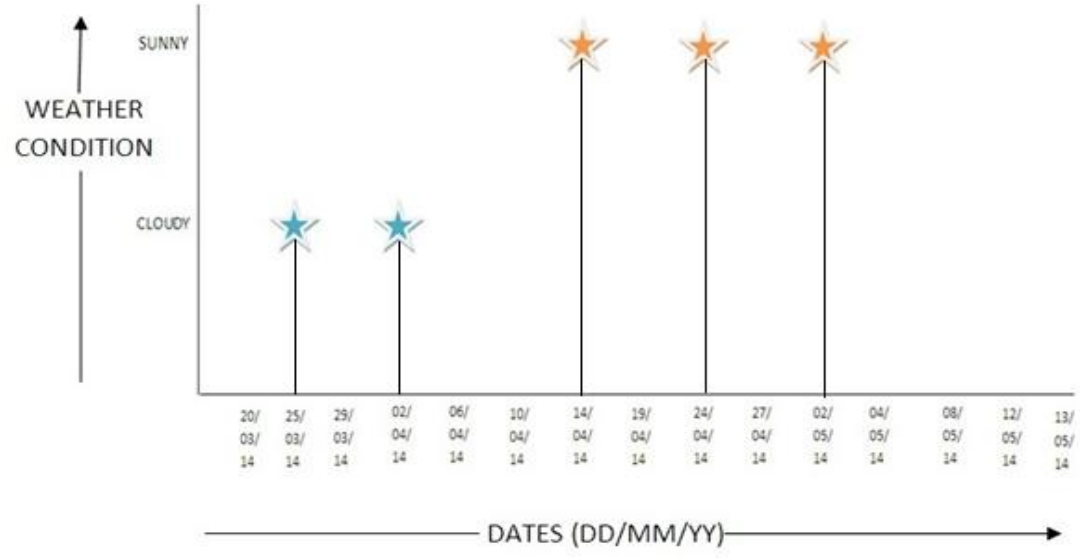

Graph 2 Indicates Weather conditions on different dates

Graph 2 Indicates the Weather conditions on different dates. The graph indicates the weather condition to be cloudy on 25/30/2014 & 02/04/2014, whereas it indicates the weather conditions to be sunny on 14/04/2014, 24/04/2014 & 02/05/2014. The system makes the final decision from graph 1&2. It suggests to water the crop when the weather condition is sunny and soil is found to be dry.

IV. CONCLUSION

Calculated The WSN and Weather Forecast based irrigation regulator system was used over a period of about six months to regulate the irrigation process for two crops – wheat and onion. The results thus obtained help us to conclude that the system can reliably be used to regulate the irrigation process. This automation has many advantages as listed below:-

4.1 It reduces human burden

During conventional agricultural practices one needs to visit the fields regularly. But by using this system there is no need to visit the fields on regular basis to check whether there is need to irrigate the crop or not.

4.2 Avoids misinterpretation

Sometimes by usually interpreting the top layer of the soil we take it as dry, but if we penetrate deep (about an inch) into the soil, we find it to be wet. In fact, it is the moisture content at the root level that matters. But by using the sensor electrodes that goes deep into soil up-to the root level, we come to know the exact moisture content. So there is no chance of wrong interpretation in this case. But there is moisture in the soil near to the roots of the crop.

4.3 Helps in saving Energy and Groundwater

In normal conventional practices we water the crop by making interpretation from the soil upper layer. And we don't have any knowledge about the weather forecast. If it rains within the next couple of days it may lead to loss of energy and groundwater. But by using this system we will have weather forecast information for next three days and proper soil moisture. The system won't water the crop unless the weather conditions are conducive. Therefore, it minimizes the energy and underground water loss.

4.4 Prevent Crop Damage

In conventional practices we water the crop without any weather information. If the weather gets turbulent within a couple of days from watering the crop, it may lead to the crop damage. As the system has weather forecast information therefore, the system saves the crop from being damaged.

4.5 Improves Crop Yield

Using this system the irrigation process is carried out only when it is required by the crop and along with that it also checks the weather forecast information for few couples of days. Therefore, it irrigates the crop with the

exact amount of water required by the crop and also prevents irrigation when it may harm the crop. Hence the crop overall yield is improved.

V. FUTURE SCOPE

A WSN and internet based irrigation regulator system has been developed. Although a lot of efforts have been made for the development of the system; still it can be further improved with some small modification. Following points may be considered for the improvement of the system in future.

A. WSNs can be equipped with other specialized sensors and hence can also be used to regulate the use of Fertilizers, pesticides etc.

B. Sensor node can be made to work on solar energy.

C. Number of sensor nodes can increase to make the system more efficient.

D. High range RF module can be used to cover a larger area.

REFERENCES

[1] Chinchalkar, S., "Determination of Crack Location in Beams using Natural Frequencies", Journal of Sound and Vibration Volume 247 (3), 2001, 417-429.

[2] NASA Satellites Unlock Secret to Northern India's Vanishing Water at: http://www.nasa.gov.com.

[3] D.L. Corwin, Apparent soil electrical conductivity measurements in agriculture. Computers and Electronics in Agriculture 46 (2005) 11-43.

[4] Ning Wang, Wireless sensors in agriculture and food industry. Computers and Electronics in Agriculture 50 (2006) 1-14.

[5] Izzat Din Abdul Aziz et al, Remote monitoring in Agriculture Greenhouse Using wireless sensor and SMS. International Journal of Engineering & technology IJET-IJENS Vol: 09 No: 09.

[6] Nannan Wen, A wireless intelligent valve controller for agriculture Integrated Irrigation System. IFIP International Federation for Information Processing 2011.

[7] Bei Wang et al, Application of wireless sensor network in farmland data acquisition system. Springer-Verlag Berlin Heidelberg 2011.

[8] Xinjian Xiang, Design of fuzzy drip irrigation control system based on ZigBee WSN. IFIP International Federation for Information Processing 2011.

[9] Max Billib betal, A Methodology to identify representative conFig.urations of sensors for monitoring soil moisture. Springer Science B.V. 2011

[10] Robert Coates et al, Wireless sensors networks with irrigation valve control. Computers and Electronics in Agriculture 96 (2013) 13-22.

NOVEL OSCILLATORS IN SUBTHRESHOLD REGIME

Neeta Pandey[1], Kirti Gupta[2], Rajeshwari Pandey[3], Rishi Pandey[4], Tanvi Mittal [5]

[1, 2,3,4,5] *Department of Electronics and Communication Engineering, Delhi Technological University, Delhi, (India)*

ABSTRACT

In this paper, the implementation of oscillators in the subthreshold region is proposed. The ring and coupled ring oscillators are implemented. The techniques of swapped body biasing (SBB) and Dynamic threshold Voltage MOSFET (DTMOS) biasing are introduced for performance improvement of coupled ring oscillators. The functionality of the oscillators in subthreshold region is verified through simulations using 180 nm CMOS technology parameters. A comparison in performance of the oscillators is carried out. It is found that coupled ring oscillator based on the two biasing techniques shows improved performance.

Keywords: Coupled Ring Oscillator, Dynamic Threshold Voltage MOS Biasing, Ring Oscillator, Subthreshold Region, Swapped Body Biasing.

I. INTRODUCTION

The development of the applications demanding low energy application has generated significant scope for subthreshold circuits [1-5]. These circuits are suitable for two type of portable devices. There are energy constraint systems at one hand where the aim is energy conservation and speed of operation is largely irrelevant. The other application need high performance for fraction of time they are operational and spend significant time in non-critical tasks. The mobile phone is apparent example of the later class as it often remains in near idle computation mode while waiting for input from wireless link or user. Oscillator is a key component in a phase-locked loop (PLL) for providing the timing basis in clock control, data recovery, and synchronization [6]. It is also an integral part of voltage controlled oscillator which is employed in a wide variety of applications such as disk-drive read channels, on-chip clock distribution, integrated frequency synthesizers and microprocessor clock generation [7]. This paper proposes the implementation of two ring oscillators in subthreshold region. The first implementation uses a chain of odd numbers of CMOS inverters operating in subthreshold region. In the second implementation, a coupled ring oscillator [6] capable of producing quadrature outputs is proposed. The paper first briefly presents the operation of a MOSFET in subthreshold region in section II. The implementations of the ring and coupled ring oscillators in subthreshold region are presented in the section III. The different biasing techniques used for implementation are described briefly in section IV. The simulation results are presented in section V using CMOS 180nm technology parameters. The conclusion drawn from the results appear in section VI.

IJEEE

II. SUBTHRESHOLD DIGITAL DESIGN

The surface of the Metal-Oxide Semiconductor (MOS) structure is weakly inverted when the gate voltage is sufficient to cause band bending at the surface ranges between φF and 2φF. This region is also called subthreshold and current flows when drain to source potential is applied. The current flow mechanism is similar to that in bipolar transistors i.e. drain current shows exponential dependence on gate to source voltage. This current is called subthreshold current and is primarily a leakage current which flows even when gate to source voltage is below threshold voltage.

In the subthreshold, the power supply voltage VDD is made less than its threshold voltage V_{th}. In this case, the drain current I_{ds} region is exponentially related to the gate voltage V_{gs} as shown in Equation (1) [3]:

$$I_{sub} = I_0 \exp\left(\frac{V_{gs} - V_T}{nV_{th}}\right)\left(1 - \exp\left(\frac{-V_{ds}}{V_{th}}\right)\right) \quad (1)$$

where V_{gs} is the gate-to-source voltage, V_{ds} is the drain-to-source voltage, n is the subthreshold slope factor and V_{th} is temperature equivalent of voltage (V_{th} = kT/q, where k is the Boltzmann constant, T the absolute temperature, and q the electron charge. The factor n of a long-channel uniformly doped device is calculated as:

$$n = 1 + \frac{C_b}{C_g} \quad (2)$$

where C_g and C_b are the gate and bulk capacitances respectively.

A MOSFET operating in subthreshold region offers several advantages. The MOSFETs operating in this region generate low levels of the drain current, thereby creates a high-value resistor. These MOSFETs show low dynamic power consumption due to the lowering of power supply and the drain current [5]. Based on these advantages, we propose the implementation of ring oscillators in the subthreshold region.

III. RING OSCILLATOR

A ring oscillator (RO) is one of the most commonly used components in many integrated systems. The unique features of RO include ease of design with the state-of-art integrated circuit technology (CMOS, BiCMOS), ability to oscillate at lower values of voltage, high frequency oscillations can be achieved, electrically tunable with wide tuning range; attainment of multiphase outputs. Two popular implementations of a ring oscillator have been used in this paper. An RO is a cascade of odd number of delay stages connected in a close loop chain. Fig. 1 shows the traditional CMOS inverter and a ring oscillator using seven inverters. The frequency of oscillation of an RO varies with propagation delay τd of the individual inverter stage and the number of inverter stages used in the ring structure. There must be a phase shift of 2π and unity voltage gain at the oscillation frequency to achieve self-sustained oscillation. In a RO with m inverter stages, a phase shift of π/m is provided by each stage while the remaining phase shift of π is provided by the dc inversion. The signal undergoes m delay

stages in a time of $m\tau d$ to provide a phase shift of π and for another time in a time period of $2m\tau d$ to obtain the remaining phase of π [8]. Therefore, the frequency of oscillation fo can be found out using (3):

$$f_o = \frac{1}{2m\tau d} \quad (3)$$

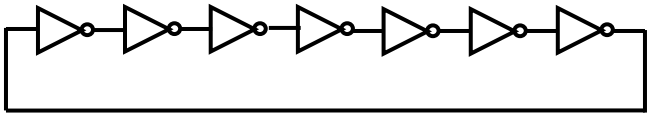

Fig. 1. Ring Oscillator with 7 inverter stages

A coupled ring oscillator (CRO) is designed by coupling two ring oscillators in such a way that only four distinguished nodes are formed. These four nodes generate quadrature outputs having a phase difference of 900 for a completely symmetrical coupling [6]. The implementation of a coupled ring oscillator employing 8 inverter stages is shown in Fig. 2.

IV. BODY BIASING TECHNIQUES

A CMOS inverter operating in the subthreshold region suffers from a drawback of reduced switching speed. This can be addressed by adopting body biasing techniques such as the swapped body biasing (SBB) [9] and the dynamic threshold MOS (DTMOS) biasing technique [10]. In SBB technique, the substrate of the NMOS devices are tied to the power supply voltage V_{DD} whereas those of the PMOS devices are tied to ground. Swapping the bulk terminals of the two MOSFETs increases the drive currents in the subthreshold operation from an exponential current increase, but degrades output node voltages when V_{DD} is greater than the zero bias threshold voltage [5]. Thus, SBB technique provides improved performance under subthreshold supply voltages. A CMOS inverter implemented using SBB technique is shown in Fig. 3. In DTMOS biasing technique, the substrate of the transistor is tied to its gate to allow the threshold voltage to change dynamically with the gate input voltage. With the increase in the gate voltage, the threshold voltage drops resulting in a much higher current drive than standard MOSFET for low-power supply voltages. A CMOS inverter implemented using DTMOS biasing technique is shown in Fig. 4. In this paper, the coupled ring oscillator (Fig. 2) is implemented using inverters with traditional biasing (Fig. 1), SBB (Fig. 3) and DTMOS biasing (Fig. 4).

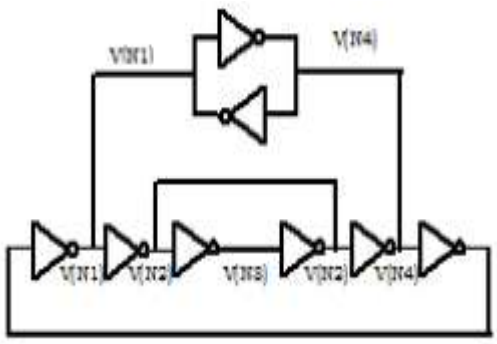

Fig. 2. Coupled Ring Oscillator Two Coupled 3-Stage Ring Oscillator

IJEEE

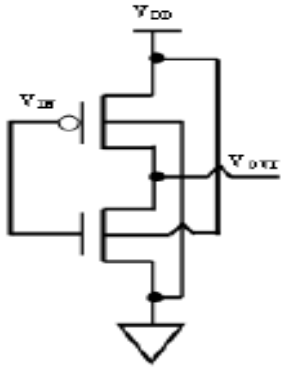

Fig.3. A CMOS Inverter Based On Swapped Body Biasing Technique

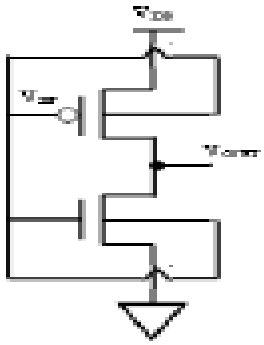

Fig. 4. A CMOS Inverter Based On DTMOS Biasing Technique

V. SIMULATION RESULTS

In the first sub-section, the functionality of ring oscillators in subthreshold region (Fig. 1) is verified. Further, the CRO is implemented using the inverters based on traditional, SBB and DTMOS biasing techniques. Then in the second section, the results of the comparison in performance of the ring oscillator and coupled ring oscillator are presented. All the simulations are carried with SPICE using 180 nm CMOS technology parameters. A power supply and load capacitor of 0.37 V and 1 fF have been taken in simulations respectively.

a. Functional Verification

The ring oscillator (Fig. 1) and the coupled ring oscillator (Fig. 2) are simulated. The waveform obtained for the ring oscillator output is shown in Fig. 5. It can be observed that the ring oscillator conforms to the functionality. The waveforms obtained at the four output nodes of the coupled ring oscillator using DTMOS biasing technique is shown Fig. 6. The waveforms for the coupled ring oscillator using traditional and SBB biasing are not shown for the sake of brevity

b. Performance Comparison

The simulation results for the ring oscillator and the coupled ring oscillator are listed in Table I. The results show that the coupled ring oscillators using SBB and DTMOS biasing techniques are better than the ring oscillators. It can be observed that the frequency of oscillation of the coupled ring oscillators increases by 16.62 MHz, 18.09 MHz in SBB and DTMOS biasing techniques respectively, with respect to traditional biasing. Though the power consumption increases by 859 nW and 757 nW respectively for both the techniques. Also, the SBB and DTMOS biasing based coupled ring oscillator outperforms the ring oscillator by reducing the propagation delay by 76.82 ns and 78.17 ns respectively.

TABLE I. PERFORMANCE COMPARISION OF OSCILLATORS

Performance Parameters	Ring Oscillator	Coupled Ring Oscillator		
		Traditional Biasing	Swapped Body Biasing	DTMOS Biasing
Frequency of oscillation (MHz)	2.19	2.954	19.571	21.040
Propagation Delay (ns)	50.53	89.822	13.008	11.654
Power Dissipation (W)	5.6×10^{-8}	1.14×10^{-7}	9.73×10^{-7}	8.71×10^{-7}

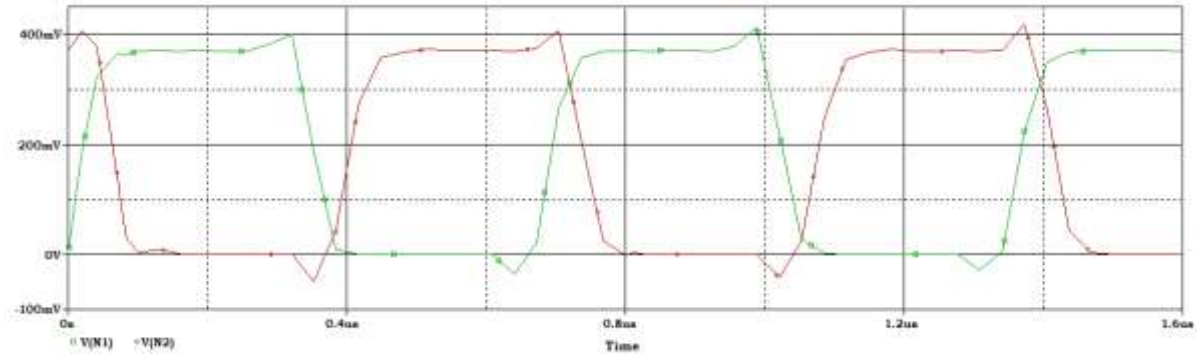

Fig. 5. Output Waveform Of Ring Oscillator Using Traditional Biasing

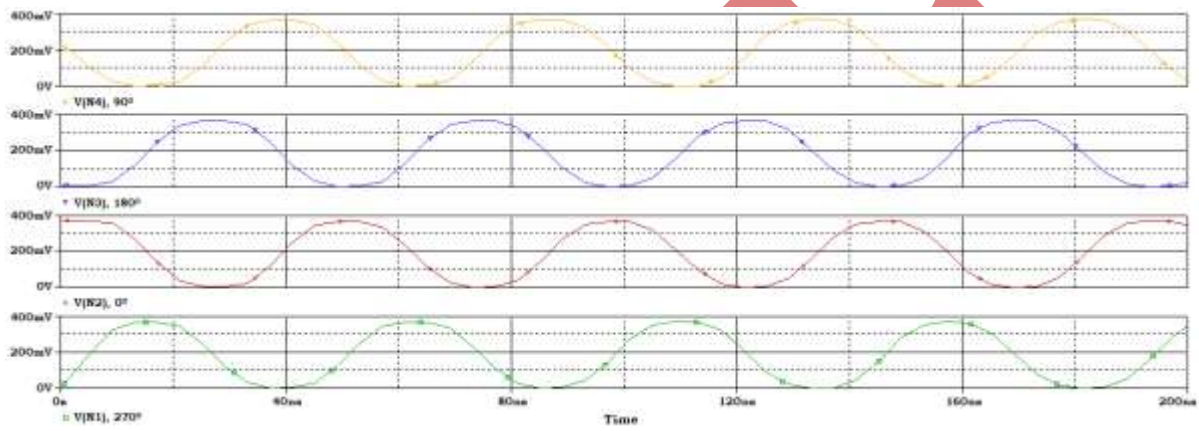

Fig. 6. Output Waveform Of Coupled Ring Oscillator Using DTMOS Biasing Technique

VI. CONCLUSION

This paper proposes the implementation of oscillators in the subthreshold regime. The ring and coupled ring oscillators are implemented. Improved CRO implementations based on swapped body biasing technique and dynamic threshold MOS biasing technique are proposed. The feasibility of the oscillators in subthreshold region is studied through simulations using 180 nm CMOS technology parameters. A comparison in performance of the oscillators show that the coupled ring oscillators based biasing techniques improves the performance significantly.

REFERENCES

[1] M. Alioto, "Understanding DC Behavior of Subthreshold CMOS Logic Through Closed-Form Analysis", IEEE Transactions on Circuits and Systems-I, Vol. 57, No. 7, July 2010, 1597-1607.

[2] H. Soeleman and K. Roy, "Digital CMOS Logic Operation in the Sub Threshold Region" CM Great Lakes Symposium on VLSI 2000: 107-112.

[3] A. Wang, B. H. Calhoun, A. P. Chandrakasan, "Sub-threshold Design for Ultra Low-Power Systems", Springer, 2006.

[4] A. Wang and A. Chandrakasan, "A 180-mV subthreshold FFT processor using a minimum energy design methodology," IEEE J. Solid-State Circuits, vol. 40, no. 1, Jan. 2005, 310-319.

[5] J. Rabaey, J. Ammer, B. Otis, F. Burghardt, Y. H. Chee, N. Pletcher, M. Sheets, and H. Qin, "Ultra-low-power design—The Roadmap to disappearing electronics and ambient intelligence," IEEE Circuits Devices Mag., pp. 23–29, Jul./Aug. 2006.

[6] J. Baker, H. W. Li, D. E. Boyce, "CMOS, Circuit Design, Layout, and Simulation", Wiley, 1997.

[7] I. A. Young, J. K. Gearson and K. L. Wong, "A PLL clock generator with 5 to 110 MHz of lock range for microprocessor," IEEE Journal of Solid State Circuits, Vol, 27, No. 11 1992. 51-52

[8] M.K. Mandal and B.C. Sarkar, "Ring Oscillators: Characteristics and applications", Indian Journal of Pure & Applied Physics Vol. 48, February 2010, 136-145.

[9] J. Nyathi, B. Bero and R. McKinlay, "A Tunable Body Biasing Scheme for Ultra-Low Power and High Speed CMOS Designs," International Symposium on Low Power Electronics and Design - 2006. October 4-6, 2006.

[10] F. Assaderaghi, D. Sinitsky, S. A. Parke, J. Bokor, P. K. Ko, and C. Hu, "Dynamic Threshold-Voltage MOSFET (DTMOS) for Ultra-Low Voltage VLSI," IEEE Transactions on Electron Devices, vol. 44, No. 3, March 1997. 414-422.

IJEE

OPEN ACCESS

International
Journal
Of Modern Engineering Research (IJMER)

Optimization of Tool Wear: A Review

Ramakant Rana[1], Kunal Rajput[2], Rohit Saini[3], Roop Lal[4]

[1]*Assistant Professor, Mechanical and Automation Engineering, Maharaja Agrasen Institute of Technology, Delhi, India*

[2,3]*Student, Mechanical and Automation Engineering, Maharaja Agrasen Institute of Technology, Delhi, India*

[4]*Assistant Professor, Mechanical Engineering, Delhi Technological University, Delhi, India*

Abstract: *The quality of the machined piece and tool life are greatly influenced by determination of maximum temperature of the cutting tool. Numerous researchers have approached to solve this problem with experimental, analytical and numerical analysis. There is hardly a consensus on the basics principles of the thermal problem in metal cutting, even though considerable research effort has been made on it. It is exceedingly difficult to predict in a precise manner the performance of tool for the machining process. This paper reviews work on the requirements for optimization of Tool wear so that its life could easily be predicted.*

Keywords: *Tool Wear, Taguchi, CNC, Optimization, Wear.*

I. INTRODUCTION

Research in metal cutting was started with Cocquilhat in 1851 which measured the work required to remove a given volume of material in drilling. The attempt made by Time led to the explanation of formation of chips in 1870 and further research was made by Tresca in 1873. Later in 1881, Mallock suggested that the cutting process was the shearing of workpiece to form the chip and emphasized the importance of the effect of friction occurring on the cutting tool face as the chip was removed. Further, Taylor investigated the effect of tool material and cutting conditions on tool life during rough operations. Latest fundamental work has been carried out by Ernst and Merchant in 1941 dealing with the mechanics of metal cutting process. The simplest and most widely used model for cutting was first by Ernest and Merchant (1941) and further contribution to study of Ernest and Merchant theory was done by Lee and Shaffer (1951), Kobayashi and Thomsen (1962). Large number of literature is available on the determination of chip-tool interface temperature, factors affecting the interface temperature and techniques of optimization of machining parameters including cutting speed, feed rate, cutting zone temperature, etc. Armerago (1969), Boothroyd (1981), Shaw (1984) and Trent (2000) wrote the most widely used text books. Kalpakjian, et al. (2006), and DeGarmo, et al. (1997) wrote books on more general introductory knowledge. The study machining process by experimental approach is expensive and time consuming peculiarly when a wide range of parameters is included like tool geometry, cutting conditions, and materials.

II. LITERATURE REVIEW

Jensen M.R. et al. [1] stated that an important problem in the machining of drawn parts is tool wear. They said that tool wear can be reduced by increasing the tool lifetime and by making more continuous production flow, by reducing the number of break-downs when the tools have to be re-polished. In their paper, an optimization of the shape of the draw-die profile with regard to wear was carried out using a conventional optimization method and explicit finite element. The optimized draw-die profile had almost twice the tool life compared to that of the initial circular draw-die, if the peak value of wear was used as the wear criteria. The relatively small resources used by them with their optimization approach made the tool wear design relevant for industrial use at the tool-design state.

Sullivan D.O' et al. [2] determined the temperature in a single point turning process. The total work done by a cutting tool in removing metal was determined from the force components on the cutting tool. Approximately, all of this work or energy is converted into heat which is dissipated into the chip, tool and workpiece material. The wear of the tool is related to the cutting forces. Initial experiments conducted involved the simultaneous measurement of forces and temperatures. These experiments focused on the use of embedded thermocouple (in the work piece) and using the infrared thermal camera to monitor the process. They concluded that in machining of aluminium Al 6082-T6 the decreased cutting tool forces and machined surface temperatures was resulted by increased cutting speed (V_C) and increased cutting tool forces and machined

surface temperature was resulted by tool wear. They left the examination of temperature distribution at the tool chip interface for the future work.

Abukhshim N.A. et al. [3] reviewed the previous research work. Research on heat generation and heat dissipation in the orthogonal machining process is critically studied. In addition, temperature measurement techniques applied in metal cutting were also reviewed. The emphasis was on the comparability of test results obtained by a thermal imaging camera in high speed cutting of high strength alloys. Finally, latest work on these topics in metal machining was also reviewed. They reviewed the methods of temperature measurement and the analytical and numerical models for the prediction of temperature and temperature distribution in metal cutting. In metal cutting the Prediction of cutting temperatures is a major challenge. They concluded that fiber-optic pyrometers and infrared thermography techniques for temperature measurement of the high speed cutting process are more promising as compared to other methods as these techniques can measure temperature, as well as, the cooling rate easily, accurately and with fast time response. They stated that technology for consideration of interactions at the tool/chip interface is mainly based on certain assumptions and not on a precise understanding of the underlying physics. They also stated that modeling and simulation of machining processes is mainly suffering from a lack of the fundamental input data.

Many researchers has been undertaking into measuring the temperatures generated during cutting operations. Investigators have attempted to measure these cutting temperatures with various techniques (see figure 1 based on [4])

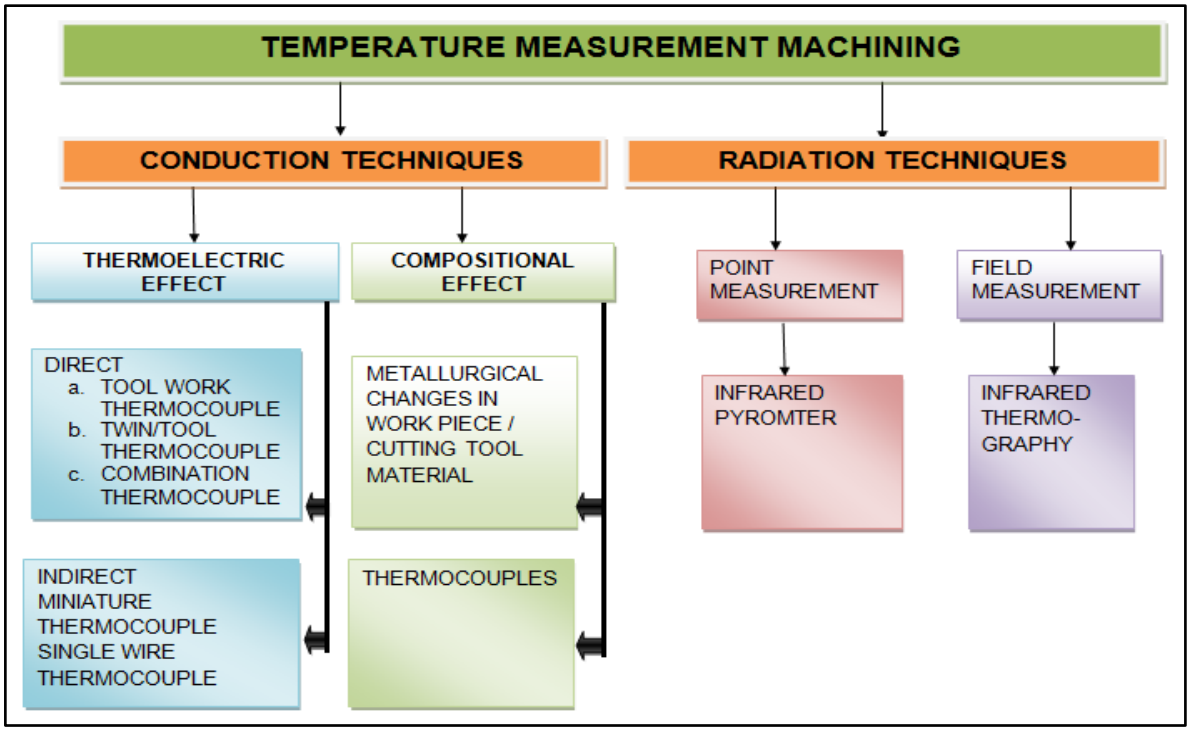

Figure 1: Temperature measurement in machining [4]

Lazoglu Ismail et al. [5] predicted the tool chip temperature in continuous and interrupted machining. They presented a numerical model based on the finite difference method to predict tool and chip temperature fields in continuous and interrupted machining and time varying milling processes. By modeling the heat transfer between the tool and chip at the tool-rake face contact zone Continuous or steady state machining operations like orthogonal cutting were studied. They determined Heat balance equations in partial differential equation forms for the chip and for the tool. The solutions of the steady-state tool and chip temperature fields were taken by finite difference method. The chip thickness was discretized along the time to determine the transient temperature variation in the case of interrupted machining.

Sutter G. et al. [6] presented an experimented setup for the measurement of temperature field in high speed machining. Their paper presented an experimental setup during an orthogonal machining operation with 42 CrMo 4 steel. The technique of temperature measurement was developed on the principle of pyrometer in the visible spectral range by using an intensified CCD camera with very short exposure time and interference filter at 0.8 micrometer. They obtained the temperature gradients in an area close to the cutting edge of the tool, along the secondary shear zone. It was established that their experimental arrangement shown in Figure 2 was quite

efficient and can provide fundamental data on the temperature field in material during orthogonal high speed machining. They showed experimentally that, for a cutting speed of 20 m/s a hot spot was located near the tool-chip interface at a distance of 300-350 μm of the tool tip. This value corresponds to about the two-thirds of the depth of cut. The reaching temperature is around 825°C. The temperature in the chip increases with increasing of the cutting speed. Their result showed that, with an increase of the cutting speed from 20–30 m/s the dependence of the temperature on the cutting speed was more noticeable. They even showed that, the temperature appeared to stabilize for the cutting speeds larger than 40 m/s. A similar tendency was observed with the increasing in the depth of cut and for a cutting speed fixed to 40 m/s by their experimental technique. The temperature in the chip was nearing a saturated value about of 840°C during the process of an un-deformed chip thickness larger than 0.5 mm.

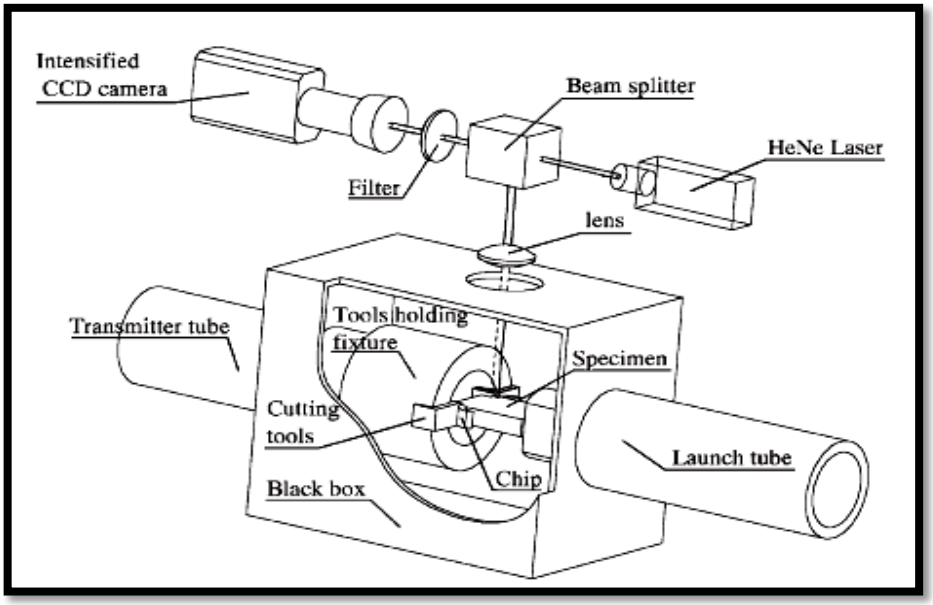

Figure 2: Experimental Apparatus's scheme used by **G. Sutter et al.** [6]

Dogu Yahya et al. [7] designed a numerical model to determine temperature distribution in orthogonal metal cutting. In their study, they developed a thermal analysis model to determine temperature distribution in orthogonal in metal cutting using FEM. Their model was used to calculate the temperature distribution as a function of heat function of heat generation. Assuming that all the work required for cutting is converted to the sensible heat energy the amount of heat generation was calculated by them. Accurate predictions of temperature field over the entire cutting zone were given by the developed model. It was also found that at the half of the contact length from cutting edge, the maximum temperatures for relatively smaller cutting speeds occurred for the analyzed cases. It was clear that the outer surface of the material will be subject to higher heat removal and sudden temperature drop.

Saglam Haci et al. [8] studied the effect of tool geometry and cutting speed on main cutting force and tool tip temperature. They investigated the temperature generated on the tip of the tool in turning and cutting speed on cutting force components and the effects of rake angle and entering angle in geometry of tool in their paper. The experiments were conducted on a CNC lathe to derive the data used for investigation. Each test was conducted with a sharp uncoated tool insert, while keeping the depth of cut and feed rate constant, during the tests. They found that the cutting speed was effective on the tool tip temperature, while the rake angle was effective on all the cutting force components. They found that, the deviation in temperature was 54%, while the average deviation between calculated and measured values of main cutting force was 0.26% in 64 numbers of experiments.

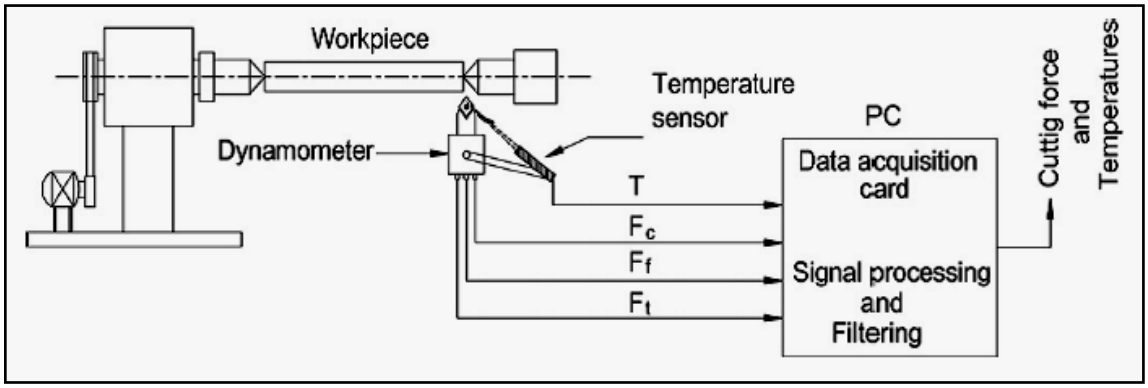

Figure 3: Experimental setup used by **Saglam et al.** [8].

They experimentally found that the main cutting edge subjected to maximum loading and unloading as it enters and leaves the cutting zone abruptly at 90^o of entering angle by using the experimental setup shown in Figure 3. They also found that the impact of load was not exerted on cutting tool when it has an entering angle different then 90^o, because the cutting edge enters and leaves the workpiece gradually. Hence, they concluded that at 60^o to 70^o the optimum entering angle was obtained. They showed that, the cutting forces were reduced and the temperature was increased when the cutting speed was raised. They also showed that, the cutting forces were decreased, for the increased positive rake angle. Their result of cutting forces and temperature evaluated together resulted that the optimum rake angle should be 12^o. Their results of analysis of variance evaluated, that the cutting speed was effective on tool tip temperature while, the rake angle had a significant effect on cutting forces components. They verified their conclusions by the correlation coefficients.

Ueda Takashi et al. [9] determined the temperature of a signal crystal diamond tool in turning. They in precision turning, investigated experimentally and theoretically the temperature on the rake face of a single crystal diamond tool. They used FEM to calculate the temperature distribution in the tool and in the work piece numerically. Two-color pyrometer with an optical fiber was used by them to measure the temperature on the rake face of a single crystal diamond tool in precision turning and then they calculated numerically using FEM. They showed that, regardless of the size of the object, the two-color pyrometer is capable of measuring the temperature when the temperature of the object is constant.

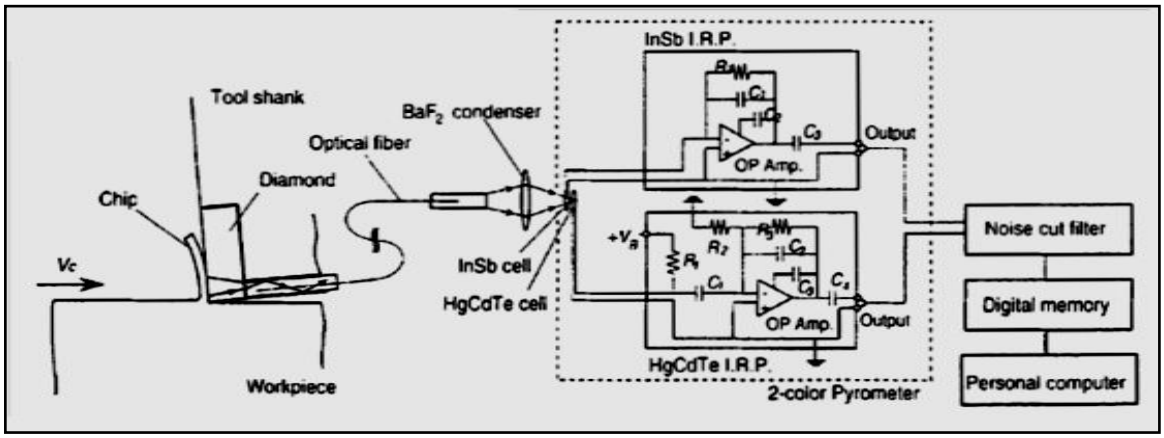

Figure 4: Experimental setup used by **Ueda Takashi et al.** [9]

They experimentally concluded that, it is possible to estimate the maximum temperature from the measured temperature, when the object has a surface of known temperature distribution. They also concluded that, when the object has a surface of known temperature distribution, it is possible to estimate the maximum temperature from the measured temperature and the increase in cutting speed increases the temperature on the rake face. Their measured values of temperatures in the experiment agreed well with their calculated results numerically using FEM.

Tanikic et al. [10] studied the metal cutting process parameters modeling using artificial neural network (ANN) and hybrid, adaptive neuro fuzzy systems. The main aim of their experiment was to conduct the qualitative analysis of metal cutting processes, and also identifying and resolving the frequently occurring problems, while improving the productivity of metal cutting by reducing the manufacturing costs. The infrared camera was used to measure and monitor the temperature at the chip tool interface. They also, modeled the

measured data by using ANN and neuro fuzzy system. Their work concluded that, the implementation of artificial intelligence based systems in metal cutting process is possible. In the end, they proposed the global system for predicting the state of cutting tool along with sub-systems for cutting temperature, cutting force and arithmetic mean deviation prediction.

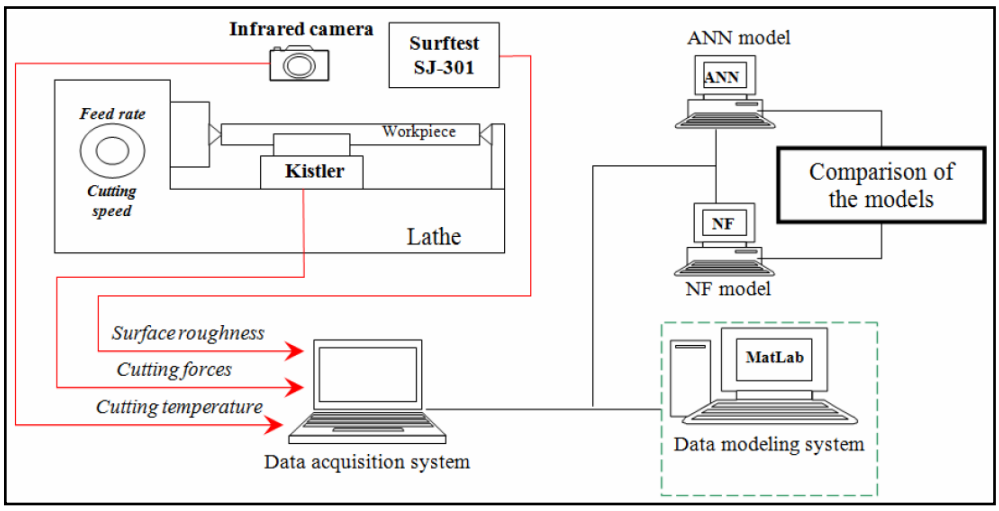

Figure 5: Component relations and information flow of material handling system

Fata [11] proposed the method of embedded thermocouple for temperature measurement along with infrared pyrometer. The experiments are conducted for dry and orthogonal machining condition with simultaneous measurement of temperature by embedded thermocouple and infrared pyrometer. With the help of these experiments a relation was established between tool temperature and cutting parameters such as cutting speed, feed rate and depth of cut. The results so obtained showed that if cutting speed, feed rate and depth of cut are increased then the tool temperature also increases which reduces the life of the cutting tool. These investigations revealed that the most effective cutting parameter in tool temperature rise is the cutting speed, especially at high range of cutting conditions. It also showed an increase in feed rate and depth of cut will lead to an almost straight line with low slope on the graph of tool temperature when plotted against them.

Adnan Jameel et al. [12] focused their study on the temperature generated at two heat zones namely primary heat zone (shear zone) and secondary heat zone (tool chip interface zone). They proposed two new objective functions for optimizing the cutting temperature problems and this system used particle swarm optimization (PSO) methodology to determine the optimal temperature. Their experiments showed that major amount of energy is converted into heat in the shear zone while the heat generated at the tool chip interface zone is due to the rubbing action at that interface. They concluded that heat distribution pattern is dependent on the size and thermal conductivity of the tool-work material and the cutting conditions. Specifically the results were obtained for mild steel work and carbide insert cutting tool in dry turning operation. Their study concluded that main cutting force, feed rate and depth of cut greatly influence the shear zone temperature while chip thickness and friction force have low effect. They also concluded that, the chip tool interface temperature increased with increase in feed rate and main cutting force while it decreased with increase in the depth of cut. Their whole study of paper concluded that feed rate has a huge effect on shear zone and chip tool interface zone temperature as compared to other parameters. Their study also concluded that till date the nearly all of optimization algorithms concentrated to optimize parameters are other than cutting temperature and according to their studies there are few papers focusing on the cutting temperature optimization.

Shirpurkar P.P. et al. [13] attempted to review the literature on optimization of machining parameters in turning processes by using different tool inserts. During their review of different conventional techniques employed for optimization of parameters were also studied by them. These techniques include geometric programming, geometric plus linear programming, non-linear programming, goal programming, sequential unconstrained minimization technique and dynamic programming. Later the latest optimization techniques were also discussed by them, specifically Taguchi technique, genetic algorithm, fuzzy logic and ant colony technique. These techniques were successfully applied in the industrial applications for optimal selection of process control variables. The paper concluded that Taguchi approach has the potential for savings in experimental time and cost on product or process, development and quality improvement and therefore is widely used in industries. According to their review, in most of the industries the skill, experience and mentality of the operators are the primary factors affecting the turning process parameters and surface roughness on the job/work piece. Therefore to attain minimum surface roughness it was very necessary to optimize the turning process parameters. Their

review concluded that the latest optimization techniques like Taguchi technique, genetic algorithm, Fuzzy logic and response surface methodology are being applied successfully in industrial applications for optimal selection of process variables in the area of machining.

Yen et al. [14] stated that the tool wear on the tool–workpiece and tool–chip interfaces in metal cutting (i.e. crater wear and flank wear) are strongly influenced by the relative sliding velocity and cutting temperature at the interface. Their study's overall objective was to develop a methodology to tool life in orthogonal cutting and predict the tool wear evolution using FEM simulations. To approach their goal, the methodology proposed by them had three different parts. In the first part, a tool wear model for the specified tool–workpiece pair was developed by them via a calibration set of tool wear cutting tests in conjunction with cutting simulations. In the second part, they modified the commercial FEM code, which was used to allow tool wear calculation and tool geometry updating. The last part was experimental validation of the developed methodology.

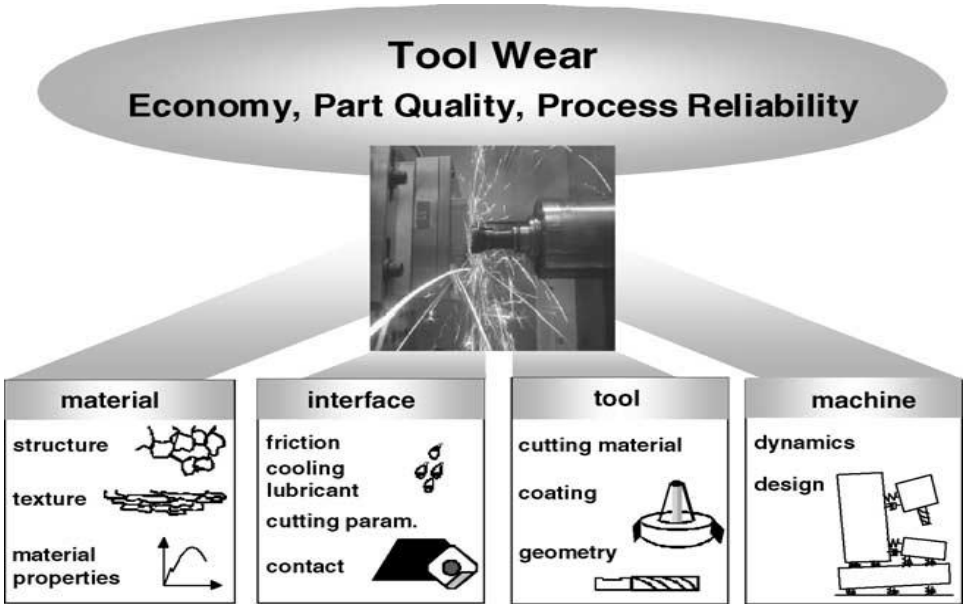

Figure 6: Four major functional elements influencing tool wear in machining processes. [14]

The maximum wear rate was clearly located on the tool rake face as shown in Figure 7. Nevertheless, they predicted small wear rates on the flank side of the tool edge radius, which were about one order of magnitude smaller than the rake face wear rates. They showed that the experimental results for uncoated carbide tools depicted that crater wear and flank wear on the tool face occur simultaneously at a similar wear rate [15].

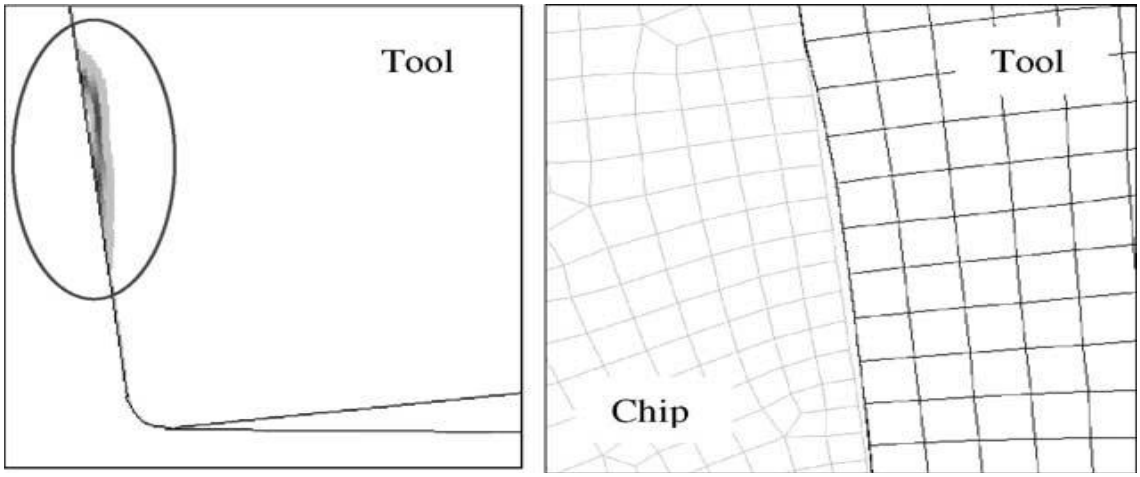

Figure 7: Result of wear rate (left) and updated rake face geometry (right) for an uncoated sharp tool. [14]

The initial results of tool wear simulations obtained by them using the developed method tend to underestimate the wear rates associated with the flank wear and crater wear, when the tool life was compared with the measured data obtained at the same conditions. They concluded that the reason to underestimate the

wear rates associated with the flank wear and crater wear may be partially due to the fact that the two wear constants in Usui's wear model were directly borrowed from the literature [16].

Thamizhmanii et al. [18] applied Taguchi method under optimum cutting condition for finding out the optimal value of surface roughness in turning SCM 440 alloy steel. They detected that the tool chattering and machine tool vibrations were the causes of poor surface finish whose effects were ignored by them for analysis. The authors concluded that that depth of cut of 1 to 1.5 mm can be used to get lowest surface roughness, and the only significant factor was depth of cut which, contributed to the surface roughness.

Kilickap [19] investigated the use of the Taguchi method and the Response Surface Methodologies (RSM) for minimizing the burr height and the surface roughness in drilling Al-7075. The optimization results showed that to minimize burr height, the combination of low cutting speed, low feed rate and high point angle were necessary. At the combination of lower cutting speed and feed rates and at higher point angles the lowest values of surface roughness were obtained. In his paper he presented an application of response surface methodology (RSM) and Taguchi method for selecting the optimum combination values of drilling parameters affecting the burr height and surface roughness in dry drilling of Al-7075. He also concluded that to perform trend analysis of the surface roughness and the burr height with respect to various combinations of drilling parameters Taguchi method is the most successful technique. The analysis of experiments perfumed by him has shown that Taguchi method can be successfully used to verify all the optimum cutting parameters.

III. SUMMARY

Experiments revealed that, the tool wear can be reduced by increasing the tool lifetime and by making more continuous production flow. The total work done by a cutting tool in removing metal was determined from the force components on the cutting tool. If cutting speed, feed rate and depth of cut are increased then the tool temperature also increases which reduces the life of the cutting tool. The chip tool interface temperature increased with increase in feed rate and main cutting force while it decreased with increase in the depth of cut. This review concluded that the decreased cutting tool forces and machined surface temperatures was resulted by increased cutting speed (V_C). It also revealed that, increased cutting tool forces and machined surface temperature was resulted by tool wear and the temperature in the chip increases with increasing of the cutting speed. Experiments also showed that, the temperature appeared to stabilize for the cutting speeds larger than 40 m/s and the temperature in the chip was nearing a saturated value during the process of an un-deformed chip thickness larger than 0.5 mm. It is now clear from the above that the outer surface of the material will be subject to higher heat removal and sudden temperature drop. The cutting forces were decreased, for the increased positive rake angle. The implementation of artificial intelligence based systems in metal cutting process is possible. The latest optimization techniques like Taguchi technique, genetic algorithm, Fuzzy logic and response surface methodology are being applied successfully in industrial applications for optimal selection of process variables in the area of machining. The maximum wear rate is located on the tool rake face. The crater wear and flank wear on the tool face occur simultaneously at a similar wear rate.

IV. FUTURE SCOPE

The future work may require validation of the proposed methodology [14] for selected cutting conditions, different from those in the calibration set by predicting tool wear curves, and comparing the results with the experiments. It may also require use of other wear rate models available in the literature (e.g. Takeyama and Murata's wear model [17]). From the above review one can optimize the turning process parameters like depth of cut, speed, feed, nose radius, material and type of tool, and even work piece material etc using Taguchi method for maximizing the tool life and minimizing the surface roughness by experimental setup. Taguchi technique will help to finalize the number of levels with orthogonal array and thus finalizing the number of experiments. Also the signal to noise ratio will help to observe the behavior of quality characteristics of work piece.

REFERENCES

[1] Jensen M.R., Damborg F.F., Nielsen K.B., Danckert J., "Optimization of the draw-die design in conventional deep-drawing in order to minimise tool wear", Journal of Materials Processing Technology 83 (1998) 106–114.

[2] Sullivan D. O' and Cotterell M., "Temperature measurement in single point turning". Cork Institute Technology. Vol. 118, 2001, pp. 301-308.

[3] Abukhshim N.A., Mativenga P.T., Sheikh M.A.,"Heat generation and temperature prediction in metal cutting: A review and implications for high speed machining", International Journal of Machine Tools & Manufacture xx (2005) 1–19.

[4] Byrne G., Thermoelectric signal characteristics and average interfacial temperature in the machining of metals under geometrically defined conditions, Int. J. Mach. Tools Manuf. 27 (2) (1987) 215-224.

[5] Lazoglu Ismail, Altintas Yusuf, "Prediction of tool and chip temperature in continuous and interrupted machining", International Journal of Machine Tools & Manufacture 42 (2002) 1011–1022.

[6] Sutter G., Faure L., Molinari A., Ranc N., Pina V., "An experimental technique for the measurement of temperature fields for the orthogonal cutting in high speed machining", International Journal of Machine Tools & Manufacture 43 (2003) 671–678.
[7] Dogu Yahya,Aslan Ersan, Camuscu Necip,"A numerical model to determine temperature distribution in orthogonal metal cutting", Journal of Materials Processing Technology 171 (2006) 1–9.
[8] Saglam Haci, Yaldiz Suleyman, Unsacar Faruk,"The effect of tool geometry and cutting speed on main cutting force and tool tip temperature", Materials and Design 28 (2007) 101–111.
[9] Ueda Takashi, Satoz Masahiko, Nakayama Kazuo,"TheTemperature of a Single Crystal Diamond Tool in Turning" Annals of the ClRP Vol. 47, issue 1, (1998) 41-44.
[10] Tanikic Dejan, Manic Miodrag, Radenkovic Goran, Mancic Dragan, "Metal cutting process parameters modeling: an artificial intelligence approach", Journal of Scientific & Industrial Research, Vol. 68, June 2009, pp. 530 – 539.
[11] Fata Ali,"Temperature Measurement During Machining Depending on Cutting Conditions", G. J. P&A Sc and Tech., 2011v01i2 (16-21) ISSN: 2249-7188.
[12] Jameel Adnan, Minhat Mohamad and Nizam Mohamad, "Optimal Parameters Selection to Reduce Cutting Temperature of Mild Steel Using Particle Swarm Optimization Intelligent Technique" Journal of Theoretical and Applied Information Technology, 31st July 2013. Vol. 53 No.3.
[13] Shirpurkar P.P., Bobde S.R., Patil V.V., Kale B.N., "Optimization of Turning Process Parameters by Using Tool Inserts- A Review", International Journal of Engineering and Innovative Technology (IJEIT) Volume 2, Issue 6, December 2012.
[14] Yen Yung-Chang, Söhner Jörg, Lilly Blaine, Altan Taylan, "Estimation of tool wear inorthogonal cutting using the finite element analysis", Journal of Materials Processing Technology 146 (2004) 82–91.
[15] Ivester R.W., Kennedy M., Davies M., Stevenson R., Assessment of Machining Models, Progress Report, Official contribution of NIST on the website http://www.nist.gov/amm/, 2001.
[16] Kitagawa T., Maekawa K., Shirakashi T., Usui E., Analytical prediction of flank wear of carbide tools in turning plain carbon steels. Part 2. Prediction of flank wear, Bull. Jpn. Soc. Precis. Eng. 23 (2) (1989) 126–134.
[17] Takeyama H., Murata T., Basic investigations on tool wear, Trans. ASME J. Eng. Ind. 85 (1963) 33–38.
[18] Thamizhmanii S., Saparudin S., Hasan S., "Analysis of surface roughness by using Taguchi method", Ach. Mater. Manuf. Eng. 20 (1–20) (2007) 503–505.
[19] Kilickap E., "Modeling and optimization of burr height in drilling of Al-7075 using Taguchi method and response surface methodology", Int. J. Adv Manuf. Technol. 49 (9–12) (2010) 911–923.

Optical Materials xxx (2014) xxx–xxx

Contents lists available at ScienceDirect

Optical Materials

journal homepage: www.elsevier.com/locate/optmat

Spectroscopic studies of Nd^{3+} doped lead tungsten tellurite glasses for the NIR emission at 1062 nm

M. Venkateswarlu [a], Sk. Mahamuda [a], K. Swapna [a], M.V.V.K.S. Prasad [a], A. Srinivasa Rao [a,b,*], A. Mohan Babu [c], Suman Shakya [d], G. Vijaya Prakash [d]

[a] Department of Physics, KL University, Green Fields, Vaddeswaram 522 502, Guntur (Dt.), AP, India
[b] Department of Applied Physics, Delhi Technological University, Bawana Road, New Delhi 110 042, India
[c] Department of Physics, Chadalawada Ramanamma Engineering College, Renigunta Road, Tirupati 517 506, AP, India
[d] Nanophotonics Laboratory, Department of Physics, Indian Institute of Technology-Delhi, Hauz Khas, New Delhi 110 016, India

ARTICLE INFO

Article history:
Received 18 June 2014
Received in revised form 1 October 2014
Accepted 16 October 2014
Available online xxxx

Keywords:
Amorphous materials
Glasses
JO parameters
Optical materials
Luminescence
Optical properties

ABSTRACT

Lead Tungsten Tellurite (LTT) glasses doped with different concentrations of Nd^{3+} ions were prepared by using the melt quenching technique to study the absorption, emission and decay spectral profiles with an aim to understand the lasing potentialities of these glasses. From the absorption spectra, the Judd–Ofelt (J–O) parameters are evaluated and in turn used to calculate the transition probability (A_R), total transition probability (A_T), radiative lifetime (τ_R) and branching ratios (β_R) for prominent emission levels of Nd^{3+}. The emission spectra recorded for LTT glasses gives three emission transitions $^4F_{3/2} \rightarrow {}^4I_{9/2}$, $^4F_{3/2} \rightarrow {}^4I_{11/2}$ and $^4F_{3/2} \rightarrow {}^4I_{13/2}$ for which effective band widths ($\Delta\lambda_P$) and stimulated emission cross-sections (σ_{se}) are evaluated. Branching ratios (β_R) measured for all the LTT glasses show that $^4F_{3/2} \rightarrow {}^4I_{11/2}$ transition is quite suitable for lasing applications. The intensity of emission spectra increases with increase in the concentrations of Nd^{3+} up to 1.0 mol% and beyond concentration quenching is observed. Relatively higher emission cross-sections and branching ratios observed for the present LTT glasses over the reported glasses suggests the feasibility of using LTT glasses for infrared laser applications. From the absorption, emission and decay spectral measurements, it was found that 1.0 mol% of Nd^{3+} ion concentration is aptly suitable for LTT glasses to give a strong NIR laser emission at 1062 nm.

© 2014 Elsevier B.V. All rights reserved.

1. Introduction

In recent years, rare earth doped materials are playing a vital role in the modern optical technology as an active constituents to produce low price integrated laser sources, integrated optical amplifiers, 3D display devices, sensors, up-conversion fibres and low loss components [1]. The above mentioned applications possessed by the rare earth doped materials have stimulated the research on rare earth doped glasses [2–6]. Among different rare earth ions, neodymium ion is one of the utmost efficient ions used to prepare solid-state lasers because of its intense emission at 1060 nm [7]. For this reason, trivalent neodymium (Nd^{3+}) ion doped variety of crystals and glasses were studied extensively under 808 and 885 nm laser diode excitation with an aim to develop high power NIR (at 1060 nm) solid state lasers [8,9]. Different glass hosts like borates, phosphates, germanates, vanadates and tellurite families have been studied extensively for this purpose [10–14]. Among all oxide glasses, Lead Tungsten Tellurite (PbF_2–WO_3–TeO_2) glass system (LTT) has unique optical properties. Tellurite based glasses besides having high linear and third order nonlinear optical constants (nonlinear refractive indices), can possess high mechanical stability, good corrosion resistance and low phonon energies equal to 750 cm^{-1}. All these novel properties make them to have their transitions range extended up to mid IR (5–6 μm) region. Tellurite based glasses are also having good capacity to accept lanthanide dopants at different concentrations [15]. The low phonon energy, extended transmission range and high refractive index of tellurite glasses allow the observation of laser emission from rare earth ions in a wide spread spectral range [5,16–20]. Such materials are also useful in optical waveguides. Tungsten oxide (WO_3) is a precise noble semi conducting and transition-metal oxide which has fascinated considerable attention for several years. It is also one of the most examined and used material for electro-chromic and photo-chromic devices in which colouration and bleaching can be reversibly obtained by

* Corresponding author at: Department of Applied Physics, Delhi Technological University, Bawana Road, New Delhi 110 042, India. Tel.: +91 85860 39007; fax: +91 01127871023.
E-mail address: drsrallam@gmail.com (A. Srinivasa Rao).

http://dx.doi.org/10.1016/j.optmat.2014.10.031
0925-3467/© 2014 Elsevier B.V. All rights reserved.

an electro-chemical process [20] and has extensive applications in smart windows, display devices and sensors. Tungsten ions are also capable to influence the luminescence characteristics of rare earth ions in tellurite glasses, for the simple reason that these ions can exist in different valence states i.e., W^{6+}, W^{5+} and W^{4+} irrespective of their starting oxidation state in glasses [21–25]. Hence, the environment around the doped rare earth ions in tellurite glass network can be changed effectively by introducing WO_3 at different concentrations. Consequently, interesting changes in the luminescent characteristics of lasing ions is expected. Now a days lead based (PbO and PbF_2) glasses are believed to be of special interest because of their effective use in IR fibre optics, laser windows and multi-functional optical components. These glasses are highly transparent in the mid infrared region up to 8 μm and more stable against atmospheric moisture. They are also believed to be more favourable material for electrochemical applications in the field of solid state batteries as power sources [26]. While both lead oxide (PbO) and lead fluoride (PbF_2) are efficient glass modifiers, the latter is having glass forming nature with strong network arrangement of PbO_2F_4 form [27,28]. Lead fluoride (PbF_2) especially with its less phonon energies (346 cm^{-1}) added to tungsten tellurite glass can reduce the phonon energies of the host glass drastically and eventually increases their radiative transition rates. It is well known that a glass host with less phonon energies encourages radiative transition rates very much and is much useful for the design and development of photonic devices. Over and above, fluoride compounds present in oxide glasses can react and remove OH group from the glass and reduces the redundant phonon energies of the base glass to enhance radiative emissions.

In the backdrop of the scientific patronages offered by lead fluoride, tungsten oxide and tellurium oxide, in the present work we prepared a germane system namely Lead Tungsten Tellurite (LTT) glass by taking the aforementioned chemicals as constituent elements and doped it with Nd^{3+} ions at different concentrations to study their optical absorption, NIR emission and decay spectral profiles in order to explore the possibility of using these new materials for future photonic devices. Particularly the absorption spectra have been analysed on the basis of Judd–Ofelt (J–O) theory as it is a standard tool in evaluating the radiative properties of the doped rare earth ions in glass hosts. Such measured radiative properties combined with emission spectral data are useful in understand the lasing potentialities of the prepared LTT glasses.

2. Experimental

2.1. Glass preparation

The LTT glasses of composition (in mol%) 15 PbF_2 + 25 WO_3 + (60 − x) TeO_2 + x Nd_2O_3 (here x = 0.1, 0.5, 1.0 and 1.5 mol%) were prepared by melt quenching technique from reagents of analar grade (purity more than 99.9%) in 10 g batches. These glasses are labelled as LTTNd01, LTTNd05, LTTNd10 and LTTNd15 depending on Nd^{3+} ion concentration 0.1, 0.5, 1.0 and 1.5 mol% respectively. Batches containing different concentrations of Nd^{3+} ions in base glass compositions were thoroughly mixed in an agate mortar to get a smooth powder. Such powders were then collected in a silica crucible and heated in a furnace at 730 °C temperature for 30 min. The melt was quenched by pouring onto a circular shaped copper plate and pressed quickly by another plate. The LTT glasses thus prepared were annealed at 400 °C for two hours to remove thermal strains and to improve the mechanical strength of the prepared glasses. Finally, the glasses were polished with emery paper before going for experimental measurements.

2.2. Physical, absorption, emission and decay spectral measurements

Archimedes principle is used to determine the densities of the Nd^{3+} doped LTT glass samples with water as an immersion liquid. Brewster's angle method with He–Ne laser operating at 632 nm is used to measure the refractive index of the prepared glasses. From the measured density and refractive indices, various other physical properties of the LTT glasses were evaluated using the relevant expressions given in our previous paper [29] and are given in Table 1. Absorption spectra for Nd^{3+} doped LTT glasses were recorded at room temperature in the wavelength range 500–900 nm with a spectral resolution of 0.1 nm using a JASCO model V-670 UV–vis–NIR spectrophotometer. The photoluminescence (PL) emission and time-resolved PL measurements were carried out using home-built set ups with 808 nm CW laser as an excitation source. The emission from sample was coupled into a monochromator (Acton SP2300) coupled to CCD (charge coupled detector) through appropriate lenses and filters. For time resolved PL measurements, a frequency generator (5 Hz), lock-in amplifier, digital storage oscilloscope and a monochromator (Acton SP2300) coupled to InGaAs detector through the appropriate lenses and filters are used.

3. Results and discussion

3.1. Physical properties

The variation of density (g/cm^3), mean atomic volume (g/cm^3/atom), refractive index, average molecular weight (g), inter ionic distance (Å) and field strength ($\times 10^{15}$ cm^{-2}) as a function of Nd_2O_3 concentration in LTT glasses have been shown in Figs. 1a–1c. From Fig. 1a it is observed that with increase in Nd^{3+} ion concentration in LTT glasses, the density and mean atomic volume values are also increasing indicating more rigid nature of the prepared LTT glasses. This is further confirmed by increase in average molecular weight and decrease in inter ionic distance values with Nd^{3+} ion concentration as shown in Figs. 1b and 1c respectively. The tendency of decrease in inter ionic distance in the present glasses indicates that the atoms are more tightly packed as the Nd^{3+} ion concentration increases in these glasses. From Fig. 1b, it is observed that refractive index of LTT glasses increases with increase in dopant ion concentration. As the density of the LTT glasses are increasing with dopant ion concentration, the denser nature of the glasses relatively increases and will increase the refractive index of the medium with dopant ion concentration. From Fig. 1c, it can also be seen that the field strength values are increasing with increase in Nd^{3+} ion concentration. This is obvious because, when the rare earth ion concentration in glass increases, the number of ions available per unit volume will also increase and this will increase the field strength. From Table 1, it is also observed that these glasses have molecular electronic polarizability of the order 10^{-23} which is a very low value and hence the present LTT glasses are said to be more stable. In general, the optical basicity of the oxide medium is nothing but the average electron donating power of all oxide atoms present in the medium. For the present system of glasses, the values of optical basicity are increasing with the increase in Nd^{3+} ion concentration. This results in increasing negative charge on the oxygen atom and thus increases covalency in the cation–oxygen bonding.

3.2. Optical absorption spectra

Optical absorption spectra for all the LTT glasses doped with Nd^{3+} ions were measured in visible and near infra-red (vis–NIR) regions at room temperature in the wavelength range 500–900 nm. Each spectrum has same resemblance in band positions with slight difference in intensities of various absorption bands. Fig. 2 shows the

Please cite this article in press as: M. Venkateswarlu et al., Opt. Mater. (2014), http://dx.doi.org/10.1016/j.optmat.2014.10.031

Table 1
Various physical properties of Nd^{3+} ions doped LTT glasses.

Physical properties	LTTNd01	LTTNd05	LTTNd10	LTTN15
Density ρ (g/cm^3)	6.607	6.612	6.619	6.626
Refractive index (n_d)	2.190	2.201	2.213	2.221
Average molecular weight $\bar{M}$ (g)	190.6	191.3	192.2	193.1
Nd^{3+} ion concentration N ($\times 10^{21}$ ions/cm^3)	2.086	10.40	20.73	30.98
Mean atomic volume (g/cm^3/atom)	8.870	8.874	8.880	8.884
Dielectric constant (ε)	4.796	4.844	4.897	4.932
Optical dielectric constant ($\varepsilon - 1$)	3.796	3.844	3.897	3.932
Reflections losses (R%)	0.139	0.140	0.142	0.143
Molar refraction (R_m) (cm^{-3})	18.89	19.02	19.18	19.31
Polaron radius (Å)	3.150	1.845	1.466	1.283
Inter ionic distance (Å)	7.838	4.588	3.646	3.189
Molecular electronic Polarizability, α ($\times 10^{-23}$ cm^3)	7.500	1.510	0.761	0.511
Field strength ($\times 10^{15}$ cm^{-2})	3.016	8.804	13.94	18.23
Optical basicity (Λ_{th})	0.464	0.468	0.473	0.477

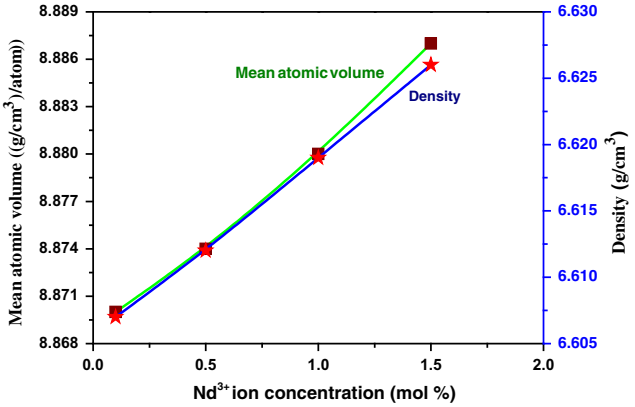

Fig. 1a. The variation of density (g/cm^3) and mean atomic volume (g/cm^3/atom) parameters as a function of Nd^{3+} ion concentration (mol%) in LTT glasses.

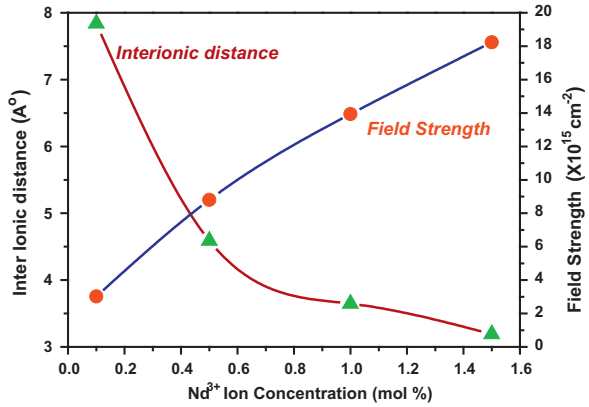

Fig. 1c. The variation of inter ionic distance (Å) and field strength ($\times 10^{15}$ cm^{-2}) parameters as a function of Nd^{3+} ion concentration (mol%) in LTT glasses.

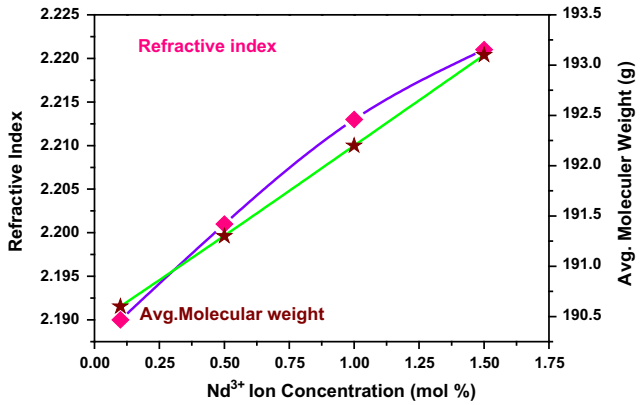

Fig. 1b. The variation of refractive index and average molecular weight (g) parameters as a function of Nd^{3+} ion concentration (mol%) in LTT glasses.

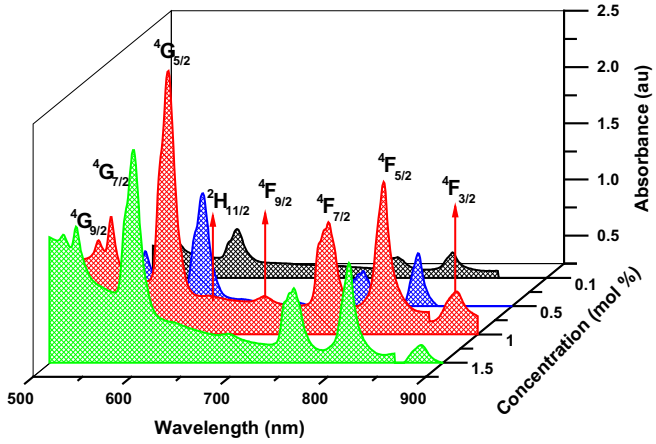

Fig. 2. Absorption spectra of Nd^{3+} ions in LTT glasses.

optical absorption spectra of Nd^{3+} ions doped LTT glasses in vis–NIR region. As shown in Fig. 2, the Nd^{3+} ions in all the LTT glasses exhibits eight absorption bands in vis–NIR region at 513, 526, 584, 627, 681, 748, 803 and 877 nm [30,31] corresponding to the transitions $^4I_{9/2} \rightarrow {}^4G_{9/2}$, $^4G_{7/2}$, $^4G_{5/2}$, $^2H_{11/2}$, $^4F_{9/2}$, $^4F_{7/2}$, $^4F_{5/2}$, and $^4F_{3/2}$ respectively [32,33]. Because of the strong absorption of the host glass in UV region, few absorption bands have disappeared in that region. From the identified band positions (cm^{-1}), nephelauxetic ratio ($\bar{\beta}$) and bonding parameters (δ) are evaluated and are given in Table 2. The essential mathematical formulae needed for the determination of nephelauxetic ratio and bonding parameter are collected from literature [34]. Depending on the field environment, the bonding parameter (δ) may be positive or negative indicating covalent or ionic bonding. From Table 2, it is observed that the bonding parameter (δ) for all the LTT glasses is found to be positive i.e., the prepared glasses are covalent in nature and the covalent nature decreases gradually with increase in Nd^{3+} ion concentration.

The intensity of absorption bands, which are usually called as oscillator strength (f_{exp}) is directly proportional to the area under the absorption band and can be determined from the absorption spectral features using the relevant equation given in literature

Table 2
Assignment of absorption bands, experimental and calculated oscillator strengths (f_{exp} and f_{cal}) (10^{-6}), rms deviation (δ_{rms}) (10^{-6}), nephelauxetic ratio ($\bar{\beta}$) and bonding parameters (δ) for Nd^{3+} ions doped LTT glasses.

Transition $^4I_{9/2}\rightarrow$	Wavelength (nm)	LTTNd01		LTTNd05		LTTNd10		LTTNd15	
		f_{exp}	f_{cal}	f_{exp}	f_{cal}	f_{exp}	f_{cal}	f_{exp}	f_{cal}
$^4G_{9/2}$	513	0.975	2.068	2.330	2.776	3.284	3.0521	2.130	2.015
$^4G_{7/2}$	527	4.650	5.064	6.340	6.660	7.610	7.263	5.16	4.732
$^4G_{5/2}$	584	16.83	16.80	27.9	27.881	29.520	29.540	18.100	18.123
$^2H_{11/2}$	627	0.113	0.156	0.510	0.294	0.547	0.328	0.270	0.207
$^4F_{9/2}$	682	0.321	0.524	1.220	1.006	1.959	1.119	0.72	0.721
$^4F_{7/2}$	747	1.426	1.791	4.130	4.206	5.206	4.685	3.530	2.984
$^4F_{5/2}$	803	7.023	6.696	10.63	10.572	11.290	11.738	7.27	7.644
$^4F_{3/2}$	878	3.867	3.857	4.52	4.405	5.08	4.842	3.430	3.246
δ_{rms}		±0.45		±0.22		±0.42		±0.29	
$(\bar{\beta})$		0.9946		0.9948		0.9950		0.9951	
δ		0.537		0.515		0.498		0.488	

[34]. From the absorption spectra, it is noticed that one particular transition namely $^4I_{9/2} \rightarrow {}^4G_{5/2}$ is more intense than other transitions and having large oscillator strengths in all the glasses under investigation. This transition is known as the hypersensitive transition, for which the selection rules $\Delta J \leqslant 2$; $\Delta L \leqslant 2$ and $\Delta S = 0$ holds good. The calculated oscillator strengths (f_{cal}) for the f–f transitions of Nd^{3+} ions from its ground state (ψ_J) to the excited state ($\psi'_{J'}$) were determined using J–O theory [35,36]. The experimental and calculated oscillator strengths reported in Table 2 are in good agreements with each other with less rms deviation. In the process of evaluating J–O parameters (Ω_λ) through a least squares fitting procedure, the necessary reduced matrix elements $\|U^\lambda\|^2$ were collected from literature [32]. The J–O intensity parameters (Ω_λ) and spectroscopic quality factors of Nd^{3+} doped LTT glasses are given in Table 3 along with the reported values [37–51]. J–O intensity parameters are highly useful in explaining the environment around the doped rare earth ions in the host glass. The local structure and bonding nature of rare earth ions can be studied on the basis of magnitudes of the J–O intensity parameters. The bulk properties of the host medium such as rigidity and viscosity of the medium in which the rare earth ions are situated can be explained on the basis of the magnitudes of Ω_4 and Ω_6. From Table 3, it is observed that Ω_4 is higher than Ω_6 and Ω_2 and follows the same trend ($\Omega_4 > \Omega_6 > \Omega_2$) for all the Nd^{3+} doped LTT glasses. Supplementarily it is perceived that the J–O parameters are increasing from 0.5 to 1 mol% of dopant ion concentration and then decreasing beyond in these glasses. Ideally, the J–O intensity parameters need not show any variation with concentration in the same host owing to the occupation of similar dopant sites. But, in the present work, the observed variation in J–O intensity parameters may be attributed to the tendency of clustering of dopant ions. Also, increasing concentration may produce site-to-site variation and subsequently the local crystal field as well as the asymmetry around the dopant ions may change and may cause variations in J–O parameters. The J–O intensity parameter Ω_2 increases from glass LTTNd01 to LTTNd10 and then decreases for LTTNd15. The intensity of hypersensitive transition and Ω_2 are high for LTTNd10 glass indicating that it has the highest covalence and asymmetry around Nd^{3+} ions.

3.3. Photoluminescence spectra and radiative properties

The NIR photoluminescence spectra of LTT glasses doped with Nd^{3+} ions when excited under 808 nm CW laser source is shown in Fig. 3. The Nd^{3+} ions excited to $^4F_{5/2}$ level in LTT glasses are immediately falling to $^4F_{3/2}$ metastable state through fast non-radiative relaxation as indicated in Fig. 4. The resultant PL spectra shown in Fig. 3 consist of three emission bands at 878, 1062 and 1339 nm corresponding to the transitions $^4F_{3/2} \rightarrow {}^4I_{9/2}$, $^4F_{3/2} \rightarrow {}^4I_{11/2}$ and $^4F_{3/2} \rightarrow {}^4I_{13/2}$ respectively. From the PL spectra, it is observed that, the intensity of all the emission transitions increases with increase

Table 3
Judd–Ofelt intensity parameters (Ω_λ where $\lambda = 2$, 4 and 6) (10^{-20} cm^2) for Nd^{3+} ions doped LTT glasses and other reported glasses.

Name of the glass	Ω_2	Ω_4	Ω_6	Trend	$\chi = \Omega_4/\Omega_6$	References
LTTNd01	1.81	5.27	2.17	$\Omega_4 > \Omega_6 > \Omega_2$	2.42	Present work
LTTNd05	4.46	5.31	5.14	$\Omega_4 > \Omega_6 > \Omega_2$	1.03	Present work
LTTNd10	4.54	5.79	5.69	$\Omega_4 > \Omega_6 > \Omega_2$	1.01	Present work
LTTNd15	2.60	3.91	3.59	$\Omega_4 > \Omega_6 > \Omega_2$	1.08	Present work
Tellurite	3.80	4.94	4.54	$\Omega_4 > \Omega_2 > \Omega_6$	1.08	[37]
Germanate	3.09	5.54	4.48	$\Omega_4 > \Omega_6 > \Omega_2$	1.23	[37]
LBNNd10 with HST	4.81	5.55	3.73	$\Omega_4 > \Omega_2 > \Omega_6$	1.48	[38]
NaTFP	3.01	5.26	4.21	$\Omega_4 > \Omega_6 > \Omega_2$	1.25	[39]
Nbl	3.12	4.84	3.28	$\Omega_4 > \Omega_6 > \Omega_2$	1.03	[39]
LaF_3	0.35	2.57	2.50	$\Omega_4 > \Omega_6 > \Omega_2$	1.03	[39]
Tellurite	3.62	4.21	2.95	$\Omega_4 > \Omega_6 > \Omega_2$	1.43	[40]
Germanate	3.09	5.54	4.80	$\Omega_4 > \Omega_6 > \Omega_2$	1.15	[41]
CaNb glass	4.40	5.20	2.70	$\Omega_6 > \Omega_4 > \Omega_2$	1.92	[42]
LBTAFNd05	5.82	1.88	4.76	$\Omega_2 > \Omega_6 > \Omega_4$	0.39	[43]
ZBLAN	5.09	3.12	7.16	$\Omega_2 > \Omega_6 > \Omega_4$	0.43	[44]
SPB1	4.81	1.97	3.94	$\Omega_2 > \Omega_6 > \Omega_4$	0.50	[45]
LBT	1.05	1.50	4.20	$\Omega_6 > \Omega_4 > \Omega_2$	0.35	[46]
30 B_2O_3–70 PbO	3.52	2.98	5.48	$\Omega_6 > \Omega_2 > \Omega_4$	0.54	[47]
Fluoride	1.95	3.65	4.17	$\Omega_6 > \Omega_4 > \Omega_2$	0.87	[48]
Silicate	4.71	4.54	5.05	$\Omega_6 > \Omega_2 > \Omega_4$	0.89	[49]
Phosphate	6.30	4.00	4.30	$\Omega_2 > \Omega_6 > \Omega_4$	0.93	[50]
TeO_2–WO_3–PbO–Nd_2O_3	4.88	4.05	3.82	$\Omega_2 > \Omega_4 > \Omega_6$	1.06	[51]

Please cite this article in press as: M. Venkateswarlu et al., Opt. Mater. (2014), http://dx.doi.org/10.1016/j.optmat.2014.10.031

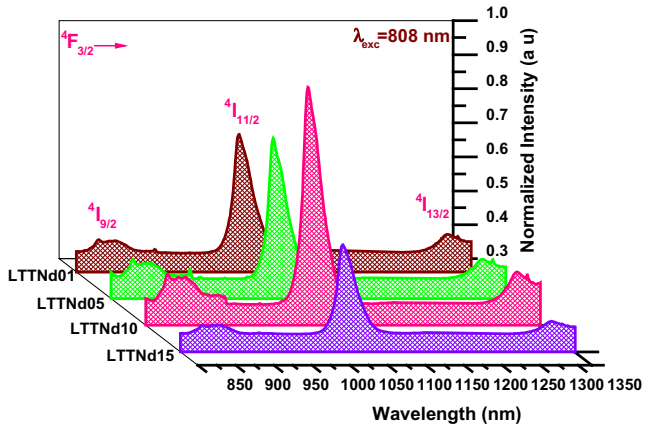

Fig. 3. Emission spectra of Nd^{3+} ions in LTT glasses.

in Nd^{3+} ion concentration up to 1.0 mol% and then decreasing beyond showing concentration quenching, which can be attributed to the interaction between the excited Nd^{3+} ions and energy transfer observed between Nd^{3+} ions. Among all the emission transitions, a transition $^4F_{3/2} \rightarrow {}^4I_{11/2}$ observed at 1062 nm has highest intensity for LTTNd10 glass. The absorption, excitation and emission mechanisms are shown in Fig. 4 along with the possible cross-relaxation channel.

The J–O intensity parameters are coupled with the emission spectral data, to evaluate different radiative properties such as radiative transition probability (A_R), total transition probability (A_T), branching ratios (β_R) and radiative lifetimes (τ_R) using the relevant expressions given in literature [34]. In general, the stimulated emission cross-section (σ_{se}) is independent on the J–O parameters and half band widths ($\Delta\lambda_{eff}$) of the emission bands, which are effected by host glass composition. In addition, the intensity of $^4F_{3/2} \rightarrow {}^4I_{11/2}$ laser transitions at 1062 nm depends only on the Ω_4 and Ω_6 parameters because of triangle rule $|J'-J| \leq \lambda \leq |J'+J|$ [39]. The A_R, A_T and τ_R values observed for all the emission transitions of Nd^{3+} ions in LTT glasses are given in Table 4. These values are useful to determine how fast an excited level gets depopulated. The radiative branching ratios (β_R) used to calculate the relative intensities of all the luminescence transitions originating from an excited state are given in Table 4 along with experimental branching ratios. The experimental branching ratios (β_{exp}) can be determined from the relative areas of the emission transitions. From Table 4, it can be seen that the experimental branching ratios are higher than radiative branching ratios for all the LTT glasses. The highest value of branching ratio (β_R) is an attractive feature for low threshold and high gain applications of lasers [34]. From Table 4, it can be observed that, the LTTNd10 glass has highest branching ratio for the transition $^4F_{3/2} \rightarrow {}^4I_{11/2}$ and can be recommended as an efficient lasing transition. The stimulated emission cross-section for all the luminescence transitions have been calculated using the formula given in the literature [34] and are tabulated in Table 5. The stimulated emission cross-section is an important parameter that influences the potential laser performance and its value signifies the energy extraction from the lasing material. From Table 5, it is observed that LTTNd10 glass possess highest stimulated emission cross-section than the other glasses for the transition $^4F_{3/2} \rightarrow {}^4I_{11/2}$ at 1062 nm. In order to understand optical amplification performance of the LTT glasses, we have evaluated gain band width ($\sigma_{se} \times \Delta\lambda_P$) and optical gain parameters ($\sigma_{se} \times \tau_R$) and are given in Table 5. From Table 5, it is observed that, among all the LTT glasses studied here, the LTTNd10 glass possesses highest values of optical gain parameters and gain band width for $^4F_{3/2} \rightarrow {}^4I_{11/2}$ transition and hence can be suggested for optical amplification also. Hence in the present system of LTT glasses, the LTTNd10 glass can be recommended as a suitable host for lasing emission at 1062 nm and also for optical amplification.

3.4. Decay curve analysis

The decay curves recorded for the luminescence from $^4F_{3/2}$ level of Nd^{3+} ion in LTT glasses are shown in Fig. 5. From Fig. 5, it can be observed that the decay profiles for all the LTT glasses are single exponential in nature irrespective of Nd^{3+} ion concentration. This may be due to fast decay of Nd^{3+} ions (or) negligible effect of ligands on Nd^{3+} ions. From the decay curves, the experimental lifetimes (τ_{exp}) are evaluated by using the relevant expression given in literature [52] and are given in Table 6 along with the radiative lifetimes (τ_R). From Table 6, it can be observed that the experimental lifetimes were found to be decreasing with increasing in Nd^{3+} ion concentration in LTT glasses. The quantum efficiency, an another

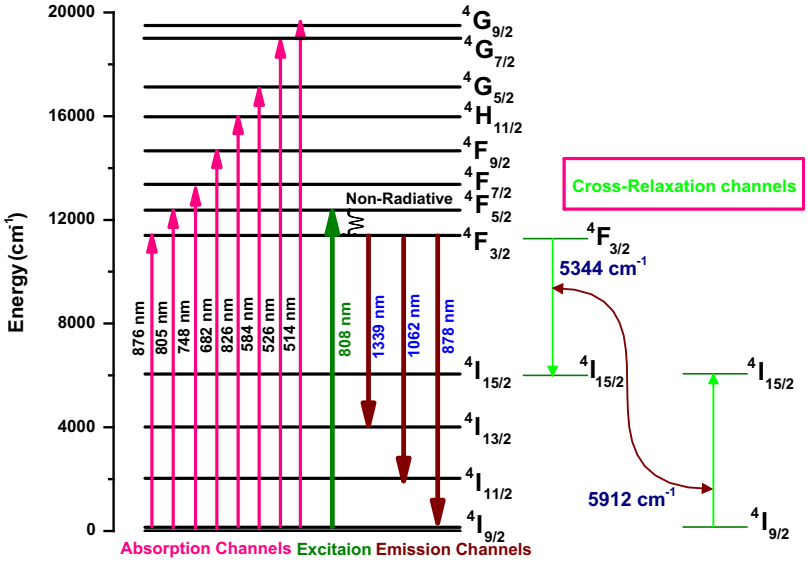

Fig. 4. Schematic energy level scheme of Nd^{3+} ions in LTTNd10 glass along with the absorption, excitation, emission and cross-relaxation channels.

Table 4
Radiative transition probabilities (A_R) (s^{-1}), total transition probabilities (A_T) (s^{-1}), experimental and radiative branching ratios (β_{exp} and β_R) and radiative lifetimes (τ_R) (μs) for the emission transitions of Nd^{3+} ions doped LTT glasses.

Transition $^4F_{3/2}$	Spectral parameters	LTTNd01	LTTNd05	LTTNd10	LTTNd15
$^4I_{9/2}$	A_R	4020.12	4663.76	5148.49	3467.25
	A_T	7342.46	10866.82	12040.22	7926.80
	β_{exp}	0.226	0.327	0.200	0.220
	β_R	0.547	0.429	0.427	0.437
	τ_R	136	92	83	126
$^4I_{11/2}$	A_R	2896.56	5169.21	5742.55	3727.74
	A_T	7342.46	10866.82	12040.22	7926.80
	β_{exp}	0.701	0.606	0.709	0.687
	β_R	0.394	0.475	0.476	0.470
	τ_R	136	92	83	126
$^4I_{13/2}$	A_R	405.68	984.97	1095.14	697.46
	A_T	7342.46	10866.82	12040.22	7926.80
	β_{exp}	0.072	0.066	0.095	0.091
	β_R	0.055	0.090	0.091	0.088
	τ_R	136	92	83	126

Table 5
Emission peak wavelength (λ_P) (nm), effective band widths ($\Delta\lambda_P$) (nm), stimulated emission cross-sections (σ_{se}) ($\times 10^{-19}$) (cm^2), gain band width ($\sigma_{se} \times \Delta\lambda_p$) ($10^{-26}$) ($cm^3$) and optical gain parameters ($\sigma_{se} \times \tau_R$) ($10^{-23}$) ($cm^2$ s) for the emission transitions of Nd^{3+} ions doped LTT glasses.

Transition $^4F_{3/2}$	Spectral parameters	LTTNd01	LTTNd05	LTTNd10	LTTNd15
$^4I_{9/2}$	λ_p	878	878	878	878
	$\Delta\lambda_p$	5.56	5.28	4.72	5
	σ_{se}	1.19	1.44	1.76	1.17
	$\sigma_{se} \times \Delta\lambda_p$	6.61	7.59	8.29	5.83
	$\sigma_{se} \times \tau_R$	1.62	1.32	1.46	1.47
$^4I_{11/2}$	λ_p	1062	1062	1062	1062
	$\Delta\lambda_p$	6.94	5.55	4.16	5.55
	σ_{se}	1.47	3.24	4.75	2.30
	$\sigma_{se} \times \Delta\lambda_p$	10.23	18.01	19.80	12.80
	$\sigma_{se} \times \tau_R$	2.00	2.98	3.94	2.89
$^4I_{13/2}$	λ_p	1339	1339	1339	1339
	$\Delta\lambda_p$	3.75	3.33	3.19	3.611
	σ_{se}	0.96	2.60	2.99	1.67
	$\sigma_{se} \times \Delta\lambda_p$	3.61	8.67	9.54	6.03
	$\sigma_{se} \times \tau_R$	1.31	2.39	2.48	2.10

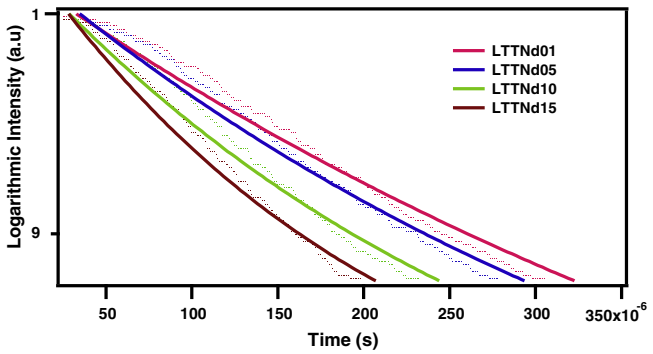

Fig. 5. Emission decay profiles for $^4F_{3/2} \rightarrow {}^4I_{11/2}$ transition of Nd^{3+} ions in LTT glasses. Solid lines are from exponential curve fits.

important parameter used to understand the lasing efficiency of a host material is defined as the ratio between emitted light intensity and absorbed pump intensity and is evaluated using the expression given in our previous paper [52]. Such quantum efficiency values along with radiative and measured lifetimes are given in Table 6. From Table 6, it is observed that, among all the LTT glasses, LTTNd10 glass possess highest quantum efficiency for the transition $^4F_{3/2} \rightarrow {}^4I_{11/2}$ (1062 nm). The experimental lifetimes for LTT are found to be less than the radiative lifetimes. The relaxation from excited state is represented by both radiative

Table 6
Radiative and experimental lifetimes (τ_R and τ_{exp}) (μs), quantum efficiency (η) and multi-phonon relaxation rate (W_{NR}) (μs^{-1}) for $^4F_{3/2} \rightarrow {}^4I_{11/2}$ emission transition of Nd^{3+} ions doped LTT glasses.

Name of the sample	τ_R	τ_{exp}	η (%)	W_{NR}
LTTNd01	136	91	67	3636
LTTNd05	92	73	79	2829
LTTNd10	83	68	82	2657
LTTNd15	126	61	48	8456

and non-radiative decay modes. The total transition probability, i.e., the reciprocal of the fluorescence decay rate measured, has the relations with the radiative and non-radiative lifetimes as follows:

$$\text{The radiative decay rate } \left(W_R = \frac{1}{\tau_R}\right) \tag{A.1}$$

$$\text{The non-radiative decay rate } W_{NR} = \left(\frac{1}{\tau_{exp}} - \frac{1}{\tau_R}\right) \tag{A.2}$$

The radiative decay rate is affected by the local crystal-field symmetry around the Nd^{3+} ion and to some extent due to local vibration density of the states of the host. The non-radiative decay rate is due to multi-phonon relaxation process. The prominent processes contributing to the reduction of radiative decay should be

Table 7
Comparison of branching ratio (β_R), stimulated emission cross-section ($\sigma_{se} \times 10^{-22}$ cm^2) and quantum efficiency (η) (%) of LTTNd10 glass for $^4F_{3/2} \rightarrow {}^4I_{11/2}$ emission transition with commercial glass systems and other Nd^{3+} doped glass hosts.

Name of the glass system	β_{exp}	σ_{se}	η (%)	References
Commercial glass systems				
LTTNd10	0.709	4.75	82	Present work
LHG-80	–	4.2	–	[53,54]
LG-770	–	3.9	–	[53,54]
Q-88	–	4.0	–	[53,54]
LHG-8	-	3.7	-	[53,54]
LG-750	-	3.6	-	[38,55]
Other glass systems				
BNa4	0.52	4.94	–	[30]
ZnAlBiB (Glass C)	0.72	3.67	–	[34]
NaTFP	0.735	3.89	71	[39]
LiTFP	0.764	3.75	62	[39]
KTFP	0.734	4.50	68	[39]
TZNLN	0.77	4.28	–	[40]
LBTAFNd05	0.62	2.60	23	[43]
$TeO_2WO_3PbONd_2O_3$	0.45	–	–	[51]
PKMAFN	0.51	4.40	–	[53]
MgTP	0.73	3.82	72	[56]
CaTP	0.73	3.95	75	[56]
SrTP	0.73	4.03	84	[56]
NdF_3 based glass	–	4.68	–	[57]
CLiBT	0.52	3.90	–	[58]
SFB	0.50	3.46	–	[59]

considered in order to explain the mechanism of non-radiative process. This non-radiative process (W_{NR}) is an undesirable for amplifying devices as they need population inversion. In the present work, the quantum efficiency of the $^4F_{3/2} \rightarrow {}^4I_{11/2}$ transition increases up to 1 mol% of Nd^{3+} ion concentration and then decreases. The non-radiative relaxation rates measured for the LTT glasses are given in Table 6. From Table 6, it is observed that, among all the LTT glasses, the LTTNd10 glass possess lowest non-radiative relaxation rate and highest quantum efficiency. Hence the LTTNd10 glass is aptly suitable for NIR laser emission at 1062 nm. Table 7 gives the comparison of experimental branching ratios, stimulated emission cross-section and quantum efficiency for LTTNd10 glass with commercial systems and other hosts [30,34,38–40,43,51,53–59]. Hence the present system LTTNd10 possess better values of branching ratios, stimulated emission cross-section and quantum efficiency than the other reported glass systems. Hence LTTNd10 glass can be recommended as suitable host to produce efficient lasing action in NIR region at 1062 nm.

4. Conclusion

Lead Tungsten Tellurite (LTT) glasses doped with different concentration of Nd^{3+} ions were prepared by employing melt quenching method and characterized by using the spectroscopic techniques such as optical absorption, emission and decay spectral measurements to optimise the concentration of the doped rare earth ions for better luminescence efficiency. From the measured branching ratios, emission cross-sections and quantum efficiency, it is concluded that the LTT glasses are better suited for NIR laser emission applications. The gain band width ($\sigma_{se} \times \Delta\lambda_p$) ($10^{-26}$)(cm^3) and optical gain parameters ($\sigma_{se} \times \tau_R$) ($10^{-23}$) (cm^2 s) measured for LTT glasses suggests the suitability of these devices for optical amplification applications. Among all the LTT glasses studied here, the LTTNd10 glass possessing better lasing potentialities and optical amplification with more branching ratio, emission cross-section, quantum efficiency, optical gain and gain band width values. Based on the luminescence characteristic parameters measured for all the LTT glasses, it is suggested that LTTNd10 glass is aptly suitable for optical amplification as well as for efficient NIR emission at 1062 nm.

Acknowledgments

Two of the authors, Mahamuda Shaik (File No. SR/WOS-A/PS-53/2011) and Swapna Koneru (File No. SR/WOS-A/PS-35/2011) are very much grateful to Department of Science and Technology (DST), Government of India, New Delhi, for endowing them with a Project under Women Scientist's scheme (DST/WOS-A program). This work is also partly supported by High impact Research initiative of IIT – Delhi, UK India Education Research Initiative (UKIERI) and DST, Govt. of India, New Delhi. One of the authors, Dr. Mohan Babu is expressing his sincere thanks to ADE-BRNS (Project No. 2012/34/72) and DST-SERB (Project No. SR/FTP/PS-109/2012) for their financial support to carry out this work.

References

[1] Gang Fua, Shiling Li, Xifeng Qin, Xiuquan Zhang, Nucl. Instrum. Methods Phys. Res., Sect. B 315 (2013) 325–327.
[2] K. Swapna, Sk. Mahamuda, A. Srinivasa Rao, M. Jayasimhadri, T. Sasikala, L. Rama Moorthy, Visible fluorescence characteristics of Dy^{3+} doped zinc alumino bismuth borate glasses for optoelectronic devices, Ceram. Int. 39 (2013) 8459–8465.
[3] Sk. Mahamuda, K. Swapna, P. Packiyaraj, A. Srinivasa Rao, G. Vijaya Prakash, Lasing potentialities and white light generation capabilities of Dy^{3+} doped oxy-fluoroborate glasses, J. Lumin. 153 (2014) 382–392.
[4] Sk. Mahamuda, K. Swapna, M. Venkateswarlu, A. Srinivasa Rao, Suman shakya, G. Vijaya Prakash, Spectral characterisation of Sm^{3+} ions doped oxy-fluoroborate glasses for visible orange luminescent applications, J. Lumin. 154 (2014) 410–424.
[5] K. Swapna, Sk. Mahamuda, A. Srinivasa Rao, T. Sasikala, P. Packiyaraj, L. Rama Moorthy, G. Vijaya Prakash, Luminescence characterization of Eu^{3+} doped zinc alumino bismuth borate glasses for visible red emission applications, J. Lumin. 156 (2014) 80–86.
[6] K. Swapna, Sk. Mahamuda, A. Srinivasa Rao, M. Jayasimhadri, Suman Shakya, G. Vijaya Prakash, Tb^{3+} doped zinc alumino bismuth borate glasses for green emitting luminescent devices, J. Lumin. 156 (2014) 180–187.
[7] C. Madhukar Reddy, N. Vijaya, B. Deva Prasad Raju, NIR fluorescence studies of neodymium ions doped sodium fluoroborate glasses for 1.06 μm laser applications, Spectrochim. Acta Part A Mol. Biomol. Spectrosc. 115 (2013) 297–304.
[8] Antonio Agnesi, Paolo Dallocchio, Federico Pirzio, Giancarlo Reali, Compact sub-100-fs Nd:silicate laser, Opt. Commun. 282 (2009) 2070–2073.
[9] I. Iparraguirre, J. Azkargorta, J.M. Fernandez-Navarro, M. Al-Saleh, J. Fernandez, R. Balda, Laser action and up-conversion of Nd^{3+} in tellurite bulk glass, J. Non-Cryst. Solids 353 (2007) 990–992.
[10] M. Yamane, Y. Ashara, Glass for Photonics, Cambridge University Press, 2000.
[11] Hrvoje Gebavi, Stefano Taccheo, Daniel Milanse, The enhanced two micron emission in thulium doped tellurite glasses, Opt. Mater. 35 (2013) 1792–1796.
[12] Hrvoje Gebavi, Stefano Taccheo, Rolindes Balda, Joaquin M. Fernandez, Daniel Milanse, Francois Auzel, The effect of ZnF_2 on the near-infrared luminescence from thulium doped tellurite glasses, J. Non-Cryst. Solids 358 (2012) 11497–11500.
[13] Guihau Liao, Qiuping Chen, Jianjun Xing, Hrvoje Gebavi, Daniel Milanse, Michael Fokine, Monica Ferraris, Preparation and characterization of new fluorotellurite glasses for photonic applications, J. Non-Cryst. Solids 355 (2009) 447–452.
[14] Hrvoje Gebavi, Daniel Milanse, Guihaua Liao, Qiuping Chen, Monica Ferraris, Mile Ivanda, Ozren Gamulin, Stefano Taccheo, Spectroscopic investigation and optical characterization of novel highly thulium doped tellurite glasses, J. Non-Cryst. Solids 355 (2009) 548–555.
[15] R. El-Mallawany, Tellurite Glasses Hand Book. Physical Properties and Data, CRC Press, USA, 2002, p. 376.
[16] Nadia G. Boetti, Joris Lousteau, Alessandro Chiasera, Maurizio Ferrari, Emanuele Mura, Gerardo C. Scarpignato, Silvio Abrate, Daniel Milanese, Thermal Stability and spectroscopic properties of erbium-doped niobic-tungsten–tellurite glasses for laser and amplifier devices, J. Lumin. 132 (2012) 1265–1269.
[17] Animesh Jha, Billy Richards, Gin Jose, Toney Teddy-Fernandez, Purushottam Joshi, Xin Jiang, Joris Lousteau, Rare-earth ion doped TeO_2 and GeO_2 glasses as laser materials, Prog. Mater Sci. 57 (2012) 1426–1491.
[18] Shaoxiong Shen, Mira Naftaly, Animesh Jha, Tungsten–tellurite-a host glass for broadband EDFA, Opt. Commun. 205 (2002) 101–105.
[19] X.Y. Wang, H. Lin, C.M. Li, S. Tanabe, Derivation of quantum yields for visible emission transitions of Sm^{3+} in heavy metal tellurite glass, Opt. Commun. 276 (2007) 122–126.
[20] D. Barreca, S. Bozza, G. Carta, G. Rossetto, E. Tondello, P. Zanella, Structural and morphological analyses of tungsten oxide nanophasic thin films obtained by MOCVD, Surf. Sci. 532 (2003) 439–443.
[21] G. Poirier, F.C. Cassanjes, Y. Messaddeq, S.J.L. Ribeiro, Crystallization of mono clinic WO_3 in tungstate fluorophosphate glass, J. Non-Cryst. Solids 355 (2009) 441–446.

[22] C. Lasbrugnas, P. Thomas, O. Masson, J.C. Champarnaud-Mesjard, E. Fargin, V. Rodriguez, M. Lahaye, Second harmonic generation of thermally poled tungsten tellurite glass, Opt. Mater. 31 (2009) 775–780.
[23] P. Subbalakshmi, N. Veeraiah, Study of Cao–WO_3–P_2O_5 glass systems by dielectric properties, IR spectra and differential thermal analysis, J. Non-Cryst. Solids 298 (2002) 89–98.
[24] Y. Gandhi, K.S.V. Sudhakar, M. Nagarjuna, N. Veeraiah, Influence of WO_3 on some physical properties of MO–Sb_2O_3–B_2O_3 (M = Ca, Pb and Zn) glass system, J. Alloys Compd. 485 (2009) 876–886.
[25] Y.B. Saddeek, Effect of B_2O_3 on the structure and properties of tungsten tellurite glasses, Philos. Mag. 89 (2009) 41–54.
[26] G. Damarawi, Transport behaviour of PbO–PbF_2–TeO_2 Glasses, Phys. Status Solidi A 177 (2000) 385–392.
[27] G. Vijaya Prakash, R. Jagannathan, Fluorescence properties of Eu^{3+} doped lead bearing fluoro-chloro phosphate glasses, Spectrochim. Acta, Part A 55 (1999) 1799–1808.
[28] B. Govinda Rao, H.G. Keshava Sundar, K.J. Rao, Investigations of glasses in the system PbO–PbF_2, J. Chem. Soc. Faraday Trans. I 80 (1984) 3491–3501.
[29] A.S. Rao, Y.N. Ahammed, R.R. Reddy, T.V.R. Rao, Spectroscopic studies of Nd^{3+} doped alkali fluoroborophosphate glasses, Opt. Mater. 10 (1998) 245–252.
[30] R.T. Karunakaran, K. Marimuthu, S. Arumugam, S. Surendra Babu, S.F. Leon-Luis, C.K. Jayasankar, Structural, Optical absorption and luminescence properties of Nd^{3+} ions in NaO–NaF borate glasses, Opt. Mater. 32 (2010) 1035–1041.
[31] T. Srikumar, M.G. Brik, Ch. Srinivasa Rao, Y. Gandhi, D. Krishna Rao, V. Ravi Kumar, N. Veeraiah, Spectral and fluorescent kinetics features of Nd^{3+} ion in Nb_2O_5, Ta_2O_5 and La_2O_3 mixed lithium zirconium silicate glasses, Spectrochim. Acta Part A Mol. Biomol. Spectrosc. 81 (2011) 498–503.
[32] W.T. Carnall, H. Crosswhite, H.M. Crosswhite, Energy level structure and transition probabilities of the trivalent lanthanides in LaF_3, Argonne National Laboratory, Argonne, USA, 1977.
[33] W.T. Carnall, P.R. Fields, K. Rajnak, Spectral intensities of the trivalent lanthanides and actinides in solution. II Pm^{3+}, Sm^{3+}, Eu^{3+}, Gd^{3+}, Tb^{3+}, Dy^{3+} and Ho^{3+}, J. Chem. Phys. 49 (1968) 4412–4423.
[34] Sk. Mahamuda, K. Swapna, A. Srinivasa Rao, M. Jayasimhadri, T. Sasikala, K. Pavani, L. Rama Moorthy, Spectroscopic properties and luminescence behaviour of Nd^{3+} doped zinc alumina bismuth borate glasses, J. Phys. Chem. Solids 74 (2013) 1308–1315.
[35] B.R. Judd, Optical absorption intensities of rare-earth ions, Phys. Rev. 127 (1962) 750–761.
[36] G.S. Ofelt, Intensities of crystal spectra of rare earth ions, J. Chem. Phys. 37 (1962) 511–520.
[37] P.R. Ehrmann, J.H. Campbell, Non radiative energy losses and radiation trapping in neodymium-doped phosphate laser glasses, J. Am. Ceram. Soc. 85 (2002) 1061–1067.
[38] L. Jyothi, V. Venkatramu, P. Babu, C.K. Jayasankar, M. Bettinelli, G. Mariotto, A. Speghini, Composition and concentration dependence of spectroscopic properties of Nd^{3+}-doped tellurite and metaborate glasses, Opt. Mater. 33 (2011) 928–936.
[39] M. Jayasimhadri, L. Rama Moorthy, R.V.S.S.N. Ravikumar, An investigation of the optical properties of Nd^{3+} ions in alkali tellurofluorophosphate glasses, Opt. Mater. 29 (2007) 1321–1326.
[40] R. Balda, J. Fernandez, M.A. Arriandiag, J.M. Fernandez-Navarro, Spectroscopy and frequency upconversion in Nd^{3+} doped TeO_2–TiO_2–Nb_2O_5 glass, J. Phys.: Condens. Matter 19 (2007) 086223–086234.
[41] Yujin Chen, Yidong Huang, Miaoliang Huang, Ruiping Chen, Zunda Luo, Effect of Nd^{3+} on the spectroscopic properties of bismuth borate glasses, J. Am. Ceram. Soc. 88 (2005) 19–23.
[42] E. Pecoraro, J.A. Sampaio, L.A.O. Nunes, S. Gama, M.L. Baesso, Spectroscopic properties of water free Nd_2O_3-doped low silica calcium aluminosilicate glasses, J. Non-Cryst. Solids 277 (2000) 73–81.
[43] B.C. Jamalaiah, T. Suhasini, L. Rama Moorthy, Il-Gon Kiman, Dong-Sun Yoo, Kiwan Jang, Structural and luminescence properties of Nd^{3+}-doped PbO–B_2O_3–TiO_2–AlF_3 glass for 1.07 μS laser applications, J. Lumin. 132 (2012) 1144–1149.
[44] A. Kedziorski, L. Smentek, New parametrization of spectra of Nd^{3+} and Sm^{3+} in glasses, J. Alloys Compd. 451 (2008) 686–690.
[45] B. Karthikeyan, R. Philip, S. Mohan, Optical and non-linear optical properties of Nd^{3+} doped heavy metal borate glasses, Opt. Commun. 246 (2005) 153–162.
[46] J. Azevedo, J. Coelho, G. Hungerford, N.S. Hussain, Lasing transition ($^4F_{3/2} \rightarrow {}^4I_{11/2}$) at 1.06 μL in neodymium oxide doped lithium boro tellurite glass, Physica B 405 (2010) 4696–4701.
[47] M.B. Saisudha, J. Ramakrishna, Effect of host glass on the optical absorption properties of Nd^{3+}, Sm^{3+}, and Dy^{3+} in lead borate glasses, Phys. Rev. 53 (1996) 6186–6196.
[48] J. Lucas, M. Chanthanasinh, M. Poulain, M. Poulain, P. Brun, M.J. Weber, Preparation and optical properties of neodymium fluorozirconate glasses, J. Non-Cryst. Solids 27 (1978) 273–283.
[49] T. Suzuki, H. Nasu, M. Hughes, S. Mizuno, K. Hasegawa, H. Ito, Y. Ohishi, Quantum efficiency measurements on Nd-doped glasses for solar pumped lasers, J. Non-Cryst. Solids 356 (2010) 2344–2349.
[50] M.J. Weber, R.A. Saroyan, R.C. Ropp, Optical properties of Nd^{3+} in metaphosphate glasses, J. Non-Cryst. Solids 44 (1981) 137–148.
[51] Bozena Burtan, Zbigniew Mazurak, Jan Cisowski, Maria Czaja, Radoslaw Lisiecki, Witold Ryba-Romanowski, Manuela Reben, Jan Wasylak, Optical properties of Nd^{3+} and Er^{3+} ions in TeO_2–WO_3–PbO–La_2O_3 glasses, Opt. Mater. 34 (2012) 2050–2054.
[52] K. Swapna, Sk. Mahamuda, A. Srinivasa Rao, T. Sasikala, L. Rama Moorthy, Visible luminescence characteristics of Sm^{3+} doped zinc alumino bismuth borate glasses, J. Lumin. 146 (2014) 288–294.
[53] S. Surendra Babu, R. Rajeswari, Kiwan Jang, Cho Eun Jin, Kyoung Hyuk Jang, Hyo Jin Seo, C.K. Jayasankar, Spectroscopic investigations of 1.06 μS emission in Nd^{3+}-doped alkali niobium zinc tellurite glasses, J. Lumin. 130 (2010) 1021–1025.
[54] C.K. Jorgensen, R. Reisfeld, Judd–Ofelt parameters and chemical bonding, J. Less Common Met. 93 (1983) 107–112.
[55] J.H. Campbell, T.I. Suratwala, Nd-doped phosphate glasses for high-energy/high-peak-power lasers, J. Non-Cryst. Solids 263 (2000) 318–341.
[56] D.V.R. Murthy, T. Sasikala, B.C. Jamalaiah, A. Mohan Babu, J. Suresh Kumar, M. Jayasimhadri, L. Rama Moorthy, Investigation on luminescence properties of Nd^{3+} ions in alkaline-earth titanium phosphate glasses, Opt. Commun. 284 (2011) 603–607.
[57] N.O. Dantas, E.O. Serqueira, M.J.V. Bell, V. Anjos, E.A. Carvalho, S.A. Lourenc, M.A. Pereira-da-Silva, Influence of crystal field potential on the spectroscopic parameters of $SiO_2{\cdot}I_2O_3{\cdot}$influence of crystal fi_2O_3, J. Lumin. 131 (2011) 1029–1036.
[58] K. Vemasevana Raju, C. Nageswara Raju, S. Sailaja, B. Sudhakar Reddy, Spectroscopic investigations of 1.06 μS emission in Nd^{3+}-doped alkali niobium zinc tellurite glasses, Solid State Sci. 15 (2013) 102–109.
[59] D. Umamaheswari, B.C. Jamalaiah, T. Sasikala, G.V. Lokeswara Reddy, L. Rama Moorthy, Investigation on 1.07 μm laser emission in Nd^{3+}-doped sodium fluoroborate glasses, J. Rare Earths 30 (2012) 413–417.

Please cite this article in press as: M. Venkateswarlu et al., Opt. Mater. (2014), http://dx.doi.org/10.1016/j.optmat.2014.10.031

ISSN: 2319-8753

International Journal of Innovative Research in Science, Engineering and Technology

(An ISO 3297: 2007 Certified Organization)

Volume 3, Issue 10, October 2014

Status of E-Waste in India - A Review

Mahesh C. Vats[1*], Santosh K. Singh[2]

Technical Officer, Defense Research and Development Organization (DRDO), Delhi, India.

Professor & Dean, Department of Environmental Engineering, Delhi Technological University (Formerly Delhi College of Engineering), Bawana Road, Delhi, India

ABSTRACT: The mammoth generation of e-waste has created a new e-waste stream in the country containing obsolete, End of life Electrical and Electronics Equipments discarded after their intended use. The innovation, dynamism in product design and globalization replacing these equipments in very duration and made it fast growing waste in the world. E-waste is being generated by both indigenous and outsourced electrical and electronics equipments besides Basel Convention. The knowhow and compatible infrastructure for e-waste treatment is limited in India and informal recycling survived under the ambit of flexible legislative framework. The presence of toxic and hazardous substances in e-wasted equipments attracted the attention of the waste managing agencies in the country because these substances endanger the human health, environment, wherever present in uncontrolled conditions. The existence and implementation of Environmentally Sound Management is partial and progressing very slowly due to obvious reasons. The formal recyclers have commissioned comprehensive e-waste treatment facilities; but inadequate in proportion to the e-waste generation in the country since the informal recyclers are treating 95% of the e-waste generated with hazardous practices. The formal e-waste collection from all sources is ambiguous. E-waste contains a good amount of valuable recyclable materials also and has potential to become lucrative business in the country.

KEYWORDS: E-waste, Globalization, Basel Convention, Recycling, Toxic and Hazardous, Environmentally Sound Management.

I. INTRODUCTION

The waste generated due to the discarded, obsolete, end of life electrical and electronics equipments is known as E-waste world over. It is well known by acronym WEEE (Waste from Electrical and Electronics Equipments). However, various definitions have been presented by different agencies.

India is generating e-waste more than 8,00,000 tonnes annually**[MoEF, Guidelines, 2008]**.The 70% e-waste is being generated by ten states in the country **Rajya Sabha Report].**The obsolete, short lived, damaged, End of life EEEs (Electrical and Electronic Equipments) all together made e-waste a fast growing waste in the country. In India, IT industry has promoted both software and hardware segment and become leader in the world. The growth rate of IT[**Information Technology]** industry was 42.4% between 1995 to 2000**[EMPA, 2006].** The use and dynamism of EEEs for information and telecommunication technology have been enhanced by manufactures and marketing agencies manifolds, resulted a huge infrastructure expansion in the country. The new technology needs new compatible infrastructure replacing the old one in a very short duration of time. In view of that EEEs in installations have increased manifolds in the country and a huge quantity of e-waste has been generated due to obsolescence. The computers, televisions, servers, music systems, mobile phones, refrigerators, air-conditioners, medical equipments and their respective assemblies and illegal outsourcing are the major contributors of e-waste in the country. There may be more obvious reasons behind their generation in huge quantity. The flow of e-waste is very rapid causing threats to the human health, environment due to its toxic and hazardous attributes. It is all due to presence of toxic and hazardous substances like mercury, lead, cadmium, chromium (VI)**[MoEF, Guidelines, 2008]** etc. in the components of these e-wasted EEEs when not handled in controlled conditions while storage,

DOI: 10.15680/IJIRSET.2014.0310071

ISSN: 2319-8753

International Journal of Innovative Research in Science, Engineering and Technology

(An ISO 3297: 2007 Certified Organization)

Volume 3, Issue 10, October 2014

transportation, recycling, recovery processes. Maharashtra among the states and Mumbai among the metropolitan cities are leading in the e-waste generation in the country.

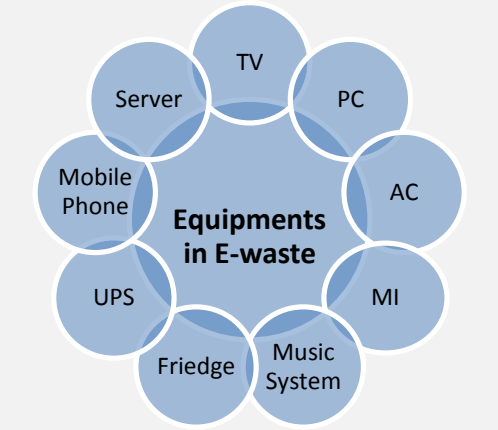

Figure 1 E-waste Equipments

In these states the various sectors like manufacturing, industrial, commercial, institutional, household, research and development are the major contributors for e-waste generation. No doubt, the e-waste collectors from all sources are the secondary source of e-waste and act as major stake holder and contribute in a big way as the e-waste collection is made from door to door by the stakeholder in the society. The recycling and recovery of components and materials out of e-waste is a pressing need of today as it provides a good support for the components refurbishment and ample quantity of secondary recyclable metals and other materials for the manufacturing of new equipments. Both informal and formal stakeholders are participating in e-waste treatment in the country. Presently the informal recyclers are dominating over formal and treating 90 to 95% of the total e-waste generated by environment unfriendly manner in the country **[Khattar, 2007].**The EEEs are being manufactured with the composition of more than one thousand substances [**MoEF, Guidelines, 2008].**The presence heavy metals like Hg, Pb, Cd, Cr (vi) etc. in the e-wasted components made them hazardous and toxic and attracted the attention of e-waste stakeholders to arrange a separate treatment place for them. Apart from hazardous contents, it has valuable and precious recoverable and recyclable metals in it. The share of metals in composition varies as steel, aluminium, copper, tin, nickel are present in bulk quantity; cadmium and mercury in small quantity and barium, nickel, gold, titanium, cobalt, palladium, manganese, silver and platinum in traces in the equipments Rajya Sabha Report**].**

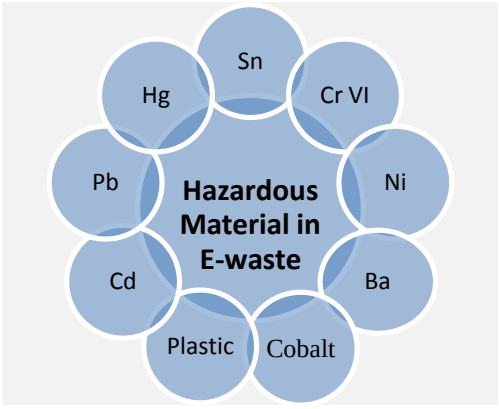

Figure 2 E-waste Hazardous Material

DOI: 10.15680/IJIRSET.2014.0310071

ISSN: 2319-8753

International Journal of Innovative Research in Science, Engineering and Technology

(An ISO 3297: 2007 Certified Organization)

Volume 3, Issue 10, October 2014

The informal recyclers are not serious about the guidelines issued by CPCB (Central Pollution Control Board) and using hazardous methods of e-waste disposal like open burning for the recovery of targeted metals like copper, aluminium, iron and steel from equipment peripherals and acid leaching for the recovery of copper and precious metals from PCB (Printed Circuit Boards), mother boards and leave all hazardous metals like Pb, Hg, Cd etc at the treating sites in open causing an explosion of pollutants in the environment. Apart from these materials, 36 chemicals are also being used in the manufacturing of these e-wasted equipment [**Amitava Bandyopadhyay, 2010]**.

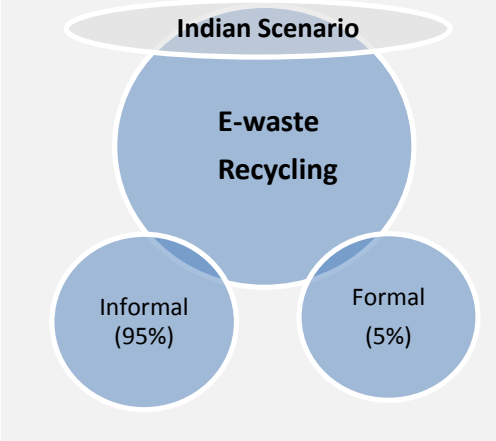

Figure 3 E-waste Recycling Status

However, CPCB has registered 23 recyclers for treating e-waste by environmentally sound methods **[Agarwal R.(1998)].** Also, the CPCB has encouraged informal recyclers to be part of formal recycling which can be carried out with compliance under single umbrella of guidelines issued in 2008**[MoEF, Guidelines, 2008].** Presently, there is no separate law for e-waste (Management and Handling) for restricting the informal recycling in the country. However a rule for e-waste management and handling is in force since 1st May 2012 to restrict the environment unfriendly methods but it is based on voluntarily clause **[E-waste (M&H) rule 2011].** In subsequent paragraphs, E-waste Inventory, E-waste sources, E-waste Treatment Scenario, Legal Support to E-waste E-waste Disposal Strategy, Challenges for ESM, and E-waste hazards in India will be discussed.

II. E-WASTE INVENTORY

The use of EEEs is increasing every day in public services, household logistics, manufacturing sectors etc to support the infrastructural requirement in the country. The e-waste generation has affinity to population and GDP **(Gross Domestic Product)** of the country. Both are increasing at varied rate. The consumption of new electronic goods is an index of societal progress and further decides the country technological rank in the world. The waste generated depends upon the demographic, geographical, socio-economic perimeters etc. [**Beigl *et al.*, 2008**]. The e-waste is being generated more in urban area than rural as 31% of people are living urban areas in the country [**Population, 2014**]. The use of these equipments like computers and its peripherals, servers, mobile phones, televisions, stereos is maximum in the society. However, other equipments are also being used for general and specific requirement. After EOL (End of Life), all equipments are supposed to be disposed of as per rule 2011. The infrastructure and inventory detail is the basic need for its disposal. A tentative estimate is available based on study conducted for e-waste generation. Presently, India is generating more than 8,00,000 tonnes annually comprising all kinds of EEEs discarded from intended use**[MoEF, Guidelines, 2008]**. Globally, 20 to 50 million tonnes per annum are being generated, which is 5% of the municipal waste at global scale [**UNEP Press Release, 2006**]. However, it will go up to 40 to 70 million tonnes by 2014/15[**IAER, 2009**]. The per capita e-

DOI: 10.15680/IJIRSET.2014.0310071

ISSN: 2319-8753

International Journal of Innovative Research in Science, Engineering and Technology

(An ISO 3297: 2007 Certified Organization)

Volume 3, Issue 10, October 2014

waste generation in India is about 1 Kg per annum. The present population of the country is 1250 billion. With this figure total e-waste accounts to 12,50000 tonnes per annum, which is merely 2.5% of the global production taking base of 40 million tonnes e-waste generated per annum. However, the per capita e-waste generation in EU is 14 to 15 times to India [**Rajya Sabha, 2010**.]. In India e-waste is increasing at the rate of 10% per annum [**Ravi Agarwal, 2010**].

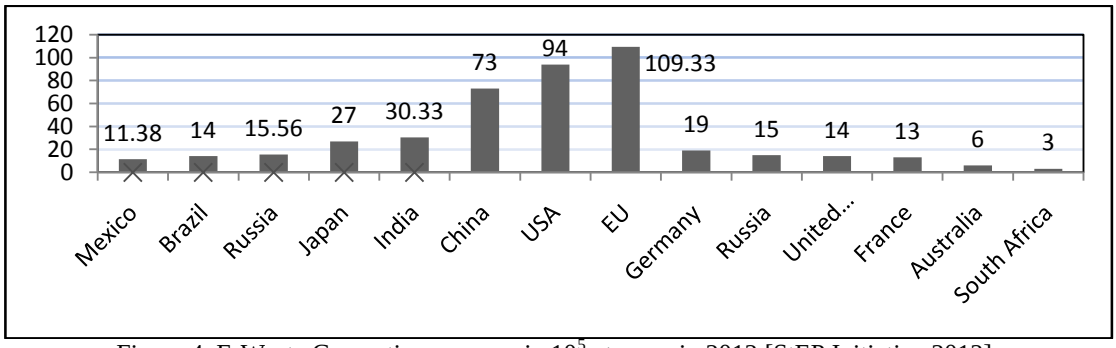

Figure 4 E-Waste Generation per year in 10^5x tonnes in 2012 [StEP Initiative 2012]

However, in EU it is estimated that 3 to 5% per year. In e-waste generation, USA is leading followed by China by 30,00,000 tonnes and 23,00,000 tonnes respectively[**Rajya Sabha ,2010**]. It has become fastest growing waste in the municipal waste stream [**Rajya Sabha ,2010**]. However, in the past 1990s, the use of EEEs was limited and life span was also more. After, globalization and invent of new EEEs products enhanced the production of these equipments manifolds. The life span of the equipments has also reduced appreciably. Based on the study made, 4,00,000 tonnes of e-waste was being produced initially in 2010[**Ravi Agarwal,2010**] and further CPCB had also reported the e-waste production in the country as 1,47,000 tonnes annually or 0.573 metric tonnes per day in 2010[**Lok Sabha,2010**]. Also, a figure of 4,34,000 tonnes annual e-waste generation was estimated for 2009[**Poonam J.Prasad,2012**] and further estimated by CPCB that it will above 8,00,000 tonnes in 2013[**Moushumi Basu,2010**]. As such, the approach for e-waste production estimation and calculation is ambiguous. E-waste quantity is being anticipated but not authenticated formally as receipt as formal collection is yet to be devised by the CPCB.

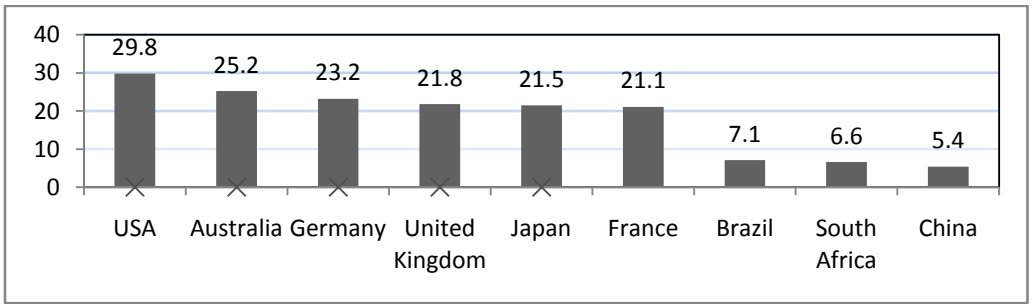

Figure 5 E-Waste Generation in Kg per Capita [Ref: StEP initiative, 2012]

Further predictions show an alarming e-waste generation at a faster rate in the country. By 2020, computer based e-waste will increase 500% and mobile phone 18 times with respect to the 2007[**Tom Young, 2010**]. A glimpse of e-waste generation in 2009 by top ten states and metropolitan cities is presented in table 1.

ISSN: 2319-8753

International Journal of Innovative Research in Science, Engineering and Technology

(An ISO 3297: 2007 Certified Organization)

Volume 3, Issue 10, October 2014

Table 1 E-waste Generation [Consumer Voice,2009].

Sr. No.	States	E-waste Generated in MTA	Metropolitan Cities and others	E-waste Generated in MTA
1.	Maharashtra	20270.59	Mumbai	11017.1
2.	Tamil Nadu	13486.24	Delhi	9729.15
3.	Andhra Pradesh	12780.33	Bangaluru	4648.4
4.	Uttar Pradesh	10381.11	Chennai	4132.2
5.	West Bengal	10059.36	Kolkata	4025.3
6.	Delhi	9729.15	Ahmadabad	3287.5
7.	Karnataka	9118.74	Hyderabad	2833.5
8.	Gujarat	8994.33	Pune	2584.2
9.	Madhya Pradesh	7800.62	Surat	1836.5
10.	Punjab	6958.46	Nagpur	1768.9

The growth rate of the mobile phones (80%) is very high compared to that of PC (20%) and TV (18%)[**CII (2006)].** However, the e-waste generation quantity given in the table is the data provided to CPCB by obvious sources, since there is no mechanism of collection of data from ratified sources. The issued instruction by CPCB to promote handing over e-waste to the registered recyclers is yet to be implemented uniformly throughout the country on every e-waste stake holders. People are yet to be ready to accept it concensously.

The e-waste is being imported from developed countries in the name of 2nd hand use of the EEEs for charity, recycling and refurbishment of these equipments. The data are not available for its quantification as it is a hidden kind of e-waste. The e-waste quantification had been made based on computers, mobile phones and television in 2007 and found that 3,82,979 tonnes e-waste generated in India and 50,000 tonnes was imported illegally**[Khattar, 2007]** from USA and EU countries in the ratio of 80 to 20 to the total quantity imported respectively**[Pratap, A, 2009]**. Out of total e-waste quantity of 3,82,979 tonnes, only 1,44,143 tonnes of e-waste has been reported back and remaining 238836 tonnes e-waste(more than 62%), either people have handed over to the informal recyclers/local collectors or kept in the house **[Khattar,2007].** However, only 19000 tonnes(13%) of e-waste has been recycled out of 1,44,143 tonnes **[Khattar,2007].**

The 70% e-waste produced in the country is being produced by ten states only and 60% by 65 cities **[**Rajya Sabha Report**].**The viable e-waste treatment facilities have been commissioned by registered recyclers as per CPCB norms in nine states of the country, other states are supposed to divert their e-waste towards the nearest installed facility easily.

III. E-WASTE SOURCES

E-waste is being produced by various sources in the country like Govt. sectors, commercial establishments, institutional sectors, research and developments, household and manufacturing sectors of the country. The above mentioned sectors are free to handover the waste who is going to bid more for it, that may be formal recyclers or informal recyclers or any local e-waste collectors or a Kabadees. The quantity may vary depending upon the demography and types of EEEs installations of the establishment. However, main stakeholder is local collectors supposed to do door to door collection of e-waste. The Government along with industrial sectors of the public and private partners contributes 70%, individual households 15% approximately **[Satish Sinha,2007].** The e-waste received from different sources predominantly comprising of the following EEEs as televisions and desktops 68%, servers 27%, mobile phone 1% and import from developed countries 2% respectively **[IMRB, 2009].** However the other equipments like refrigerator, air conditioner, music system, recorder, monitoring and control, Medical equipments, ovens etc are also contribute in the e-waste generation marginally as their life is more and their use is limited in the society.

DOI: 10.15680/IJIRSET.2014.0310071

ISSN: 2319-8753

International Journal of Innovative Research in Science, Engineering and Technology

(An ISO 3297: 2007 Certified Organization)

Volume 3, Issue 10, October 2014

Figure 6 E-Waste Sources

IV. E-WASTE TREATMENT SCENARIO

Presently, the e-waste is treated by both informal and formal recyclers sharing total e-waste quantity in 95 to 5 ratios in the country **[Khattar, 2007; Raghupathy, L, 2009].** From the total e-waste generated in the country 60% e-waste remains in warehouses/storages and only 40% is made available for recycling process. In recycling process 95% E-waste is being used for the refurbishment and only 5% need process of disposal [**MAIT**]. The enormous energy may be saved by adapting recycling of e-waste.

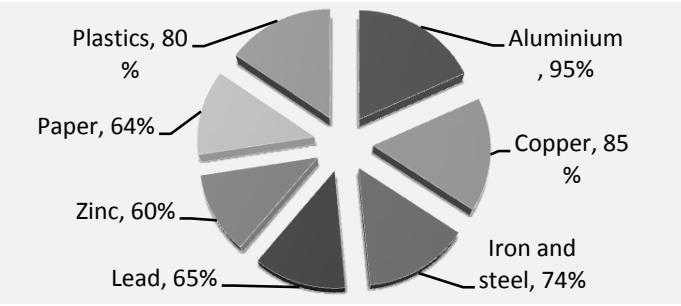

Figure 7 Energy saving %age by recycled material **[Cui, 2003]**

It is presented in fig 7 as in recycling of aluminium 95%, copper 85%, iron and steel 74%, lead 65%, Zinc 60%, plastics 80% energy can be saved and for extraction of virgin material CO^2 emission takes place for each tone of metal. It is presented in figure 8. So, this environmental loading also can be avoided if recovery of metals is done from e-waste and put in the recycling of the metals for further use. The informal recyclers get the e-waste from local waste collectors at very cheap price and recover the targeted metals like copper, aluminium, iron and steel with rudimentary and primitive methods and put a heavy environmental loading of pollutants on atmosphere. They are using open burning, acid leaching for the recovery of metals, which are non-environment friendly methods. The informal recyclers treat 95% of the e-waste generated by all sources **[Khattar, 2007].**These activities of e-waste treatment are cause of concern of the ambience and society as these are detrimental to the air quality, human health as the pollutants persist in the environment years together and harm it

DOI: 10.15680/IJIRSET.2014.0310071

ISSN: 2319-8753

International Journal of Innovative Research in Science, Engineering and Technology

(An ISO 3297: 2007 Certified Organization)

Volume 3, Issue 10, October 2014

continuously. The dispersion of pollutants due to treatment in uncontrolled conditions and further transportation ahead, resulting various kinds of diseases to the human beings effecting kilometers distant human being and environment.
The recovery of materials: metals etc. are a lucrative business and acts as feedstock for the manufacturing of the new equipment, which is going to meet the user equipment demand at very cheap rate [**Rajya Sabha, 2010].** The state of the art is available to recover metals to the maximum from the e-wasted equipment easily. Umicore in Belgium and Attero in India are the appropriate examples recovering gold up to 99% efficiently **[Gupta, R,2009].**

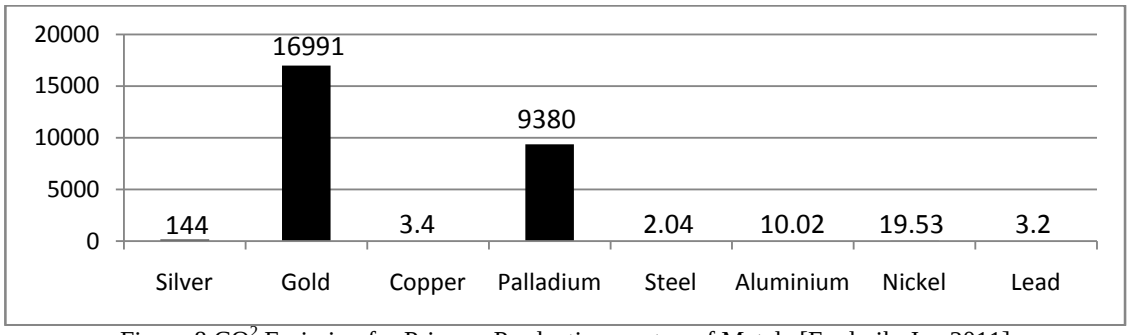

Figure 8 CO^2 Emission for Primary Production per ton of Metals [Frederik, Jan 2011]

The formal recycling in the country is in the transition and CPCB is registering recyclers every year and presently registered 23 recyclers have been registered for the treatment of e-waste produced in the country [**MoEF Registered Recyclers**]. The registered recyclers have to comply the e-waste management guidelines and adhere to rule 2012**[E-waste (M&H) rule 2011].** A fixed quantity of e-waste is being allotted to them; however they are not getting it easily and always strive to get it from import channels so that the state of the art facility may be run at full load.
The informal recovery system is less environ efficient comparably to the formal in terms of the state of the art technology. For example: for the recovery of 1 g gold and 6 g of silver, the informal recyclers are using more than 50 litres water, 3 and 21 Kg Chemicals and explode 1.3 g and 3 g of mercury in the environment due to uncontrolled treatment[**Keller, M. (2006**)]. However, the metal yield by using chemical processes 10 to 20% more if it is carried out by informal recyclers**[Keller, M. (2006)]** but they are not carrying out it in the ambit of ESM. The e-waste generated reporting process is not in place. The inadequate record keeping by all e-waste stakeholders made the e-waste treatment very tedious task. The infrastructure cannot be created based on estimated quantity of e-waste.

Table 2 Registered Recyclers and E-waste Allotments [MoEF Recyclers].

Sr. No.	States	No. of Registered Recyclers	Total Quantity of E-waste Allotted for recycling by CPCB
1.	Andhra Pradesh	02	11800 MTA
2.	Karnataka	07	3140.6 MTA and 120000 nos. cartridges
3.	Gujarat	01	12000 MTA (Shredded PCBs and mother boards.
4.	Maharashtra	03	8060 MTA
5.	Haryana	01	1200 MTA
6.	Rajasthan	01	450 MTA
7.	Tamil Nadu	06	38927 MTA
8.	Uttar Pradesh	01	1000 MTA
9.	Uttarakhand	01	12000 MTA

DOI: 10.15680/IJIRSET.2014.0310071

ISSN: 2319-8753

International Journal of Innovative Research in Science, Engineering and Technology

(An ISO 3297: 2007 Certified Organization)

Volume 3, Issue 10, October 2014

People should look forward to hand over the e-waste to the registered recyclers rather than treat it themselves otherwise they would be victimized by the toxic and hazardous substances in the e-waste. However, for the informal recycler's research scholar are striving to get environment friendly, low cost, effective, handy e-waste processing and treating techniques [**Sepúlveda et al., 2010**]. New techniques may bridge the informal and formal processing methods and environmentally sound e-waste management may be established easily.

V. EMPLOYMENT PROSPECTIVE OF E-WASTE

The rapidly growing e-waste can be utilized as source of recyclable and recoverable materials and enormous employment opportunities can be explored via this profession. It is evident that the demand of virgin material for the manufacturing of the new EEEs is increasing every day. The use of EEEs have increased manifold in our day to day work. The materials mined from natural resources consume ten times energy with respect to recovery of materials from e-waste. E-waste confirms the availability of these materials but natural resources confirm it partially. In view of that the recovery of recyclable materials from e-waste releases environmental pressure on all natural resources until unless it is carried out by environment friendly techniques and methods. The environment friendly recovery infrastructure adopted by Umicore in Belgium and Attero in India employed specialized, skilled, semiskilled and unskilled manpower in proportion to the e-waste treated. Even before treatment, presently e-waste engages enormous unskilled manpower for the collection, segregation, manual dismantling, packaging, transportation of e-waste. So, there is and would be a huge demand of all kind of manpower if e-waste profession is organized professionally in the country. The glimpse of employment flow for the e-waste processing has been presented in the table 3.

Table 3 Manpower Detail for e-waste processing on Annual Basis [Amitava, 2010]

E-waste processed in one year	**Manpower employed in Numbers**	**Working Hours per day**	**Daily Wages Rate**	**Per Annum Employment Business**	**Working Place**	**Safety Measures**
10,000 tonne to 20,000.	25000	8 to 10	Rs 350/-	3193750000 or Rs.319 crore	Basements/close units	Minimum

The table shows for the 10,000 MT to 20,000 MT e-waste processing 319 core has been spent which arrives as Rs. 160 per Kg maximum as processing charges.

There is lot of possibilities of multi-crore business of e-waste treatment and concurrently e-waste recycled material market like other types of materials can be created very easily. There is a wide scope of this type of market as e-waste is growing at a rapid rate in the country.

The refurbishing of EEEs and their components is not established and organized as such in the country, but if it is organized properly then low cost EEEs can be made available to the second hand use easily. The installation of these equipments comes under non-sophisticated equipments as these reassembled kind of equipments but a separate kind of market can be established like Nehru Place in India where both assembled and branded equipments are being marketed.

The e-waste pre-processing is cheap in developing countries due to the availability of human resource at reasonable cost. The availability of update environment friendly recovery technology will strengthen and explores more employment opportunities in the country.

VI. LEGAL SUPPORT TO E-WASTE

Before 1989, e-waste was not in inception so far; afterwards, it covers under Hazardous Waste Management (HWM) rules (1989,2000, 2003) indirectly since electronics equipment mentioned in schedule-1, contain hazardous material in their composition. A ray of hope came in 2008 when it is addressed separately. CPCB has issued guidelines to manage e-waste by environmentally sound manner to all state pollution control Boards in April 2008. These are applicable to all e-waste

DOI: 10.15680/IJIRSET.2014.0310071

ISSN: 2319-8753

International Journal of Innovative Research in Science, Engineering and Technology

(An ISO 3297: 2007 Certified Organization)

Volume 3, Issue 10, October 2014

stake-holders viz. generators, collectors, transporters, dismantlers, recyclers etc. In 2011, under Environmental Protection Act 1986, E-waste (Management and Handling) rule was introduced and enforce from 1st may 2012. It confirms the environment friendly handling, transportation, storing and recycling of e-waste, obviating any kind of implications occurrence with the existence of hazardous substances **[E-waste (M&H) rule 2011]**. It is applicable on producers, marketing agencies, refurbishing centres, collection centers, dismantler and recyclers of EEEs and its components mentioned in schedule1. The responsibilities of each stakeholder i.e. Producer, Collection centre, Consumer or bulk consumer, dismantler, other stakeholders have been explained accordingly so that it can be strengthened further. The SPCBs (State Pollution Control Boards) compliance report regarding implementation of these rules need to be furnished to CPCB latest by 30th September every year. The e-waste storage duration is permitted for 180 days, the further storage of it would be offensive until unless it is permitted by SPCB concerned in unavoidable circumstances.

EPR (Extended Producer Responsibility) is in place but its strengthening process is still underway and hope so it will work comprehensively very soon. The applicability option is voluntarily, so there is a laxity for the informal recyclers to opt it. Violation of any kind rule pertaining to e-waste does not penalize the culprit. However, CPCB has made lot of efforts in bridging the informal to formal by inviting all kinds of professionals in the workshops on common platform. But by the introduction of EPR the electronics producer has taken financial responsibility for the disposal of all equipment produced under his control. In fact the responsibility has shifted from municipality to OEM (Original Equipment Manufacturer)[**Yu, Welford & Hills, 2006**]. Take back is inclusive of the EPR and however the producer can apply RoHS (Restriction of Hazardous Substances) concurrently and implemented by incorporating green product design in the forth coming manufacturing.

However, India has ratified the Basel convention, prohibiting trans-boundary movement of e-waste. Despite Basel Convention the developed nations are dispatching e-waste to the developing Nations continuously in the name of recycling, charity, second hand use. The CPCB has strived in organizing various seminars and conferences with the objective to disseminate the information among all stakeholders. The role of non-governmental organizations cannot be ignored as they have conducted various qualitative and quantities studies for quantification of waste. Also, the comprehensive e-waste treatment initiative by Attero in Roorkee is an example to move forward towards the environmental sustainability and overcome e-waste threat to a maximum.

The take back initiatives by the OEMs (Original Equipment Manufacturers) have started by Nokia, Wipro and Dell in the country.

VII. E-WASTE DISPOSAL STRATEGY

In CPCB guidelines issued in 2008, the Environmentally Sound Management (ESM) has been suggested to deal with the e-waste at SPCB (State Pollution Control Board) level in the country. The e-waste is being treated in phase manner and divided in to various activities. For each activity and material the treatment is different. The objective of the strategy is to dispose of the e-waste in sustainable and environmental friendly manner with the help of infrastructure having controlled conditions and adhering to the occupational health norms suggested by OSHA (**Occupational Health Standards in Ambience**). The treatment of e-waste is well monitored by the SPCB time to time and adequacy report of the installed infrastructure is being scrutinized on regular basis by the SPCB confirming viable infrastructure is sound to dispose of e-waste in an effective manner. For comprehensive treatment, the e-waste undergoes various stages of treatments i.e. 1st Level, 2nd Level and 3rd Level treatments are presented below.

ISSN: 2319-8753

International Journal of Innovative Research in Science, Engineering and Technology

(An ISO 3297: 2007 Certified Organization)

Volume 3, Issue 10, October 2014

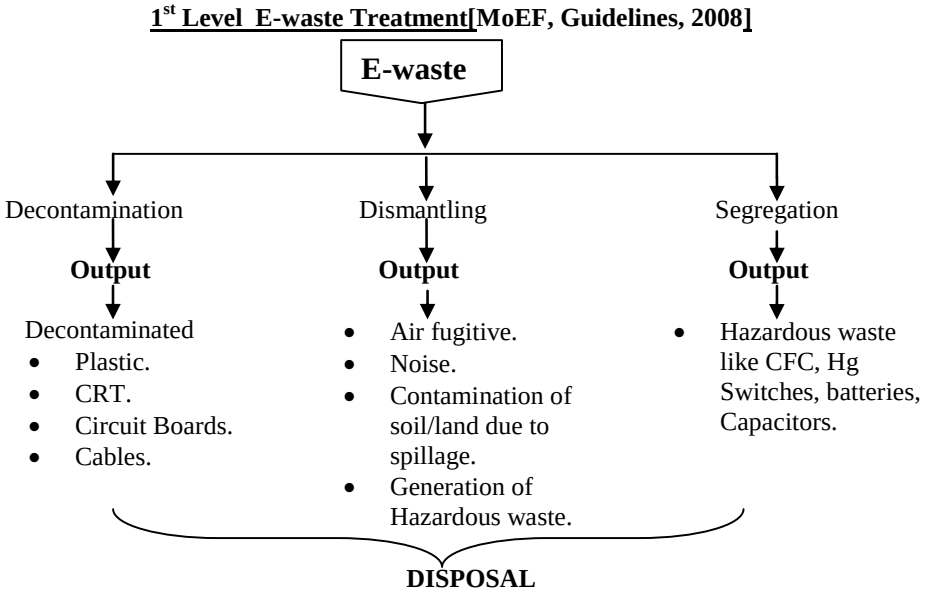

Fig. 9 Flow Chart 1st Level Treatment

In 1st level treatment the e-waste is being decontaminated, dismantled and segregated. The further outputs are represented in fig. 10

After 1st level e-waste treatment, the disposal becomes the input of the 2nd level treatment. In 2nd level treatment e-waste is being hammered, shredded and special Processes like CRT treatment, electromagnetic separation, eddy current separation and density separation are to be carried as per need. The flow chart has been drawn in fig.10.

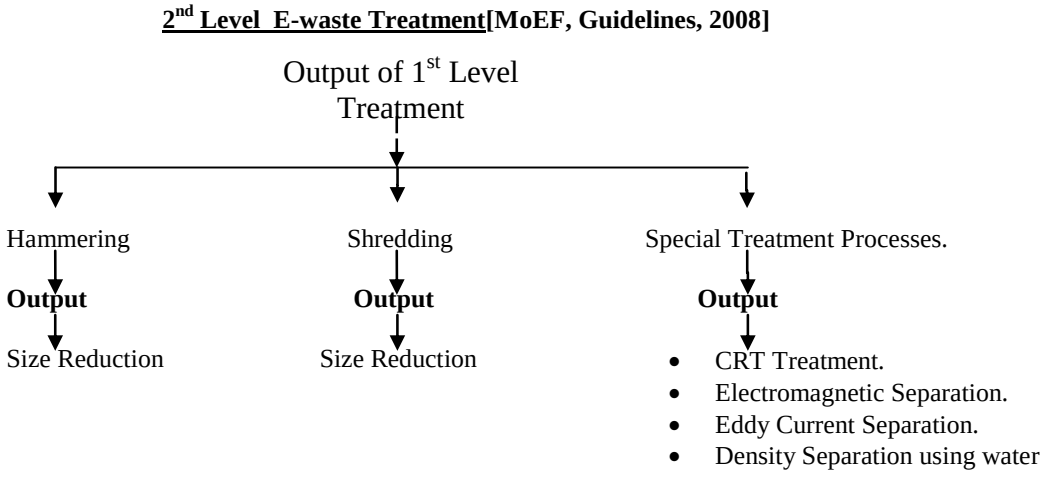

Fig: 10 Flow chart of 2nd level e-waste treatment.

DOI: 10.15680/IJIRSET.2014.0310071

ISSN: 2319-8753

International Journal of Innovative Research in Science, Engineering and Technology

(An ISO 3297: 2007 Certified Organization)

Volume 3, Issue 10, October 2014

. **3rd Level Treatment of E-waste[MoEF, Guidelines, 2008].**

Treatment of E-waste **[**Ministry of Environment**]** is based upon the input (residual fractions), technologies used and its final output. Apart from eddy current separation, magnetic separation etc. the e-waste feedstock is treated with incineration; refining, smelting and distillation to get heat energy and concentrated metals.

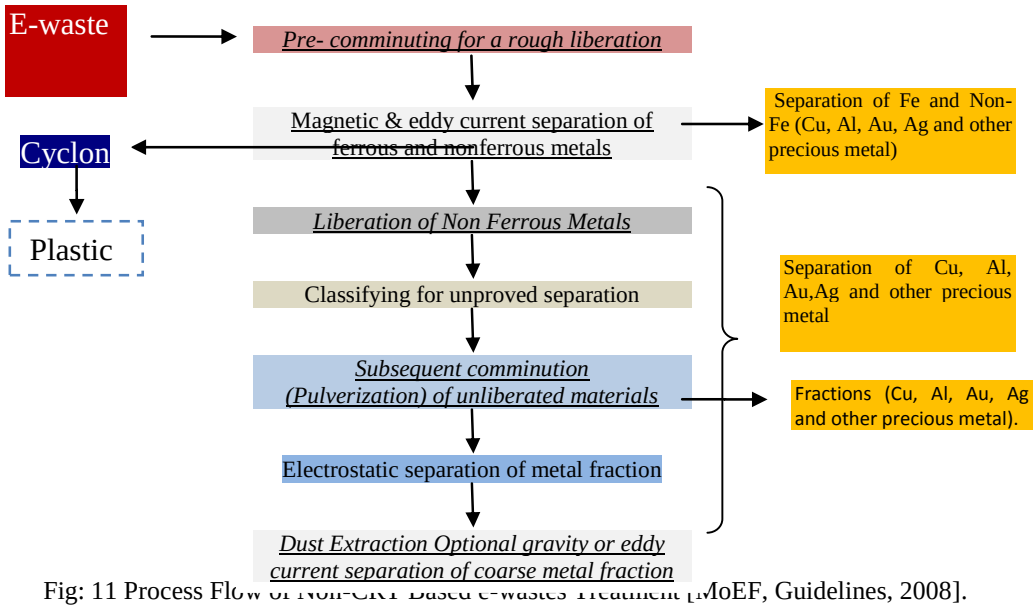

Fig: 11 Process Flow of Non-CRT Based e-wastes Treatment [MoEF, Guidelines, 2008].

The techniques are available with developed Nations to recover recyclable material like plastics, ferrous metals, non-ferrous metals and their efficiencies are high and vary material to material. For example magnetic separation achieves a target of ferrous metal recovery is 90% to 95% from e-waste and eddy current separation of non-ferrous metals is more than 90% **[MoEF, Guidelines, 2008].**

In the recovery of materials from e-waste, an appreciable amount of energy can be saved with respect to the virgin material recovered by exploitation from natural resources. A ready reckoner of few materials is presented in the fig 7. The monetary benefits and fulfilling the demand of these materials.

VIII. CHALLENGES FOR ESM

The informal recyclers with primitive and environment unfriendly e-waste disposal methods lead to pollutants explosion in the atmosphere. After recovery of target material, it is being left either in open or put in the municipal waste resulting contamination of air, water and soil. The heavy metals leak out from the components if not handled properly and harm our natural resources through leachate. The ESM is not in practice fully in India as on ground only registered recyclers are complying ESM. However, more recyclers have expressed their interest in ESM but their numbers are not increasing in the proportion to the e-waste generation. As more than 90% e-waste generated find their way to maximum to Local collectors (Kabadees) and rest to landfilling. It is very true that e-waste treatment is a business driven profession and even under the ambit of ESM, the compliance from e-waste stakeholders is lacking since they are not working cohesively. The ESM implementation is a big challenge in the country to treat e-waste. These are the hurdles hampering implementation of ESM.

- No legislative frame work for EPR (Extended Producer Responsibility), Take back, RoHS as Environmental Protection Strategy is in place in mandatory mode.

DOI: 10.15680/IJIRSET.2014.0310071

ISSN: 2319-8753

International Journal of Innovative Research in Science, Engineering and Technology

(An ISO 3297: 2007 Certified Organization)

Volume 3, Issue 10, October 2014

- Mammoth e-waste generation in the country.
- Apathy towards e-waste collection from sources.
- Unanimity for common e-waste disposal point/Centre in towns, metros.
- Perennial e-waste Sources are not classified.
- Carelessness in EEEs disposal.
- Sloppy E-waste Collection and Refurbishment System.
- Clumsiness in Recycling and Recovery of the materials.
- Ineptness of proficient Incinerating Facility.
- Deficit Secured Land Fills.
- Timidity of recyclers towards allotted quantum of e-waste.
- Deprivation of financial and technical assistance for creating infrastructure.
- Ineptness appealing approach to fascinate people to come forward for e-waste solution.
- Ineptness of familiarity with e-waste treatment technology.
- Formal e-waste collection and storage system is not in place.
- No formal reporting of e-waste generated by major e-waste generators to CPCB on annual basis.

A formal e-waste treatment and disposal structure has been defined by CPCB. For e-waste treatment, awareness about their ill effects helps to deal with it. The above mentioned gaps need to be filled for implementation of ESM uniformly in the country.

IX. SUGGESTIONS FOR E-WASTE ESM MODEL

The management of e-waste as per Indian scenario may be divided into three main nodal sections viz: Collection, Recycling and Recovery and Disposal. However, the sections are further divided to the sub sections as per their further activities involved. To optimize the use of available resources and infrastructure of both informal and formal stake holders a few suggestions applicable on Indian scenario are presented so that their potential may be utilized for the Environmentally Sound Management [ESM] of e-waste fully.

- The e-waste collection should be emphasized by creating local, urban, District level, and state level collection points so that the maximum amount of e-waste may be collected. Initially, the investment is high and approach is new, but after some time it will be established and well known for e-waste collection point. To attract people for voluntarily disposal, the awareness about the monetary benefits to be given to the people concerned and ill effects to them and their family and ambience should be spell out in terms of type of diseases caused due to e-waste and respective expenditure will be incurred for disease treatment should also be told in their local language by arranging workshops at grass root level. By this way we can motivate people to come forward for e-waste disposal
- The registered recyclers' representative will train the local collectors formal and informal about the e-waste and its detrimental effects on human beings, atmosphere, water, air, soil and ambience in absolute by conducting seminars, workshops with the help of Doctors.
- Set the door to door e-waste collection, its storage and further packaging mechanism in the locality by one to one contact or by phones with the help of formal and informal collectors keeping the incentives to the informal as per minimum monetary expectations.
- The segregation of the various equipment, components and packaging by pasting slip with all details need to be done on local stations and dispatch it to the registered recyclers.
- Transport the e-wasted equipment to the registered recycler's destination.
- After recovery, recycling and refurbishment the remaining material after decontamination disposed of either through incineration or secured landfilling.
- Use the potential of local collectors and fix the rates item-wise which are to be given to the user after receipt of items concerned and its collection charges upto collection point.

DOI: 10.15680/IJIRSET.2014.0310071

ISSN: 2319-8753

International Journal of Innovative Research in Science, Engineering and Technology

(An ISO 3297: 2007 Certified Organization)

Volume 3, Issue 10, October 2014

- The informal recyclers are used only up to collection of e-waste and for further treatment the e-waste should be handed over to the formal recyclers only.

The remaining modalities in between sections and sub-sections will work as per existing ESM in India. To make a sound e-waste management, a new working culture with new approaches suit to the locality need to be devised. It is a new field of profession and once people get its exposure then it would be a profit making and environment friendly profession in future.

X. E-WASTE HAZARDS

The handling of e-waste in uncontrolled conditions the hazardous and toxic potency of encapsulated materials in EEEs made it hazards prone. The backyard recycling with minimum safety measures and open burning recovery process made the situation very hazardous in nature. The health condition of the people engaged with bare hands and without masks is very poor and infected with chronic and acute diseases. Professionals in developing countries are employing men, women and children for the sorting and recovery of the materials and keep them in closed backyard. In general, in e-wasted equipment, the metal constitutes more than 60%, plastic 30% and hazardous pollutants 2.7% **[Agarwal R, 2006].** In PCB, BFRs (Brominated Fire Resistants' constitute 5 to 10% and antimony 1 to 2% to the weight of PCB **[Dr. B. J. Mohite, 2013].**
The recycling and reuse of the e-waste equipment and components is 25% all over the world and left 75% is waste **[Widmer R, 2005].** The leftover is being disposed of either in landfills or in municipal dustbins. It has been reported that among total metals, 75% are heavy metals present in landfills where e-waste has been landfilled **[Leke L, 2011].** The landfills are considered a good source of manure and people are taking its use in the vegetation and vegetables thereby the heavy metals get into the human food chain easily and may cause neurological and bone disorders. Even with the ingestion, inhalation and dermal routes, the heavy metals may cause blood and bone disorders, damage to the neurological and kidney, decline mental capacity. The high concentration of heavy metals can be felt in plants, animals, human bodies, water, and air. Due to run off and air transportation the soil concentration changes. **[Yilmax A.B, 2005, Asuqo F.E, 2004, Awokunmi, 2010]** The constituents, health effects and sources of constituents are presented in table. Most of them are carcinogenic.

Table 4. Health Hazards of Constituents in E-Waste [Poonam J.Prasad].

Constituents	Health Effects	Source of Constituents
Lead	• Cause to damage the central and peripheral nervous systems, blood systems, and kidney. • It effects badly on child brain development, damage to the circulatory system and kidney.	Available in solder in Printed circuit boards, glass panels, and gaskets in computer monitors.
Cadmium	• Irreversible toxic effects on human health. • It accumulates in kidney and liver. • Damage neural.	Available in chip resistors and semi-conductors.
Mercury	• Cause chronic damage to the brain. • Cause respiratory and skin disorders due to bioaccumulation in fishes.	Available in relays and switches, and printed circuit boards.
Chromium	• It causes bronchitis.	Available in galvanized steel plates and decorator or hardener for steel housing.
Plastics and PVC	• While burning produces dioxin that causes reproductive and developmental problems.	Available in Cabling and computer body.
Brominated flame-retardants	• It disrupts endocrine system functions.	Available in electronic equipment and circuit Boards.
Barium phosphorus and heavy metals.	• It cause muscle weakness and damage to heart, liver, and spleen.	Present in front panel of CRTs.

DOI: 10.15680/IJIRSET.2014.0310071

ISSN: 2319-8753

International Journal of Innovative Research in Science, Engineering and Technology

(An ISO 3297: 2007 Certified Organization)

Volume 3, Issue 10, October 2014

Copper	• It causes stomach cramps, nausea, liver damage, or Wilson's disease.	Present in copper wires, printed Circuit board tracks.
Nickel	• Causes allergy to the skin results dermatitis while allergy to the lung results in asthma.	Present in nickel-cadmium rechargeable batteries.
Lithium	• It can pass into breast milk and may harm a nursing baby.	Present in Lithium-ion battery
Beryllium	• It is Carcinogenic (lung cancer). • The inhalation of fumes and dust causes chronic beryllium disease or beryllicosis.	Present in Motherboards.

XI. CONCLUSION

It is fact that e-waste generation is increasing very fast due to obsolescence of the EEEs. People are either store the obsolete equipment in their home or sell it to the local collectors for monetary benefits. Presently there is no legislative binding framework for e-waste management. In view of that there is no e-waste collection mechanism at place. The CPCB has taken lead in declaring e-waste as a new waste stream made new e-waste rules came in force since 1st may 2012 governing all stakeholders of e-waste but it is volunteer kind of law applicable on registered recyclers but encourage informal recyclers to work in ambit of CPCB guidelines issued in 2008, so that ESM may be established effectively. But the informal recycling dominates over formal recycling in the country. The technology is changing every hour of the day due to availability of new technology due to globalization and replacing the old EEEs in large numbers. The infrastructure for e-waste treatment is money intensive but a lucrative business these days as recovery of metals is possible up to 99% from the e-wasted EEEs. Umicore in Belgium and Attero in India are the appropriate examples of metal recovery. People engaged in this profession are not aware about the ill effects of e-waste causing them chronic and acute diseases.

The e–waste management has become a complex and poses hazards to the environment in various ways and patients of chronic and acute diseases are increasing exponentially, however there may be obvious reasons for them. It is evident that air pollution is root cause of these diseases. Recently AIIMS (All India Institute of Medical Sciences) revealed that Arthritis is caused by air pollution. The environment health condition is declining due to the partially managed e-waste in the country. The solution may be sought by splitting it into three parts as user realization, local collectors and controlled treatment may possibly solve e-waste registered recycler's demand of not getting ample quantity of e-waste regularly so that the treating plant may be run at full load.

The ESI(Environmental Sustainable Index) rank was 101in 2005 and 66th in environmental governance, need further improvement by creating e-waste treatment infrastructure by PPPs(People, Private Partnership model in the country via Foreign Direct Investment(FDI) because European countries have technology and India has cheap manpower can collectively make the e-waste treatment viable and economical.

The technology boom is in 21st century will bring more challenges ahead so our preparedness should be equipped with new infrastructure, awareness and technology for e-waste treatment. For the reduction of environmental loading **5Rs (Report, Reduce, Reuse, Recycle and Recover)** principles should be followed in the country and a multi-crore lucrative business can be explored easily.

REFERENCES

1. Agarwal R.(1998) India: ' *The World's Final Dumpyard!'*, January, Basel Action News, vol. 1 at www.ban.org accessed on 14th September, 2006.
2. Amitava Bandyopadhyay '*Electronics waste management: Indian practices and guidelines'* Vol. No. 1, Issue No. 5, pp.793-804, 2010.
3. Asuqo F.E., EWA- OBOHO I., Asuquo E.F., UDOH P.J. '*Fish species used as biomarkers for heavy metals and hydrocarbon contaminations Cross river Nigeria*'. Environmentalist, Vol. No. 24, Issue No. 29, 2004.
4. Awokunmi E.E., ASAOLU S.S., IPINMORATI K.O. '*Effect of heavy metals concentration of soil in some dumpsites*' Afric. J. Environ. Sci. Tech. Vol. No. 4, Issue No. 8, 495, and 2010.

ISSN: 2319-8753

International Journal of Innovative Research in Science, Engineering and Technology

(An ISO 3297: 2007 Certified Organization)

Volume 3, Issue 10, October 2014

5. Beigl, P.G., Wassermann, F., Schneider, and Salhofer, S., Forecasting MSW Generation in Major European Cities, European Commission's Fifth Frame work Programme (EVK4-CT-2002-00087), pp 1-6, 2008.
6. CII (2006), '*E-Waste Management Green Business Opportunities'*, Volume No. 12, Issue No 1, Confederation of Indian Industry, Delhi.
7. Consumer Voice '*E-Waste Management in India*', April 2009.
8. Country level '*WEEE assessment'* study by the International Resource Group Systems South Asia Pvt. Ltd (IRGSSA), (m/s IRG Systems South Asia Pvt. Ltd), 2005.
9. Cui, J.; Forssberg, E. Mechanical recycling of waste electric and electronic equipment: A review. *J. Hazard. Mater*, *99*, 243–263, pp. 16–24, **2003**.
10. Dr. B. J. Mohite 'Issues *and Strategies in Managing E-Waste in India'* IJRMBSS I ISSN No. : 2319-6998 I Vol. 1 I Issue 1 I Mar. 2013.
11. E-waste (*Management and Handling) rule* 2012.
12. EMPA. The e-waste guide; Accessed on Aug 2006: http://www.ewaste.ch/.
13. EU. Directive 2002/96/EC of the European parliament and of the council of 27 January 2003 on waste electrical and electronic equipment (WEEE) — joint declaration of the European parliament, the council and the commission relating to article 9. Official Journal L037:0024-39 [13/02/2003; 2002a http://europa.eu.int/eur-lex/en/].
14. Frederik Eisinger, Ronjon Chakrabarti, Christine Krüger, Johannes Alexeew 'Carbon Footprint of E-waste Recycling Scenarios in India' Berlin, January 2011.
15. Gupta, R.: *Interview on e-waste in India and the Basel Ban.* [Interview] (Personal communication, 11 December 2009).
16. IAER Newsletter '*International News on Electronic Recycling*', January 2009, http://www.isrielectronics.org/communications/NL0109.html].
17. Indian market Research Bureau (IMRB) survey of '*E-waste generation at Source*' in 2009.
18. Keller, M. (2006): *Assessment of Gold Recovery Processes in Bangalore, India, and Evaluation of an Alternative Recycling Path for Printed Wiring Boards*, Diploma Thesis, Zurich: ETH
19. Khattar, V., Kaur, J, Chaturvedi, A. and Arora, R. "*E-Waste Assessment in India: Specific focus"*, 2007.
20. Leke L., Akaahan T., Simon A. '*Heavy metals in soil sand auto mechanic shops and refuse dumpsites in Markurdi, Nigeria'.* J. Appl. Sci. Environ. Manage., 15, (1), 207, 2011
21. Lok Sabha Unstarred Question no.650, dt. 28.07.2010.
22. Ministry of Environment and Forests "*Guidelines for environmentally sound management of e-waste"* March 12, 2008.
23. MoEF "*Implementation of e-waste rules in India*"2011, CPCB Delhi 32.
24. Ministry of Environment and Forests, CPCB Registered Recyclers.
25. Moushumi Basu, *'New e-waste management plan lucrative for states', The Pioneer*, New Delhi, 18 May 2010].
26. Pratap, A.: *Interview on e-waste in India and the Basel Ban.* [Interview] (Personal communication, 14 December 2009).
27. Poonam J. Prasad '*Environmental System Design &Modelling'* 2012 Intl. Journal of Environmental Technology and Management, Vol. 15, pp. 363-376.
28. Raghupathy, L.: *Interview on e-waste in India and the Basel Ban.* [Interview] (personal communication, 9 December 2009).]
29. Rajya Sabha Unstarred Question No. 24, '*Generation of E-waste'* dated 26.07.2010
30. Rajya Sabha Website, http://rajyasabha.nic.in/rsnew/publication_electronic/E-Waste_in_india.pdf
31. Ravi Agarwal, *'A Policy? Rubbish', The Hindustan Times*, 4 May 2010].
32. Sandeep Joshi, *'Growing e-waste is causing concern', The Hindu*, 28 February 2009.]
33. Satish Sinha, *'Downside of the Digital Revolution', Toxics Link*, 28 December 2007, http://www.toxicslink.org].
34. Sepúlveda, A. et al. 2010. "A review of the environmental fate and effects of hazardous substances released from electrical and electronic equipments during recycling: Examples from China and India", in *Environmental Impact Assessment Review*, Vol. 30, No. 1, pp. 28–41.
35. StEP initiative, 2012].
36. Tom Young, *'E-waste a growing problem for China and India'*, 22 February 2010, http://www.computing.co.uk].
37. UNEP Press Release, *'Basel Conference addresses Electronic Wastes Challenge'*, 27 November 2006 http://www.unep.org/].
38. Widmer R.,Heidi O.K.,Deepali S.M. Heimz B. '*Global perspective on e-waste*'. Environ. Impact Assess. 25, 436, 2005.
39. Yilmax A.B. *'Comparison of heavy metals of Grey mullet'* (M.Cephalus L) and Sea bream (S.Aurata L.) caught in Iskenderun bay (Turkey). Turk. J. Vet. Anim. Sci. 29, 257, 2005.]
40. Yu, J.; Welford, R.; Hills, P. 2006. "Industry responses to EU WEEE and ROHS Directives: Perspectives from China", in *Corporate Social Responsibility and Environmental Management*, Vol. 13, No. 5, pp. 286–299.

DOI: 10.15680/IJIRSET.2014.0310071

International Journal of Advanced Research in Electronics and Communication Engineering (IJARECE)
Volume 3, Issue 11, November 2014

Throughput Calculation according to User Location in LTE-A Network

Kishor Pratap Singh, Pradeep Kumar Chopra

***Abstract*— LTE-A is a very advanced and very adaptive intelligent network. Use of femto cells increases its capacity without increasing the installation cost of the network. Mostly femto cells are deployed by home users itself so a service has not to worry about installation cost. But due to co-channel operation interference increase between femto & macro users which can be reduced by using cross-tier interference cancellation strategy. In this paper analysis of LTE-A system has been done. This paper proposes a simulator that consists of practical deployment conditions, random user distribution, random building generation, MIMO and different coordinated multipoint schemes. This simulator takes into account both types of cross-tier interference, i.e., the macrocell interference to users attached to femtocell and the femtocell interference to users attached to macrocell.**

***Index Terms*— COMP, Frequency Reuse, LTE-A, MIMO, Throughput.**

I. INTRODUCTION

The need for high data speed is rapidly increasing day by day and the main reason for this increment is the availability of smart devices, and social networking facilities. Enhancement in data rate is constantly required in wireless communication technology. Long Term Evolution-Advanced (LTE-A) is the promising solution for wireless broadband services. LTE-Advanced is also known as 4G wireless networks [1]. It is an evolution of LTE Rel-8. This paper focuses on LTE-Advanced systems and femtocell technologies. Femtocells, also referred to as femto or Femto Base Stations (FBSs) or Home Node-Bs (HNBs) are data access points installed by the subscribers to provide better indoor voice and data coverage and to increase system capacity [2]. The integrated femtocell / macrocell networks offer an efficient way to increase access capacity by improving coverage and quality of service. Femtocells are an attractive solution for providing better coverage and capacity and low cost for deployment and maintenance [3]. However, their performance is restricted by the cross-tier interference with macrocell base station coverage or between adjacent femtocell base station coverage, especially in the case of co-channel deployment. A simulator is designed that consists of practical deployment conditions, random user distribution, random building generation, MIMO and different coordinated multipoint schemes.

Coordinated multi-point (COMP) transmission / reception are considered for LTE-Advanced technology as a tool to improve the coverage of high data rates, the cell-edge throughput and to increase the system throughput [4]**.** This can be achieved using coordination between nearby base stations and the serving base station. MIMO can be used to increase the throughput of cell center and edge users. In MIMO 8x8 antenna array is used. Cell center users will get different data streams at each MIMO link and cell edge users will get same data on each MIMO link. Interfering elements like walls are taken as random to create a practical scenario and to get close to genuine results as much as possible. Use of new techniques gives very high enhancement in throughput. As the enhancements in the wireless technologies are coming data rates for end users are increasing and data cost decreasing for users. As the bandwidth increase implemented with highly adaptive systems throughput increases due to decrease in interference from nearby transmissions. So implementation of LTE-A is a very good decision for serving users with high data rates.

COMP is also known as network MIMO or Co-operative MIMO. The primary difference between standard MIMO and COMP is that in the COMP, the transmitters are not physically co-located as shown in Fig. 1.1

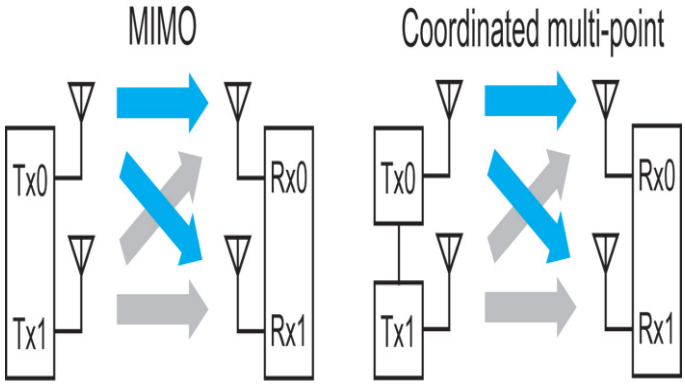

Fig. 1.1 Standard MIMO versus COMP

The paper is organized as follows. In Section 2 simulator architecture is described. In section 3 results of the work are shown. Finally, the paper is concluded in Section 4, and future scope is discussed in Section 5.

Manuscript received Nov, 2014.
***Kishor Pratap Singh**, Deptt. Of E.C.E.,A.K.G. Engineering College, Uttar Pradesh Technical University,Ghazaibad, India.*
***Pradeep Kumar Chopra,** Deptt. Of E.C.E.,A.K.G. Engineering College, Uttar Pradesh Technical University,Ghazaibad, India.*

 All Rights Reserved © 2014 IJARECE

II. SIMULATOR ARCHITECTURE

Firstly, User input is given in the form of the random location coordinates of femtocells, femto users, fixed macro cell coordinates, the number of expected users required, channel bandwidth, desired femtocell range. Based on the selection of user input, path-loss and gain are calculated s shown in Fig. 2.1.

For edge users for which the path-loss of the original base station is more than the adjacent base station, COMP is applied. For edge users MIMO is also applied, whose results are shown separately.

Afterwards, depending on the interference technique chosen, the signal to interference + noise ratio (SINR) is calculated, followed by the throughput evaluation.

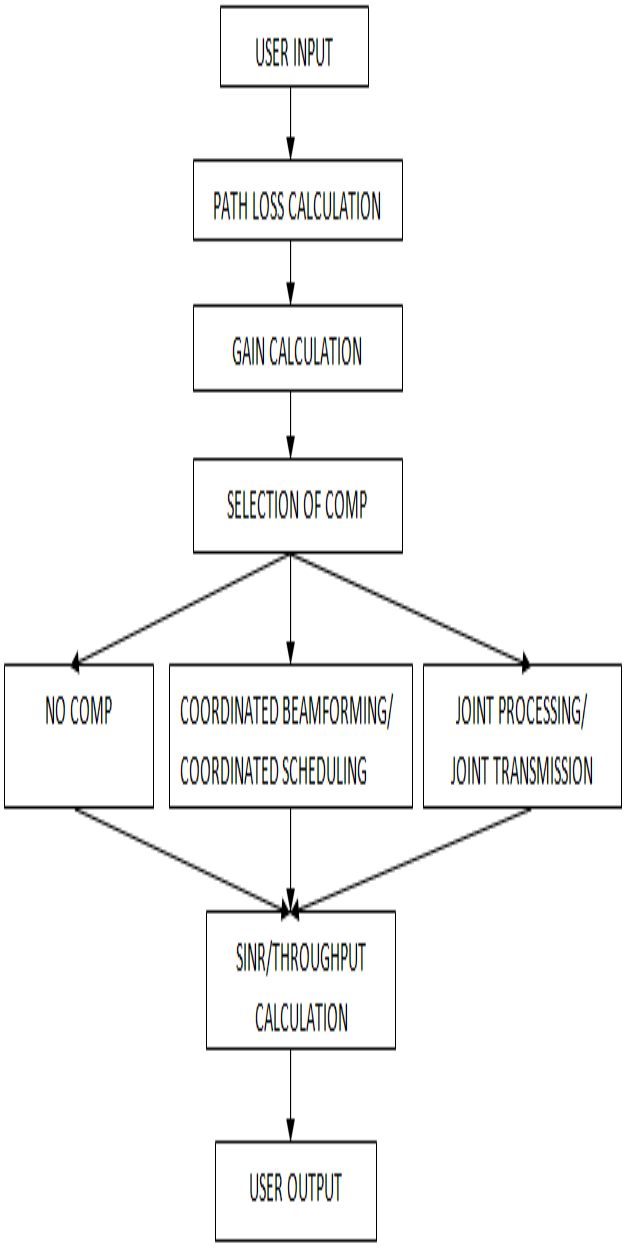

Fig. 2.1 Flowchart

III. SIMULATION RESULT

A. SIMULATOR DETAILS

The red circles shows the femto cells, the hexagonal structure shows macro cell, square structures shows the buildings which are used for interference calculation, in the middle of the picture there is an macro enodeB, blue dots shows femto users, green dots shows macro users, outdoor walls are shown between users and base stations. Distances between users and base stations are also shown. Simulator is easy to use and flexible to change for end users. The simulation parameters are shown in Table 3.1.

Table 3.1 Simulation Parameter Table

PARAMETERS	VALUE
MACROCELL RADIUS	250 m
FEMTO CELL RADIUS	20 m
FREQUENCY	2 GHz
MACRO BS POWER	46 dBm
FEMTO BS POWER	20 dBm
OUTDOOR WALL LOSS	15 dB
INDOOR WALL LOSS	7 dB
BANDWIDTH (MHz)	20
MODULATION SCHEME	64 QAM
SUBCARRIER SPACING	15 KHz
WHITE NOISE POWER DENSITY	-174 dBm / Hz

B. DEPLOYMENT SCENARIO

In this the simulation is done on centre macro base station. Adjacent base stations as well as adjacent to adjacent base stations are taken, to take into account the interference from adjacent base stations. If the scenario is co-channel the interference will be from adjacent base stations on the centre base station users. If the scenario is IFR, the interference will be from adjacent to adjacent base stations because same frequencies are not allocated to adjacent base stations. Fig. 3.1 shows the perfect deployment of base stations but practically this is not possible at all times in an urban area scenario, as shown in Fig. 3.2, due to social and other factors. There are coverage gaps left in between which can be overcome by relaying at the cell edges to increase the coverage of macro cells in the areas of low and no coverage. These two types of scenarios are shown to understand the practical network deployment. By seeing these scenarios a viewer can easily understand how the network has been deployed in the practical environment.

ISSN: 2278 – 909X
All Rights Reserved © 2014 IJARECE

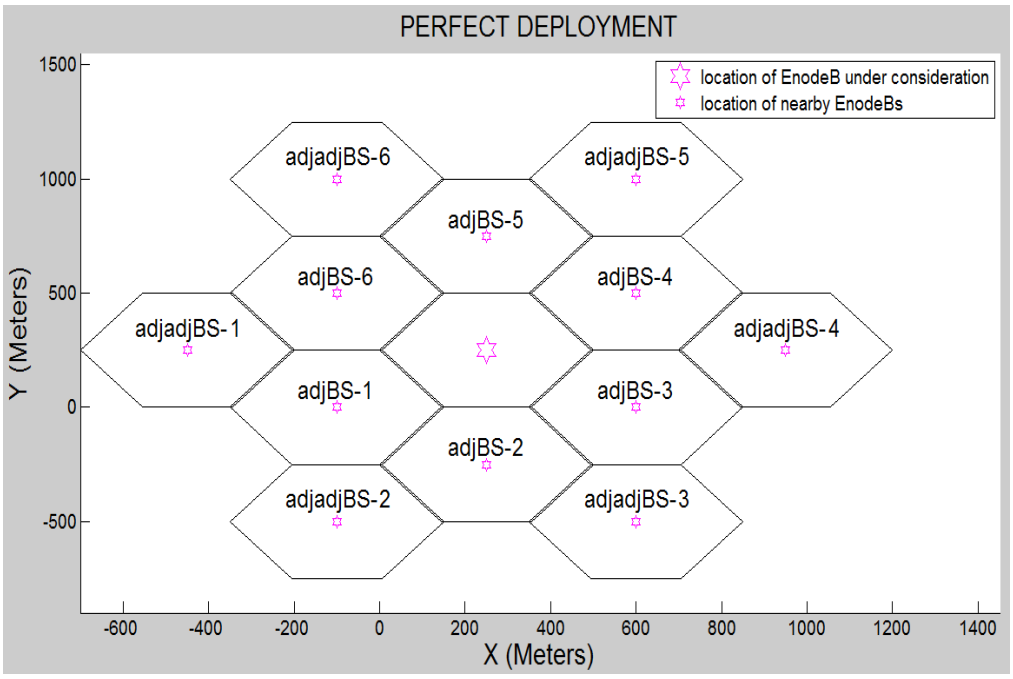

Fig. 3.1 Perfect deployment

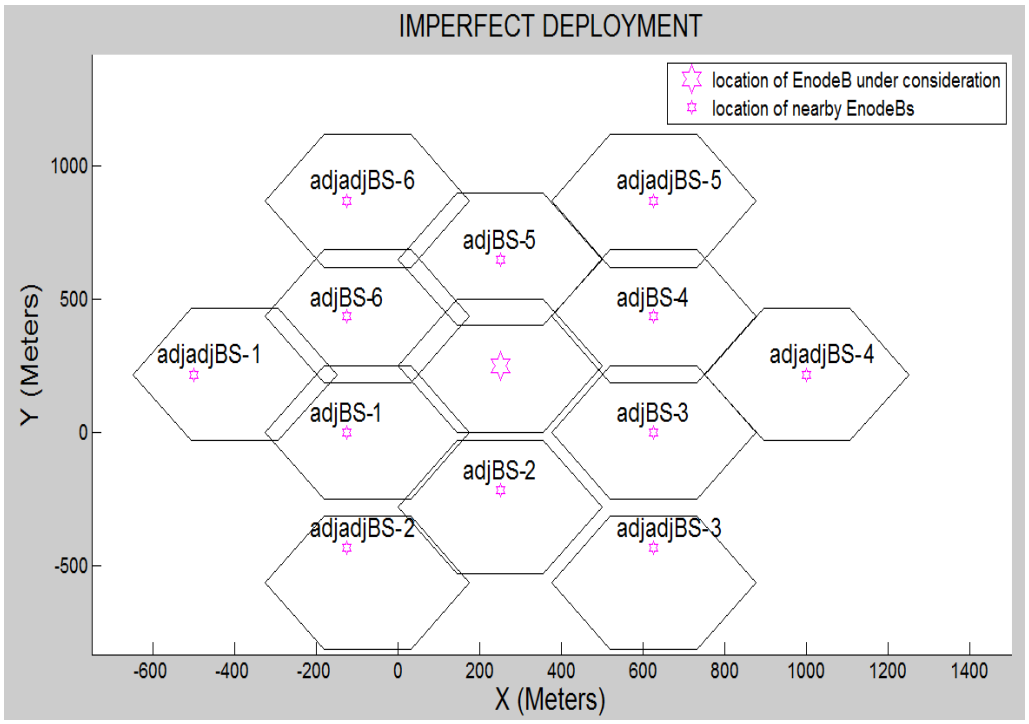

Fig. 3.2 Imperfect deployment

C. THROUGHPUT AT DIFFERENT USER POSITIONS

In this different positions of femto and macro users, with different no. of walls in between users and base stations, with user distances from their serving base stations, users indoor or outdoor are shown and their effect on throughput. Fig. 3.3 shows the first position of users. In this femto user is 19 m away from FBS and is indoor user with no wall in between user and its serving base station having throughput 46.0858 Mbps whereas macro user is 67 m away from MBS and is indoor user with one wall in between user and its serving base station with throughput 95.463 Mbps. With user new position which is shown in Fig. 3.4. In this femto user is 5m away from FBS and is indoor user with no wall in between user and its serving base station having throughput 108 Mbps whereas macro user is 215 m away from MBS and is indoor with one wall in between user and its serving base station having throughput 48.3328 Mbps.

 All Rights Reserved © 2014 IJARECE

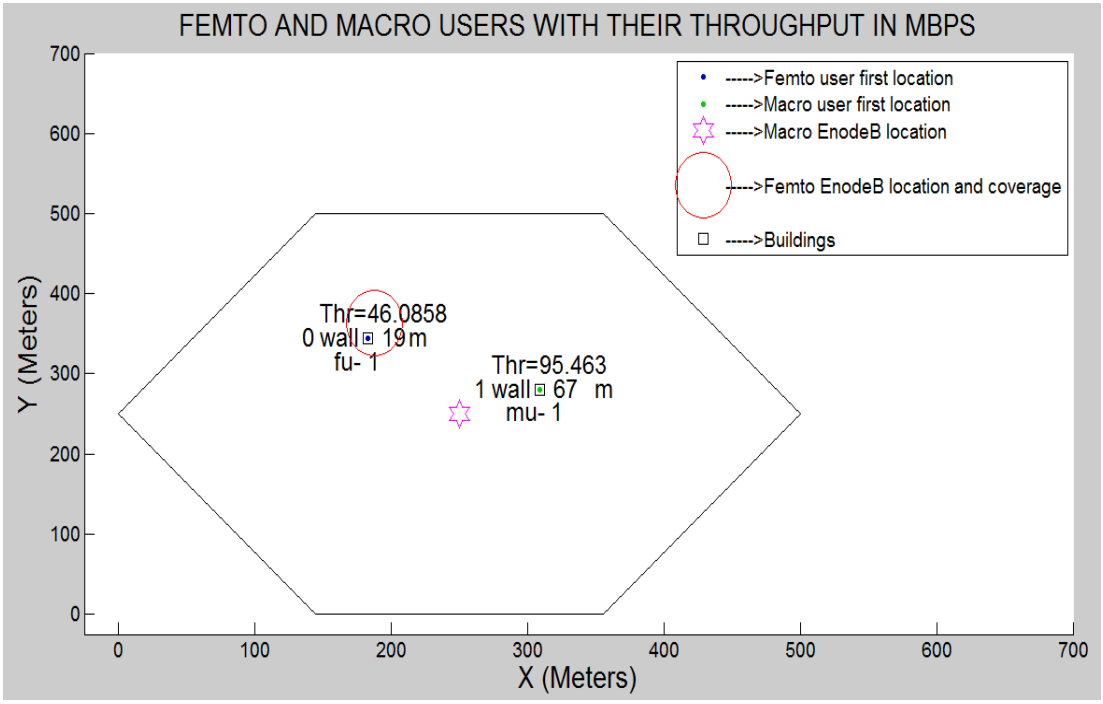

Fig. 3.3 First position of users

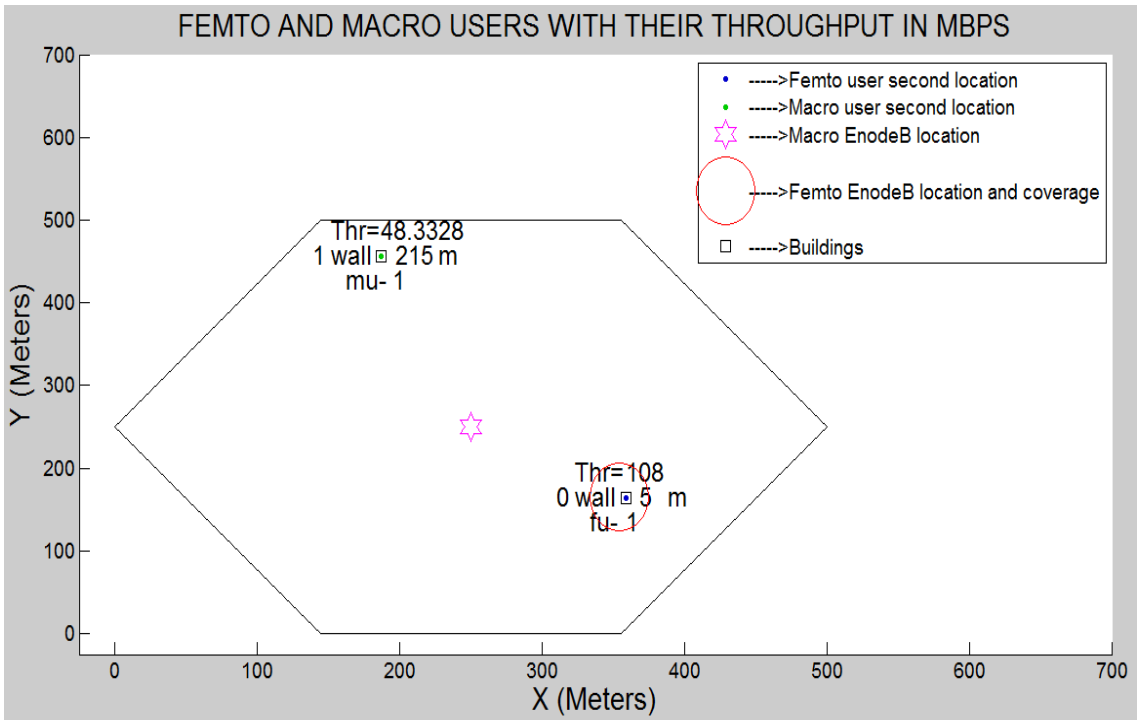

Fig. 3.4 Second position of users

D. THROUGHPUT AT DIFFERENT COORDINATED MULTIPOINT MECHANISMS

COMP mechanism is used to increase the throughput of macro edge users in which users are served from one or more adjacent base stations simultaneously when the path loss of serving cell is more as compared to adjacent base station. Coordinated multipoint (COMP) is of two types coordinated beam-forming / coordinated scheduling (CB / CS) and joint processing / joint transmission (JP / JT). Fig. 3.5 shows throughput of macro user at edge when it is 245m away from MBS with no COMP applied and is indoor user with one wall in between user and its serving base station having throughput approx 0.62317 Mbps. Fig. 3.6 shows throughput of macro user at edge when it is 245m away from MBS with coordinated beam-forming / coordinated scheduling (CB / CS) COMP applied and is indoor user with one wall in between user and its serving base station having throughput approx 6.6534 Mbps. In this the user is served from one base station but not from center base station but from adjacent base station 3, Fig. 3.7 shows throughput of macro user at edge when it is 245m away from MBS with joint processing / joint

ISSN: 2278 – 909X All Rights Reserved © 2014 IJARECE

transmission (JP / JT) COMP applied and is indoor user with one wall in between user and its serving base station having throughput approx. 19.9009 Mbps. In this the user is served from three base stations simultaneously i.e. centre base station and adjacent base stations 3 and 4. MIMO diversity is used at the edge with all the same conditions as in comp and the throughput is 4.9722 Mbps as shown in Fig. 3.8

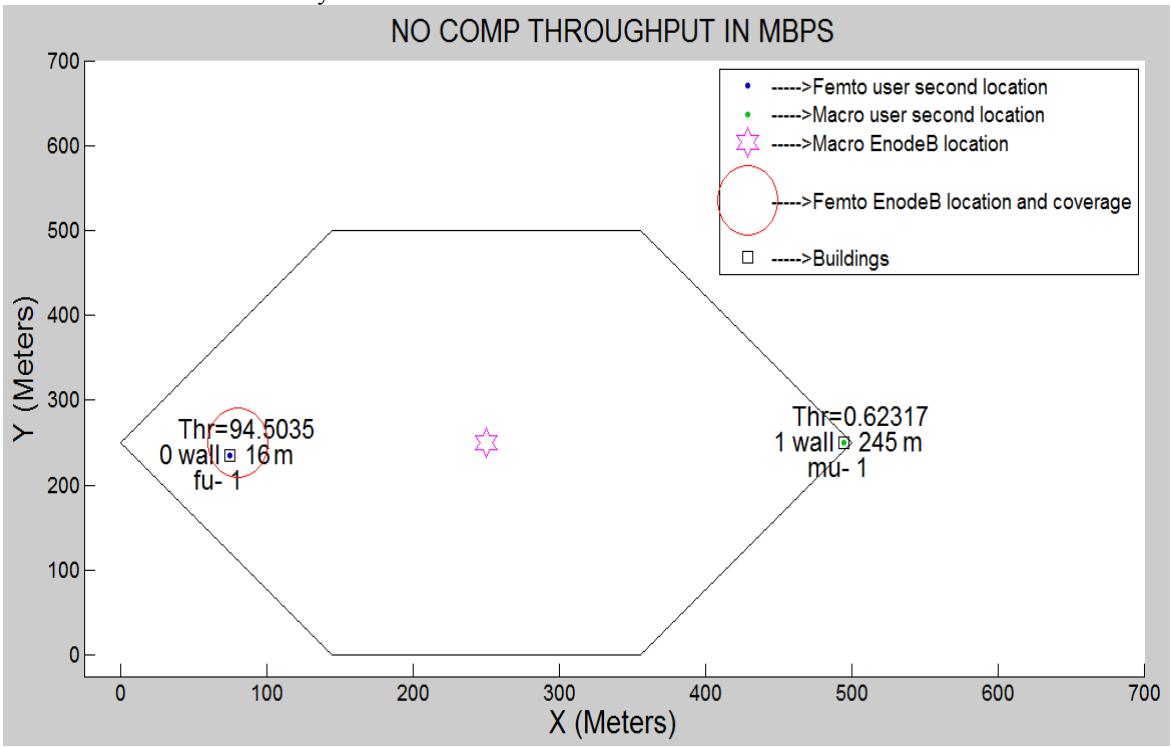

Fig. 3.5 Throughput with no COMP applied

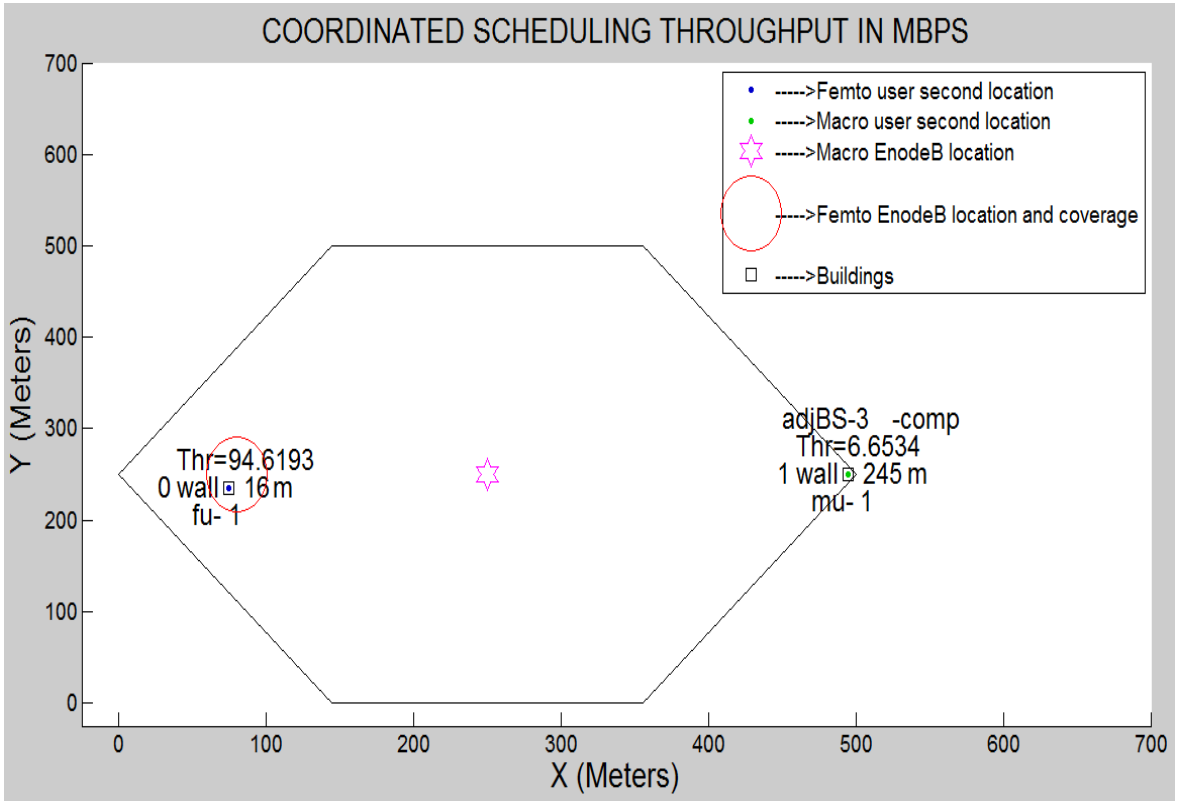

Fig. 3.6 Throughput with single COMP applied

 All Rights Reserved © 2014 IJARECE

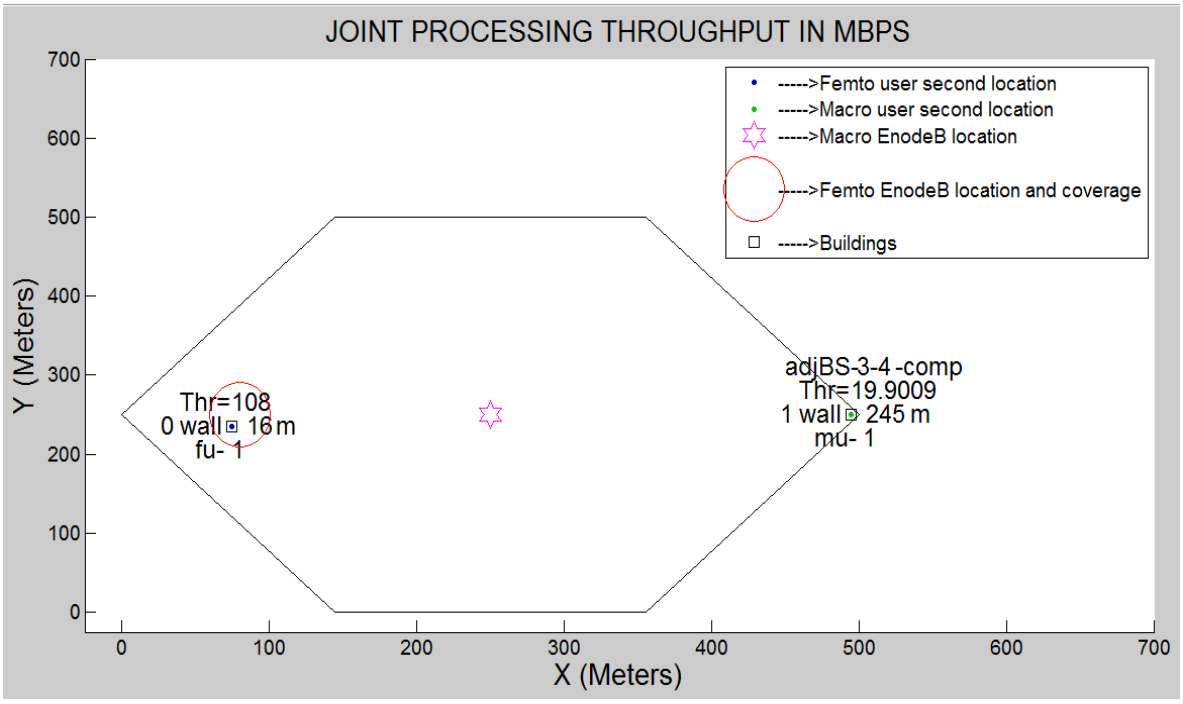

Fig. 3.7 Throughput with joint COMP applied

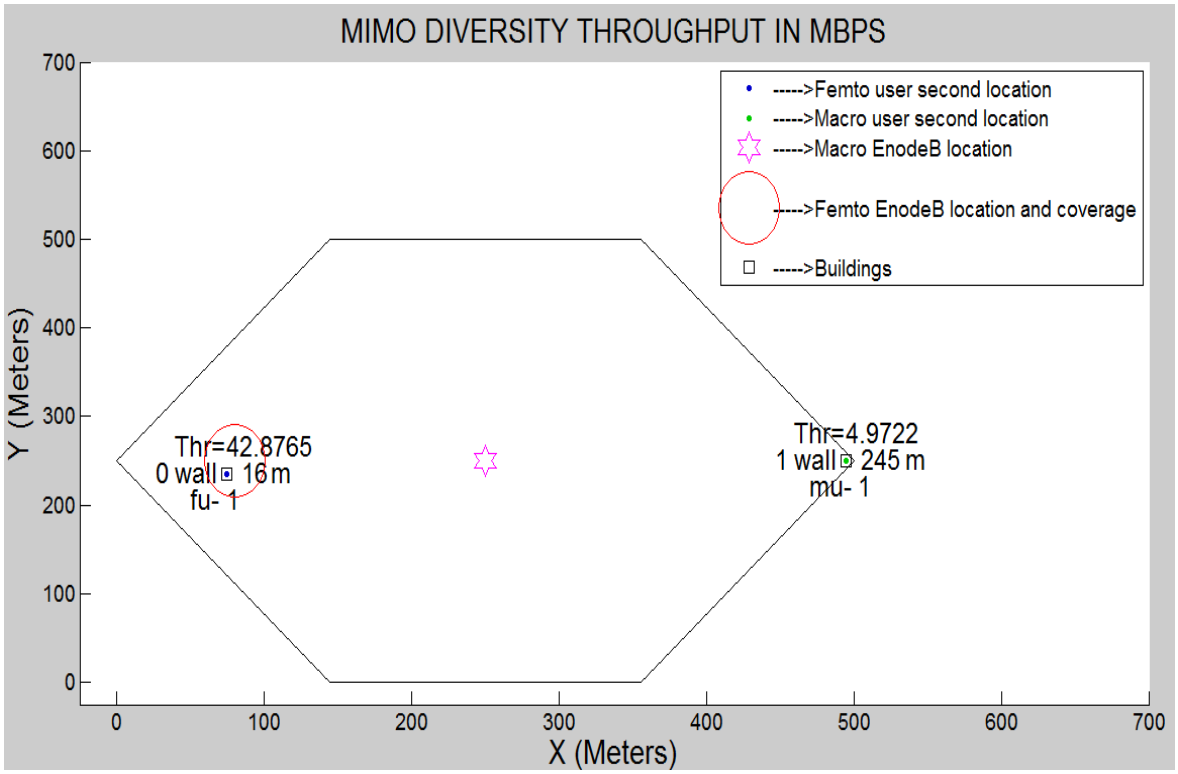

Fig. 3.8 Throughput with MIMO applied at edge

IV. CONCLUSION

In this paper, analysis of LTE-A system has been done. This paper presented a simulator consists of MIMO and COMP. This simulator takes into account most of the all major types of interference. With the use of COMP, MIMO user throughput gets increased due to reduction in interference. This paper gives a clear view of throughput a user get in a practical network area which also helps in deployment of original network.

V. FUTURE SCOPE

Future scope is to make more adaptive and more optimized network by including release 11, 12, 13 features and also to include original terrain in the simulator to get exactly the same result as a user get at a particular location in the included terrain. Advanced fractional frequency reuse in combination with power control can be applied to increase capacity.

ISSN: 2278 – 909X All Rights Reserved © 2014 IJARECE

With the current simulator consisting of MIMO and COMP the throughput is increased to a large extent. For more enhancements in throughput, advanced power control algorithm and interference mitigation techniques can be used .Also with the help of adaptive beam forming excellent data rates can be achieved.

ACKNOWLEDGEMENT

I sincerely thank Electronics and Communication Engineering Department of Ajay kumar Garg Engineering College, Ghaziabad for providing the opportunity and guidance for research work.

REFERENCES

[1] Christos Bouras, Georgios Diles, Vasileios Kokkinos, Konstantinos Kontodimas and Andreas Papazois, 2013 " A Simulation Framework for Evaluating Interference Mitigation Techniques in Heterogeneous Cellular Environments" *Springer Journal,* pp. 1 – 25.

[2] Ian F. Akyildiz, David M. Gutierrez-Estevez, Elias Chavarria Reyes, 2010 "The evolution to 4G cellular systems: LTE-Advanced", *Elsevier Journal,* pp. 217-244.

[3] Christos Bouras, Vasileios Kokkinos, Konstantinos Kontodimas andAndreas Papazois, 2012 "A Simulation Framework for LTE-A Systems with Femtocell Overlays" *Proceedings of the* 7th *ACM Workshop on Performance monitoring and measurement of heterogeneous wireless and wired network,* pp. 85-90.

[4] Satnam Singh, Amit Kumar, Dr.Sawtantar Singh Khurmi, Tanvir Singh, 2012 "Coordinated Multipoint (COMP) Reception and Transmission for LTE-Advanced/4G", *International Journal of Computer Science And Technology (IJCST),* Vol. 3, No. 2**,** pp. 212-217.

Kishor Pratap Singh received his B.Tech degree in Electronics & Communication Engineering from Indian Institute of Technology (Gautam Budh Technical University, Lucknow) Bareilly, U.P., India in 2011 and is shortly finishing his M.Tech degree in Electronics & Communication from Ajay Kumar Garg Engineering College (Uttar Pradesh Technical university, Lucknow), Ghaziabad, U.P., India. His interest areas are advanced wireless communication, digital signal processing.

Prof. Pradeep Kumar Chopra entered the field of education in the year 2004 after 24 years of exemplary service in the technical branch of the Indian Air Force, He earned his Bachelors degree in Engineering (Electronics) from Delhi college of Engineering in the year 1979 and Masters in Technology from IIT Delhi in the year 1985. He also has a Masters degree in Defence Studies from Madras University. While he was in the Indian Air Force he was part of, and headed a number of important technical projects. For his exemplary services he was awarded "Vishist Seva Medal" by the President of India in the year 1993. He took premature retirement from the IAF in the year 2004 and entered the field of education. He is the Dean and Head of Dept. (Electronics and Communication) in Ajay Kumar Garg Engineering College in Ghaziabad. AKGEC is rated as the No 1 Engineering College in U.P., Affiliated to Uttar Pradesh Technical University, Lucknow.

 All Rights Reserved © 2014 IJARECE